Anglia Ruskin University

Cambridge Chelmsford Peterborough

MODELLING WHEELED CONSTRUCTION PLANT PERFORMANCE IN CLAY AND SANDY TERRAIN: A TERRAMECHANICS PERSPECTIVE

A THESIS SUBMITTED TO THE FACULTY OF SCIENCE AND TECHNOLOGY, DEPARTMENT OF ENGINEERING AND THE BUILT ENVIRONMENT OF ANGLIA RUSKIN UNIVERSITY IN PARTIAL FULFILMENT OF THE REQUIREMENTS FOR THE AWARD OF THE DEGREE OF DOCTOR OF PHILOSOPHY

Franco Muleya

August 2014

Supervisors: Dr Sunny Nwaubani: PGCert, MSc, PhD, FHEA, MABSE
Dr David Reid, BSc, MSc, PhD, CEng, CMath, MICE, FIMA

ACKNOWLEDGEMENTS

My sincere gratitude goes out to my supervisors Dr Sunny Nwaubani and Dr David Reid for the unfailing, tremendous and consistent support from the inception of the research right through to the completion of this research. I would also like to thank Anglia Ruskin University particularly the Department of Engineering and the Built Environment for the scholarship and Graduate Teaching Assistantship (GTA) awarded to me in order to enable me carry out the research. I also want to extend my gratitude to the acting head of department Peter Crabtree for the special support and understanding during my research period at the University.

Special thanks and heartfelt gratitude go out to my wife Linda, my daughter Mukomi and my son Mulambo Siachintu 'State Counsel' for their solid and consistent support throughout the research period. I want you to kNow that I am immensely grateful for your physical and emotional support that you rendered to me all the time be it day or night. I would also like to thank my father Moses Muleya and my mother Ellen Muleya, my brothers Wezzy and Alvin for their encouragement and support. I would also like to extend my heartfelt appreciation and thanks to my parents in law Fred and Israel Zandonda for their outstanding support during this immensely demanding and testing time.

I would like to further extend my appreciation to my friends for their support. These include Matyola Moomba, Joseph Phiri, Bruce Mwiya, Obby Phiri, Alice Lungu and Dr Roy Chileshe all from the Copperbelt University, Thank you so much for your amazing and unfailing support. I also want to thank my colleagues and fellow research students at in the department such as Oluwafemi Akande, Mohammed Hussein, Chucks Wokocha and Diagarajen Carpanen. I also wish to thank Mr and Mrs Mumbuluma for their support during my first days of arriving in Chelmsford. Special thanks go out to Mr and Mrs Chitambala for their tremendous support throughout my research period. Thank you to all Chelmsford SDA church Pastors, Elders and members for their prayers and encouragement led by Sr Verbena Newyear. I would like to extend special thanks to my sister Ngoza Phiri for her immeasurable financial and moral support. Thank you so much. Last but not the least I would like to offer special thanks to the team of elite technicians that worked

with me in planning, building and running of laboratory experiments. Thank you for spending those long hours of hard work with me. These technicians include Steve Read, Andy Ferady and Dan Jackson. Special thanks for Dominic Martin as well for his insights and valuable contribution to the success of my work. I would also like to thank Graham Wing of Chelmer Laboratories in Chelmsford, Essex, for facilitating some of my key laboratory soil tests. Thank you very much.

Dedication

This thesis is dedicated to my beautiful, loving and hardworking wife Linda, our two beautiful children Mukomi and Mulambo SC.

ABSTRACT

This research has investigated the effect of tyre rutting of wheeled construction plant performance traversing in wet and deformable terrain, specifically clay and sand. The purpose was to translate the wheel rutting into performance reduction measured in drawbar-pull. The ultimate goal was to translate the power loss into practical effects on cost, time and other economic variations on construction projects that are characterised by movement of wheeled plant on long haulage deformable roads.

In order to achieve this aim, mathematical modelling was deployed based on Newton's laws of motion, principles of energy conservation and numerical integration. The model is based on a single rigid wheel because construction plant tyres are inflated to high pressure in order to support heavy loads thereby translating the flexible tyres into rigid mode. The results from the mathematical model were verified using a three stage robust verification process which included computational analysis based on two existing semi-empirical methods and real experimental data. Laboratory experiments using Mobility SF- 3713 were also used to check the validity of the results.

The results from the mathematical model verify that a flexible tyre can operate in rigid mode if it encounters softer and wet ground. Results further indicate that the soil cohesion, angle of shearing resistance and moisture content play key roles in the subsequent power loss created by motion resistance. All the results from computational analysis and the experiments were found to be consistent with the mathematical model results.

The study concludes that there is ample evidence to suggest that there is significant power loss associated with wheeled construction plant traversing in soft terrain which can be assessed. The study further concludes that a combination of economic decisions on variables must be considered with respect to existing ground conditions. This will considerably reduce uncertainty levels in cost and resource management on construction projects.

Keywords: ***Modelling, wheel-soil interaction, drawbar-pull, rut depth, performance, Construction***

TABLE OF CONTENTS

TABLE OF FIGURES

LIST OF TABLES

DEFINITION OF TERMS

Wheel-slip (i) is the proportional measure by which the actual travel speed of the wheel falls short of (or exceeds) the "theoretical" speed”

Wheel Rutting (mm) is the longitudinal vertical deformation of a surface or terrain a wheel path, measured relative to a straight edge placed at right angles to the traffic flow and across the wheel path.

Rolling (motion) resistance (R) is the force opposing motion of the wheel that arises from the non-recoverable energy expended in deforming the surface and wheel. It is convenient to consider this force as acting in the horizontal direction.

Tractive force (H) is the horizontal reaction on a driven wheel by the soil in the contact area; it is equal and opposite to the horizontal force generated by the wheel on the soil.

Drawbar-pull (DP) is the horizontal force at the axle generated by a driven wheel; it may be assumed that:

Drawbar-pull = Tractive force - Rolling resistance

Cohesion (C) is a measure of the forces that cement particles of soils

Angle of shearing resistance (φ) is the measure of the shear strength of soils due to friction

Mohr-Coulomb Failure Criteria This theory states that a material fails because of a critical combination of normal stress and shear stress, and not from their either maximum normal or shear stress alone.

A **normal stress** is force that is applied vertically and held constant

A **shear stress** is a force that is applied until failure takes place

The **shearing strength** of a soil sample is generally defined as its maximum resistance to shearing forces

HCS: (Higher Cohesion Soil)

LCS: (Lower Cohesion Soil)

Distance conversion factor: 1m/s = 3.6km/h

NOMENCLATURE

Roman symbol	Description	Unit
A	Area	m^2
b	Wheel width or plate size	m
b_{ti}	Tyre width	m
c	Cohesion	Pa
d	Diameter	m
DP	Drawbar-pull	N
e	Void ratio	$--$
F	Force	N
g	Gravity	m/s^2
H	Thrust /Horizontal component of tension force	N
i	Slip ratio	$--$
j	Soil deformation /Shear displacement	m
k	Empirical coefficient	$--$
K	Shear deformation modulus	m
k_φ	Friction sinkage parameter	N/m^{n+2}
k'_φ	Dimensionless friction modulus	$--$
k'_a	Pressure-sinkage modulus	$--$
k_c	Cohesion sinkage parameter	N/m^{n+1}
$k'c$	Dimensionless cohesion modulus	$--$
l	Length	m
lc	Contact length	m
m	Mass	kg
n	Sinkage exponent	$--$
p	Pressure	Pa
p_g	Ground pressure	Pa
p_{cr}	Critical inflation pressure	Pa

Roman symbol	Description	Unit
p_{gcrr}	Critical ground pressure	Pa
p_i	Tyre inflation pressure	Pa
r	Radius	m
R	Resistance	N
T	Torque	Nm
t	Time	s
V	Velocity	m/s
V_v	Total volume	m^3
V_v	Translational velocity	m/s
Vp	Rotational velocity	m/s
w	Width	m
W	Weight	N
z, z_0	Sinkage	m
z_r	Sinkage of a tyre in rigid operating mode	m
z_e	Sinkage of a tyre in elastic operating mode	m

Greek symbol	Description	Unit
γ	Density	$N/m3$
η	Rear of wheel sinkage relationship	$--$
θ	Angle	rad
σ	Normal stress	Pa
τ	Shear stress	Pa
φ	Angle of shearing resistance	deg
ω	Angular frequency or velocity	rad/s
λ	Ratio	$--$
δ	Tyre deflection	m

LIST OF APPENDICES

COPYRIGHT

CHAPTER 1

INTRODUCTION TO THE RESEARCH

1.0. CHAPTER 1

Introduction to the Research

1.1 Research Background

According to Reid (2000), ground conditions can vary greatly on a construction site due to external factors such as the effect of weather conditions on the physical properties of the soil. This in turn has a marked effect upon the efficiency and power output of the tracked and wheeled plant employed. Contractors have to price the cost of ground works based upon the expected conditions but need to consider the effects of such variations.

One of the main sources of wheeled construction plant power loss is the rolling resistance between the moving wheels and the ground as plant wheels traverse through the unprepared terrain on construction sites and soft haulage roads. This relationship forms part of Terramechanics which Reid (2000) defines as the study of performance of off-road vehicles in relation to the operating environment and its terrain. Terramechanics is concerned with the measurement of the mechanical properties and characteristics of terrain as they affect vehicle mobility and the mechanics of vehicle-terrain interaction. According to the Department of Defence, vehicle mobility is also defined as the overall capacity of a vehicle to move from place to place while retaining its ability to perform its primary mission, Sandu et al (2010).

According to Reid (2000), a prolonged dry spell of weather can result in a compact surface capable of effectively supporting heavy construction traffic operating in clay terrain conditions. After a heavy shower, the surface layers of the same soil may loosen and distort when trafficked by site plant, resulting in reduced efficiency and output from the plant due to energy losses caused by wheel slip and rutting of the surface. Barnes (2010) equally highlights that the effects of weather on an earthworks project with softening during wet weather. Formation of permanent ruts by rolling wheels of Off-Road Vehicles (ORVs) presents a particularly complex and challenging problem when analysed within the framework of mechanics, Hambleton and Drescher, (2009). Part of the economic success of a construction project often hinges on the correct selection of wheeled plant to minimise these operational efficiency losses. After analysing the energy efficiency of flexible tyres in off-road conditions, a study undertaken by Senatore and Sandu (2011) concluded that it is possible under the given conditions to improve the fuel economy by reducing the power lost at the wheels. The choices available can only be assessed through an understanding of the relative effects of each of the problem variables. Figures 1.1 and 1.2 show the geometry and ground contact profile of a rigid and flexible wheel operation in deformable terrain. Figure 1.1 illustrates rutting of the wheel into the soil without deflection. This is common for solid wheels and fully inflated tyres traversing in soft ground. Figure 1.2 illustrates the partial rutting due to deflection experienced by the wheel. The latter is common when a flexible tyre is not fully inflated and encounters soft but firmer terrain. A detailed discussion of this relationship is presented in chapters 2, 5 and 6.

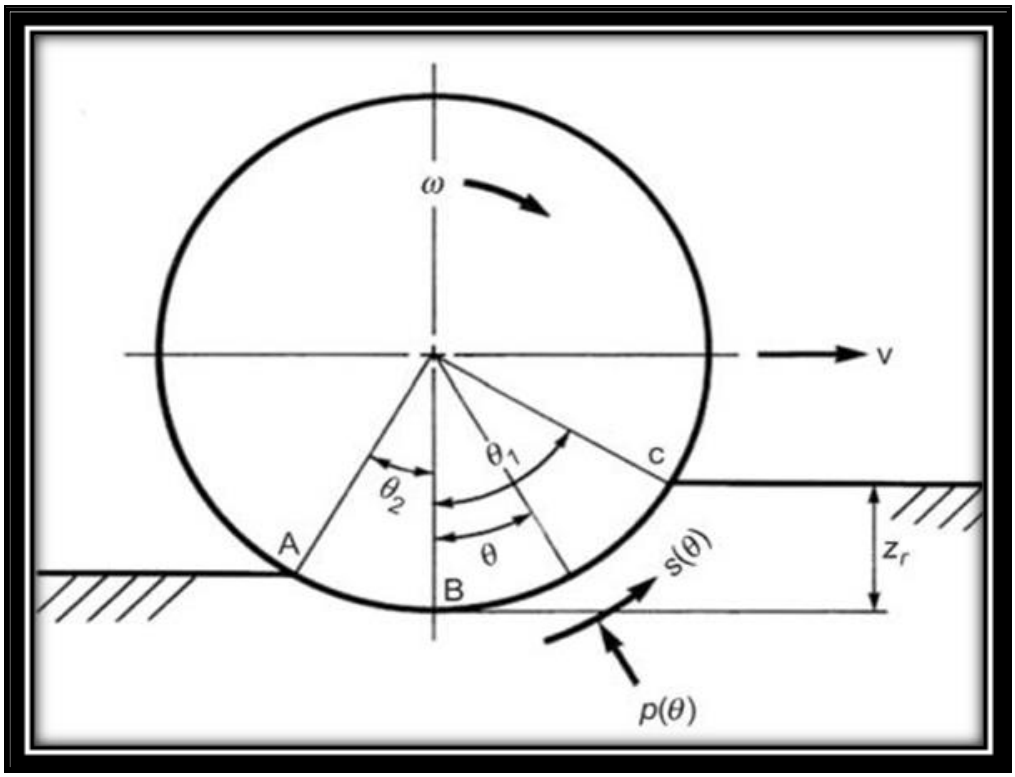

Figure 1.1: Rigid tyre in deformable ground Wong (2010)

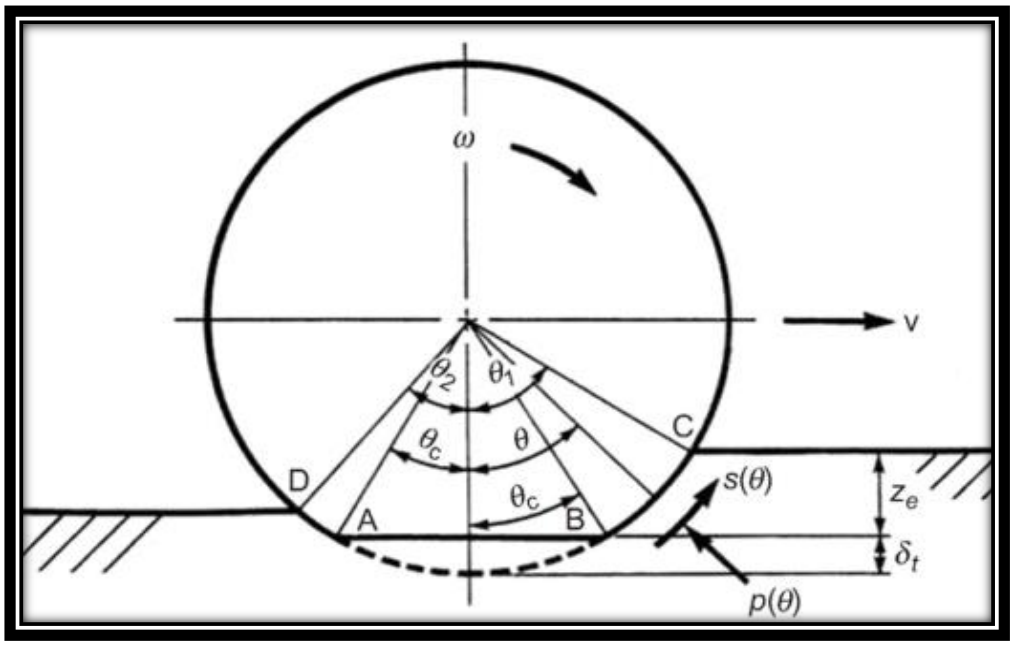

Figure 1.2: Flexible tyre in deformable ground Wong (2010)

Tyre-terrain interaction is a very complex research topic in terramechanics and has been regarded as a critical issue to the design of off-road vehicles, (Xia, 2010).

1.2 Overview of Terramechanics

Systematic research and studies in Terramechanics began in the 1950's primarily driven by military and agricultural engineers mostly based on the classical work of Dr Miecyslaw Gregory Bekker using semi empirical constants, (Scott and Ellery, 2005; Sandu, C. et al 2010). After the Second World War empirical methods which were more applicable in important branches of military off-road transportation and agricultural engineering had been given precedence over a more scientific approach. Since 1942, Bekker had been conducting basic research first in the Canadian Department of National Defence and later in the United States Army Ordinance Corps, Sohne (1976). It was Bekker who was first to maintain that off-road transportation should not be developed exclusively by empirical methods but by scientific ones.

Terramechanics models fall into three categories of increasing complexity: purely empirical methods, semi-analytical methods and physics-based approaches, Madsen, et al, (2013). The Bekker model and the extension made by Wong and Reece are both semi-empirical models developed in the terramechanics literature. These are two fundamental models used in performance evaluation of rovers, Azimi et al (2013). Terramechanics can be used for intended purposes such as evaluating vehicle mobility in a specific, area, industry, defined terrain and existing circumstances. It can also be used to understand wheel-soil interaction in an effort to circumvent environmental, economic and operational constraints, Wong (2010).

Today there are many analytical methods that have been developed such as the elastic theory approach, limit equilibrium approach, spring method, Finite Element Models, mathematical modelling and energy models. These methods are described and discussed in detail in the literature review chapter. From the background and literature review studies, it has been observed that most of these Terramechanics studies have been extensively carried out and applied to the military, agriculture, forestry and planetary exploration sectors. This research on the other hand was seeking to utilise terramechanics by developing a model that will be useful in predicting the power loss arising from wheel rutting. This aspect is very critical for the management of costs and variations during the construction period that involves traversing of wheeled plant in deformable clay and sandy terrains.

1.2.1. Current practices in Terramechanics

One of the first institutes to use Terramechanics was the Canadian Department of Defence and the United States Army Corps of Engineers Waterways Experiment Station (WES). The Waterways Experiment Station performed a number of tests on vehicles in different terrain to determine a ‘GO’ or ‘NO-GO’ basis for their missions. This approach had a number of drawbacks regarding its reliability, (Madsen et al, 2013 and Wong, 2010). Wheeled and tracked vehicles have continued to be studied in the military sector. Details of the various research studies undertaken in the military sector are described and analysed in detail in the literature review chapter.

In forestry management, Terramechanics has been used to attain eco-efficient wood harvesting on sensitive sites that utilise wheeled and tracked machinery during the harvesting process, Saarilahti (2002). Terramechanics has also been used to develop models for determining wood production, soil compaction, environmental damage, operational costs, routing, site machine matching and production Saarilahti (2002). Exiting literature clearly indicates that Terramechanics application has been extensive in addressing the economic implications of forestry plant operation during logging.

Terramechanics has been extensively studied and applied to the agricultural sector to improve tractor traction and economical wheel movement during tillage. Studies in this sector range from early empirical approaches, experimental studies, mathematical modelling and computer simulation. Terramechanics has been used in this sector to understand the relationship between moving tractor tyres, soil compaction and its effect on crop production, Xia (2010). Details of some of the major studies are also discussed in chapter 2.

The study of the wheel-soil interaction relationship has been used in analysing driving wheel performance in rigid and deformable soils as part of the development of exploration and planetary rovers (robots) moving on planets such as the moon and Mars, Ding et al (2011). The National Aeronautics and Space Administration (NASA) in the United States of America has for a long time now used Terramechanics in the design of rigid and flexible wheels for planetary exploration rovers for robust mobility on planets, (Lagnemma 2011).

In open cast mining road haulage of large volumes of ore is a major characteristic throughout the life of a mine. These haulage roads are normally built with rock and well-compacted hard gravel, Thomson, R.J and Visser, A.T (2000). This results in negligible wheel sinkage of wheeled haulage trucks eliminating the problem of power and traction loss that would arise for this tyre-soil interaction. Terramechanics can however be used during the process of constructing the stable haulage roads which are deformable in nature during the initial stages of road construction projects. Detailed for this section are also discussed in the literature review chapter.

1.3. Terramechanics and the construction industry

It is very clear from the literature and research background information discussed that significant modelling work has been done in the field of Terramechanics covering the military, forestry, agricultural and planetary exploration sectors. Variables such as wheel sinkage, wheel power losses, and trend analysis of variables among others have been extensively researched and explored using semi-empirical methods, mathematical modelling, laboratory experiments, full scale field tests and computer simulation programs.

In addition it is also evident from the number of publications that the benefits of these research studies have played a significant and key role in decision making regarding operations and correct selection of plant. However, literature on this subject reveals that there has been very little research and application of Terramechanics in the construction and mining industries despite being heavy users of wheeled and tracked plant operating in off-road construction sites,

deformable haulage roads and the construction phase of surface or open cast mining operations.

1.4. Research problem and knowledge gap

Records exist regarding previous research work involving modelling construction plant such as predicting the average hourly maintenance cost of tracked hydraulic excavators operating in an open cast mining, Edwards et al (2000). Another record of related research includes an estimation of construction daily productivity of dozer operations modelled by comparing linear regression analysis and neural network model, Seung and Sunil (2006). Edwards et al (2002) equally presents the classification of plant operator maintenance proficiency into good, average and poor.

In all the above studies and many others, the wheel-soil interaction study and how the energy efficiency of the plant varies with the ease of mobility of the wheels traversing in different soils, including the underlying economic aspect of the relationship has not been fully addressed. Furthermore, construction plant power loss resulting from wheel-soil interaction has not been fully addressed. Obtaining accurate solutions to tyre/terrain interaction challenges can directly help to understand how tyre types and natural terrain conditions affect plant mobility and traction performance on construction related projects. This will also help in many levels of decision making regarding off-road vehicle design, operations and economic analysis.

This doctoral study was aimed at addressing the wheel-soil challenges associated with off-road construction related sites. Reid (2000) presented the development a

mathematical model that predicts the rut depth caused by a constant velocity wheel moving in sandy and clay soils. Despite the successful establishment of this wheel-soil interaction in construction related terrain, the rut depths predicted have limited practical application. The model can however be used as the first important step in soil trafficability and vehicle mobility studies for construction related vehicles operating in off-road conditions.

The conclusion of Reid's mathematical model strongly demonstrated the need to further develop a simple mathematical model that would provide the practising engineer with solutions to wheel-soil interaction problems such as subsequent plant power/efficiency loss. Such a model could be used as a basis for assessing mechanisms for establishing contractors claims and eliminate initial overestimating, Reid et al (2012). This research was therefore seeking to bridge this knowledge gap by developing a mathematical model that has the ability to predict construction plant power loss resulting from changing ground conditions and increased rut depth in sandy and clay related soils from initial site survey to contract completion. This research also considered the effect of multiple wheel pass rather than single wheel pass alone as seen in many experimental research works carried out in other sectors mentioned above.

1.4.1. Current wheeled plant management in industry for off-road conditions

A survey carried out through with three large plant manufacturers revealed that power loss and traction performance tests are not carried out in wet and deformable terrain due to health and safety restrictions. The absence of these tests presents a gap in knowledge because the window of opportunity to establish

the behaviour of wheeled plant operating in soft and deformable ground conditions is taken away.

Further interviews with large construction companies operating wheeled plant also revealed that practices differ from each contractor in terms of cost variations management arising from changing ground conditions. Some use the factor loads to establish the price unit rates while some are mainly interested in the cycle time of the plant. Fuel consumption factors and costs are generally passed on to the client. A guiding tool to establish the whole ranges of parameters is not available at present.

Another survey was carried out with construction plant hiring companies which established that plant hire rates are the same regardless of the terrain in which the wheeled plant operates in. This results in underestimating contract pricing in terms of hidden wear/tear costs. The risk of underestimating the hire rates is also high.

The above survey confirms the absence of a model or tool that can be used to regulate contract cost management arising from soft and deformable terrain when using wheeled construction plant. The current practice results in uncertainty in the form of unfair contract pricing and variation management of ground conditions. This also leads to poor estimation of economic performance of wheeled equipment.

1.5. Soil parameter challenges

Soil is a complex, highly variable, anisotropic material whose physical properties depend to a great extent on its state of compaction and degree of saturation.

Different industrial sectors have different compaction requirements, as illustrated in (Xia, 2010), where soil compaction is strongly desired in civil/pavement/geotechnical engineering but extremely unwelcome in agriculture. Soil compaction should therefore be alleviated and counteracted as much as possible when operating agricultural vehicles on land during seed planting and tilling as presented by Xia (2010). In addition, soil compaction also has an adverse effect on crop production. Tyre-terrain interaction is a very complex topic in classical soil mechanics in which problems are classified into two broad groups. These are characterised as settlement calculations and stability calculations. Clay and sandy soils were considered for investigation in this research.

When loaded, each type of soil responds differently when subjected to changes due to different properties, (Reid, 2000). It is for this reason that this research was seeking to develop this soil-wheel interaction study further by providing practising engineers on construction related projects with tools and solutions that would enable them to make informed decisions in minimising plant power loss arising from wheel-soil interaction. Clay and sandy soils each behave differently when subjected to moisture and other physical conditions. Their measurable engineering properties are discussed in detail later in the thesis.

According to Barnes (2010) The suitability of a soil as it affects the operation and efficiency of earth moving plant was assessed by the Transport and Road Research Laboratory in the United Kingdom in the 1980's and a reasonable relationship was found to exist between

- The soil condition and the moisture content value

- The type of plant including factors such as the number of driven wheels, tyre width, maximum engine power available and total mass of plant
- The efficiency of operation as represented by the speed of travel which could be achieved on the haul road.

1.6. Selection of wheeled plant for the study

The focus of this research was on wheeled plant and not tracked plant. This is because tracked plant has better floatation due to its larger contact area of the tracks run by belts and the ground, Bygdén and Wästerlund (2007). Tracked equipment is also characterised by lower velocities. The combination large track/ground contact area and lower velocities reduces track sinkage thereby reducing motion resistance which lead to better traction. Wheeled plant on the other hand has opposite characteristics to tracked plant. Wheeled equipment has less tyre/terrain contact area compared to tracked equipment. Most wheeled equipment such as dump trucks, front end loaders, tipper trucks, concrete mixer trucks all move at relatively higher velocities of more than 10m/s or 36km/h. This results in higher risks of deeper sinkage and subsequent motion resistance which leads to power loss prompted by lost traction such as drawbar-pull.

A tool is required to accurately estimate the whole range of effects of changing ground conditions on wheeled plant operating on construction sites and deformable haulage roads because these effects can have cost and time implications on construction projects. Despite manufacturers having developed bigger and wider wheels for such plant, such a tool would also protect the client from paying unnecessary over estimates and protect the contractor from financial and time losses arising from uncertainty created by changing ground conditions.

This is so because there are other vehicle and terrain factors that affect plant mobility besides the size of tyres. Figure 1.3 shows a tracked excavator in action while the figure 1.4 shows a wheeled truck rutting in deformable ground. These two figures provide examples of practical application of tracked and wheeled plant in line with the research purpose.

Figure 1.3: Multipurpose tracked equipment in deformable terrain (http://www.agg-net.com/news/pgc-calls-on-jcb-for-massive-groundworks-project)

Figure 1.4: Rut formation by a wheeled tipper truck in deformable terrain (http://www.volvoce.com/dealers/en-gb/vcegb/products/articulatedhaulers/pages/introduction.aspx)

1.7. Research aim

The aim of this research was to investigate the effect of ground conditions on the power loss of wheeled construction plant arising from the wheel-soil interaction. The focus of this study was on clay and sandy terrain.

1.8. Research objectives

(I) To produce a predictive mathematical model that relates the loss of power and efficiency of wheeled construction plant to prevailing geotechnical ground conditions and soil properties using a single wheel model.

(II). To critically review the existing literature in terramechanics and identify the knowledge gap associated with the subject's application to the construction sector.

(III). To formulate a research design and methods approach that will result in the successful execution of this doctoral research

(IV). To demonstrate that the flexible tyre can operate in a rigid mode under certain off-road conditions using numerical computational analysis.

(V). To verify the mathematical model results using computational analysis method based on the Canadian Defence Department experimental real data obtained by permission from the publishers.

(VI). To verify the mathematical model and computational analysis model results by carrying out laboratory tests using a special battery powered instrumented vehicle called MOBILITY SF-3713 operated under controlled laboratory conditions. Measurements of variables during laboratory tests were taken using physical measurements, instrumentation and data computation.

(VII). To conduct a critical results analysis and interface of the variable trend and performance implications of this relationship between ground conditions and power losses associated with wheeled construction plant.

(VIII). To present the main contribution to knowledge and identify areas of further research based on the research findings and conclusions.

In addition to the aim and objectives laid down, three key research questions were outlined from the onset of the research as follows:

- How does wheeled construction plant performance and efficiency vary with response to prevailing ground conditions?

- Can this mathematical model be used to predict costs, time variations and estimated completion dates resulting from research results?

- Can the effects of varying ground conditions on cost associated with construction plant be modelled and quantified?

1.9. Research Design and Methods

Experiments, mathematical modelling and computer simulations have been used either in isolation or in combination in many scientific investigations and research. In this research, the rut depth mathematical model was further developed to incorporate construction wheel plant power loss. The individual elements of a mathematical model are capable of isolated analysis allowing the user to identify and assess their separate contribution and effects on rut depth development and its subsequent effects, Reid (2000).

According to Gerda (2001) mathematical modelling is the use of mathematics to describe real-world phenomena, investigate important questions about the observed world, explain real-world phenomena, test ideas and make predictions about the real world situations. The computational analysis model was employed using real data from the Canadian Defence Department as part of the study. The aim of using this computational model was to verify and compare the results with the power loss mathematical model. Research shows that computational analysis has the capacity to model and analyse real data, Senatore and Sandu (2011). The mathematical model was used to provide an insight into the relative effects of each of the variables and how they interact; leading to a deeper understanding of the underlying principles involved hence the decision to use both methods in this research.

Further verification of the mathematical and computational analysis models was achieved through laboratory experiments using a wheeled vehicle MOBILITY SF-3713 on different test beds namely non-deformable terrain, clay soil and sandy

soil. A total of 303 laboratory experiments were carried out in different configurations on hard ground, clay soil bed and sand soil bed based on various speeds, tyre pressures and applied loads. Details of the research design and methods are discussed in the research methodology section in chapter 3. Figure 1.6 is an adopted structure of the model verification process from Walker (2010).

This model validation process which is discussed in detail in the research methodology chapter clearly illustrates the importance and options of model verification available. A combination of all or any of the two routes in the given verification process provides important and reliable verification of the results. Replacing this research in Walker's FEM model validation process, the mathematical model is represented by the power loss model (POWERSEV), the simulation model is represented by computational analysis while the physical model is represented by the laboratory experimental analysis. As mentioned above, details of these individual approaches are discussed in chapter 3.

The main variables that were considered in order to achieve the aim and its objectives are:

- Wheel rut depth
- Power loss measured in form of drawbar-pull
- Vehicle self-weight
- Applied load
- Wheel radius
- Wheel width
- Velocity

- Soil cohesion
- Soil angle of shearing resistance
- Moisture content
- Wheel slip/skid ratio

1.10. Significance and relevance of the study

This research is significant because a terrain variation management tool is very important for the construction industry because it relies on unit pricing of operations. Clients and their consultants require a tool in place to establish and verify variations arising from power losses resulting from changing ground conditions. Currently the pricing of variations is based on estimating and experience which is not accurate all the time because changes in ground conditions are difficult to forecast and price in advance.

The results from this research are also relevant and critical to the contractors because they would be a basis for providing data for selecting the type of plant and determining contract durations depending on the given ground conditions for each day or period of time. Insurance and plant hire companies can benefit from the results through the availability of a quantitative tool in place for determining insurance premiums and other quantitative risk assessments associated with plant operating in off-road conditions. Plant hire companies equally need to have an accurate and measurable basis for establishing plant hire rates for different terrain conditions that the plant is to operate in. Currently standard hourly rates apply regardless of the terrain in which the hired plant will operate in. This presents a risk of underestimating the wear and tear factors associated with the specific plant at each given time.

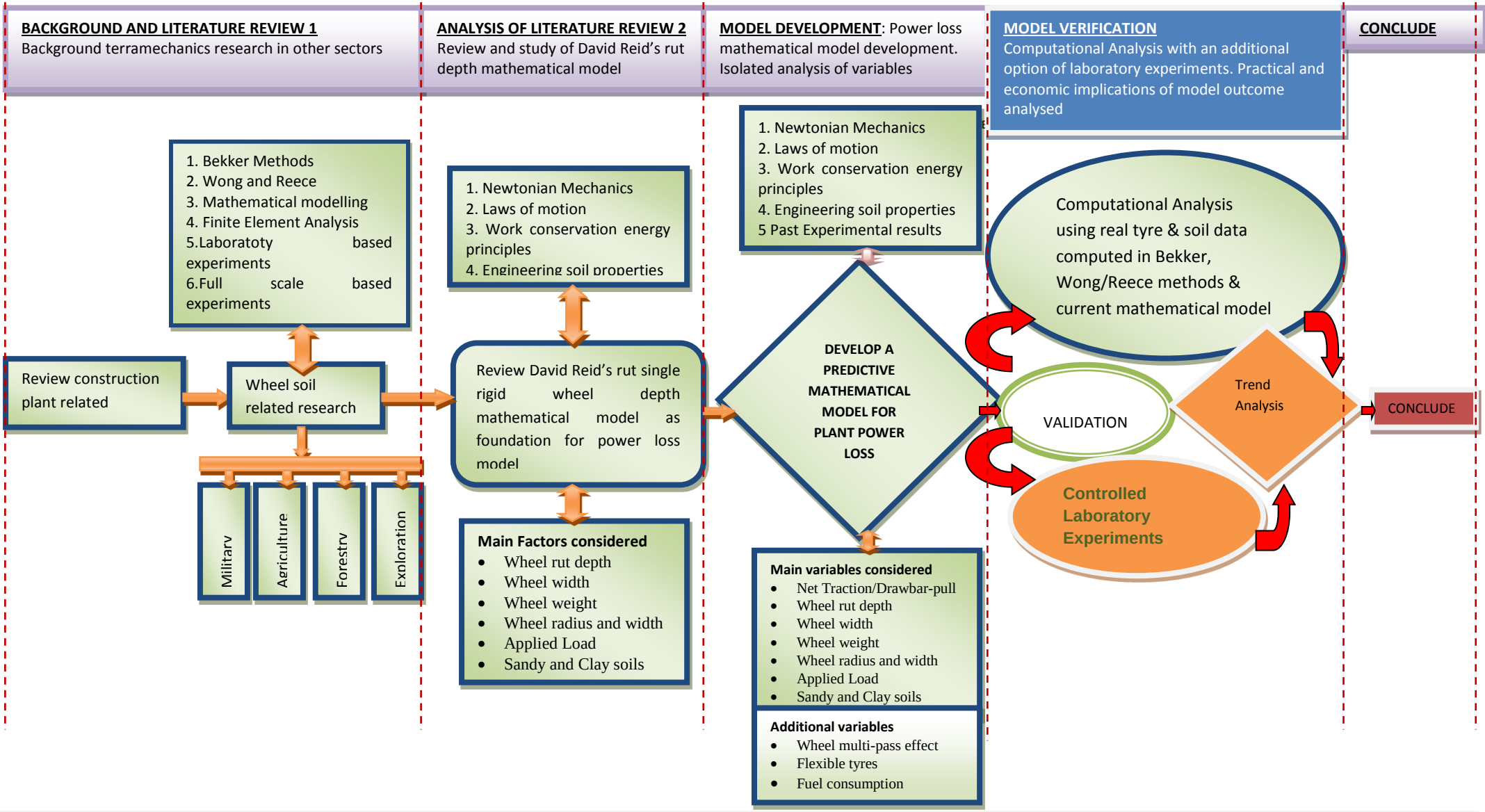

Figure 1.5: Flow chart showing the research design road map

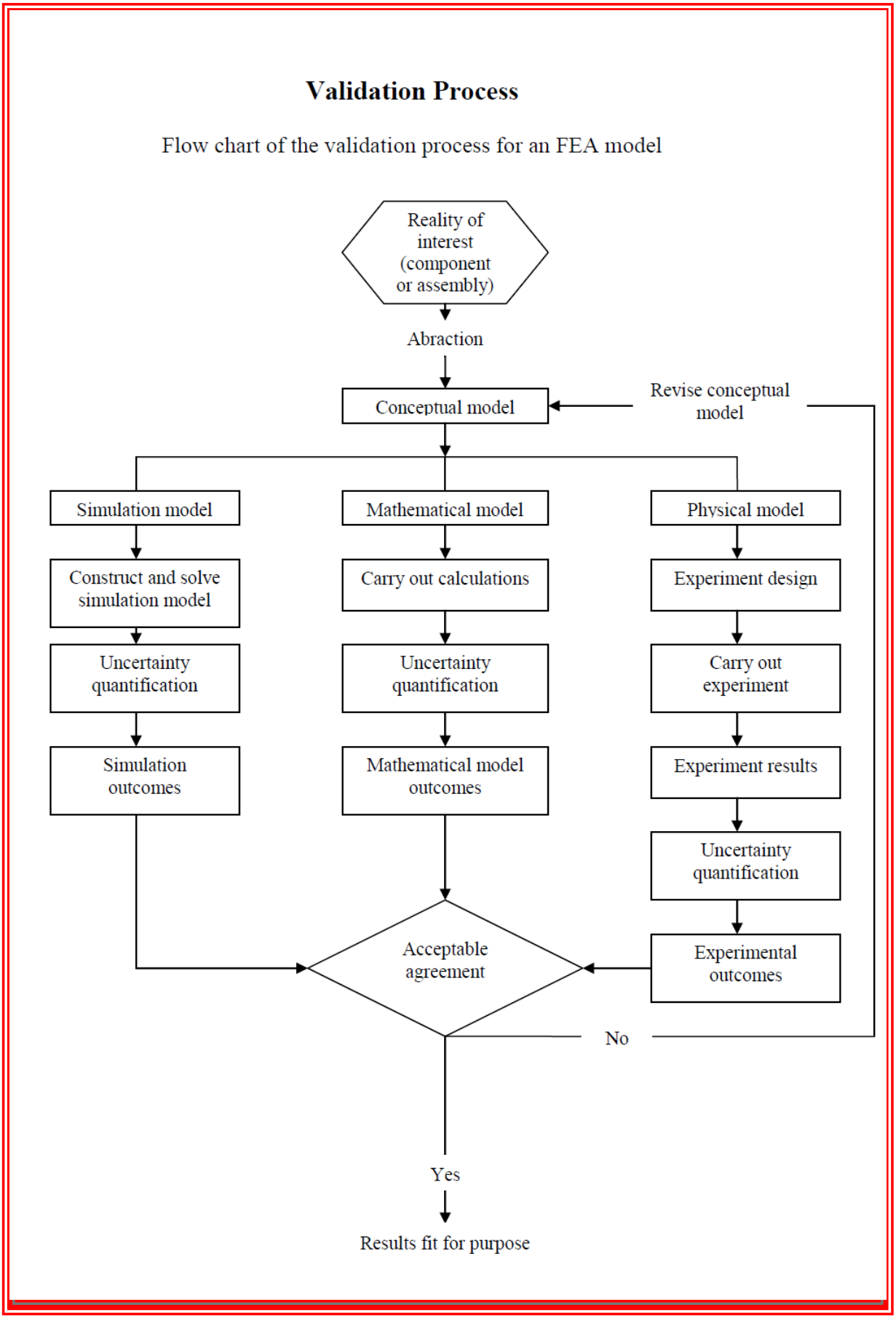

Figure 1.6: Validation Model, Walker (2010)

1.11. Thesis outline and content

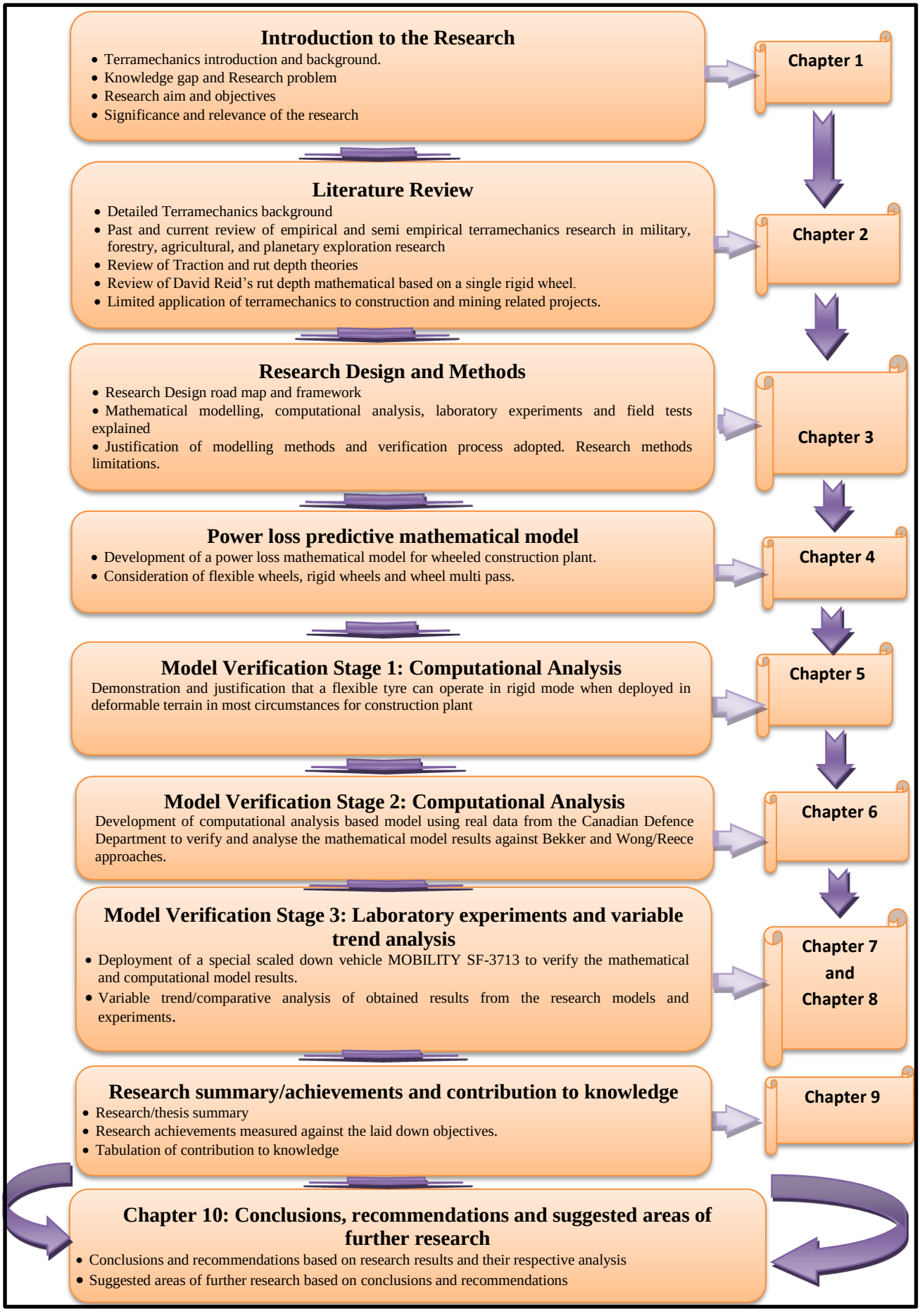

Figure 1.7: Thesis outline

CHAPTER 2

LITERATURE REVIEW

TERRAMECHANICS BACKGROUND AND APPLICATIONS IN OTHER INDUSTRIES

2.0. CHAPTER 2

Literature review
Research background and applications in Terramechanics

2.1. Introduction

This chapter discusses the principles that underpin the wheel-soil relationship. It also discusses the history of Terramechanics and how its applications have evolved over time. The chapter further considers the difference between Terramechanics and contact mechanics which some researchers still find difficult to distinguish today. It finally takes a detailed review and analysis of Terramechanics applications and research outputs in various key sectors of engineering and economics. Terrain-vehicle mechanics involves the study of tractive performance of a vehicle over unprepared terrain, ride quality over undulating surfaces and obstacle negotiation and avoidance Wong (1984). It is concerned with the measurement of the mechanical properties/characteristics of deformable terrain that affect vehicle mobility.

Terramechanics was developed by M.G Bekker in the 1950s to characterise vehicle ground interaction using semi empirical relationships according to Sandu et al (2010). Terramechanics provides guiding principles for the rational design, evaluation, testing, selection/operation of off-road vehicles and terrain working machinery (Wong, 1984). Ground conditions also affect the performance of construction plant on a construction site and long deformable haulage roads due to the wheel-soil interaction caused by changing ground or terrain conditions.

Other factors that affect the performance of wheeled and tracked plant include: traction, rolling resistance and wheel/track sinkage. In the absence of reliable

measuring instruments and models, accurate estimation and quantification of wheel-soil interaction is extremely difficult. The terrain conditions in the agricultural, military, forestry and planetary exploration sectors are often different from those found or desired on a construction site. The Agricultural sector is mainly concerned with loose soils as desired terrain while the construction site requires stable terrain to support plant mobility, safety and cost management. The application of terramechanics to construction sites can guide practising engineers and planners to attain maximum traction performance and output from wheeled construction plant.

The chapter presents a review of the processes and results from some of the available landmark research that has been done in the military, agricultural, forestry and planetary exploration sectors. These studies cover field experiments/tests, laboratory experiments, mathematical modelling, regression analysis and computer simulation packages such as Finite Element Modelling (FEM). The chapter concludes by analysing the potential benefits of terramechanics when fully applied to construction sector, particularly construction sites characterised with natural off-road terrain and deformable haulage roads.

2.1.2. Modelling Terrain behaviour

The understanding of terrain behaviour under vehicular load is of great importance to the study of vehicle-terrain interaction. Wong (2010) outlines three methods of modelling terrain behaviour namely; elastic medium, plastic medium and critical state soil mechanics.

2.1.2.1 Modelling terrain as an Elastic medium (Elasticity Theory)

The behaviour of dense terrain such as compact sand under certain circumstances may be compared to an ideal elastoplastic medium with a stress-strain relationship shown in figure 2.1. This means that the theory of elasticity may only be applied to dense terrain with vehicular load applied not exceeding a certain level so that the terrain is considered elastic. The corresponding stress in the medium is lower than (A) in figure 2.1 where the terrain will exhibit elastic behaviour. The slope OA is dependent upon the degree of saturation of the soil which varies throughout the year.

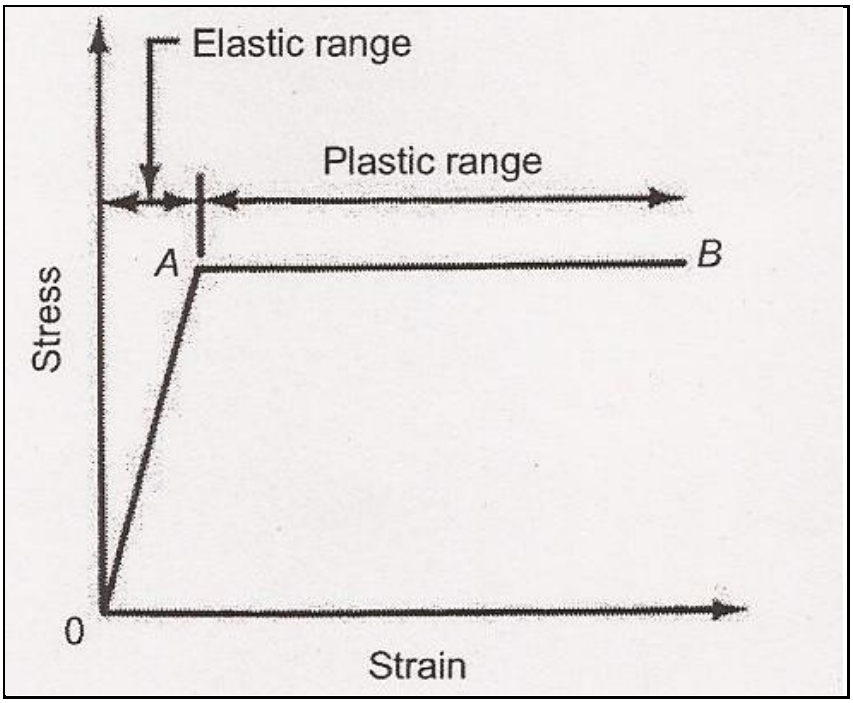

Figure 2.1: Stress-strain relationship of an idealised elastoplastic material, Wong (2010)

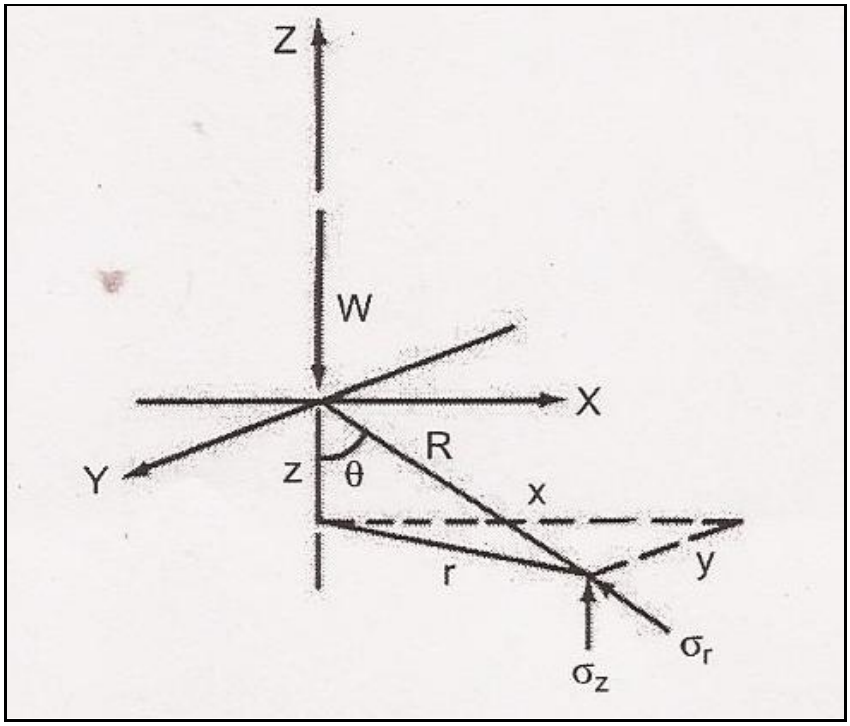

Figure 2.2: Stresses in a semi-infinite medium subject to a point load on the surface, Wong (2010)

For a homogenous isotropic elastic medium subject to a point load on the surface, the stress distribution in the medium may be predicted using the Boussinesq equation defined by coordinates in figure 2.2.

$$\sigma = \frac{3W}{2\pi\left[1+(\frac{r}{z})^2\right]5/2_z2} \qquad \text{Eqn 2.1}$$

$$\frac{3W}{2\pi rR^{\,2}\left[\frac{z}{R}\right]^3} = \frac{3W}{\pi rR}cos^3\theta \qquad \text{Eqn 2.2}$$

Where $r = \sqrt{x^2 + y^2}$ and $R = \sqrt{z^2 + r^2}$

2.1.2.2 Modelling terrain as a Plastic Medium (Theory of Plastic equilibrium)

According to Wong (2010) the theory of plastic equilibrium can only be used in modelling terrain when estimating the maximum vehicle load that the terrain can support without causing its failure. The theory however cannot be used to predict sinkage of the vehicle because of its normal load or the slip of the vehicle due to the shearing action of its running gear. An infinitely small increase in stress beyond point (A) as illustrated in figure 2.1 produces a rapid increase in strain which constitutes plastic flow. The state preceding plastic flow is usually referred to as plastic equilibrium. The transition from the state of plastic equilibrium to that of plastic flow represents the failure of the terrain material.

The Mohr Coulomb failure criterion is one of the most widely used today. It postulates that the material at a point will fail if the shear stress at that point satisfies the following condition:

$$\tau = C + \sigma \tan \emptyset \qquad \text{Eqn 2.3}$$

Where τ = shear stress, c is the cohesion and σ is the normal stress on the shearing surface and $\emptyset$ is the angle of internal shearing resistance of the material. Cohesion is defined as the bond that cements particles of the material together, regardless of the normal pressure between the particles Wong (2010). As for the other property, particles of frictional material can be held together only when normal pressure is present between them. The shear strength of saturated clay or similar does not depend on the normal pressure whereas the shear strength of dry sand or similar increases with the increase in the normal pressure.

Saturated clay and its shear strength is given by

$$\tau = c \qquad \text{Eqn 2.4}$$

and for dry sand, its shear strength is expressed by

$$\tau = \sigma \tan \emptyset \qquad \text{Eqn 2.5}$$

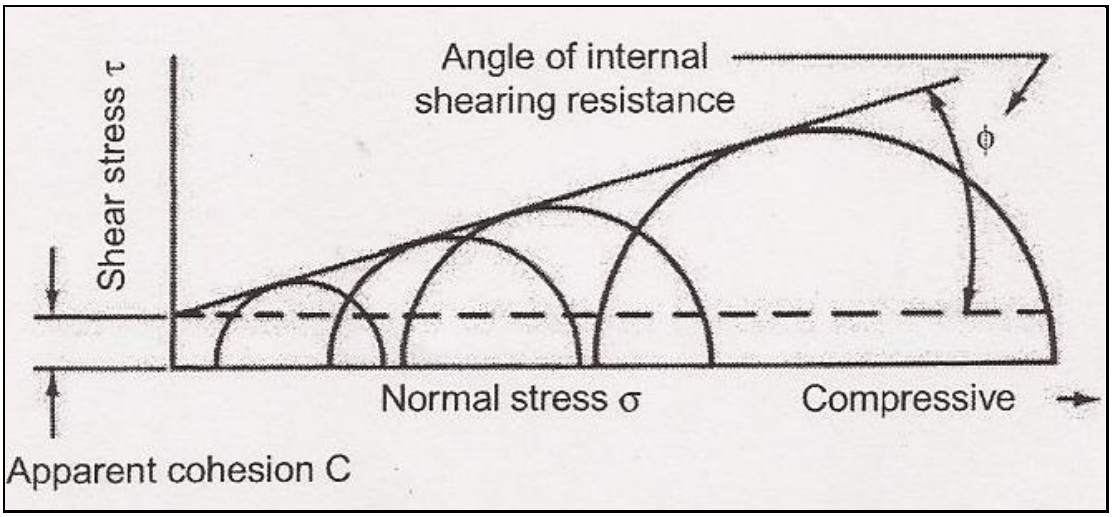

Figure 2.3: Mohr-Coulomb failure criterion, Wong (2010)

Terrains that cover most of the trafficable earth surface generally have both cohesive and frictional properties and their shear strength is described by equation 2.3. This means that most of these soils contain a combination of clay and sandy soils. This is the reason why plastic equilibrium theory has been adopted as the option of modelling the terrain in the development of the mathematical model in this research. The meaning of the Mohr-Coulomb failure criterion may be further illustrated with the aid of the Mohr circle of stress. If specimens of a terrain are subjected to different states of stress, for each mode of failure a Mohr circle can be constructed as shown in figure 2.3. The cohesion of the terrain is defined by the intercept of the straight line with the shear stress axis and the angle of internal shearing resistance being represented by the slope of the straight line Wong (2010). This criterion implies that if a Mohr circle representing the state of the

stress at a point in the terrain touches the enveloping line, failure will take place at that point.

2.1.2.3 Modelling terrain based on critical state soil mechanics

According to Wong (2010), in an attempt to overcome the limitations of elastic and plastic methods of modelling terrain, the concept of critical state soil mechanics was developed by Roscoe and his team at Cambridge University (Wong, 2010). The soil is usually described as dense or loose. The method has the capacity to predict both the stress and strain in the terrain under vehicular load. The complexity and variability of terrain behaviour in the field makes its applications limited because of its four assumptions below that it embraces:

1. The soil is homogenous and isotropic.
2. The mechanical behaviour of soil depends only on effective stress which is defined as the difference between total stress and pore water pressure.
3. The mechanical behaviour of the soil can be described by a macroscopic model
4. The mechanical behaviour of the soil is not time dependant and the soil is not viscous.

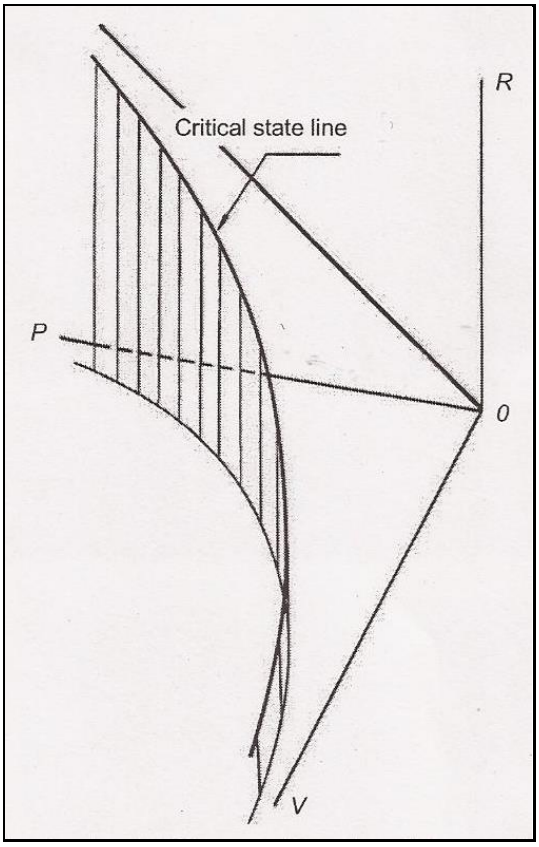

Figure 2.4: Critical State line in the P-R-V Wong (2010)

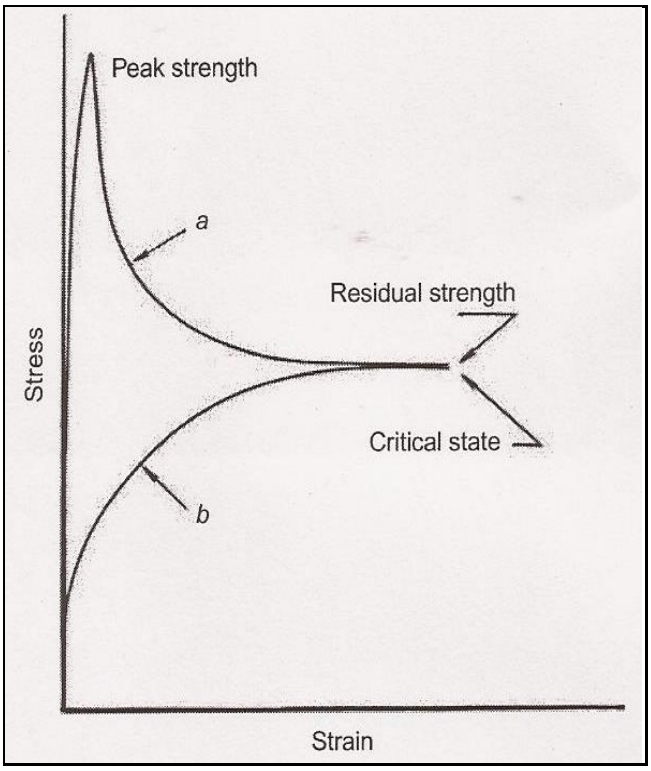

Figure 2.5: Stress-Strain relationship of soil in (a) dense state and (b) loose state, Wong (2010)

This method establishes the relationship between the specific volume *V*, spherical pressure *P* and the deviatoric stress *R* of the soil. The specific volume *V* is equal to 1+*e*, where *e* is the void ratio of the soil, which is the ratio of the volume of the voids to the volume of the solids. The *P-R-V* space is illustrated in figure 2.4. Figure 2.5 illustrates the two types of behaviours of soil deformation. The line identified by *a* represents the stress-strain relationship of the material in the dense state while line *b* represents the behaviour of the material initially in a loose condition. The spherical pressure *P* and the deviatoric stress *R* are defined and based on figure 2.4 as follows:

$$P = \frac{\sigma_1+\sigma_2+\sigma_3}{\sqrt{3}} \qquad \text{Eqn 2.6}$$

And

$$R = \frac{1}{\sqrt{3}}[(\sigma_1 - \sigma_2)^2 + (\sigma_2 - \sigma_3)^2 + (\sigma_3 - \sigma_1)^2]^{1/2} \qquad \text{Eqn 2.7}$$

where σ_1, σ_2 and σ_3 are principal stresses acting on a cubic element of the soil

One of the greatest challenges of using critical state soil mechanics is that it is based on the assumption that the soil is homogenous and isotropic. In practice however, an off-road vehicle may encounter a variety of terrains. These include snow, organic terrain, such as tundra or muskeg which under most circumstances cannot be possibly idealised as homogeneous and isotropic Wong (2010). Heavily loaded vehicles may also damage terrain thereby making it impossible for the soil to behave as a homogenous material. This is the major reason why critical soil mechanics has so far found few practical applications to the study of vehicle-terrain interaction in the field.

2.1.2.4 Modelling terrain using Finite Element Method (FEM)

The Finite Element Method has been applied to study the interactions between tyre and soil, tyre and snow and track and soil Wong (2010). The Finite Element Method (FEM) was originally developed for structural analysis; however it has been expanded to cover many fields of engineering over the years Wong (2010). FEM is the idealisation of a continuum such as a soil mass under certain circumstances as an assemblage of a finite number of elements. The two widely used models in terrain modelling are the Drucker-Prager cap model and the Cam Clay critical state soil model although the Mohr-Coulomb yield models also employed in some cases Wong (2010).

The limitation of Finite Element Method (FEM) is that it is not suitable for simulating significant soil flow or large discontinuous soil deformation because its principle is based on a continuum body Wong (2010).

2.1.2.5 Modelling terrain using the Discrete (Distinct) Element method (DEM)

The Discrete Element Method was initially developed for the study of rock mechanics as an alternative to modelling a granular material as continuum Wong (2010). It represents the terrain as an assemblage of discrete elements. It assumes that in its basic form each element has stiffness characterised by a spring constant and poses damping characterised by a viscous damping coefficient. The Discrete Element Method is still in its developmental stage when applied to the study of vehicle-terrain interactions. Several issues need to be resolved before it can be considered to be a practical tool for vehicle – terrain studies Wong (2010).

While most literature review under this subject focuses more on the equations and dynamics of the subject, this literature review takes a unique focus of the application of terramechanics in various fields before reverting back to modelling of wheel-soil relationship with a view of establishing its importance to the construction industry.

2.2. Flexible and rigid wheels in Terramechanics.

Flexible wheels do not present any problems with wheel sinkage when operating on hard gravel, concrete and pavement provided they are inflated to the required and recommended tyre pressure. The tyres however are subjected to some form of wheel deflection especially if the tyre inflation pressure is low and the applied load is high. Furthermore these flexible tyres do not encounter any motion resistance arising from wheel sinkage because the rut depth is negligible. Xia (2010) makes the point that high inflation tyres on relatively stiffer deformable terrain can reduce energy cost, however for relatively soft soil; the results might turn out to be completely different.

Modern conventional tyres of road equipment and ordinary cars are flexible and run in a flexible mode when moving on hard and stable surface. However when fully inflated to a high pressure and operating in soft soil they behave like a rigid wheel because of the wheel sinkage that is experienced. According to Senatore and Sandu (2011), the rigid wheel can be considered a first approximation of a flexible tyre. If the terrain stiffness is significantly lower than the total tyre stiffness (carcass stiffness plus the inflation pressure) then the flexible tyre can be

approximated as a rigid wheel thereby greatly simplifying the analysis Senatore and Sandu (2011). The study of rigid wheels is relevant because some vehicles such as lunar rovers are natively equipped with rigid wheels.

The simulation of the vehicle–soil interaction is dominated by the tyre model (i.e. flexible or rigid) as shown in figure 2.6. When the average ground pressure is larger than the critical pressure, which is dependent on the wheel load, the tyre deflection can be ignored compared with the sinkage and the tyre can be modelled as rigid; otherwise, the tyre should be considered flexible, and that the tyre deformation must be accounted for in the simulation. Simplified graphical representations of these two types of tyre models are illustrated in figure 2.6. The critical ground pressure is obtained by equation 2.8 and the wheel load the wheel load by equation 2.9 and equation 2.10.

$$p_{cr} = \left(\frac{k_c}{b_w} + k_\emptyset\right)^{\frac{1}{2n+1}} \left[\frac{3W_{fl}}{(3-n)b_w\sqrt{D}}\right]^{\frac{2n}{2n+1}} \quad \text{Eqn 2.8}$$

$$W_{fl} = k_1\left(z_{1fl} - x_4 - s_{fl}\right) + 9.8\left[\frac{(W_{load}+m_2)b}{2L}\right] + m_1 \quad \text{Eqn 2.9}$$

$$W_{fl} = k_1\left(z_{1fl} - x_5 - s_{fl}\right) + 9.8\left[\frac{(W_{load}+m_2)b}{2L}\right] + m_1 \quad \text{Eqn 2.10}$$

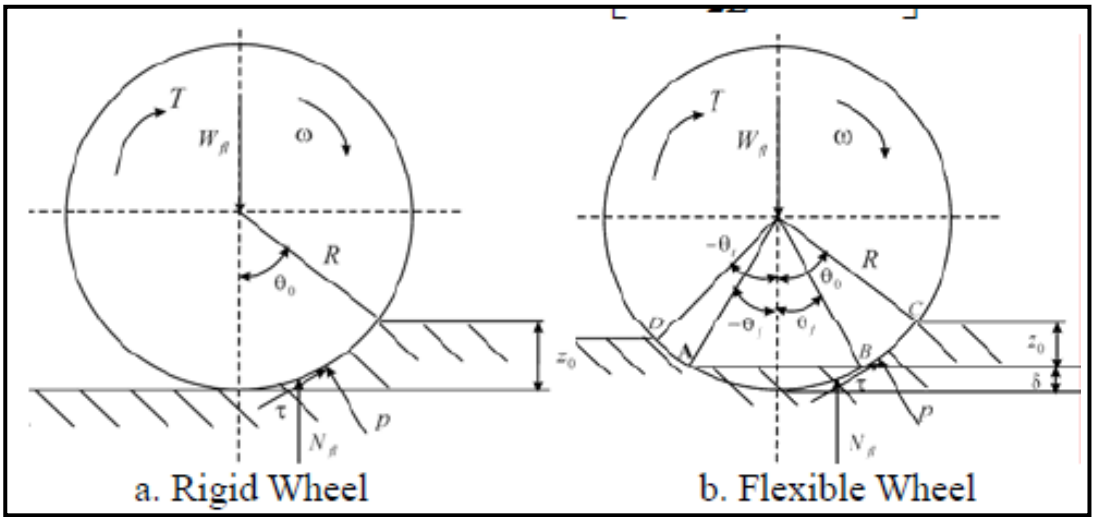

Figure 2.6: Simplified graphical representations of the two types of tyre models, Li and Corina (2006)

For the rigid tyre model, the maximum sinkage is given by equation 2.11, resistance force by equation 2.13, wheel load by equation 2.14, tractive force by equation 2.15 and drawbar-pull by equation 2.16.

$$z_0 = \left[\frac{3W_{fl}}{b_w(3-n)\left(k_c/b_w+k_\emptyset\right)\sqrt{D}}\right]^{\frac{2n}{(2n+1)}} = R(1-\cos\theta_0) \qquad \text{Eqn 2.11}$$

$$j = R[(\theta_0-\theta)-(1-i)(\sin\theta_0-\sin\theta)] \qquad \text{Eqn 2.12}$$

$$R_c = \frac{1}{(n+1)\left(k_c+b_w k_\emptyset\right)^{1/(2n+1)}}\left[\frac{3W_{fl}}{(3-n)\sqrt{D}}\right]^{\frac{2n+2}{2n+1}} \qquad \text{Eqn 2.13}$$

$$N_{fl} = Rb_w\left[\int_0^{\theta_0}\tau(\theta)\sin\theta d\theta + \int_0^{\theta_0}p(\theta)\cos\theta d\theta\right] \qquad \text{Eqn 2.14}$$

$$F = \int_0^{\theta_0}\tau(\theta)\cos\theta\cdot R\cdot b_w\, d\theta \qquad \text{Eqn 2.15}$$

$$F_d = Rb_w\left[\int_0^{\theta_0}\tau(\theta)\cos\theta\, d\theta - \int_0^{\theta_0}p(\theta)\sin\theta\, d\theta\right] \qquad \text{Eqn 2.16}$$

For rigid tyre models, the sinkage, the normal pressure, the shear stress and the forces on wheels can be calculated directly as described in the previous section. For flexible tyre models, the sinkage and the entry angle are calculated first, and the initial tyre deformation and the exit angle are initialized. The forces are then calculated. In this study by Li and Sandu (2006), an algorithm real time prediction of vehicle terrain interaction under uncertain vehicle parameters was developed. The tyre model was identified as rigid or flexible at each moment of the simulation taking into account the uncertainties in soil parameters.

Ishigami et al (2011), provides a unique illustration of the transition of rigid wheel to flexible wheel under different conditions illustrated in figure 2.7.

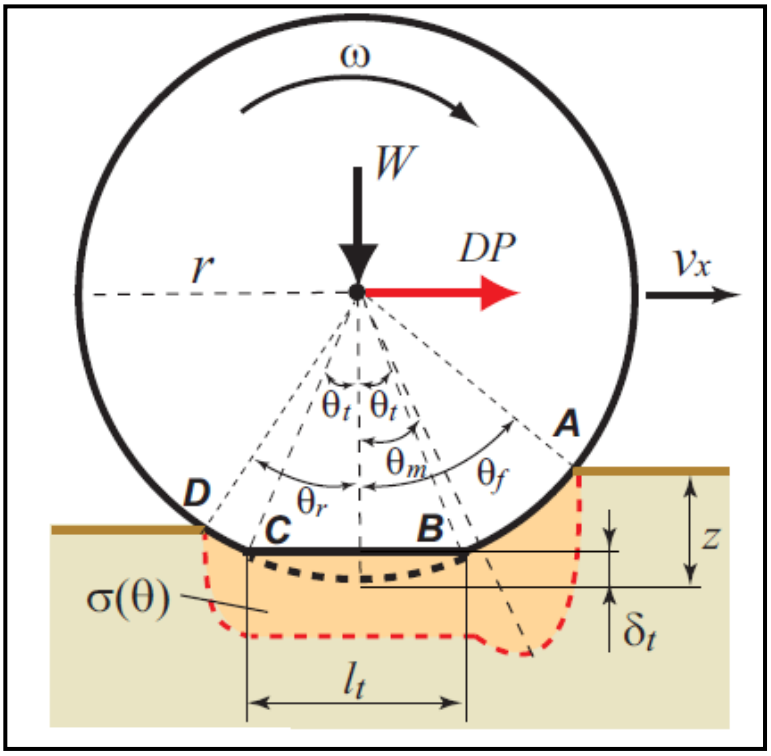

Figure 2.7: Wheel-terrain model: Normal stress distribution of driving wheel Ishigami et al (2011)

$$\sigma(\theta)\begin{cases}\sigma_f = \sigma_m(\cos\theta - \cos\theta_f)^n \\ \sigma_t = \begin{cases}(k_c/l_t + k_\emptyset)(z-\delta_t)^n & (if\ l_t < b) \\ (k_c/b + k_\emptyset)(z-\delta_t)^n & (if\ l_t \geq b)\end{cases} \\ \sigma_r = \sigma_m\left\{\cos\left[\theta_f - \frac{(\theta-\theta_r)(\theta_f-\theta_m)}{(\theta_m-\theta_r)}\right]\cos\theta_f\right\}^n\end{cases}$$ Eqn 2.17

$$\theta_f = \cos^{-1}(1 - z/r)$$ Eqn 2.18

$$\theta_r = \cos^{-1}(1 - \lambda z/r)$$ Eqn 2.19

$$s = \begin{cases}(r\omega - v_x)/r\omega & (|r\omega| \geq |v_x|)\text{: driving} \\ (r\omega - v_x)/v_x & (|r\omega| < |v_x|)\text{: braking}\end{cases}$$ Eqn 2.20

Equations 2.17 to 2.20 provide the wheel sinkage taking into account the terrain rebound factor due soil elasticity denoted in equations 2.18 and 2.19. θ_f and θ_r are entry and exit angle respectively with σ_t being the normal stress assumed to be uniformly distributed along the soil dependant parameters. Equation 2.20 denotes the two slips in driving and braking modes.

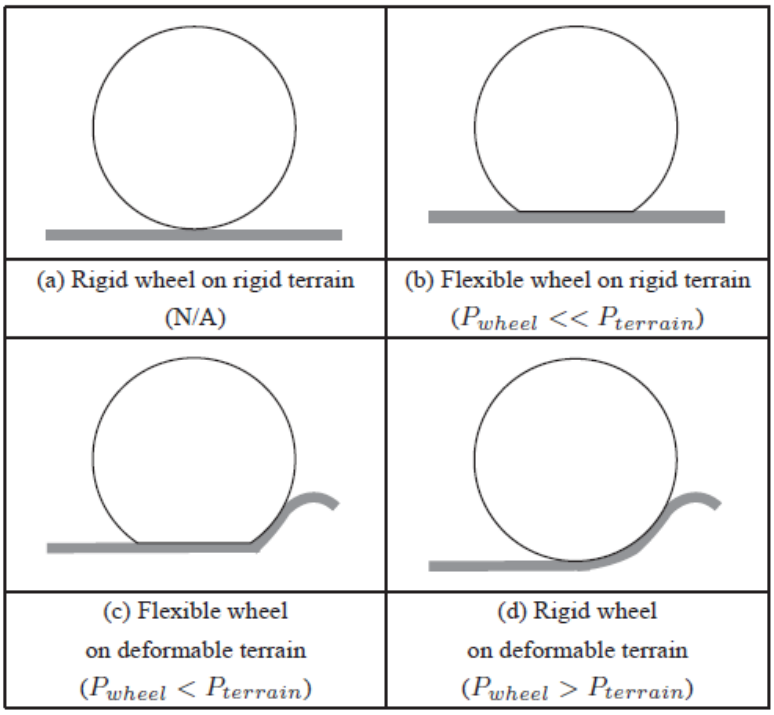

Figure 2.8: Four categories for wheel-terrain interaction, Ishigami et al (2011)

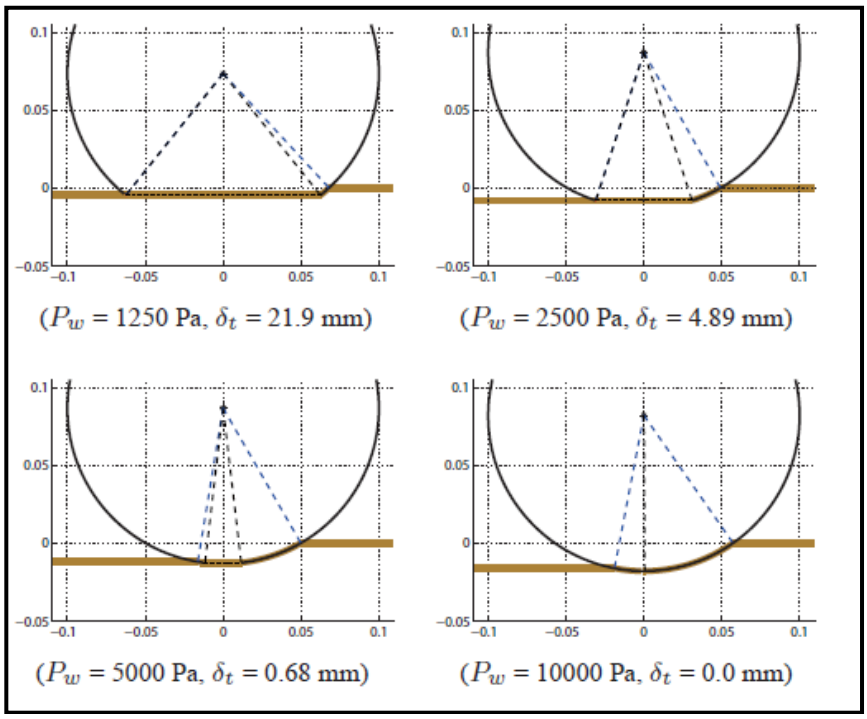

Figure 2.9: Wheel deflection and contact patch with varied wheel pressures Ishigami et al (2011)

Figure 2.8 and Figure 2.9 shows the simulation results for the wheel deflection and sinkage. From the graphs, the wheel deflection increases as the wheel pressure decreases. The wheel sinkage also decreases with decreasing the wheel pressure. This is because low wheel pressure easily deflects the wheel shape which generates larger flat section of wheel, resulting in less wheel sinkage. The wheel having *Pw*=10000 Pa can be assumed as “rigid wheel” since its deflection is 0 mm, while others are “flexible wheels” as seen from Figures 2.10 and 2.11.

The wheel sinkage of the most rigid wheel (black line) increases as the slip ratio increases. This is due to the fact that the shear deformation of wheel increases with increasing the slip ratio. However, the sinkage of the other wheels is one of the most constants regardless of slip ratio since the flat section of the wheel mostly supports the vertical load of wheel. These results confirm that the proposed model can appropriately calculate wheel deflection/sinkage in accordance with the

wheel pressures. It can also be seen that the tyre with the lowest inflation pressure generates relatively small drawbar-pull in particular; the drawbar-pull at low slip ratio takes significantly negative value. This is attributable to the resistance force due to the wheel deflection that is calculated around −20 N. On the other hand, the wheels with *Pw* = 2500 and *Pw* =5000 Pa generate positive drawbar-pull regardless of slip ratio (Ishigami et al, 2011). This is explained in terms of the force generated at the flat section of the wheel.

The shearing direction at the flat section is parallel to the direction of wheel traveling, resulting in the increase of the thrust. In addition, the resistance force due to the wheel deflection is not notable for these semi-flexible wheels. Therefore, the gross net traction becomes large as compared to the rigid wheel or the wheel with *Pw* =1250 Pa. It should be emphasized that the wheel with *Pw* =2500 Pa has a maximum drawbar-pull for every slip ratio as compared to the other wheels athough the pressure of the wheel is moderate between the four wheels. *This result implies that an optimal wheel pressure for drawbar performance may exist*

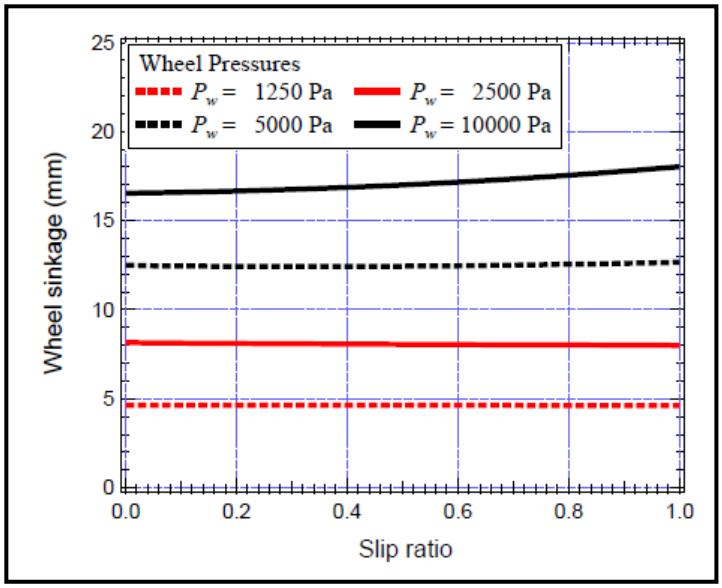

Figure 2.10: Wheel sinkage with varied wheel pressure Ishigami et al (2011)

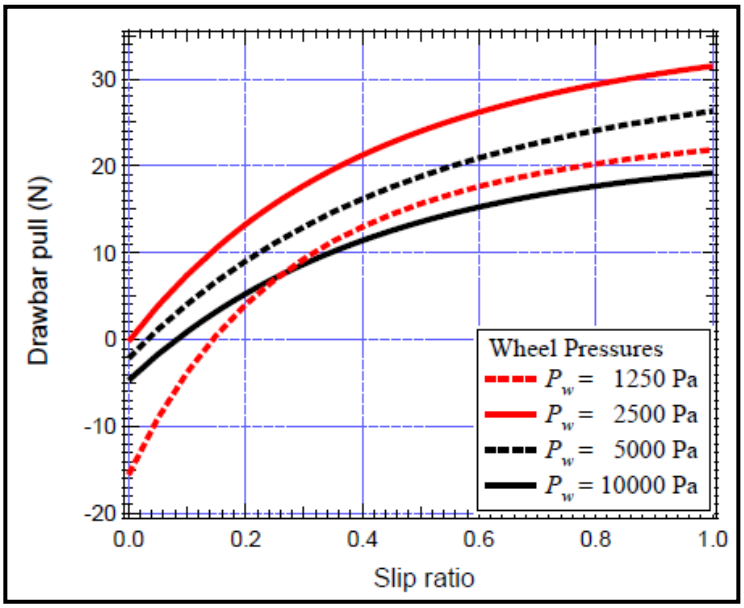

Figure 2.11: Drawbar-pull with varied tyre pressure Ishigami et al (2011)

From the results and discussions, the wheel traction characteristics are determined by the relationship between the drawbar-pull and the resistance torque: a rigid wheel has small drawbar-pull as well as small resistance torque, whereas a flexible wheel requires large drawbar requiring large resistance torque. An optimal wheel pressure can be found based on a wheel load, terrain stiffness, and wheel structure. Establishing the running mode of the wheel is critical for the modelling of wheeled construction plant performance. It is also critical for decision making when it comes to running the vehicles in relatively soft soils.

Chapter 5 demonstrates that a flexible wheel can be modelled as rigid wheel if the pressure of the carcass exceeds the average ground pressure. This represents the tyres for construction vehicles that are normally fully inflated at an average of 100 PSI making the tyres to run in a rigid mode when operating in soft soils, appendices (19 and 20). Despite this study and its results being based on simulation, the calculation of outcomes was based on the established equations as

discussed throughout this chapter. The equations used range from 2.21 to 2.27 as tabulated below:

$$W = rb\left[\int_{\theta_2}^{\theta_1} \sigma(\theta)\cos\theta \cdot d\theta + \int_{\theta_2}^{\theta_1} \tau(\theta)\sin\theta \cdot d\theta\right] \quad \text{Eqn 2.21}$$

$$DP = rb\left[\int_{\theta_2}^{\theta_1} \tau(\theta)\cos\theta \cdot d\theta + \int_{\theta_2}^{\theta_1} \sigma(\theta)\sin\theta \cdot d\theta\right] \quad \text{Eqn 2.22}$$

$$T = r^2 b\left[\int_{\theta_2}^{\theta_1} \tau(\theta) \cdot d\theta\right] \quad \text{Eqn 2.23}$$

$$\tau(\theta)(c + \sigma(\theta)\cdot\tan\emptyset)\left[1 - e^{\frac{-r}{k}[\theta_1 - \theta - (1-i)(\sin\theta_1 - \sin\theta)]}\right] \quad \text{Eqn 2.24}$$

$$i = 1 - (V/r\omega) \quad \text{Eqn 2.25}$$

$$\tau_{max} = c + \sigma_{max}\cdot\tan\emptyset \quad \text{Eqn 2.26}$$

$$\sigma(z) = \left(\frac{k_c}{b} + k_\emptyset\right) z^n \quad \text{Eqn 2.27}$$

2.2.1. Drawbar-pull, motion resistance and wheel slip.

From the Bekker theory, Drawbar-pull is defined as the difference between soil thrust and motion resistance and that it defines trafficability. When the forces of the wheels on the soil push the soil, the resulting force is called soil thrust. Soil thrust is modified by the slip of the wheel against the soil and is basically the difference between the vehicles translational velocity and the wheel rotational velocity. Drawbar-pull, the thrust or net pull is the lateral forward force a wheel can develop when moving Saarilahti (2002)

2.2.2. Bulldozing effect

Wong (2010) clearly mentions that the problem of bulldozing effect occurs when the tyre is experiencing 100% skid (Locked position, figure 2.13). In this case, a

wedge shaped soil body is formed in front of the wheel because the soil flows forward. As for the slip situation the pattern is different because the wedged soil body forms behind (figure 2.13) for 100% slip case as the soil flows backwards. Normal wheel drive therefore does not result in bulldozing because the front is normally clear. This is illustrated in figures 2.12 to 2.14.

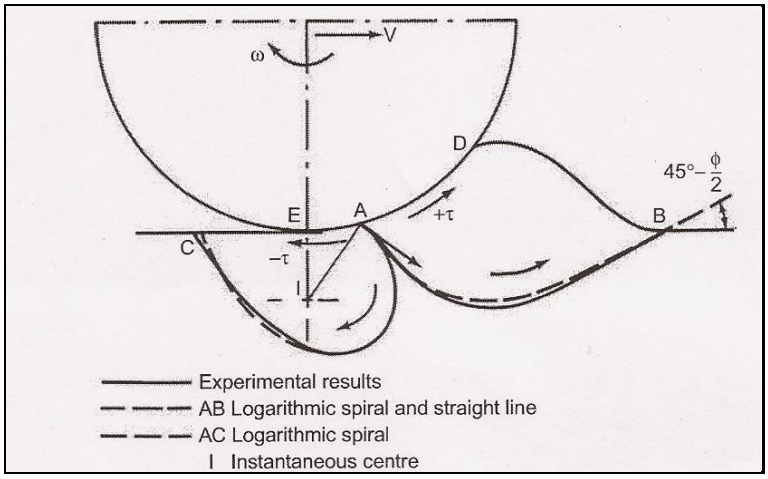

Figure 2.12: Flow patterns and bow wave under the action of a towed rigid wheel in sand, Wong (2010)

Figure 2.12 illustrates the flow patterns and bow wave under the action of a driven rigid wheel in dry sand. It is noticeable that the resistance is less compared to the action of a towed wheel as illustrated in figure 2.14. The front bow for the towed wheel is much bigger than the driven wheel.

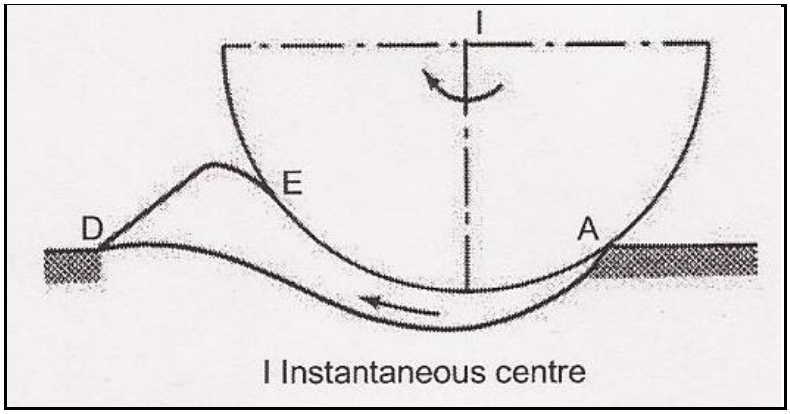

Figure 2.13: Flow patterns beneath a driven rigid wheel at 100% slip in sand Wong (2010)

Figure 2.13 illustrates the soil flow patterns for a wheel full slip or drive conditions which is not affected by inertia. The absence of a bow in front is noticeable.

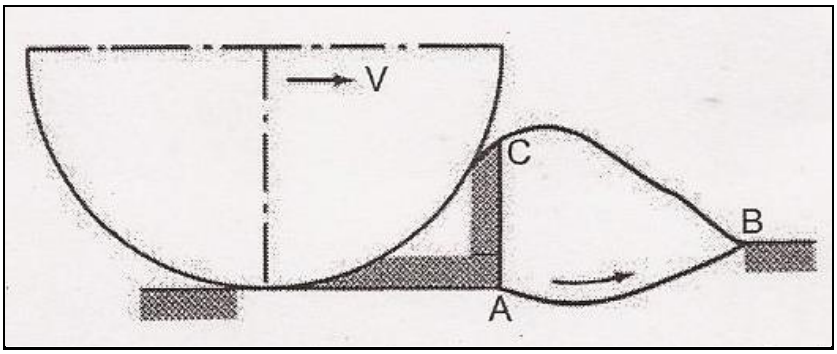

Figure 2.14: Flow patterns and soil wedge formed in a locked rigid wheel at 100% skid in sand, Wong (2010)

Figure 2.14 illustrates the soil flow patterns for a locked rigid wheel in braking mode affected by inertia. The presence of a bow in front is noticeable due to the skidding condition of the wheel. All the soil flow patterns illustrated from figure 2.12 to 2.14 are based on experimental and logarithmic approaches.

2.2.3. Difference between Terramechanics and contact mechanics

Many researchers mistake Terramechanics for contact mechanics. Terramechanics is the study specifically of the interaction between natural soil or undisturbed terrain/soil and wheels or tracks of a vehicle. Equilibrium forces are used to calculate the sinkage, motion resistance and drawbar-pull as shown in equations 2.21 to equation 2.27. As seen from the literature above, soil can become inhomogeneous under certain conditions such as attainment of failure point. Other conditions such as moisture content and can make the soil anisotropic according to Johnson (1995). This is particularly true for clay soil whose cohesion strength reduces with the introduction of moisture content. Dry sand on the contrary is in anisotropic condition until moisture is added to bring it to a saturated

state. From the experimental study, Blahova, Sevelova and Pilarova (2013) equally states soil cohesion reduces with the increase of water content. The research further established that optimum moisture content exists for maximum angle of shearing resistance granular soils. In contact mechanics, the elastic deformation in the contact region is obtained in the Hertz theory by assuming that each solid deforms as elastic, isotropic and homogenous provided it is still within its elastic limit.

If the material is either solid anisotropic or inhomogeneous or if their thickness is not large compared to the size of the contact area their compliance under the contact pressure, they will differ from that assumed in the classical theory. Practical examples of contact between anisotropic solids are found with single crystal and extruded polymer filaments; between inhomogeneous materials with foundations built on stratified rock or soil, Johnson (1995). Johnson further states that detailed discussion of the contact of anisotropic solids is beyond the scope of contact mechanics discussed in his book '*Contact Mechanics'*. Inhomogeneous materials are of interest in soil mechanics in the calculation of settlement of foundations. Foundation soils are normally compacted increasing chances of stability. Natural terrain however is mostly inhomogeneous and can easily deform and fail under vehicular loading.

Clearly the complex structure of a pneumatic tyre does not lend itself to the analytical treatment which is possible for solid isotropic bodies Johnson (1995). This research is focussed on Terramechanics because of the non-linear nature of the natural soil which wheeled vehicles have to traverse.

2.3. Terramechanics in the military sector

2.3.1. Stability of the HMMWV after up armouring

Terramechanics has been utilised in the military to study the performance of wheeled and tracked equipment traversing in different types of terrain. It was originally used by army engineers for military intelligence and reconnaisance in determining go/no go decisions for military vehicles operating in natural and deformable terrain (Reid, 2000). The pioneers of this work were the United States Army Waterways Experimental Station (WES) and the Canadian Defence Department. According to Grujicic et al (2009) a series of parallel Finite Element Modelling (FEM) and Multi Body Dynamics (MBD) simulations of several High Mobility Multi-purpose Wheeled Vehicle (HMMWV) manoeuvres (as shown in figures 2.15 to 2.17) were carried out on a sandy road in order to assess the effect of up armouring on the vehicles off-road performance. Virtually all the United States military branches use the (HMMWV) as the standard utility vehicle for logistical support and convoy operations particularly during off-road travel Grujicic et al (2009).

There are also exceptions to this traditional use of the HMMWV such as offensive and defensive missions, where these missions require the HMMWV to be fully or partially armoured. While the additional armour increased vehicle blast/ballistic protection performance, it also degraded its riding stability performance because suspension and steering components and tyres were not modified in most cases to keep pace with the added weight of installed armour which can be up to 2000kg. This contributed to the increase in HMMWV instability related accidents

and soldier injuries/fatalities. This additional weight caused the roadside or small bridges to collapse causing the vehicle in ditch/water and soldier injuries/fatalities Grujicic et al (2009). The results obtained from this study not only showed the undesirable effects of vehicle up armouring such as rollover propensity but clearly revealed a very high computational cost associated with the use of the Finite Element Analysis as compared to Multi Body Dynamic calculations.

The results from this research indicate that tipping over of construction vehicles can be simulated for different situation such as loaded and unloaded plant operating in different ground conditions. This would give guidelines regarding measuring and predicting risks associated with each respective construction terrain and equipment.

Figure 2.15: HMMWV before up armouring, Grujicic et al (2010)

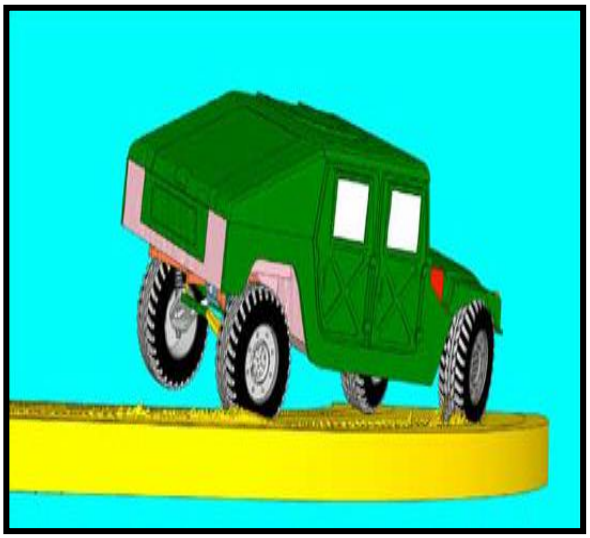

Figure 2.16: Finite Element Analysis of HMMWV, Grujicic et al (2010)

Figure 2.17: Up-armoured HMMWV operating as a common light tactical vehicle (http://usarmy.vo.llnwd.net/e2/-images/2007/05/11/4877/index.html)

The results also indicate that the computational calculated results between the costly Finite Element Modelling (FEM) and Multi Body Dynamics (MBD) were in reasonably good agreement with the relative difference between the two sets being 15%.

2.3.2. Performance of lightweight military vehicles on sandy soil

In another military related study reported by Sandu et al (2010), experiments aimed at understanding vehicle mobility of small unmanned ground lightweight vehicles for military and space exploration were carried out. These experiments

involved testing the significance of payload, ground speed, and sand grain size, sand moisture content on contact pressure and tyre sinkage. Extensive tests were carried out using a wheeled lightweight All-Terrain Vehicle (ATV) as shown in figures 2.18 and 2.19.

Figure 2.18: Lightweight wheeled military test vehicle, Sandu et al (2010)

Figure 2.19: Preparation of sand bed before each run, Sandu et al (2010)

Results indicate that the tread imprint sinkage was mostly affected by the vehicle speed while the borderline was affected by the carried payload and two interactions: sand-grade moisture and sand grade speed. The results from this research suggest that similar studies can be used on wheeled construction plant

operating in different terrain conditions to determine economical speeds for the given particular terrain. This would also lead to accurate establishment rut depths arising from different plant speeds thereby making it easy to predict plant performance and its effects on project costs/time. The results from this study are presented in table 2.1 below with the analysis of the carcass/tread sinkage data and the peak, average and different pressures. It is worth mentioning that the soil parameters were based on the Mohr-Coulomb failure criteria using Coulomb's equation

Table 2.1 however does not provide comprehensive data presentation apart from the significance of the data. A more numerical or graphical representation would have presented a much clearer interpretation of the experiments. Such a table or graph would have provided measurable and comparable variable effect to determine the level of significance of variables rather than a general approach of grouping the significance levels as shown in table 2.1.

Significance of parameters in carcass imprint and tread imprint sinkage, peak pressure, average pressure and difference pressure models (H for highly significant $p \leq 0.05$, B for borderline-significant $0.05 < p \leq 0.10$)

	Parameter significance									
	Sand	Speed	Payload	Sand *moist	Sand *speed	Sand *payload	Moist *speed	Speed *payload	Sand *moisture *speed	Sand *moisture *payload
Carcass sinkage		H	. B	B	B					
Tread sinkage				B			H			
Peak pressure	H	H	H		H	H	H	B		H
Average pressure	H	H	H		H		B		H	
Difference pressure	H	H	H		H	H	H			H

Table 2.1: Significance levels of parameters from the ATV experiment, Sandu et al (2010)

It is worth noting that the Mohr Coulomb formula was used for determining the soil characteristics as shown in equation 2.28 below.

$$\tau = \underset{\text{Cohesion}}{C} + \underset{\text{Internal friction}}{\sigma \tan(\emptyset)} \qquad \text{Eqn 2.28}$$

Where τ is shear stress, σ is normal stress representing inter particle interactions, φ is angle of internal friction and C is soil cohesion.

2.3.3. Physical simulation of terrain properties

A study by Bacon et al (2008) considered the United States Army's capacity to successfully operate and accomplish any mission on a global scale in all possible environments including wet, dry or a combination of different terrains. The study constituted an attempt to characterise the dessert terrain of a test course at Yuma Proving Ground (YPG) which is the Department of Defence desert environment test centre located within the Sonoram desert in Arizona. Results from this study indicated that vehicle endurance course is marginally representative of a region interest in the YPG to some areas in Afghanistan as seen in figures 2.20 and 2.21. Testing of military vehicles in environmental conditions similar to those under which they will be deployed is critical to ensuring their functionality. This approach is expensive and therefore requires huge research funding if was to be applied to the construction sector.

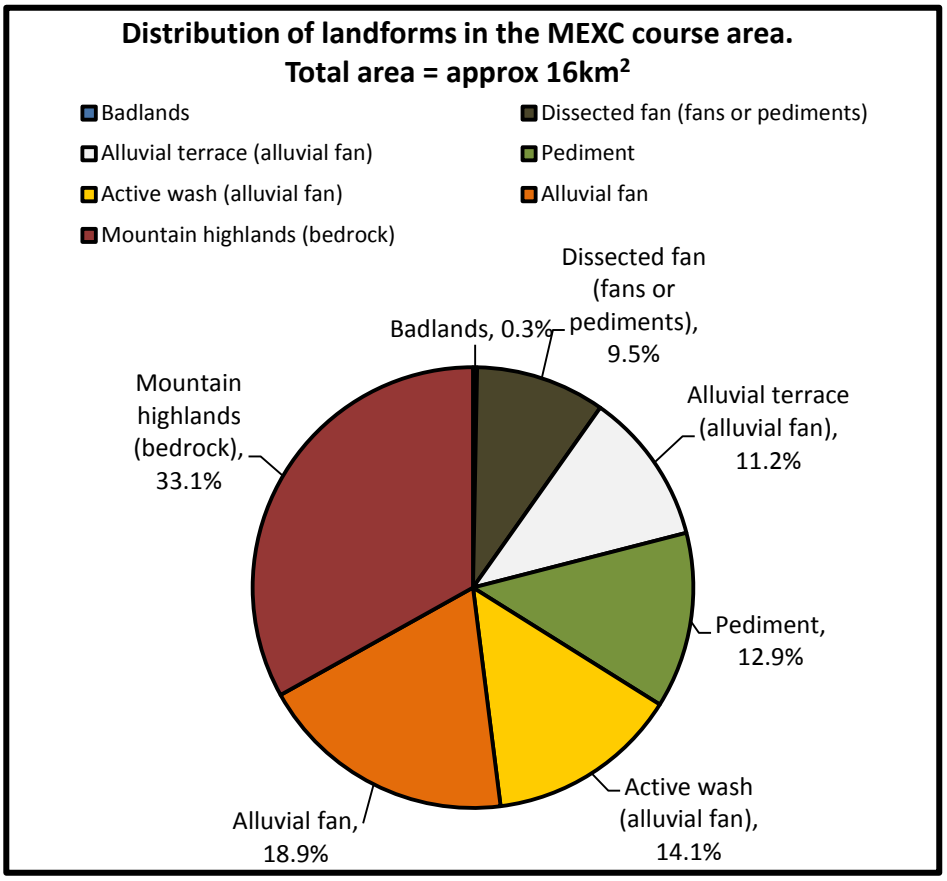

% Area	Landform
0.3	Badlands
9.5	Dissected fan (fans or pediments)
11.2	Alluvial terrace (alluvial fan)
12.9	Pediment
14.1	Active wash (alluvial fan)
18.9	Alluvial fan
33.1	Mountain highlands (bedrock)

Figure 2.20: Distributions of landforms in the experimental MEXC area **16Km²**, Bacon et al (2008)

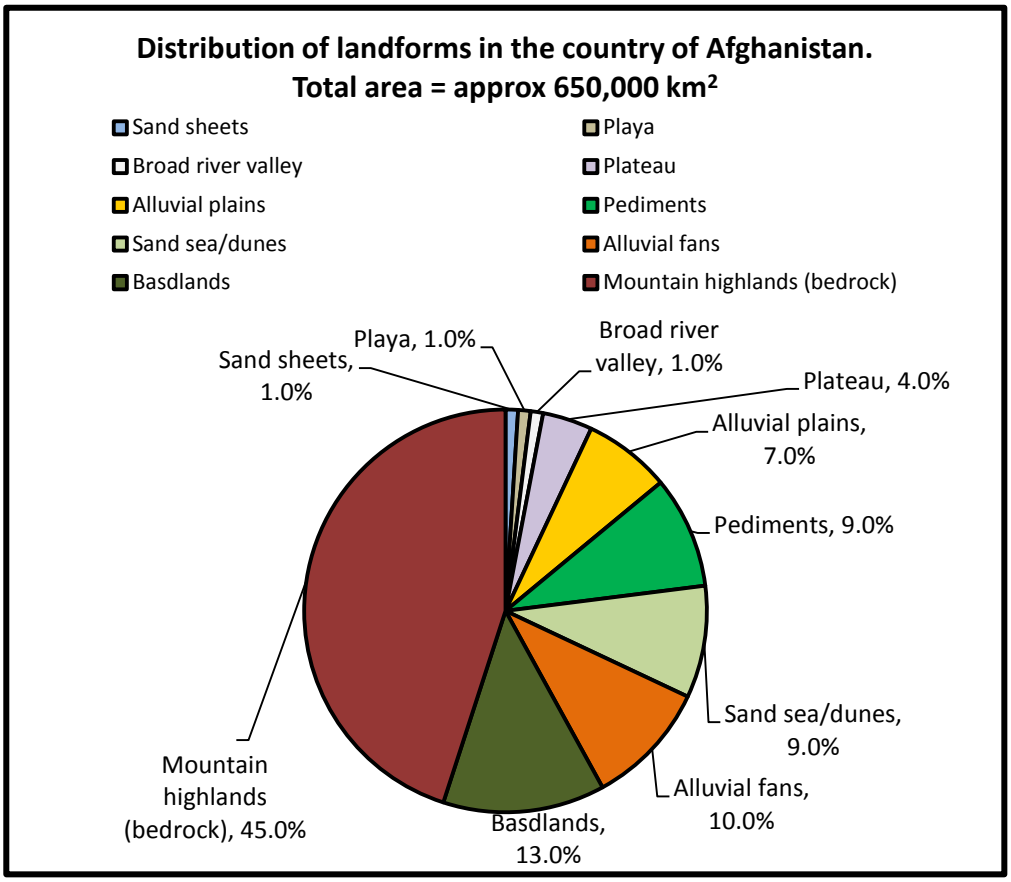

% Area	Landform
1.0	Sand sheets
1.0	Playa
1.0	Broad river valley
4.0	Plateau
7.0	Alluvial plains
9.0	Pediments
9.0	Sand sea/dunes
10.0	Alluvial fans
13.0	Badlands
45.0	Mountain highlands (bedrock)

Figure 2.21: Distributions of landforms in the country of Afghanistan total area **650,000km^2,** Bacon et al (2008)

Based on the results shown in the two comparative figures above it is evident that MEXC provides a good basis for testing of vehicle endurance at MEXC YPG in order to assess the performance of vehicles in similar terrain in Afghanistan. The study also demonstrates that physical simulation by experiments can be used to

create similar terrain and measurements similar to that where live operations are intended to take place.

2.3.4. Assessment of impact of military vehicles traffic on natural terrain

In this research study the impact of military vehicle traffic on natural areas was considered. Anderson et al (2005) studied the types of environmental impacts associated with off-road vehicles and to identify knowledge gaps that limit the use of study results in land management decision making processes. This study concluded that researchers of off-road vehicles impacts from all disciplines including military, re-creational, agricultural, mining and others are coming together to form a more cohesive impacts assessment discipline.

The study further concludes that no single study provides vehicle data impact suitable to support all land management decisions. It has been strongly observed that as coordination and cooperation grows, researchers will be better equipped to provide the kind of research, data and information needed to make more effective plans and decisions to conserve natural resources Anderson et al (2005).

2.3.5. Assessment of impact of military vehicle traffic on vegetation

An assessment technique for evaluating military vehicular impacts to vegetation in the Mojave Desert in South-Eastern California in the United States of America was developed, Hansen and Ostler (2005). This technique was used to evaluate different vehicle types with rubber wheels and metal tracks in different soils and intensity training levels. The technique also provides tabular data that can be sorted to show a variety of trends related to military vehicular traffic impacts. 20 tracks and nearly 500 shrubs were sampled in the six study areas to evaluate the

vegetation damage assessment technique. The research design provided a relatively comprehensive data set upon which to evaluate the impacts to perennial vegetation as sown in table 2.2. The impact to relatively undisturbed vegetation is greater than impacts to vegetation that has been run over several times thereby selecting branching patterns and equipment sizes that are better able to withstand vehicular traffic. Plant damage assessment technique provides rapid means of assessing impacts of vehicular traffic in areas from moderately to heavily distributed impact. Despite the importance of the data in table 2.2, the clarity of the research results could have been much better by adding more measurement parameters to the table.

Percent survival expressed as a mean value for plants by prior damage class after vehicular impact

Prior damage class	Percent survival (mean)	SE Mean (+-))	*N*
Low	51.4	6.5	35
Moderate	29.3	2.6	139
High	25.9	2.5	144
Very High	32.8	3.7	91

(SE Mean is the standard error of the mean and *N* is the number of measurement

Table 2.2: Survival rate of plants after vehicular impact, Hansen and Ostler (2005)

Vegetation damage is also greater with dry soil conditions than moist conditions. The study concludes that this technique is also suitable for assessing other non-military off road traffic impacts Hansen and Ostler (2005). This study also presented the degree to which rubber tyre wheels have less impact that metal tracks. The construction sector is yet to benefit from similar studies and its impact on project cost and time.

2.4. Terramechanics in the Agricultural sector

Over time, research tools that have been used in agricultural terrain mechanics have developed from empirical to reliable methods such as experiments, mathematical modelling and Finite Element Modelling. One of the main reasons for wheel-soil studies in agriculture is to reduce soil compaction which in turn promotes healthy crop production.

2.4.1. Tractor drawbar-pull experiments on sandy and sandy loam soils

An experimental based research was carried out in one of Hungary's arable area with field tests done in 1959 and 1960 as one of the early experiments on drawbar-pull, Zombori (1967). These soils were not suitable for tractor operation because of their low strength (looseness) which limited the available drawbar-pull. Drawbar-pull tests on traction devices were carried out by means of a standard dynamometer on sand and sandy loam soils. The test was carried out on two wheel drive, four wheel drive and tracked tractors.

The results indicate that ballast weights applied on the driving wheels of a two wheel drive tractor always resulted in an increase in pull in sandy and sandy loam. It was also established that a decrease in the tyre inflation pressure resulted in an increase in drawbar-pull for a constant travel reduction on loose soils as shown in figure 2.22. The tyres were also best utilised at a rear dynamic load of 1500Kg where the dynamic traction ratio is maximum Zombori (1967). The results from the study suggest that construction plant performance could also benefit from this research by modelling and studying how wheeled construction plant would respond to different ground conditions found on construction sites under loaded and unloaded conditions.

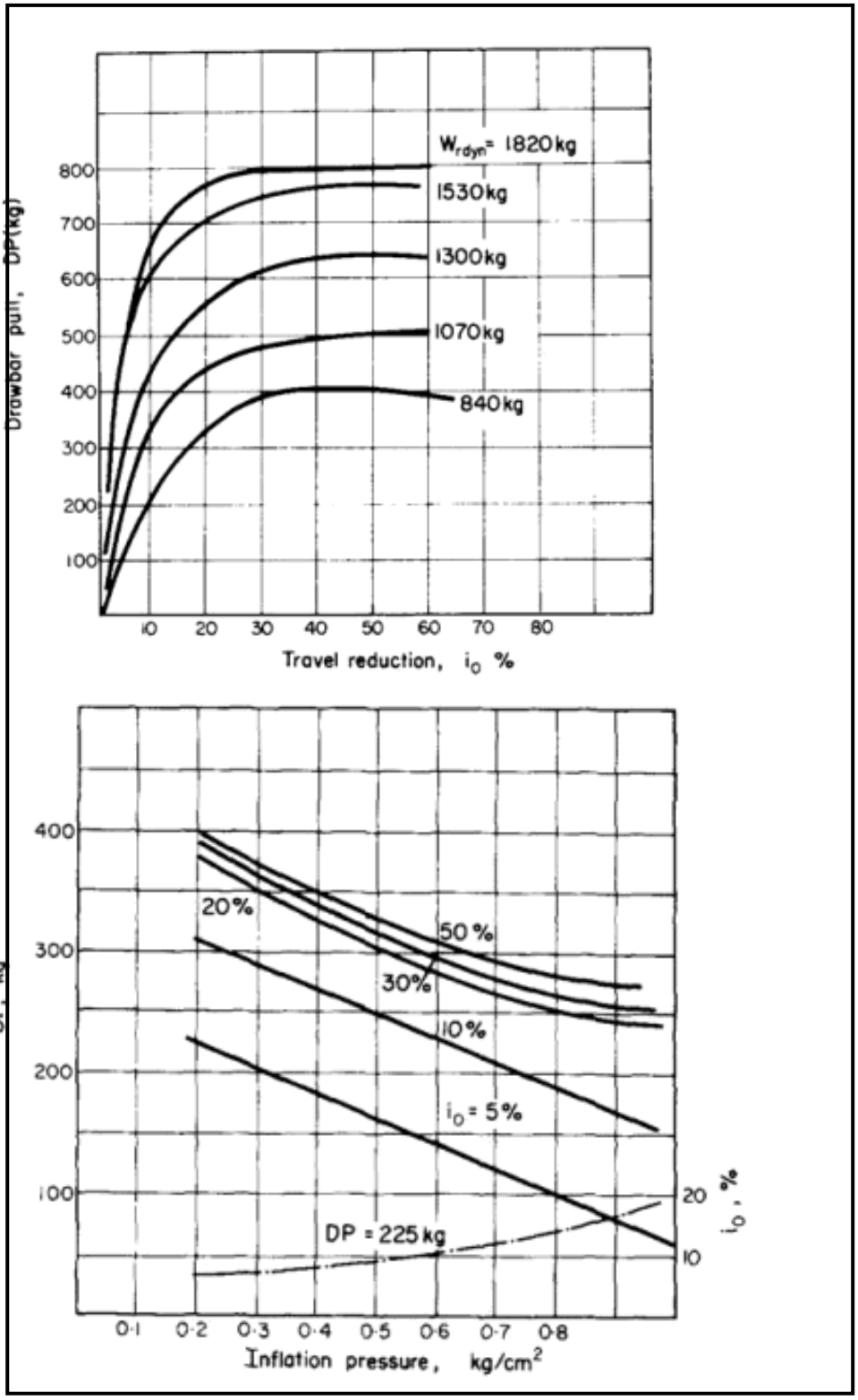

Figure 2.22: Zombori's experiment showing drawbar-pull in relation to dynamic load and tyre pressure, Zombori (1967)

The effects of weight increase on wheeled construction plant traversing on construction sites needs to be investigated. The importance of this investigation rests in the fact that the agricultural sectors requires loose soil to support high

yield crop production while the construction sites and deformable haulage roads require compact and hard surface to support wheeled and tracked plant traversing on the given terrain. Zombori's results further indicate that light track layers are far superior to wheeled tractors on sandy soils due to wider contact area. The power loss predictive mathematical model (POWERSEV) developed in chapter 4 of this thesis however focuses on wheeled plant as stated in the introductory chapter.

2.4.2. Influence of tyre inflation pressure on drawbar-pull characteristics on a tractor set.

Cupera and Smerda (2010) presents an agricultural based research aimed at establishing the influence of tyre inflation on drawbar-pull characteristics and performance on a tractor set using regression analysis and Mohr Coulomb's soil failure theory. The results indicate that 20% to 55% of the energy transferred to the drive tractor wheels is wasted in the wheel–soil interaction during crop production Cupera and Smerda (2010). This research also identified two essential ways on reducing slip in Terramechanics: The first one lies in increasing the tractors weight by adding ballast weight. The other possibility is to enlarge the contact area between tyres and the surface.

These results validated Zombori's experimental analysis (Zombori, 1967) undertaken 43 years earlier. Larger contact area makes rolling resistance smaller in soft soils. Reducing tyre pressure in tyres with wide treads (low profile) increased the front foot print thereby showing a positive impact on the specific tractive fuel consumption that decreased in the range from 3.4% to 16% depending on travel speed. This also resulted in fuel savings of 4.7% litres per hectare as seen in table 2.3. The study established that the slip should not exceed

15% because it causes a decrease of engine power efficiency transmitted to the surface. The tractor transferred larger drawbar-pull to the surface at the same ground speed and lower tyre inflation pressure resulting in significant increase in performance. Graphical analysis of the results in table 2.3 could provide a much clearer interpretation of the data regarding the effect of wider tread and narrow tread tyres on performance and fuel consumption.

The results of the ploughing set measurement

Width (mean)	Depth (Mean)	Tractor speed		Slip	Effective performance		Fuel consumption	
m	m	m s^{-1}	kph	%	h ah^{-1}	m^{-3} s^{-1}	1 ha^{-1}	ml m^{-3}
1. Radial-ply tyres with wide tread (low-profile), front 75kpa, rear 65kpa								
Mean	*2.71*	*…...0.25*	*1.31*	*4.70*	*19.11*	*1.27*	*0.895*	*24.33*	*9.61*
II. Radial-ply tyres with wide tread (low-profile), 180kpa								
Mean	*2.68*	*…...0.26*	*1.21*	*4.35*	*21.99*	*1.17*	*0.83*	*26.68*	*10.38*
Radial-ply tyres with narrow tread (standard), inflation 250kpa								
Mean	*2.64*	*…...0.25*	*1.23*	*4.44*	*24.73*	*1.17*	*0.81*	*26.55*	*10.67*
Radial-ply tyres with narrow tread (standard), inflation 170kpa								
Mean	*2.60*	*…...0.25*	*1.29*	*4.66*	*20.74*	*1.21*	*0.832*	*25.53*	*10.34*

Table 2.3: Results of the ploughing set measurements, Cupera and Smerda (2010)

Reducing tyre pressure however does not guarantee better drawbar characteristics in all cases. Reducing tyre pressures for appropriate tyres improve drawbar-pull characteristics and consequently fuel consumption, Cupera and Smerda (2010).

The terrain conditions described in this study are purely agricultural based and loose in nature. Construction sites mostly require more compact terrain for safe vehicular movement. The development of models and experimental analysis for construction sites and deformable haulage roads would provide valuable insights regarding the effects of wheel-soil interaction on construction plant performance. This will also result in improved measurement and evaluation of terrain mechanics

effect on wheeled construction plant performance during the construction period. The parameters of interest during this construction period include tyre inflation, fuel consumption, plant weight and traction efficiency. As for tyre inflation pressure, construction plant wheels are normally operated with highly inflated tyres because of the heavy loads that they are designed to carry. This research also has great potential to be extended to construction tracked equipment such as tracked excavators.

2.4.3. Finite Element Modelling for Wheel-Terrain interaction

Another study by Xia (2010) presents the design of a three dimensional Finite Element Model for wheel-terrain interaction as well as a finite strain hyperelasticity model for modelling of rubber materials using the Drucker-Prager/Cap model implemented in ABAQUS to model the soil compaction. The main purpose was to demonstrate that many factors relating to soil compaction and tyre mobility can be directly predicted based on the FEM of wheel-terrain interaction as indicated in figures 2.23 and 2.24 below. The research offered a novel future of modelling the special density change which has been an issue of great significance in the application of Finite Element techniques to agricultural, geotechnical and pavement engineering.

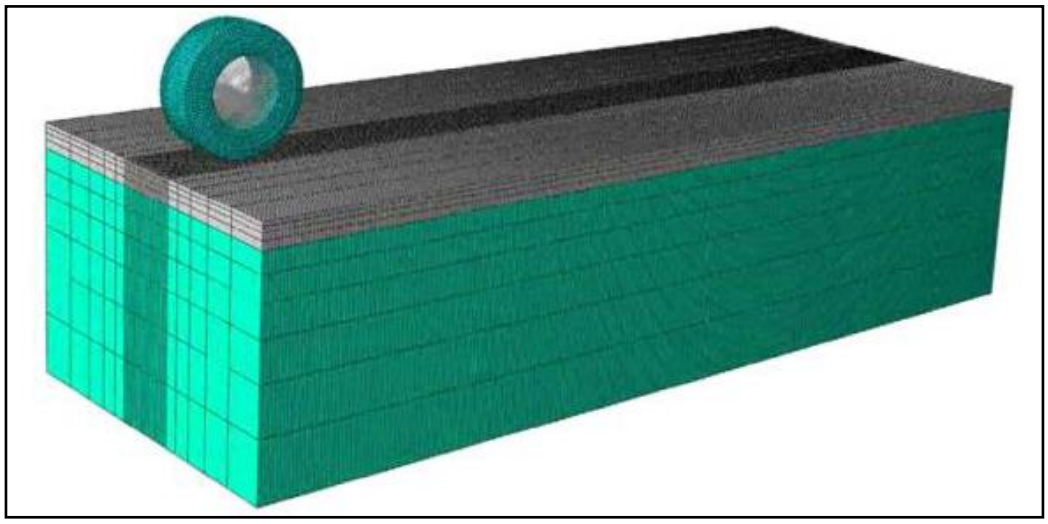

Figure 2.23: Finite Element Model of tyre/terrain interaction, Xia (2010)

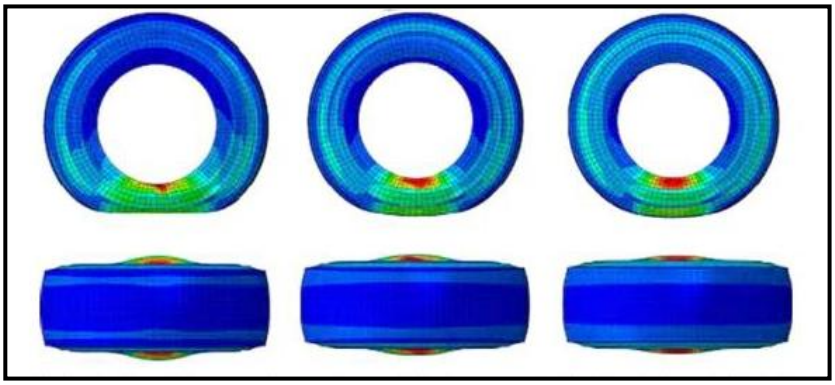

Figure 2.24: Tyre foot printing on soft ground versus inflation pressure 0.3MPa, 0.5MPa and 0.7MPa, Xia (2010)

Rolling radius, acceleration, torque, traction can be obtained from Finite Element wheel-terrain interaction model. The research results indicate that using field experiments to test tyre performance can be extremely expensive and time consuming. Lower tyre inflation will have a relatively higher contact area with ground. The contact area will decrease with increasing tyre inflation pressure. The density will increase with increasing inflation pressure leading to a stiffer tyre and eventually lead to relatively smaller contact area with terrain, which produces a higher compaction on soil.

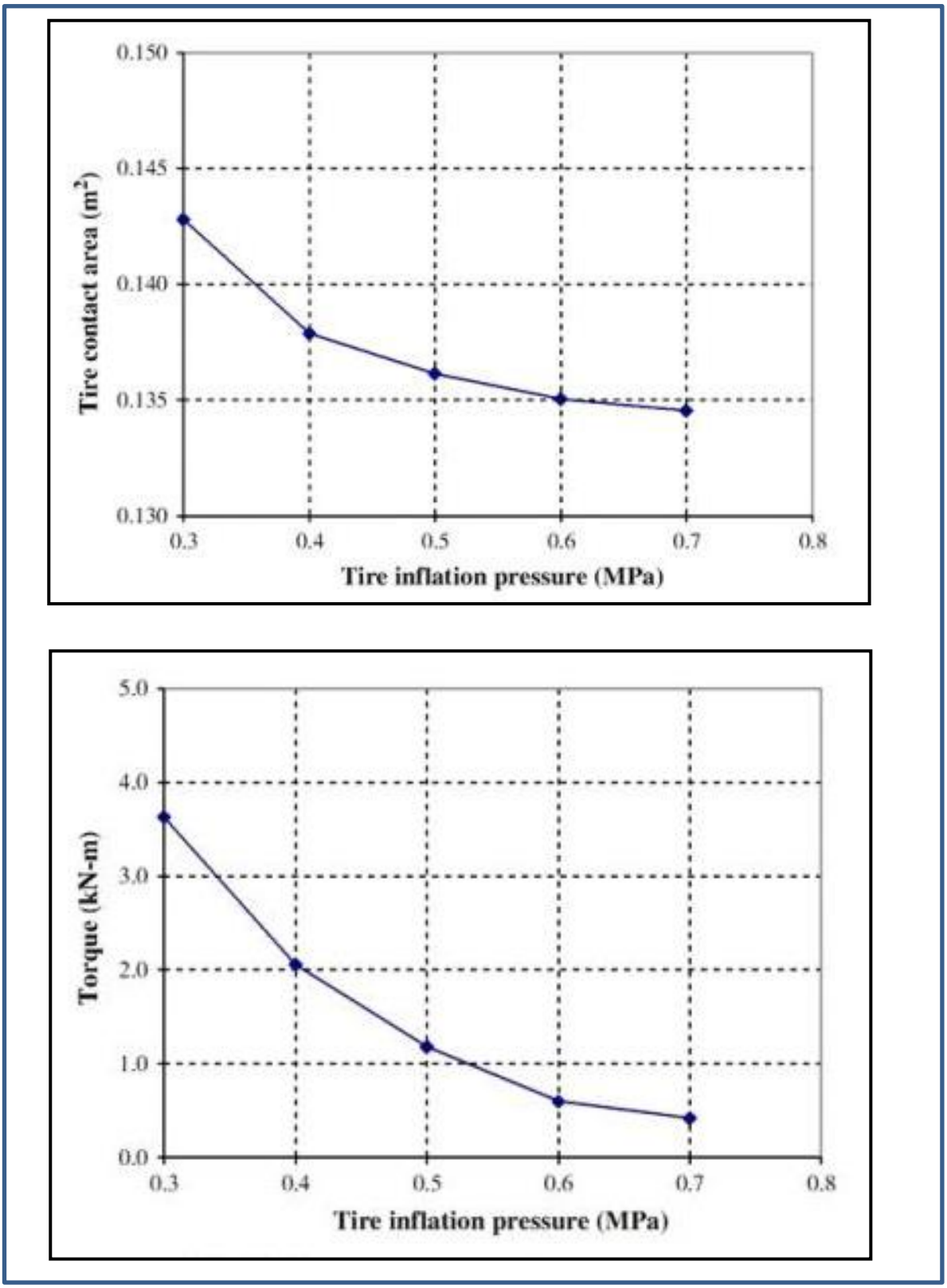

Figure 2.25: Tyre inflation pressure against tyre contact area and torque, Xia (2010)

The top panel of Figure 2.25 shows the relationship between tyre contact area and tyre inflation while the bottom panel represents the relationship between tyre pressure and the torque generated. The contact area was calculated based on the contact algorithms from the Finite Element output. High inflation tyre on relatively stiffer deformable terrain can reduce energy cost; however for relatively soft soil the result might turn out to be completely different Xia (2010). This delivers a relatively lower required torque and power to maintain the vehicle speed. It must also be noted that higher inflation pressure will require higher toque to maintain vehicle speed. While this is true for the agricultural environment, its influence and impact to the construction sector is yet to be established.

2.4.4. Field and laboratory experiments on agricultural tractors.

In most times, the selection of a right type of tyre involves a decision making process in which a balance should be made between good traction for acceleration stage and energy reduction. Modelling and experimental analysis of this process with a focus on typical construction site terrain would provide potential benefits in managing project time, plant selection and project cost. The figures 2.26 and 2.27 show the two tractors under field and laboratory tests respectively. Both field and laboratory experiments have their own advantages and disadvantages. Field experiments provide real data through the use of instruments as denoted in figure 2.26. Alternatively laboratory experiments provide the opportunity to control, change and monitor the test environment easily. On the other hand field experiments provide limited configurations while laboratory experiments may require implementation of scaling factors in order to simulate the real terrain and the associated vehicle factors.

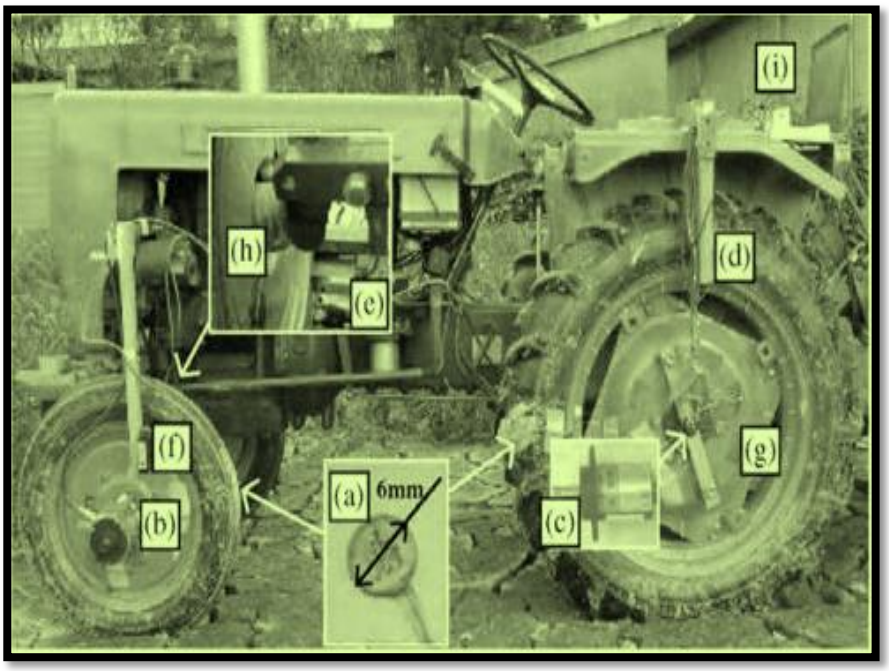

Figure 2.26: Agricultural tractor prepared for field tests, Nguyen et al (2008)

Figure 2.27: Tractor being tested for drawbar-pull in a test laboratory (http://pubs.ext.vt.edu/442/442-072/442-072.html)

2.5. Terramechanics in planetary exploration studies

Terramechanics is a subject that has been considered during the design of planetary and exploration rovers on exploration missions to the moon and planet Mars. Rigid and flexible wheeled rovers have been studied to understand the relationship between wheels and terrain in the determination of traction efficiency for planetary and exploration vehicles.

2.5.1. Experimental study of performance for wheeled planetary rovers in deformable soil

Results from an experimental study by Ding et al (2010) on the analysis of driving wheels performance for planetary exploration rovers moving in deformable soils are useful in optimal wheel design and improvement/verification of wheel-soil interaction mechanics model. Below are the formulae used to calculate *s* the slip ratio and the entry angle θ, S being represented by equation 2.30

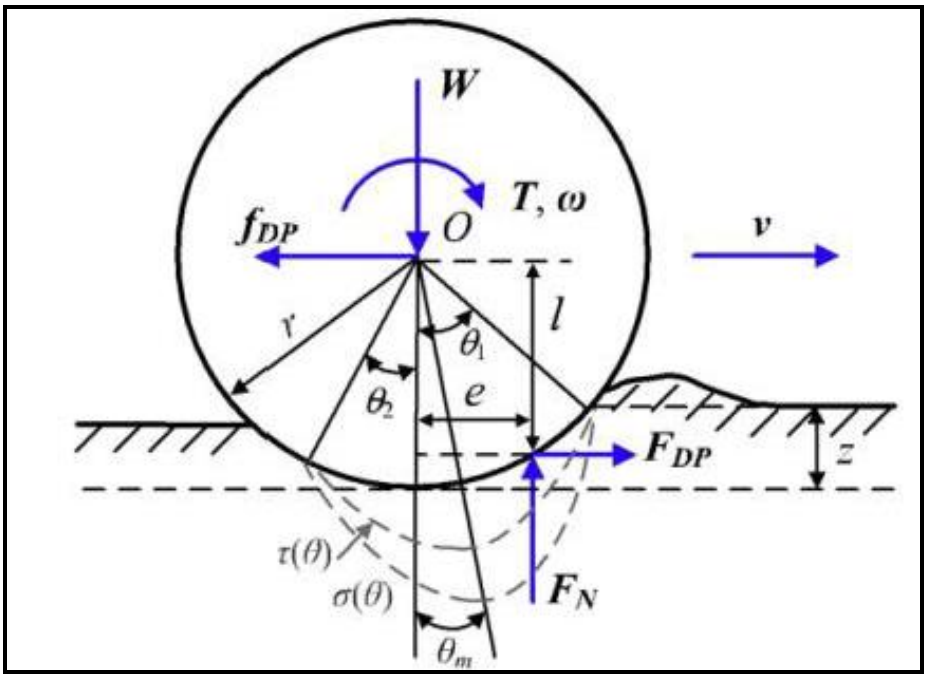

Figure 2.28: Forces and torque acting on a driving wheel, Ding et al (2010)

$$r_s = (r + \lambda_s h)(0 \leq \lambda_s \leq 1) \qquad \text{Eqn 2.29}$$

$$s = \begin{cases} (r_s\omega - v)/r_s\omega \ \ (r_s\omega \geq v, 0 \leq s \leq 1) \\ (\ r_s\omega - v)/v \ (r_s\omega < v, -1 \leq s < 0 \end{cases} \qquad \text{Eqn 2.30}$$

$$\theta_1 \ = arcos(1 - z/r) \qquad \text{Eqn 2.31}$$

Conclusions from this research indicate that increasing wheel width and radius can improve the drawbar-pull performance of the rover wheel. Figure 2.29a and 2.29b indicate the slip ratio relationship with sinkage and drawbar-pull. Figure 2.30 shows the set up for the single wheel laboratory experiment. The study further revealed that the slip ratio and entrance angle of the wheel are the two important variables that must be considered while deducing the wheel-soil interaction model.

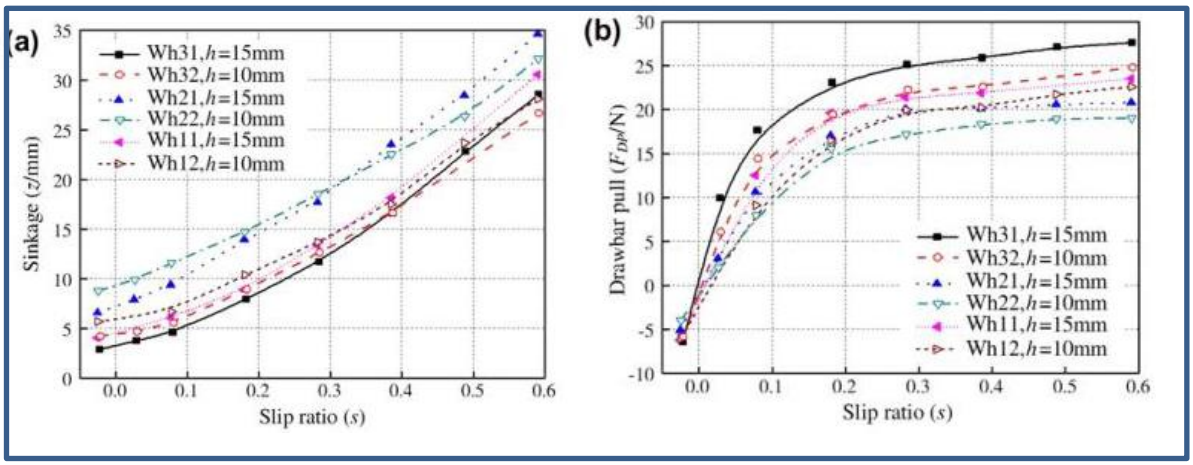

Figure 2.29: (a) Slip ratio against sinkage and (b) Slip ratio against drawbar-pull, Ding et al (2010)

Figure 2.30: Experimental set up based on a single wheel, Ding et al (2010)

Figure 2.29a demonstrates that the increase in slip results in increased sinkage. This increase in slip ratio results in increased drawbar-pull (Figure 2.29b) with maximum efficient slip being between 0.3 and 0.5 as cited in other studies. The research further considered the effect of wheel lugs which is outside the scope of the research at hand. Wheel lugs are commonly used by planetary rovers in explorations missions.

2.5.2. Modelling and simulation of planetary rovers on soft terrain.

Another study on advanced modelling and simulation methods of planetary rover mobility on soft terrain was developed with the aim of producing develop a Computer Aided Engineering (CAE) tool. This tool was designed to support the integrated conceptual design process of multi–axle vehicles in consideration of dynamic behaviour of the soil in interaction with the vehicle suspension, Gibbesch and Schafer (2004). In this research the accuracy of wheel- soil simulations could

not be higher because physical properties of natural soil are extremely non–deterministic.

The greatest challenge is the variability of moisture content which gives the soil an extremely non-linear behaviour. One important observation made in this research is that moisture content is not in the interest of planetary rovers because Martian soil consists of no moisture. The research concludes by emphasising that consideration of moisture content in field experiments on earth cannot be completely disregarded and therefore it is important to consider the non-linear effects Gibbesch and Schafer (2004). The discretisation of the soil allows plastic behaviour of the soil to be simulated with compression and movement of soil particles which is currently not possible with commonly used analytical methods based on Bekker's formulae hence the introduction of computer simulated models Gibbesch and Schafer (2004)).

2.5.3. Application of Bekker theory and Drawbar-pull to wheeled, tracked and legged vehicle locomotion

A study into the application of the Bekker theory was carried out for planetary exploration through wheeled, tracked and legged vehicle locomotion. The aim of this research was to modify the Bekker theory to make it applicable to planetary exploration rovers that are much lighter than the vehicles used to formulate the original theory which was based on heavy vehicles such as tanks and tractors. This was achieved by developing the Rover Mobility Performance Evaluation Tool (RMPET) whose main aim was to evaluate the performance of wheeled, tracked and legged rovers using the Bekker theory, Ellery and Scott (2005). Results summarised in table 2.4 below indicate that the software was able to assess the performance of vehicles on a variety of soil conditions including Martian and Lunar

soil stimulants. It would also benefit designers for small rovers for terrain negotiation operating in earth based terrain and beyond. The research further highlighted that the mobility system for unmanned robotics planetary exploration vehicles is the backbone of robotic planetary exploration, Ellery and Scott (2005).

Soil	Specific Gravity (ρg)	Soil Cohesion (Pa)	Friction Angle (°)	k_c $(N/m^{n+1})^*$	k_ϕ $(N/m^{n+2})^*$	Consistency $(k=k_c+bk_\phi)$	Deformation Coeff (n)**	Drawbar Pull (N)
DLR soil simulant A	4.24	188	24.8	2370	60300	8400	0.63	112.7
DLR soil simulant B	4.24	441	17.8	18773	763600	95133	1.1	155.0
VL1 drift	4.29	1600	18	1400	820000	83400	1.0	151.28
VL1 blocky	5.97	5500	30.8	1400	820000	83400	1.0	319.5
VL2 crusty-cloddy	5.22	1100	34.5	1400	820000	83400	1.0	378.8
PL drift	4.36	380	23.1	1400	820000	83400	1.0	215.2
PL cloddy	5.70	170	37	1400	820000	83400	1.0	421.45
Dry sand	5.67	1040	28	990	1528000	153790	1.1	293.2
Sandy loam	5.67	1720	29	5270	1515000	156770	0.7	298.8
Clayey soil	5.67	4140	13	13190	692200	82410	0.5	79.2
MER-B 'sandy loam'	4.24	4800	20.0	28000	7600000	788000	1.0	202.7
MER-B 'slope soil'	4.24	500	20.0	6800	210000	27800	0.8	137.2

* as there is no experimental data from VL1, VL2 and PL (lunar values for those soils have been used)[5]
** as there is no experimental data from VL1, VL2 and PL (assumed n=1 for those soils)

Table 2.4 Summary of soils investigated in this study, Ellery and Scott (2005)

$$\tau = C_0 + \sigma \tan \emptyset \qquad \text{Eqn 2.32}$$

$$DP = H - R = H - (R_c + R_b + R_g + R_{other}) \qquad \text{Eqn 2.33}$$

$$Z = \frac{1}{n}\left(\frac{3W}{(3-n)k\sqrt{d}}\right)^{2/(2n+1)} \qquad \text{Eqn 2.34}$$

$$R_b = \frac{B\sin(\alpha+\varphi)}{2\sin\alpha\cos\varphi}\left(2zC_0k_c + \gamma z^2 k_\gamma\right) + \left[\frac{\pi\gamma l^2(90-\varphi)}{540}\right] + \frac{\pi C_0 l^2}{180} + C_0\, l^2 \tan\left(45 + {}^{\varphi}/_{2}\right) \qquad \text{Eqn 2.35}$$

The above equations are representing various parameters such as shear stress for equation 2.32. Drawbar-pull is represented by equation 2.33, sinkage for equation 2.34 and Resistance for equation 2.35. Other equation parameters can be found on the nomenclature page before the introductory chapter. The study concluded that benefits of producing the most drawbar-pull from a minimal weight vehicle is very attractive to space robotics, because maximising performance with minimal weight is one of the most important factors, Ellery and Scott (2005). This interpretation however may be different from the requirements for the construction vehicles that are generally characterised by heavy loads.

2.5.4. Algorithm development for terrain estimating and sensing for planetary rovers

In another study, research results are presented based on a multi sensor terrain for planetary rovers. An algorithm was developed for terrain estimation and sensing which relied on simplified form of terramechanics equations using linear least estimator to compute terrain parameters in real time. Results from the experiment indicate that this approach and method is computationally efficient and is thus suitable for implementation on a rover with limited on board resources, Lagnemma et al (2004). Simulation and experimental results show that the algorithm can accurately and efficiently identify key terrain parameters for a variety of soil types with Drawbar-pull being an indicator of a rover's ability to move through terrain. This research was carried out at the Field and Space robotics laboratory Massachusetts Institute of technology, USA. It was further supported by the National Aeronautics and Space Administration (NASA) jet propulsion laboratory through the Mars Technology program, Lagnemma et al (2005). Figures 2.31 and 2.32 illustrate the above described experiment.

Figure 2.31: Planetary wheel-terrain interaction test bed in the laboratory, Lagnemma et al (2004)

Figure 2.32: Example of wheel sinkage in deformable terrain, lagnemma et al (2004)

Lagnemma (2005) presents the design vehicle for robust mobility on Mars surface based on terramechanics principles. The research also presents Curiosity Mars

Rover test model at NASA. The presentation analyses the design and performance prediction for the mars exploration rover. *This study recommends the use of laboratory based validation against experimental data*. Figures 2.33 and 2.34 illustrate the MARS exploration rovers associated with NASA research.

Figure 2.33: NASA's Mars Science Laboratory (MSL) Rover Design/Test Model in the sandy Mars yard at JPL Lagnemma (2005)

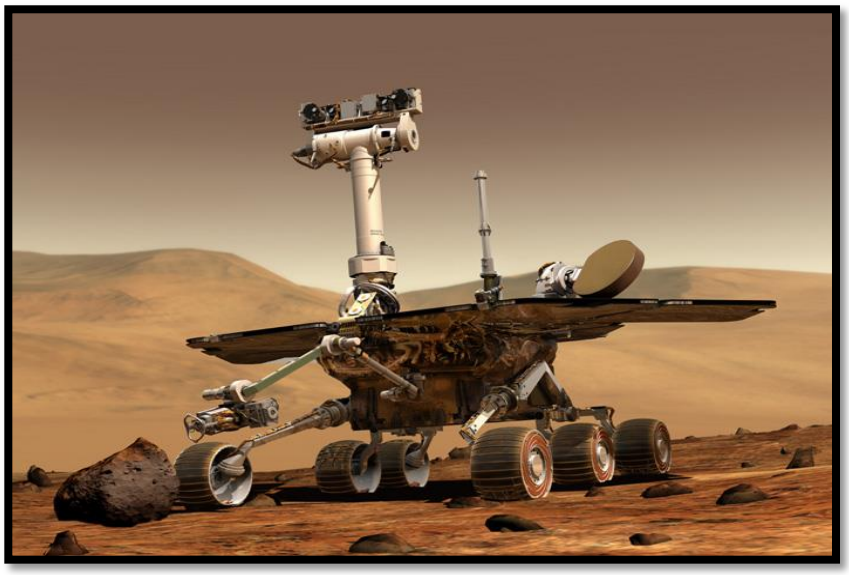

Figure 2.34: Artists impression of the MARS exploration, Lagnemma (2005)

2.6. Terramechanics in forestry studies and research

Wheel-soil studies have been used to attain eco-efficient wood harvesting on sensitive sites that utilise wheeled and tracked machinery during the harvesting process in Agro forestry, Saarilahti (2002).

2.6.1. Terramechanics and eco-efficient wood harvesting in forest research.

In one detailed research in Finland, a wheel-soil interaction model was designed to develop a protocol for eco-efficient and wood harvesting on sensitive sites that matches the machines to the site, Saarilahti (2002). The matching of the two elements (machine and site) needed to meet the environmental and economic criteria. The modelling included all the three relevant levels namely: wheel-soil, machine terrain and transport-environment. In order to attain the main objective, interactive sub models were developed with each of the models to be updated with increasing experience, Saarilahti (2002). There is need to formulate criteria for matching machine and site in order to meet specified economic and environmental requirements for construction projects as well particularly those that involve a great deal of soft ground traversing.

2.6.2. Machinery soil compaction, root damage and logging operations

In another terramechanics based forestry research, a study was carried out in an acid and loamy leached forest soil of the loessic belt of central Belgium Rohand et al (2004). In forest ecosystems, the increase in size, power and weight of forestry machinery is one of the main causes of soil degradation (soil compaction), the soil being subjected to severe stresses due to mechanical forces exerted by tractor tyres and skidding. The study provides clear evidence that soil compaction caused

by logging operations result in increased in bulk density, reduction in macro porosity and consequently reduced soil aeration and water holding capacity Rohand et al (2004). The study concludes that these effects result in poor rooting, inducing lower uptake of nutrients and water and possibility of tree growth. Just like the agricultural environment, soil compaction and root damage increase the risk for infection by root pathogens, Rohand et al (2004). Consideration of crop production and desire for health roots is not applicable to a construction site except in cases where the environmental impact assessment requires preservation of selected natural species.

2.6.3. Effect of wheel/track skidding on the degradation of the soil.

Another important research aimed at examining the impact of timber production works on the terrain was carried out by Makineci et al (2007) with particular focus on herbaceous cover, forest floor and soil on the skid road in the Belgrad forest in Turkey. The study further states that skidding or yarding requires the construction of relatively dense network of forest roads including skid roads, haul roads and landings. Harvesting works being carried out in the forest areas cause losses, mixing and compaction of the soil to a great extent. Degradation in the soil after timber harvesting also has much important effects on the contents of the nutrients as it has impact on the physical properties of the soil, Makineci et al (2007).

The results from this study indicate that long term harvest using skidding techniques on these sites had adversely affected soil action concentrations, physical soil conditions and mass of herbaceous cover and forest floor. The research further concludes that prompt action should be taken in order to prevent

and minimise such negative impacts of the skid roads. The skid roads should not be used for long periods without taking any corrective actions after they have been built. Such rehabilitation works on degraded skid roads will be very useful in the protection of the ecosystem.

2.6.4. Wheeled forest forwarders and traction efficiency

Research on logging machines and self-loading forwarders in forests has been focussed on improving profitability and forest environmental care. Problems that may result from deep rut formation include reductions in tree growth and the disruption of ecosystems. Forwarders transporting logs from the forest to the roadside travel many times, empty or loaded on the same strip road, Jun Gyu et al (2004). The number of forestry machine passes is a significant factor influencing rut formation which is influenced by the wheel-soil interface pressures. Higher load gives better traction in soft soil.

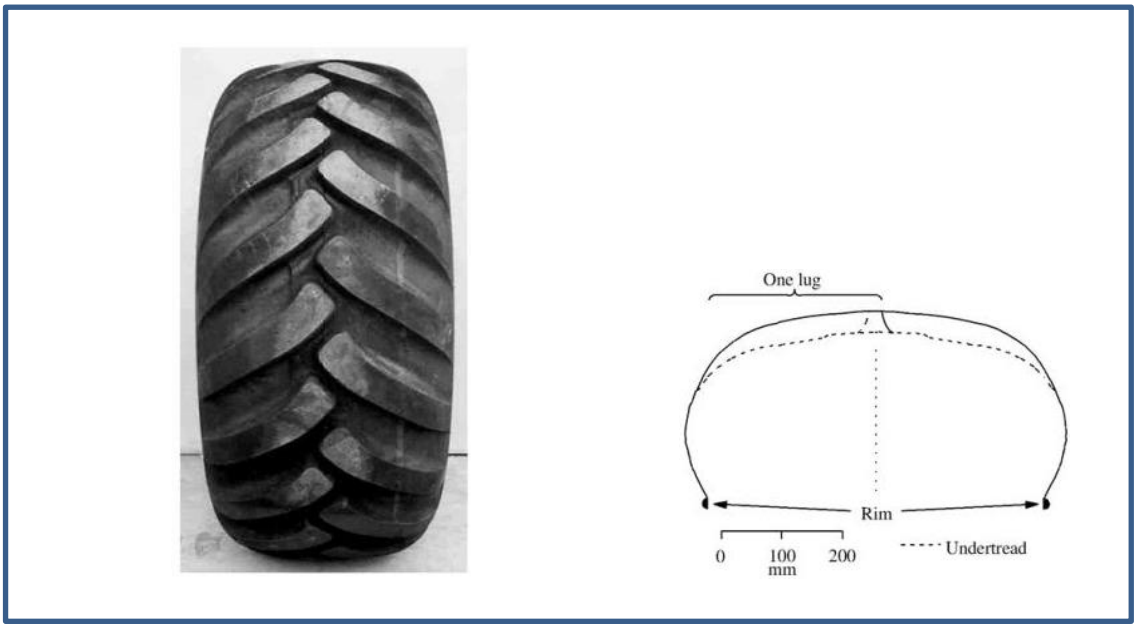

Figure 2.35: Trellebord 600/55-26.5 forwarder tyre on top and circumferential projections of lugs tyre and under tread of unloaded tyre section onto a cross sectional plane, Jun Gyu et al (2004)

Mean net tractions and tractive efficiencies at 5% travel reduction

	Treatment				Dynamic load (KN)		Inflation Pressure (KPa)	
	23.9-100	23.9-240	40-100	40-240	23.9	40	100	240
Net Traction (KN)	7.0	5.8	13.4	10.9	6.4	12.1	10.2	8.3
Tractive Efficiency (%)	75.0	68.9	78.4	71.6	71.9	75.0	76.7	70.2

Table 2.5: Mean net tractions and tractive efficiencies at 5% travel reduction, Jun Gyu et al (2004)

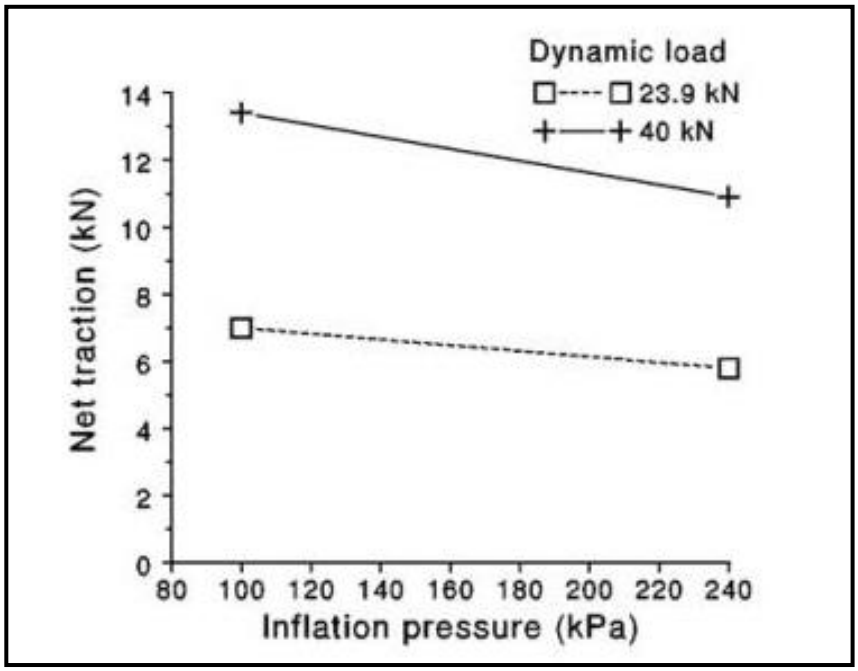

Figure 2.36: Interaction of dynamic load and inflation pressure for net traction, Jun Gyu et al (2004)

The research concluded that as inflation tyre pressure decreased at constant dynamic load, the net traction and tractive efficiency of the forwarder tyre decreased with increasing inflation pressure at constant dynamic load. The tyre and its profile details used in the experiment are given in figure 2.35 and table 2.5 (Jun Gyu et al, 2004). The relationship between inflation pressure and sinkage are given in figure 2.36. At constant inflation pressure, net traction and tractive efficiency increased with increasing dynamic load. The influence of this

relationship would be of great interest when applied to a construction project with particular focus to project cost and time.

2.6.5. Managing forest soft terrain and rutting using basic WES principles.

Due to the increased awareness of environmental issues, need has been created to evaluate the usefulness of mobility models for Nordic forestry conditions. A research was conducted to establish wheel rut depth for timber transport on moraine soils in West central and Southern Finland. Mobility is not an acute problem in today's logging in Finland, but the environmental impacts are of great interest. The field tests were carried out in connection with normal forest operations in West-Central and Southern Finland and because the study was done to investigate the usefulness of the WES-method. Test sites were selected so that the variations in wheel slip or changes in dynamic wheel load were minimised.

$$Z_{RUT} = d\left(a + \frac{b}{N_{CI}}\right)$$

Eqn 2.36

In equation 2.36, the sinkage is calculated by finding z, where *a* and *b* are empirical constants. The results of regression analysis can be seen that the highest coloration coefficient squared (r2=0.863) was obtained by using Cone Index (CI) of layer 7 (0.163). The correlational relationship is shown in figure 2.37.

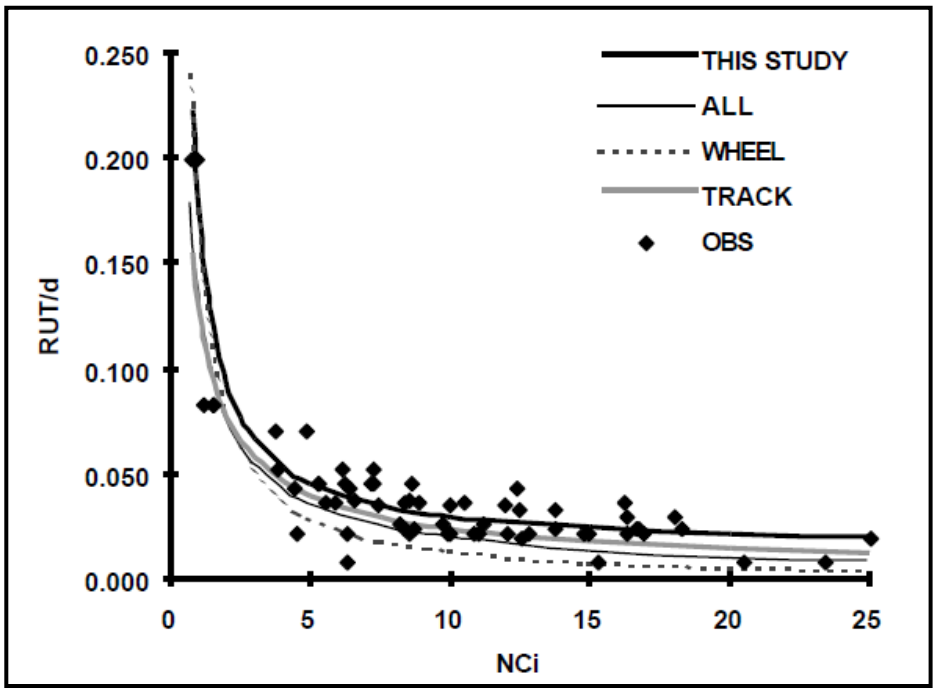

Figure 2.37: Comparison of models for the study (Saarilahti and Anttila, 1999)

Simple rigid wheel rut depth models based on the WES-principles, the use of soil penetration resistance and wheel numeric, seem to be reliable enough to avoid too risky operations on Finnish forest sites and too risky soils. The same models seem to apply both for mineral and organic soils, Saarilahti and Anttila (1999). The same methods have great potential of benefiting the construction sites and road haul operations during construction phase of a project.

2.6.6. Investigating the rutting and soil displacement by wheeled skidder in a forest.

In another field based research study, the rutting and soil displacement caused by 450C Timber Jack wheeled skidder in the Asalem forest of Northern Iran were investigated. The study shows that skidding machinery in logging operations causes destructive effects especially on soil but has many advantages such as extracting long and heavy logs, optimum use of useful logging time Naghdi et al (2009). Logging always leads to a wide range of disturbing effects on the forest

ecosystem. Soil surface disturbance, changes in chemical/physical properties of soil and damage to natural regeneration stand as the three main effects of logging operations and wood extraction on soil and forests.

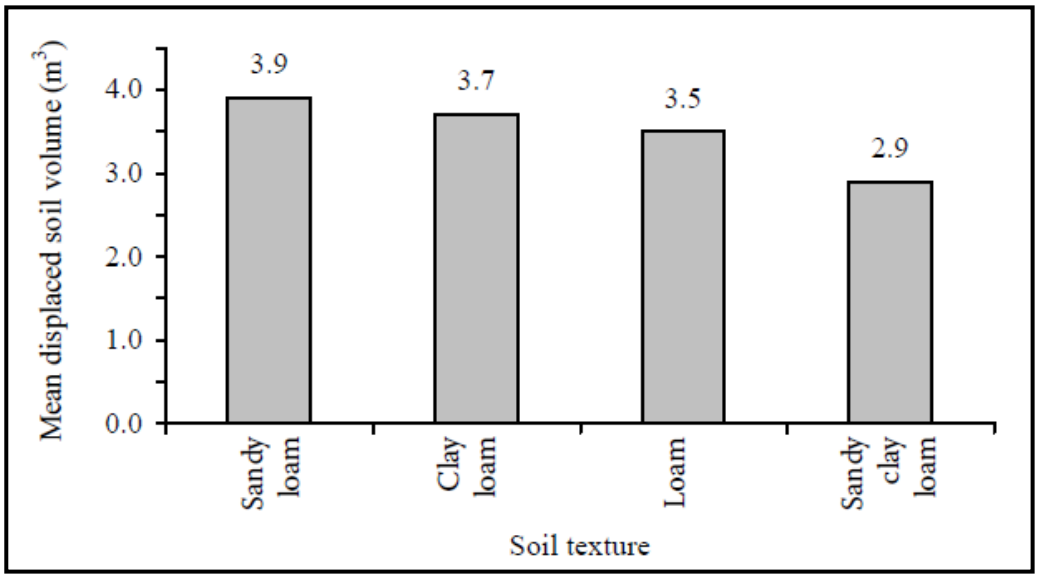

Figure 2.38: Mean displaced soil volume concerned with soil texture in longitudinal slope 15 to 25%, Naghdi et al (2009)

Soil texture testing of samples in the laboratory considered four types of soil: loam, clay loam, sandy loam and sandy clay loam. The soil moisture content was from 18% to 22%. The results from this study indicated that the maximum volume of displaced soil in slope class 2 (15–25%) was in sandy loam soil. Figure 2.38 provides a summary of the displaced volume against soil type/texture where the significant displacement is seen to be in the sandy loamy soil. There was no significant correlation between the mean rut depth and soil texture (r = –0.194, n = 18, P > 0.05). No correlation was observed between the volume of displaced soil and the type of soil texture (r = 0.19, n = 18, P > 0.05), Naghdi et al, 2009).

Soil compaction is the first consequence arising from skidder traffic because due to the weight of the machine with load, engine vibrations and wheel slip. The soil in

skid trails will be compacted, therefore water and air infiltration decreases resulting in run-off increases. Appropriate and precise scheduling of skidding operations in order to minimise damage to soil requires the knowledge of soil/terrain conditions and machine characteristics, Naghdi et al (2009). The study concludes that it is necessary to kNow the relationship between forest soils and their susceptibility to damage arising from skidding machinery operations. Determining and decreasing soil damage is a necessary part of sustainable management strategies. This is very useful knowledge to the construction industry in order to select the appropriate wheeled plant and time in order to attain maximum efficiency and output of the project associated with soft terrain on construction sites and deformable long haulage roads.

2.6.7. Minimising rutting and soil displacement in forestry logging

An investigation into the use of bogie tracks and planning to minimise rutting and soil disturbance in forestry logging operations is carried out**.** With increased soil moisture content the soil softens and thus increased rutting may be the case. Soil compaction may cause up to 50% growth reduction and it seems that the effect is greater on poorer sites compared to fertile sites, Bygdén and Wästerlund (2007). On dry sites some compaction may even improve growth by increasing the capillary forces. With tracks the rut depths decreased 30–40% compared to 700-mm wide tyres without tracks while rolling resistance was the same or somewhat reduced with tracks compared to wheels, Bygdén and Wästerlund (2007). The investigation concludes that increasing the contact area with tracks mounted on the bogie machine is today a good solution to minimize rutting and compaction. A good solution to further minimise the impact is to extend the contact area against the ground by putting tracks on the bogie. The carrying capacity increases much

with tracks, especially on wet soils thus, to avoid rutting on sensitive soils, tracks are highly recommended.

Figure 2.39: Ruts after 14 tonnes machine with tracks (left) and 10 tonnes on wheels with grove depths 25 – 30cm one passage each, Bygden and Wasterlund (2007)

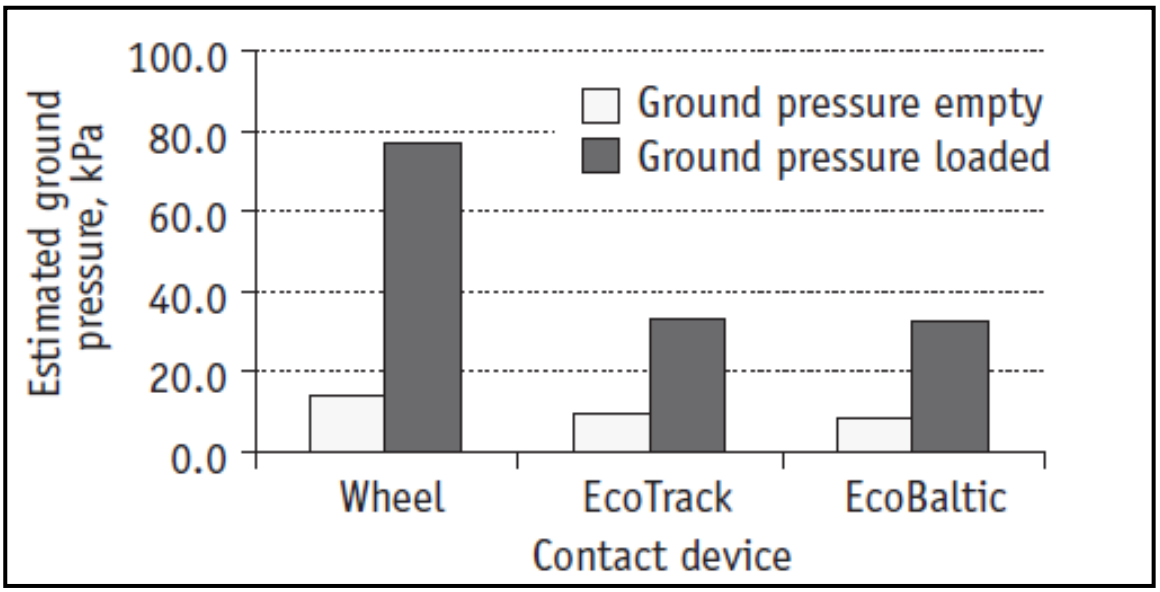

Figure 2.40: Estimated ground pressure for the alternative available kPa, Bygden and Wasterlund (2007)

Figures 2.39 and 2.40 illustrate the process of measuring ruts made by moving wheels in a forest plantation and how wheels produce deeper ruts than tracks. It is evident that rutting and soil disturbance can be minimised by planning and using bogie tracks. With increased soil moisture the soil softens and thus increased rutting may be the case. However, soils are not just loaded beneath a tyre but also subjected to shear forces. The shear forces are measured in the field with a bevameter, a shear ring annulus.

Based on Mohr-Coulomb diagrams the soil strength is determined by using two different sizes of the shear annulus. The equation is: $\tau = c + \sigma \tan\varphi$ where τ is the shear strength (N/m^2), c is apparent cohesion; σ is the load and $\tan\varphi$ the soil friction. Pressure sinkage parameters are presented in figure 2.41 below.

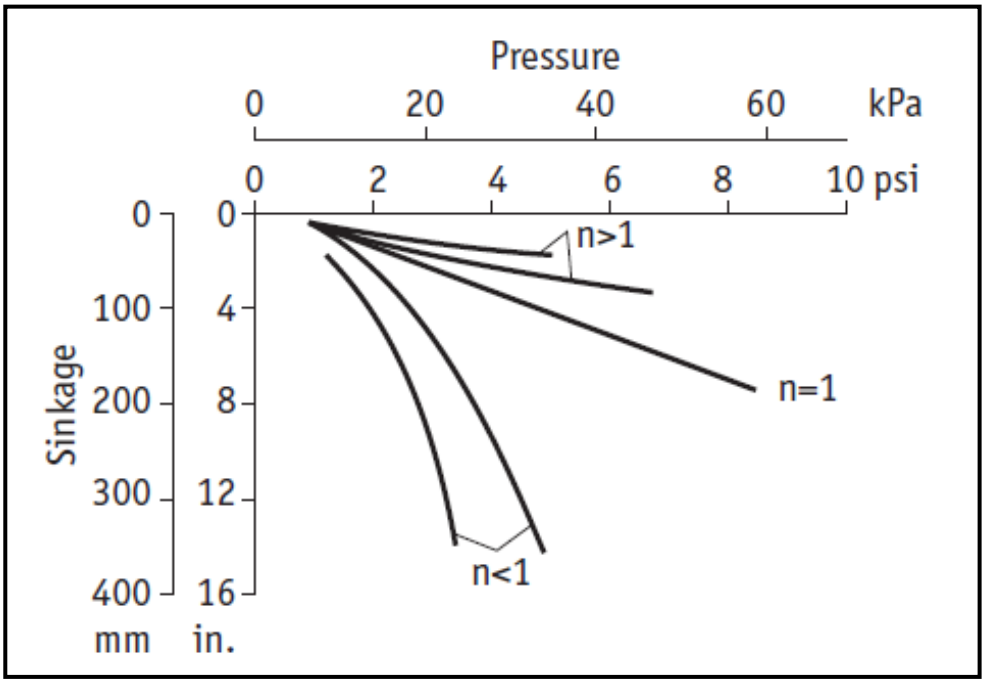

Figure 2.41: Principle pressure sinkage relationships for different types of soil, Bygden and Wasterlund (2007)

2.6.8. Estimating wheel slip for a forestry machine forwarder

A report produced by Hellström et al (2008) on the estimating of wheel slip for a forest machine shows that preliminary field tests were carried out on a Valmet 830 forwarder. On asphalt, the forest machine is assumed and defined to have no slip, so these results can be used for calibration. The field tests with a forestry machine showed that slip over time could be calculated accurately, Hellström et al (2008). Figure 2.42 shows a typical boggie tyre negotiating terrain while figure 2.43 shows the effect of rutting on the terrain. No significant difference between asphalt and a hard gravel surface can be detected. This means that the wheel slip is very low, both on hard gravel and asphalt surfaces. Tests on loose sand show a significant slip and also that the measuring method is able to detect and estimate slip. The outcomes from this study suggest that wheel slip principles could be useful in the wheel-soil studies that focus on the construction site terrain.

$$S = \frac{v_w - \|V\|}{v_w} = 1 - \frac{\|V\|}{v_w} \qquad \text{Eqn 2.37}$$

An idealised rolling wheel with radius r moves at a speed $v_w = \omega r$, in a direction perpendicular to the wheel axle rotating at angle velocity ω. In reality, both magnitude and direction may differ from this idealised situation. The actual wheel velocity vector is denoted by V .The longitudinal slip of a wheel denoted in equation 2.37, is the difference between v_w and $\|V\|$. By normalising the difference the definition of slip coefficient S is arrived at.

These results strongly verify the fact that wheel sinkage and slip are more significant on deformable or loose soil. Asphalt and hard gravel have negligible

rutting resulting in negligible wheel power loss from sinkage related issues provided tyres have been inflated to the correct levels.

Figure 2.42: Bogie negotiating a stone and reducing obstacle height, Hellstrom et al (2008)

The slip coefficient defines the state of the wheel on whether it is in the driving mode (positive value referred to as slip) or in the braking mode (negative value referred to as skid).

Figure 2.43: Example of rut depth measurement in a forest plantation, Saarilahti (2002)

2.6.9. Effect of wheels and boggie tracks on rut formation, cone index and rolling resistance on forest soils.

In a research by Gunnar Bygden et al (2003) an experimental investigation and comparison is undertaken to determine the effects of wheels and two types of bogie tracks on rut formation, cone index, and vehicle rolling resistance on some typical forest soils in Sweden. Terrain transport of timber in Scandinavian forestry is often done with the help of a forwarder carrying the timber cut into assortments from stump to roadside.

A forwarder is a machine type used in the CTL (Cut-to-length) method that carries the cut timber in the forest to the landing (for an overview of machine development). The carrying capacity can be between 8 and 18 tonnes and commonly in Nordic forestry the machines have 8 driven wheels (8WD) for improved mobility on soft ground and articulated steering.

With a softer soil the distribution of the stress is narrower but penetration is deeper. With increased soil moisture the soil softens and thus increased rutting may be the case. It is not the axle load that causes most deep compaction. It is the tyre dimensions, contact stresses, number of passes, soil density and water content distributions, the resulting soil strength and the previous stress that cause most deep compaction effects. The static theory also states that a long contact area is better than a round one of the same area however; soils are not just loaded beneath a tyre but also subjected to shear forces (Gunnar Bygden et al, 2003). The shear forces are measured in the field with a Bevameter, a shear ring annulus. Based on Mohr-Coulomb diagrams the soil strength is determined by using two different sizes of the shear annulus.

The equation is: $\tau = C_0 + \sigma \tan \emptyset$ *as already discussed and illustrated in equation 2.3.*

where τ is the shear strength (N/m^2), C is apparent cohesion, σ is the load and

tanφ is the friction. To engage the whole shear strength in the soil usually the same degree of slippage is needed, e.g. on clay soils. Often the maximum traction is obtained at about 10–30% slippage. Unfortunately the shear strength is mainly measured on non-vegetated areas, which may be erroneous on forest soils. Experiments on forest ground have indicated that root armouring could have a significant (20–50%) effect on the shear strength. Thus, it is proposed that the equation above should have an additive component comprising the root contribution (Sr): $\tau = c + \sigma \tan\varphi + Sr$

Results from this study suggest that compared to rather wide and soft tyres, tracks on the bogie reduced rut depth by up to 40% and cone index in the ruts by about 10%, although the tracks increased the mass on the trailer by 10–12%. The study concludes that further studies are needed to show the effect of track tension on rolling resistance and flotation and of the effects of tracks on heavy vehicles on subsoil compaction. Transport machines used in forestry are often built to carry heavy loads; however, the use of heavy machinery on moist soils gives a high risk for rutting. *Rutting is neither good for future forest growth nor for the operation. Increased rutting implies an increased waste of energy through increased rolling resistance and through unnecessary remoulding of the soil,* Gunnar Bygden et al (2003).

A common measure to decrease rutting on soft soils is to increase flotation of the machines and bogie tracks are one way to achieve this. This is highly likely to be the same for construction related operations hence the potential need to save significant sums of resources and time during the construction period. The reduction of rutting and improved traction need to be translated in monetary value

in order to demonstrate to clients on the significance of applying this field of study to construction related projects.

In a robust research focussing on environmentally sound forest practices to sustain tropical forests, Brown and Sessions (1999) undertook a study on, a study focussing on Research on Variable Tyre Pressures for Tropical Forests. The study observes that in order for a vehicle to move, it must be able to produce a thrust that is larger than the sum of the resisting forces (i.e., grade, friction, rolling, and air resistances). As torque at the wheel overcomes rolling and other resistances, the vehicle will move.

Brown and Sessions (1999) further highlight that A traction evaluation conducted by FERIC on a flat, gravel surface showed that drawbar-pull could be increased 39% by lowering the tyre inflation pressure from 90PSI (620KPa) to 30PSI (207KPa). Both FERIC's and Weyerhaeuser's operational studies found that CTI trucks experienced large traction gains in slippery, muddy conditions. The study concludes that Significant benefits to the road, vehicle, driver and environment are all possible when tyre inflation pressures are set to match the hauling condition; defined by speed, load, terrain, and road surface strength. Low tyre pressures can be used on non-paved, low speed roads in order to minimise road and vehicle damage, maximize vehicle traction and mobility.

In order to match the tyre inflation pressures with changing haul conditions, commercially developed "Central Tyre Inflation" systems are available to allow the driver to change tyre pressures from inside the cab, or stationary "airing stations"

can be set up to manually alter tyre pressures. The construction sector needs automated systems to manage the tyre pressure based on the set parameters in order to optimise efficiency and reduce unnecessary costs.

2.6.10. Computer simulation as a tool for operator training, development and procurement

A computer simulation program called WinMaku was developed with the aim of offering a tool to facilitate development, procurement and operator training in ensuring that vehicles cope with all possible conditions in off-road mobility, Korlath (2007). The study highlights that the presented simulation tools serve as training tools for operators. It also serves as a cost effective method to assess possible development steps, allowing customers to run a pre-selection process prior to expensive and time consuming field tests. Finally it supports mission planning by providing data like expected fuel consumption or time needed to pass a certain mission profile.

Other factors considered by the simulator included tyre size, tyre type, engine power, torque characteristics, gear shifting, engine load, tyre inflation, slip, vehicle types, and gear selection, Korlath (2007). The conclusion however states that while WinMaku provides first indication of mobility performance of a vehicle in loose terrain without time consuming and expensive field tests, it is clear that the presented tool WinMaku could not predict off-road mobility performance of vehicles with a precision comparable to Finite Element Modelling. The simulation is based on the theories of Bekker and Wong which offers the possibility of obtaining the first estimate for off-road mobility.

It is evident that in-depth research and application of terramechanics has been used for various environmental and operational mitigation measures regarding sustainable forestry management. Such tested and experimentally validated software can provide great and useful data for construction plant operating in deformable ground. It is very clear that wheeled plant operating in off-road construction sites with deformable terrain can be better managed and planned with the availability of wheel-soil interaction predictive and management tools.

2.7. Terramechanics in the mining sector.

As stated in the introductory chapter, Thompson and Visser (2000) and Thompson, Visser and Heyns (2004), open cast mining haulage roads are subject to functional and operational design like a conventional road such as asphalt or concrete. The only time the sector has to deal with natural terrain roads is during construction of the haulage roads.

Compacted natural gravel, crushed stone and gravel mixtures have been widely used in strip coal mines for haul road construction, especially for base and wearing course layers. The functional design of a haul road is the process of selecting the most appropriate wearing course natural gravel or crushed stone and gravel mixtures that are commensurate with safety, operational, environmental and economic considerations, Thompson and Visser (2000). In surface mining operations a mine haul road network of 10–40km in length typically is gravel surfaced and comprises a number of road segments, each with variable traffic volumes and construction/material qualities. The design of these roads

encompasses structural, functional and maintenanace aspects as discussed by Thompson and Visser (2000), (Thompson, Visser and Heyns, (2004). This operational stage of mining haulage falls outside the subject of terramechanics because there is insignificant rutting due to the compacted surface and that this field of study is only applicable to wheels moving in natural deformable terrain as opposed to a structurally and functionally designed road such as tarmac, concrete and well compacted gravel.

2.7.1. Mine research and rescue robots

A study by Wang et al (2007) presents the design and building of a mine research and rescue robot with features designed to withstand rough and deformable terrain. Besides the comprehensive electrical and mechanical system of the robot, the operation in terms of trafficability is purely based on the principles of Terramechanics including some key concepts from Bekker and the Mohr-Coulomb formula. The robot was designed to use tracks to the wider contact are with the ground which delivers maximum drawbar-pull, Wang et al (2007). On a soil with significant cohesion, a notable portion of the thrust is derived from cohesion of the soil and is dependent on tyre contact area, hence contact length, whereas on a soil with a significant angle of internal shearing resistance, a major portion of the thrust is derived from friction and is independent of contact area.

2.7.1.1 Bulldozing

Bulldozing is the accumulation of soil mass in front of a mobile robot Wang et al (2007). If the robot runs in the soft terrain such as sand, soft soil or snow the resistance is caused by soil compaction, bulldozing and dragging. For most scenarios, the resistances originating from bulldozing, soil trapping and dragging

are neglected. So the robot's resistance is compaction resistance. Mining conditions that are similar to construction could be categorised together signifying that some of the outcomes from this research could also be directly beneficial to the mining sector. Figure 2.44 gives the three different conditions that mainly constitute the soil inertia and resistance pattern

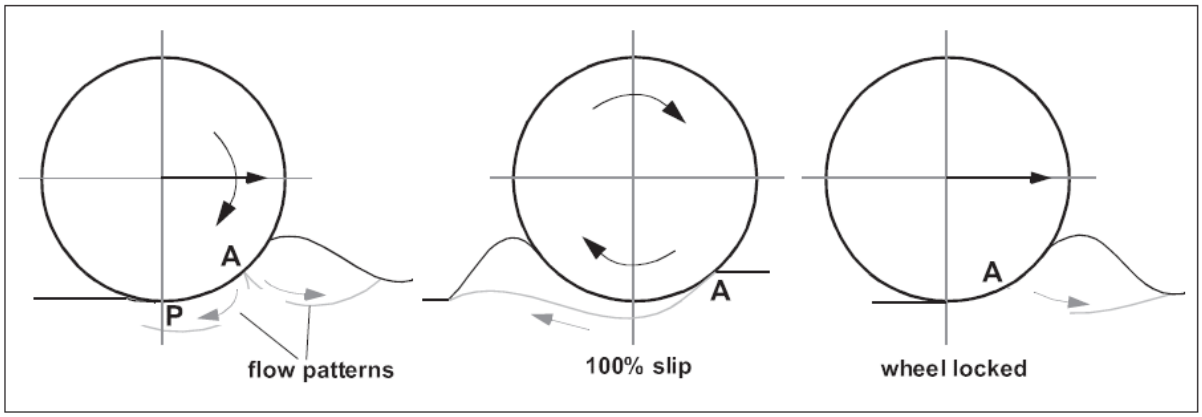

Figure 2.44: Soil flow at the wheel-soil interface during sustained driving (left), 100% slip (middle) and braking effect (right), Apostolopoulos (2001)

2.8. Extending terramechanics to the construction sector.

In a study aimed at establishing the traction efficiency of a wheeled tractor in construction operations an observation was made that, it is essential to determine directions and values of power flow through the wheels using sensors and instrumentation, Jerzy Zebrowski (2010). These in turn depend on the forces and moments applied to a given wheel as well as the type and condition of the ground under the wheel. Zebrowski's study concluded that the analysis of the flow of power through a wheel as well as the whole vehicle presented in this paper can serve as a basis for elaboration of algorithms to describe differential gear locks and front wheel drive in vehicles. Jerzy Zebrowski (2010). The study however did not link the results to the effect on project cost and time implications on ground condition variations during the construction period.

Janulevičius et al (2010) presents an interesting research focussing on the tractor engine load and fuel consumption on road construction works. The aim of this study was to analyse how well the Massey Ferguson MF 8480 tractor is adapted to the provided work and optimal engine speed as well as load and fuel consumption are chosen during the operational work of the tractor. Results indicate that the operational economy and productivity of the tractor is mostly evident when its engine power is utilised at least 80% and engine speed is as low as possible, Janulevičius et al (2010). The study concludes that more work needs to be done by Studying engine speeds and load modes using information collected in the integrated microprocessors which may reveal the operation quality of the tractor. Focus on different wet terrain could be a good extension of the study so that the effects of rutting, motion resistance and traction are also quantified and evaluated.

As indicated earlier in the introductory chapter, a mathematical model was developed to predict rut depth caused by moving wheels (Reid, 2000). The fundamental starting point and foundation for this model was the basic laws of Newtonian Mechanics particularly the Laws of Motion and the Conservation Work-Energy Principle. The model powered by a programme RUTSEV was based on a single rigid wheel just like many previous models before. (Sandu and Senatore, 2011) adds on to state and confirm that a fully inflated flexible tyre behaves like a rigid wheel when operating in soft soils. A rigid wheel can be considered a first approximation of a flexible tyre especially if the pressure distribution along the contact patch does not exceed the inflated carcass stiffness, Sandu and Senatore (2011).

This mathematical model was developed and validated to predict rut depth for a wide range of typical clay and sandy soils recorded in Reid (2000). Rut depth was seen to increase with increases in wheel self-weight, applied load, wheel slip and forward velocity. Rut depth was further seen to decrease with increases in wheel radius, wheel width, wheel skid. Increase in area between the wheel and the soil and lead to reductions in the rut depth produced, Reid (2000). For clay soils, rut depth decreases as the value of soil cohesion increases. For sandy soils, rut depth decreases with increasing angle of shearing resistance with negligible ruts formed when high angles of shearing resistance are in combination with slow moving wheels. The model is underpinned by equations 2.38 to 2.40 adopted as primary database from (Reid, 2000). The definition of symbols used in the equations can be found in appendix 25. The development of these equations can be found in appendix 26.

Slip/skid values are shown to have negligible effect for slow moving wheels. Increasing slip is shown to increase rut depth with higher velocities particularly on weak sand terrains leading to larger rates of increase. Skid was seen to decrease rut depth and for all velocities. Although the model provides an estimate for rut depth alone, it does not provide the full effect on the power available at the wheels.

$$d_n = d_{n-1} - \frac{f(d)}{f'(d)} \qquad \text{Eqn 2.38}$$

Where d_n is the rut depth.

$$f(d) = Ctd^2 - \frac{WVv^2d^2}{2gr^2(1-i)^2\arccos^2\left(\frac{r-d}{r}\right)} + 2C(2rd-d^2)^{0.5}d^2$$

$$+(W+L)\left(\frac{2}{\pi}-1\right)d+2(W+L)\left(\frac{(1-\sin\phi)}{(1+\sin\phi)}\right)\tan\phi.d$$

$$+\left(\frac{(W+L)\tan\phi\left(2rd-d^2\right)^{0.5}}{2r}\right)d \qquad \text{Eqn 2.39}$$

$$f'(d)=2Ctd-\left\{\frac{W\omega^2 d\left(\arccos\left(\frac{r-d}{r}\right)-\frac{d}{r\left(1-\left((r-d)/r\right)^2\right)^{0.5}}\right)}{g.\arccos^3\left(\frac{r-d}{r}\right)}\right\}$$

$$+4dc\left(2rd-d^2\right)^{0.5}+\frac{Cd^2(2r-2d)}{\left(2rd-d^2\right)^{0.5}}+\left(\frac{2}{\pi}-1\right)(W+L)$$

$$+\frac{(W+L)\tan\phi(2rd-d^2)^{0.5}}{2r}+\frac{(W+L)\tan\phi.d(2r-2d)}{4r(2rd-d^2)^{0.5}}$$

$$+2(W+L)\left(\frac{(1-\sin\phi)}{(1+\sin\phi)}\right)\tan\phi \qquad \text{Eqn 2.40}$$

While a range of rut depths under different soil conditions successfully produced, the POWERSEV power plant performance model was developed out of RUTSEV (the rut depth model) into a full performance model which has been verified using computational analysis and laboratory experiments presented in chapters 5, 6 and 7. Table 2.6 presents details of the idealised wheel used in RUTSEV

wheel self-weight, W	100N
applied load, L	5000N
wheel radius, r	0.8m
wheel width, t	0.3m
horizontal translational velocity, V_V	10m/s

Table 2.6: Parameters for the RUTSEV wheel model

The rut depth model has set the background for the wider aspects of vehicle mobility such as drawbar-pull, tractive effort, translational rolling resistance and all economic aspects associated with the construction site terrain and haul roads. Vehicle operation on unpaved surfaces is a field of interest in military, agriculture, construction, exploration, recreation and mining as critically observed by (Sandu and Senatore, 2011). These factors were considered in the development of the mathematical model to predict wheeled plant power loss presented in chapter 4.

2.9. Wheel Multi Pass Effect

Many studies have been carried out to determine the effect of wheel multi pass using mathematical modelling and Finite Element Analysis, (FEA). The most reliable approach for determining wheel multi pass is experimental because of the highly unpredictable behaviour of deformable terrain under repetitive loading (Sandu and Senatore 2011). Multi-pass effect has a strong impact on the evaluation of traction of off-road vehicles. Repetitive loading on deformable soils has shown that during the unloading and reloading process the pressure–sinkage relation can be approximated with a straight line.

The study by Sandu and Senatore (2011) demonstrates that the terrain changes its properties after each pass and the variations are a function of the slip. If the first wheel is towed (zero torque pass) the terrain properties vary mildly, while the passage of a slipping tyre produces stronger effects on the soil, Sandu and Senatore (2011). The greatest variation occurs between the first and second pass: successive runs have less impact on the behaviour of the terrain. Terrain density increases after each pass and, considering the obtained results and related work from Bekker also the cohesion of the material is considered to have increased, Sandu and Senatore (2011).

In a research carried out by Rashidi et al (2010) Laboratory tests were performed to verify the prediction of soil sinkage by multiple loadings using the FEM. A sandy-loam soil was chosen for characterising the agricultural soil. The sandy-loam soil was consisted of 33% sand, 45% silt and 22% clay.

Properties	Symbol	Unit	Amount
Modulus of elasticity	E	MPa	150
Poisson's ratio	●	-----	0.3
Cohesion	c	KPa	80
Angle of internal friction	●	deg	30

Table 2.7: Soil parameters used for Finite Element Analysis of the soil-rectangular plate system, Rashidi et al (2010)

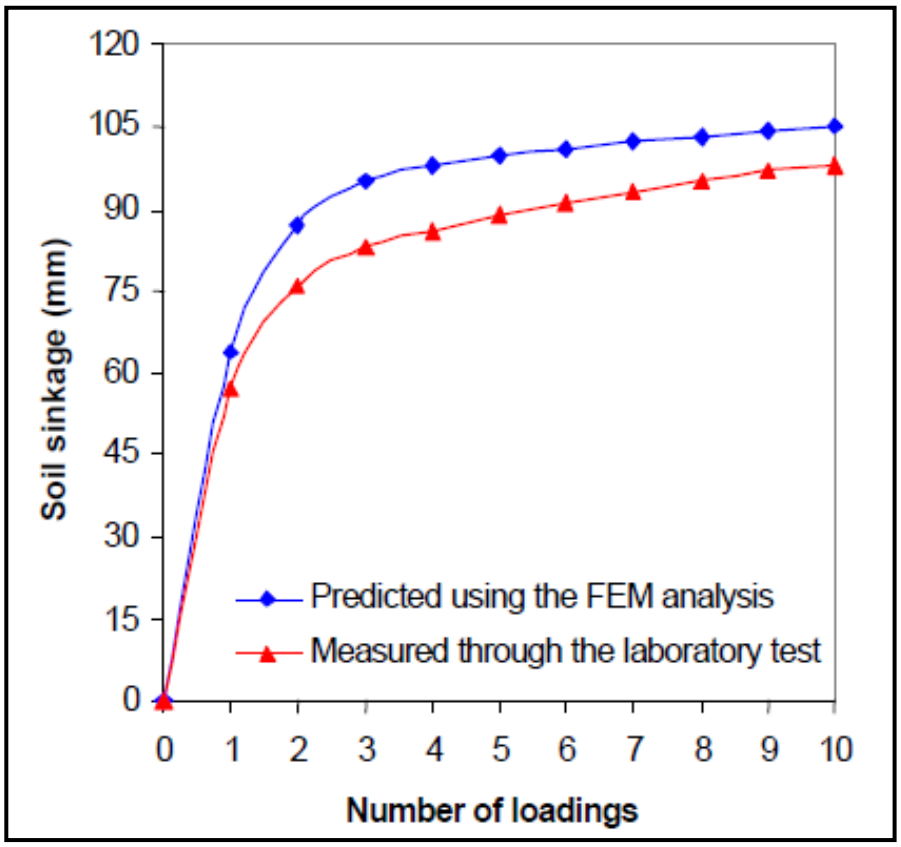

Figure 2.45: Soil sinkage values under the rectangular plate as related to number of loadings predicted using the FEM analysis compared with those measured through laboratory test, Rashidi et al (2010)

The FEM analysis was finally verified through laboratory tests. Results of the laboratory test proved that the FEM program called PRESSINK is a relatively accurate and powerful technique to predict soil sinkage by multiple loadings. Results of the study as shown in table 2.7 also indicate that the number of loadings noticeably affected soil sinkage. Moreover, figure 2.45 confirms that the first three loadings caused critical soil sinkage and the amount of soil sinkage owing to the first three loadings was about 89% and 82% of the total soil sinkage based on the FEM analysis and laboratory test results respectively, Rashidi et al (2010).

The Transport Research Laboratory had conducted research into this problem to determine that the overall plant efficiency is related to the depth of a rut after a single pass of the machine in the 1980's. Shallower ruts represent less damage while deeper ruts exceeding 100mm will represent severe damage to the terrain, Barnes (2010).

2.10. Tyre Manufacturers approach

The Tyre manufacturer Good Year provides useful guidelines regarding the size and usage of tyres in off-road conditions. According to the manual, tyres operating in soft soil or sand have lower inflation recommendation. Tyres operated on paved or hard gravel surfaces have higher inflation recommendation. The manual goes on to recommend the following speeds for haulage units as follows:

- Earthmoving, mining, logging, etc.: 30mph as maximum speed
- Dozer/Loader units, shovels, loaders: 5mph
- Road graders: 25mph

Appendices 19 and 20 show various recommended speeds in relation to tyre inflation pressure. It can be noted that high pressure tyres must move at slowest speed possible. The high inflation pressure can also be generally seen from the table.

A Goodyear Tyre and Rubber Company study showed that a 10 PSI (69 kPa) reduction in truck tyre pressure will cause a one percent loss in fuel economy on paved roads. On softer roads, this relationship is less well defined because rolling resistances are not always the lowest with high tyre pressures. Low pressure tyres penetrate into the soil less than high pressure tyres and therefore have less rolling resistance from the soil, Brown and Sessions (1999).

Although so much has been provided regarding off road tyre specification, what has not been done is to relate/link each average speed to specific group of terrain. Off-road conditions can vary from one condition to the other including dry, wet, rocky and organic surfaces. The mathematical model (POWERSEV) provided additional information and analysis to take into account engineering properties of the respective soil and the recommended vehicle and tyre settings in order to run the vehicles in the most economic mode possible.

2.11. Chapter Summary

Results from research publications as seen from the review of the many cases above strongly reveal that despite the complexity of terramechanics, tyre-soil studies in off-road terrain have delivered enormous benefits to many sectors through field/laboratory experiments, mathematical modelling and computer simulations. The construction industry however has experienced limited research in this study area particularly on construction sites characterised with typical off-road deformable terrain. The rut depth model related to construction is extended to address the far reaching effects of rut depth on the power loss through the further development of the mathematical model which is addressed in chapter 4. The following summarises the outcomes and conclusions drawn from the literature review presented in this chapter:

1. From the studies carried in the four major sectors discussed in this chapter, it is evident that the research results have improved the understanding of the tyre-soil interaction and its effects on wheeled equipment performance. This has

resulted in economic choices of both wheeled and tracked plant for respective soils at each time and circumstances.

2. The literature review indicates that there is a direct relationship between weight of the vehicle applied on the driving wheels and the traction effort of the vehicle operating in agriculture terrain. Similar studies on the construction sites and deformable haulage road activities would provide valuable results because of the dynamic nature of site plant movement.

3. The established relationship between soil resistance, wheel sinkage, traction effort, fuel consumption and tyre pressure in military, agriculture, forestry and planetary exploration studies provides a strong basis for detailed studies in Terramechanics on construction sites whose unique variables include plant movement patterns terrain, moisture content, variance in size of plant and plant weight.

4. The literature shows that Terramechanics studies on wheeled construction plant operating on construction sites and deformable roads would provide measurable effects of terrain on project completion and cost. The results would present an improved and reliable perspective of plant management in economic selection of plant with respect to the given ground conditions. This conclusion follows the evidence of adverse effects of rutting arising from heavy wheeled equipment operating in natural deformable terrain as seen from the cases reviewed in this chapter.

5. The literature also reveals that original mathematical models can be adopted and modified for the construction sector in developing new models for the construction projects related wheel-soil studies.

6. The outcome from extensive research in this area suggest that contractors and plant hire firms could model the plant output and hourly rates arising from wheel-tyre interaction once more detailed studies are done. With the combination of mathematical modelling and computational analysis, laboratory experiments, full scale field tests, different plant performance measurements and soil parameters can be modelled for use in forecasting, costing, planning, plant selection and soil behaviour on construction sites and deformable haulage roads. This will in the long run eliminate uncertainty in the pricing of earthworks related contracts.

7. The reviewed literature in this chapter clearly suggests that there is need to carry out full scale field tests in combination with laboratory tests as a way of model verification. The construction industry is no exception to this especially that significant work still need to be done in the area of terramechanics.

8. Full scale validation is expensive and requires contribution and cooperation of all key stakeholders.

9. This literature review has clearly revealed that applications of terramechanics are unique to each sector. This suggests that the construction sector needs to invest in laboratory and full scale of testing wheel-soil studies to obtain full benefits and data that is to be used for effective management of time and costs arising from wheeled equipment operating on wet and deformable terrain.

CHAPTER 3

RESEARCH DESIGN AND METHODS

3.0. CHAPTER 3

Research Design and Methods

3.1 Introduction.

This chapter discusses the plan and layout for implementing the research aim and its objectives. The chapter outlines the research design, its approach, the tools/methods and instruments used in delivering the results from the laid down objectives. The chapter further justifies the selection of modelling as the main research tool used in this study. The chapter begins by defining the key research design terms and outlining the underpinning research paradigms before narrowing down to the experimental and non-experimental modelling instruments that have been extensively used in this particular research.

A research paradigm is a perspective about research held by a community of researchers that are based on a set of shared assumptions, concepts, values, and practices. More simply, it is an approach to thinking about and doing research, Johnson and Christenden (2012). The chapter further presents various model verification options including the justification for using computational analysis and laboratory experiments as the main model verification processes. This research has adopted a 3-stage robust model verification process in order to increase the confidence levels of the research outcome.

3.2 Research Design

The online business dictionary defines research design as a detailed outline of how an investigation will take place. A research design will typically include how

data is to be collected, what instruments will be employed, how the instruments will be used and the intended means for analysing data collected, Rajasekar et al (2006).

The Association for Qualitative Research (AQR) defines research design as the essential parameters of a research project, including factors such as its basic approach (qualitative, quantitative or some combination). The work plan helps to outline the procedures to be followed throughout the research from inception to completion. The choice of research strategy drastically influences the specification of the research methods that are deployed for investigating a problem. It is this choice that also determines the research design, which is the framework for collecting, analysing and interpreting data, Dainty (2008). The research design and roadmap for this entire study is presented and summarised in figure 3.1.

3.3. Research methods

Research methods are the various procedures, schemes, algorithms and similar tools that are used in research. All the methods used by a researcher during a research study are termed as *research methods*. They are essentially planned, scientific and value-neutral. They include theoretical procedures, experimental studies, numerical schemes, statistical approaches among others.

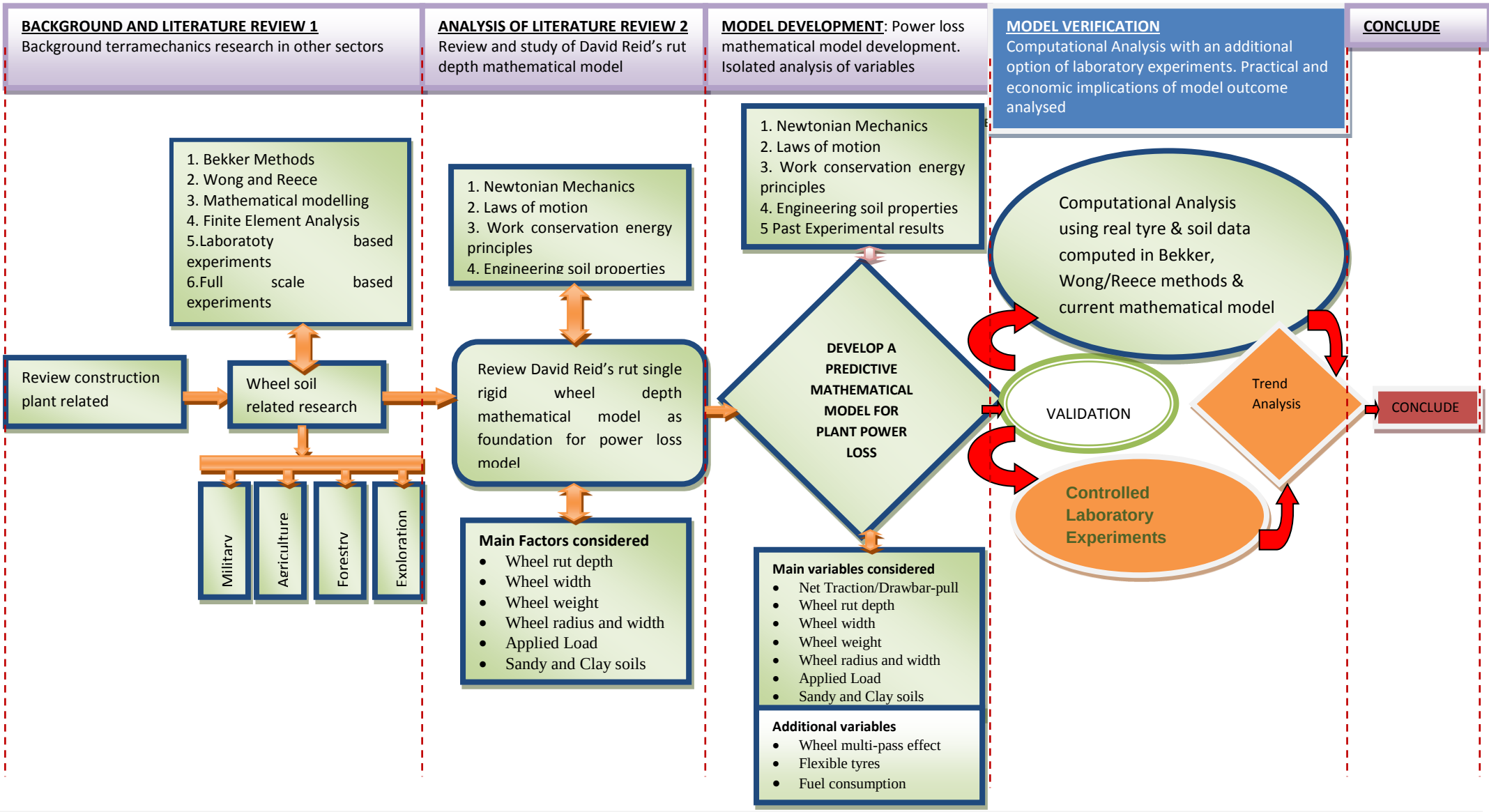

Figure 3.1: Research background, modelling methods and research design road map

Research methods are useful in the collection of samples, data and finding a solution to a problem. Particularly, scientific research methods call for explanations based on collected facts, measurements and observations and not on reasoning alone. They accept only those explanations which can be verified by experiments, Rajasekar et al (2006). The adopted quantitative methods in this research involve the measurement of soil and wheel parameters in order to establish the power losses measured in terms of drawbar-pull based on the wheels translational resistance.

3.4. Research Paradigms adopted for this research

3.4.1. Quantitative research

Quantitative model based research can be classified as a rational knowledge generation approach. It is based on the assumption that objective models can be built to explain part of the behaviour of real life operational processes or that can capture part of the decision making problems faced by managers and engineers in real life operational processes. In other types of quantitative research such as survey research, relationships are defined between the variables that are under study. Quantitative research is based on the measurement of quantities or amounts. The process in this case is expressed or described in terms of one or more quantities, Ellis and Levy (2009).

Quantitative research relies on the collection of quantitative data. Quantitative research often uses what might be called a “narrow-angle lens” because the focus is on ***only one or a few causal factors*** at the same time. In Quantitative research, the research attempt to hold constant the factors that are not being studied. *This is often accomplished under laboratory conditions* in which the

researcher randomly assigns participants to groups, manipulates only one factor, and then examines the outcome, Johnson and Christenden (2012). This is typical of the research data contained in this study as demonstrated in the mathematical modelling and experimental work in chapters 4, 5, 6 and 7.

Quantitative researchers attempt to operate under the assumption of objectivity. They assume that there is a reality to be observed and that rational observers who look at the same phenomenon will basically agree on its existence and its characteristics. They try to remain as neutral or value-free as they can attempting to avoid human bias whenever possible. *Quantitative research generally reduces measurement to numbers*, Johnson and Christenden (2012). Quantitative research has been adopted as the main research paradigm because of the generation of quantities based on solutions derived from various mathematical equations, computational analysis and measurable variables from laboratory experiments

The nature of this research involved the development of a model that would predict the loss of power for wheeled plant traversing in deformable ground. The primary data for this research was rooted in the rut depth mathematical model which automatically eliminates the qualitative research approach as the main method because the project suggests significant involvement of numerical values and measurements. The essence of having a model in place was to have a tool that could predict power loss as model output from the input of variables that can be varied to determine the effect on the power loss measured in form net traction or drawbar-pull. These variables include wheel rut depth, wheel diameter, wheel width, applied load, soil cohesion, internal shearing resistance or friction angle, net traction measured as drawbar-pull and motion resistance. *The quantitative*

*approach turned out to be the most appropriate for this research***.** Qualitative methods were only been applied at a smaller scale to support the case and its results.

3.4.2. Types of Quantitative Research branches applied in this study

3.4.2.1. Experimental Research

The purpose of experimental research is to determine cause-and-effect relationships. The experimental research method enables the researcher to identify causal relationships because it allows the researcher to observe, under controlled conditions, the effects of systematically changing one or more variables. Specifically, in *experimental research***,** the researcher takes control and *manipulates* the independent variable, actively intervening in the world, and then observes what happens. *Thus, manipulation, an intervention studied by an experimenter, is the key defining characteristic of experimental research*. The use of manipulation in studying cause-and-effect relationships is based on the activity *theory of causation* (Cook & Shadish, 1994), (Johnson and Christenden, 2012).

The essence of experimental research is to determine if a cause-effect relationship exists between one factor or set of factors: the independent variable(s) and a second factor or set of factors: the dependent variable(s) (Cook & Campbell, 1979). Experimental research seeks to determine if a specific treatment influences an outcome. The experimenter measures and compares the performance of the participants on the dependent variable to determine if changes in the independent variables are very likely to cause similar changes in performance on the dependent variable, Ellis and Levy (2009). In this research, the experimental part is represented by the running of MOBILITY SF-3713 under laboratory controlled

conditions using different configurations of soil, weight, speed, tyre pressure and power measured in drawbar-pull as net tractive effort. Details are discussed in chapter 6. MOBILITY SF-3713 is a mobility scooter that has been structurally and electronically modified to meet the requirements of the objectives of the study.

3.4.2.2. Correlational Research

The primary focus of the correlational type of research is to determine the presence and degree of a relationship between two factors. Although correlational studies are in a superficial way similar to causal-comparative research – both types of study focus on analysing quantitative data to determine if a relationship exists between two variables – the difference between the two cannot be ignored (Creswell, 2014). These designs have been elaborated into more complex relationships among variables found in techniques of structural equation modelling, hierarchical linear modelling and logistic regression. More recently quantitative strategies have included elaborate structural equation models that incorporate casual paths and the identification of the collective strength of multiple variables, Ellis and Levy (2009).

The correlational non-experiment quantitative method is represented by the developed mathematical model (POWERSEV) which is discussed in chapter 4 and the computational analysis model verification process in chapters 5 and 6. Both chapters involved equation based mathematical modelling. This approach is also a less expensive way of establishing relationship existence between soil, speed, tyre pressure and wheel traction. The approach also provides flexibility and unlimited

configuration of variables, however, simulation of wheeled plant require introduction of scaling factors.

3.5. Qualitative research adopted to support the research methods

Qualitative research is concerned with qualitative phenomenon involving quality. It is non-numerical and descriptive which *applies reasoning* and usage of words with the aim of getting the meaning, feeling and description of the situation, (Johnson and Christenden, 2012). Pure *qualitative research* relies on the collection of qualitative data (i.e. non-numerical data such as words and pictures), (Johnson and Christenden, 2012). This approach has not been adopted as the primary research paradigm because the research at hand is primarily driven by quantities and measurements. Some case studies (qualitative tools) discussed below in form of existing results on the similar subject have been used to support some quantitative results from the modelling and experimental procedures. Figures 3.2a and 3.2b provides a summarised but detailed distinction between quantitative and qualitative research methods

3.5.1. Case Study Research

A case study is “an empirical inquiry that investigates a contemporary phenomenon within its real life context using multiple sources of evidence” Noor (2008). The evidence used in a case study is typically qualitative in nature and it focuses on developing an in-depth rather than broad, generalised understanding. Case studies can be used to explore, describe, or explain phenomena by an exhaustive study within its natural setting, Ellis and Levy (2009). Case studies can therefore be used as useful complimentary tools in reinforcing quantitative approach method. Case studies in this research have also been used in the

literature review to build and support the background and justification of the case. This modelling construction plant performance research is not dependant on subjective individual opinions but on objective independent measurable data compilation and analysis through mathematical modelling, computational analysis and experimental analysis. Qualitative expert views have only been used in the determination of knowledge and usage in terramechanics application in the construction sector and not in the process of establishing the main research outputs.

3.6. Mixed Methods Research as the ultimate approach for the research

Mixed research involves the mixing of quantitative and qualitative research methods, approaches, or other paradigm characteristics. The exact combination that is considered appropriate depends on the research questions and the situational/practical issues facing a researcher. Although there are many designs that exist for in mixed methods, this chapter considers the explanatory sequential mixed methods as the most appropriate method because its primary or main paradigm is quantitative method supported by qualitative method as secondary or supportive paradigm as discussed below in 3.5.1. A mixed method approach of more than one quantitative method provides an opportunity to validate the results especially when a non-experimental model is used as the primary model. Field experiments, laboratory experiments, surveys, mathematical modelling, computer modelling/simulation, algorithms are all tools available in the quantitative research methodology route.

3.6.1. Explanatory sequential mixed methods

In this approach, quantitative research results are analysed after which the results are explained further with qualitative research. It considered being explanatory because the initial quantitative results are explained further with the qualitative data. This type of research design is popular in fields with a strong quantitative orientation. Unequal sizes of samples in both stages can present a problem when it comes to evaluating the final conclusion, (Creswell 2014). This is the approach that has been adopted in this research. Modelling and experiments have been used to process and analyse the main results while interviews and observations have only been used to support the knowledge gap and main results outcome.

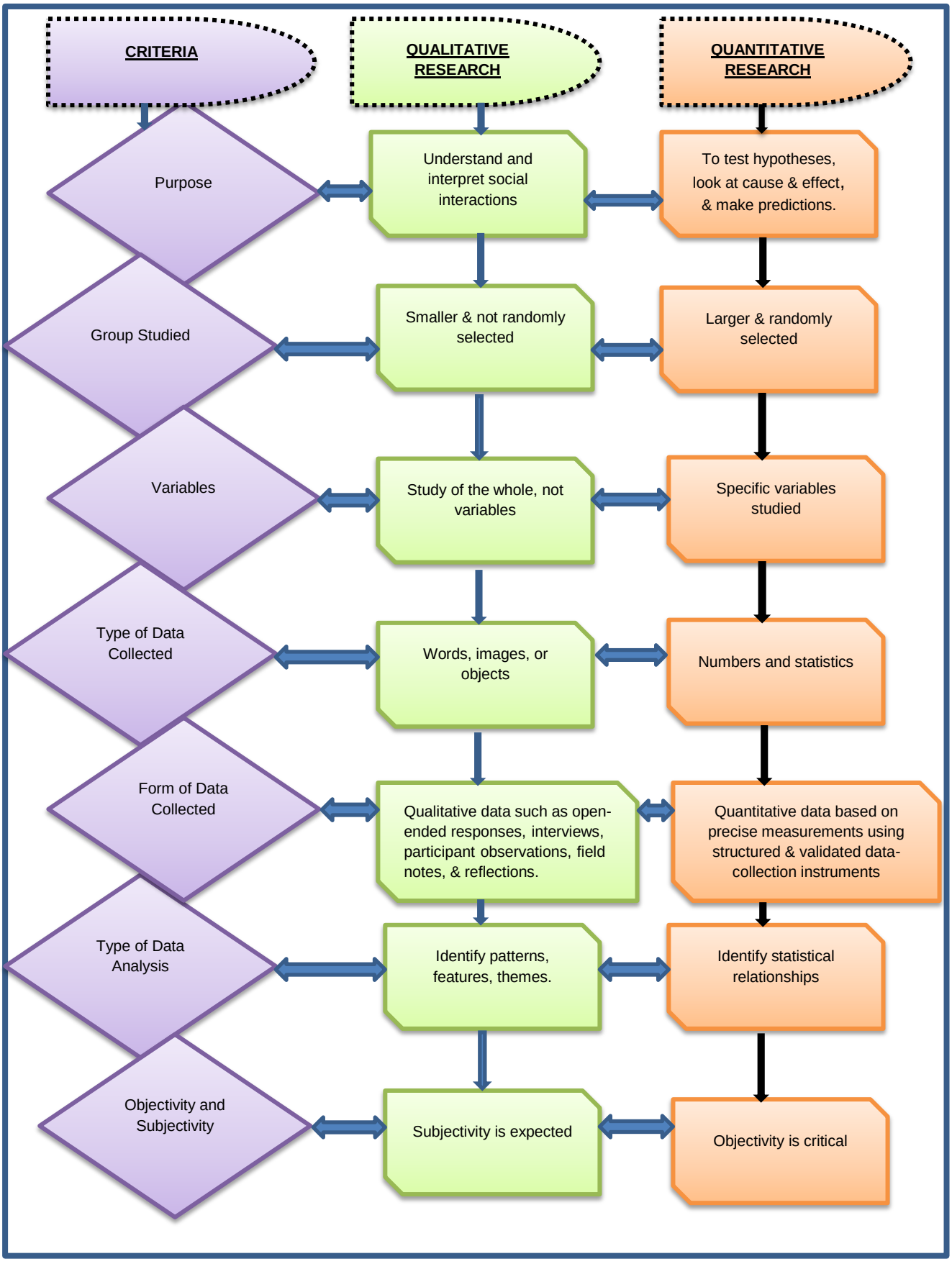

Figure 3.2a Qualitative methods versus quantitative research methods, adapted from (Johnson and Christenden, 2012)

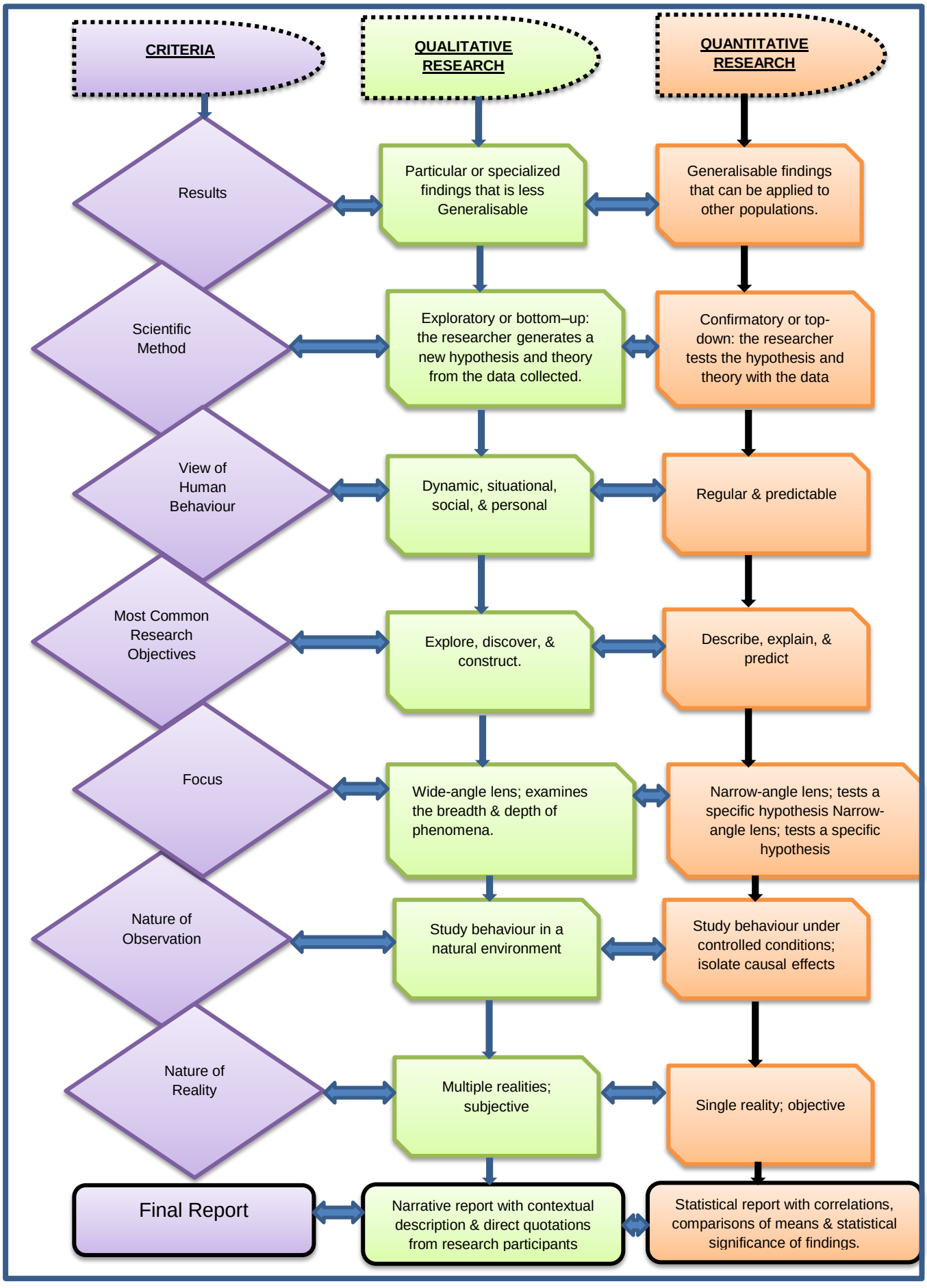

Figure 3.2b Qualitative methods versus quantitative research methods continued, adapted from (Johnson and Christenden, 2012)

3.7. Selection of appropriate quantitative tool and instruments for the research.

3.7.1. Modelling

The principles of modelling involve several categories of systems representation for a functional system or phenomenon in particular mathematical and physical (e.g. scale modelling) prototypes. In Jordan and Lategan, (2010), modelling is also referred to as simulation where it describes the representation of an actual situation by a mathematical model or alternatively by laboratory apparatus in the case of a physical model. The term modelling is also used to describe the practice of functionally dividing an operational unit into a number of different sub units, the operational parameters of each of which can be defined as an element of the whole unit, Jordan and Lategan (2010). Mathematical modelling has been used for the main model development with details explained in 3.7.1.1. Physical modelling on the other hand has been used in the form of laboratory experiments under stage three of the robust model verification process.

3.7.1.1. Mathematical modelling and solutions

Mathematical modelling is the process of describing the behaviour of an element of a physical system, or a comprehensive system or phenomenon by means of a mathematical expression, definition and quantification of the interrelationship of those variables with a substantial effect on the functioning of the system to be modelled, Jordan and Lategan (2010). The expected behaviour of the system under consideration can be predicted by means of mathematical modelling, whilst the accuracy of the predictions is a function of the correctness of the mathematical formulae used to describe the system, as well as that of the boundary conditions and the initial conditions in the case of unsteady or time dependant phenomena.

According to Gerda (2001), mathematical modelling is the use of mathematics to describe real-world phenomena, investigate important questions about the observed world, explain real-world phenomena, test ideas and make predictions about the real world as illustrated in figure 3.3. Instead of undertaking expensive experiments in the real work, a modeller undertakes experiments on mathematical representations of the real world at a significantly reduced cost. From the equations that describe the problem, a mathematical solution can be derived in the form of another mathematical equation (e.g. equation of motion as the solution to the differential equation or as an algorithm such as simplex algorithm or linear programming, Jordan and Lategan (2010).

A mathematical system is a mathematical structure (e.g. set of equations or relations) than can be used as a mathematical model for a class of system. From a mathematical system very general results can be obtained e.g. on the stability of the system that will be valid for all kinds of models and systems for which this mathematical system is a valid model, (Jordan and Lategan, 2010). It is clear that mathematical modelling is an extremely useful tool that can be used in a very wide variety of applications and is only limited by the mathematical abilities

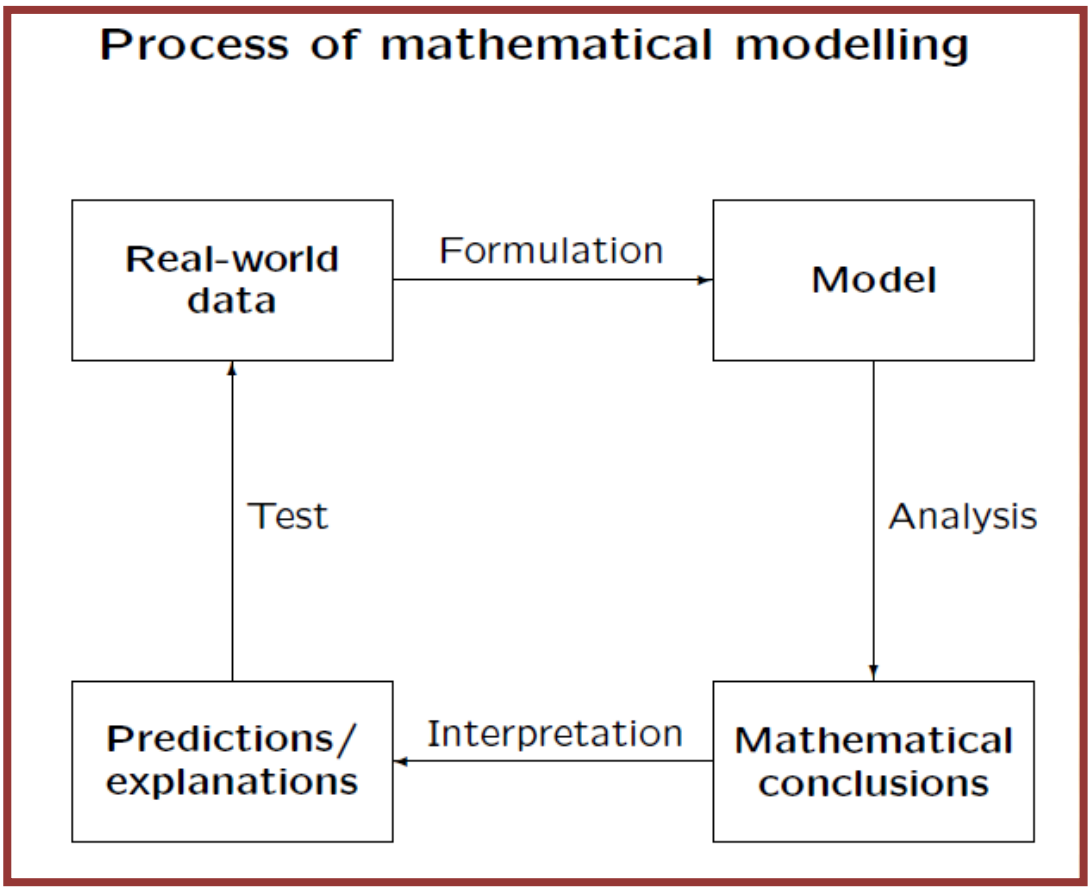

Figure 3.3: Generic process of mathematical modelling, Gerda (2001)

and understanding of the modeller. Mathematical simulations are often executed using standard mathematical software such as Matlab, MathCAD, Mathematica or Maple. Alternatively application specific software can be used for this purpose, (Jordan and Lategan, 2010). With the foundation of this research rooted in modelling and mathematics first principles, mathematical modelling was identified as the most suitable primary model to predict the power loss of plant wheel traversing in deformable ground. The individual elements of a mathematical model are capable of isolated analysis allowing the user to identify and assess their separate contribution and effects on rut depth development and its subsequent effects, (Reid, 2000). This provides an insight into the relative effects of each of the variables and how they interact, leading to a deeper understanding of the underlying principles involved.

3.7.1.2. Physical Modelling (Laboratory Experiments)

Although physical modelling is used predominantly in engineering applications, it can also be used for the execution of controlled experiments in other natural science disciplines. To some extent mathematical modelling has superseded scale modelling and facilitated a shorter reaction time in terms of possible changes in the design of a modelled system. However the use of physical modelling is still very much the order of the day particularly in terms of modelling of hydrodynamic and geographical phenomena. It is still popular in the verification of mathematical modelling outcomes. In these cases there is often no analytical solution available and scale modelling is the only viable method to accurately investigate the characteristics of the prototype, (Jordan and Lategan, 2010).

A physical model typically consists of a scaled down in some cases scaled up version of the complete system or specific portions thereof. Often the system is simplified by limiting the accuracy to which some non-critical elements of the system are modelled. However a thorough understanding of the underlying functional principles of the system is required to ensure the safe identification of non-critical variables, Jordan and Lategan (2010). Experiments, which mainly constitute physical modelling, are however very useful when it comes to verification or validation of non-experimental approaches such as Causal comparative and Correlational design.

3.7.1.3. Advantages of modelling

According to Jordan and Lategan, (2010), the ever increasing use of mathematical and physical modelling techniques is enough proof of the immense value of these practices for modern day researchers, practising engineers and technologists. The

following are examples indicative of the advantages that normally flow from modelling and simulation in research activities.

- The resultant ease of performing controlled pseudo-experiments.
- The determination of the anticipated effect of any change in the operating conditions that will influence the functioning of the eventual man-made system or otherwise.
- Time compression in the sense that a simulated experiment can take a small fraction of time to an actual system under test.
- Sensitivity analysis for observation of the behaviour limits of a system.
- Experimentation without requiring the financial outlay for the real system

Usually modelling is an effective training tool, according to (Jordan and Lategan, 2010). Figure 3.4 gives an illustration of incorporating specific research instruments in the physical and mathematical modelling part of the research process.

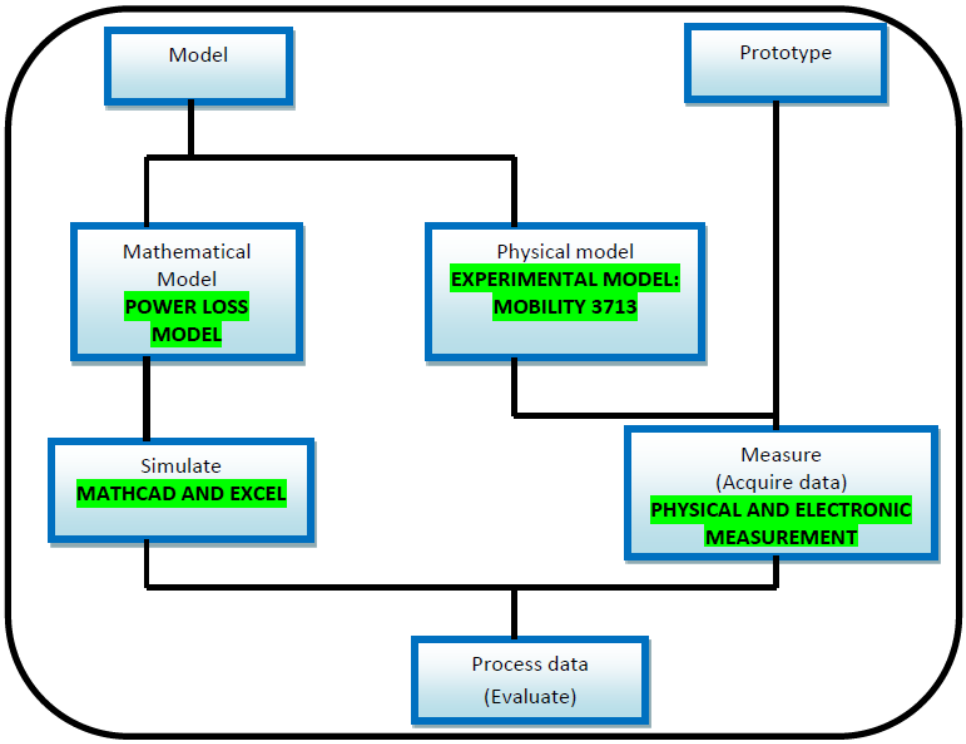

Figure 3.4: Modelling flow chart, adapted from Jordan and Lategan (2010)

3.8. Mathematical model development

The mathematical model builds its equations from mathematics first principles. It then deploys the principle of motion equilibrium to determine the power loss based on applied numerical integration. The model is based on a 1.8m diameter and 300mm wide rigid wheel moving in an imaginary straight line. Figure 3.5 is a generic flow chart summarising the route path for mathematical model with the corresponding stage application to the research. Figure 3.6 shows flow chart for the actual mathematical development based on the 1.8m diameter rigid wheel.

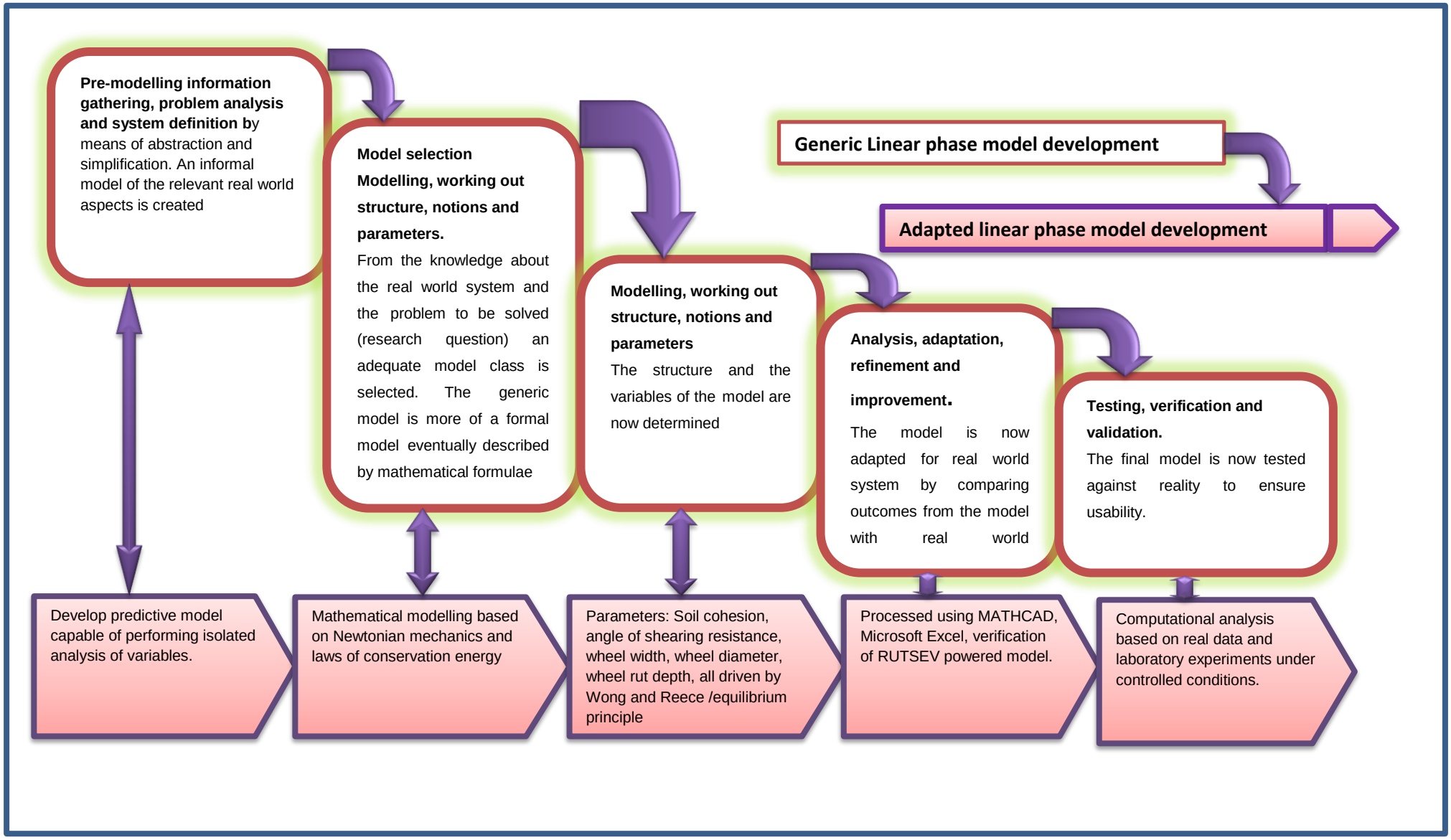

Figure 3.5: Mathematical model linear phase model, adapted from Jordan and Lategan (2010)

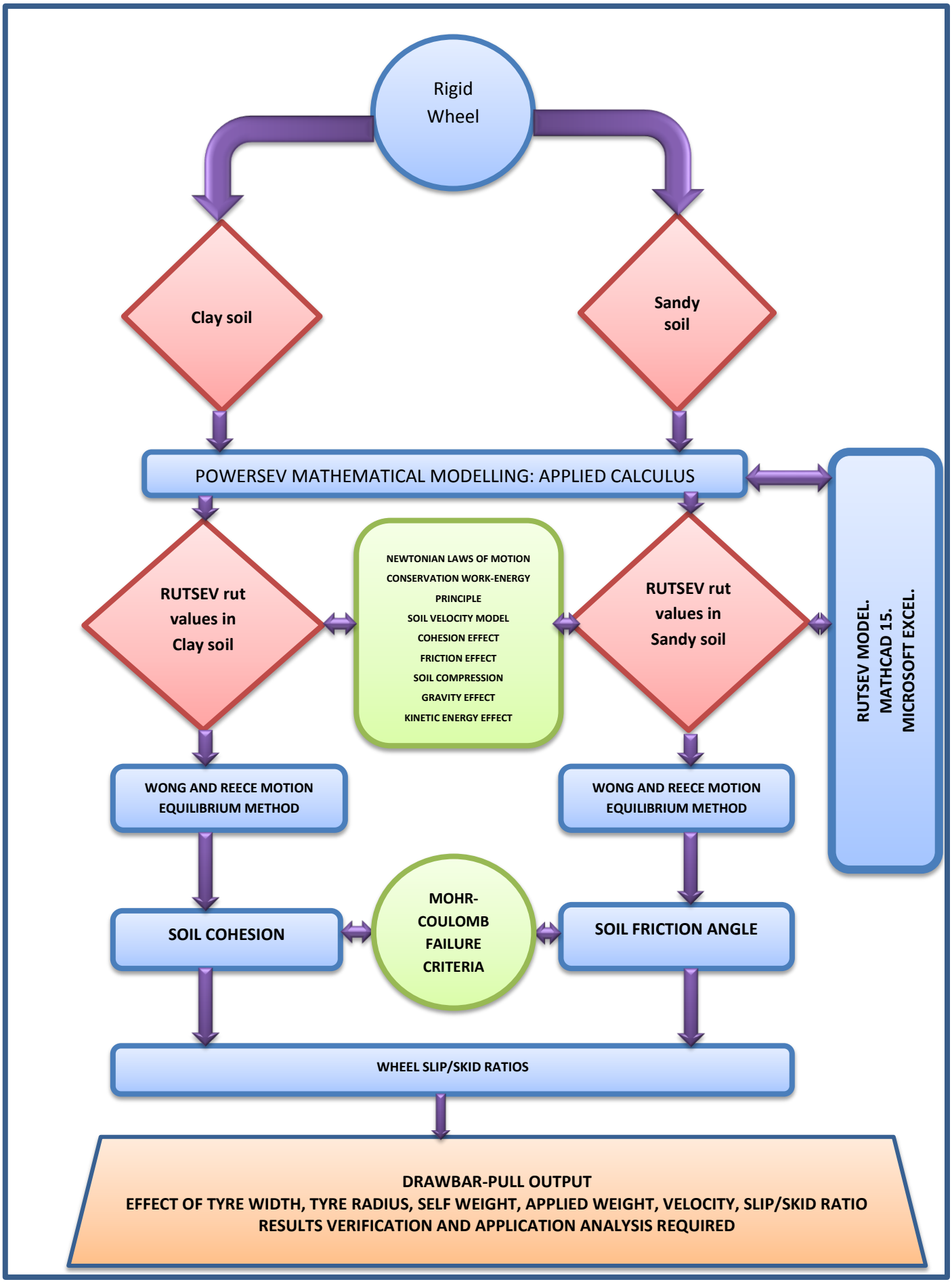

Figure 3.6: Mathematical model development design based on the rigid wheel

3.9. Model Verification

Model Verification is the process of determining that a model implementation accurately represents the developer's conceptual description of the model and the solution to the model, Ben et al (2004). Validation assessment is the process of determining the degree to which a model is an accurate representation of the real world from the perspective of the intended uses of the model. The goal of validation is to quantify confidence in the predictive capability of the model by comparison with experimental data, Ben et al (2004). Figure 3.7 illustrates a detailed model development, verification and validation process.

Figure 3.8 is an adopted structure of the model validation from Walker (2010). This model validation clearly illustrates the importance and options of validation available. A combination of all or any of the two routes in the given validation process provides important and reliable validation of the results. Experiments, mathematical modelling and computer simulations have been used either isolated or in combination in many scientific investigations and research.

3.9.1. Adopted model verification route and analysis

Model verification forms part of the key section of the research. From the traffic light system in figure 3.9 the model verification route is discussed and justified. The traffic light system is presented to illustrate, discuss and justify the model verification route adopted based on the detailed analysis of the available terramechanics quantitative methods. The individual options for model verification are all based on figure 3.9 and are discussed from 3.9.1.1 to 3.9.1.5.

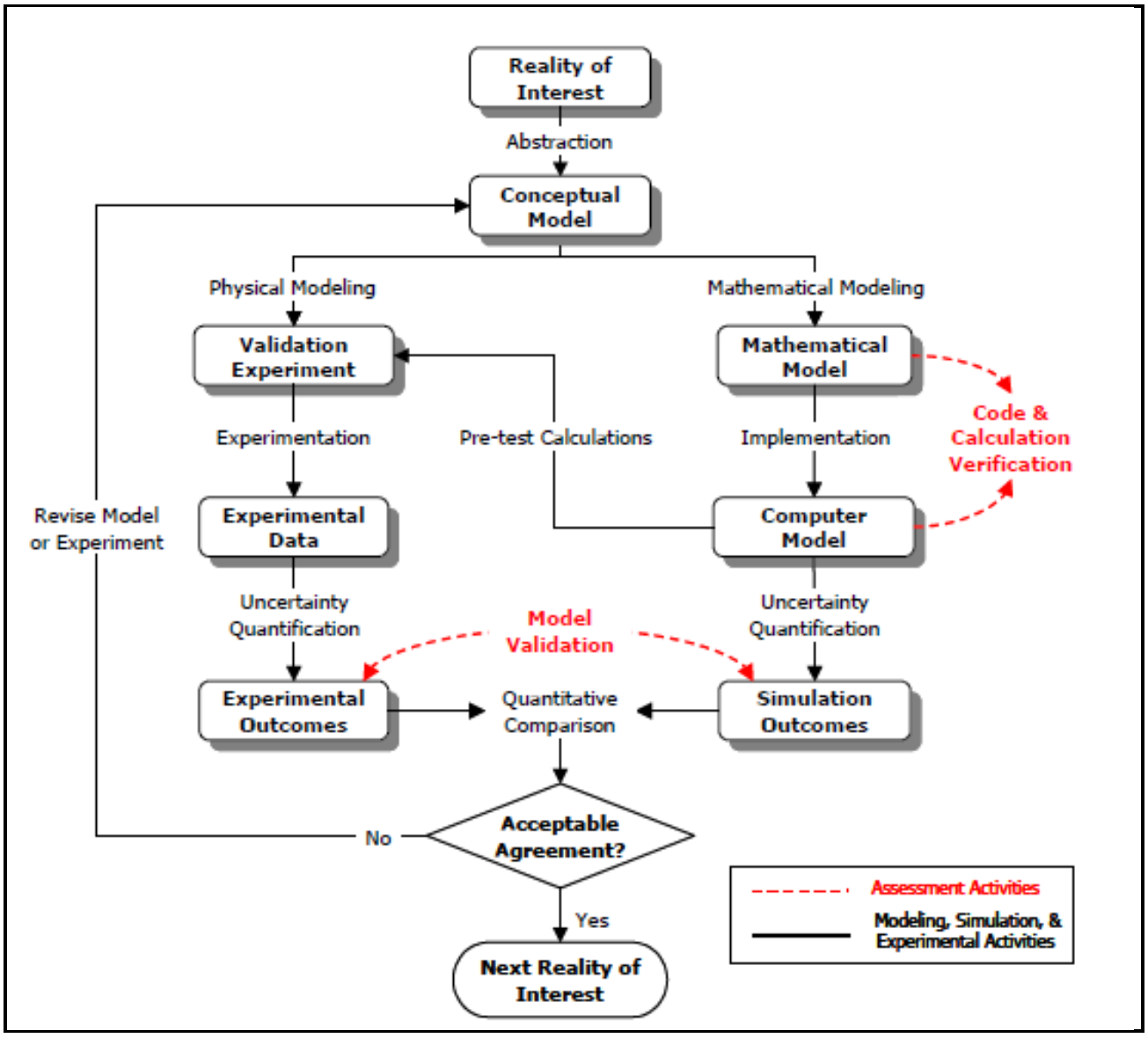

Figure 3.7: Detailed model development, verification and validation process, Ben et al (2004).

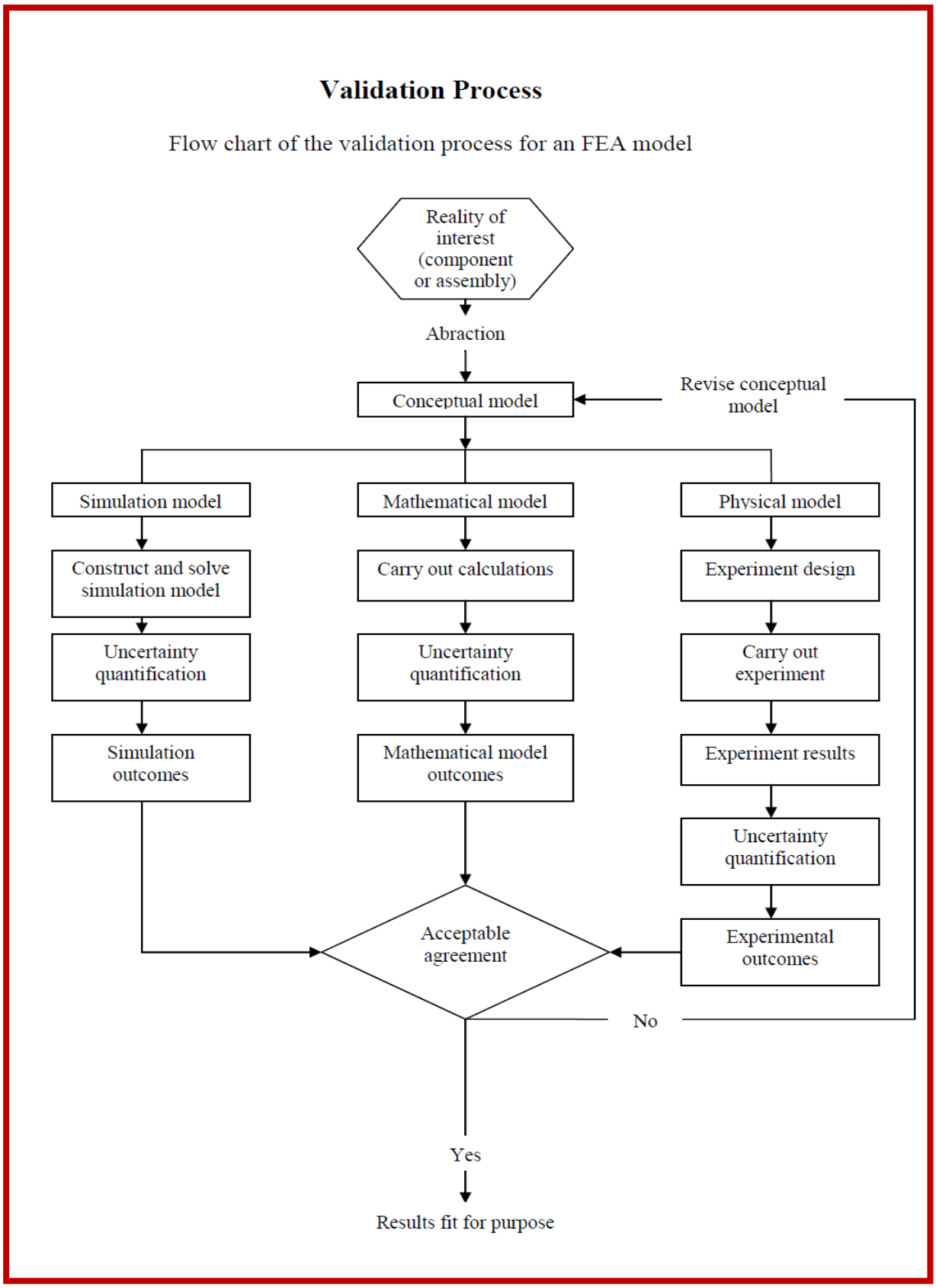

Figure 3.8: Typical model validation process (Walker, 2010)

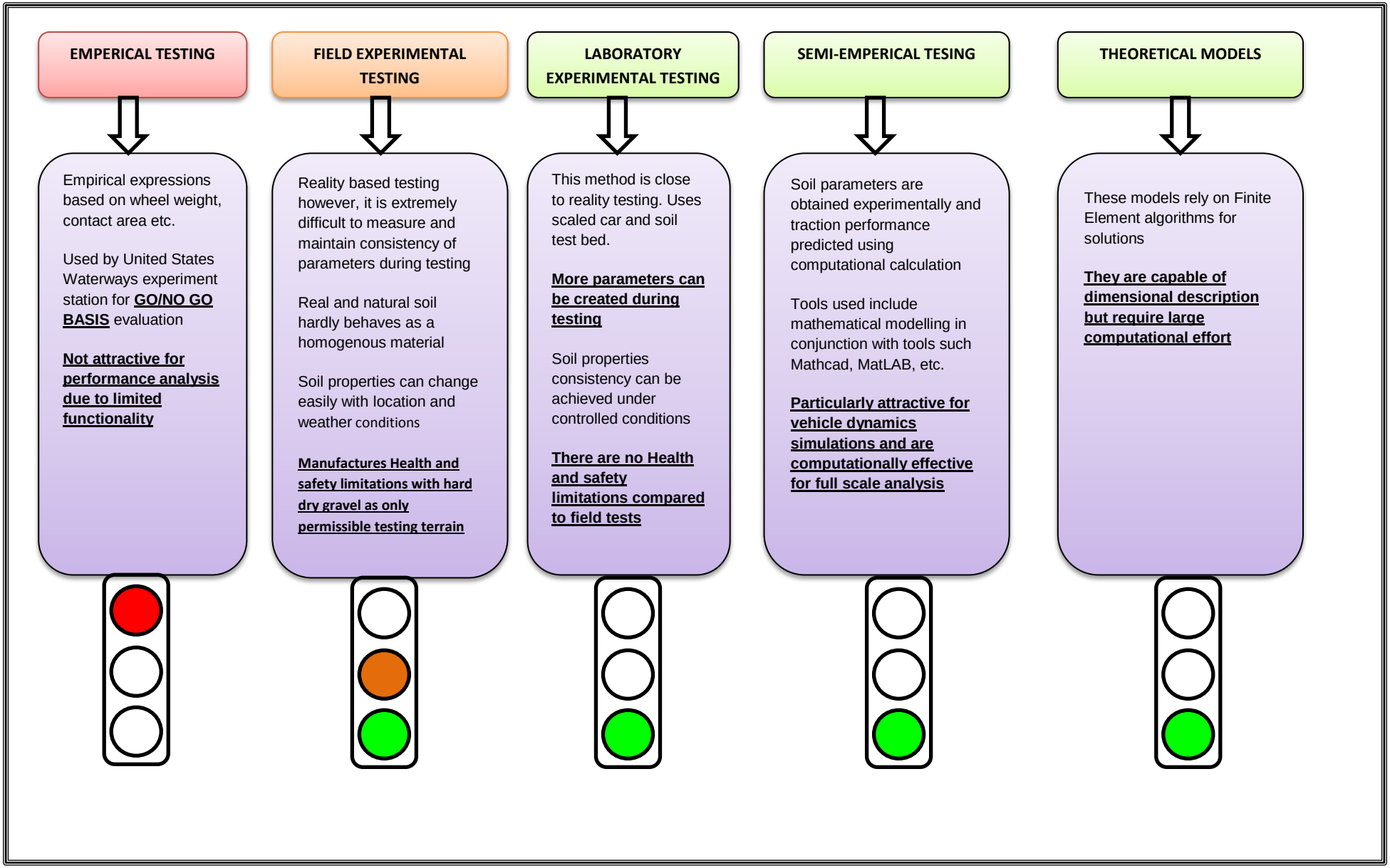

Figure 3.9: Research model verification, identification and analysis

3.9.1.1. Empirical testing

Empirical expressions are based on wheel weight, contact area etc. They were used in military combat missions to determine if wheeled and tracked armoured cars and tanks could safely be allowed to drive through particular terrain at each given time. They were first used by the United States Waterways Experiment Station (WES) for *GO/NO GO BASIS* evaluation as discussed in the literature review section in chapter 2. This approach is not attractive for performance analysis due to limited functionality and therefore it cannot be used for model verification in this study. The go or no go basis is not adequate enough to take into account additional factors such as performance of mobility in various soil and driving conditions. This method could therefore not be used for model verification in this research due to its limitations as illustrated in figure 3.9.

3.9.1.2. Field experimental testing

Live field experiments provide real time based testing however, as observed in chapter 2 of the literature review, it is extremely difficult to measure and maintain consistency of parameters during testing because natural soil hardly behaves as a homogenous material. Soil properties can easily change with location and weather conditions. The live field tests also present very limited configurations at a given time location and time. These configurations include soil type, soil properties, tyre diameter and tyre width. Normally there is only one set of configuration that can be obtained at each given time. Resetting the parameters is also difficulty and expensive.

The above description does not make the live experiments to be attractive practically and economically applicable as the main model verification at this stage. This approach was dropped from the verification list and therefore it was not used for mathematical model verification as illustrated in figure 3.9. In addition wheeled plant manufactures' Health and Safety regulations currently do not allow plant to be tested on deformable or wet ground except on hard gravel. This condition makes the option unsuitable because one of the main variables and key interest in this research is wheel sinkage and the subsequent power loss in deformable and wet terrain.

The wheel sinkage associated with testing cannot be attained on hard gravel terrain which is the only permissible and approved testing terrain for the manufacturing companies testing sites. Contractors on the other hand have tight deadlines and Heath/Safety policy that severely limit the experiments. Funding is required to secure purpose acquired sites to run such experiments in partnerships with contractors and plant manufacturers as seen in some military experiments in 2.3.3 of chapter 2. These results can be used to build advanced and more accurate purpose driven models for the construction industry which would also further provide additional validation and refinement of model results.

3.9.1.3. Laboratory experimental testing

Like the live field experiments, the laboratory tests provide an opportunity to verify the non-experimental model results. The advantage of laboratory experiments over the live field experiments is that many configurations can be attained by

changing the soil types and vehicular parameters. Other advantages of the laboratory experimental testing are listed below:

- This method was close to reality testing by using a scaled up or scaled down car and soil test bed.
- More parameters for the soil and scaled car can be created during the testing procedures.
- Acceptable levels of material consistency can be achieved under controlled conditions
- There are no Health and safety limitations compared to the live field test approach.
- The scaled down MOBILITY SF-3713 model was deployed in this research to provide reality range results which are consistent with the theory and principles of terramechanics. It also provides far reaching insights regarding the response to construction related operations.
- It must be emphasised that laboratory experimental results still require further validation through live site experiments.

This method has been selected as the secondary verification method due to the practical nature of the experiment and the high confidence levels that it constitutes. Laboratory experiments on the other hand have a tendency to reduce the correlation significance compared to live experiments although they present a better configuration arrangement compared to site experiments. Scaled and correction factors may have to be deployed when analysing data for live projects due to the difference in the value of plant and working figures. Figure 3.10 shows the laboratory experimental design.

The combination of non-experimental and experimental verification provides a well balanced approach of verifying the mathematical model. The strength of the laboratory experiment lies in the fact that while many laboratory models reviewed

in the literature were based on a single wheel laboratory model guided by a rail in a straight line, as seen in figures 2.30 and 2.31. This machine was run under free environment conditions that are close to live experiments. There are some exceptions like by NASA's laboratory rover as shown in figure 2.33 of the literature review chapter 2 under planetary exploration sub heading 2.5.4 which were ran free of guiding rails. The laboratory machine MOBILIY SF-3713 provided the opportunity to measure the effect of wheel multi pass. The pneumatic tyres also provided an opportunity to evaluate the effect of variable tyre pressures on rut depth and wheel power loss in different soil types. This made it suitable to verify the primary verification model which was based on the flexible tyre behaving as a rigid wheel when it exceeds a particular level of inflation pressure. The machine was designed to run on the following settings:

- Various speeds.
- Fully inflated and partially inflated flexible tyres measured in PSI.
- Run on different terrains namely: pavement as reference terrain, clay test bed and sandy test bed.
- Various applied loads
- The main outputs are rutting measured in millimetres, contact patch and drawbar-pull measured with load cell dynamometer. These outputs are recorded for analysis in relation to mathematical model results presented in chapter 4.

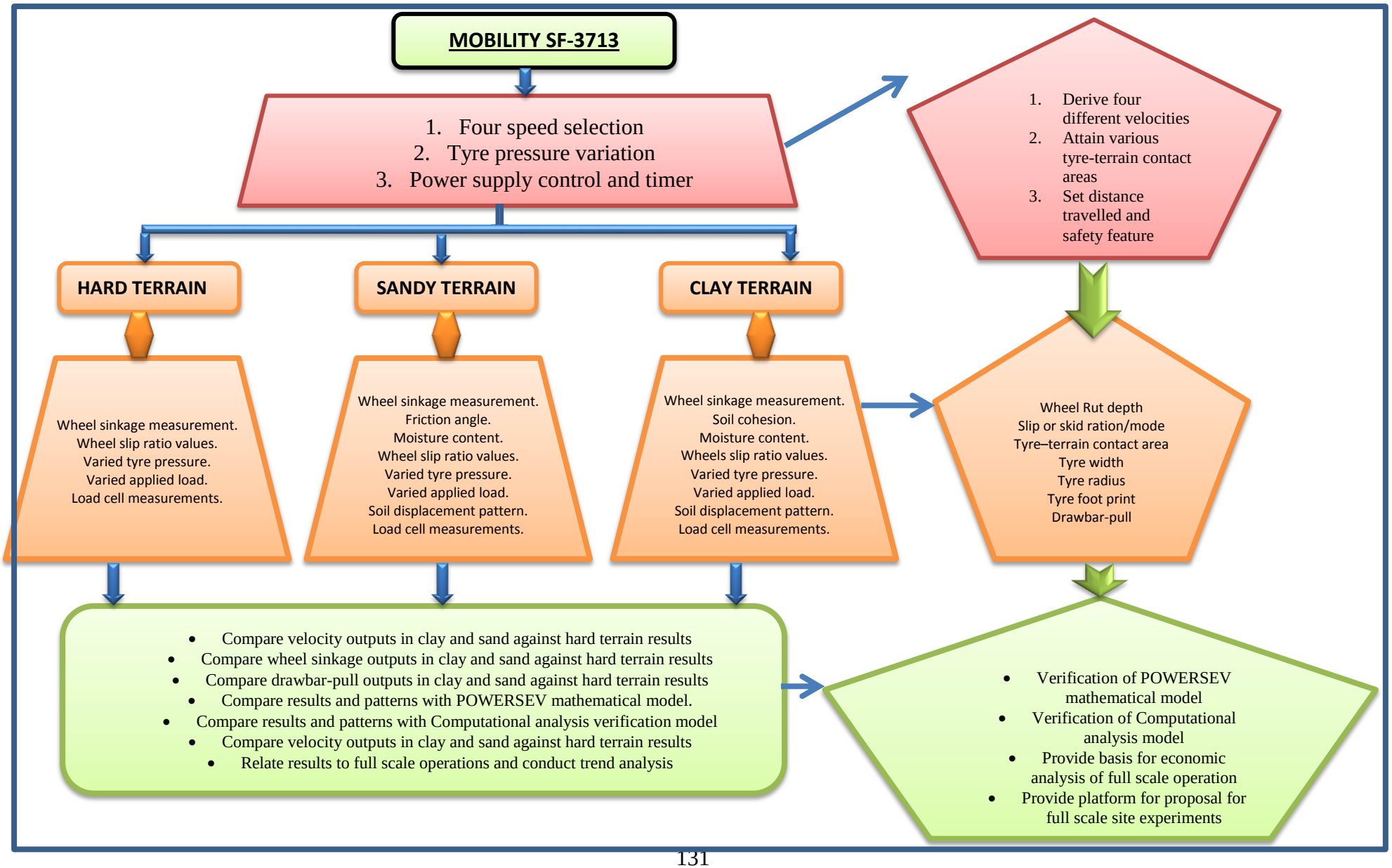

Figure 3.10: Laboratory experiment design

3.9.1.4. Semi-empirical testing

In semi-empirical testing soil parameters are obtained experimentally with values being computed to predict traction performance using computational calculations. Systems that are used in computation calculations include mathematical modelling in conjunction with tools such Mathcad, MatLAB and other similar software. This option is particularly attractive for vehicle dynamics simulations and is computationally effective for full scale analysis. This approach has been used as the primary model verification route because of the unlimited configurations available. The non-experimental quantitative approach therefore provides the opportunity to run, model or simulate live conditions in unlimited configurations. The model verification data is obtained from the 1m diameter flexible wheel operating in deformable ground obtained from the Canadian Defence Department as recorded by (Wong, 2010). Details and outcomes of this application are discussed in chapter 5 and 6. The computational analysis process and verification method is presented in figure 3.9.

3.9.1.5. Theoretical models

Theoretical models rely on Finite Element algorithms for solutions. They are capable of dimensional description but require large computational effort. Research shows that Finite Element Modelling produces more accurate results and has the ability to capture non-linearity and the complexity of the changeable ground conditions. This method requires specialised training and engaging the software developer through what is called focus groups. Physical verification is still required to validate the model results through field experiments or laboratory work. Computer simulations mainly rely on the black box approach denying the modeller to understand the basic operations embedded in the software.

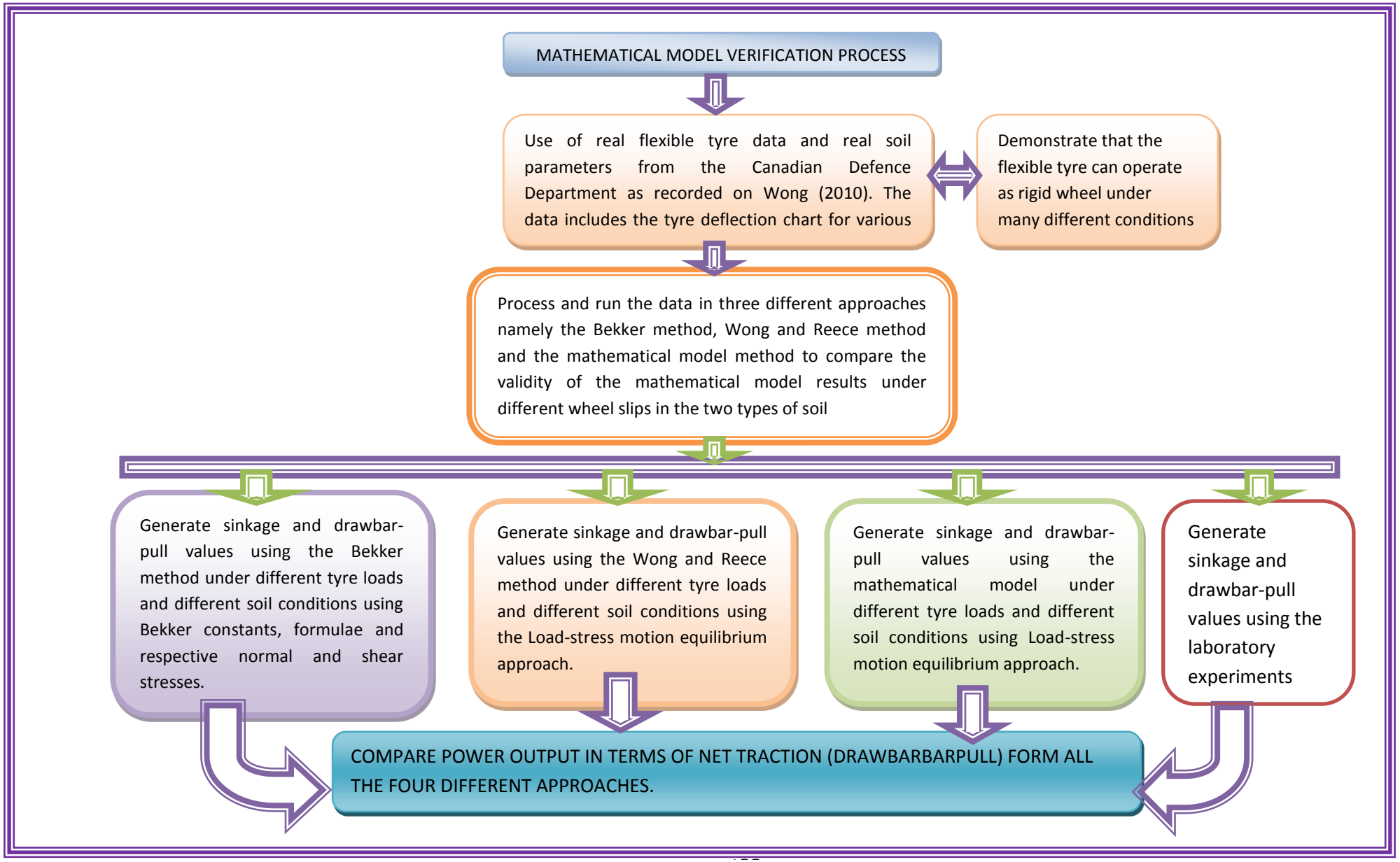

Figure 3.11: Semi-empirical computational analysis verification method

3.10. Variable trend and comparative analysis

The results from the mathematical model have been linked to the operational and cost implications of construction projects that involve significant usage of wheeled construction plant including road haul works. This involved some qualitative analysis where existing results of plant performance trends were be linked to the rut depth and power loss results. The effects of the results and how they influence the pricing of works resulting in tender evaluation have been discussed. The cumulative sinkage and associated power loss were also linked to the effect of construction planning and programming in terms of time and resource allocation.

This also includes parameters such most economic tyre diameter and width for a particular terrain and load. A major comparative analysis was done between the model results and the experimental outcomes. Details of this discussion are contained in chapter 8 where all the results were compared, discussed and linked to the variable trend effect on construction projects that utilise wheeled plant in deformable terrain.

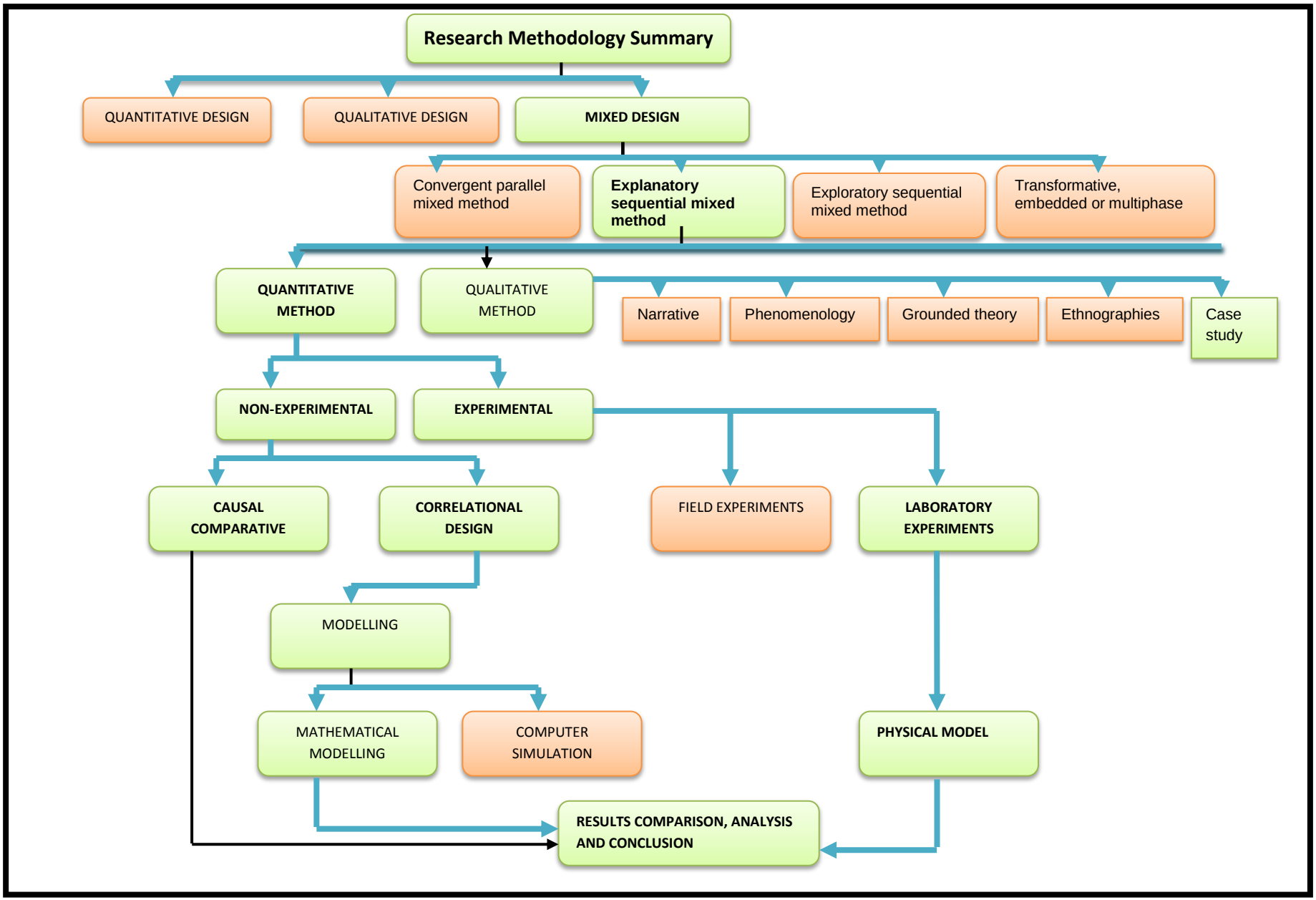

Figure 3.12: Summary of Research Methodology including model verification

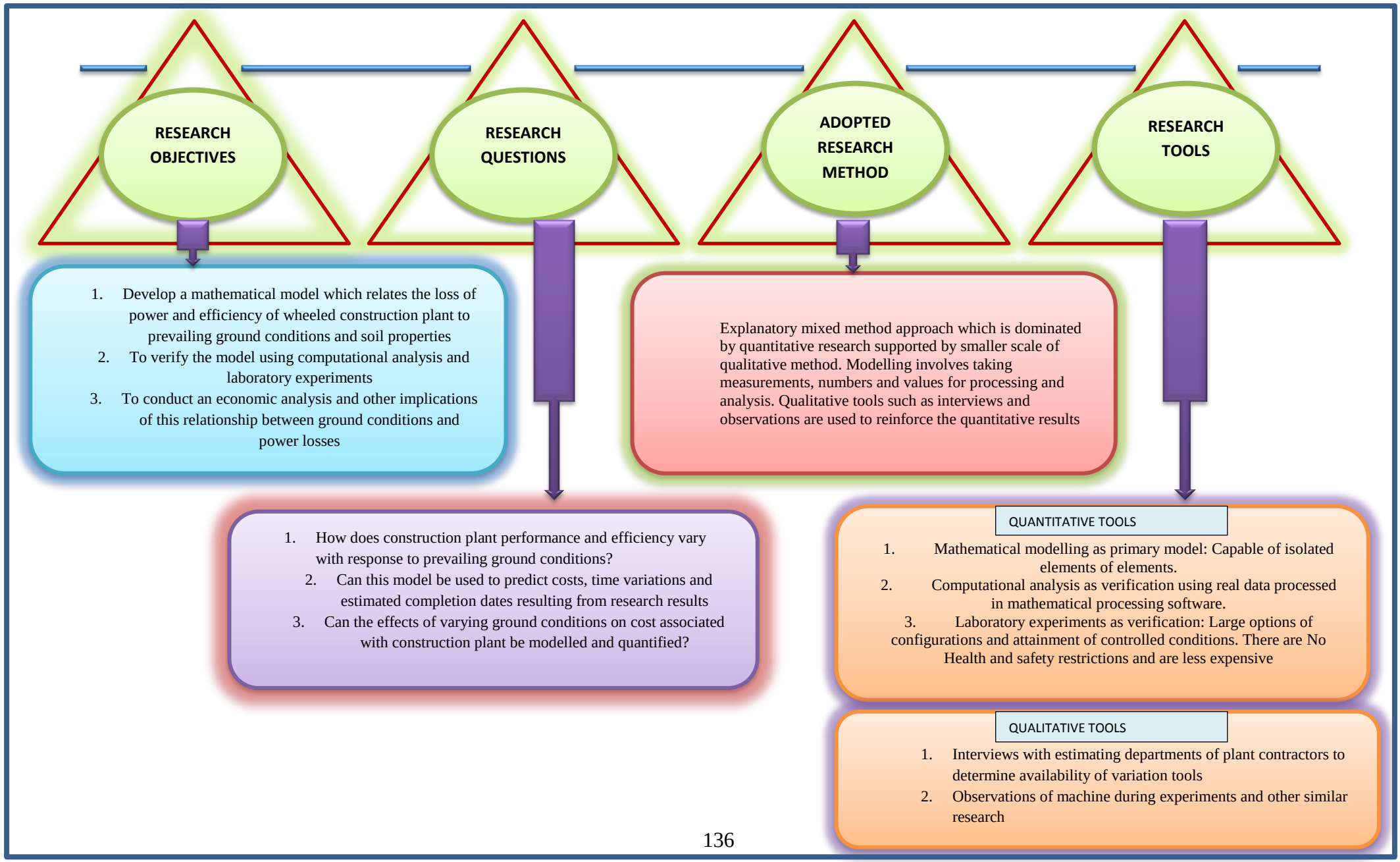

Figure 3.13: Interface between research objectives, research questions, research methods and tools

3.11. Chapter Summary.

This chapter has outlined and justified the research paradigms and tools used in the execution of the research from commencement to completion. The chapter has also discussed the challenges associated with the available methods and instruments of model verification which is one of the challenges encountered by this research. The challenges and successes associated with the methods have been discussed and illustrated. Figure 3.12 provides a summary of the research route layout from commencement to completion of the research. Figure 3.13 provides the relationship between the research objectives, research questions and the justification of the adopted research methodology used.

CHAPTER 4

MATHEMATICAL MODEL DEVELOPMENT

4.0. CHAPTER 4

Development of the mathematical model to predict wheel power loss

4.1 Introduction to mathematical model development

This chapter presents the results of an investigation into the inter-relationship between the dynamic characteristics of off-road vehicles, focussing on wheels and the physical properties of soils. The chapter focuses on developing a mathematical model for predicting wheel power loss measured in form of drawbar-pull using Newtonian principles of mechanics and the law of conservation energy. The model provides criteria for the prediction of the likely pulling performance and efficiency of wheeled construction plant as it traverses through a spectrum of off-road soil conditions. The model is developed as a continuation of the work started in 2000 by Dr David Reid in which a motion and energy based mathematical model driven by a program called RUTSEV was developed to predict rut depth of a wheel moving at a constant velocity.

With the limited practical application of the rut depth model results, this extended wheel pulling power based POWERSEV model developed for this research by the author provides more usable results to the practising engineer. The model was aimed at determining the relationship between wheel rut depth, soil cohesion, friction angle, wheel size and wheel velocity. This mathematical model is based on the 1.8m diameter theoretical rigid wheel moving in an imaginary straight line at a constant velocity in clay and sandy soils. As established in the literature review chapter, a rigid wheel can be considered a first approximation of a fully inflated

flexible tyre due to reduced sinkage resistance which results in negligible tyre deformation when moving in deformable terrain.

4.2. Wheel Power loss and motion resistance

The main variable of interest in this research was the wheel power loss which is measured in terms of drawbar-pull. The wheel power loss is caused by the motion resistance experienced as a result of wheel rutting. Slip also occurs is an internal resistance and leads to considerable power losses. Wheel slip is given by

$$i = \frac{Vp - Vv}{Vp} = \frac{\omega r - Vv}{\omega r} \quad \therefore Vv = \omega r(1-i) \qquad \text{Eqn 4.1}$$

Where V_v = Translational Velocity, V_p = Rotational Velocity and i = slip

Interpretations of all symbols for the equations are given in the introductory section of the thesis under the nomenclature section. Motion resistance to the wheel movement is dominated by soil compaction and bull dozing of the soil. It can absorb between 5-35% of gross engine power depending on the soil and vehicle speed, Cupera and Smerda (2010). Traction must exceed the resistance in order to produce positive drawbar-pull.

4.3. The mathematical model development

Final rut depths from the RUTSEV motion and work based conservation model data base were used in the development of the model to predict wheel power losses. The rut depths produced by the 800mm radius and 300mm wide rigid wheel were used to produce hundreds of runs based on different wheel slips and cohesion values for clay soils and angle of shearing resistance of resistance for pure sandy soils. The model's assumption was that the wheel was moving in a

theoretically straight line and at constant velocity. The runs were based on slip ratios ranging from 0.6 to -0.9. Higher positive slips exceeding 0.6 produced unrealistic results. The wheel rut depths in combination with the tyre motion equilibrium equations were used to develop the POWERSEV driven model for calculating drawbar-pull as summarised below.

Power loss mathematical model boundaries, limitations and assumptions:

1. The model is simple and based on the single rigid wheel of radius 800mm and width 300mm.
2. The terrain under consideration is clay and sandy soils.
3. The soil cohesion rage runs from 20,000N/m^2 to 200,000N/m^2 for clay soils
4. The angle of shearing resistance ranged from 15^o to 20^o for sandy soils.
5. The wheel in the mathematical model obeyed the Newton's laws of motion.
6. The soil properties such as density, moisture content and soil cohesion were assumed to be uniform at every given time of running the model. The specific details are presented in the next section.
7. The wheel moved in straight line and does not consider turning and cornering effects.

Specific soil profile expected behaviour and assumptions based on Barnes (2010) and Farrar and Darley (1975) TRRL report 688:

1. For cohesive soils in particular and granular soils to a lesser extent, their condition is affected by changes in moisture content.
2. Sandy soils are generally considered to be in a suitable condition provided their natural moisture content lies close to the optimum moisture content.
3. Staying with sandy soils, the moisture content is more than the optimum then the soil may be loosely spread to allow evaporation while if it is too dry additional water may be required to bring to its optimal moisture content.

With these details above, the following assumptions were adopted and supported by figure 4.1

1. The soil cohesion and shear strength increases with reduced moisture content for clay soils as illustrated in figure 4.1. Increase in water content reduces the value of soil cohesion
2. An optimal angle of shearing resistance exists with the optimal amount of moisture content in sandy soil.
3. Compaction resistance increases with increased number of passes as illustrated in section 2.9 of chapter 2 and will therefore not be assessed separately.

The three assumptions above were further verified by the work done by Blahova, Sevelova and Pilarova (2013) in which the influence of water content on soil cohesion and angle of shearing resistance was studied experimentally.

The Mohr- Coulomb relationship

The Mohr-Coulomb relationship is the most appropriate strength criterion adopted in soil mechanics. It simply relates the shear stress at failure on a failure plane or slip surface to the normal effective stress acting on that plane. Soil failure criterion is further given by figure showing three categories peak strength, critical state and residual strength as recorded in Barnes 2010. This relationship shown in figure 4.2 was used in determining the shear and stress values as tabulated in the chapter equations. The subject has been discussed in general detail in section 2.1.2.2 of chapter 2.

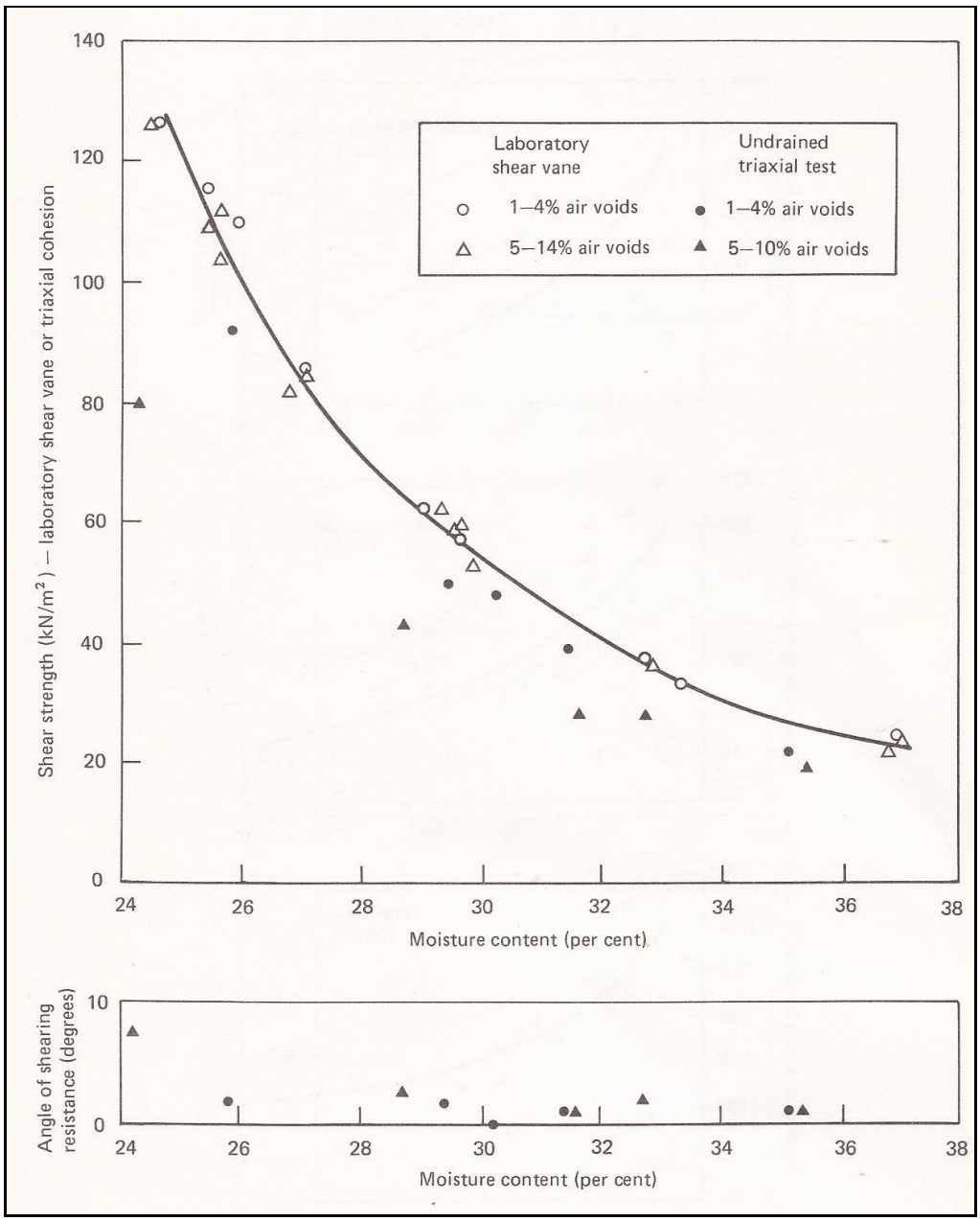

Figure 4.1: Relationship between soil cohesion, shear strength and moisture content for compacted London Clay specimens, TRRL: Farrar and Darley (1975).

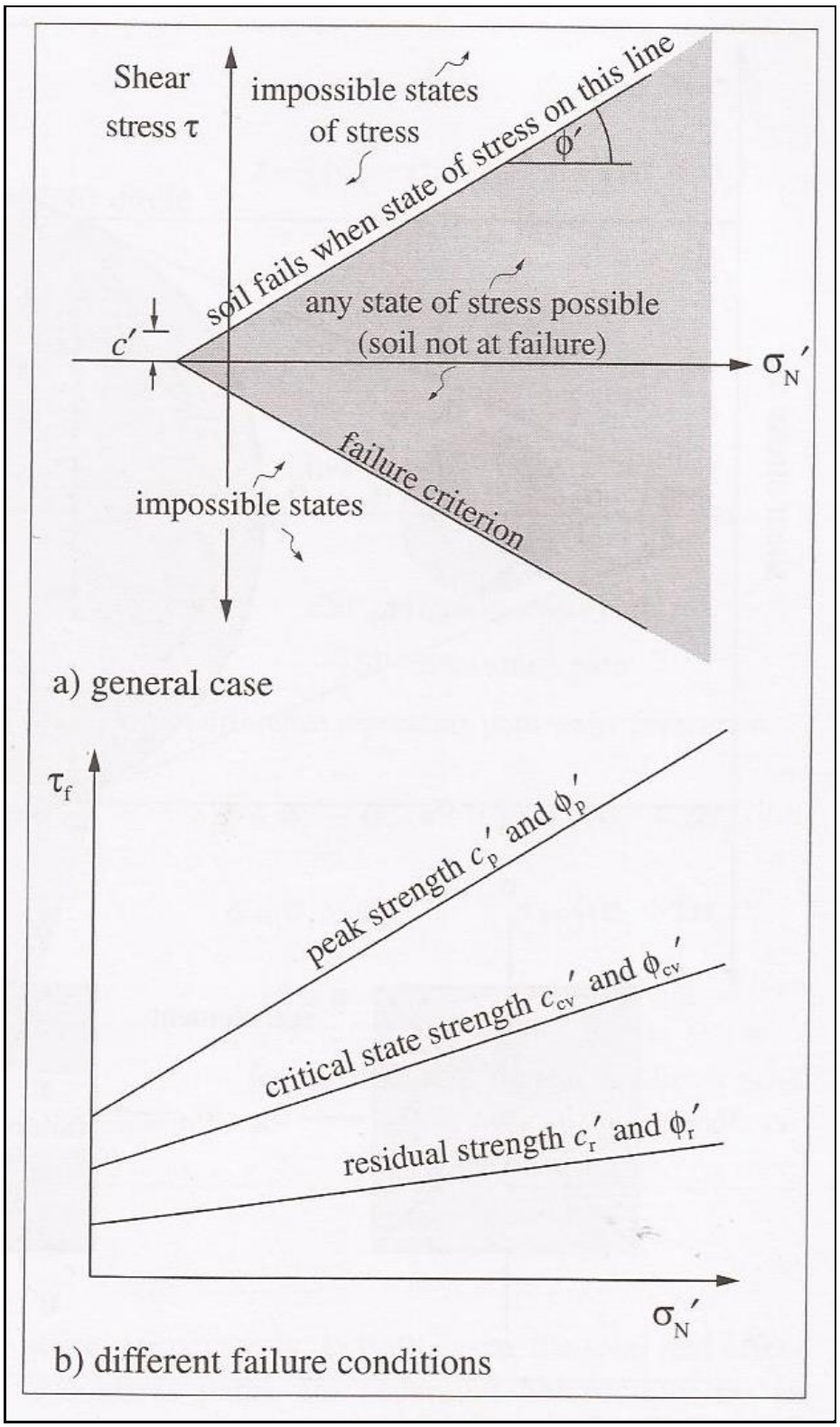

Figure 4.2: Mohr-Coulomb failure condition, Barnes (2010)

Figure 4.3 below provides the first principle of motion and forces through a schematic drawing of a rigid wheel moving with a constant velocity and the associated forces acting on it. Figure 4.3 also shows the free-body diagram of the wheel on the right. These figures are based on Wong and Reece semi empirical equilibrium formula.

t = wheel width (m)
d = wheel sinkage (m)
r = wheel rolling radius (m)
T = input torque (kNm)
θ defines the position of a point on the contact arc (rad).

V_v = forward velocity (m/s)
V_p = peripheral velocity (m/s)
θ_1 = wheel entry angle (rad)
θ_2 = wheel exit angle (rad)

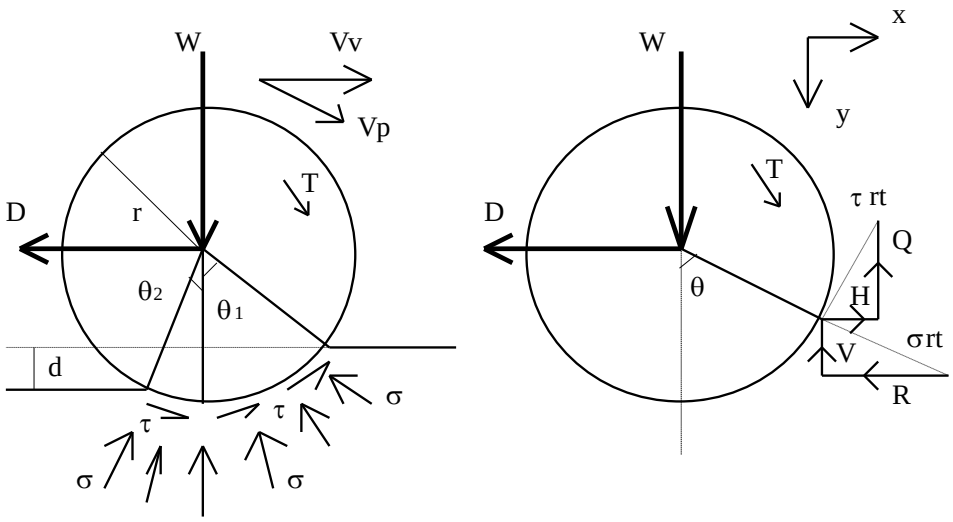

Figure 4.3: Forces acting on a solid wheel and free-body diagram of wheel on the right, Reid (2000)

σ represents radial soil reaction

τ Represents tangential stress distribution from the free-body diagram it can be seen that, if θ_2 is neglected, then the following relationships hold:

4.3.1. Wheel weight

Wheel weight (W), radial support force (V) and the shear support force (Q)

$$W = V + Q = rt\left(\int_0^{\theta_1} \sigma(\theta)\cos\theta.d\theta + \int_0^{\theta_1} \tau(\theta)\sin\theta.d\theta\right) \quad \text{Eqn 4.2}$$

Using the trigonometry

$$V = rt\sigma \int_0^{\theta_1} \cos\theta \cdot d\theta \quad \text{Eqn 4.3}$$

Using trigonometry

$$Q = rt\tau \int_0^{\theta_1} \sin\theta \cdot d\theta \qquad \text{Eqn 4.4}$$

$$W = V + Q \qquad \text{Eqn 4.5}$$

Integrating the equation 4.2 produces the following results for the given range of wheel contact.

$$V = Radial\ support\ force = rt\sigma \sin\theta_1 \qquad \text{Eqn 4.6}$$

$$Q = Shear\ support\ force = rtC[1 - \cos\theta_1] \qquad \text{Eqn 4.7}$$

$$\boldsymbol{W = rt\left[\sigma \sin\theta_1 + C(1 - \cos\theta_{1)}\right]} \qquad \text{Eqn 4.8}$$

4.3.2. Drawbar-pull

Drawbar-pull (D), tractive effort (H) and the translational rolling resistance (R);

$$D = H - R = rt(\int_0^{\theta_1} \tau(\theta)\cos\theta.d\theta - \int_0^{\theta_1} \sigma(\theta)\sin\theta.d\theta) \qquad \text{Eqn 4.9}$$

$$H = rt\tau \int_0^{\theta_1} \cos\theta \cdot d\theta \qquad \text{Eqn 4.10}$$

$$R = rt\sigma \int_0^{\theta_1} \sin\theta \cdot d\theta \qquad \text{Eqn 4.11}$$

Integrating the equation 4.9 in order to obtain the results from the given range of wheel contact, the following equations are generated:

$$H = Tractive\ effort = rtC \sin\theta_1 \qquad \text{Eqn 4.12}$$

$$R = Translational\ rolling\ resistance = rt\sigma[1 - \cos\theta_1] \qquad \text{Eqn 4.13}$$

$$D = H - R \qquad \text{Eqn 4.14}$$

$$D = rt\tau \int_0^{\theta_1} \cos\theta \cdot d\theta - rt\sigma \int_0^{\theta_1} \sin\theta \cdot d\theta \qquad \text{Eqn 4.15}$$

$$\boldsymbol{D = Drawbarpull = rt[C \sin\theta_1 - \sigma(1 - \cos\theta_1]} \qquad \text{Eqn 4.16}$$

4.3.3. Tangential stress

Tangential stress or shear stress is calculated using the Mohr- Coulomb formula $\tau = C + \sigma \cdot \tan \emptyset$. The maximum tangential shear stress for the entire contact as given by

$$\boldsymbol{\tau = C + \sigma \cdot \tan \emptyset \cdot \left(1 - e^{-j/k}\right)} \qquad \text{Eqn 4.17}$$

Where

C = soil cohesion

σ = normal stress

$\emptyset$ = Soil angle of shearing resistance

J = Soil shear displacement.∴ $j = r((\theta_1 - \theta) - (1-i)(\sin\theta_1 - \sin\theta))$ Eqn 4.18

K = Soil shear deformation modulus

As mentioned earlier in pure clays, $\emptyset$ = 0, making $\tau = C$. In pure sands C = 0, making $\tau = C + \sigma \cdot \tan \emptyset$. In Loam soils a combination of both may occur with values for C and $\emptyset$.

In this case where C = 0, τ becomes:

$$\tau = \sigma \cdot \tan \emptyset \cdot \left(1 - e^{-j/k}\right) \qquad \text{Eqn 4.19}$$

Using Wong and Reece equations 4.2 and 4.9, values for σ and eventually τ can then be established to obtain values for gross traction, motion resistance and drawbar-pull using the given $\emptyset$ and d (rut depth). Below are the equations derived from the sequence above.

$$W = rt[\sigma \sin(\theta + \tau\,(1 - \cos\theta] \qquad \text{Eqn 4.20}$$

$$W = rt\left[\sigma \sin\theta + \sigma \tan \emptyset \cdot \left(1 - e^{-\frac{j}{k}}\right)(1 - \cos\theta\right] \qquad \text{Eqn 4.21}$$

Since all values, for (–j/k) are over 100, $e^{-\frac{j}{k}} = 0$

$$W = rt[\sigma \sin\theta + \sigma \tan\varphi\,(1 - \cos\theta)]$$ Eqn 4.22

$$W = rt[\sigma \sin\theta + \sigma \tan\varphi - \sigma \tan\emptyset \cdot \cos\theta]$$ Eqn 4.23

$$W = rt\sigma[\sin\theta + \tan\varphi - \tan\emptyset \cdot \cos\theta]$$ Eqn 4.24

For **sandy soils**, $\boldsymbol{\sigma = Wrt/[\sin\theta + \tan\emptyset - \tan\emptyset \cdot \cos\theta]}$ Eqn 4.25

$W = rt[\sigma \sin\theta + C(1 - \cos\theta\,]$, when $\emptyset = 0$ Eqn 4.26

For pure clay soil equation 4.25 applies for calculating radial stress

$$\boldsymbol{\sigma = W - rtC(1 - \cos\theta)/rt \sin\theta}$$ Eqn 4.27

$$H = rt\sigma \cdot \tan\emptyset \cdot \sin\theta$$ Eqn 4.28

$$R = rt\sigma(1 - \cos\theta)$$ Eqn 4.29

4.3.4. Application of the equations

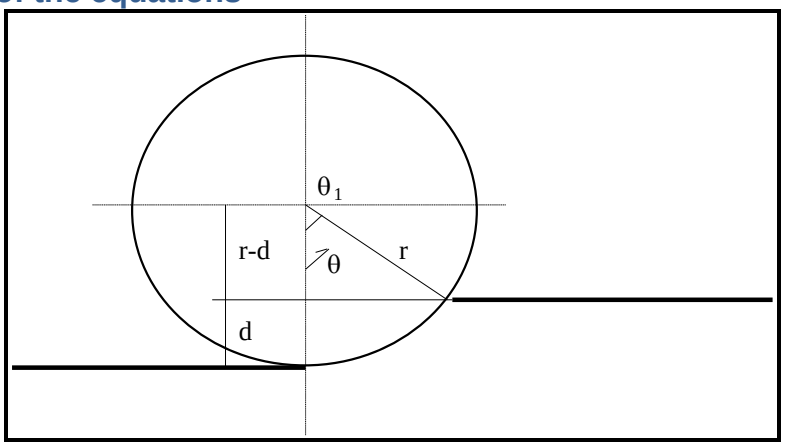

Figure 4.4: Details showing the relationship between d, theta and r

From the above figure, the contact angle θ_1 and the rut depth d are related by the equation below:

$$\cos\theta = \frac{r-d}{r}$$ Eqn 4.30

$$\cos\theta = 1 - \frac{d}{r}$$ Eqn 4.31

$$\theta = acos\left[1 - \frac{d}{r}\right]$$ Eqn 4.32

Using equation 4.27, if the rut depth d, is established from equations 4.33 to 4.35, the contact arc angle θ can be calculated. Equations 4.33 to 4.35 were adapted from Reid (2000) which constituted part of the database used for the development of POWERSEV mathematical model developed by the author. The description of variables and notation in equations 4.33 to 4.35 is presented in appendix 24. A summary of the development of the same equations is presented in appendix 25.

Other variables that can be calculated include radial support stress σ can be found from equation 4.20, $W = rt[\sigma \sin\theta + \tau\,(1 - \cos\theta)]$ given wheel parameter weight, radius r, width of tyre t and cohesion value C for clay soils and $\emptyset$ for sand soils. For clay soils, tractive effort (H), translational resistance (R) and drawbar-pull, (D) can also be found from equations 4.12 and 4.13 and 4.16 respectively. For sandy soils tractive effort is calculated from equation 4.28, while translational resistance is calculated from equation 4.29.

$$d_n = d_{n-1} - \frac{f(d)}{f'(d)} \qquad \text{Eqn 4.33}$$

Where d_n is the rut depth.

$$f(d) = Ctd^2 - \frac{WVv^2d^2}{2gr^2(1-i)^2\arccos^2\left(\frac{r-d}{r}\right)} + 2C(2rd-d^2)^{0.5}d^2 + (W+L)\left(\frac{2}{\pi}-1\right)d + 2(W+L)\left(\frac{(1-\sin\phi)}{(1+\sin\phi)}\right)\tan\phi.d + \left(\frac{(W+L)\tan\phi\left(2rd-d^2\right)^{0.5}}{2r}\right)d \qquad \text{Eqn 4.34}$$

$$f'(d) = 2Ctd - \left\{ \frac{W\omega^2 d\left(\arccos\left(\frac{r-d}{r}\right) - \frac{d}{r\left(1-\left((r-d)/r\right)^2\right)^{0.5}} \right)}{g.\arccos^3\left(\frac{r-d}{r}\right)} \right\}$$
$$+ 4dc\left(2rd - d^2\right)^{0.5} + \frac{Cd^2(2r-2d)}{\left(2rd-d^2\right)^{0.5}} + \left(\frac{2}{\pi} - 1\right)(W+L)$$
$$+ \frac{(W+L)\tan\phi(2rd-d^2)^{0.5}}{2r} + \frac{(W+L)\tan\phi.d(2r-2d)}{4r(2rd-d^2)^{0.5}}$$
$$+ 2(W+L)\left(\frac{(1-\sin\phi)}{(1+\sin\phi)}\right)\tan\phi \qquad \text{Eqn 4.35}$$

4.4. Presentation and discussion of the model results (Clay)

The rut depths values were used to establish the corresponding drawbar-pull values in relation to soil cohesion, angle of shearing resistance, wheel velocity, moisture content, wheel self-weight, applied load, wheel radius and wheel width. The mathematical model results were then compared with results from the computational analysis and laboratory experiments using MOBILITY SF-3713 which are discussed in detail in chapters 5 and 6 and 7. Table 4.1 below is a summary of the mathematical model data used to generate values for power loss in terms of drawbar-pull. Table 4.2 presents a summary of the mathematical model (POWERSEV) equations used in the generation of desired results.

Model boundaries and specifications for POWERSEV

Velocity	0.2m/s, 10m/s, 20m/s and 30m/s
Soil Cohesion	20,000 N/m^2 to 200,000 N/m^2
Angle of shearing resistance	15^o to 20^o
Wheel radius	800mm
Wheel width	300mm
Slip	-0.9, -0.6, -0.3, 0, 0.3, 0.6, 0.9
Wheel self-weight	100N
Applied load	5000N

Table 4.1: Mathematical model key formulae

Mathematical model key formulae in use for POWERSEV

Drawbar-pull (D)	$D = H - R = rt(\int_0^{\theta_1} \tau(\theta)\cos\theta.d\theta - \int_0^{\theta_1} \sigma(\theta)\sin\theta.d\theta)$
Total traction for clay (H)	$H = rtC\sin\theta_1$
Total traction for sandy soil (H)	$H = rt\sigma \cdot \tan\varphi \cdot \sin\theta$
Rolling Resistance for clay soil (R)	$R = rt\sigma(1-\cos\theta)$
Rolling Resistance for sand soil (R)	$R = rt\sigma[1-\cos\theta_1]$
Sigma for clay soils	$\sigma = W - rtC(1-\cos\theta)/rt\sin\theta$
Sigma for sandy soils	$\sigma = Wrt/[\sin\theta + \tan\varphi - \tan\emptyset \cdot \cos\theta]$
Angle θ based on given rut depth	$\theta = acos\left[1-\frac{d}{r}\right].$
Theory and Principle used	*Newtonian principles of mechanics, The equilibrium model and Wong/Reece mathematical approach.*
Programmes used running and processing equations	***MATHCAD 15 AND MICROSOFT EXCEL***

Table 4.2: Power loss mathematical model equations

Example 1: Generation of results for drawbar-pull for velocity 10m/s and slip 0.3 in clay soil.

Ruts			Eqn 4.32				Eqn 4.27	Eqn.4.12	Eqn.4.13	Eqn.4.16
d (m)	d(m)	r (m)	alpha	W (N)	t (m)	C (N/m^2)	sigma(N/m^2)	H (N)	R (N)	D (N)
112	0.112	0.8	0.5355	5100	0.3	20000	36156	2449	1215	1235
94	0.094	0.8	0.4896	5100	0.3	25000	38937	2822	1098	1724
82	0.082	0.8	0.4567	5100	0.3	30000	41212	3175	1014	2161
73	0.073	0.8	0.4305	5100	0.3	35000	43265	3506	948	2558
66	0.066	0.8	0.4090	5100	0.3	40000	45130	3818	894	2925
61	0.061	0.8	0.3930	5100	0.3	45000	46525	4136	851	3285
56	0.056	0.8	0.3764	5100	0.3	50000	48291	4411	811	3599
52	0.052	0.8	0.3625	5100	0.3	55000	49838	4681	777	3904
49	0.049	0.8	0.3518	5100	0.3	60000	51001	4962	750	4213
46	0.046	0.8	0.3408	5100	0.3	65000	52400	5214	723	4490
43	0.043	0.8	0.3294	5100	0.3	70000	54068	5434	697	4736
41	0.041	0.8	0.3215	5100	0.3	75000	55078	5688	677	5011
39	0.039	0.8	0.3135	5100	0.3	80000	56254	5922	658	5264
37	0.037	0.8	0.3053	5100	0.3	85000	57614	6132	640	5493
36	0.036	0.8	0.3011	5100	0.3	90000	57989	6407	626	5780
34	0.034	0.8	0.2926	5100	0.3	95000	59676	6576	609	5968
33	0.033	0.8	0.2882	5100	0.3	100000	60246	6822	596	6226
32	0.032	0.8	0.2838	5100	0.3	105000	60893	7056	585	6471
31	0.031	0.8	0.2793	5100	0.3	110000	61621	7278	573	6705

Table 4.3: Example of results from one of the model equation runs using MATHCAD and 15 and Microsoft Excel

4.4.1. Effect of soil cohesion on drawbar-pull

Results from the mathematical model show that increase in soil cohesion results in rut depth reduction as anticipated from the literature review. Figures 4.5 to 4.7 show that available drawbar-pull increases with increase in soil cohesion in clay soil. The wheel slips in the given figures 4.5 to 4.10 are for 0, 0.3, 0.6, -0.3 and -0.6. The results show that the higher the soil cohesion the higher the drawbar-pull at the wheel. Higher velocities are seen to produce higher available drawbar-pull than low velocity provided the wheel slip does not exceed the uneconomical cap of 0.4. Higher slip/skid ratio also produced higher drawbar-pull with increasing soil cohesion values. Table 4.3 confirms that increase in drawbar-pull is generated by increase in gross traction and reduction in motion resistance due to reduced rut depth as illustrated in figure 4.10. The figure also shows that high velocities in low cohesion soils result in energy wastage. High velocities would only be economical in high cohesion and more stable terrain.

Figures 4.12 to 4.19 further illustrate the results through comparative graphs. Results suggest that it would be more economical to operate wheeled plant in high cohesion soils when traversing in clay dominated terrain. Soils with low soil cohesion will require stabilisation to avoid power and traction losses or alternatively plant would be required to move at very low velocities. Figure 4.12 and figure 4.13 compares drawbar-pull for slip/skid ratio of 0 and 0.3 respectively with the 0.3 slip wheel providing the higher drawbar-pull. Figure 4.14 and Figure 4.15 compares drawbar-pull for slip/skid ratio of 0.6 and -0.3 respectively with the 0.6 slip (also in figure 4.7) wheel providing the higher drawbar-pull and the risk of high and uneconomical resistance resulting in uneconomical drive.

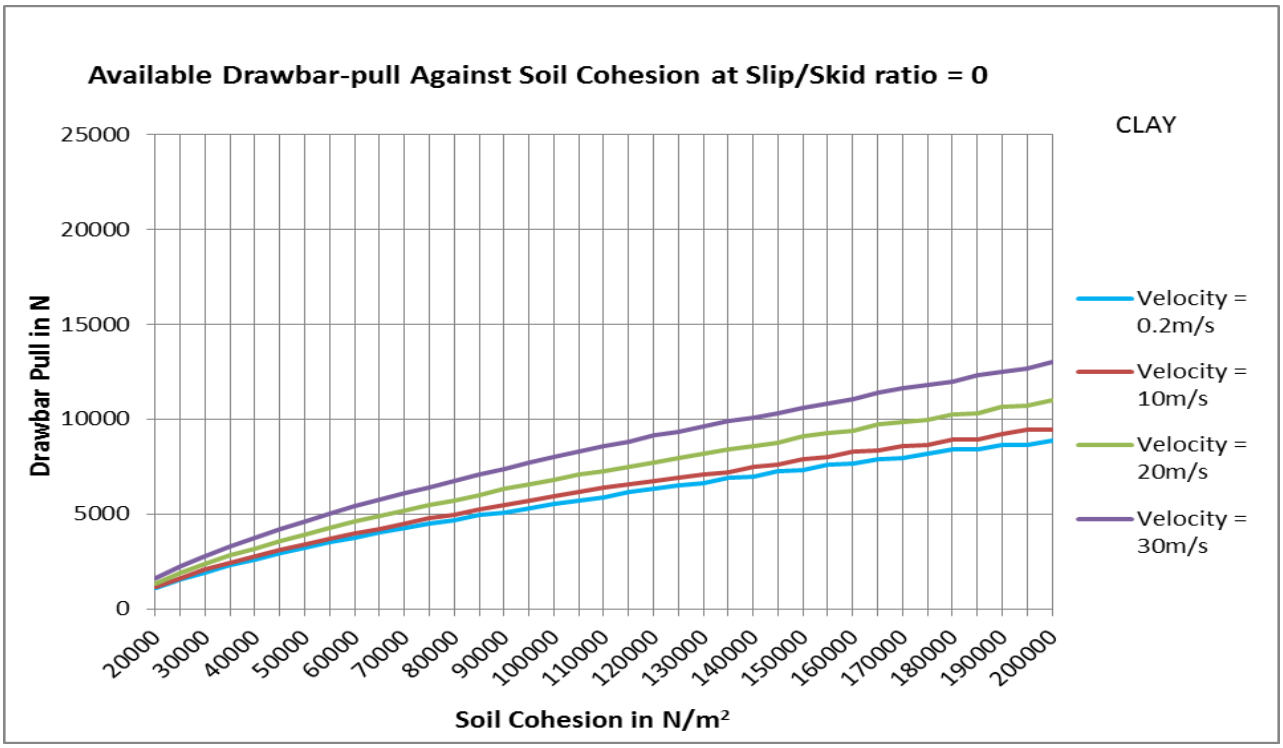

Figure 4.5: Graph showing available drawbar-pull against soil cohesion at slip/skid ratio = 0

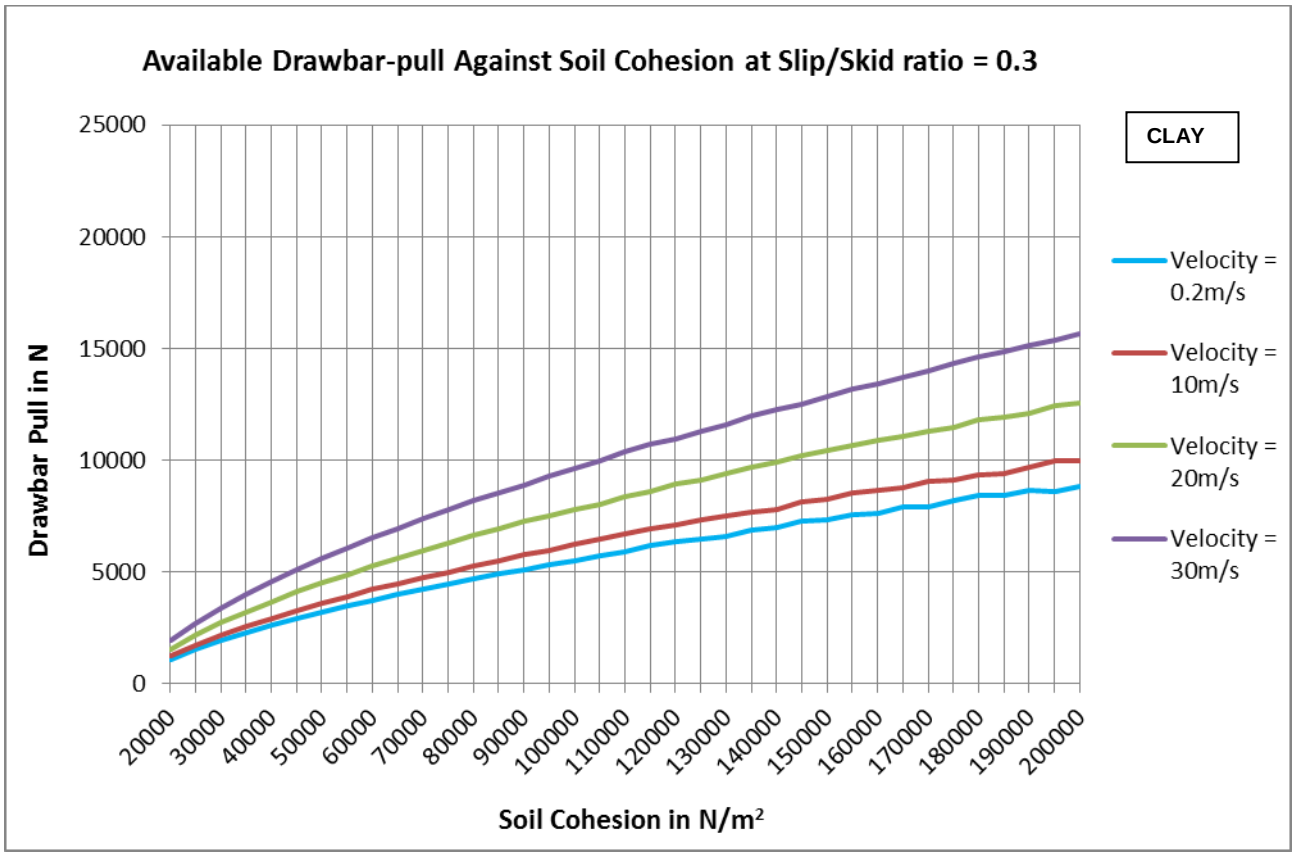

Figure 4.6: Graph showing available drawbar-pull against soil cohesion at slip/skid ratio = 0.3

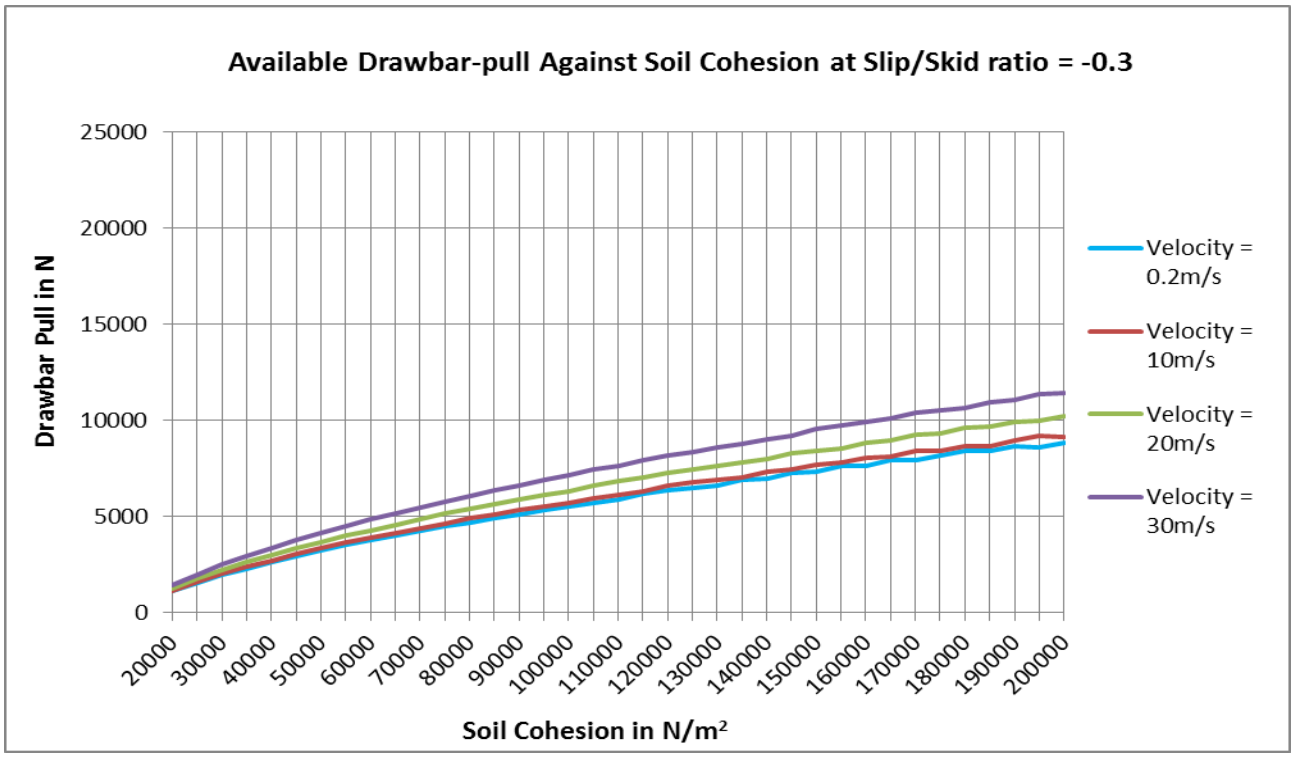

Figure 4.7: Graph showing available drawbar-pull against soil cohesion at slip/skid ratio = -0.3

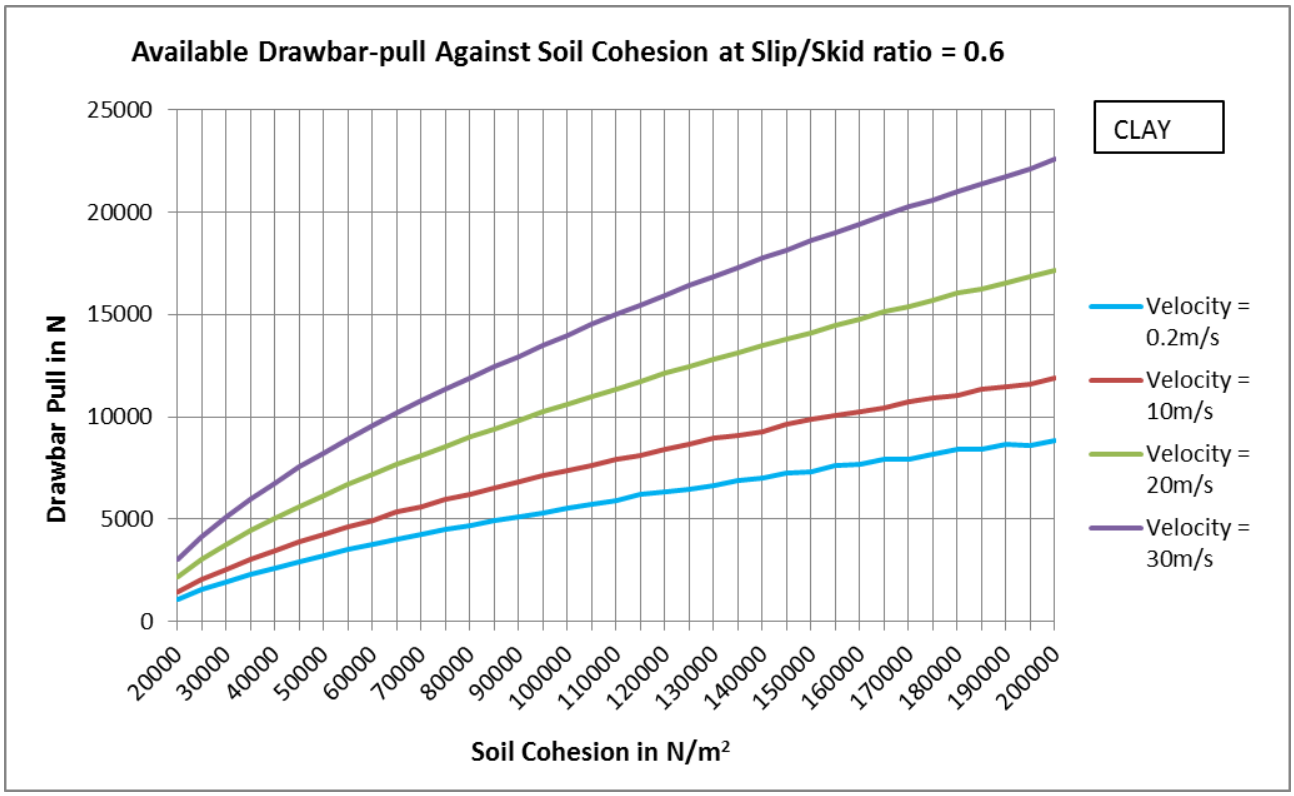

Figure 4.8: Graph showing available drawbar-pull against soil cohesion at slip/skid ratio = 0.6

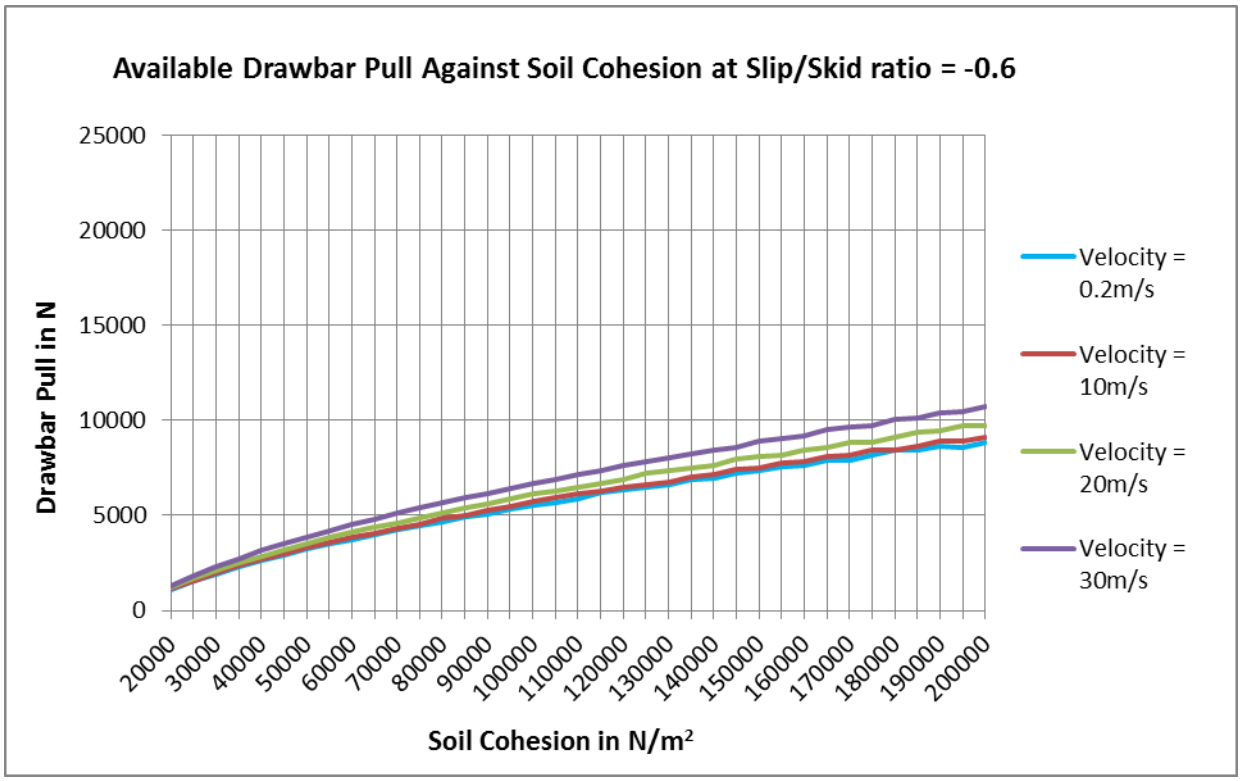

Figure 4.9: Graph showing available drawbar-pull against soil cohesion at slip/skid ratio = -0.6

Figures and 4.16 and 4.17 compares drawbar-pull for slip/skid ratio of -0.6 (also in figure 4.8) and -0.9 respectively with the -0.9 slip providing lesser drawbar-pull due to higher skidding arising from significant braking effect. Braking effect generally carries less or no drawbar-pull transmitted to the wheel with full braking effect amounting to -1. This also results in creation of a front soil bow as discussed in section 2.2.2 and 2.7.1.1 of the literature review chapter. Figure 4.18 compares drawbar-pull and the corresponding rut depth which is inversely proportional to drawbar–pull as shown in the two graphs.

Figure 4.10 further shows that reduction in rut depth will result in increased available drawbar-pull. This is because rut depth reduction is associated with increased soil cohesion and compaction. The results suggest that slow moving wheeled vehicles will attain economical traction as compared to higher velocity wheels moving in soft soils. Deeper rutting of the soil by high velocity wheels results in more energy being wasted in the process of overcoming the rolling resistance.

DRAWBAR-PULL/NET THRUST AGANIST SOIL COHESION SLIP/SKID RATIO COMPARISON

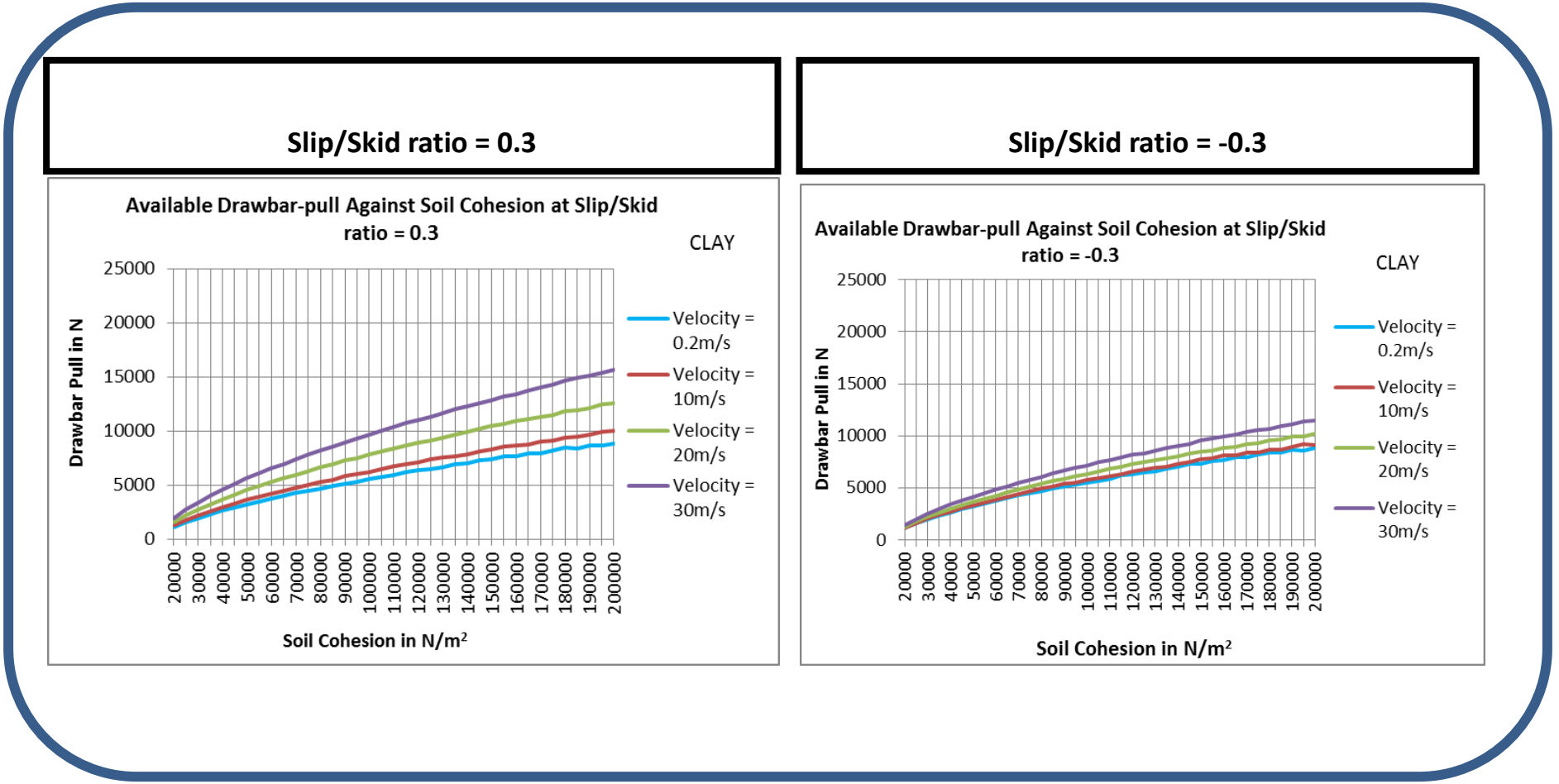

Figure 4.10: Graph showing comparison between drawbar-pull, soil cohesion and wheel slip for 0.3 and -0.3

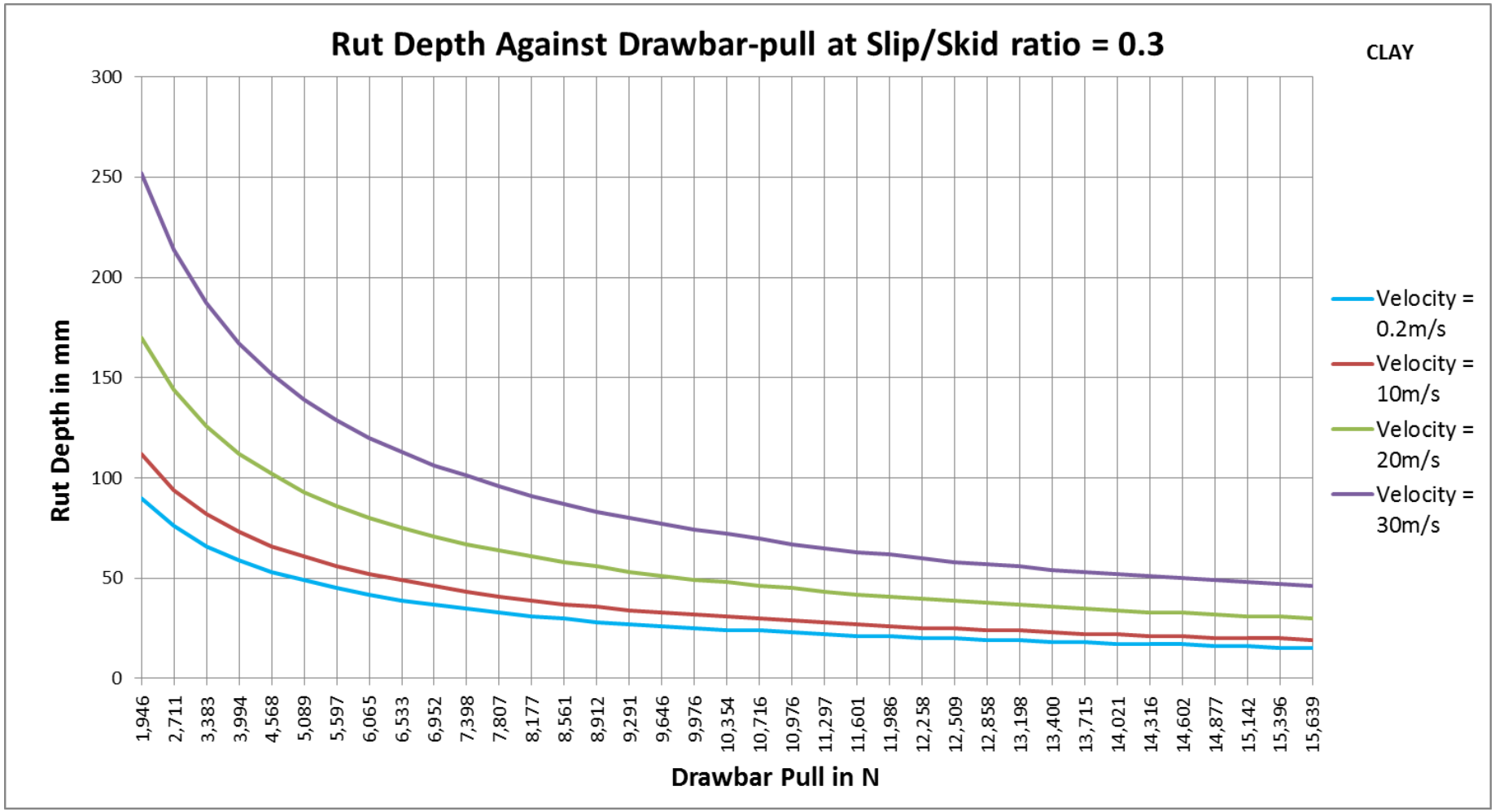

Figure 4.11: Graph showing rut depth against drawbar-pull at slip/skid ratio = 0.3

The increasing effect of soil cohesion, wheel velocity, wheel slip/skid ratio and the resultant effect on draw bar-pull can be clearly seen in the following series of graphs in figures 9 to 16 which provide a side by side comparison of each changing variable.

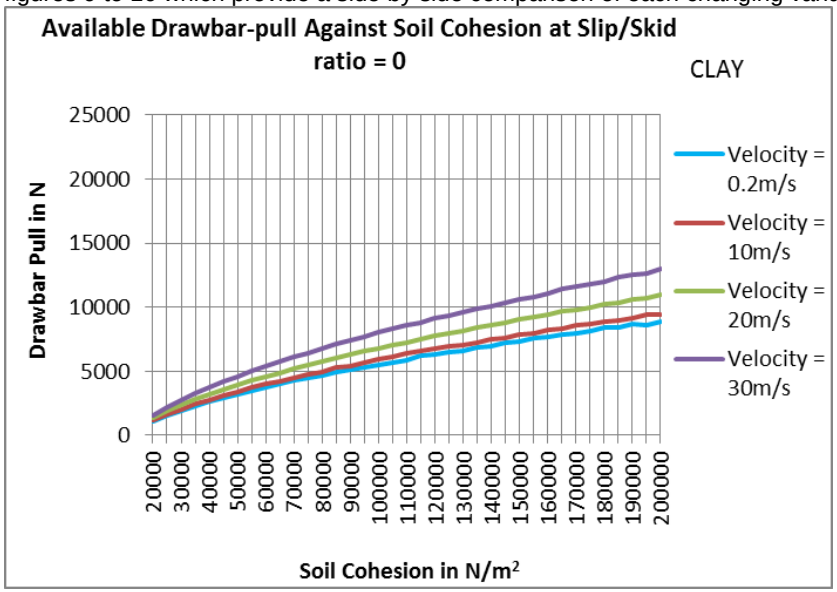

Figure 4.12: Graph showing available drawbar-pull against soil cohesion at slip/skid ratio = 0

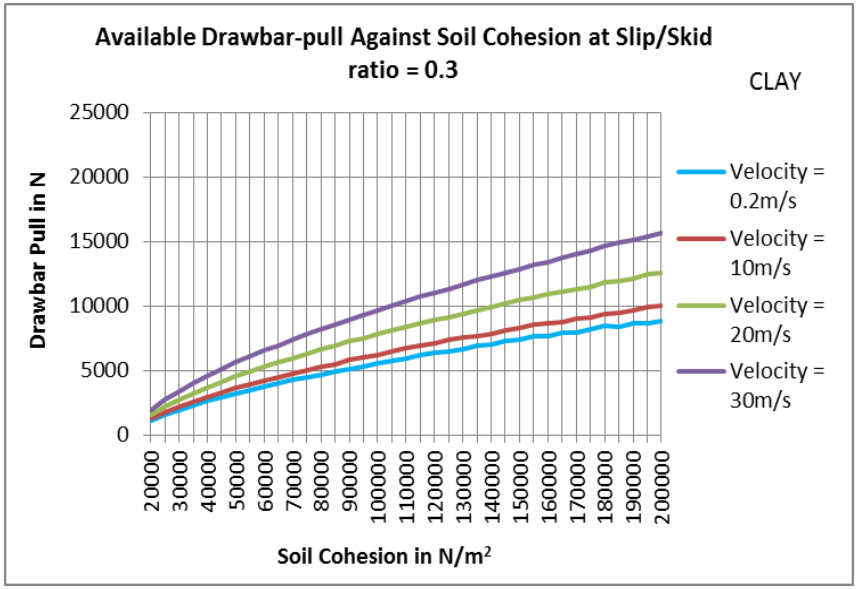

Figure 4.13: Graph showing available drawbar-pull against soil cohesion at slip/skid ratio = 0.3

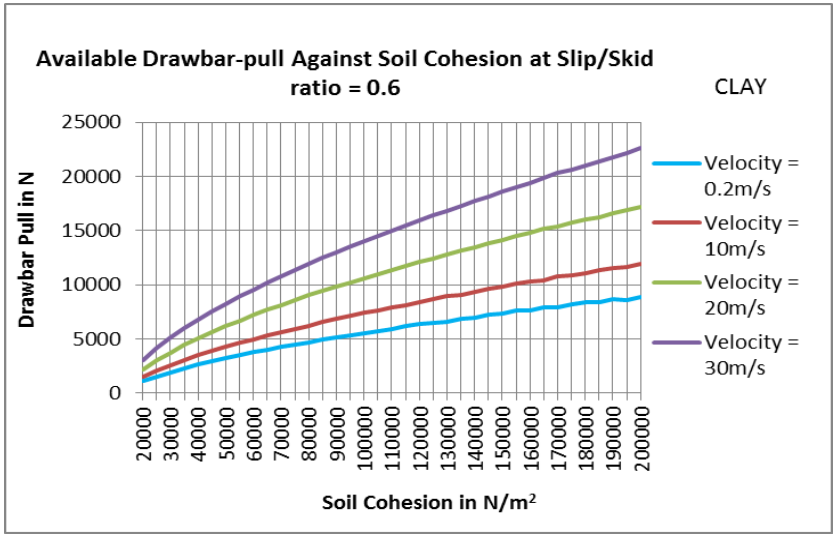

Figure 4.14: Graph showing available drawbar-pull against soil cohesion at slip/skid ratio = 0.6

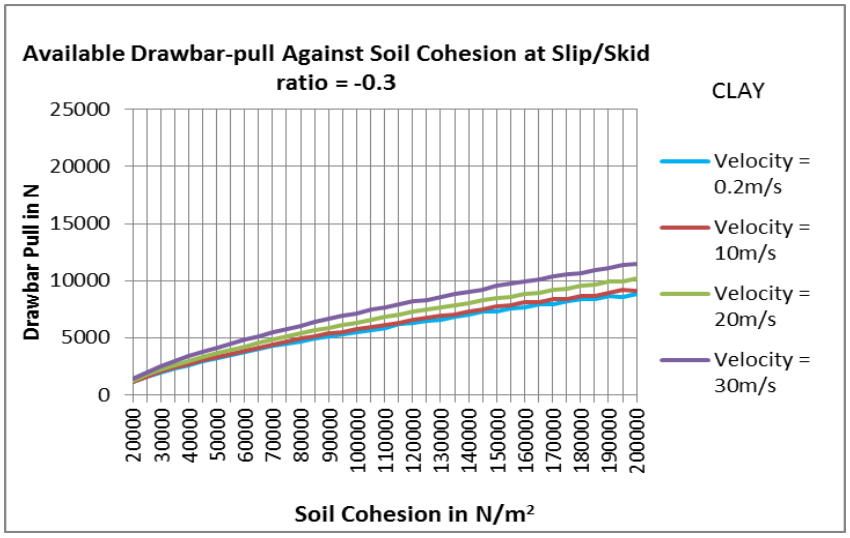

Figure 4.15: Graph showing available drawbar-pull against soil cohesion at slip/skid ratio = -0.3

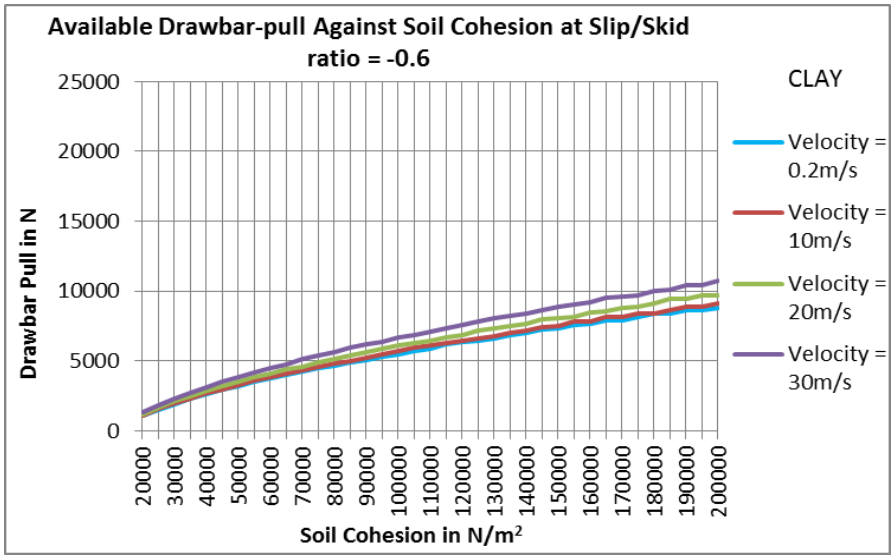

Figure 4.16: Graph showing available drawbar-pull against soil cohesion at slip/skid ratio = -0.6

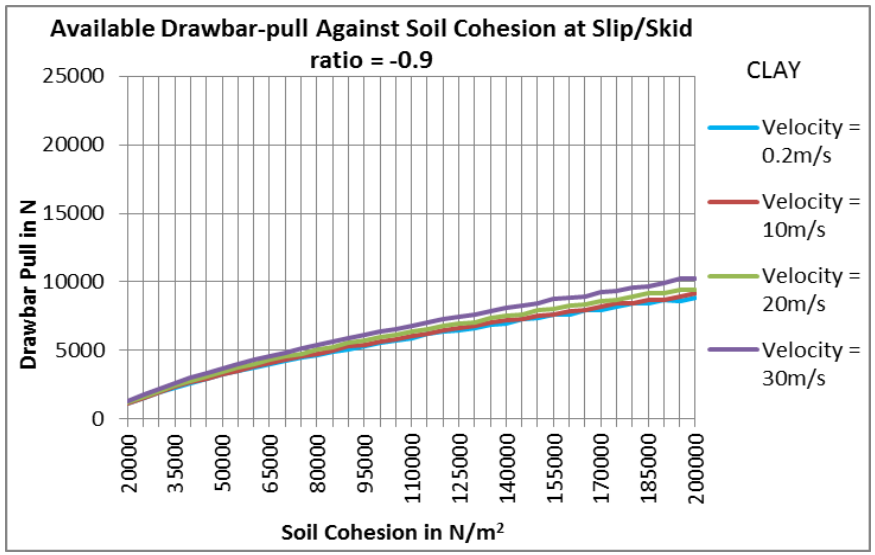

Figure 4.17: Graph showing available drawbar-pull against soil cohesion at slip/skid ratio = -0.9

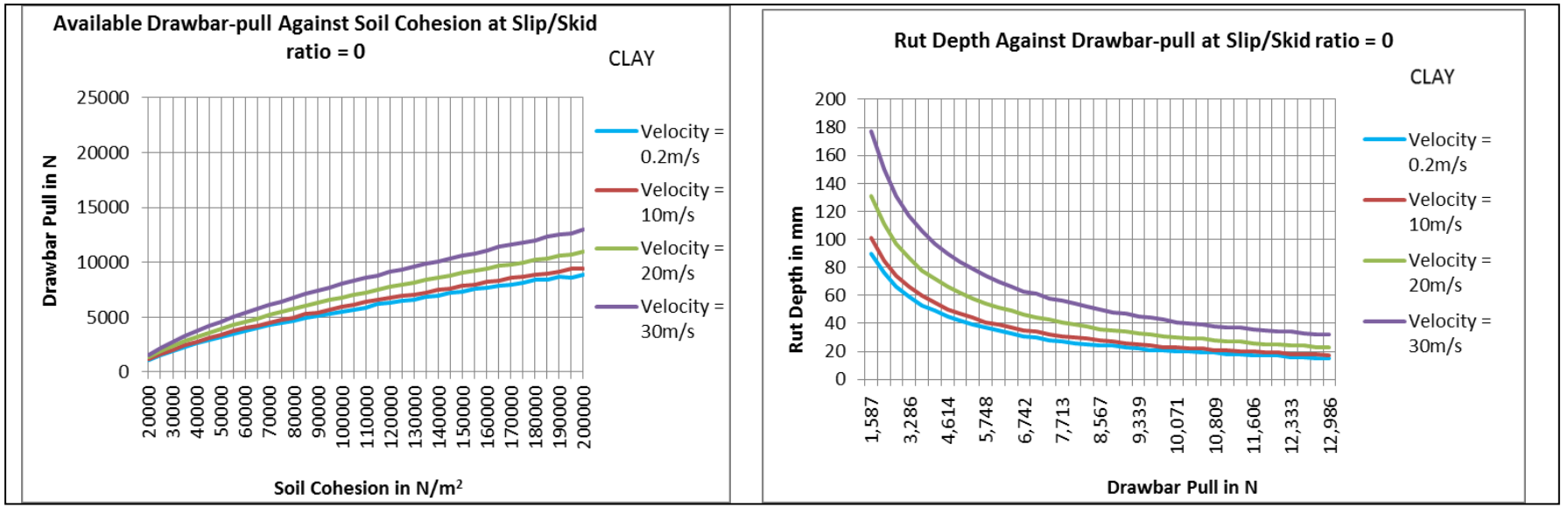

Figure 18: Graph showing available drawbar-pull against soil cohesion at slip/skid ratio = 0 compared with corresponding effect on rut depth shown in the figure on the right

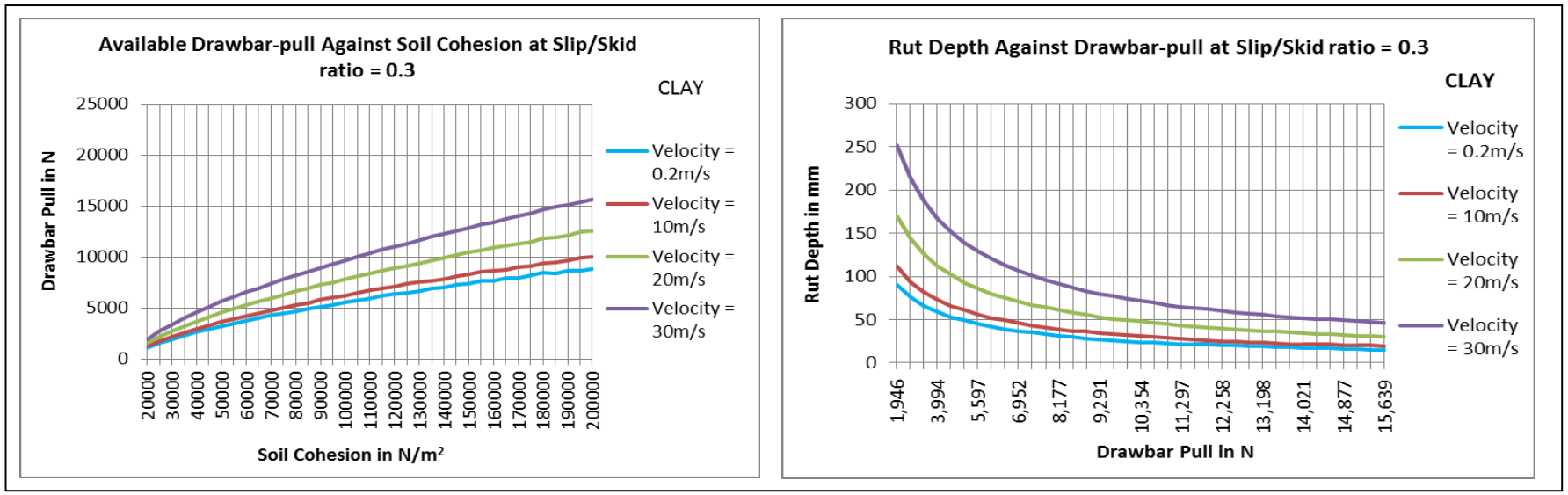

Figure 4.19: Graph showing available drawbar-pull against soil cohesion at slip/skid ratio= 0.3 compared with corresponding effect on rut depth shown in the figure on the right

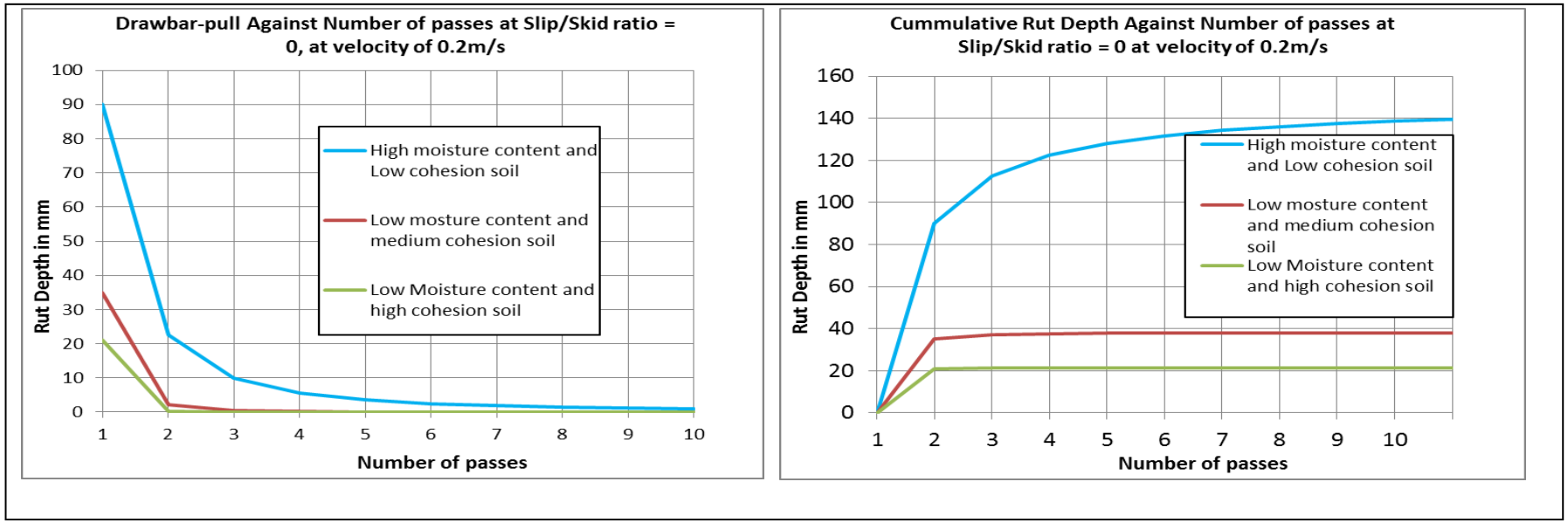

Figure 4.20: Graphs showing rut depth against number of wheel passes at slip/skid ratio = 0. The graph on the left shows the additional depth after each pass while the graph on the right shows the cumulative increase of the rut depth after each pass

Further model results analysis

SLIP/SKID RATIO = -0.6

Velocity	Net Drawbar-Pull at Soil Cohesion 20000N/m^2	Net Drawbar-Pull at Soil Cohesion 200000N/m^2
0.2m/s	1099N	8843N
10m/s	1124N	9136N
20m/s	1205N	9696N
30m/s	1316N	10733N

Table 4.4: Relationship between velocity, drawbar-pull, soil cohesion and slip/skid ratio -0.6

SLIP/SKID RATIO = -0.3

Velocity	Net Drawbar-Pull at Soil Cohesion 20000N/m^2	Net Drawbar-Pull at Soil Cohesion 200000N/m^2
0.2m/s	1099N	8843N
10m/s	1136N	9136N
20m/s	1252N	10227N
30m/s	1415N	11452N

Table 4.5: Relationship between velocity, drawbar-pull, soil cohesion and slip/skid ratio -0.3

SLIP/SKID RATIO = 0

Velocity	Net Drawbar-Pull at Soil Cohesion 20000N/m^2	Net Drawbar-Pull at Soil Cohesion 200000N/m^2
0.2m/s	1099N	8843N
10m/s	1168N	9420N
20m/s	1344N	10978N
30m/s	1587N	12986N

Table 4.6: Relationship between velocity, drawbar-pull, soil cohesion and slip/skid ratio 0

SLIP/SKID RATIO = 0.3

Velocity	Net Drawbar-Pull at Soil Cohesion 20000N/m^2	Net Drawbar-Pull at Soil Cohesion 200000N/m^2
0.2m/s	1099N	8843N
10m/s	1235N	9965N
20m/s	1552N	12565N
30m/s	1946N	15639N

Table 4.7: Relationship between velocity, drawbar-pull, soil cohesion and slip/skid ratio 0.3

SLIP/SKID RATIO = 0.6

Velocity	Net Drawbar-Pull at Soil Cohesion 20000N/m^2	Net Drawbar-Pull at Soil Cohesion 200000N/m^2
0.2m/s	1099N	8843N
10m/s	1458N	11909N
20m/s	2162N	17151N
30m/s	3029N	22581N

Table 4.8: Relationship between velocity, drawbar-pull, soil cohesion and slip/skid ratio 0.6

In addition to the graphical interpretation of the results contained in figures 4.5 to 4.19, numerical and tabular interpretations of the results are shown in tables 4.4 to 4.8. From the tables above the following observations were deduced:

1. Negative slip provides the lowest drawbar-pull output while the highest slip ratio gives the highest drawbar-pull for the same given velocity and soil cohesion. It must be noted however that the most efficient slip lies between 0.3 and 0.5.
2. The highest velocity in any slip provides a higher drawbar-pull output, however velocities resulting in a slip of more than 0.5 results in high resistance thereby making high velocities to be unrealistic and uneconomical.
3. Low cohesion soils provide low drawbar-pull caused by deep wheel rutting.
4. High cohesion soil on the other hand provides high drawbar-pull prompted by shallow rut depths.
5. Rolling resistance decreases with increasing soil cohesion due to the corresponding reduction in wheel rutting.

4.4.2. Effect of wheel multi pass on rut depth.

Using Abebe's et al (1989) forestry management approach and formula expressed in equation 4.36, the effect of wheel multi pass on rut depth was determined using

information from table 4.9 established from previous experiments based on terrain similar to that of off-road conditions. Results indicate that the deepest rut is created by the first pass followed by second and third passes which are very significant. The subsequent passes result in diminishing values of rut depths. The first three passes are the most important in determining the effect of multi pass. This can be illustrated in figure 4.19 which shows the diminishing cumulative values of rut depths from the model.

$$Z_N = Z_1 \cdot 1/n^a \qquad \text{Eqn 4.36}$$

Where

Z_N = sinkage after pass N, m

Z_1 = First pass sinkage, m

n = number of passes

a = multi-pass coefficient from table 4.9.

Soil and load conditions	**Multi pass coefficient**
Loose soil, low load	2 to 3
Medium bearing soil, medium load	3 to 4
Bearing soil, heavy load	4 to 5

Table 4.9: Abebe's coefficient table

Figure 4.20 also shows cumulative rut depth from the model results and the diminishing effect of wheel multi pass from equation 4.36. The fourth and subsequent passes have negligible effect for very medium and high cohesive soils. A similar pattern of cumulative rut depth was established by Rashidi and

Gholani (2011) using Finite Element Modelling and laboratory experiments as illustrated in figure 4.21.

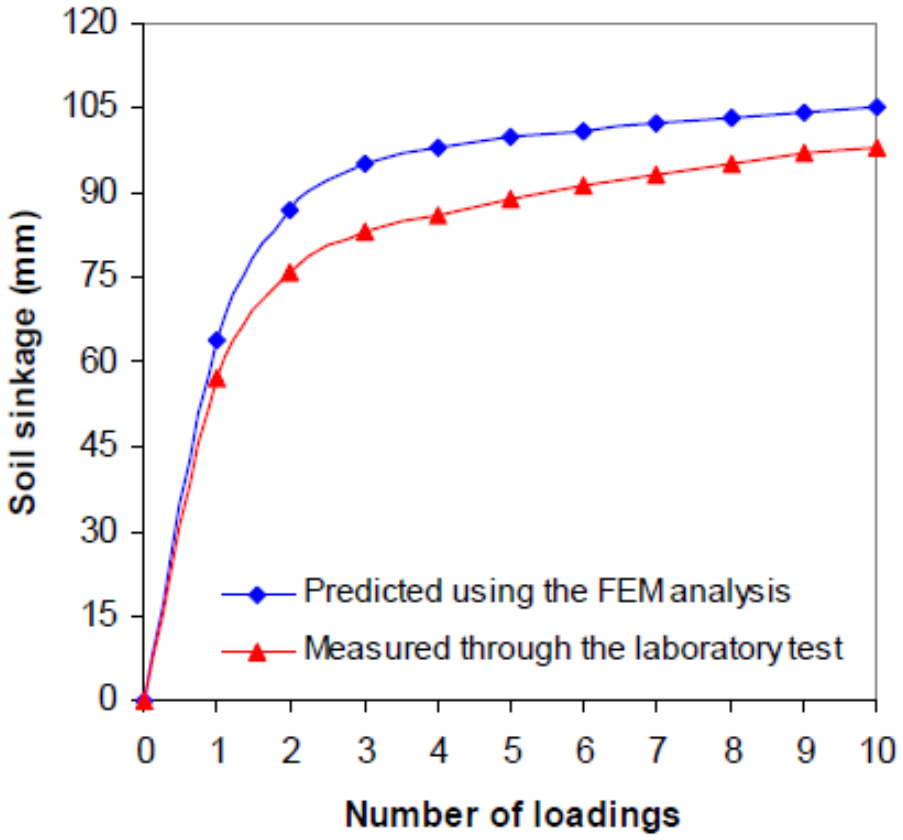

Figure 4.21: Experimental and simulation graph for wheel multi pass from Rashidi and Gholami (2010)

4.4.3. Effect of wheel Self-Weight in clay terrain

The effect of increasing wheel self-weight is illustrated in figure 4.22. With low velocity of the moving wheel, an increase in self-weight has negligible effect on drawbar-pull. This is because of the corresponding negligible rut depths produced by low velocity wheels. The drawbar-pull power gradient on the graph increases as the wheel velocity increases reflecting the corresponding increase in the traction transferred to the wheel. The wheel rut depth does not negatively affect drawbar-pull because wheel self-weight does not produce rut depth deep enough to reduce the drawbar-pull. The addition of self-weight to the wheel results in increased

wheel traction thereby increasing the total available drawbar-pull. This result is also supported by the agricultural industry where agriculture tractors have addition of self-weight known as ballast to improve wheel traction as discussed in chapter 2. This therefore means that the heavier the weight of the wheel the more traction it will produce thereby providing more drawbar-pull in full-drive conditions.

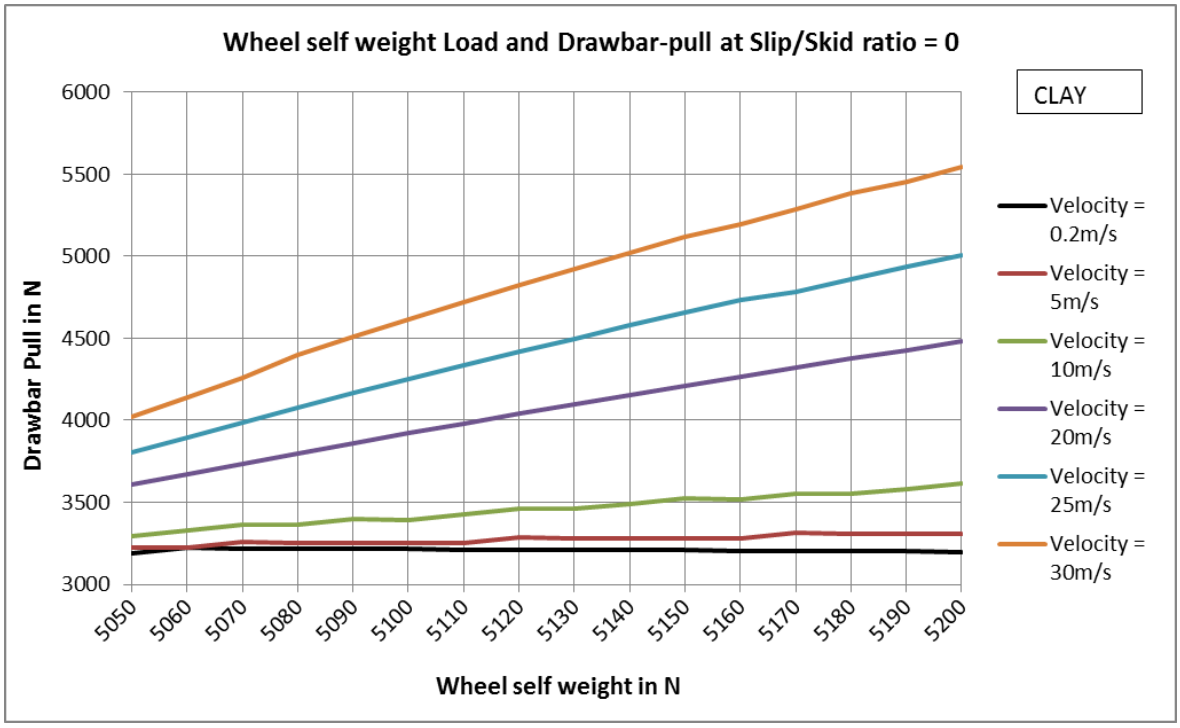

Figure 4.22: Graphs showing wheel self-weight against drawbar-pull at slip/skid ratio =0

4.4.4. Effect of Applied Load in clay terrain

Figure 4.23 illustrates variations in applied load between 1100N and 10,100N for a range of velocities ranging from 0.2m/s to 30m/s. Unlike the self-weight parameter, applied load does not contribute to the traction increase from the rotational kinetic energy except for lower velocities up to a particular load which varies for each different run. Applied load increase the vertical load resulting in deeper rut depths. As the applied load and velocity increase, the drawbar power begins to reduce as most of the wheel traction is wasted in overcoming the motion resistance due to deeper wheel ruts that are formed. This result suggests that wheels operating in

low cohesion terrain should not be overloaded and must move at an economical velocity of not more than 10m/s or 36km/h. High velocities generate more drawbar-pull which reduces with increase in applied load. Terrain must be stabilised if plant is to move at higher velocities without losing power and protecting the terrain from the effect of deep rutting. Lower velocities on the other hand show better performance of drawbar-pull with increase in applied load for full drive conditions, but only up to a specific value of load, 6100N in this case as seen in figure 4.23. Figure 4.24 further shows the reduction of drawbar-pull output when the wheel width is reduced, presenting a simulation of higher inflation pressure for flexible tyre or smaller wheel. This signifies the importance of larger wheel/terrain contact area required in the generation of drawbar-pull.

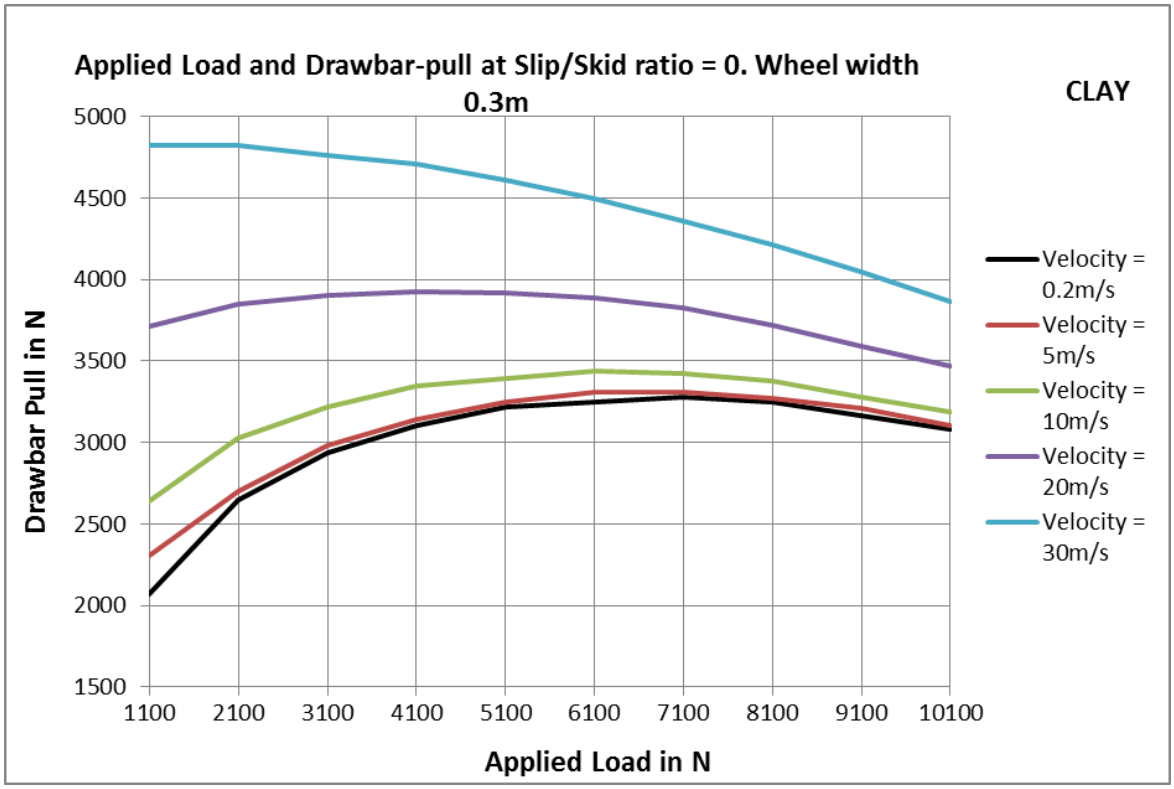

Figure 4.23: Graph showing applied load against drawbar-pull at slip/skid ratio = 0

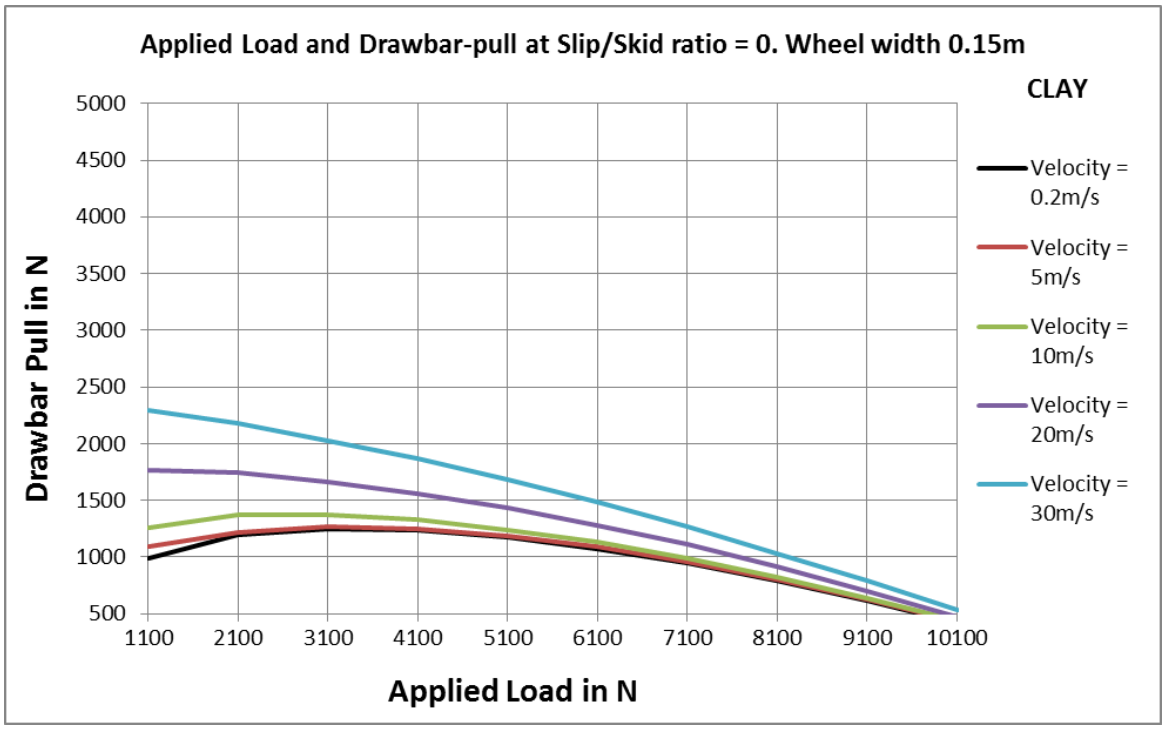

Figure 4.24: Graph showing applied load against drawbar-pull at slip/skid ratio = 0 but with smaller wheel width

4.4.5. Effect of Wheel Radius in clay terrain

The effect of increasing the wheel radius on drawbar-pull is illustrated in figure 4.25. The increase in wheel radius results in increased drawbar-pull. This is because of the increase in contact surface area which significantly reduces the pressure on the soil. This results in subsequent reduction in rut depths leading to reduced motion resistance thereby increasing the total traction and the drawbar-pull within the defined model parameters. As expected, the drawbar-pull increases with the increase in the wheel velocity because the power transferred from the engine to the wheels is not affected by resistance.

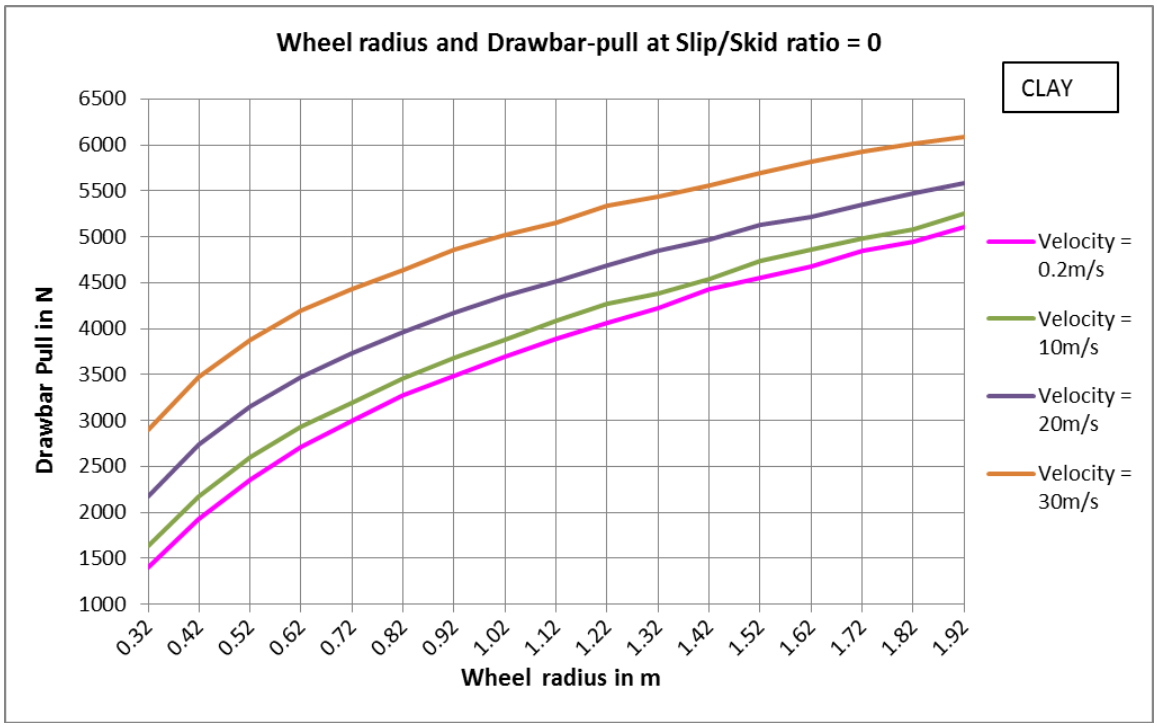

Figure 4.25: Graphs showing wheel radius against drawbar-pull at slip/skid ratio = 0

4.4.6. Effect of wheel width in clay terrain

Figure 4.26 illustrates the linear nature of the increase in drawbar-pull to the linear increase in the wheel width contact surface that results in reduced rut depths. Higher wheel velocity produces higher drawbar-pull due to reduced motion resistance results from reducing rut depths. It can be concluded from this result wheels operating in deformable or natural terrain on construction sites and haulage roads need to have wider wheel widths in order to maintain high pulling power. Wider wheels increase the contact area thereby reducing sinkage. While construction plant manufacturers produce wider tyres for off-road conditions, this model demonstrates that there are additional factors to be considered in off-road terrain management such as wheel self-weight, applied load, velocity, tyre width, tyre diameter, drawbar-pull and the overall properties and nature of the soil at specific time of operation.

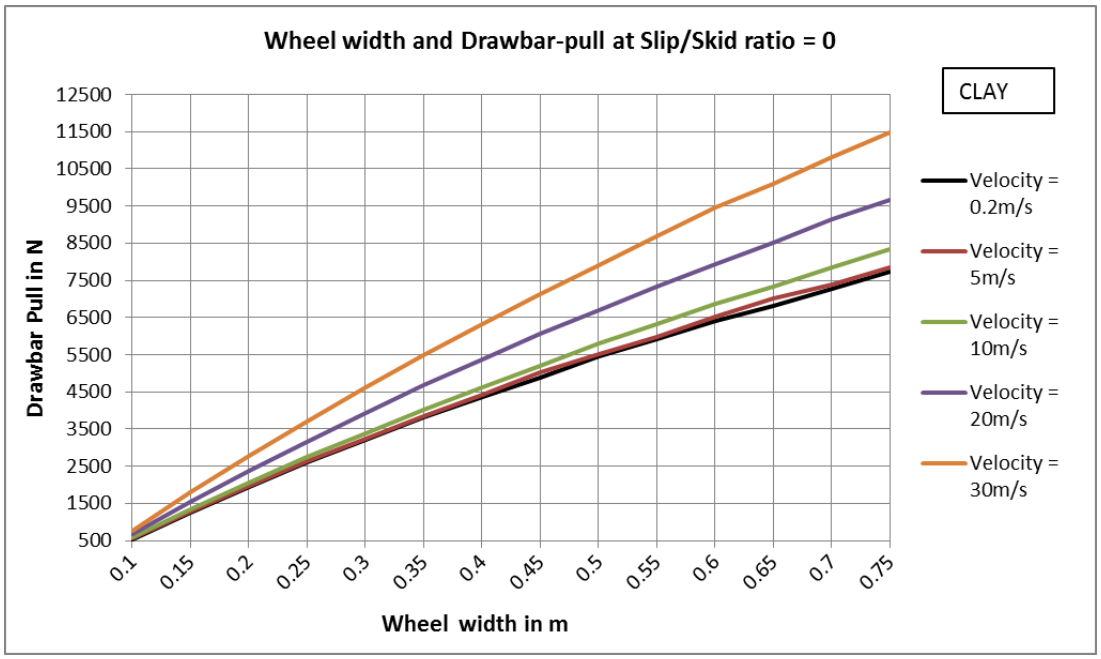

Figure 4.26: Graphs showing wheel width against drawbar-pull at slip/skid ratio = 0

4.4.7. Effect of Slip/kid wheel width in clay terrain

The effect of slip/skid ratio is illustrated in figure 4.27 below. The figure clearly illustrates that in the skid zone very little drawbar-pull is generated while the slip zones generates more drawbar-pull. This is because the braking mode produces no significant power while the driving mode generates power to the wheels which is manifested in drawbar-pull.

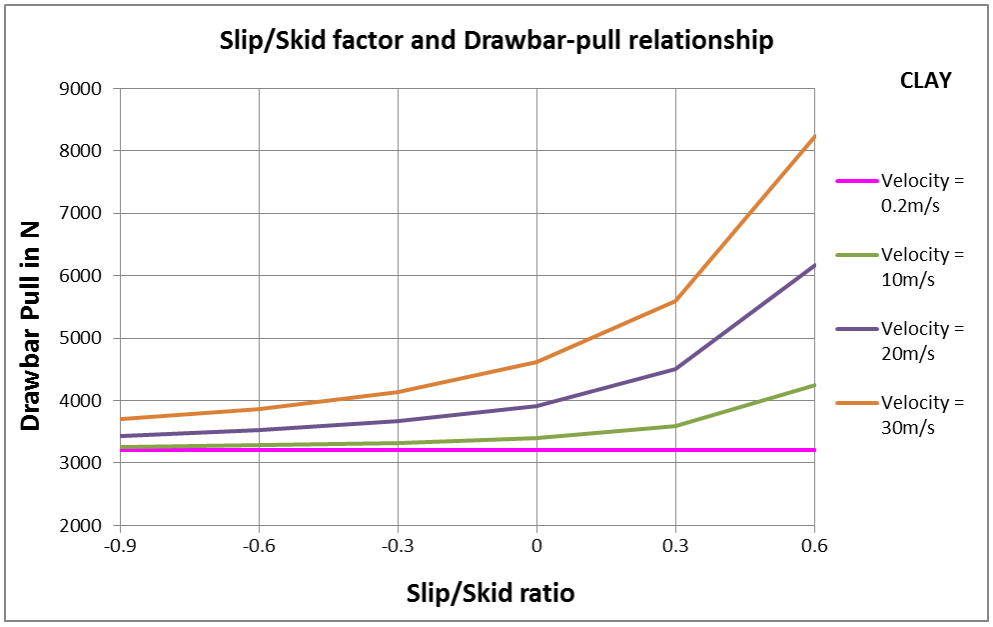

Figure 4.27: Graphs showing slip/skid ratio against drawbar-pull

- **DRAWBAR-PULL INCREASES WITH INCREASE IN WHEEL RADIUS (Slip/Skid ratio =0)**
- **HIGH VELOCITY PRODUCE HIGH DRAWBAR-PULL**

- **DRAWBAR-PULL INCREASES WITH INCREASE IN WHEEL WIDTH (Slip/Skid ratio =0)**
- **HIGH VELOCITY PRODUCE HIGH DRAWBAR-PULL**

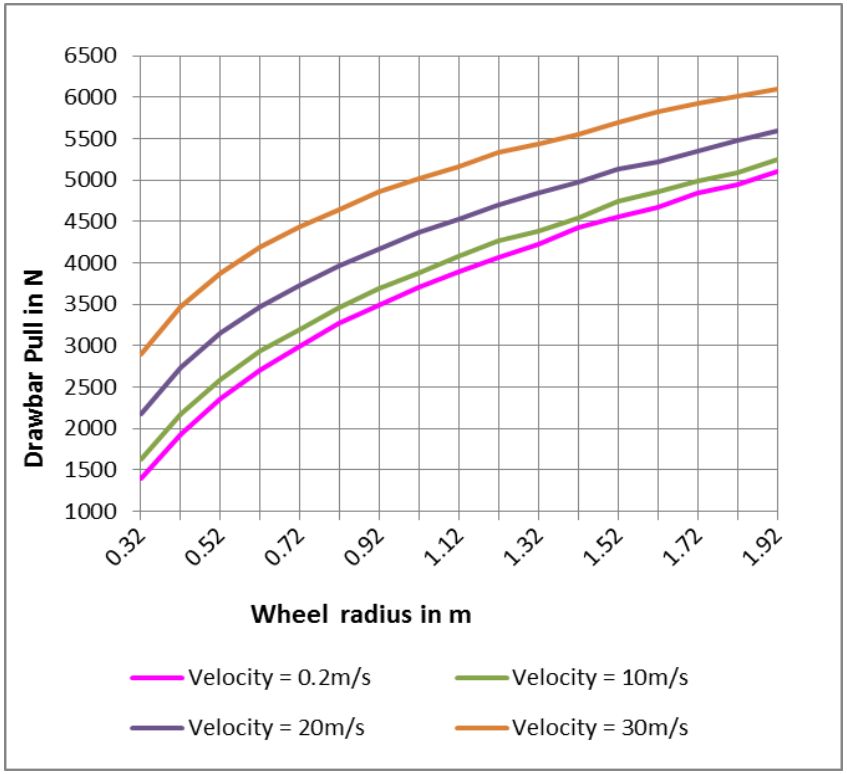

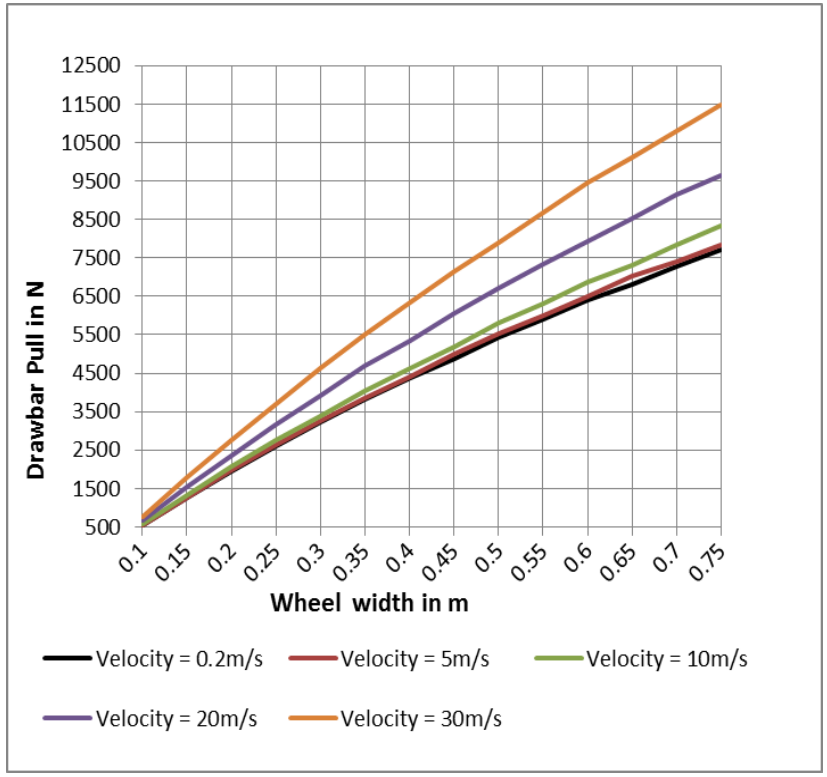

Figure 4.28: Graph showing drawbar-pull against wheel radius compared with wheel width at skid ratio = 0

.

4.5. Presentation and discussion of the model results (Sand)

4.5.1. Drawbar-pull outputs in the sandy terrain

Example 2: Generation of results for drawbar-pull for velocity 0.2m/s and slip 0.3 in sandy soil

Angle of shearing resistance	Rut depth			Eqn 4.32				Eqn 4.25	Eqn.4.28	Eqn.4.29	
φ(deg)	d (m)	d(m)	r (m)	alpha	W (N)	t (m)	φ(rad)	sigma(N/m2)	H (N)	R (N)	D (N)
15	53	0.05	0.8	0.366	5100	0.3	0.2618	3420	79	54	24
15.5	39	0.04	0.8	0.3135	5100	0.3	0.2705	3969	81	46	35
16	28	0.03	0.8	0.2654	5100	0.3	0.2793	4667	84	39	45
16.5	20	0.02	0.8	0.2241	5100	0.3	0.2880	5508	87	33	54
17	14	0.01	0.8	0.1874	5100	0.3	0.2967	6571	90	28	62
17.5	10	0.01	0.8	0.1583	5100	0.3	0.3054	7766	93	23	69
18	6	0.01	0.8	0.1226	5100	0.3	0.3142	10013	95	18	77
18.5	4	0	0.8	0.1	5100	0.3	0.3229	12255	98	15	84
19	2	0	0.8	0.0707	5100	0.3	0.3316	17321	101	10	91
19.5	1	0	0.8	0.05	5100	0.3	0.3403	24488	104	7	97
20	1	0	0.8	0.05	5100	0.3	0.3491	24488	107	7	100

Table 4.10: Example of results tabulation for sandy soils

Figure 4.29 at full drive (i=0) shows that for increase of angle of internal friction will result in increase in drawbar-pull. This however only applies to slow moving wheels because an increase in velocity results in deeper wheel rutting which requires unrealistic traction to overcome motion resistance.

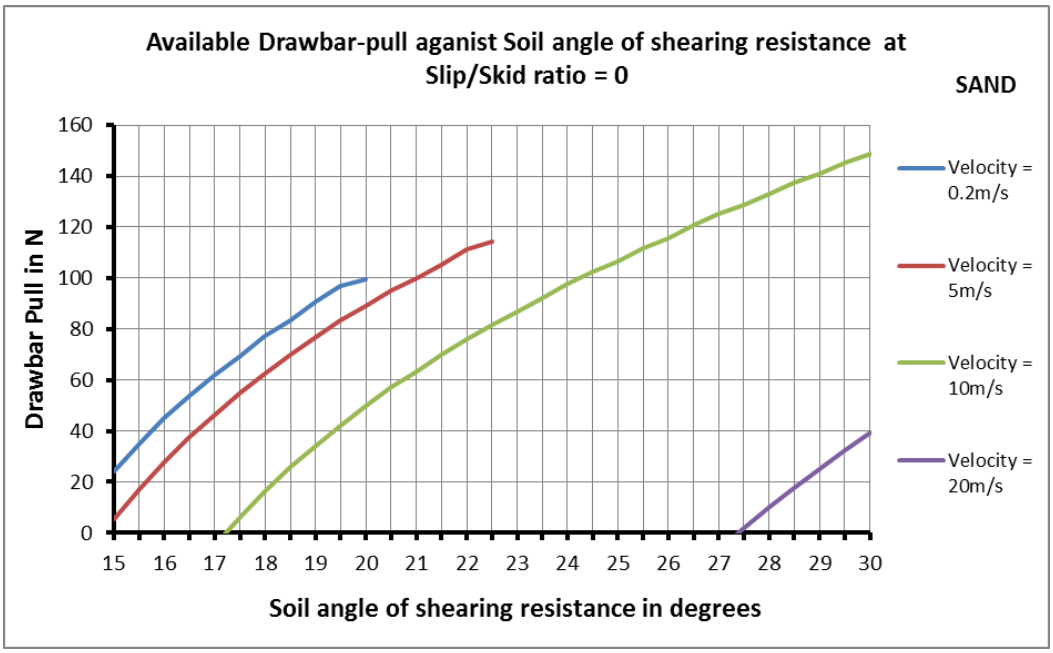

Figure 4.29: Graphs showing drawbar-pull against soil angle of shearing resistance at slip/skid ratio = 0

Figure 4.30 shows a wheel moving at a slip ratio of 0.3. Velocities of 10m/s can only be attained in soils of more than 17 degrees angle of internal friction. For velocities of 20m/s the angle of internal friction must be more than 21 degrees under the existing research parameters. Higher velocities result in the wheels digging into the ground reducing the pulling power at the wheels.

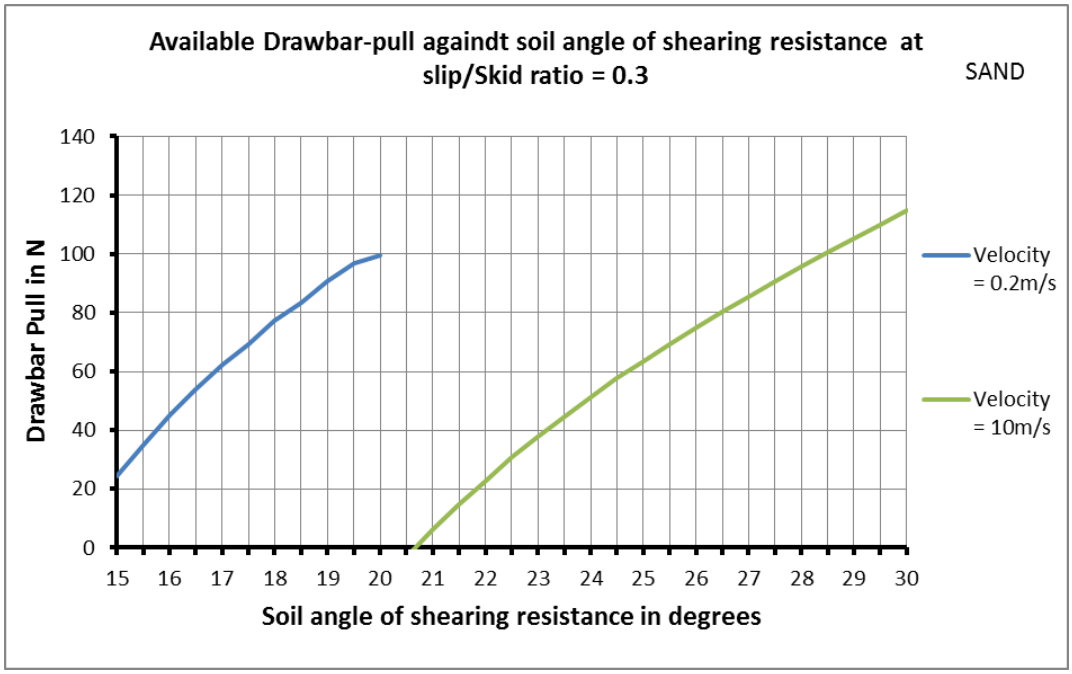

Figure 4.30: Graphs showing drawbar-pull against soil angle of shearing resistance at slip/skid ratio = 0.3

Figure 4.31 shows the wheel with slip of -0.3 in braking mode. A drawbar-pull for 0.2m/s can be attained at an angle of shearing resistance of 15 degrees under the given parameters. The minimum angle of shearing resistance required for the wheel to move at 10m/s must be more than 16 degrees. This is because as the wheel attempts to skid it will easily sink because of the loose nature of sand resulting in reduced pulling power. A bow is formed in front of the tyre as described in the literature review. Higher internal angle of friction are required to maintain drawbar-pull under skid conditions. This result suggests that soils with low angle of shearing resistances will require stabilisation and addition of moisture to make it dense otherwise it will be uneconomical for wheeled construction plant to operate in such terrain.

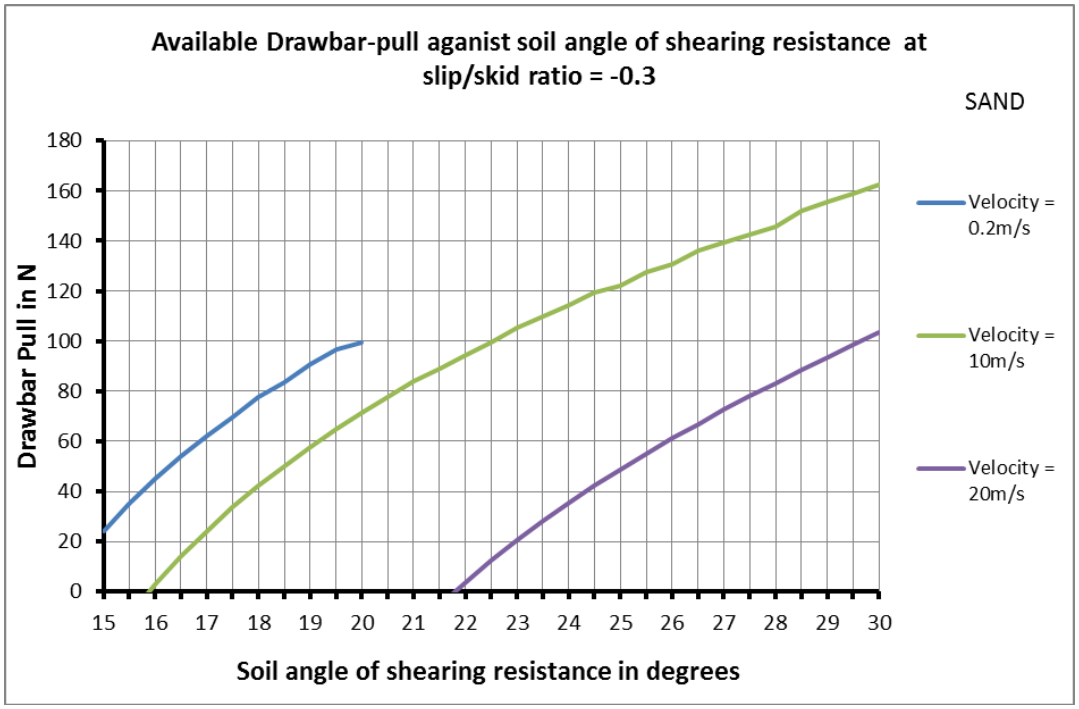

Figure 4.31: Graphs showing drawbar-pull against soil angle of shearing resistance at slip/skid ratio = -0.3

4.5.2. Effect of Applied Load in sandy terrain

The figure 4.32 below shows the effect of applied load on sand on the 0.3m wide model wheel. Reducing the wheel width to 0.15m results in reduced drawbar-pull out as shown in figure 4.33. The reduced width simulates the smaller wheel or highly inflated tyre which reduces the contact area. This result is also verified by the laboratory experiments in chapter 7.

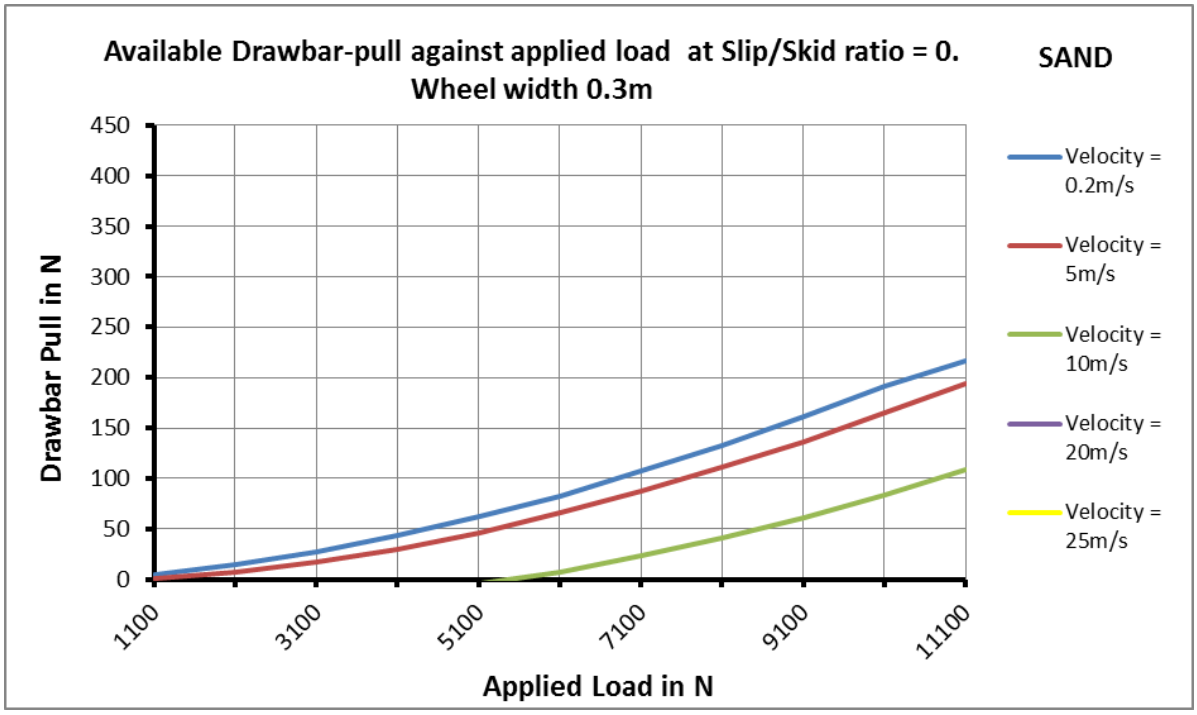

Figure 4.32: Graphs showing applied load against drawbar-pull at slip/skid ratio = 0

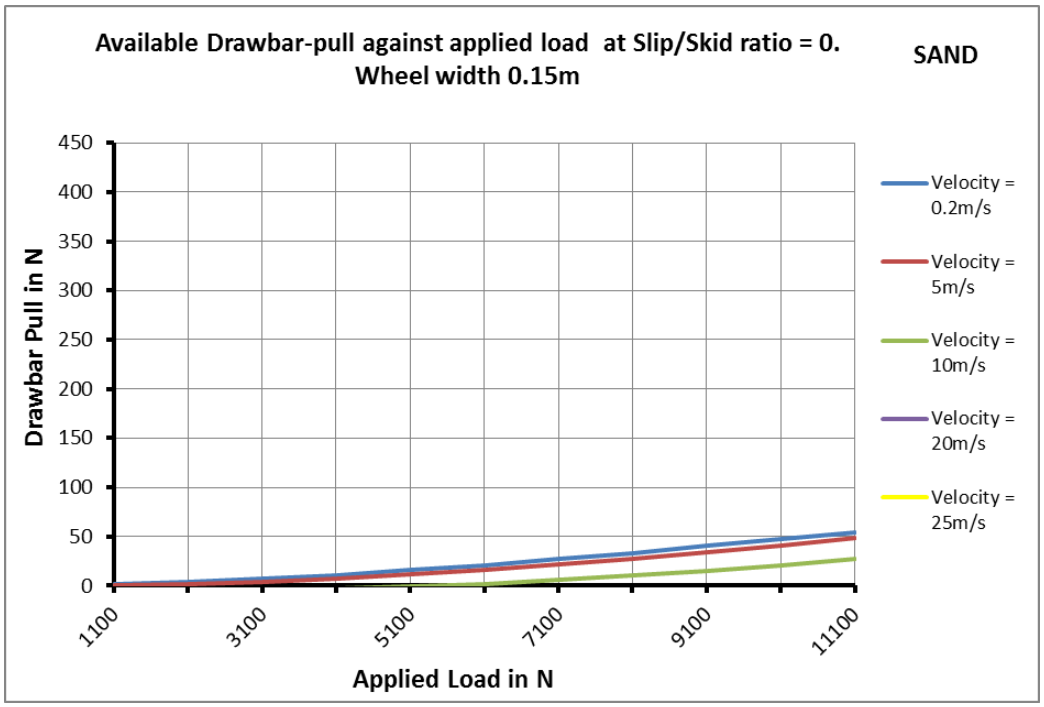

Figure 4.33: Graphs showing applied load against drawbar-pull at slip/skid ratio = 0, but with smaller tyre width

4.5.3. Effect of Wheel Radius in sandy terrain

Figure 4.34 below shows that increase in radius results in increase in drawbar-pull subject to the level of moisture content.

Figure 4.34: Graphs showing wheel radius against drawbar-pull at slip/skid ratio = 0

4.5.4. Effect of wheel self-weight in sandy terrain

Figure 4.35 below shows that increase in radius results in diminishing increase in drawbar-pull subject to the level of moisture content.

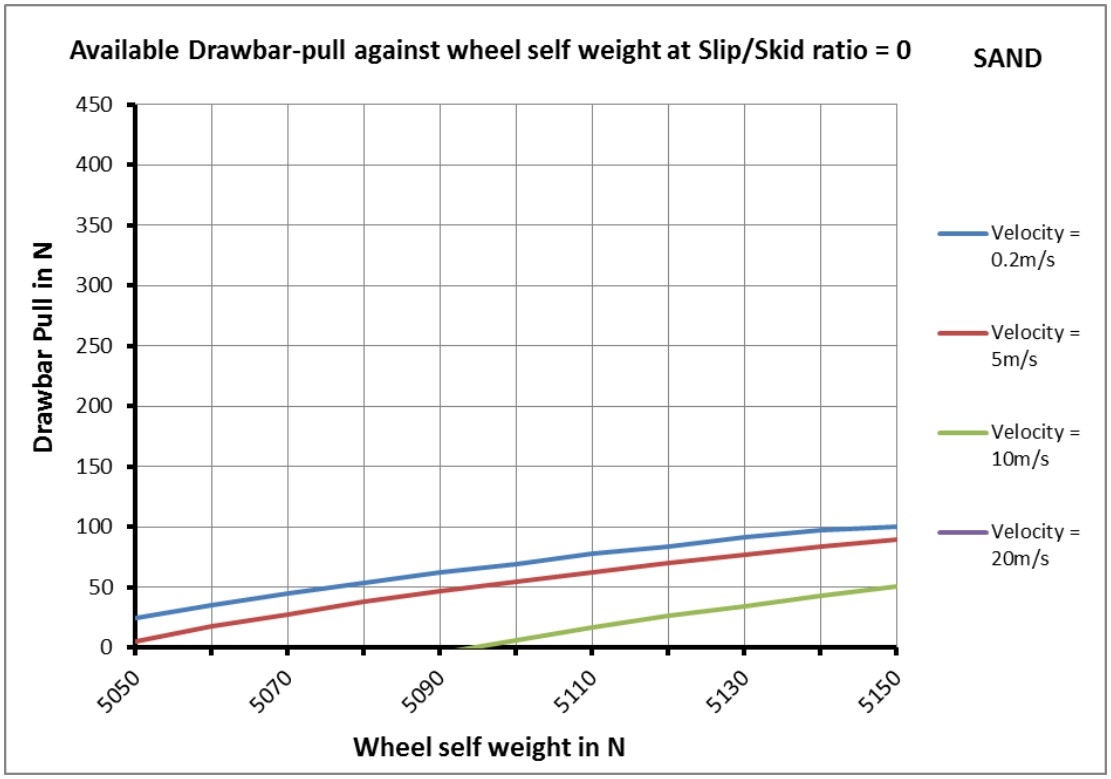

Figure 4.35: Graphs showing wheel self-weight against drawbar-pull at slip/skid ratio = 0

4.5.5 Effect of wheel width in sandy terrain

Figure 4.36 below shows that increase in radius results in increase in drawbar-pull subject to the level of moisture content. Loose sand soil has very lower cohesion value resulting in making tyre mobility extremely difficult. Addition of moisture content makes the sand soil to be more dense and stable to support vehicle mobility.

Figure 4.36: Graphs showing wheel width against drawbar-pull at slip/skid ratio = 0

4.6. Chapter summary

The following findings have been drawn based on the results of the POWERSEV mathematical model within the set boundaries of the model.

1. Increase in soil cohesion resulted in decreased rut depths which further translated into increased drawbar-pull. The increased net traction was attributed to the reduction in motion resistance.
2. Increase in wheel velocity with increasing values of soil cohesion resulted in increased drawbar-pull provided the slip/skid ratio did not exceed 0.5.
3. The results suggest that it is more efficient to operate wheeled construction plant in higher cohesive soils with relatively higher velocities. Low cohesion soils require stabilisation to avoid plant power loss due to high motion resistance. Lower wheel velocities are also recommended on this type of soil.

4. For sandy soils increase in shearing resistance angle resulted in increased drawbar-pull due to subsequent reduction in rut depth.
5. For sandy soils with low angles of internal friction (15 degrees in this case), lower velocities of the wheel are recommended in order to attain drawbar-pull or net traction effort. Higher wheel velocities resulted in the wheel digging into the soil thereby resulting in unrealistic velocities to overcome motion resistance. A typical soil bow is also formed in front of the tyre under these conditions.
6. Increasing the slip ratio in lower angles of internal friction soils resulted uneconomical drawbar-pull results. Drawbar-pull in sandy soil could only be attained at significant or higher shearing angle of resistance and significant moisture content. Velocity and slip ratio have significant influence of drawbar-pull in sandy soils.
7. From conclusion 6, it is can be seen clearly that construction sites with sandy soils characterised by low angle of shearing resistance values would require stabilisation and additional moisture in all vehicular routes/roads to avoid wheeled plant power losses during traversing on the sites. This also applies to long haulage roads characterised by natural or deformable terrain. This conclusion was been verified through the experimental procedure presented and discussed in chapters 7 and 8.
8. The wheel multi-pass effect of the wheels on the ground was mostly significant in the first two to three passes after which the increase in rut depths is insignificant. The experimental approach is recommended for establishing more accurate effects of wheel multi-pass for each particular terrain given at each time.

9. Increase in vehicle or wheel self-weight resulted in increased drawbar-pull due to the traction that it added to the wheel. Increased velocity with increased self-weight further resulted in increased drawbar-pull. This result suggests that large diameter, wider and heavier tyres must be recommended during operations on construction sites that are characterised by deformable natural terrain.

10. Increase in applied load resulted in reduced drawbar-pull particularly for the wheels moving at higher velocities. A wheel moving at lower velocity would generate some drawbar-pull which diminishes with increase in velocity. This result shows that heavily loaded wheeled construction plant operating in low cohesive or low angle of internal friction must travel at lower velocities to avoid loss in pulling power that arises from deep wheel rutting.

11. Increase in wheel radius in relation to contact surface reduced the resultant rut depth. This effect increased the drawbar-pull values at the wheel. Higher velocities would transfer the traction effort to the wheels as motion resistance in reduced.
12. Increase in wheel width increases wheel contact surface which reduces rut depths resulting in increased drawbar-pull. Motion resistance is also reduced in this case.

13. The results show that wider wheels would produce higher drawbar-pull. The results suggests that wheeled construction plant traversing in off-road construction sites and similar haulage roads should use wider wheels as much as possible in order to attain maximum pulling power efficiency.

Reducing wheel pressure like in agriculture may not be desirable due to heavy loads carried by construction plant.

14. Drawbar-pull will increase with slips of up to 0.4. Slips beyond this ratio signify higher velocities which result in deep rutting thereby reducing drawbar-pull. Increase in wheel skids resulted in gradual reduction in drawbar-pull. Operator awareness is important in this case in order to save on fuel consumption and the wear and tear rate of the engine.

15. These model results have been verified by computational analysis and scaled down laboratory based experiments which are discussed in chapters 5, 6 and 7

CHAPTER 5

MATHEMATICAL MODEL VERIFICATION STAGE 1 FOR THE RIGID WHEEL MODEL

COMPUTATIONAL ANALYSIS

5.0. CHAPTER 5

MATHEMATICAL MODEL VERIFICATION STAGE 1: COMPUTATIONAL ANALYSIS.

5.1. Introduction

The aim of this chapter is to present and demonstrate that a flexible tyre can behave in a similar manner to a rigid wheel when fully inflated and when operating in softer and deformable ground. The chapter also demonstrates that a rigid wheel can be used to analyse the performance of a flexible tyre under certain circumstances described later in the chapter. The analysis contained in this chapter strongly supports the deployment of the pseudo rigid wheel in the mathematical modelling part contained in chapter 4. This chapter also constitutes the first part of the 3 stage robust model verification adopted for this research.

Model verification is critical for the validation of any research results. The mathematical model presented in chapter 4 is based on a pseudo or theoretical wheel operating in clay and sandy soil whose results require full verification. Computational analysis involves the processing of data (usually real data) to generate a model that will predict the behaviour of factors or parameters under consideration. Semi-empirical methods are very attractive methods of model verification because they provide good understanding of the physics underlying the problem and yet they are computationally effective for full scale analysis, Sandu and Senatore (2011). As mentioned in the research design and methods chapter, computational analysis in terramechanics has advantages over other

verification methods namely field tests and empirical tests as described in chapter 3.

5.1.1. Procedure

The flexible real tyre data was computed into terramechanics equations outlined later in the chapter to obtain tyre sinkage, tyre contact length and tyre deflection. The analysis took the powerful form of isolated analysis by introducing different loads and different terrain parameters in order to demarcate the border line between rigid and flexible mode of the tyre. Real data of the flexible wheel was run on the two terrains and the results were recorded and plotted in graphical format. The pseudo mathematical wheel data is also ran in the same terrain with results recorded and plotted graphically. The results of the two were then compared to study the pattern of the behaviour and similarities of the wheels and terrain provided.

5.1.2. Characteristics of computational analysis

- Unlimited model configurations
- The results are based on real data obtained through field experiments processed using computational tools such as Mathcad, Mat lab, Mathematica and the like.
- They have proved to be accurate in predicting full scale results.
- They are far less expensive compared to laboratory and field experiments.
- Parameters can be easily changed in order to perform isolated analysis of variables.

5.2. Source and nature of experimental data for computational analysis

5.2.1. Experimental tyre data

The data for verifying the mathematical model results was obtained with permission from the Canadian Defence Department research results published in

Wong (2010). The radial tyre used was a 12.5/75R20 which has a diameter of 1m and a width of 0.327m. It also had a sectional height of 0.245m. The parameters for tyre pressure and average ground pressure are given in table 5.1.

EXPERIMENTAL TYRE PROPERTIES AND DATA *Tyre source: Canadian Defence Department*	
Flexible Tyre type	2.5/75 R20
Flexible Tyre diameter	1m
Flexible Tyre width	0.327m
Flexible Tyre section height	0.245m
Tyre pressure	150kPa to 600kPa (22PSI to 87PSI)
Tyre Load	10kN to 25kN

Table 5.1: Experimental tyre data, Wong (2010)

5.2.2. Mathematical model tyre Data

The data for the mathematical model tyre remains the same as in chapter 4 (1.8m diameter and 0.3m wide) except that in this case it is assumed to be flexible in flexible nature in order to identify the parameters that would create the boundary between the rigid mode and flexible mode. The results obtained from running the two tyres computationally and mathematically were compared in order to ascertain the pattern of behaviour between the two sets of tyres when run in the same soil/terrain profiles.

MATHEMATICAL MODEL TYRE PROPERTIES AND DATA	
Flexible Tyre type	1m radial tyre
Flexible Tyre diameter	1.8m
Flexible Tyre width	0.30m
Flexible Tyre section height	0.245m
Tyre pressure	150kPa to 600kPa (22PSI to 87PSI)
Tyre Load	10kN to 25kN

Table 5.2: Mathematical model tyre data

5.2.3. Experimental and modelling soil data

The data used for the soil was again based on experimental data obtained from the Canadian Defence Department published in Wong (2010). The same data was used for the mathematical model in order to compare the performance of the two tyre operations under similar conditions. The soil data is in two parts. The first one is the medium profile soil which has a higher value of soil cohesion and internal shearing angle. This soil profile is therefore harder and more stable than the second one. The second soil profile is clayey in nature and has lower values of soil cohesion and angle of shearing resistance. The data was originally obtained experimentally and subsequently used for computation analysis using the NWVPM for evaluation of tyre performance, a study that is not related to this research. The NWVPM is a computer aided practical tool used for parametric analysis in off-road vehicle performance and design Wong (2010).

EXPERIMENTAL AND MATHEMATICAL MODEL SOIL PROPERTIES AND DATA: MEDIUM SOIL ***Tyre source: Canadian Defence Department***	
Soil cohesion (C)	8.62KPa
Angle of shearing resistance (Ø):	22.5^0
Pressure-sinkage parameter 1 (K_c)	$29.76kN/m^{n+1}$
Pressure-sinkage parameter 2 (K_ϕ)	$2083kN/m^{n+1}$
Exponent of sinkage (n)	0.8
Shear deformation parameter (K)	0.0254m

Table 5.3: Experimental and mathematical model medium soil properties and data, Wong (2010)

EXPERIMENTAL AND MATHEMATICAL MODEL SOIL PROPERTIES AND DATA: CLAYEY SOIL *Tyre source: Canadian Defence department*	
Soil cohesion (C)	7.58KPa
Angle of shearing resistance (Ø):	14^0
Pressure-sinkage parameter 1 (K_c)	$30.08kN/m^{n+1}$
Pressure-sinkage parameter 2 (K_Φ)	$499.7kN/m^{n+1}$
Exponent of sinkage (n)	0.6
Shear deformation parameter (K)	0.0254m

Table 5.4: Experimental and mathematical model clayey soil properties and data, Wong (2010)

5.3. Average ground pressure and inflation pressure

If the average ground pressure p_g derived from a generalised deflection chart (figure 5.1) for a given tyre at a particular combination of inflation pressures and load is greater than p_{gcr} as determined by equation 5.2 then the tyre is assumed to be in the rigid mode of operation Wong (2010). On the other hand if the value of p_g is less than p_{gcr} the tyre is assumed to be in elastic mode of operation. At this stage the lower portion of the tyre circumference in contact with the terrain is assumed to be flattened. Under these circumstances the ground contact pressure acting on the flat portion is assumed to be equal to $p_{g.}$ Wong (2010). Figure 5.1 below shows the tyre deflection chart. Figure 5.2 shows the average ground pressure and inflation pressures for various loads as obtained from Wong (2010)

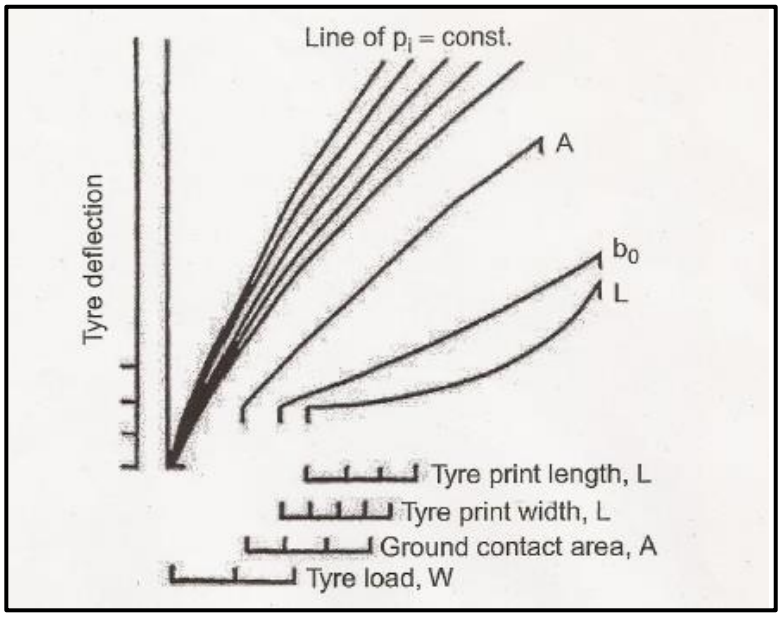

Figure 5.1: Generalised tyre deflection chart Wong (2010)

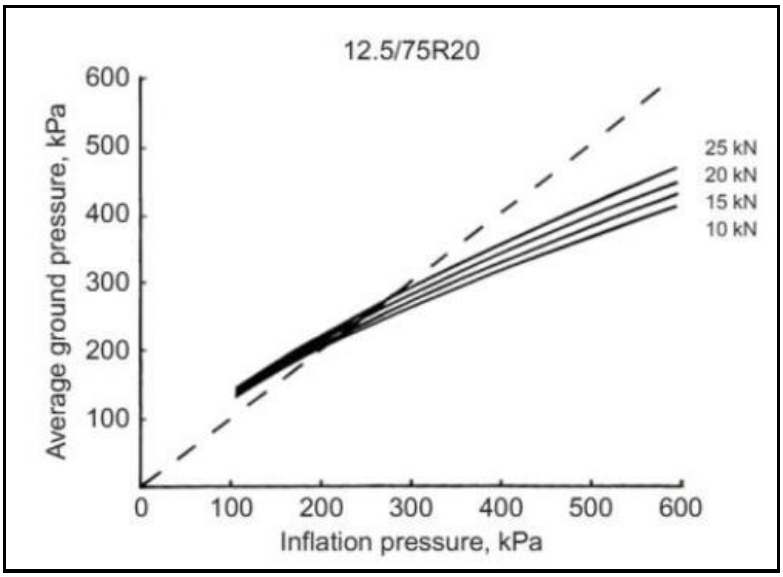

Figure 5.2: Average ground pressure and inflation pressures for various loads derived from deflection chart in figure 5.1 Wong (2010)

The above principles are based on the reasoning that if the terrain is relatively soft and the sum of the inflation pressure p_i and the pressure produced by the carcass stiffness p_c is greater than the pressure exerted by the terrain at the lowest point of the tyre circumference, the tyre can be assumed to remain round like a rigid rim, (Wong, 2010). On the other hand if the ground is firm and the sum of p_i and p_c is less than the critical ground pressure $_{pgcr}$ then the portion of the tyre in contact

with the terrain will have a significant deflection and the tyre is assumed to be in an elastic or flexible mode of operation. If the tyre behaves like a rigid rim, using the Bekker pressure sinkage equation, the normal pressure p_g at the lowest point of contact is given by equation 5.1, Wong (2010).

$$p_g = \left[\frac{k_c}{b} + k_\emptyset\right] z_r^n \qquad \text{Eqn 5.1}$$

The critical ground pressure formula is given in equation 5.2

$$p_{gcr} = \left[\frac{k_c}{b} + k_\emptyset\right]^{1/(2n+1)} \left[\frac{3W}{(3-n)b_{ti}\sqrt{D}}\right]^{2n/(2n+1)} \qquad \text{Eqn 5.2}$$

The wheel sinkage for rigid wheel is given by equation 5.3

$$z_r = \left[\frac{3W}{b_{ti}(3-n)\left(k_c/b_{ti}+k_\emptyset\right)\sqrt{D}}\right]^{2/2n+1} \qquad \text{Eqn 5.3}$$

The wheel sinkage for flexible/elastic wheel is given by equation 5.4

$$z_e = \left[\frac{p_g}{k_c/b+k_\emptyset}\right]^{1/n} \qquad \text{Eqn 5.4}$$

The contact length for the rigid wheel is given by equation 5.5

$$l_t = \sqrt{(D/2)^2 - (D/2 - z_r)^2} \qquad \text{Eqn 5.5}$$

The contact length for the flexible wheel is given by equation 5.6

$$l_t = \frac{W}{b_{ti}p_g} \qquad \text{Eqn 5.6}$$

The deflection of the flexible tyre is given by equation 5.7

$$\delta_t = D/2 - \sqrt{(D/2)^2 - (l_t/2)^2} \qquad \text{Eqn 5.7}$$

All the description of symbols used in the equations above can be found in the nomenclature section. Figures 1.1, 1.2 and 6.1 further demonstrate the notation used in these equations.

5.4. Procedure for classifying rigid and flexible wheels.

Using equation 5.2 the critical ground pressure was calculated and compared with average ground pressure which was derived from figure 5.2. Figure 5.2 was developed from the generalised deflection chart in figure 5.1. The average ground pressure was derived from chart's Y-axis from the given inflation pressure from the X-axis in figure 5.2.

Results obtained from the equations 5.3 to 5.7 were all used to compare the behaviour of the flexible tyre and rigid tyre with the critical ground pressure being the boundary line. The wheel sinkage, contact length and deflection were calculated based on the rigid and flexible wheel status. Figures 5.3 to 5.22 illustrate the behaviour of flexible tyre as it translates into rigid mode based on the increasing values of tyre pressure. The transition of the modes can be clearly seen in the figures illustrated from figure 5.3 to 5.28. It must be noted at this stage that a rigid wheel does not experience any significant deflection thereby pushing soil underneath down with negligible or no deflection. When the tyre is in flexible mode it will experience deflection due to the higher pressure from the ground than in the tyre. As the tyre pressure increases the deflection reduces and until it becomes negligible. The contact length also reduces with increased tyre pressure. The contact length is maximum at lowest tyre pressure possible and highest critical ground pressure. A rigid wheel has negligible contact length. The entire analysis is

covered in figures 5.3 to 5.22. Table 5.5 provides a typical example of the iterative data processed initially in Mathcad and eventually exported to Microsoft excel for fine graphical production.

5.5. Computational analysis of the experimental tyre in medium (Higher cohesion soil) soil.

The experimental tyre was run on the medium and clayey soil using information given in tables 5.1, 5.3 and 5.4.

5.5.1. Experimental tyre with 25kN load in higher cohesion soil

		EXPERIMENT TYRE SET 1: 25KN					
Tyre type: 12.5/75R20							
Normal load: 25KN							
Inflation pressure: 150 - 600Kpa							
Tyre diameter: 1m							
Section height: 0.245m							
Tyre width: 0.327							
Pressure sinkage parameters: K_c=29.76KN/m^2, K_ϕ=2083 KN/m^3 and n=0.8, D=1m							
Critical ground pressure: 335Kpa							
Medium soil							
Inflation Pressure	**AV Pg**	**Contact length**	**Sinkage**	**Deflection**			
150	180	0.425	0.044	0.047			
200	220	0.348	0.057	0.031			
250	260	0.294	0.070	2.20E-02			
300	290	0.264	0.080	0.018			
						0.095m	zr
350	330	0.207	0.095	0.011			
400	360	0.204	0.095	0.011			
450	390	0.201	0.095	1.000E-02			
500	420	0.199	0.095	1.000E-02			
550	450	0.197	0.095	9.80E-03			
600	480	0.196	0.095	9.70E-03			

Table 5.5: Typical tabular format of experimental results for the 25kN load in higher cohesion soil

Experimental tyre with 25kN load in higher cohesion soil

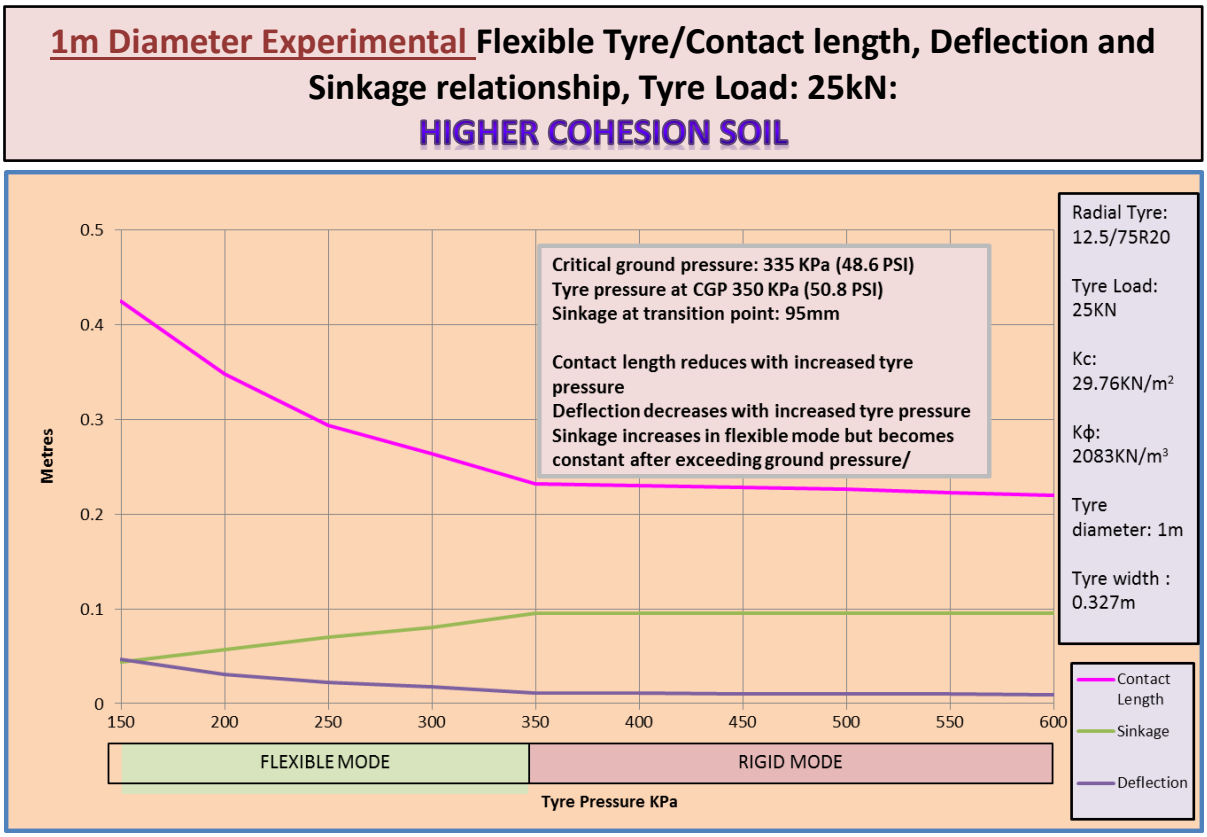

Figure 5.3: Experimental tyre under 25kN load in higher cohesion soil

From figure 5.3 above the following results and interpretation were derived:

The tyre remains in flexible mode until its pressure exceeds 335KPa which is the critical ground pressure. This graph was processed from the data provided in table 5.5.

5.5.1.1. Tyre Contact Length

The contact length reduces with increase in tyre pressure in the flexible mode. In the rigid mode which takes effect after the tyre pressure exceeds the critical ground pressure, the contact length remains constant even with increase in tyre pressure. The tyre behaves like a rigid rim because the tyre pressure has no more significant effect on contact length.

5.5.1.2. Tyre Sinkage

The tyre sinkage increases with increase in tyre pressure in the flexible mode. The tyre sinkage remains constant with increase in tyre pressure in the rigid mode. Tyre sinkage is minimal with longer contact length during the flexible mode. In the rigid mode both parameters are constant. Traction can be easily maximised in the flexible mode as compared to the rigid mode. Other factors need to be considered for traction efficiency in the rigid mode, these include velocity, slip ratio, tyre width, tyre radius and terrain profile.

5.5.1.3. Tyre Deflection

The tyre deflection decreases with increase in tyre pressure in the flexible mode. The tyre deflection remains constant in the rigid mode thereby behaving like a rigid wheel. The graph above demonstrates that deflection is directly related to contact length and sinkage. The graph in figure 5.3 above also demonstrates the three parameters gradually change with tyre pressure in the flexible mode but they all remain constant after entering the rigid mode.

A fully inflated tyre will behave like a rigid wheel thereby justifying the use of the rigid wheel based mathematical model presented in chapter 4. The tyre inflation guide from Goodyear as presented in appendix 19 and 20 indicates that some heavy duty trucks need an average tyre pressure of 102PSI or 700KPa when operating in off-road conditions. This inflation pressure is higher than the average provided in the graphs generated through the mathematical model.

5.5.2. Experimental tyre with 20kN load in higher cohesion soil

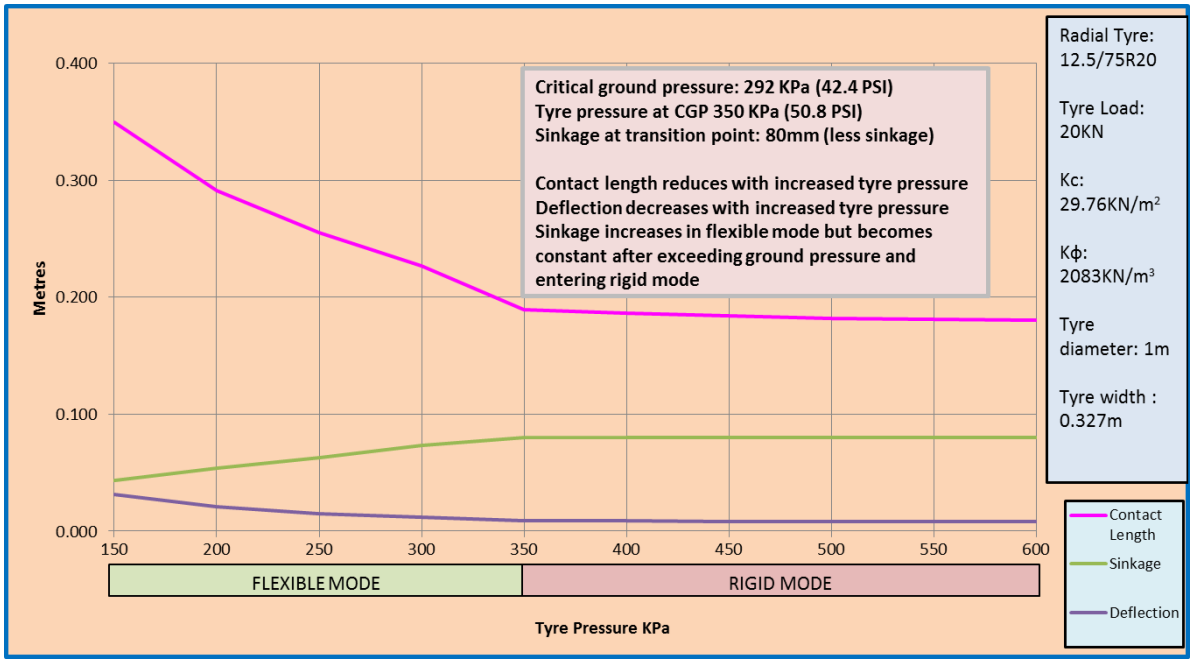

Figure 5.4: Experimental tyre under 20kN load in higher cohesion soil

The contact length, sinkage and deflection graphs and interpretation in figure 5.4 above are very similar to those discussed for the 25kN load graph with the following exceptions: Reduction in the load results in reduced sinkage from 95mm for the 25kN load to 80mm for the 20kN load. 80mm sinkage is the transition point from flexible mode to rigid wheel model.

5.5.3. Experimental tyre with 15kN load in higher cohesion soil

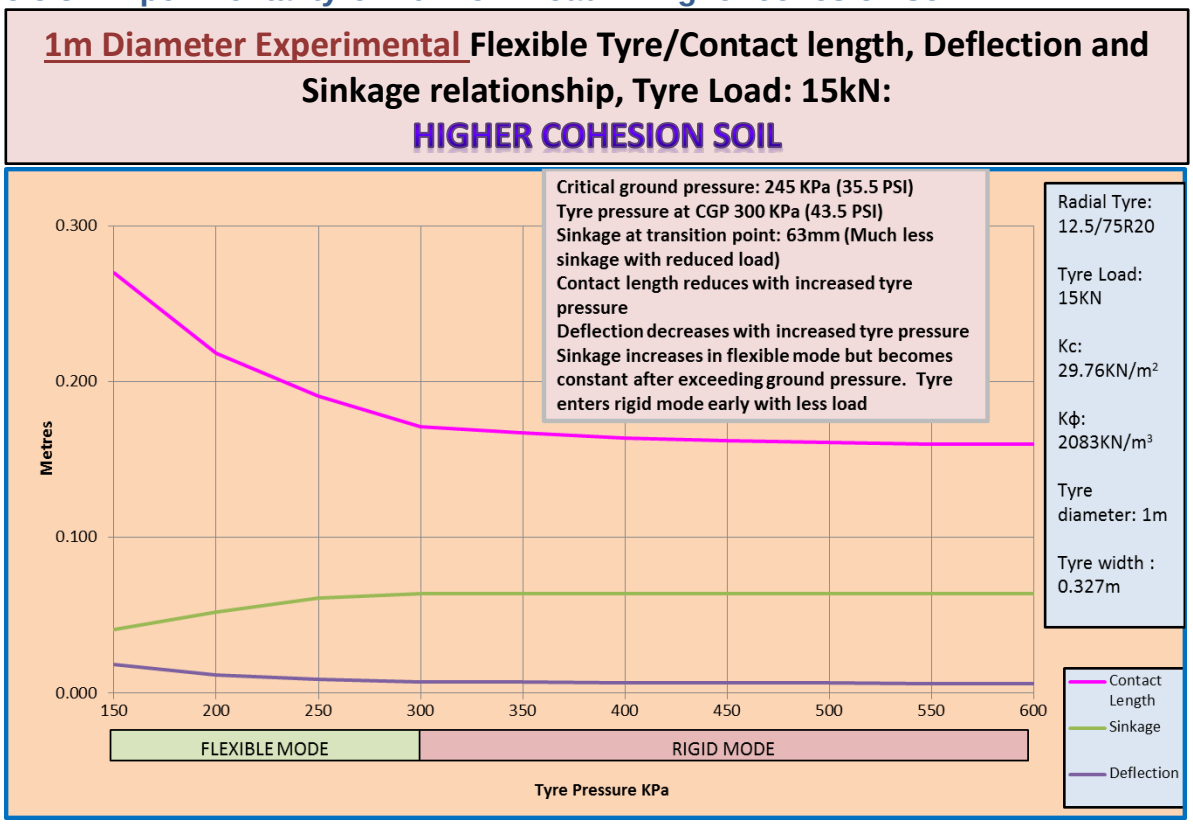

Figure 5.5: Experimental tyre under 15kN load in higher cohesion soil

The contact length, sinkage and deflection graphs and interpretation in figure 5.5 above are very similar to those discussed for the 25kN load in slide with the following exceptions: Reduction in the load results in reduced sinkage from 80mm for the 20kN load to 63mm for the 15kN load. 63mm sinkage is the transition point from flexible to rigid wheel format.

The tyre pressure at the transition point is 200kPa (29PSI) for the 10kN load. This is because reduced load results in less pressure thereby reducing the deflection and contact length. The tyre enters the rigid mode earlier than in the 25kN load and 20kN load. Wider contact length is also influenced by higher loads on more stable terrain. With reduced load, there is reduced pressure exerted on the ground resulting in the tyre operating in rigid mode for most of the time that is made to

make a complete run. This load provides the shortest flexible mode for the tyre as shown in the next three slides. The models accuracy for the contact length for this load is not as good as compared to the other three loads.

5.5.4. Experimental tyre with 10kN load in higher cohesion soil

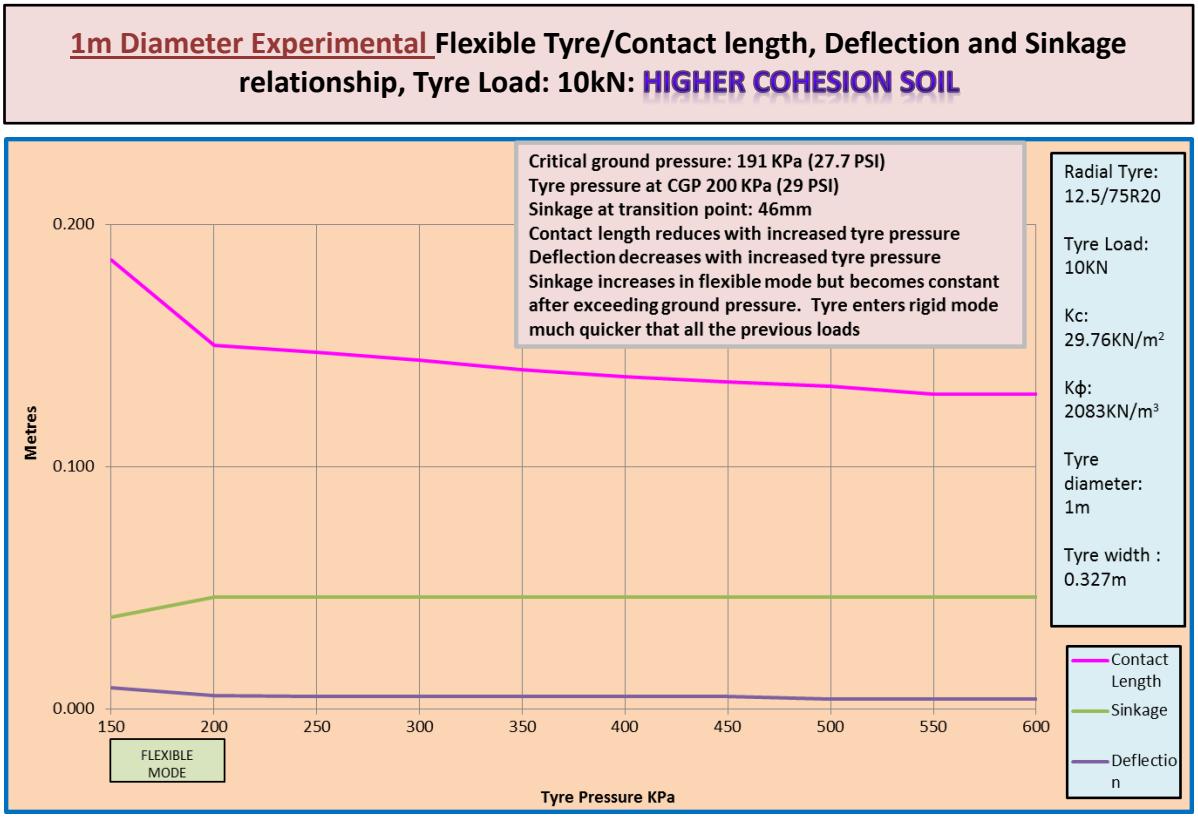

Figure 5.6: Experimental tyre under 10kN load in higher cohesion soil

The contact length, sinkage and deflection graphs and interpretation are very similar to those discussed for the 25kN load slide with the following exceptions: Reduction in the load results in reduced sinkage from 63mm for the 15kN load to 46mm for the 10kN load. 46mm sinkage is the transition point from flexible to rigid wheel format. Contact length graph is not as accurate as the other two graphs.

5.5.5. Experimental tyre contact length analysis for all loads higher cohesion soil

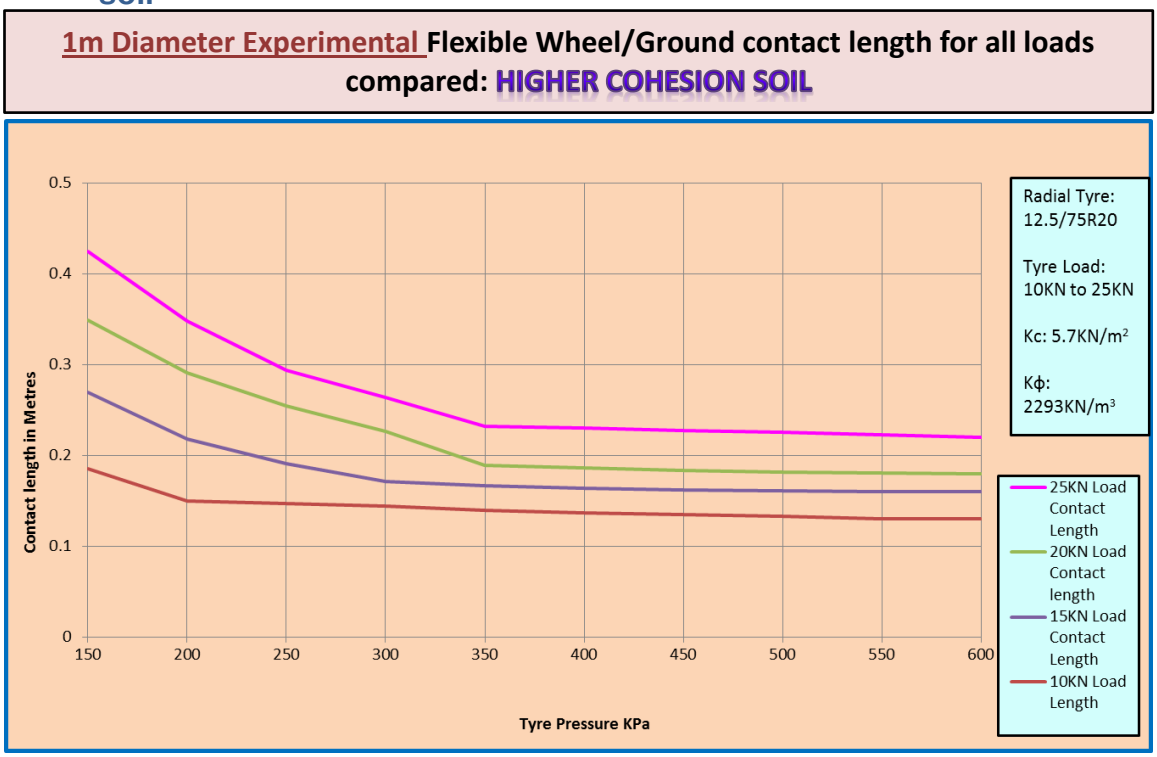

Figure 5.7: Experimental tyre contact length analysis for all loads in higher cohesion soil

5.5.6. Experimental tyre wheel sinkage analysis for all loads in higher cohesion soil

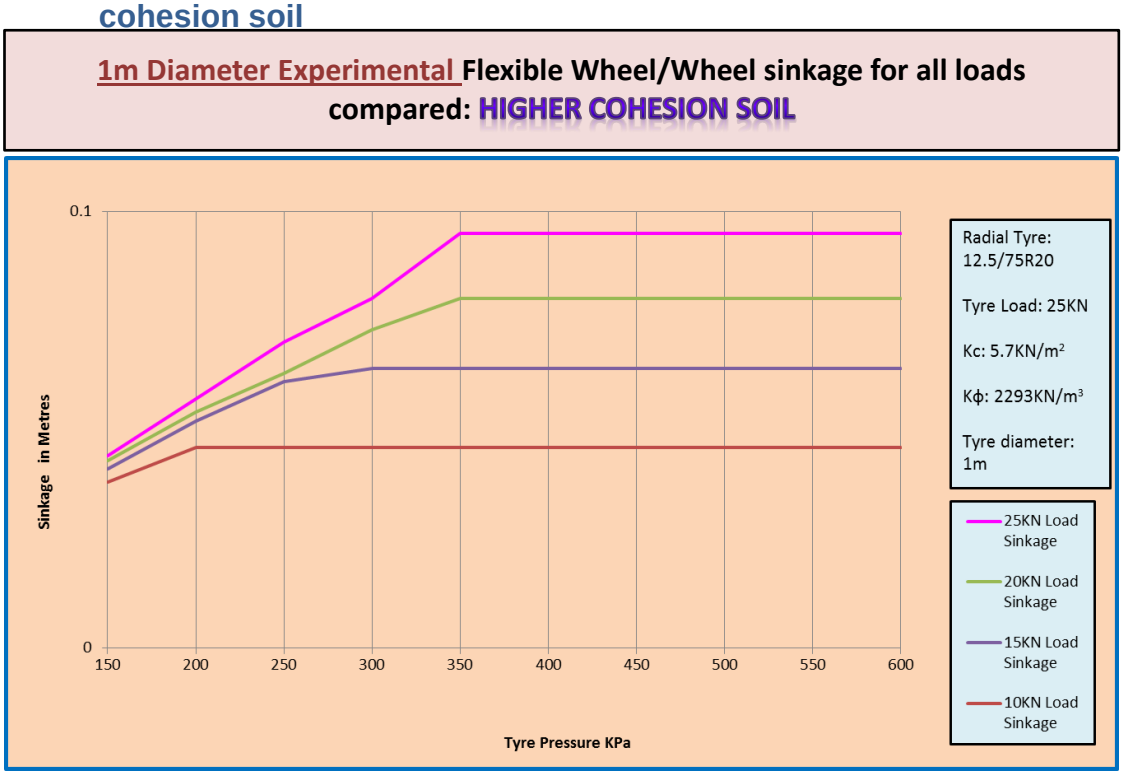

Figure 5.8: Experimental tyre sinkage analysis for all loads in higher cohesion soil

5.5.7. Experimental tyre deflection for all loads higher cohesion soil

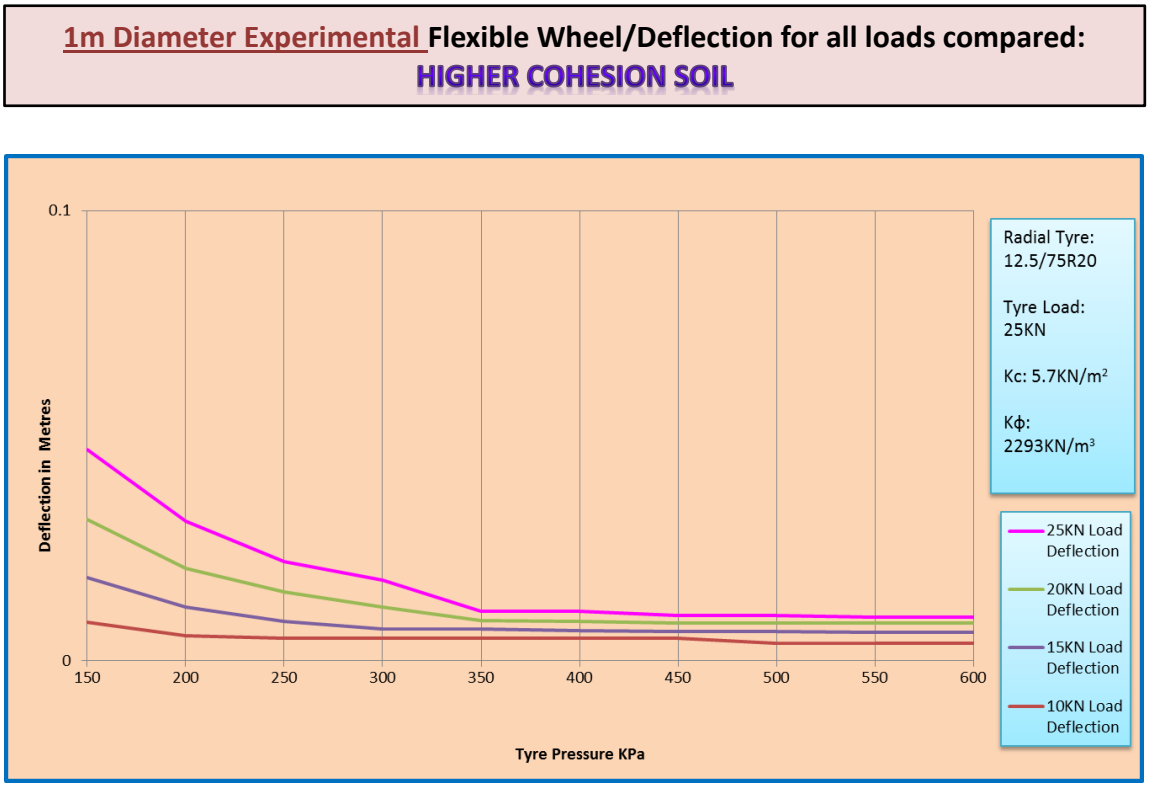

Figure 5.9: Experimental tyre deflection analysis for all loads in higher cohesion soil

Figure 5.7 to 5.9 present combined graphical summaries of the results in order to see the effect of isolated analysis from a broader perspective.

5.6. Computational analysis of the experimental tyre in clayey (Lower cohesion) soil.

5.6.1. Experimental tyre with 25kN load in lower cohesion soil

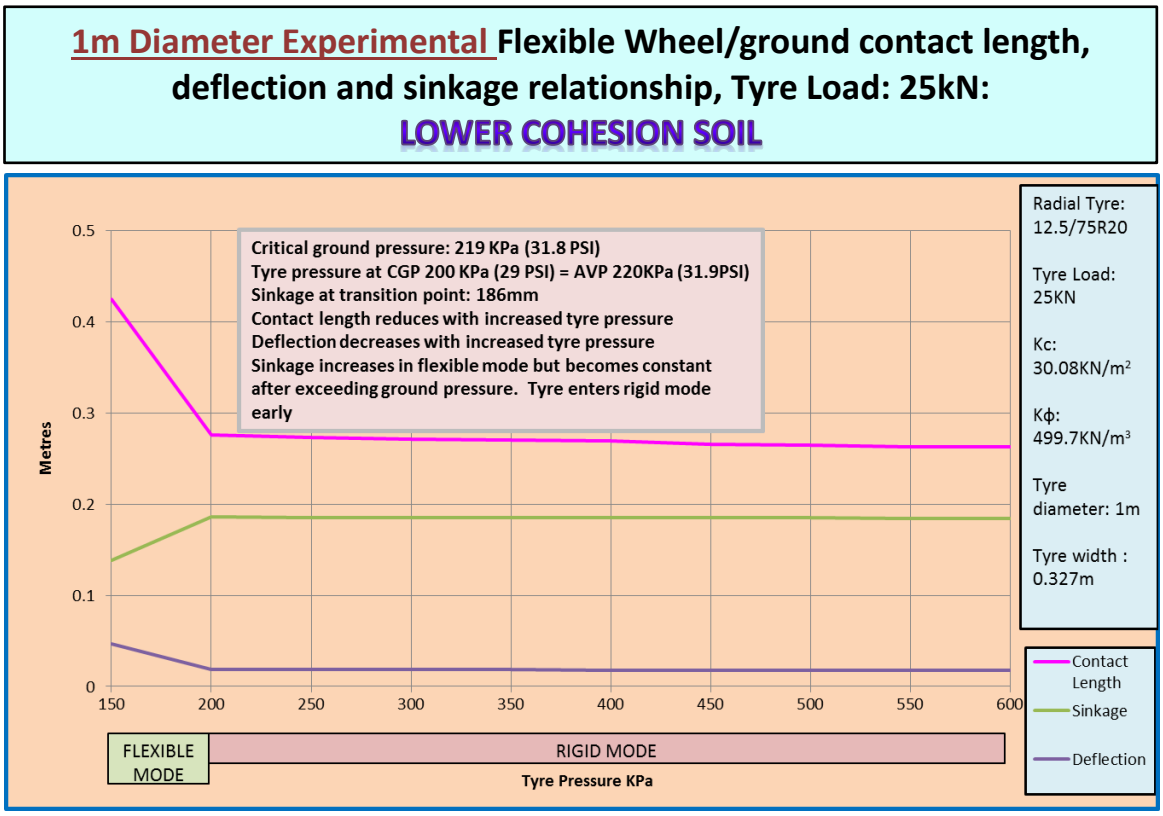

Figure 5.10: Experimental tyre under 25kN load in lower cohesion soil

The contact length, sinkage and deflection graphs and interpretation are very similar to those discussed for the tyre operating in high cohesion soil but with the following exceptions as shown in figure 5.10: In the low value cohesion soil, the sinkage values are deeper and more immediate than in the higher cohesion soil. The contact length, deflection and deflection only vary for a short phase in the flexible mode after which the tyre enters in rigid mode. The gradient of the graphs is also steep due to the combination of high load, low soil cohesion and low shearing angle.

This result suggests that the rigid wheel mathematical model is best suited in the estimation of flexible tyre plant performance operating in deformable ground particularly in low cohesion soils.

The tyre enters the rigid mode after 220kPa (31.9 PSI) which represents a sinkage of 186mm. This tyre pressure is too low to run tyres for heavy equipment hence the tyres will need to have higher pressure resulting in rigid mode. All parameters are not affected by the increase in tyre pressure after the tyre switches from flexible mode to rigid mode which takes effect after overcoming the critical ground pressure.

5.6.2. Experimental tyre with 20kN load in lower cohesion soil

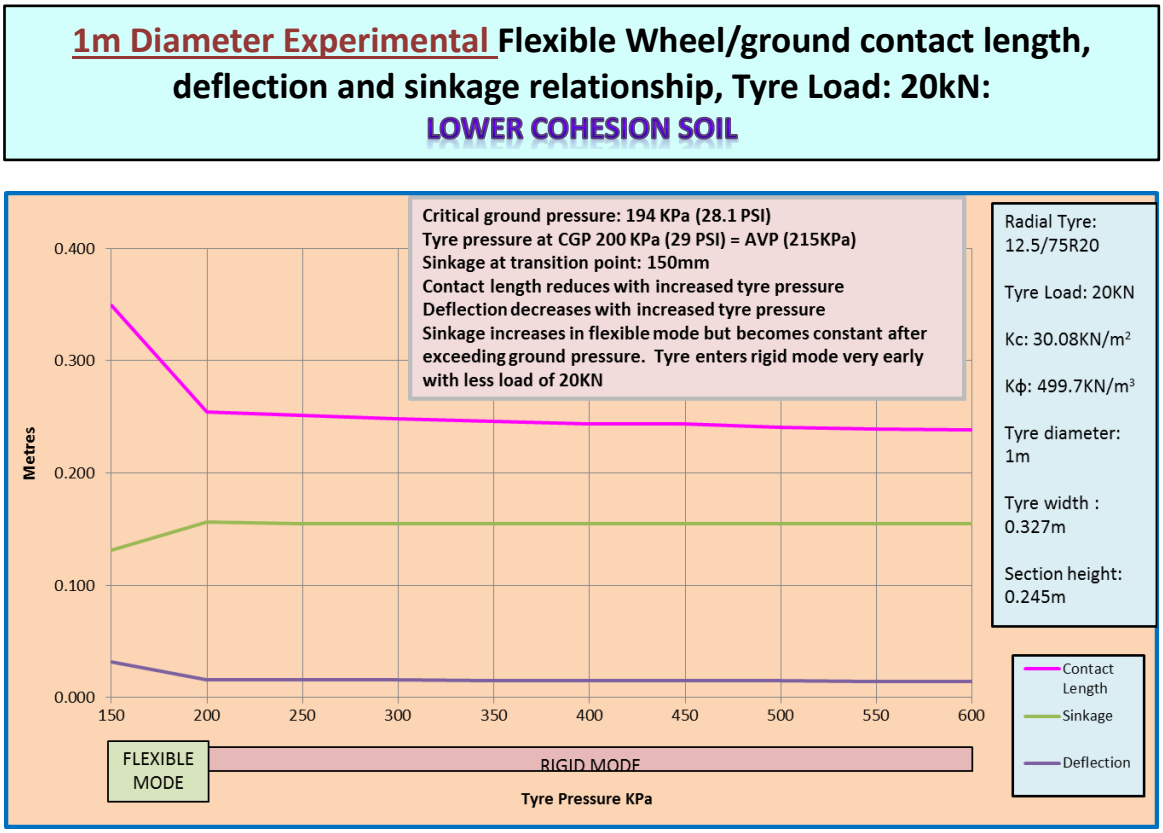

Figure 5.11: Experimental tyre under 20kN load in lower cohesion soil

Contact length, sinkage, deflection graphs and their interpretation in figure 5.11 are very similar to those discussed for the tyre operating in high cohesion soil but with the following exceptions: The reduced load from 25kN to 20kN results in the reduction in the tyre sinkage from 186mm to 150mm. The tyre almost immediately gets into rigid mode due to the combination of low soil cohesion and high load. Flexible tyres in low cohesion will mostly operate as rigid wheel. Increase in tyre pressure does not affect the contact length, sinkage and deflection.

5.6.3. Experimental tyre with 15kN load in lower cohesion soil

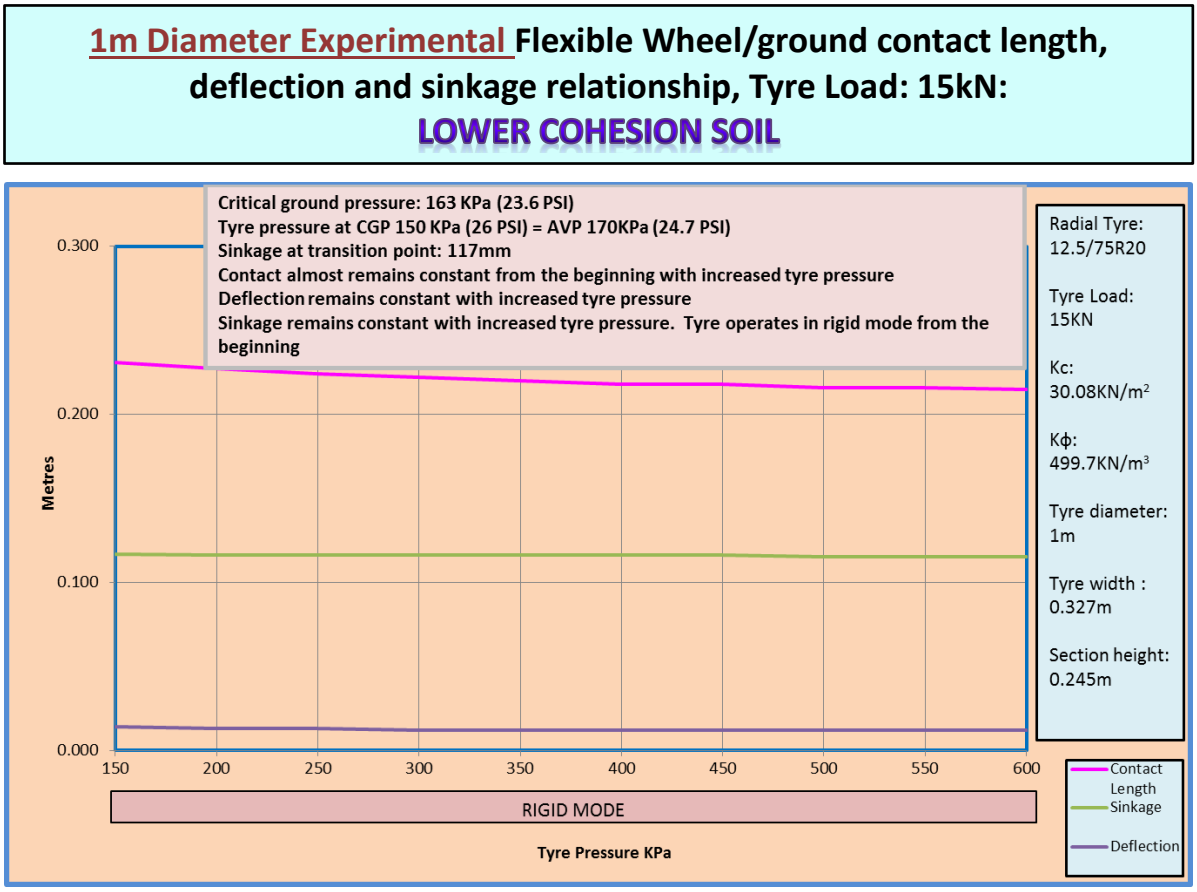

Figure 5.12: Experimental tyre under 15kN load in lower cohesion soil

For the 15kN load in the low cohesion soil, the change in contact length is negligible as shown in figure 5.12 above. There is no change on in sinkage and deflection. All parameters remain constant even with increase in tyre pressure.

The tyre remains in rigid mode from the beginning as seen in figure 5.12. The lower load is not strong enough to create deflection in the already low cohesion and low internal shearing angle soil.

5.6.4. Experimental tyre with 10kN load in lower cohesion soil

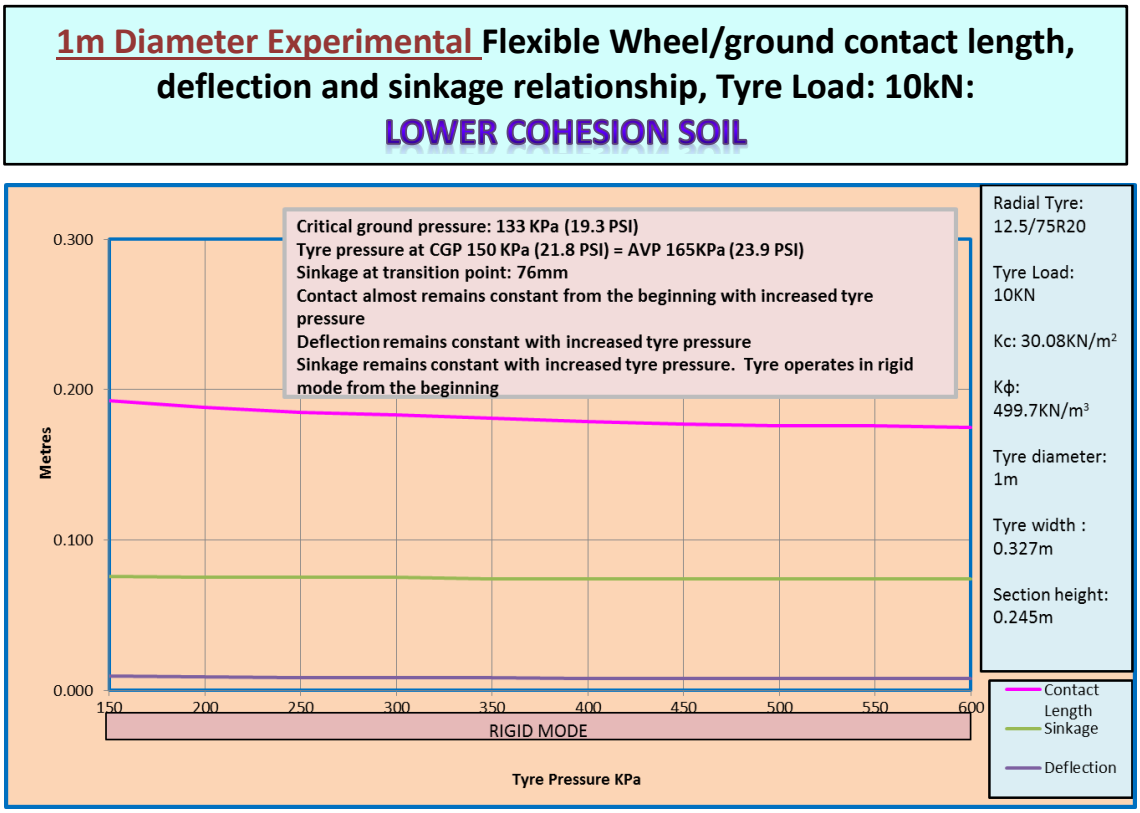

Figure 5.13: Experimental tyre under 10kN load in lower cohesion soil

The tyre with 10kN load behaves the same as the 15kN load in low cohesion soil in the previous description. All parameters remain constant making the tyre operate in rigid mode from the beginning as shown in figure 5.13 above.

5.6.5. Experimental tyre contact length analysis for all loads in lower cohesion soil

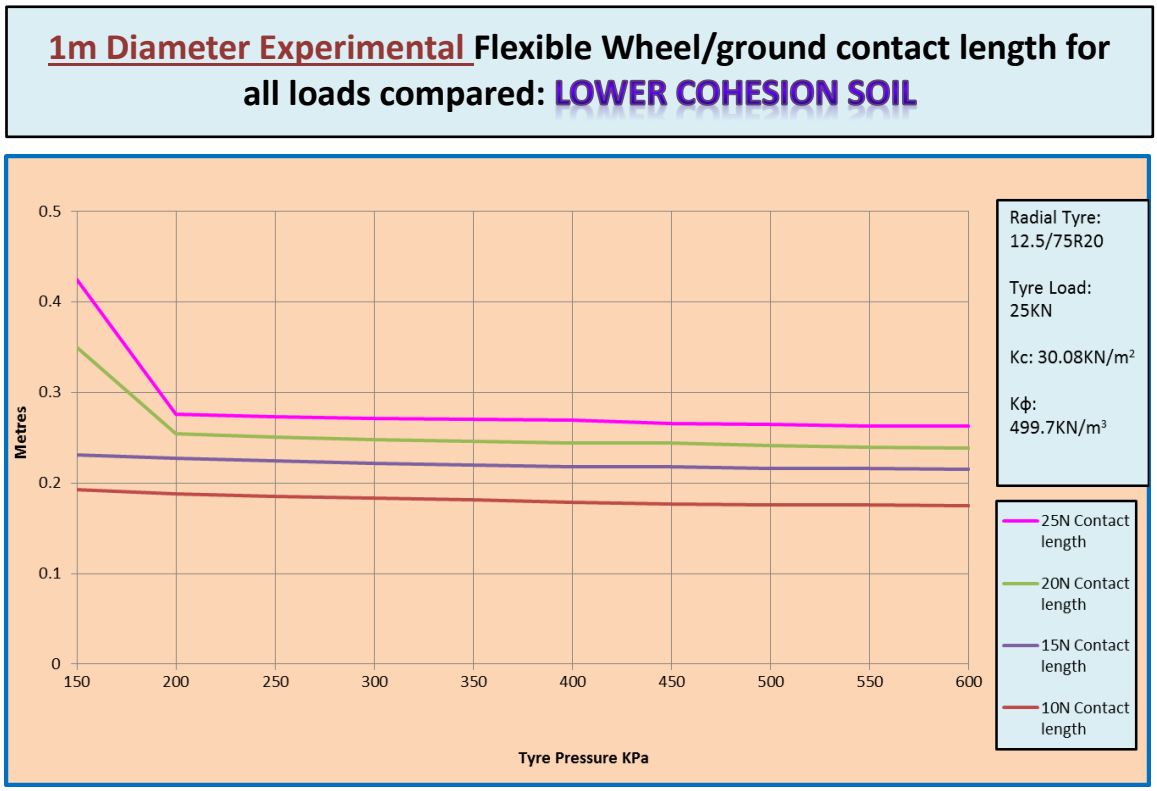

Figure 5.14: Experimental tyre contact length analysis for all loads in lower cohesion soil

5.6.6. Experimental tyre wheel sinkage analysis for all loads in lower cohesion soil

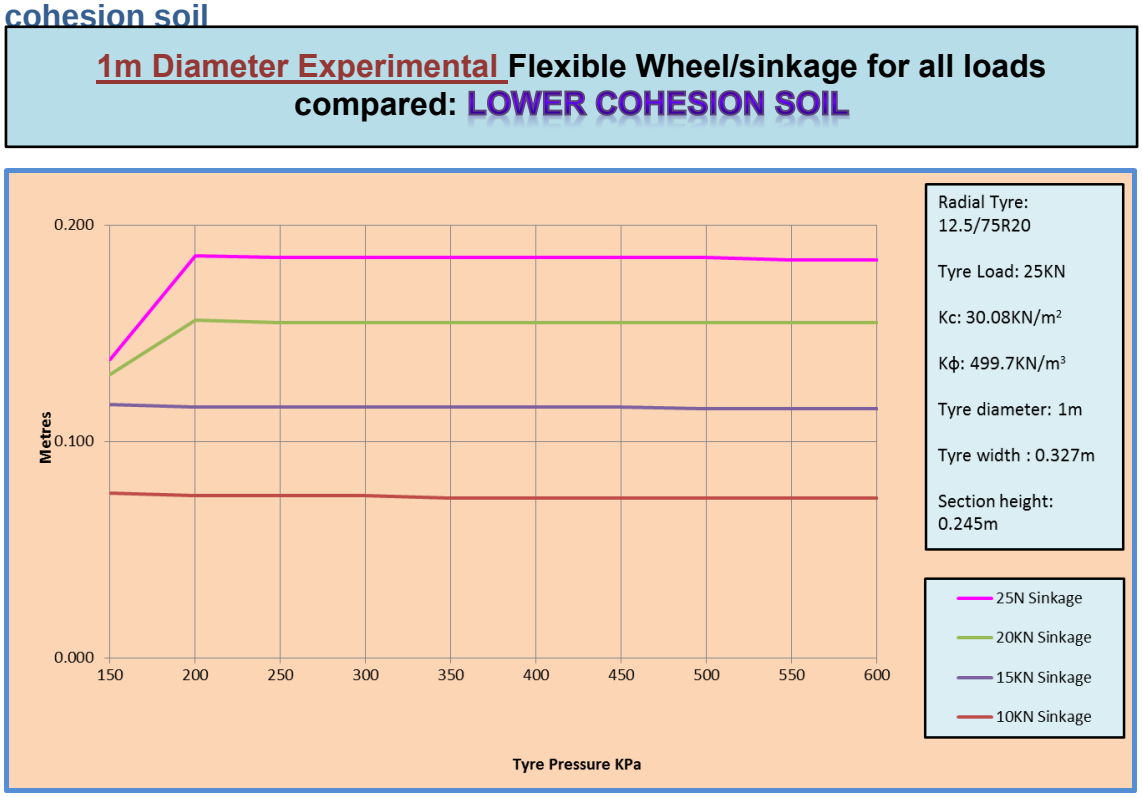

Figure 5.15: Experimental tyre sinkage analysis for all loads in lower cohesion soil.

5.6.7. Experimental tyre deflection analysis for all loads in lower cohesion soil

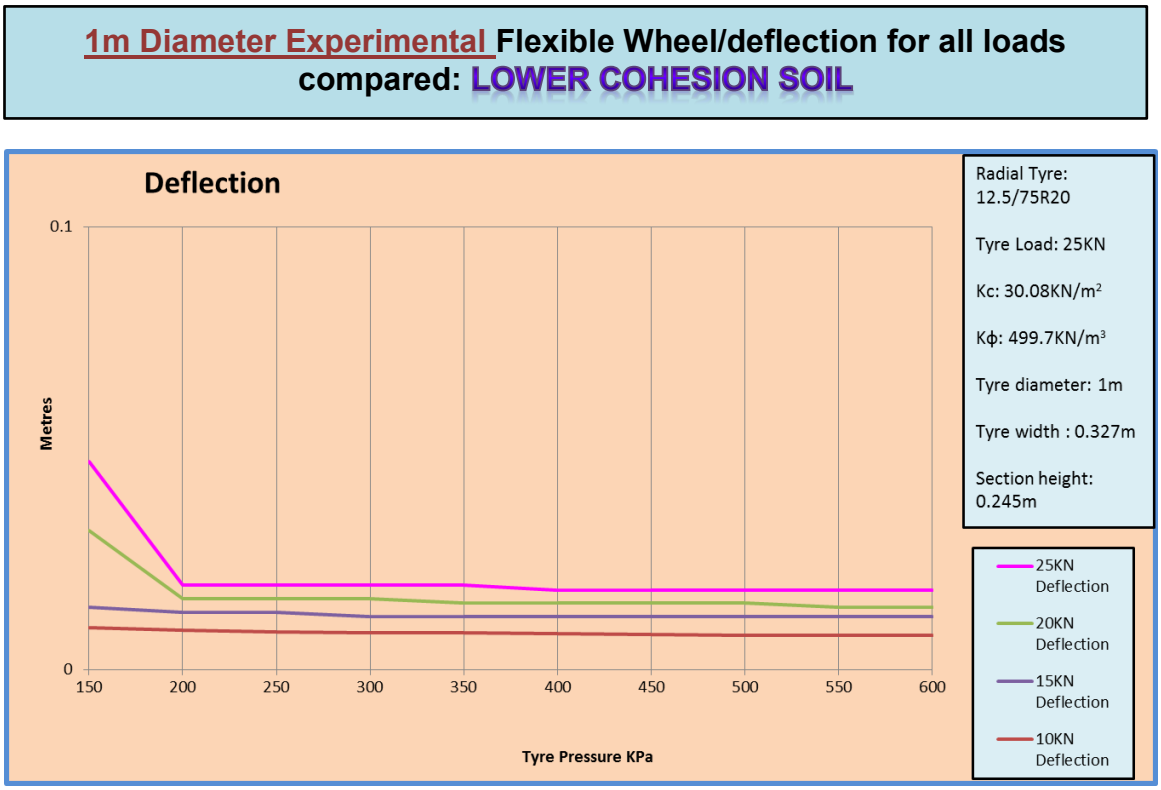

Figure 5.16: Experimental tyre deflection analysis for all loads in lower cohesion soil

Figures 5.14 to 5.16 present a combined summary of the results. Contact length reduces with increase in tyre pressure and higher critical ground pressure only for a short period in the flexible mode and for 25kN and 20kN loads only. Wheel sinkage increases with increase in tyre pressure and high load only for the 25 and 20kN loads only. Deflection reduces with increase in tyre pressure for the first two graphs as described above. The results confirm that a flexible wheel will operate as a rigid wheel when the load is below a particular load and when the ground has less critical ground pressure than tyre pressure.

From figures 5.17 and 5.18, a rigid model can therefore be used as for a flexible tyre under the given or similar conditions as summarised below:

Higher Cohesion soil:
The flexible tyre operates in rigid mode after inflation pressure exceeds the following tyre inflation pressures:

- 350kPa for the loads of 25kN and 20kN

- 300kPa for the loads of 15kN
- 200kPa for the loads of 10kN

Lower Cohesion soil:
The flexible tyre operates in rigid mode after inflation pressure exceeds the following tyre inflation pressures:

- 200kPa for the loads of 25kN and 20kN
- The 15kN and 10kN load runs all run in rigid mode from the from the minimum 150kPa

From the above interpretation of the graphs and tyre manufacturers' manuals, it can be deduced that the effect of the weight of wheeled construction plant (loaded or unloaded) and it's fully inflated tyres results in the tyres to operate in rigid mode when traversing through deformable and wet ground.

Figures 5.17 to 5.22 present the graphical summative illustrations by comparing higher cohesion and lower cohesion behaviour under different loads and conditions. The respective explanation is presented in the next section 5.7

5.6.8. Comparison of contact length, wheel sinkage and deflection between higher cohesion and lower cohesion soils.

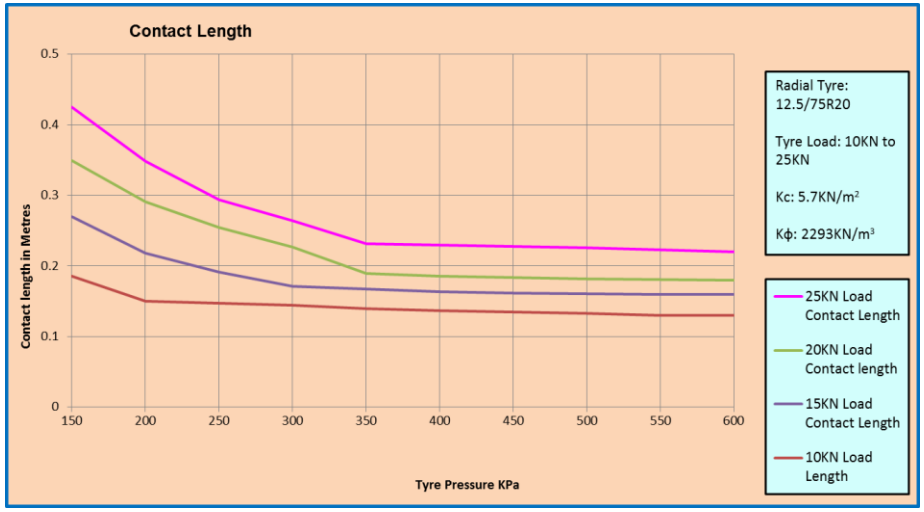

Figure 5.17: Contact length for HCS (Medium soil) for all loads

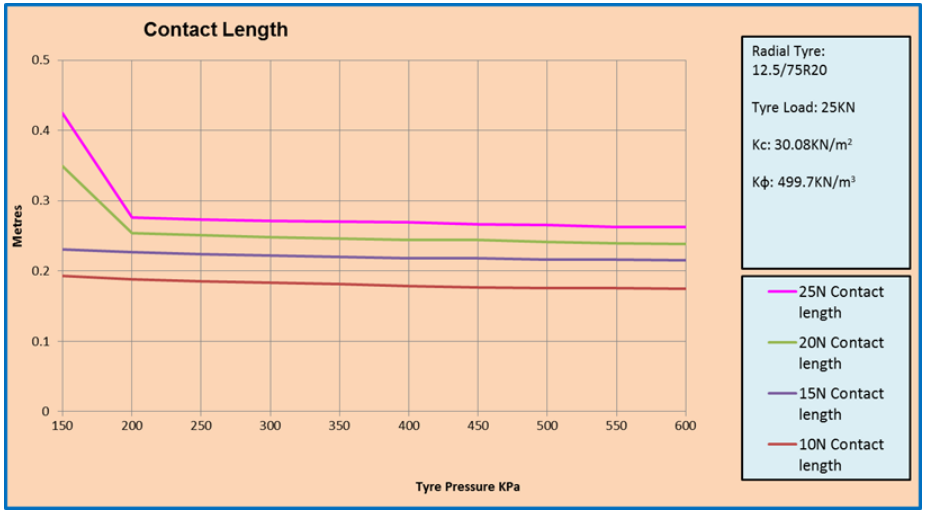

Figure 5.18: Contact length for LCS (Clayey soil) for all loads

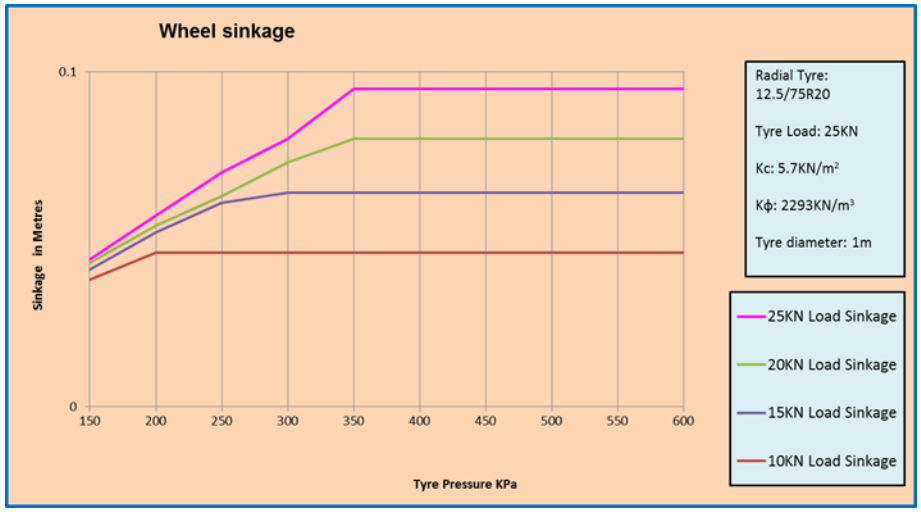

Figure 5.19: Wheel sinkage for HCS (Medium) for all loads

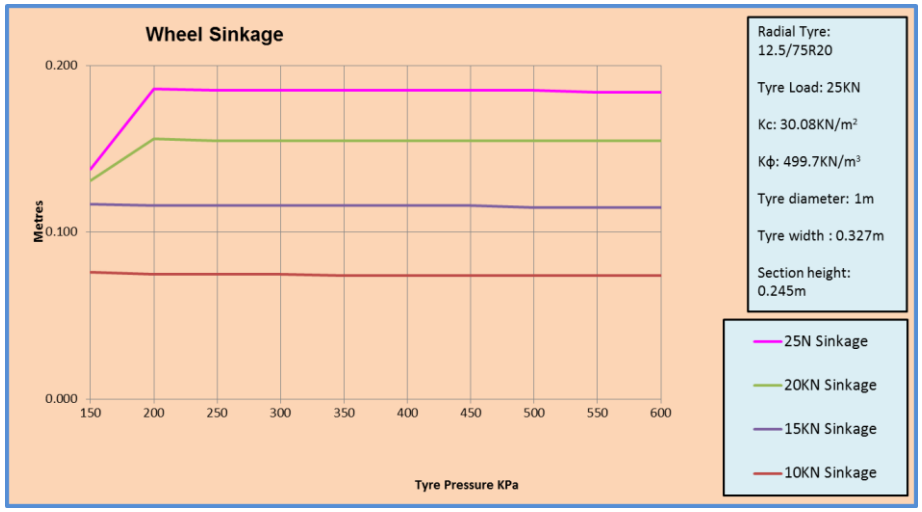

Figure 5.20: Wheel sinkage for LCS (Clayey soil) for all loads

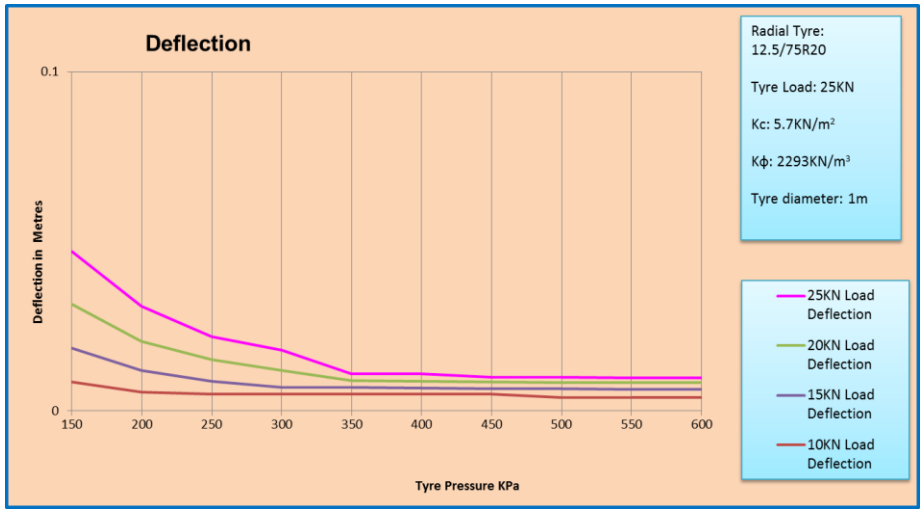

Figure 5.21: Tyre deflection for HCS (Medium soil) for all loads

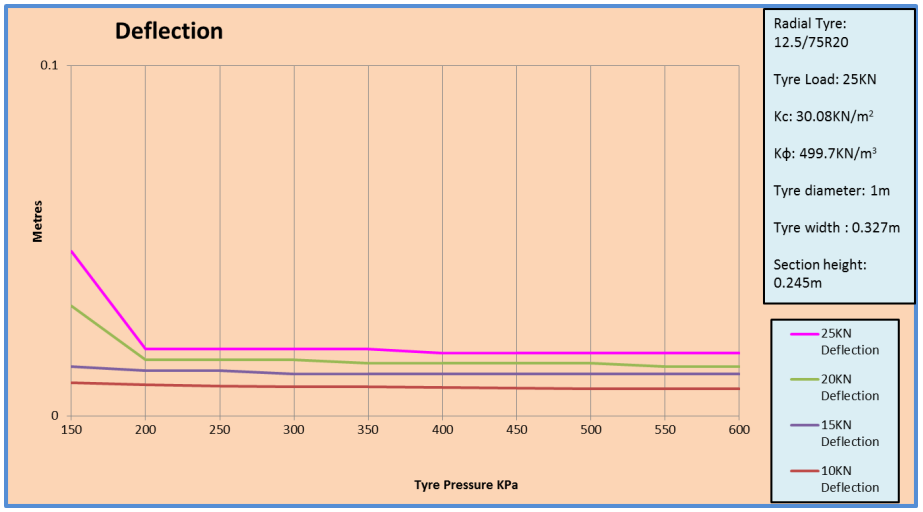

Figure 5.22: Tyre deflection for LCS (Clayey soil) for all loads

5.7. Summary of graphical interpretation

5.7.1. Contact Length

The contact length for all test runs is presented in figures 5.17 and 5.18. The results clearly point out that for the higher value soil cohesion the flexible mode of the tyre lasts longer with maximum load of 25kN producing the longest stretch. All the loads in this terrain produced a flexible mode before entering the rigid mode.

In the lower value cohesion and angle of shearing resistance soil, on the other hand the flexible mode for the tyre only exist for the 25kN and 20kN loads and only for a short stretch of tyre pressure increase. The 15kN and 10kN loads only exist in rigid mode. A combination of weak terrain and higher tyre load produces the rigid wheel format. Flexible mode is most common for tyres running on hard surface or semi-hard terrain while the rigid mode is most common for wet and deformable terrain.

5.7.2. Wheel Sinkage

The same principle discussed above for the contact length applies to the wheel sinkage as illustrated in figures 5.19 and 5.20. In wheel sinkage however, in the higher value soil cohesion, the sinkage values increase until they reach the rigid mode after which they become constant. In lower value soil cohesion, sinkage values are higher immediately and for a short stretch before they become constant in rigid mode. This is due to reduced motion and compaction resistance, a typical property of a weaker soil.

5.7.3. Deflection

Deflection equally operates on the same principle as the tyre contact length as seen in figures 5.21 and 5.22. Heavy Wheeled Construction plant tyres can have up to 700 kPa as recorded in the good year tyre chart in appendix 19 and 20. This signifies that operations in deformable and wet terrain must be properly investigated in order to determine the most economic parameter to use at each particular time.

5.8. Computational analysis of the mathematical model tyre in medium soil (Higher cohesion soil).

The aim of this section of work is to establish the validity of using the mathematical model rigid wheel model as a flexible wheel.

The following are the pseudo tyre properties and its associated parameters.

- Tyre type: Flexible tyre
- Flexible Tyre diameter: 1.8m
- Flexible Tyre width: 0.3m
- Tyre pressure: 150 to 600kPa (22PSI to 87PSI)
- Tyre Load: 10kN to 25kN

5.8.1. Mathematical model tyre with 25kN load in higher cohesion soil

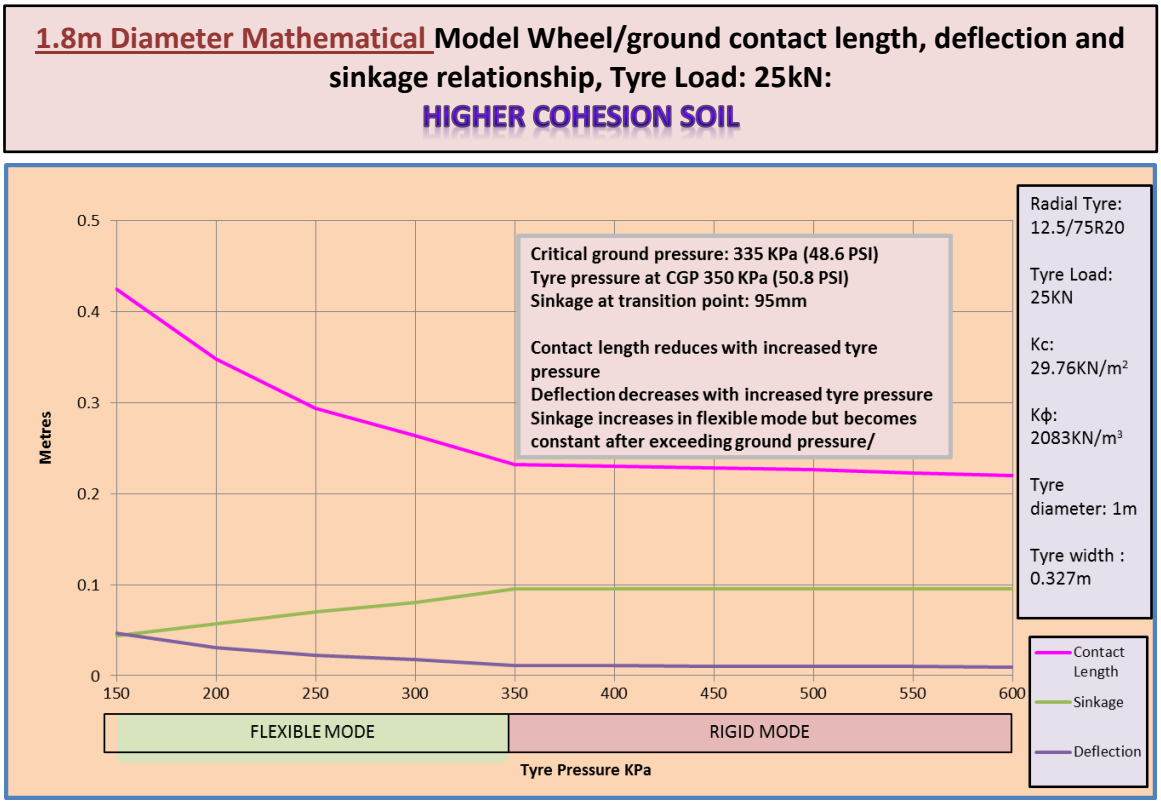

Figure 5.23: Mathematical model tyre under 25kN load in higher cohesion soil

Like the experimental tyre model, the mathematical model begins to run in flexible mode until the increasing tyre pressure overcomes the average ground pressure at 354kPa as shown in figure 5.23 above.

Contact length, wheel sinkage and deflection all remain constant after entering the rigid mode. High load has significant effect on all the three factors even in the mathematical model tyre. Flexible tyre mode exists for a combination of high load and much harder/stable terrain. The computational and mathematical model behaviour of the tyres is basically the same justifying the relevance of the developed mathematical model.

5.8.2. Mathematical model tyre with 10kN load in higher cohesion soil

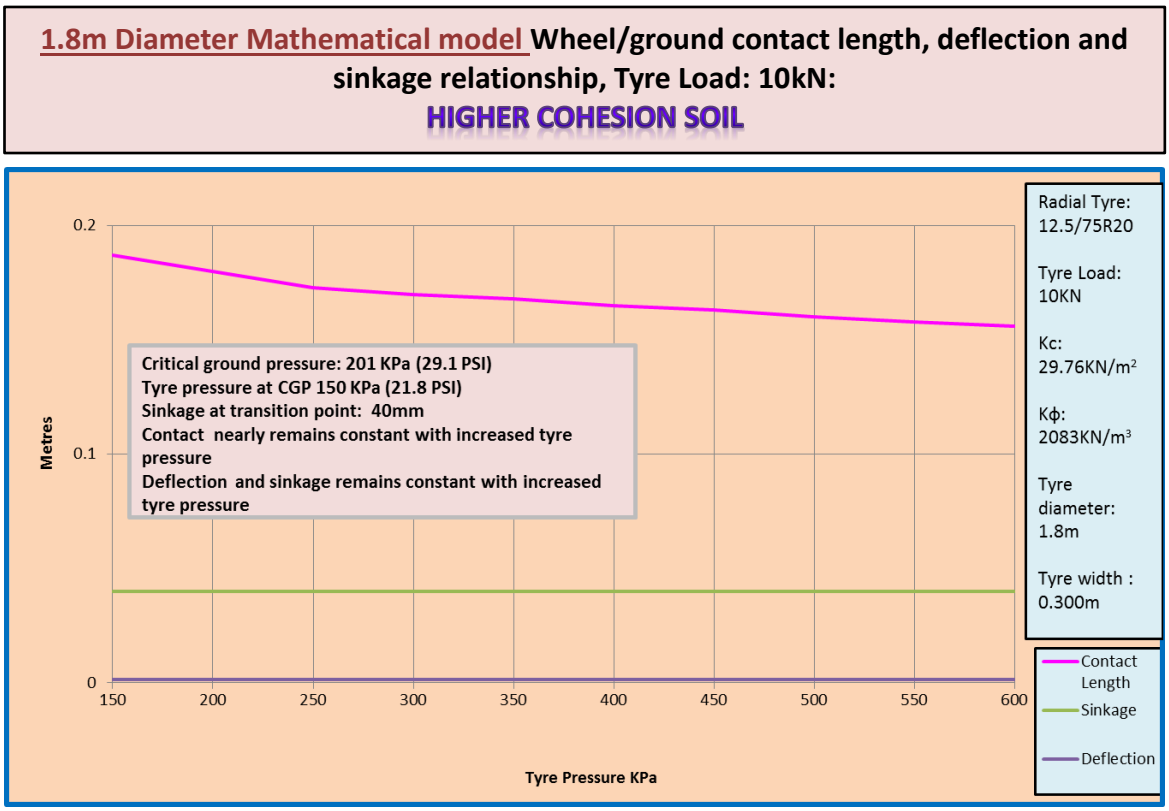

Figure 5.24: Mathematical model tyre under 10kN load in higher cohesion soil

The model tyre starts as a rigid wheel. The contact length gradient can be neglected because deflection and the sinkage all remain constant with increase in tyre pressure. Lower loads applied in weak ground do not produce any significant deflection, sinkage thereby making the tyre to run in rigid wheel format deploying the rigid wheel modelling approach for a flexible tyre.

5.8.3. Mathematical model tyre with 5.1kN load in higher cohesion soil

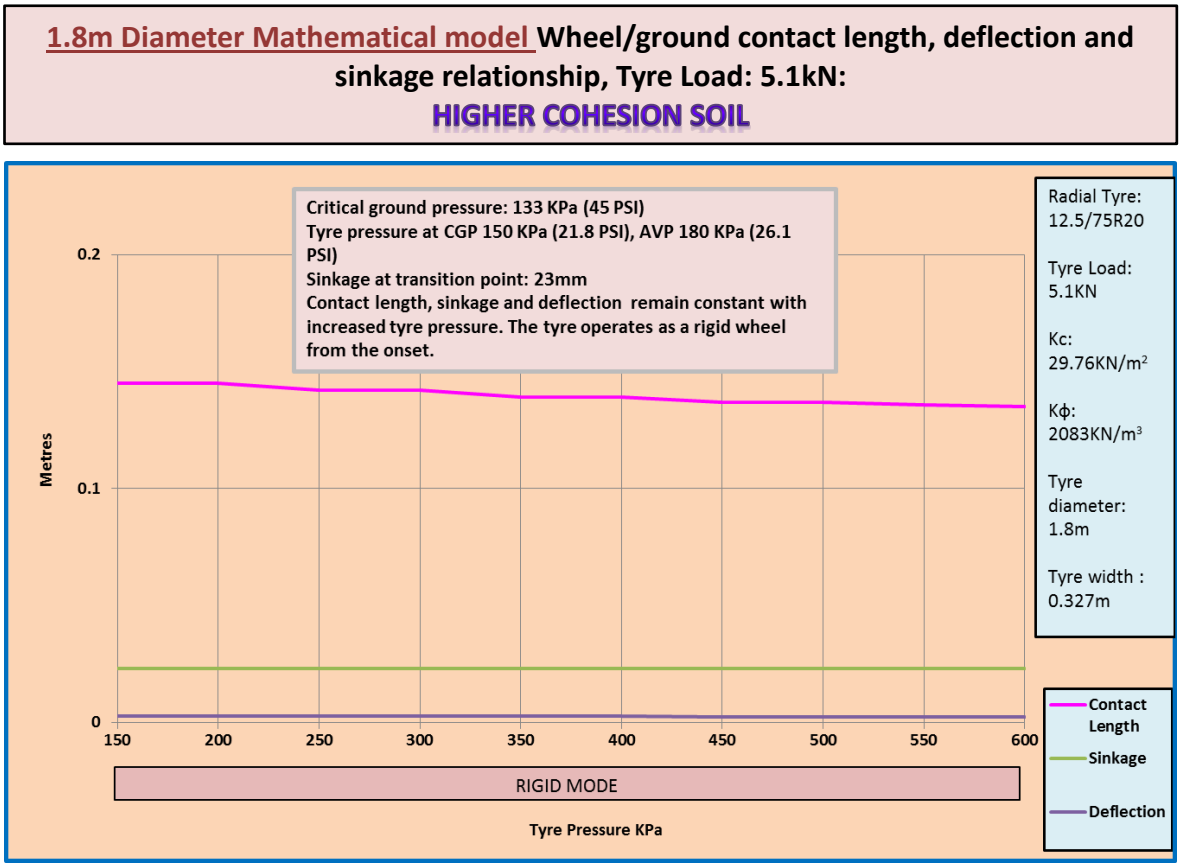

Figure 5.25: Mathematical model tyre under 5.1kN load in higher cohesion soil

The contact length, wheel sinkage and deflection all remain constant with increase in tyre pressure. The tyre remains in rigid mode from the onset as the 10kN is not large enough to cause deflection. The tyre operates in rigid mode throughout as seen in figure 5.25. The rigid wheel in the mathematical model can also be substituted for a flexible tyre at 5.1kN. The tyre in the original mathematical model used 5.1kN as the load. This result strongly suggests that the mathematical model discussed and presented in chapter 4 is fully justified and qualified for use in both rigid and flexible tyre modes for most of the off-road conditions.

5.9. Computational analysis of the mathematical model tyre in clayey (Lower Cohesion Soil).

5.9.1. Mathematical model tyre with 25kN load in lower cohesion soil

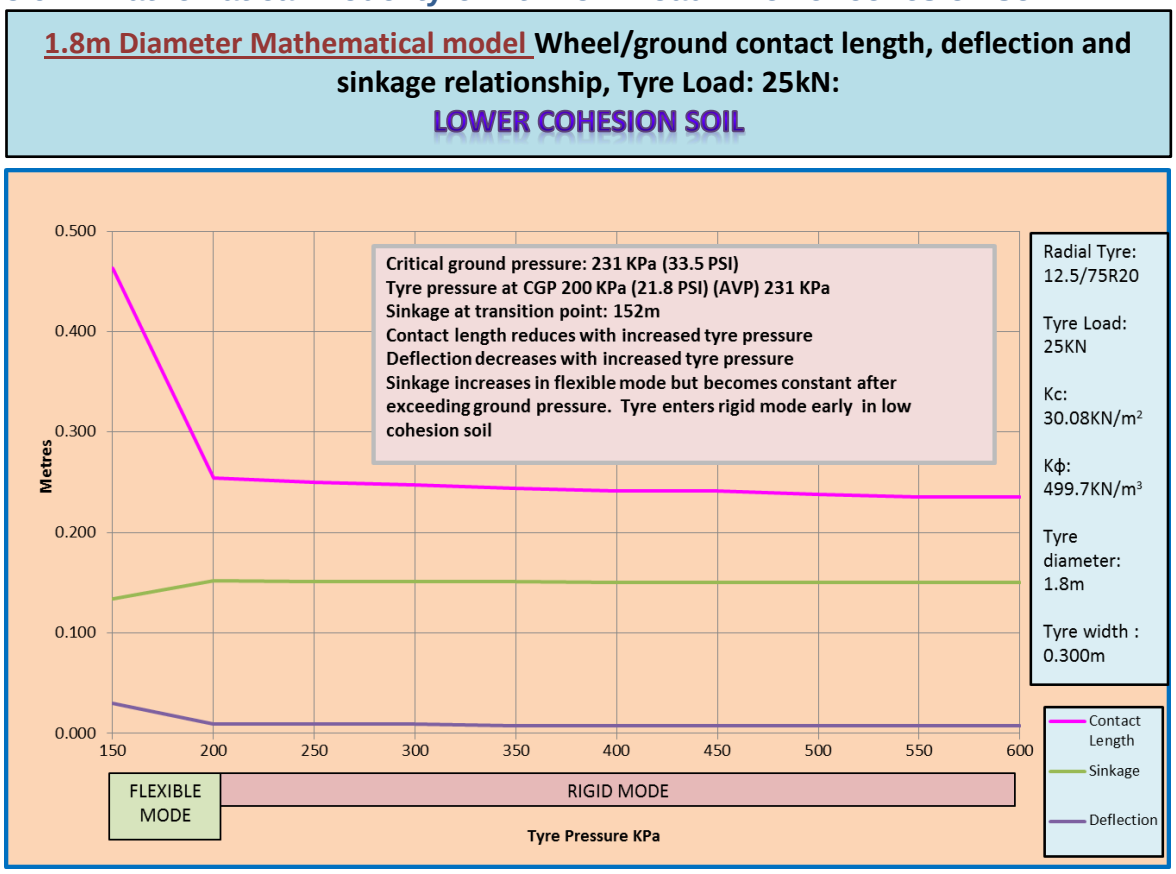

Figure 5.26: Mathematical model tyre under 25kN load in lower cohesion soil

The high load in lower soil cohesion makes a significant change in contact length, wheel sinkage and deflection up to the point of 200kPa of tyre pressure as seen in figure 5.26. After this sharp gradient the tyre goes into rigid mode having exceeded the critical ground pressure. The tyre only stays in flexible mode for a short period of time within the lower section of the tyre pressure. The tyre only operates as a flexible tyre under unrealistically low tyre pressure for heavy construction related vehicles.

This result shows that the lower cohesion soil cannot withstand higher applied load for a longer time before it is overcome by the tyre load and mobility.

5.9.2. Mathematical model tyre with 10kN load in lower cohesion soil

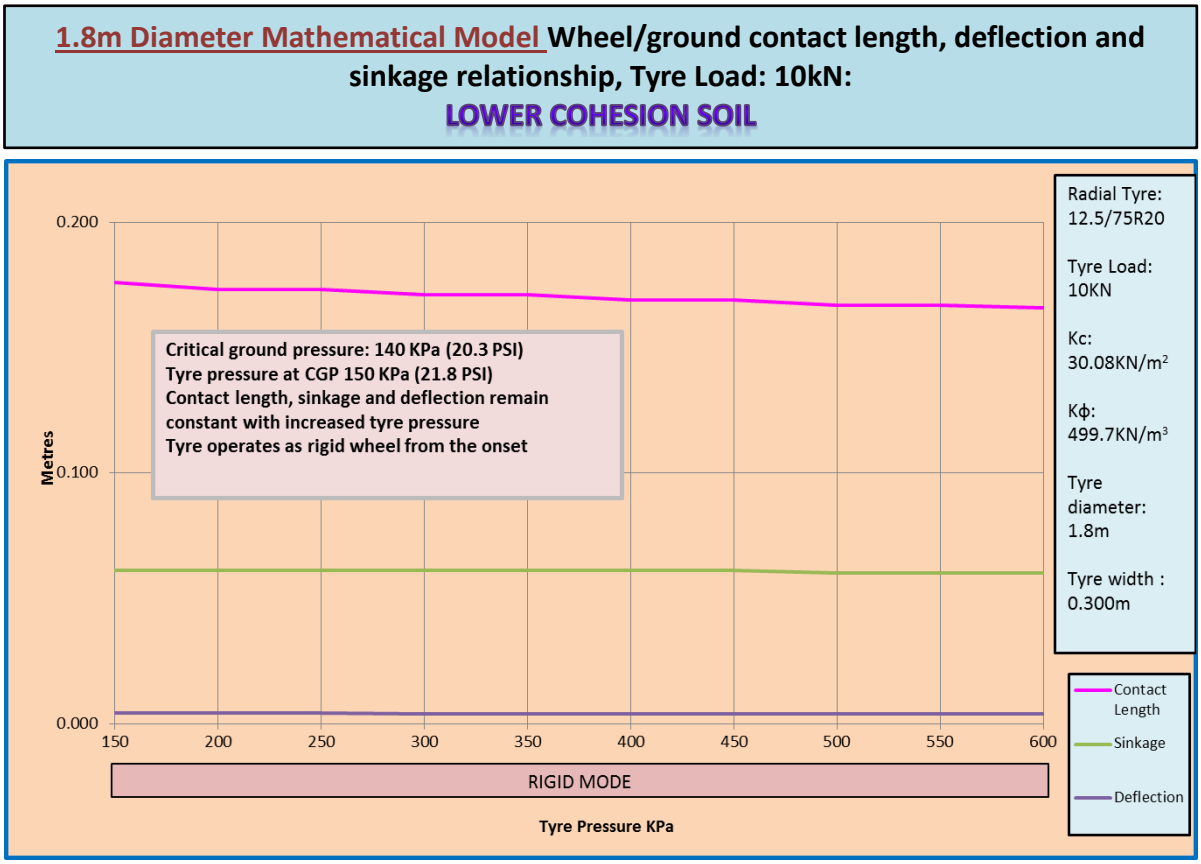

Figure 5.27: Mathematical model tyre under 10kN load in lower cohesion soil

From figure 5.27 above the 10kN load in low cohesion soil, increase in tyre pressure does not affect tyre contact length, wheel sinkage and deflection. The contact length change with increase in tyre pressure is negligible. The tyre operates in rigid mode from beginning. Reducing the applied load from 25kN to 10kN has an influence on the mode of the tyre. The 10kN load is not large enough to produce significant sinkage or displacement in deflection and contact length.

5.9.3. Mathematical model tyre with 5.1kN load in lower cohesion soil

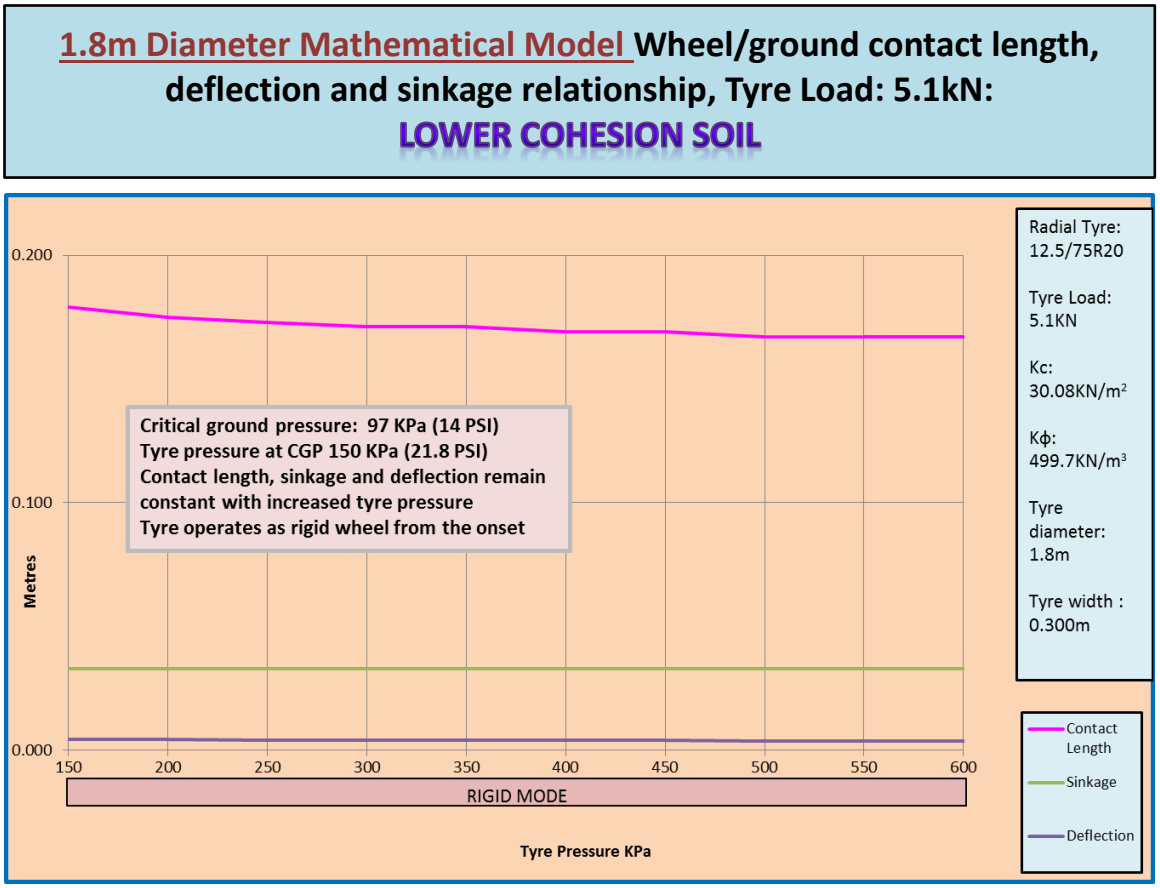

Figure 5.28: Mathematical model tyre under 5.1kN load in lower cohesion soil

The rigid wheel mathematical model was based on 5.1kN. Modelling the tyre as a flexible tyre still provides the same result as it also behaves as a rigid wheel from the beginning. All the three parameters under discussion remain constant as shown in figure 5.28. This provides support for the rigid wheel based mathematical model presented in chapter 4.

5.10. Results summary and chapter overview.

While tyre deflection is significant on hard and un-deformable surface like paved roads, the results clearly indicate that a deformable and wet terrain will mostly be

overcome by the tyre pressure and its carcass thereby making heavy and fully inflated tyres for construction plant to operate in rigid mode for most of the time. This means that the rigid wheel mathematical model formulae can be confidently deployed in the use of construction plant performance regarding the relationship between moving tyres and the deformable terrain. This conclusion is also supported by the outcome of laboratory experimental results discussed in Chapter 7. It is worth mentioning at this stage that top soil or vegetable soil was not included in the main testing and discussion because it does not have measurable engineering properties that would facilitate a comprehensive engineering analysis of its behaviour. In addition topsoil is normally not stable enough to constitute terrain that can support vehicular mobility.

It is evident from all the results in this chapter that the mathematical model tyre operates as a rigid rim for most of the time under normal and average tyre pressure that is expected for the wheeled construction plant operating in deformable ground. The results provide a strong verification and justification for the use of the mathematical modelling model that is based on the pseudo rigid wheel discussed in chapter 4. The results also indicate that the average tyre pressures and suggested velocities provided by tyre manufacturers (appendix 19 and 20) alone cannot be adequate to make economic decisions regarding operating of wheeled plant in off-road conditions. Other factors such terrain profile, tyre size, applied load, moisture content and wear/tear have to be considered as well if the plant is to be operated at optimal specifications and economy.

CHAPTER 6

MATHEMATICAL MODEL VERIFICATION STAGE 2

DRAWBAR-PULL COMPUTATIONAL ANALYSIS

6.0. CHAPTER 6

MATHEMATICAL MODEL VERIFICATION STAGE 2: DRAWBAR-PULL COMPUTATIONAL ANALYSIS.

6.1. Introduction

This aim of this chapter is to demonstrate that the mathematical model developed in chapter 4 is supported by existing terramechanics theories developed by Bekker and Wong/Reece as discussed in chapter 2. In this stage 2 of the robust model verification process, the experimental tyre data was run in the Wong/Reece approach, the Bekker theory and the developed mathematical model driven by the POWERSEV program. The results were then compared to evaluate the mathematical model performance, being the main subject of this research. These results are presented on one graph for each run in order to highlight the similarity and pattern of each of the outlined categories under study.

The tyre data used was from the Canadian Defence Department published in Wong (2010). The data was run using Wong/Reece approach, the Bekker theory and the mathematical model. Results indicate that the mathematical model results fall within the range of the two existing benchmarks. The same soil and tyre profiles that were used during the determination of sinkage and flexible tyres in chapter 5 were applied in the generation of drawbar-pull results in order to maintain consistency of the study.

6.2. Computation of Formulae and approach used

The formulae used to obtain the required pulling power in the form drawbar-pull were split into three stages: The Bekker theory, The Wong and Reece approach and the mathematical modelling approach driven by POWERSEV. Equation 6.1 represents wheel sinkage and is based on figure 6.1. Equation 6.2 represents ground pressure. The interpretation of the Greek symbols contained in the formulae can be found in the nomenclature section on page xxxvii of the preamble section

6.2.1. Bekker approach

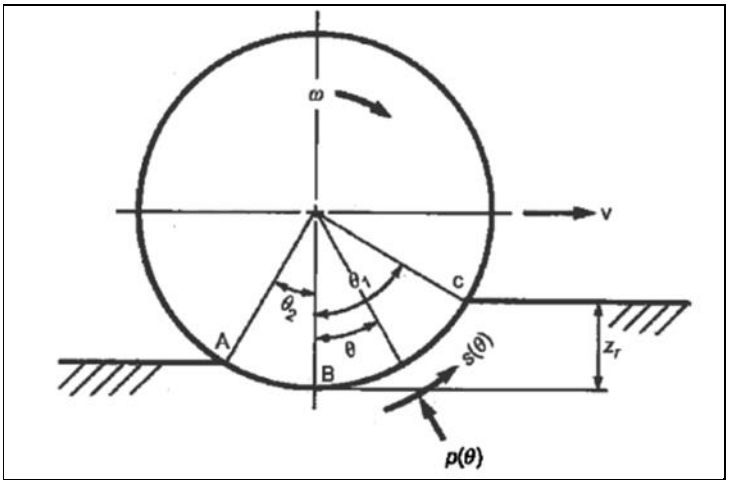

Figure 6.1: An improved model for tyre-terrain interaction for a tyre in the rigid operating model showing z_r as sinkage

$$z_r = \left[\frac{3W}{b_{ti}(3-n)(k_c/b_{ti}+k_\emptyset)\sqrt{D}}\right]^{2/2n+1} \quad \text{Eqn 6.1}$$

$$p_g = \left[\frac{k_c}{b} + k_\emptyset\right] z_r^n \quad \text{Eqn 6.2}$$

6.2.2. Wong and Reece Approach without rebound factor from exit angle

$$W = V + Q = rt(\int_0^{\theta_1} \sigma(\theta)\cos\theta.d\theta + \int_0^{\theta_1} \tau(\theta)\sin\theta.d\theta)$$ Eqn 6.3

Wheel sinkage

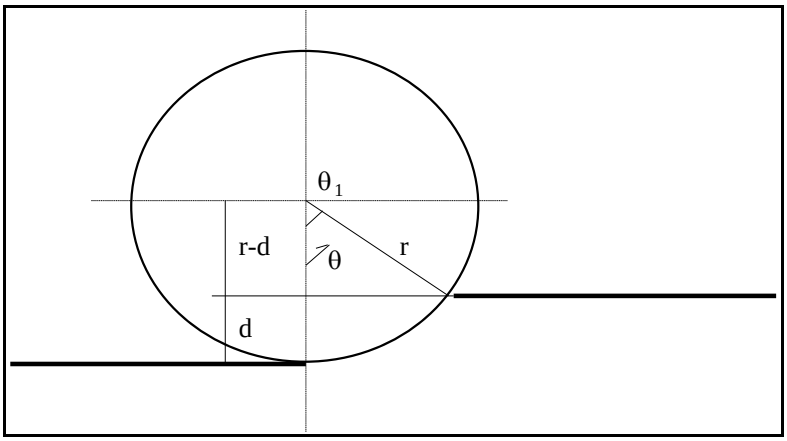

Figure 6.2: Details showing the relationship between d, theta and r

Equations 6.4 to 6.6 are based on figure 6.2.

$$\theta = acos\left[1 - \frac{d}{r}\right]$$ Eqn 6.4

$$\theta = acos\left[1 - \frac{\lambda d}{r}\right]$$ Eqn 6.5

$$d = r(1 - cos(\theta)$$ Eqn 6.6

Normal Pressure

$$\sigma = Wrt/[\sin\theta + \tan\varphi - \tan\varphi \cdot \cos\theta]$$ Eqn 6.7

$$\sigma = W - rtC(1 - \cos\theta)/rt\sin\theta$$ Eqn 6.8

6.2.3. For rebound cases the following formulae applies

$$H = rt\tau \sin(\theta_1) + rt\tau \sin(\theta_2) \quad \text{Eqn 6.9}$$

$$R = rt\sigma(1 - \cos(\theta_1)) - rt\sigma(1 - \cos(\theta_2)) \quad \text{Eqn 6.10}$$

$$W = rt\left[\int_0^{\theta_1}(\sigma(\theta)\cos(\theta) + \tau(\theta)\sin(\theta)\,d(\theta) + \int_0^{\theta_2}(\sigma(\theta)\cos(\theta) - \tau(\theta)\sin(\theta)\,d(\theta)\right] \quad \text{Eqn 6.11}$$

6.2.4. Mathematical modelling formulae

Equations 6.12 to 6.14 were adapted from Reid (2000) which constituted part of the database used for the development of POWERSEV mathematical model. The description of variables and notation in equations 6.12 to 6.14 is presented in appendix 24. A summary of the development of the same equations is presented in appendix 25.

$$d_n = d_{n-1} - \frac{f(d)}{f'(d)} \quad \text{Eqn 6.12}$$

Where d_n is the rut depth.

$$f(d) = Ctd^2 - \frac{WVv^2d^2}{2gr^2(1-i)^2\arccos^2\left(\frac{r-d}{r}\right)} + 2C(2rd-d^2)^{0.5}d^2$$

$$+ (W+L)\left(\frac{2}{\pi}-1\right)d + 2(W+L)\left(\frac{(1-\sin\phi)}{(1+\sin\phi)}\right)\tan\phi.d$$

$$+ \left(\frac{(W+L)\tan\phi(2rd-d^2)^{0.5}}{2r}\right)d \quad \text{Eqn 6.13}$$

$$f'(d) = 2Ctd - \left\{\frac{W\omega^2 d\left(\arccos\left(\frac{r-d}{r}\right) - \frac{d}{r\left(1-((r-d)/r)^2\right)^{0.5}}\right)}{g.\arccos^3\left(\frac{r-d}{r}\right)}\right\}$$

$$+4dc\left(2rd-d^2\right)^{0.5}+\frac{Cd^2\left(2r-2d\right)}{\left(2rd-d^2\right)^{0.5}}+\left(\frac{2}{\pi}-1\right)\left(W+L\right)$$

$$+\frac{(W+L)\tan\phi(2rd-d^2)^{0.5}}{2r}+\frac{(W+L)\tan\phi.d(2r-2d)}{4r(2rd-d^2)^{0.5}}$$

$$+2\left(W+L\right)\left(\frac{\left(1-\sin\phi\right)}{\left(1+\sin\phi\right)}\right)\tan\phi \qquad \text{Eqn 6.14}$$

6.2.5. Common/General formulae applied

Shear stress:

$$\tau = C+\sigma\cdot\tan\varphi\cdot\left(1-e^{-j/k}\right) \qquad \text{Eqn 6.15}$$

Shear displacement:

$$j=[(\theta_1-\theta)-(1-i)sin(\theta_1)-sin(\theta)] \qquad \text{Eqn 6.16}$$

Tractive effort:

$$H=rt\tau\int_0^{\theta_1}\cos\theta\cdot d\theta \qquad \text{Eqn 6.17}$$

Translational resistance:

$$R=rt\sigma\int_0^{\theta_1}\sin\theta\cdot d\theta \qquad \text{Eqn 6.18}$$

6.3. Mathematical model verification using drawbar-pull results by comparing with Bekker and Wong/Reece models: Higher Cohesion Soil

6.3.1. Drawbar-pull analysis for the experimental tyre with 25kN load in higher cohesion soil.

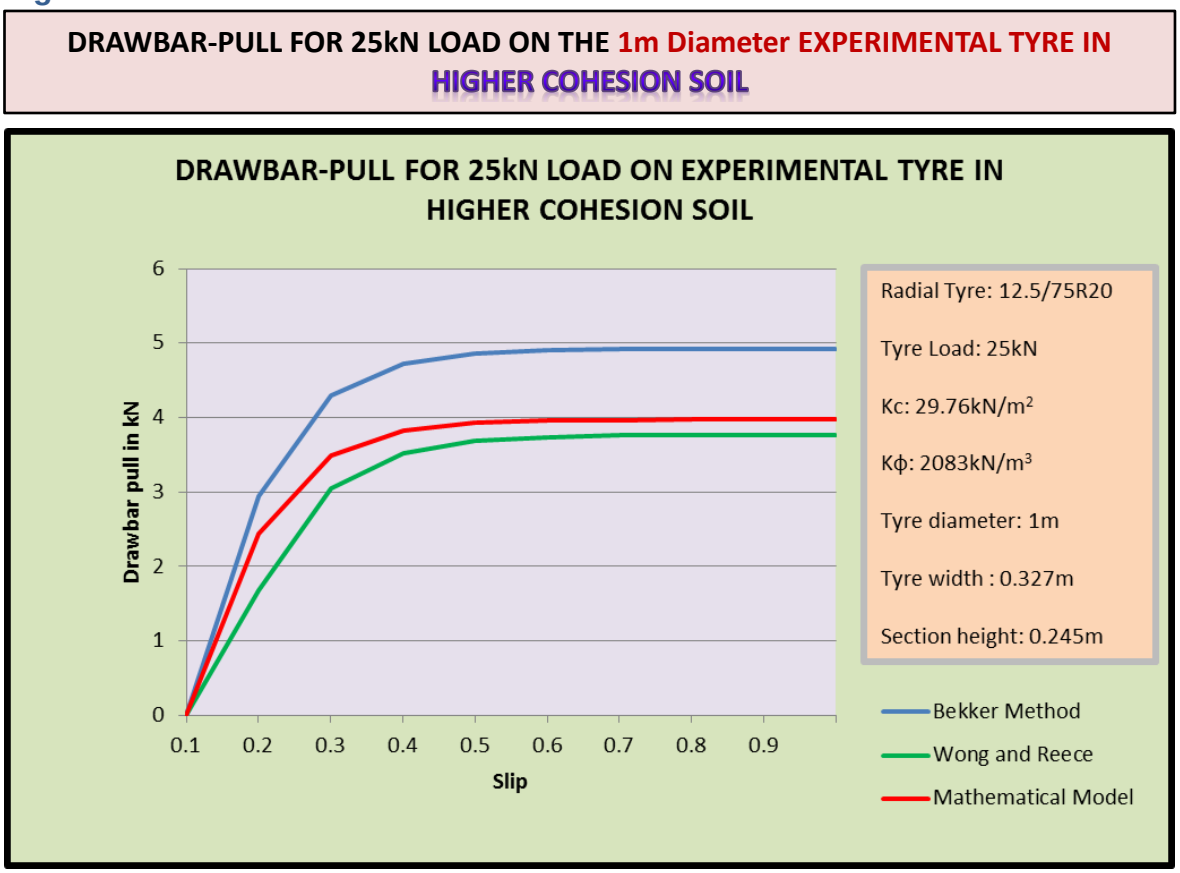

Figure 6.3: Drawbar-pull analysis for the experimental tyre with 25kN load in higher cohesion soil

The mathematical model drawbar-pull graph in figure 6.1 generally falls between the Bekker method and Wong-Reece approach. The three drawbar graphs confirm that the wheel slip efficiency falls between 0.3 and 0.5.

- Drawbar-pull at slip 0.5
- Bekker method: 4.91kN
- Wong and Reece: 3.74kN
- Mathematical model: 3.96kN

Bekker Method (KN)	4.91	Bekker Method (KN)	4.91	Mathematical Model (KN)	3.96
Wong and Reece Method (KN)	3.74	Mathematical Model (KN)	3.96	Wong and Reece Method (KN)	3.74
Difference (KN)	**1.17**	Difference (KN)	**0.95**	Difference (KN)	**0.22**
Difference (%)	31.3	Difference (%)	24.0	Difference (%)	5.9

Table 6.1: Drawbar-pull output comparative analysis between Bekker method, Wong/Reece method and POWERSEV mathematical model under 25kN load in the experimental tyre in higher cohesion soil

After slip value of 0.5 there is no significant return for more wheel traction. The results from figure 6.1 confirms that the mathematical model results falls within the accepted range of the two main approaches used in terramechanics so far. The results go further to add credibility of the research approach used and overall results obtained. The graph in figure 6.1 also confirms the outcome of the mathematical model that the maximum efficient slip value is between 0.3 and 0.5. The difference between the Bekker method and Wong/Reece and mathematical model results can be attributed to the fact that while the later utilises mathematical and computational analyses while the Bekker method relies on constants which are not as accurate in terms of response and sensitivity to changes in parameters

Table 6.1 also numerically illustrates that the mathematical model lies between the Bekker approach and Wong/Reece method. The data also illustrates that the mathematical model compares well to the other two models.

6.3.2. Drawbar-pull analysis for the experimental tyre with 20kN load in higher cohesion soil.

DRAWBAR-PULL FOR 20kN LOAD ON THE 1m Diameter EXPERIMENTAL TYRE IN HIGHER COHESION SOIL

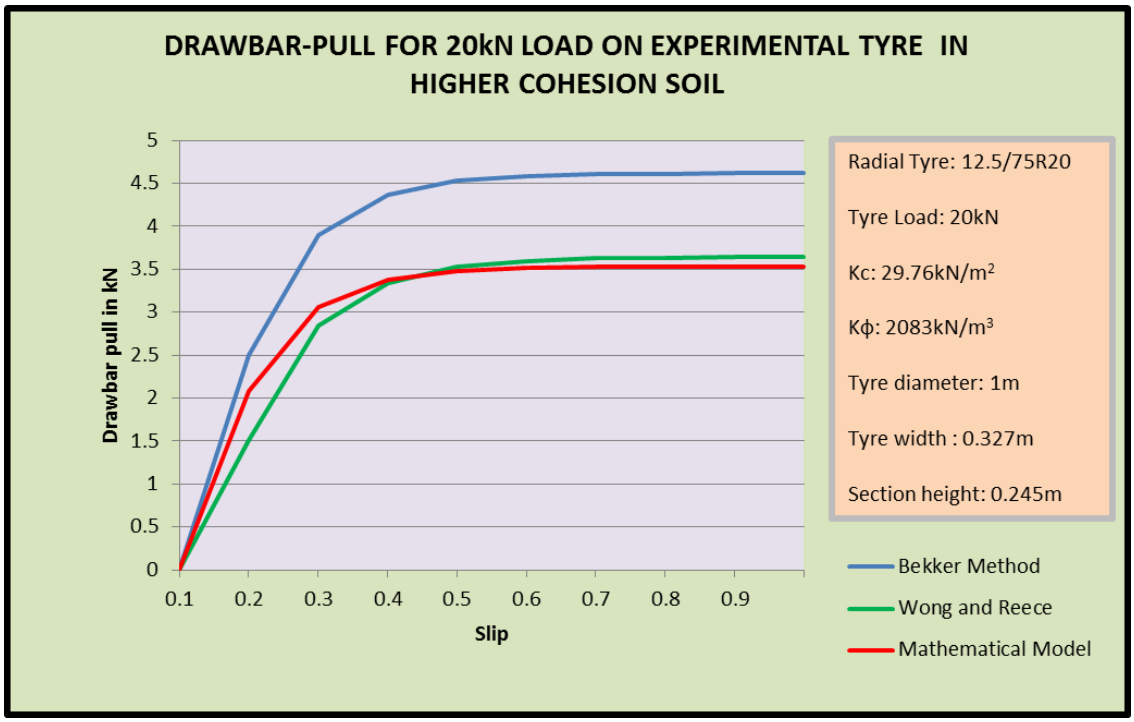

Figure 6.4: Drawbar-pull analysis for the experimental tyre with 20kN load in higher cohesion soil

The drawbar-pull for the mathematical model graph generally falls between the Bekker method and Wong-Reece approach until after 0.5 slip when it crosses the Wong Reece graph based on the given applied load of 20kN. The three graphs have the maximum wheel slip efficiency falls between 0.3 and 0.5 as shown in figure 6.2.

- Drawbar-pull at slip 0.5
- Bekker method: 4.59kN
- Wong and Reece: 3.60kN
- Mathematical model: 3.53kN

After slip value of 0.5 there is no significant return for more tyre traction.

Bekker Method (KN)	4.59	Bekker Method (KN)	4.59	Mathematical Model (KN)	3.53
Wong and Reece Method (KN)	3.60	Mathematical Model (KN)	3.53	Wong and Reece Method (KN)	3.60
Difference (KN)	**0.99**	Difference (KN)	**1.06**	Difference (KN)	**0.07**
Difference (%)	27.5	Difference (%)	30.0	Difference (%)	1.9

Table 6.2: Drawbar-pull output comparative analysis between Bekker method, Wong/Reece method and POWERSEV mathematical model under 20kN load in the experimental tyre in higher cohesion soil

Table 6.2 illustrates the reliability of the mathematical model results which are very close to existing methods despite the reduction in the load from 25kN to 20kN. In this case while the mathematical model is close to Wong/Reece approach with a difference of 1.9%, the Wong/Reece approach is still closer to the Bekker method. Overall the results are generally acceptable with 30% difference or less.

6.3.3. Drawbar-pull analysis for the experimental tyre with 15kN load in higher cohesion soil.

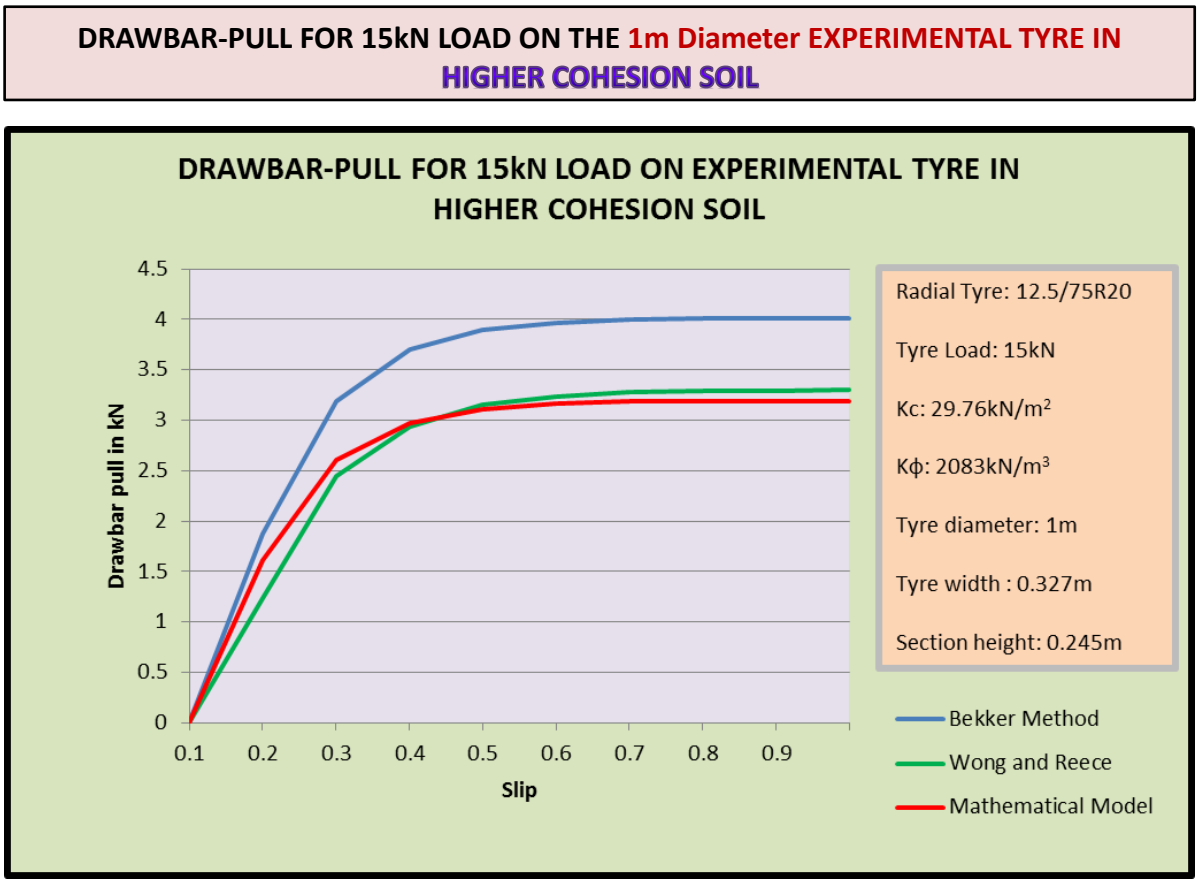

Figure 6.5: Drawbar-pull analysis for the experimental tyre with 15kN in higher cohesion soil

Like in the 20kN load the drawbar-pull for the mathematical model generally falls between the Bekker method and Wong-Reece method until after 0.3 slip before it crosses the Wong Reece graph. The three drawbar-pull graphs have the maximum wheel slip efficiency falls between 0.3 and 0.5 as seen in figure 6.3 above.

- Drawbar-pull at slip 0.3
- Bekker method: 3.70kN
- Wong and Reece: 2.94kN
- Mathematical model: 2.98kN

After slip value of 0.5 there is no significant return for more tyre traction. The mathematical model results fall within the acceptable traction efficiency.

Bekker Method (KN)	3.70	Bekker Method (KN)	3.70	Mathematical Model (KN)	2.98
Wong and Reece Method (KN)	2.94	Mathematical Model (KN)	2.98	Wong and Reece Method (KN)	2.94
Difference (KN)	**0.76**	Difference (KN)	**0.72**	Difference (KN)	**0.04**
Difference (%)	25.9	Difference (%)	24.2	Difference (%)	1.4

Table 6.3: Drawbar-pull output comparative analysis between Bekker method, Wong/Reece method and POWERSEV mathematical model under 15kN load in the experimental tyre in higher cohesion soil

The reason for Bekker's approach not being close to the other two methods is explained in 6.3.2. One unique observation from the results is that drawbar-pull reduces from maximum 3.5kN for 20kN load to 3.2kN for 15kN load. The load has significant influence on the amount of drawbar-pull generated. This is also supported by the outcome of the mathematical model in chapter 4 and the experimental analysis in chapter 7.

Table 6.3 shows that despite reducing the load further to 15kN the mathematical model still stays between the two control results. The table provides an alternative view of the graphical illustration given in figure 6.3.

6.3.4. Drawbar-pull analysis for the experimental tyre with 10kN load in higher cohesion soil.

DRAWBAR-PULL FOR 10kN LOAD ON THE 1m Diameter EXPERIMENTAL TYRE IN HIGHER COHESION SOIL

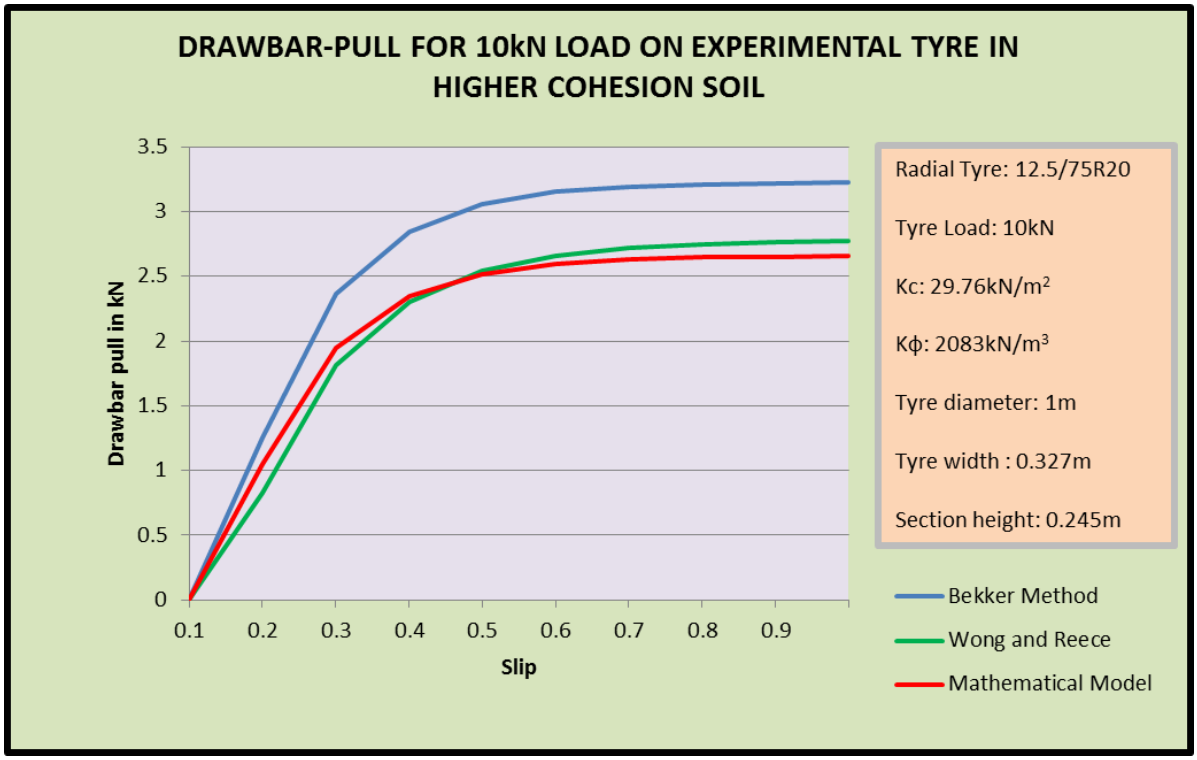

Figure 6.6: Drawbar-pull analysis for the experimental tyre with 10kN load in higher cohesion soil

The results for the 10kN load are the same as those for 15kN except for different values:

- Drawbar-pull at slip 0.3
- Bekker method: 2.85kN
- Wong and Reece: 2.30kN
- Mathematical model: 2.34kN

Bekker Method (KN)	2.85	Bekker Method (KN)	2.85	Mathematical Model (KN)	2.30
Wong and Reece Method (KN)	2.30	Mathematical Model (KN)	2.34	Wong and Reece Method (KN)	2.34
Difference (KN)	**0.55**	Difference (KN)	**0.51**	Difference (KN)	**0.04**
Difference (%)	23.9	Difference (%)	21.8	Difference (%)	1.7

Table 6.4: Drawbar-pull output comparative analysis between Bekker method, Wong/Reece method and POWERSEV mathematical model under 10kN load in the experimental tyre in higher cohesion soil

From table 6.4, with the load reduced to 10kN the mathematical model results still provides the most desirable average result but closer to Wong/Reece results because both deploy the principle of motion equilibrium. The major difference is in the rut depth calculation which forms the key part in the level of accuracy

After slip value of 0.5 there is no significant return for more traction. Any increase in velocity beyond this point results in wastage of energy. The mathematical model results graph fall within the acceptable traction efficiency between 0.3 and 0.5 where higher drawbar-pull is attained efficiently. Even the lowest applied load produces drawbar-pull that lies within the limits of the reference graphs. A direct effect of reduced load is again noticed in reduced drawbar-pull values.

6.3.5. Comparison of results outcome

Figures 6.5 and 6.6 illustrate the difference in the drawbar-pulls generated as results of reduced applied load from 25kN to 20kN respectively. Figures 6.7 and 6.8 illustrate the difference in drawbar-pull resulting from reduced applied load of 15kN and 10kN respectively. The significance of the difference is further illustrated in the following graphs:

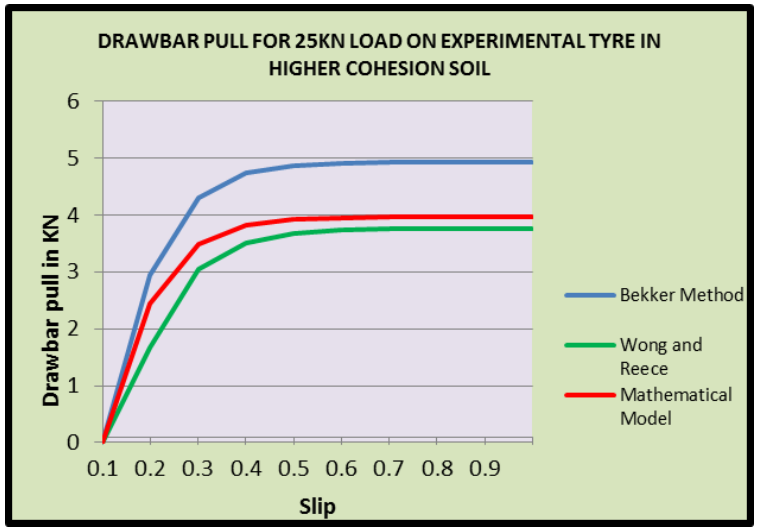

Figure 6.7: Drawbar-pull analysis for the experimental tyre with 25kN load in HCS

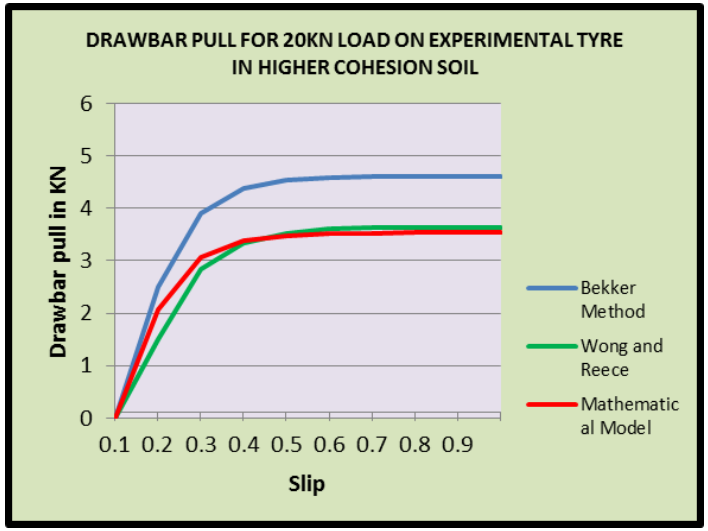

Figure 6.8: Drawbar-pull analysis for the experimental tyre with 20kN load in HCS

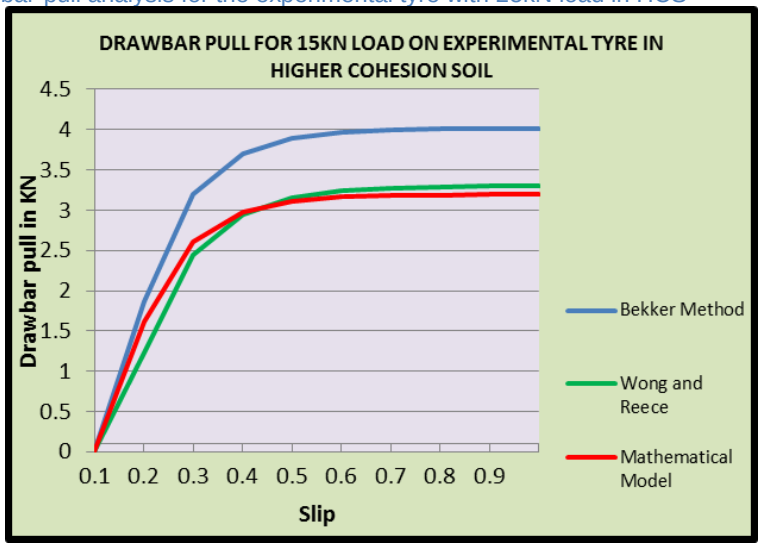

Figure 6.9: Drawbar-pull analysis for the experimental tyre with 15kN load in HCS

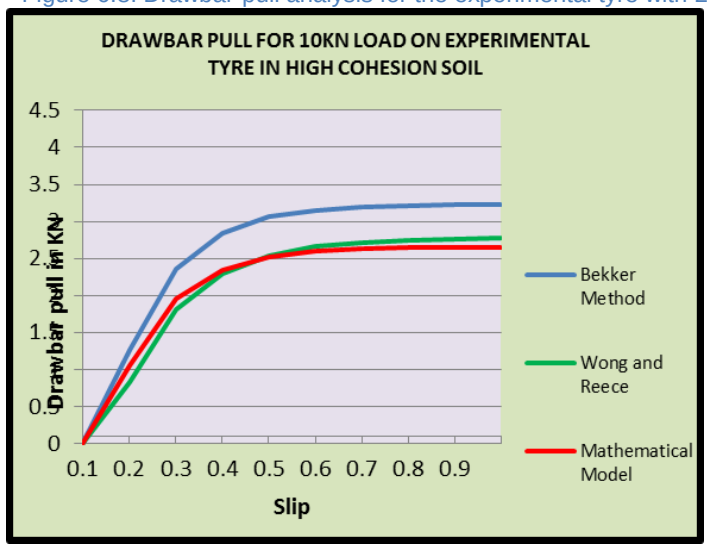

Figure 6.10: Drawbar-pull analysis for the experimental tyre with 10kN load in HCS

6.3.6. Effect of the rebound factor

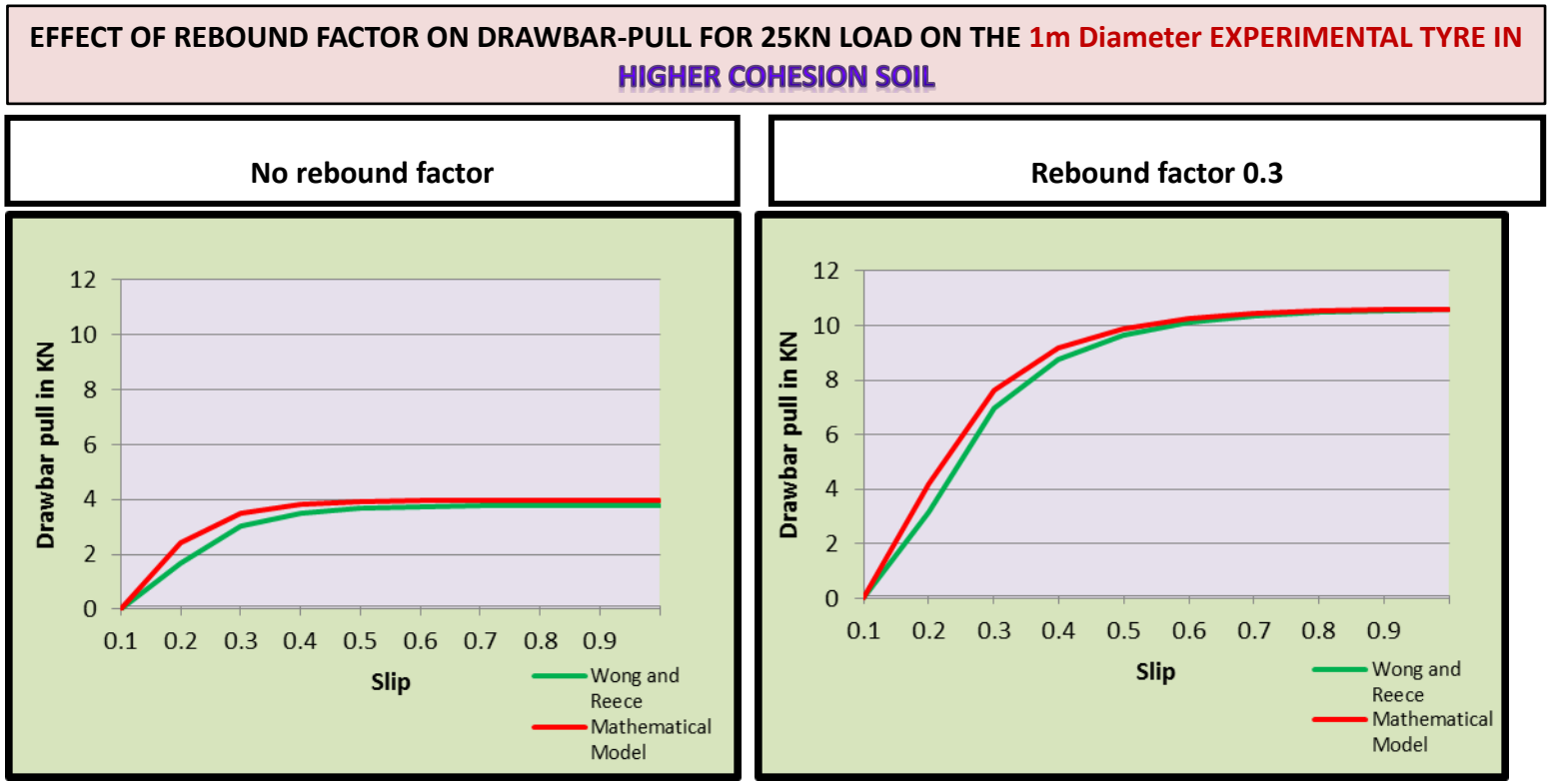

Figure 6.11: Drawbar-pull analysis for the tyre with 25kN load in HCS with no rebound factor

Figure 6.12: Drawbar-pull analysis for the tyre with 25kN load in HCS with 0.3 rebound factor

The rebound factor can range from 0.1 to 0.9. The data can be obtained from the experimental soil assessment. The rebound factor is influenced by the opposite reaction generated by the effect of the wheel exit angle. The rebound factor results in increased drawbar-pull as seen in figures in 6.9 and 6.10. The effect of the rebound factor is illustrated in figures 6.9 and 6.10. The rebound factor will vary from terrain to terrain and in most cases is obtained through experiments.

The mathematical model developed is consistent with the Bekker method and Wong and Reece approach. The maximum tractive efficiency is between 0.3 and 0.5. High soil cohesion results in less wheel rut and more drawbar-pull. Lower cohesion soils resulted in deep wheel ruts thereby reducing the available drawbar-pull. These results strongly indicate that the mathematical model developed in chapter 4 is credible, justified and verified.

6.4. Mathematical model verification using drawbar-pull results by comparing with Bekker and Wong/Reece models: Lower Cohesion Soil with the experimental tyre

6.4.1. Drawbar-pull analysis for the experimental tyre with 25kN load in lower cohesion soil.

The 25kN load on the tyre in low cohesion produces deep wheel ruts and negative drawbar-pull for all three methods. This result suggests that it's almost impossible and uneconomical to drive under the given conditions. These results confirm the results by other scholars as shown in the literature review chapter. Deep rutting for the wheels or tyres is very uneconomical because significant energy is wasted and lost in the process of attempting to overcome motion resistance by the mobile tyre. The results for the 20kN load are similar to those of the 25kN load where ruts are

deeper and drawbar-pull is negative. However the lower load results in less rutting and improved drawbar-pull values compared to the 25kN load.

The results for the 15kN load are similar to those of the 20kN load where ruts are deep enough to produce negative drawbar-pull. However the lower load results in less rutting and improved drawbar-pull values compared to the 20kN load.

6.4.2. Drawbar-pull analysis for the experimental tyre with 10kN load in clayey soil (LCS)

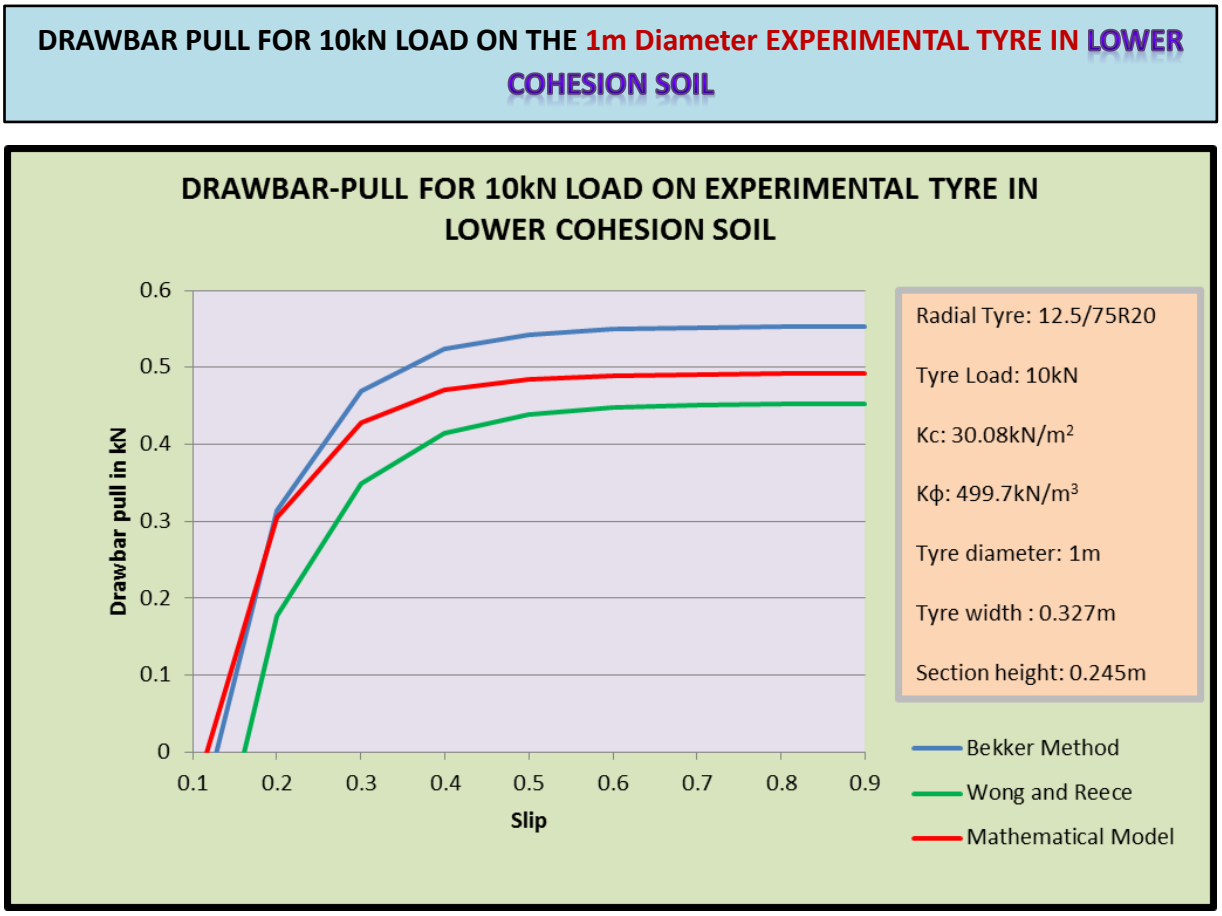

Figure 6.13: Drawbar-pull analysis for the experimental tyre with 10kN load in lower cohesion soil

The 10kN load applied produces some positive net drawbar-pull due to reduced rutting resulting in reduced motion resistance. This result suggests that unloaded wheeled plant may traverse in wet and deformable ground without encountering much energy loss. The mathematical model drawbar-pull generally falls between

the Bekker method and Wong-Reece approach as seen in figure 6.11. The three drawbar graphs confirm that the wheel slip efficiency falls between 0.3 and 0.5. The lower load produces low rutting with positive drawbar-pull despite being in lower values.

Drawbar-pull at slip 0.5

- Bekker method: 0.52kN
- Wong and Reece: 0.44kN
- Mathematical model: 0.48kN

After slip value of 0.5 there is no significant return for more tyre traction.

Bekker Method (KN)	0.52	Bekker Method (KN)	0.52	Mathematical Model (KN)	0.48
Wong and Reece Method (KN)	0.44	Mathematical Model (KN)	0.48	Wong and Reece Method (KN)	0.44
Difference (KN)	**0.08**	Difference (KN)	**0.04**	Difference (KN)	**0.04**
Difference (%)	18.2	Difference (%)	8.3	Difference (%)	9.1

Table 6.5: Drawbar-pull output comparative analysis between Bekker method, Wong/Reece method and POWERSEV mathematical model under 10kN load in the experimental tyre in lower cohesion soil

The mathematical model still compares extremely well with the other two control models even in smaller drawbar-pull value outputs arising from lower cohesion soil. This confirms that the mathematical model is effectively functional both in high and low cohesion values of soils. The difference between the mathematical model results and the other two control models both in terms of value and percentages is noticeable in table 6.5. The table also illustrates the relationship between lower load and the subsequent lower drawbar-pull output. Deep tyre rutting is experienced in low cohesion from high load. Lower loads results in reduced wheel rutting making positive drawbar-pull available at the tyre. Slip values higher than 0.5 result in expensive, uneconomical and impractical runs for most of the times. Lower velocity and lower loads are more appropriate for lower cohesion soils. From the graph in figure 6.11 the correct selection of velocity plays an important role in the attainment of economic performance of wheeled plant.

The graph further shows that beyond a certain point there is no more pulling power that is generated at the wheels despite the increase in velocity. Any attempt to drive faster would result in significant energy waste which in turn is translated to projects costs. These are costs that will either reduce the contractors profit or incur unnecessary expenditure on the part of the client. Despite the high values of drawbar-pull being produced, they are cancelled out by motion resistance which is determined by the nature of the soil at any given time such as moisture content, soil cohesion and angle of shearing resistance.

6.5. Mathematical model verification using drawbar-pull results by comparing with Bekker and Wong/Reece models: HCS with mathematical model tyre

6.5.1. Drawbar-pull analysis for the model tyre with 25kN load in medium soil (HCS)

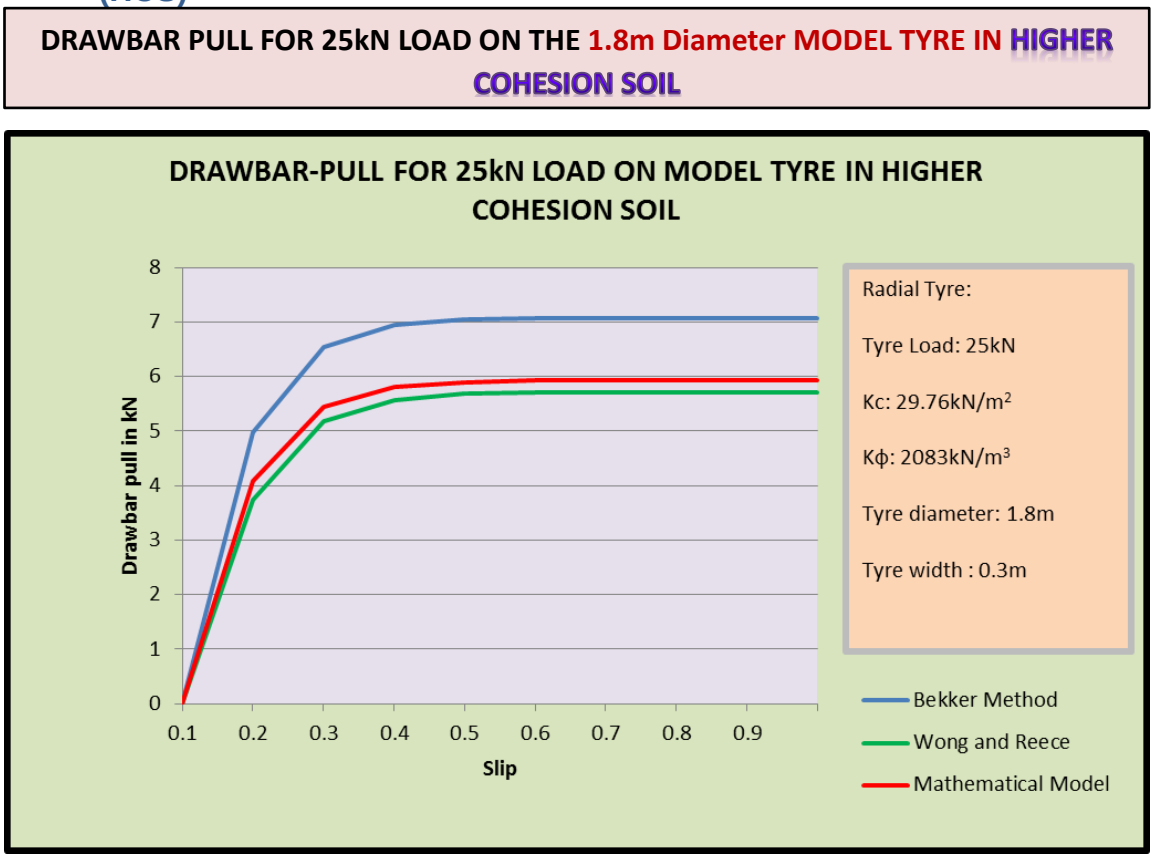

Figure 6.14: Drawbar-pull analysis for the mathematical model tyre with 25kN load in higher cohesion soil

From the figure 6.12, the mathematical model drawbar-pull generally falls between the Bekker method and Wong-Reece approach which is acceptable. Table 6.6 also confirms this outcome through numerical data presentation in terms of drawbar-pull values and percentage differences between the models. The three drawbar graphs confirm that the wheel slip efficiency falls between 0.3 and 0.45.

- Drawbar-pull at slip 0.5
- Bekker method: 7.07kN
- Wong and Reece: 5.71kN
- Mathematical model: 5.92kN

After slip value of 0.5 there is no significant return for more traction.

Bekker Method (KN)	7.07	Bekker Method (KN)	7.07	Mathematical Model (KN)	5.92
Wong and Reece Method (KN)	5.71	Mathematical Model (KN)	5.92	Wong and Reece Method (KN)	5.71
Difference (KN)	**1.36**	Difference (KN)	**1.15**	Difference (KN)	**0.21**
Difference (%)	23.8	Difference (%)	19.4	Difference (%)	3.7

Table 6.6: Drawbar-pull output comparative analysis between Bekker method, Wong/Reece method and POWERSEV mathematical model under 25kN load in the mathematical model tyre in higher cohesion soil

Higher loads indicate higher drawbar-pull for the mathematical model at 5.92kN. The drawbar-pull for the 20kN load is reduced to 3.18kN. This suggests that there is higher traction available at the wheels in stable clay condition. This conclusion is also strongly supported by the outcome of laboratory experiments presented in chapter 7.

6.5.2. Drawbar-pull analysis for the model tyre with 10kN load in medium soil (HCS)

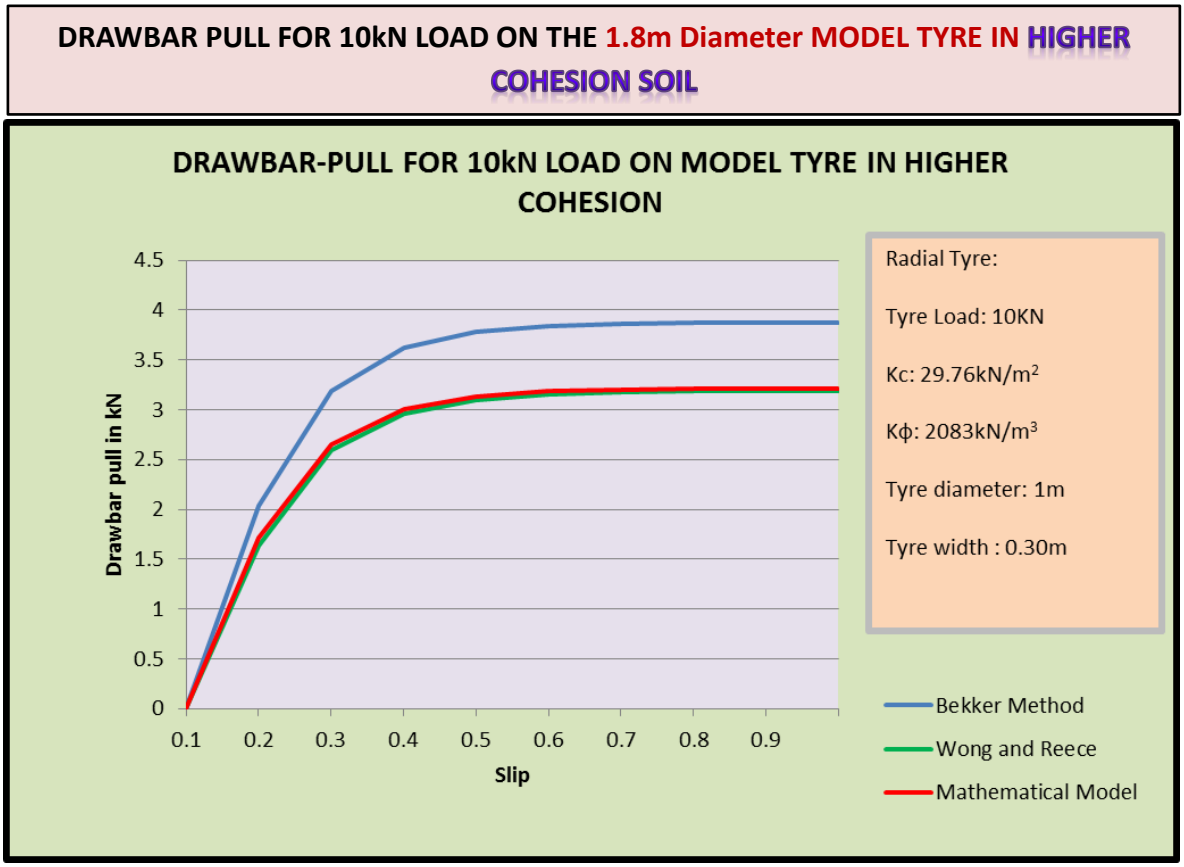

Figure 6.15: Drawbar-pull analysis for the mathematical model type with 10kN load in higher cohesion soil

Like the 25kN load mathematical model drawbar-pull generally falls between the Bekker method and Wong-Reece approach. The three drawbar graphs confirm that the wheel slip efficiency falls between 0.3 and 0.5 as shown in figure 6.13. Table 6.7 below also confirms this result by tabulating the drawbar-pull in terms of values and percentage differences.

- Drawbar-pull at slip 0.5
- Bekker method: 3.84kN
- Wong and Reece: 3.15kN
- Mathematical model: 3.18kN
- After slip value of 0.5 there is no significant return for more traction.

Bekker Method (KN)	3.84	Bekker Method (KN)	3.84	Mathematical Model (KN)	3.18
Wong and Reece Method (KN)	3.15	Mathematical Model (KN)	3.18	Wong and Reece Method (KN)	3.15
Difference (KN)	**0.69**	Difference (KN)	**0.66**	Difference (KN)	**0.03**
Difference (%)	21.9	Difference (%)	20.8	Difference (%)	1.0

Table 6.7: Drawbar-pull output comparative analysis between Bekker method, Wong/Reece method and POWERSEV mathematical model under 10kN load in the mathematical model tyre in higher cohesion soil

6.5.3. Drawbar-pull analysis for the model tyre with 5.1kN load in medium soil (HCS)

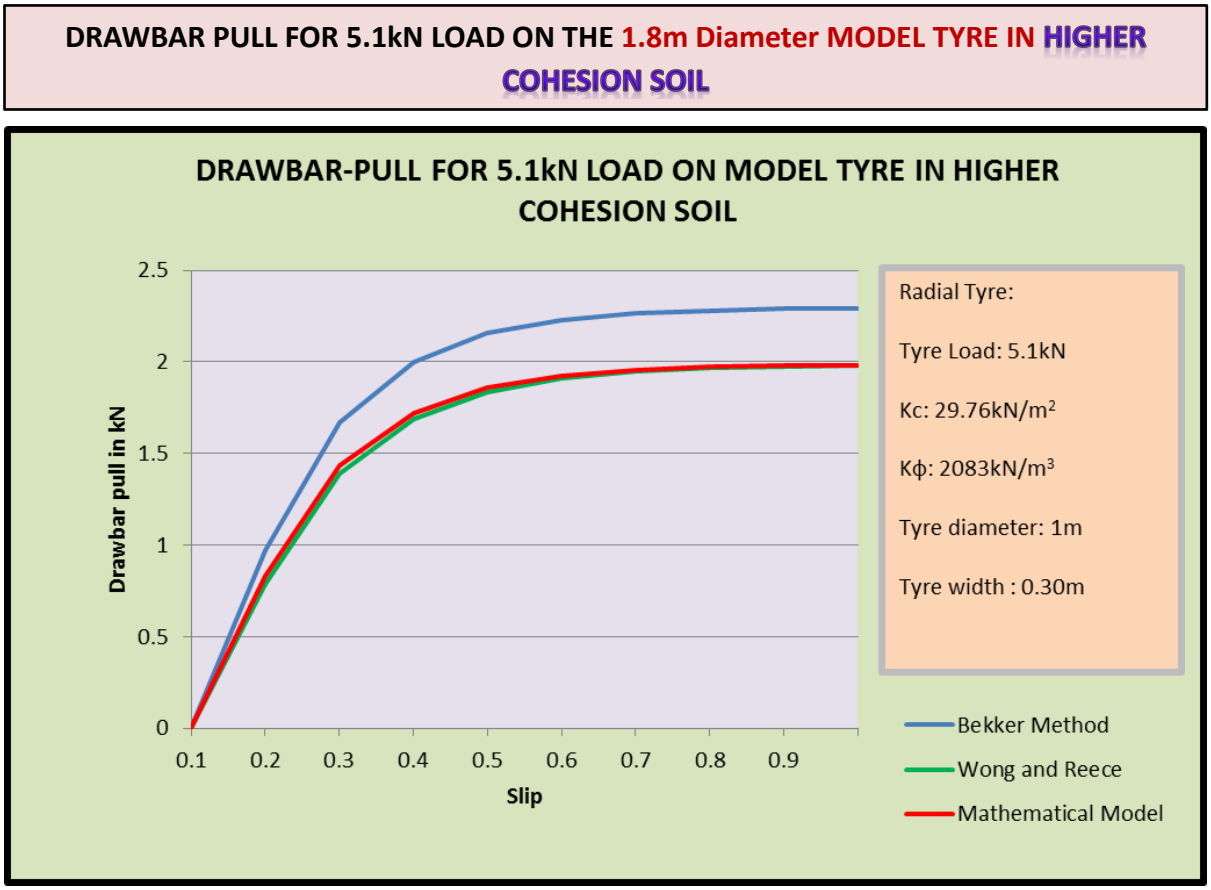

Figure 6.16: Drawbar-pull analysis for the mathematical model tyre with 5.1kN load in higher cohesion soil

Like the 10kN load mathematical model drawbar-pull generally falls between the Bekker method and Wong-Reece approach. The three drawbar graphs confirm that the wheel slip efficiency falls between 0.3 and 0.5. These results confirm the outcome of the original mathematical model developed.

- Drawbar-pull at slip 0.5
- Bekker method: 2.23kN
- Wong and Reece: 1.91kN

- Mathematical model: 1.93kN

After the slip value of 0.5 there is no significant return for more traction. The original mathematical model tyre results and verification results based on Bekker and Wong/Reece approaches shows consistency of the outcome results as illustrated in table 6.8 and figure 6.14. The 5.1 kN used is the exact load used in the mathematical model which also performs consistently with the outcome of this computational analysis model.

Bekker Method (KN)	2.23	Bekker Method (KN)	2.23	Mathematical Model (KN)	1.93
Wong and Reece Method (KN)	1.91	Mathematical Model (KN)	1.93	Wong and Reece Method (KN)	1.91
Difference (KN)	**0.32**	Difference (KN)	**0.30**	Difference (KN)	**0.02**
Difference (%)	16.8	Difference (%)	15.5	Difference (%)	1.0

Table 6.8: Drawbar-pull output comparative analysis between Bekker method, Wong/Reece method and POWERSEV mathematical model under 5.1kN load in the mathematical model tyre in higher cohesion soil

6.6. Mathematical model verification using drawbar-pull results by comparing with Bekker and Wong/Reece models: LCS with model tyre

6.6.1. Drawbar-pull analysis for the model tyre with 25kN load in clayey soil (Lower Cohesion Soil)

Like the results for the 25kN load on the tyre in low cohesion soil results in deep wheel ruts and negative drawbar-pull are produced for all the three methods. However due to the bigger tyre diameter as compared to the experimental tyre, the drawbar-pull is positive for the Bekker and mathematical models after the slip of 0.2. These results confirm the results by other scholars as shown in the literature review.

6.6.2. Drawbar-pull analysis for the model tyre with 10kN load in clayey soil (LCS)

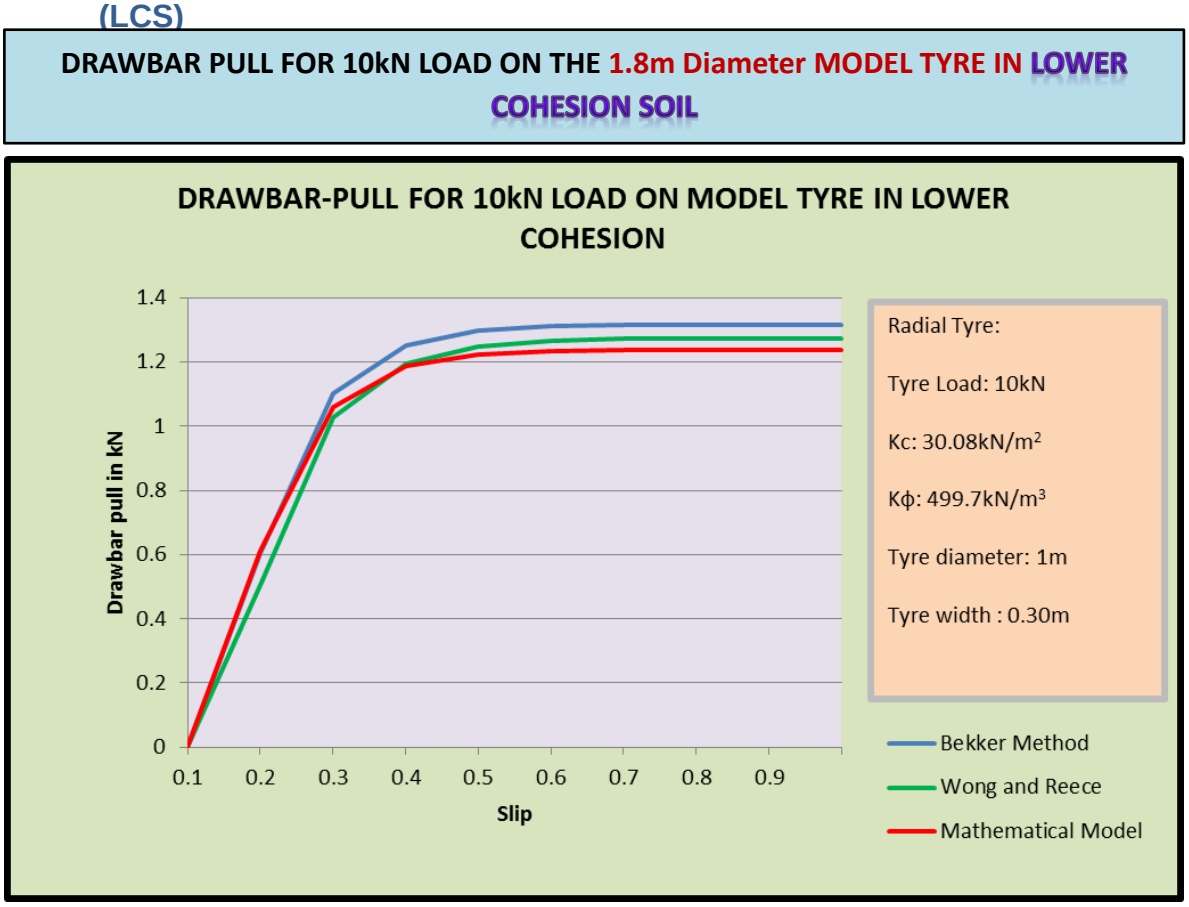

Figure 6.17: Drawbar-pull analysis for the mathematical model tyre with 10kN load in lower cohesion soil

The lower cohesion soil produces less drawbar-pull (1.19kN) compared to higher cohesion soil (1.93kN) which is more stable. The drawbar-pull for the mathematical model generally falls between the Bekker method and Wong-Reece approach until after 0.3 to 0.4 slip when before it crosses the Wong Reece graph as shown in figure 5.42. In the three drawbar-pull graphs, the maximum wheel slip efficiency falls between 0.3 and 0.5.

- Drawbar-pull at slip 0.3
- Bekker method: 1.25kN
- Wong and Reece: 1.19kN
- Mathematical model: 1.19kN

After slip value of 0.5 there is no significant return for more wheel traction.

Bekker Method (KN)	1.25	Bekker Method (KN)	1.25	Mathematical Model (KN)	1.19
Wong and Reece Method (KN)	1.19	Mathematical Model (KN)	1.19	Wong and Reece Method (KN)	1.19
Difference (KN)	**0.06**	Difference (KN)	**0.06**	Difference (KN)	**0.00**
Difference (%)	5.0	Difference (%)	5.0	Difference (%)	0.0

Table 6.9: Drawbar-pull output comparative analysis between Bekker method, Wong/Reece method and POWERSEV mathematical model under 10kN load in the mathematical model tyre in lower cohesion soil

In table 6.9, there is no difference between the mathematical model and Wong/Reece approach. The difference between the mathematical model and Bekker method is only 5% which is very much acceptable

6.6.3. Drawbar-pull analysis for the model tyre with 5.1kN load in clayey soil (Lower Cohesion Soil)

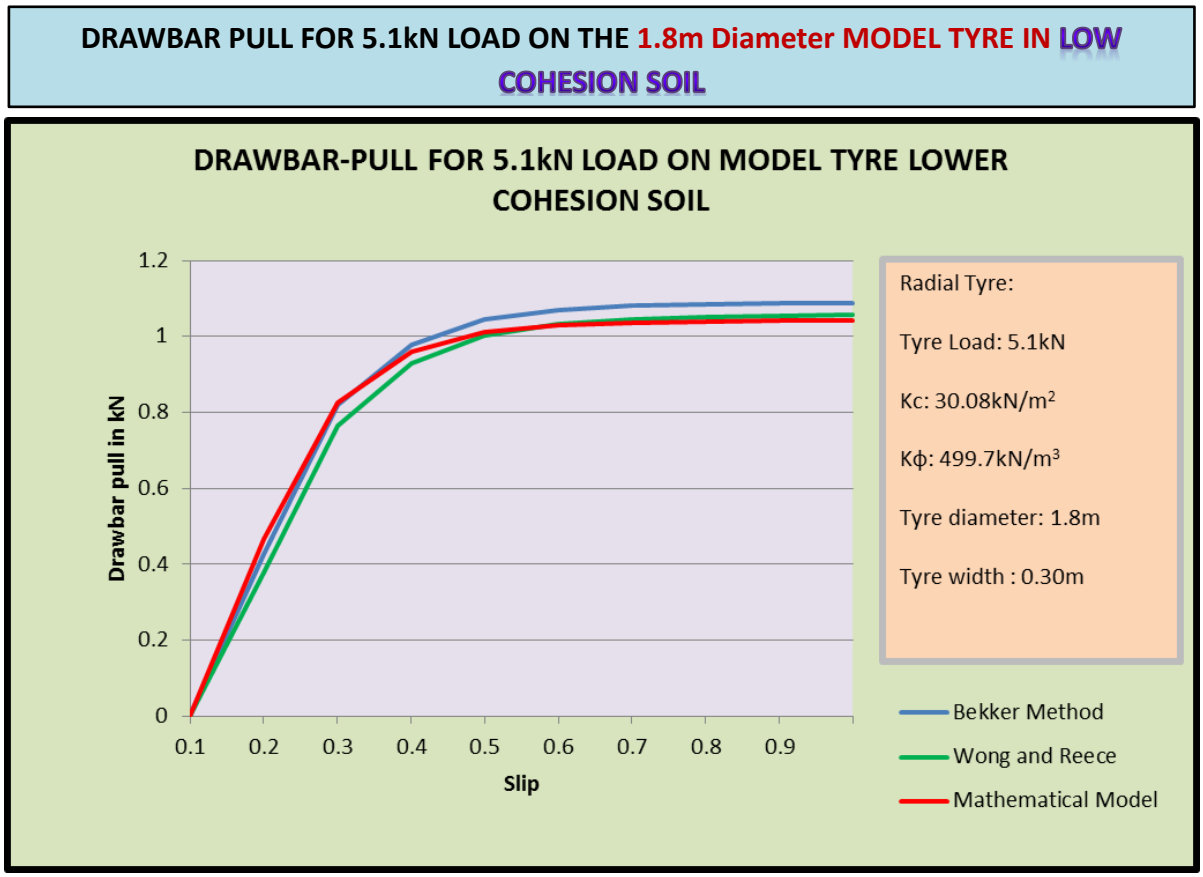

Figure 6.18: Drawbar-pull analysis for the mathematical model tyre with 5.1kN load in lower cohesion soil

Just like the 10kN tyre load, the 5.1kN load based drawbar-pull for the mathematical model generally falls between the Bekker method and Wong-Reece approach until after 0.4 slip when before it crosses the Wong Reece graph. The

three drawbar-pull graphs have the maximum wheel slip efficiency falls between 0.3 and 0.5. The drawbar-pull values reduces because of reduced load

- Drawbar-pull at slip 0.3
- Bekker method: 1.04kN
- Wong and Reece: 1.00kN
- Mathematical model: 1.01kN

After slip value of 0.5 there is no significant return for more tyre traction.

Bekker Method (KN)	1.04	Bekker Method (KN)	1.04	Mathematical Model (KN)	1.01
Wong and Reece Method (KN)	1.00	Mathematical Model (KN)	1.01	Wong and Reece Method (KN)	1.00
Difference (KN)	**0.04**	Difference (KN)	**0.03**	Difference (KN)	**0.01**
Difference (%)	4.0	Difference (%)	3.0	Difference (%)	1.0

Table 6.10: Drawbar-pull output comparative analysis between Bekker method, Wong/Reece method and POWERSEV mathematical model under 5.1kN load in the mathematical model tyre in lower cohesion soil

Positive drawbar-pull is attained by the reduced load of 5.1kN which is as a result of reduced tyre motion arising from reduced motion resistance and reduced rut depth. In the case of higher loading, the large value of drawbar-pull is lost through motion resistance. The maximum drawbar-pull produced is just above 1kN for the mathematical model. Table 6.10 shows that the model is close to both reference models with the highest difference being with the Bekker method at 3%. There is more drawbar-pull in higher value cohesion soil than in lower cohesion soil. Almost all runs are in rigid wheel mode because the evidence from the tyre mode analysis suggests that the higher values of tyre pressure are mainly found in off-road vehicles operating in deformable terrain.

6.6.4. Comparison of tyre loads effects on drawbar-pull

EFFECT OF LOAD ON DRAWBAR PULL IN 25kN AND 10KN LOAD ON THE 1m Diameter MODEL TYRE IN LOWER AND HIGHER COHESION SOIL

EFFECT OF 25kN TYRE LOAD ON DRAWBAR PULL FOR SLIP RATIO 0.4 IN EXPERIMENTAL TYRE IN HIGH COHESION SOIL

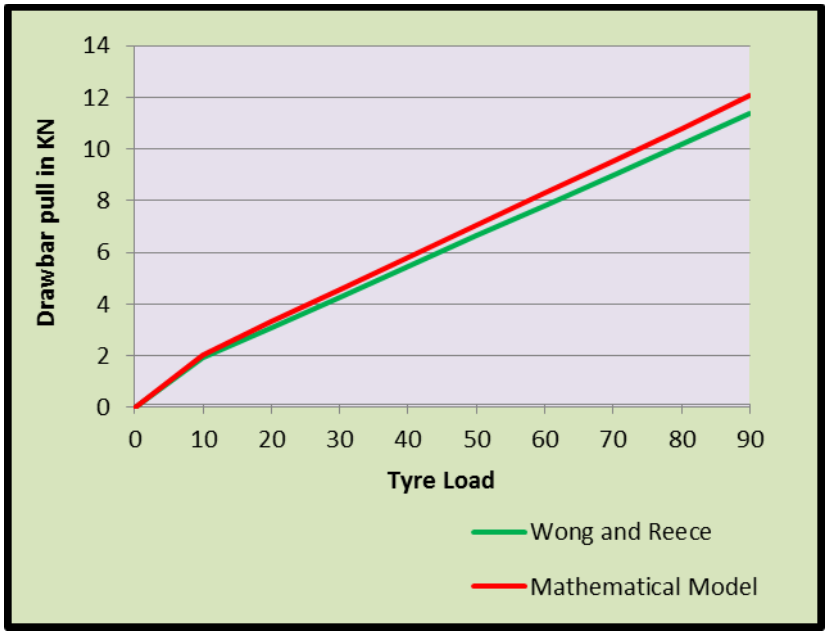

Figure 6.19: Tyre load effect on drawbar-pull in higher cohesion soil

EFFECT OF TYRE WEIGHT ON DRAWBAR PULL FOR 10kN LOAD ON EXPERIMENTAL TYRE IN LOW COHESION SOIL SLIP RATIO 0.4

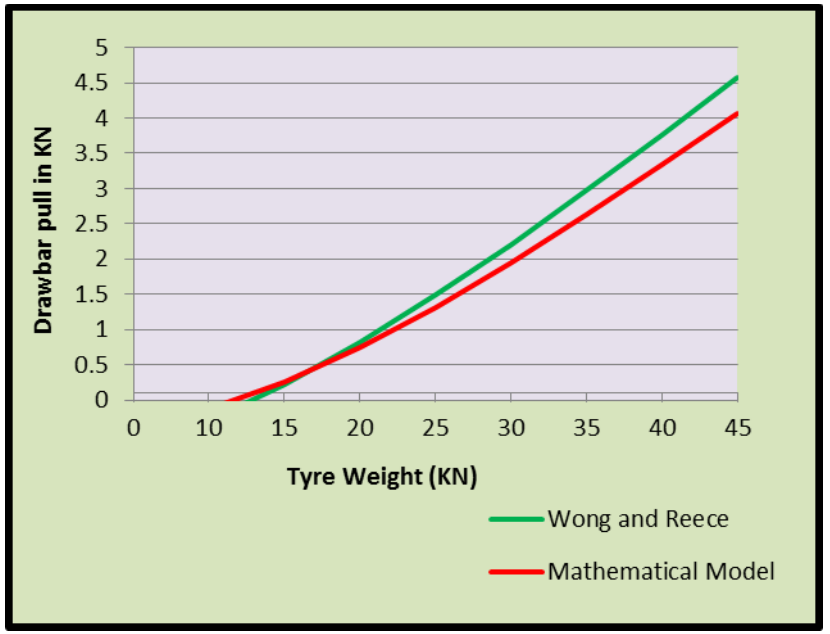

Figure 6.20: Tyre load effect on drawbar-pull in lower cohesion soil

Increase in load results in increase in drawbar-pull of which the ultimate/available drawbar-pull is determined by the motion resistance.

6.6.5. Comparison of tyre radius effects on drawbar-pull in medium and clayey soils.

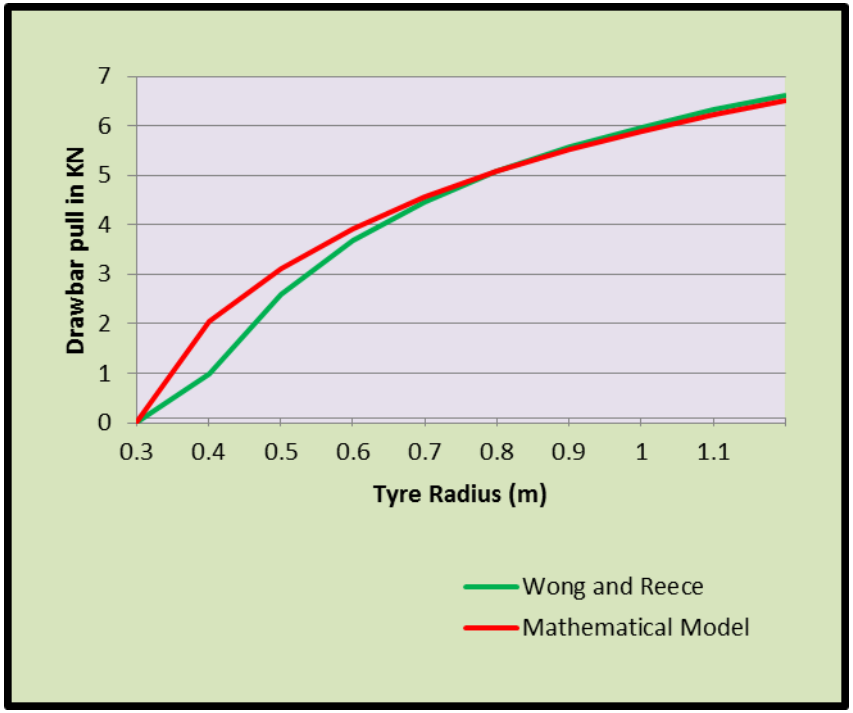

Figure 6.21: Tyre radius effect on drawbar-pull in higher cohesion soil

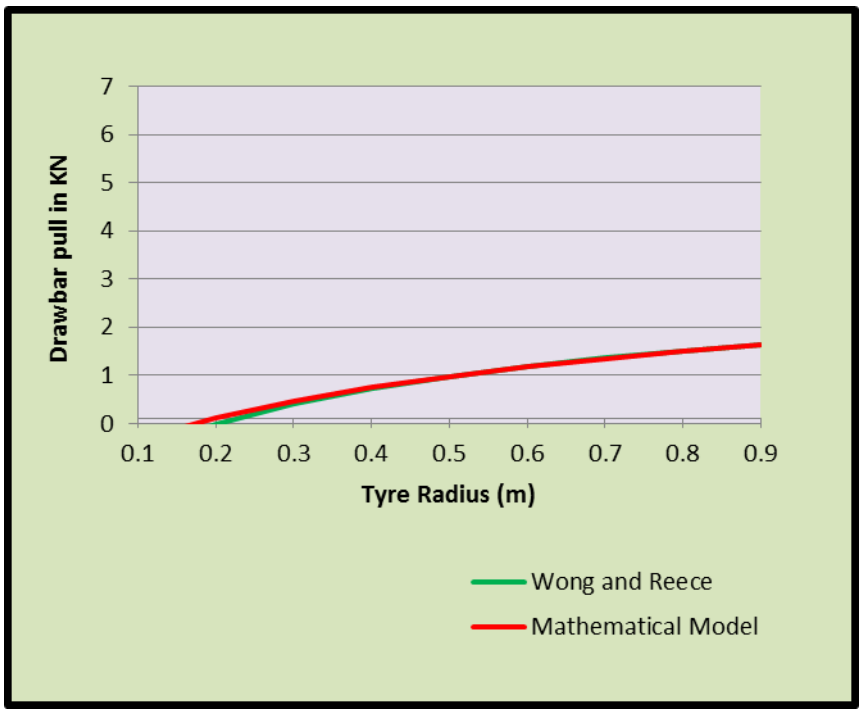

Figure 6.22: Tyre radius effect on drawbar-pull in lower cohesion soil

Figure 6.19 and figure 6.20 indicate that increasing wheel radius improves drawbar-pull at the wheels. This result verifies the mathematical model results in section 4.4.5 of chapter 4 under the subtitle 'Effect of wheel radius'. From the results above drawbar-pull increases with increase in diameter and self-weight. The mathematical model has shown accuracy in predicting drawbar-pull and traction efficiency. The mathematical model has also demonstrated the strength in isolated analysis of the variables. The verification results have confirmed the outcome of various studies discussed in the literature review including the outcome of Reid's rut depth model results.

6.7. Strengths of the mathematical model

The good level of accuracy in the mathematical model results is driven by POWERSEV can be attributed to the following:

a) Detailed approach towards wheel sinkage calculation/prediction and subsequent analysis
b) It is built from first mathematical principles based on numerical integration and motion equilibrium.
c) It applies the Newtonian Mechanics particularly the Laws of Motion and the Conservation Work-Energy Principle.
d) The model is able to perform isolated analysis of variables under different terrain and wheel parameters.

The tyre pressure charts from good year attached in appendix 19 and 20 show that the tyre pressures for off-the road tyres are so high that they all would operate as rigid wheel in highly deformable terrain. Lowest pressure for some off road haulage tyres can be from 475kPa or 69PSI for the slow speed service which automatically qualifies the tyres to operate in rigid mode.

6.8. Chapter Summary

This chapter has strongly demonstrated that the mathematical model powered by POWERSEV compares well with other existing approved and acceptable models namely the Bekker and the Wong/Reece semi-empirical models. The mathematical model has further proved that it is able to process different values of the soil and tyre parameters at hand. It is also able to handle high and low cohesion soils, high and low angle of shearing resistance, heavier and lighter applied loads including the respective slip ratios.

The chapter has also shown that this mathematical model is best suited for big and high pressured tyres for wheeled construction plant operating in rigid mode in deformable terrain. Tyres provide better traction due to increased contact area however; fully inflated tyres moving in deformable terrain will hardly deflect thereby requiring other options of assessing or improving traction. Low pressure but safely inflated can utilise tyres can use deflection and increased contact area to attain traction on stable terrain.

From the graphs presented in the chapter, more drawbar-pull is generated in high value soil cohesion and angle of shearing resistances. This result is confirmed by

the laboratory analysis based results from MOBILITY SF-3713 in chapter 7. The drawbar-pull output values attained are optimum at 0.5 slip ratio. The ultimate result from the graphs as earlier highlighted is that increase in velocity does not necessarily improve drawbar-pull performance. This result is very critical in decision making regarding selection of wheeled plant and the optimum operational factors such as speed, gear selection, and tyre size and tyre pressure. The mathematical model shows consistency and reliability for all described situations in higher and lower value cohesion and angle of shearing resistance soils. It is worth mentioning that scaling factors would be relevant especially when handling larger values of parameters for live running projects.

CHAPTER 7

MATHEMATICAL MODEL VERIFICATION STAGE 3:

LABORATORY EXPERIMENTS: MOBILITY SF-3713

7.0. CHAPTER 7

MATHEMATICAL MODEL VERIFICATION STAGE 3: LABORATORY EXPERIMENTS

7.1. Introduction

This chapter presents the third and final stage of the model verification process. This part of the verification process constitutes laboratory experiments based on a modified four wheeled scooter machine MOBILITY SF-3713 (Figure 7.1) which is also discussed in section 3.8.1.3 of chapter 3. These experiments provide practical results in relation to the outcomes recorded in the mathematical modelling chapter and the first two stages of the mathematical model verification process.

The aim of this chapter is to increase confidence levels of the mathematical model and the model verification results by conducting laboratory experiments in order to assess the consistency and accuracy of the mathematical model. These experiments provide the practical outcome of the results. The purpose of the laboratory experiments is to:

1. Verify/confirm that the flexible tyres can operate in rigid and/or flexible modes
2. Verify/confirm that speed has an effect on power output in terms of traction/drawbar-pull.
3. Verify/confirm that tyre pressure has a significant effect on the performance of wheeled machine in terms of velocity, rut depth and drawbar-pull.

4. Verify/confirm that time is greatly affected by the changing effects of the terrain and tyre mode at each given time.
5. Verify the extent and nature of wheel rut depth created by the wheeled machine under different operating conditions and terrain.
6. Verify the effect of the rut depth on drawbar-pull being one of the research primary and main variables in this research.
7. Verify the effect of the varying weights on the performance of the machine.
8. Verify the difference between the performance of the machine on hard surface and deformable terrain (Sand and clay soils in this study).

The above purposes were achieved through the use of a machine in form of a mobility scooter that was significantly modified physically and electronically to meet the project objectives and requirements. The shop rider sovereign mobility scooter was named MOBILITY SF-3713 following the major modifications that were conducted on the machine. The laboratory conditions provided more control of the experimental procedures such as protection from external factors which included weather, temperature and soil test bed re-building.

7.2. Experimental equipment and Procedure: MOBILITY SF-3713

Figure 7.1 shows the special instrumented vehicle MOBILITY SF-3713 that was used for the laboratory experiments by running it on three different types of terrain namely non deformable hard pavement, wet clay and wet sand terrain beds. The labelled photograph containing the identification and description of the various parts of the vehicle can be found in appendix 24.

Figure 7.1: Instrumented Mobility SF-3713 vehicle

7.2.1. Speed selection and control on the hard ground

Velocity plays a key role in determining the travel time, slip ratio and tyre performance of the machine. In order to attain various velocities MOBILITY SF-3713 was selected because it has ten different speeds for which one speed can be selected at any given time using the speed selector as shown in figure 7.2. Speeds 1, 3, 5 and 7 were selected for this experiment. Speed 1 was the slowest while speed 7 was the maximum speed selected after considering the maximum length of the laboratory space used and the safety of the machine, operatives and the building. In addition any speed exceeding speed selection 7 would also compromise the accuracy of the results. The numerical velocity values of the speed selections varied depending on the respective factors (such load, inflation pressure and terrain) in place for each run. It is worth mentioning at this stage that the values obtained from the experimental runs were on the hard ground and were

used as benchmarks or reference points against deformable terrain runs in order to establish the effect of deformable terrain on the velocity of MOBILITY SF-3713.

7.2.2. Determining the actual velocity for each speed selector

Each speed mark was selected from the speed selector unit on MOBILITY SF-3713 at each given time to determine the actual velocity by using the general formula of distance divided by time. Marks were made on the ground at 0 metres, 3 metres and 9 metres as distance control points. The first 3 metres was used to allow the machine to accelerate to the constant velocity. Trials were conducted with longer distances and 3 metres was found to be long enough to bring the machine to constant velocity. The timer was activated at 3 metres and stopped at 9 metres travelling a total distance of 6 metres. The timer was also stopped at 9 metres. The velocity was then calculated by dividing the distance travelled in metres by the time taken in seconds. There were two timers, one on board the video camcorder and the other operated independently by the operative for quality control purposes. The process was repeated twice in order to get an average velocity for each of the four speed marks under consideration.

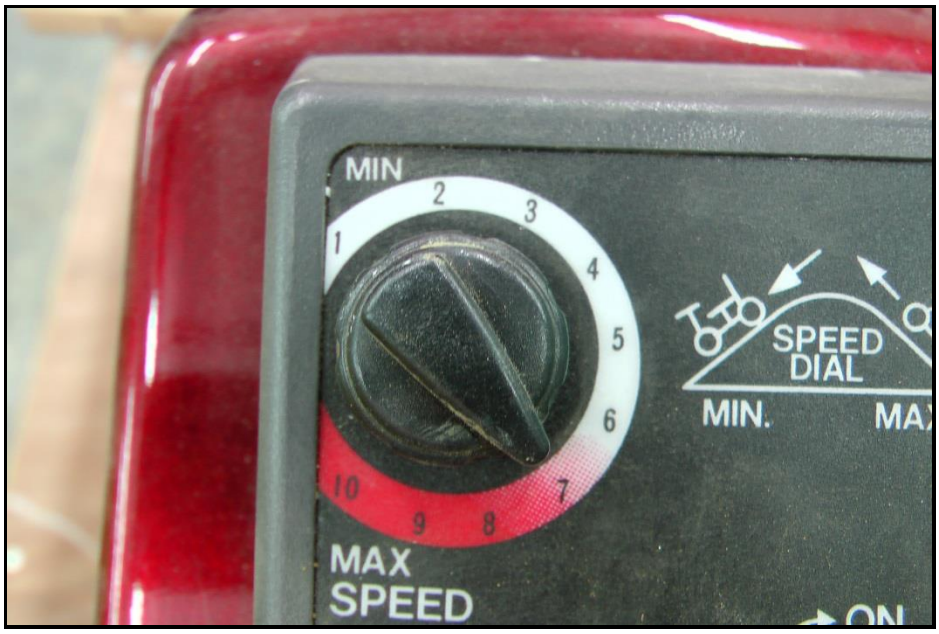

Figure 7.2: Speed selection unit

7.2.3. Speed selection and control on the sand and clay terrain

The same procedure for selecting speeds marks and determining actual velocities on hard ground described in section 7.2.2 was used for sand and clay terrain test beds. The only difference is that the velocity was affected by the sand and clay test beds due to the motion resistance encountered resulting from tyre rutting. The velocity of MOBILITY SF-3713 was compared with that of the hard ground and to establish the subsequent effect of reduced performance. The maximum distance travelled and time taken was recorded for all the four speeds which were compared with the earlier results from the hard ground.

7.2.4. Battery power meter

The machine had a battery meter that was used to monitor the level of the power supply in order to maintain consistency in terms of power supply to the motor as shown in figure 7.3 below. The power source was from two 12 volts batteries as shown in figure 7.4 whose capacity is equivalent to 20 miles of distance coverage.

Figure 7.3: Battery power meter

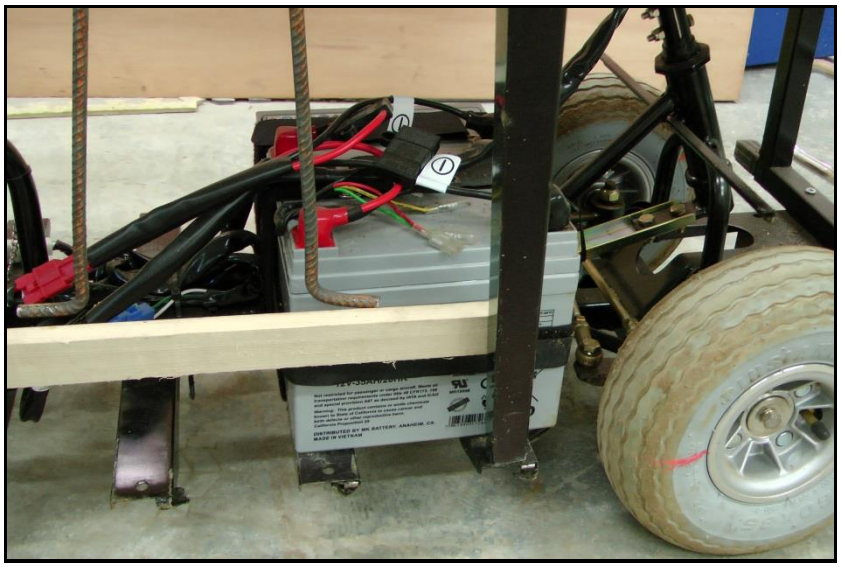

Figure 7.4: Two white 12 volts batteries housed at the bottom for stability

7.2.5. Braking system of the machine

In order to bring the machine to a stop after reaching the required distance, an electronic modification was done by introducing a cable switch. This switch was

operated by means of pulling the cable from a socket in order to cut supply. This approach created a safer stoppage mechanism of the machine without distorting the surface of the bed. Figures 7.5 to 7.7 below illustrates is the cable switch and mechanism (shown on the left of each photo) used for bringing the machine to a stop by simply pulling it off from the socket.

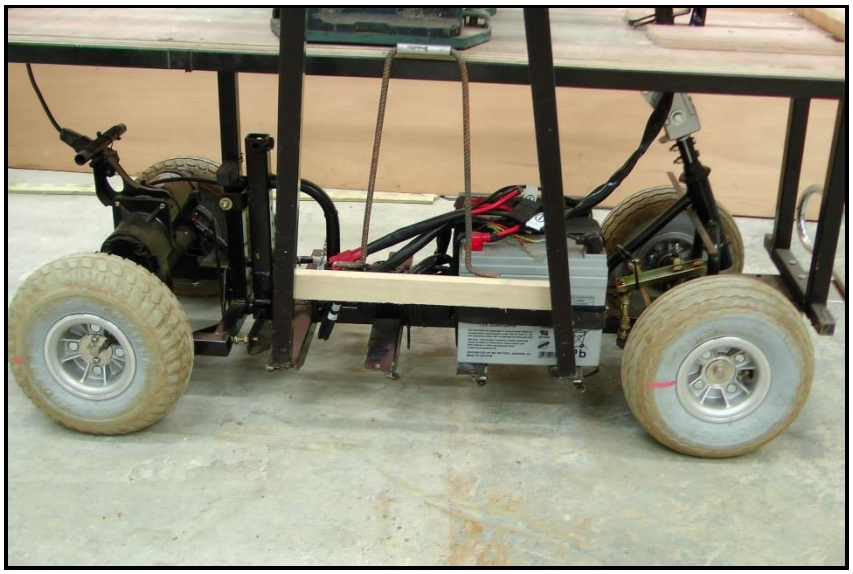

Figure 7.5: Cable connected to the motor for cutting power supply

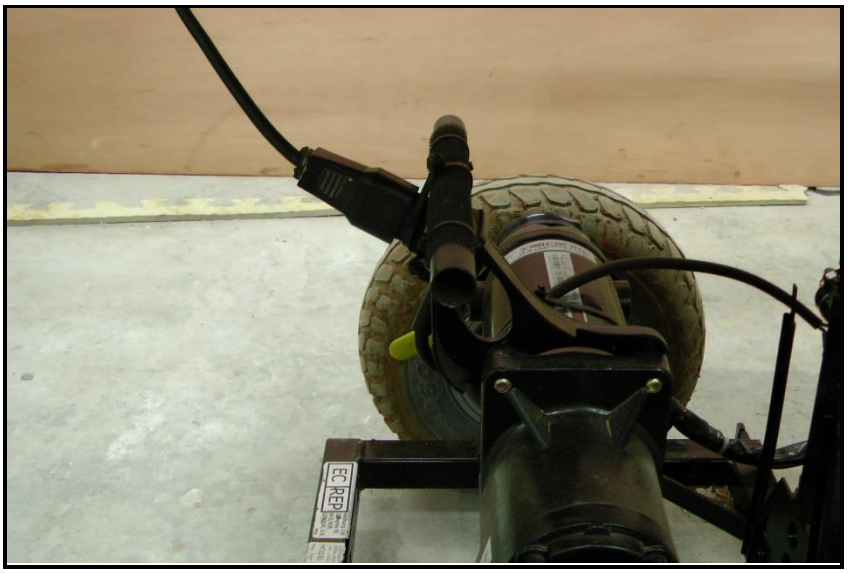

Figure 7.6: Closer view of the cable connected to the motor for cutting power supply

Figure 7.7: Perspective view of the cable connected to the motor for cutting power supply

7.2.6. Rut depth measurement

All rut depth measurements were 0mm for all the runs on hard non-deformable ground. This resulted in significant effects in tyre deflection and contact patch area whose results are demonstrated in figure 7.28. The slip was also recorded from the rotational difference between rear and front tyres obtained from the camcorder (figure 7.20) that was mounted on the machine.

7.2.7. Rut depth measurement for sand and clay terrain

Rut depth measurements for sand and clay solid were measured in millimetres using a ruler. The rut depths were taken at various points for both tyres after which the average rut depth was established. The pattern of the wheel rutting in relation to speed, soil type, weight and tyre pressure were all recorded and compared with the benchmark results from the hard ground experiments. The rear tyre measurements were taken as primary measurements being the ones that are

powered by the motor. All the effects on the performance of the special vehicle from the difference in front and rear tyre treads were assumed to be negligible.

7.2.8. Tyre Pressure measurement and variation

In order to verify the concept surrounding the effect of tyre pressure variation on the performance of the wheeled machinery, the tyres on the MOBILITY SF-3713 are pneumatic and of size 260 x 85mm. Three values of tyre pressure were selected for analysis namely 45PSI being the maximum, 10PSI and 3PSI. The 10PSI was selected in order to record the difference between the medium and the lowest tyre pressures. The 3PSI tyre pressure was selected as the lowest working tyre pressure because the effect of tyre pressure reduction was only significant with the lowest possible tyre pressure due to the small size of the tyre. Tyre foot prints were also taken in order to establish tyre contact area for every respective weight and tyre pressure as seen in figure 7.28. The tyre inflation pressure source was industrial compressed air while the digital tyre pressure gauge was used to obtain the accurate tyre pressure at each given time. Figures 7.8 to 7.10 provide the equipment used inflation, reading and regulation of the tyre pressure.

Figure 7.8: Digital tyre pressure gauge/reader

Figure 7.9: Demonstration of digital tyre pressure gauge reading

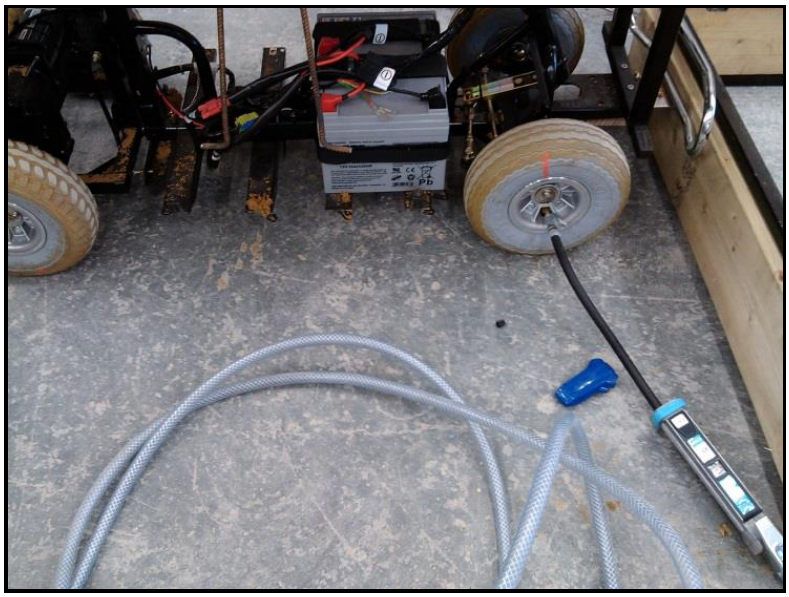

Figure 7.10: Tyre inflation in progress using compressed air

7.2.9. Tyre Pressure variation in sand and clay terrain beds

The tyre pressure variation procedure in deformable sand and clay soils was the same as for the hard ground. The difference is that there were only two tyre

pressure in use namely 45PSI and 3PSI as explained in section 7.2.8. The 10PSI was not used because of its insignificance in isolated analysis due to the smaller size of the tyre. The difference in rut depth influenced by tyre factor variation was recorded. While the effect of tyre pressure was seen in the deflection and contact area on the hard ground, the effect on deformable terrain was seen in rut depth which was recorded and analysed. The velocity and soil reaction patterns were also recorded for analysis.

7.2.10. Performance of machine: Drawbar-pull values

Drawbar-pull values measured in Newtons constitutes one of the major research outputs. While the effect of tyre pressure and applied load were seen in rut depth in deformable terrain and reduced speed on hard ground, the pulling power measured in form of drawbar-pull provided a more precise result and interpretation of the actual power available both on the hard ground and in soft terrain (Sand and clay in this particular case).

The drawbar-pull values for all experiments encompassing different tyre pressures, weights and velocities were measured by attaching the slack-less chain to the machine and a secure point in order to obtain the maximum drawbar-pull available with the given conditions. The drawbar-pull values were obtained and recorded using a special load cell dynamometer called PCE-1000 shown in figures 7.11 to 7.14 and has a maximum capacity of 100Kg or 1000N. The load cell was connected to a digital gauge/reader via a cable. Values of drawbar-pull were equally compared with results from the mathematical model and computational analysis.

Figure 7.11: Dynamometer load cell and PCE-1000 force gauge

Figure 7.12: Dynamometer load cell in use

Figure 7.13: Dynamometer load cell and PCE-1000 force gauge in use

Figure 7.14: Mobility SF-3713 pulling its own weight to measure maximum force available using the dynamometer load cell PCE force gauge

7.2.11. Effect of wheel weight/Applied load

In an effort to establish and verify the effect of applied load, 4 blocks of 20kg each were used in combination to determine the cumulative effect of applied load. The MOBILITY SF-3713 was run with applied loads of 0Kg, 20kg, 40kg, 60kg and 80kg in all the three terrain profiles namely hard ground, sand and clay terrains. Appendix 15 shows the weighing process of the loads. The readings from the applied load variations were also recorded with corresponding variations in tyre pressures, velocities, rut depths and drawbar-pull.

Figure 7.15: Two sand filled moulds on the machine acting as weights each weighing 20kg

7.2.12. Sandy terrain

The timber and steel formwork for the sandy terrain bed was 3 metres long, 1 metre wide and 0.20metres high. The sand ordered had moisture content of 6.3% in order to obtain the credible results that would be consistent with the outlined objectives. The sand bed mould was filled with sand in layers of 50mm which was compacted in order to simulate a realistic natural terrain that would be representative of the moist dense sandy terrain. The sand bed was prepared every time after running the experiment in order to create a bed of undisturbed terrain. Sand was much easier to handle in preparation, handling and disposal due to its non-cohesive nature.

Figure 7.16: Laboratory sand bed for the Mobility SF-3713 on the left and the right pane shows the sand bed is shown with the acceleration allowance for the machine

The 6.3% moisture content was determined by weighing 1000g on a scale and putting it in the oven for 48 hours at a constant temperature of 110 degrees. The sample was later weighed again. The difference was the moisture content by mass. MOBILITY SF-3713 was also to run on the dry, loose and un-compacted sand in order to confirm the behaviour of the machine when operated in un-compacted sand. The vehicle slipped continually without moving a metre. The levelling of the sand in the sand bed was achieved by marking a horizontal line representing a uniform height around the formwork. The horizontal level was achieved by tamping the top of the material with a flat piece of timber. Below is the profile for sand soil used in the experiments. The graphical presentation in figure 7.17 is in form of the sieve analysis based on BS EN 1997-2:2007 which is the Eurocode 7 Geotechnical design part 2 of ground investigation and testing. The

angle of shearing resistance was found to be 31^{o} which is consistent with average for soil of this nature.

Sieve size (1)	Mass retained(g) (2)	Percentage retained (%) (3)	Cumulative percentage passing (4)	Cumulative percentage retained (5)
10.00mm	11.4	0.5	99.5	0.5
5.00mm	21.4	0.8	98.7	1.3
2.36mm	243.4	9.6	89.1	10.9
1.18mm	249.7	9.9	79.2	20.8
600µm	554.4	22.0	57.2	42.8
300µm	1287.5	51.0	6.2	93.8
150µm	105.3	4.2	2.0	98.0
<150µm	51	2.0	0.0	100.0
Total	**2524.1**	**100.0**		

Table 7.1: Sand soil sieve analysis data

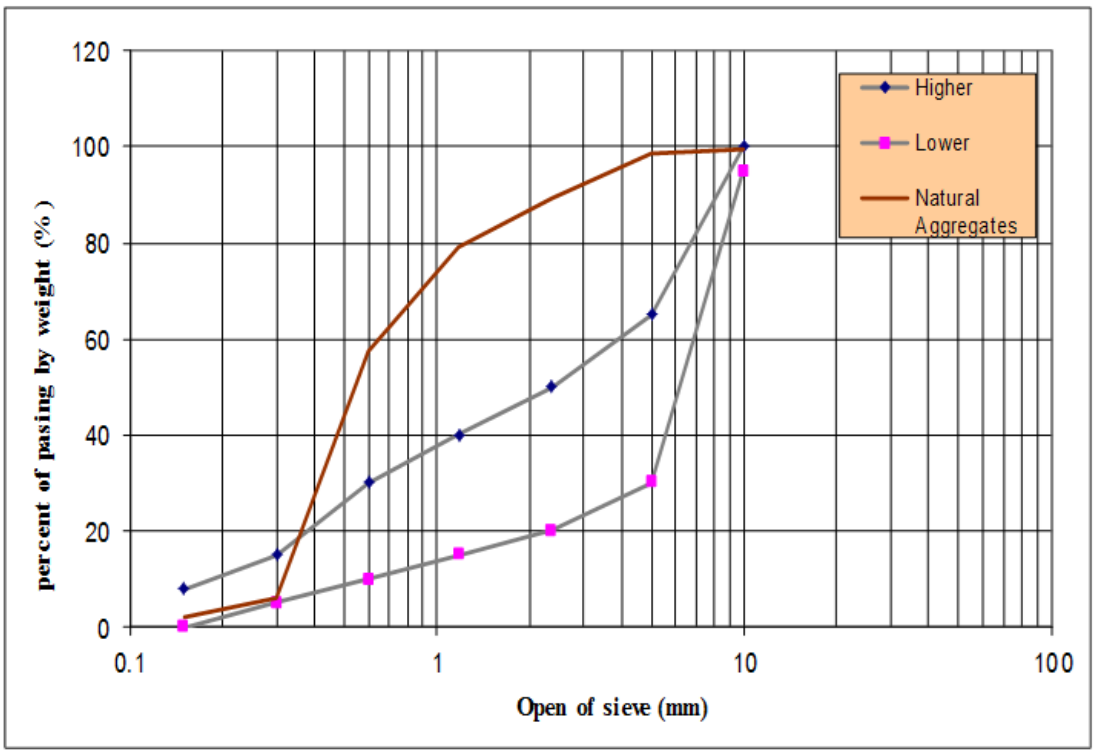

Figure 7.17: Sand soil profile through sieve analysis tabulation and graph

7.2.13. Clay terrain

The procedure used for the design and assembly of the clay bed is similar to that of the sand bed. The only difference is that due to the cohesive nature of moist clay, it is very challenging to handle because of its cohesive property compared to the sandy soil. It took nearly twice the time taken the clayey based experiments. Just like in the sand bed, the machine was allowed to accelerate for a distance of 3 metres on an elevated and supported board before entering the clay soil bed. Average rut depths were measured and recorded. The video was switched on at the beginning and end of each run using a remote controlled switch. The tyres had to be cleaned after each run to maintain the same traction conditions throughout the experiments.

The clay material used was compacted enough to represent natural terrain. It had moisture content of 31% and a bulk density of 1.98Mg/m^3. The soil cohesion established through tri-axial machine was 74KN/m^2. Full details of the soil test results can be found in the appendix 18. The quantity of the soil material was assumed to be constant during experiments. This was facilitated by the marked level line in the solid timber moulds that were acting as terrain beds.

7.2.14. Experiment Limitations

Despite meeting the requirements the study's outlined objectives, the experiments set up had the following limitations

- The experiments were run on one specification of soil moisture content as supplied.

- There was just one configuration of each soil, however the non-deformable terrain acted as a control or reference point to justify the validity of the two deformable terrains.
- The special vehicle was not powered by fuel thereby taking away the opportunity to monitor the respective fuel consumption for each run.
- The total running distance of 9 metres did not provide the longer term effects of the terrain on the machine. The experiment however was adequate enough to meet the laid down objectives of the study which was to verify the outcome of the mathematical model within the boundaries of the study.
- Like the mathematical model the vehicle was designed to move in one direction without turning or cornering in order to get consistent results with the mathematical model results.

Figure 7.18: Laboratory experiment clay bed

Figure 7.19: Mobility SF-3713 traversing through the prepared laboratory clay bed

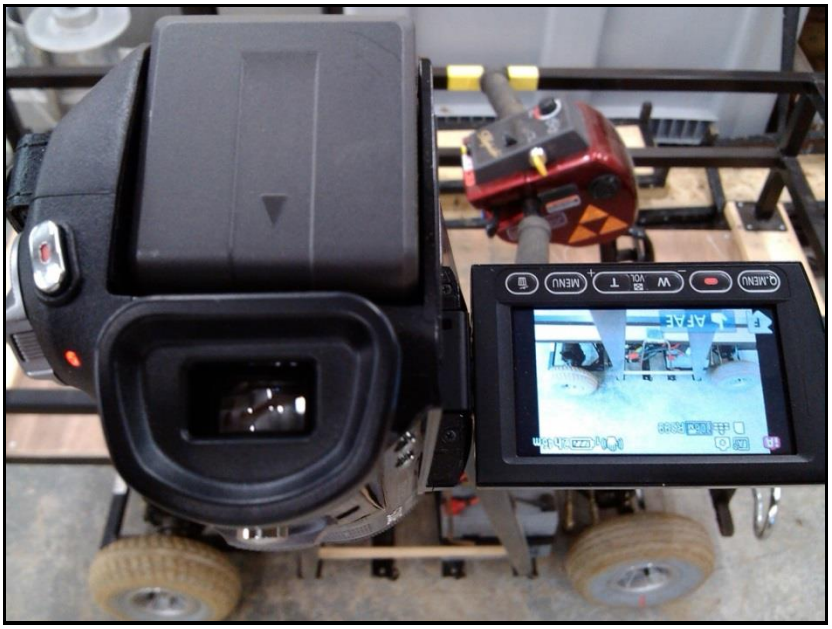

Figure 7.20: Camcorder fitted to the stand on Mobility SF-3713 to record travel time and wheel slip differences

7.3. (ISOLATED ANALYSIS 1) Individual Terrain Analysis

7.3.1. Velocity data of the machine with all loads and speeds selections on hard terrain

	Velocity (m/s)					
Applied Load & Tyre Pressure	0N, 3PSI	400N, 3PSI	800N, 3PSI	0N, 45PSI	400N, 45PSI	800N, 45PSI
Speed Selection						
1	0.73	0.70	0.67	0.82	0.80	0.78
3	0.95	0.90	0.87	1.05	1.03	1.01
5	1.17	1.13	1.05	1.26	1.25	1.23
7	1.42	1.39	1.32	1.61	1.58	1.53

Table 7.2: Velocity data of the machine based on all loads and speed selections on the hard non-deformable ground

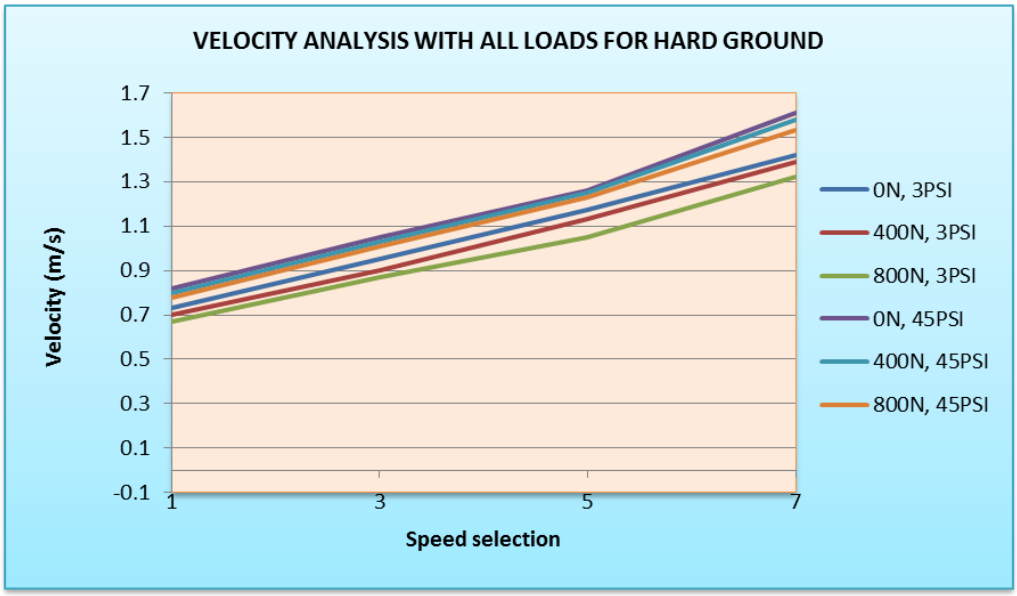

Figure 7.21: Velocity analysis of the machine for all loads on the hard ground

For the hard ground, the velocity variation was minimal. With the highest speed selection, the highest velocity was attained with the combination of the highest tyre pressure of 45PSI and 0N applied load at 1.61m/s. The lowest velocity was attained from the combination of 3PSI and the maximum load of 800N which was 1.32m/s. This is because the larger contact area reduces the speed. The middle loads also fall in the middle of the graphical analysis as seen in figure 7.21 above.

The maximum velocity at highest load still provided higher velocity of 1.53m/s. For the hard ground fully inflated tyres gave better velocity and reduced energy loss. Figure 7.22 below demonstrates the foot print between the smallest contact area and the largest contact area which all had significant influence on the velocity of the special wheeled vehicle.

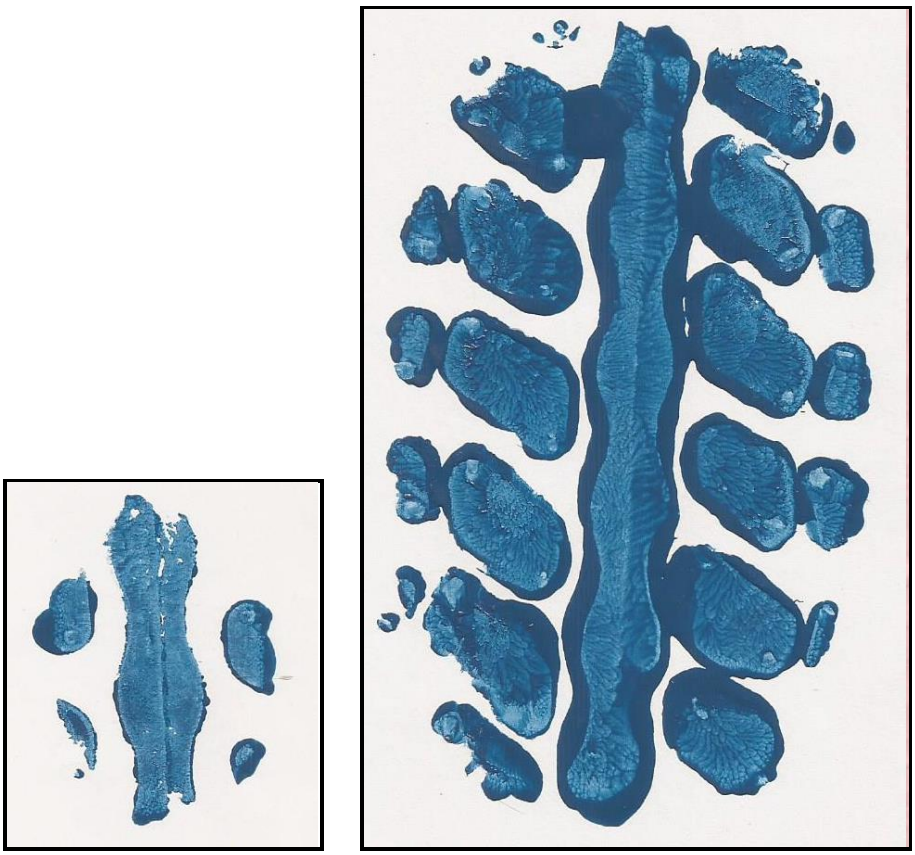

Figure 7.22: Tyre foot print with 45PSI and 0N load on the left pane and on the right it is the tyre foot print with 3PSI and 800N applied load. Note the difference in contact area

7.3.2. Velocity data of the machine with all loads and speed selections on sandy terrain

	Velocity (m/s)					
Applied Load & Tyre Pressure	0N, 3PSI	400N, 3PSI	800N, 3PSI	0N, 45PSI	400N, 45PSI	800N, 45PSI
Speed Selection						
1	0.69	0.76	0.52	0.53	0.31	0.45
3	1.00	0.98	0.98	0.76	0.21	0.12
5	1.27	1.24	1.21	0.88	0.57	0.24
7	1.59	1.52	1.71	1.28	0.67	0.35

Table 7.3: Velocity data of the machine based on all loads and speed selections on the sand bed

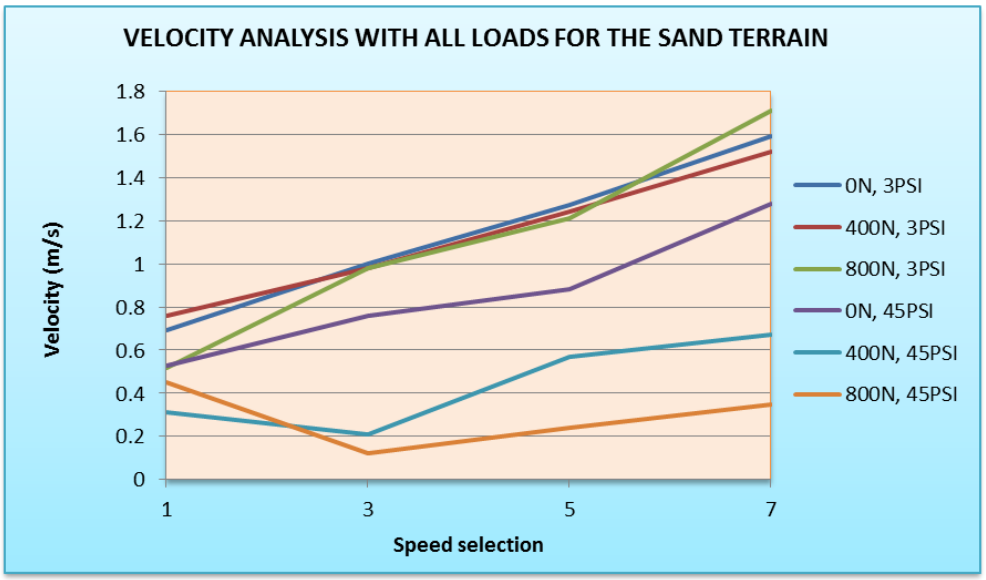

Figure 7.23: Velocity analysis of the machine for all loads on the sand terrain bed

Figure 7.23 above shows the results from the special vehicle operating in a sandy terrain bed in which the highest velocity attained was 1.71m/s on average from the combination of the lowest tyre pressure tyre with the highest load of 800N. All fully inflated tyres provided lower velocity with the slowest tyre being the 45PSI under maximum load. From this result, wheeled and loaded plant is likely to provide poor power output/efficiency in the sandy soil bed.

7.3.3. Velocity data of the machine with all loads and speed selections on the clayey terrain bed.

	Velocity (m/s)					
Applied Load & Tyre Pressure	0N, 3PSI	400N, 3PSI	800N, 3PSI	0N, 45PSI	400N, 45PSI	800N, 45PSI
Speed Selection						
1	0.69	0.57	0.47	0.77	0.59	0.50
3	0.83	0.7	0.63	0.81	0.75	0.52
5	1.03	0.9	0.79	1.06	0.88	0.77
7	1.27	1.09	1.00	1.31	1.14	0.93

Table 7.4: Velocity data of the machine based on all loads and speed selections on the clay terrain bed

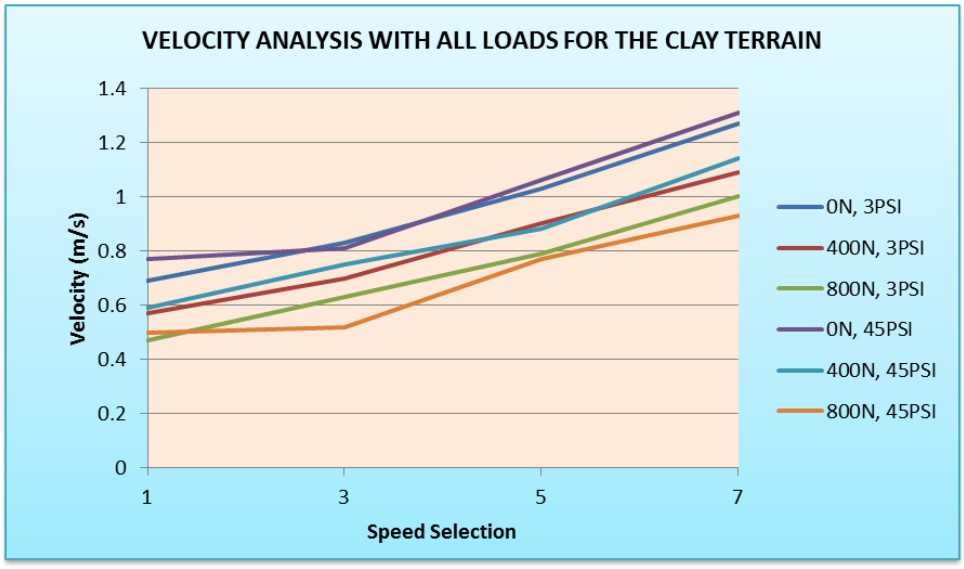

Figure 7.24: Velocity analysis of the machine for all loads on the clay terrain bed

From the clayey terrain in figure 7.24 above, the highest velocity of 1.31m/s was attained with maximum tyre inflation pressure with no load; however this tyre pressure provided the lowest velocity of 0.93m/s when fully loaded with 800N. The 400N load in both lower and higher tyre inflation pressure provided the most economic velocity as seen from the graph in figure 7.24. Running wheeled and unloaded plant throughout is not acceptable and does not achieve any economic value.

7.3.4. Rut depth data of the machine with all loads and speed selections on hard terrain

	Rut Depth (mm)					
Applied Load & Tyre Pressure	0N, 3PSI	400N, 3PSI	800N, 3PSI	0N, 45PSI	400N, 45PSI	800N, 45PSI
Speed Selection						
1	0	0	0	0	0	0
3	0	0	0	0	0	0
5	0	0	0	0	0	0
7	0	0	0	0	0	0

Table 7.5: Rut depth data of the machine based on all loads and speed selections on the hard non-deformable terrain

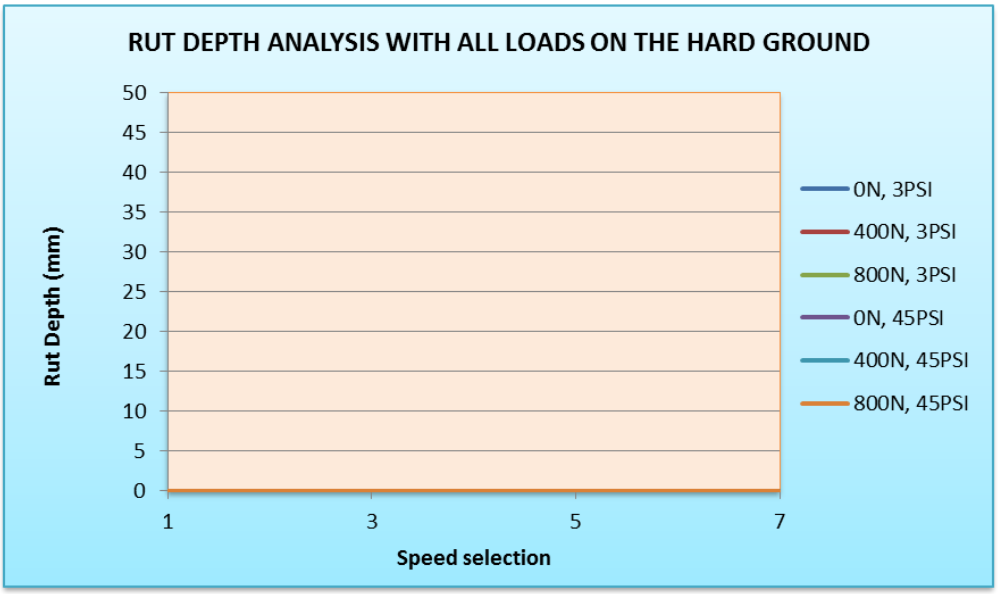

Figure 7.25: Rut depth analysis of the machine for all loads on the non-deformable ground

From figure 7.25 above, the rut depth for all experiments on the ground was 0mm simply because the ground was not deformable. The effect of the weight however was seen in the tyre foot print changes which also signify tyre deflection and contact area. The details and illustrations of the respective tyre foot prints are given in figure 7.28. Figure 7.26 shows the image for the fully inflated tyre on a hard surface while figure 7.27 shows the tyre with low inflation pressure.

Figure 7.26: Image for fully inflated vehicle tyre at 45PSI showing very small contact length and patch on the non-deformable hard ground

Figure 7.27: Image for the lowly inflated vehicle tyre at 3PSI tyre pressure showing a longer contact length and patch on the non-deformable hard ground

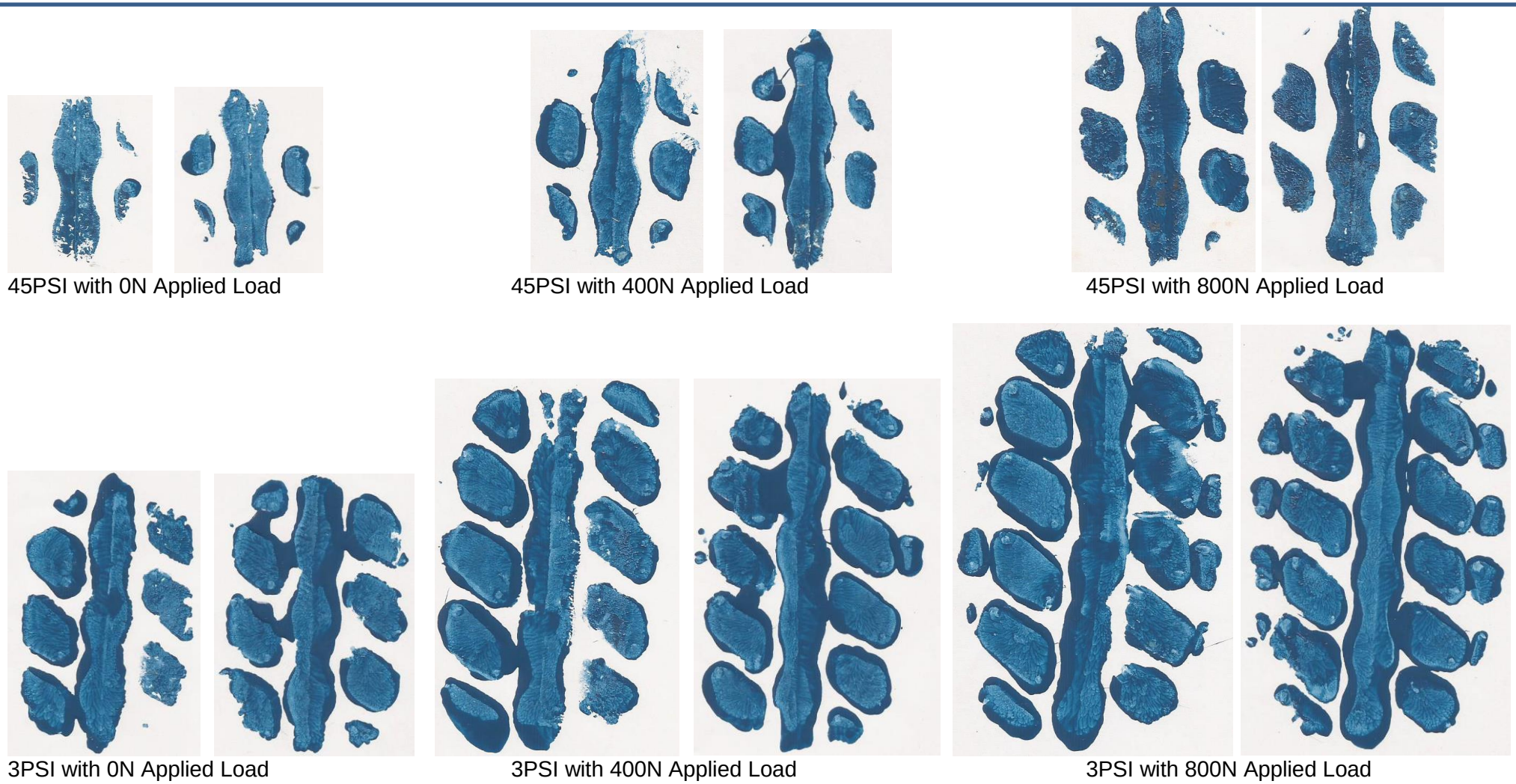

Figure 7.28: Tyre foot prints for the machine under different loads and tyre pressures

7.3.5. Rut depth data of the machine with all loads and speed selections on the sand terrain bed

	Rut Depth (mm)					
Applied Load & Tyre Pressure	0N, 3PSI	400N, 3PSI	800N, 3PSI	0N, 45PSI	400N, 45PSI	800N, 45PSI
Speed Selection						
1	13	4	1	21	25	40
3	2	3	3	25	31	34
5	2	3	4	27	36	42
7	3	4	4	22	32	47

Table 7.6: Rut depth data of the machine based on all loads and speed selections on the sand terrain bed

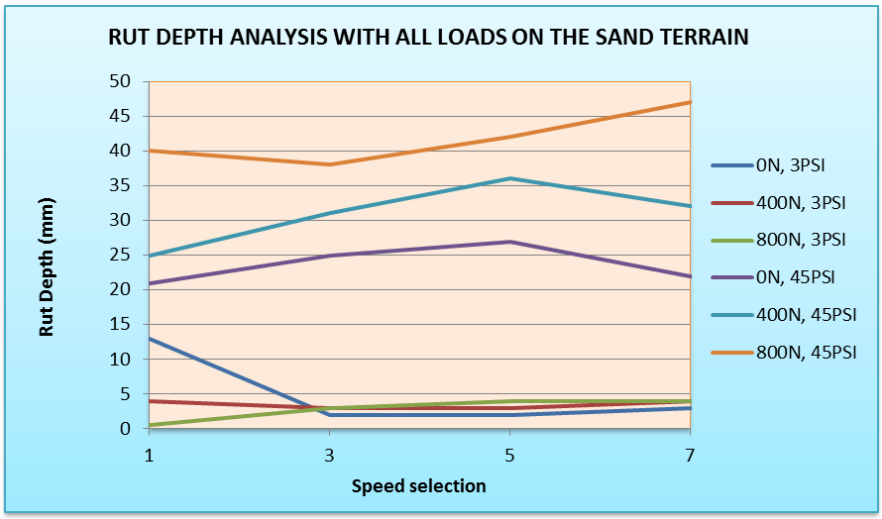

Figure 7.29: Rut depth analysis of the machine for all loads on the sand terrain bed

The deepest wheel rut depth in the sand terrain was 47mm produced from the one from the combination of 45PSI tyre with maximum load of 800N as seen from the graph in figure 7.29. From the graph the ultimate lowest rut depth came from the lowest tyre pressure of 3PSI regardless of the load. The 0N load however shows deep rutting. Additional load provided more grip and stability resulting in the energy turning the wheel rather digging into the ground. Lower tyre pressure and wider tyre/terrain contact area provided better performance through reduced rutting. Figure 7.30 and figure 7.31 shows the behaviour of the tyre with maximum

tyre pressure and minimum tyre pressure respectively all subjected to the maximum load in the sand terrain bed.

Figure 7.30: Deepest rut depth illustration in sand bed terrain with machine running on maximum speed, maximum tyre pressure 45PSI and maximum load 800N

Figure 7.31: Lowest rut depth illustration in sand terrain bed with the machine running on maximum speed, minimum tyre pressure 3PSI and maximum load 800N

Figure 7.32: Rear view of the rut depth illustration of deep rutting on the left pane similar to (Figure 7.30) and lowest rutting on the right pane similar to (Figure 7.31) on sand terrain bed

7.3.6. Rut depth data of the machine with all loads and speed selections on clayey terrain

	Rut Depth (mm)					
Applied Load & Tyre Pressure	0N, 3PSI	400N, 3PSI	800N, 3PSI	0N, 45PSI	400N, 45PSI	800N, 45PSI
Speed Selection						
1	11	14	18	8	14	20
3	6	14	20	7	17	26
5	4	15	23	7	14	24
7	8	15	17	4	16	30

Table 7.7: Rut depth data of the machine based on all loads and speed selections on the clay terrain bed

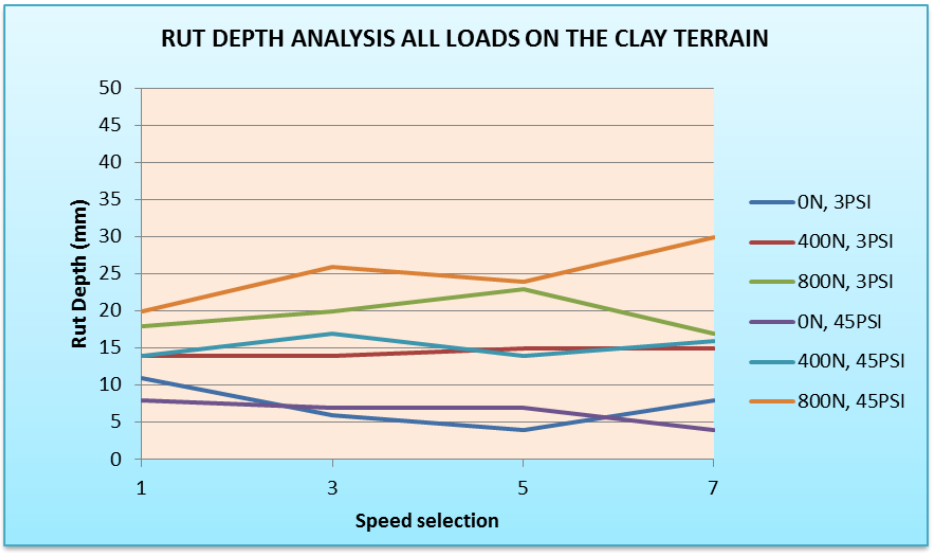

Figure 7.33: Rut depth analysis of the machine for all loads on the clay terrain bed

Figure 7.33 above displays data from the experiments for rut depths arising from all loads and tyre pressures in the clayey terrain. The deepest rut depth in the clay terrain (30mm) came from maximum load of 800N and tyre pressure of 45PSI. The medium/average load for both lower and higher tyre pressure provided the most economical performance. The least rut depth of 4mm came from the runs without load for both tyres. Velocity was equal for both tyre pressures (3PSI and 45PSI) and the most feasible option has to be determined by considering other factors.

Figure 7.34: Deepest rut depth illustration in the clay terrain bed with the machine running on maximum speed, maximum tyre pressure 45PSI and maximum load 800N

Figure 7.35: Shallowest rut depth illustration in the clay terrain bed with the machine running on maximum speed, minimum tyre pressure 3PSI and minimum load 0N

7.3.7. Drawbar-pull data of the machine with all loads and speed selections on the hard terrain

	Drawbar-Pull (N)					
Applied Load & Tyre Pressure	0N, 3PSI	400N, 3PSI	800N, 3PSI	0N, 45PSI	400N, 45PSI	800N, 45PSI
Speed Selection						
1	410	615	605	380	530	520
3	420	640	620	380	630	600
5	420	640	640	380	630	630
7	410	660	670	330	630	630

Table 7.8: Drawbar-pull data of the machine based on all loads and speed selections on the hard non-deformable terrain

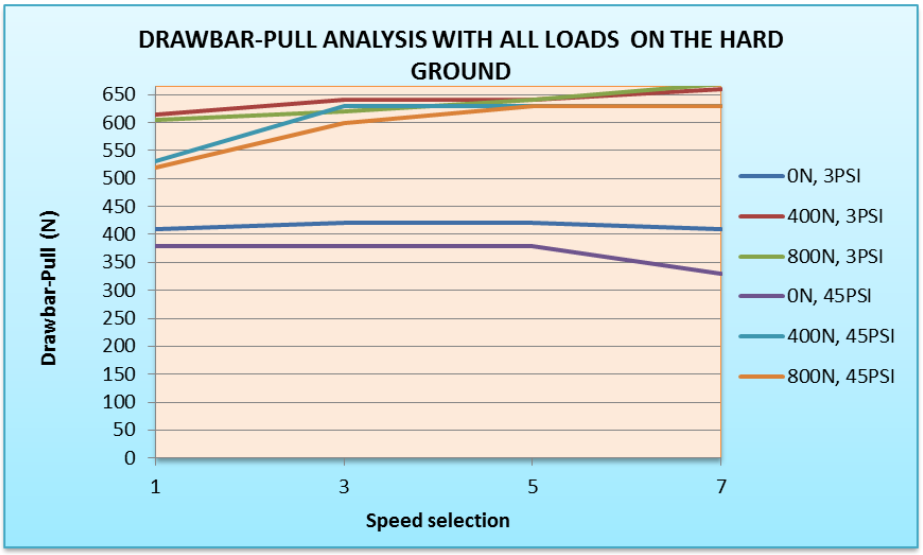

Figure 7.36: Drawbar-pull analysis of the machine for all loads on the non-deformable hard ground

The highest drawbar-pull on the hard ground (630N to 670N) was attained from the all combinations of tyre pressure and load except for the 3PSI with 0N load which produced 410N. The combination of 45PSI and 0N load produced 330N as indicated in figure 7.36. The applied load is very critical in the generation of drawbar-pull and the much needed traction for stability. Traction is not only

essential for off road conditions but pavement roads as well, a point made in the literature review as well.

7.3.8. Drawbar-pull data of the machine with all loads and speed selections on the sandy terrain bed

	Drawbar-Pull (N)					
Applied Load & Tyre Pressure	0N, 3PSI	400N, 3PSI	800N, 3PSI	0N, 45PSI	400N, 45PSI	800N, 45PSI
Speed Selection						
1	200	210	330	5	5	50
3	150	200	250	0	0	90
5	90	150	300	1	1	150
7	23	160	330	0	0	45

Table 7.9: Drawbar-pull of the machine based on all loads and speed selections on the sand terrain bed

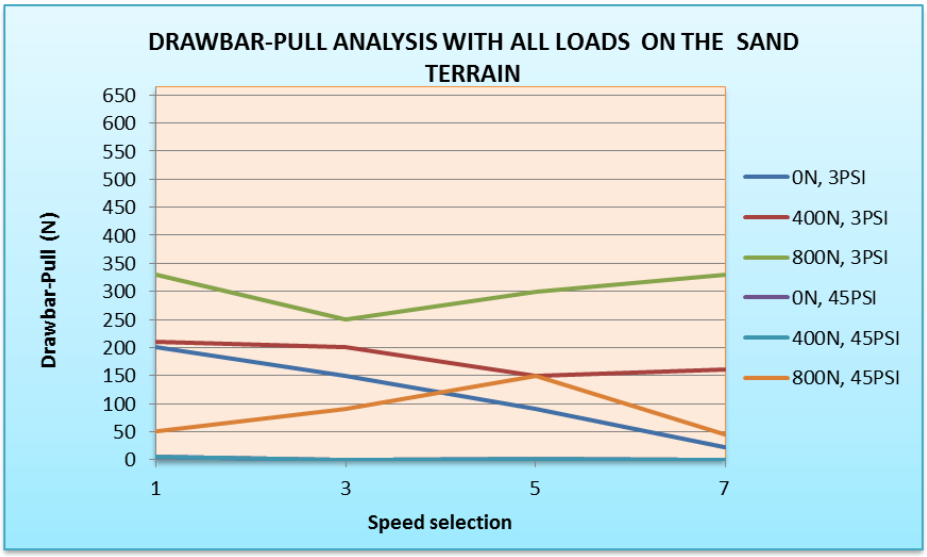

Figure 7.37: Drawbar-pull analysis of the machine for all loads and tyre pressures on the sand terrain bed.

In the sandy terrain bed, the maximum drawbar-pull (330N) was generated from the lowest tyre pressure of 3PSI running with maximum load of 800N as illustrated in figure 7.37 above. This result implies that heavily loaded wheeled construction plant must run with maximum tyre/terrain contact area when operating in sandy soil. The lowest drawbar-pull (0N) is obtained from the combination of maximum tyre pressure of 45PSI and 800N load because the energy required to turn the

wheels in attempting to overcome motion resistance is too high due to deep tyre rutting as seen in figure 7.37. The sandy terrain needs to be dense and contain some moisture because loose soil wet or dry will not facilitate the wheeled vehicle to move as observed in the experiments.

7.3.9. Drawbar-pull data of the machine with all loads and speed selections on the clayey terrain bed

	Drawbar-Pull (N)					
Applied Load & Tyre Pressure	0N, 3PSI	400N, 3PSI	800N, 3PSI	0N, 45PSI	400N, 45PSI	800N, 45PSI
Speed Selection						
1	500	450	430	300	530	550
3	430	500	520	530	550	480
5	500	530	530	280	430	330
7	550	530	500	190	440	330

Table 7.10: Drawbar-pull data of the machine based on all loads and speed selections on the clay terrain bed

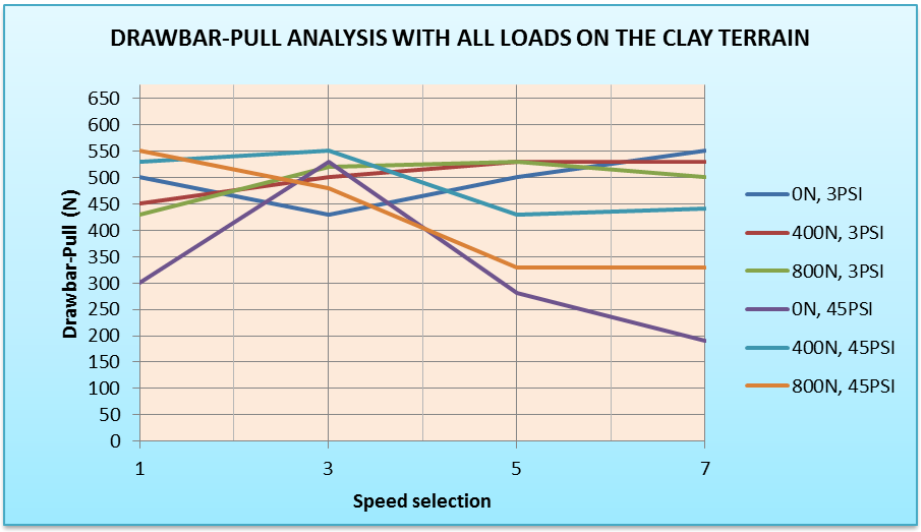

Figure 7.38: Drawbar-pull analysis of the machine for all loads and tyre pressures on the clay terrain bed

Figure 7.38 above shows the drawbar-pull results in clay terrain for all applied loads and tyre pressures. The drawbar-pull values for all combinations were significant and close to each other. It is in this terrain that most combinations had significant and higher drawbar-pull. The lowest values (190N) are from the

combination of 45PSI with no load at maximum velocity. The average loaded tyre was required to provide maximum drawbar-pull in this particular case. The results suggest that in clay soil the larger contact area is still essential in the generation of drawbar-pull. Drawbar-pull results in the clay terrain bed are closer to that of the hard ground as seen from the experiment results. The conclusion can be drawn that the drawbar-pull output in clay terrain is better than in the sand terrain as already established by the mathematical model in chapter 4.

7.4. (ISOLATED ANALYSIS 2) Integrated Terrain Analysis

7.4.1. Velocity data of the machine with 0N applied load for all speed selections and terrains

	Velocity in m/s					
Tyre Pressure & Terrain type	45PSI hard	3PSI hard	45PSI sand	3PSI sand	45PSI clay	3PSI clay
Speed Selection						
1	0.82	0.73	0.53	0.69	0.77	0.69
3	1.05	0.95	0.76	1.00	0.81	0.83
5	1.26	1.17	0.88	1.27	1.06	1.03
7	1.61	1.42	1.28	1.59	1.31	1.27

Table 7.11: Velocity data of the machine based on 0N applied load for all speed selections and the three terrains

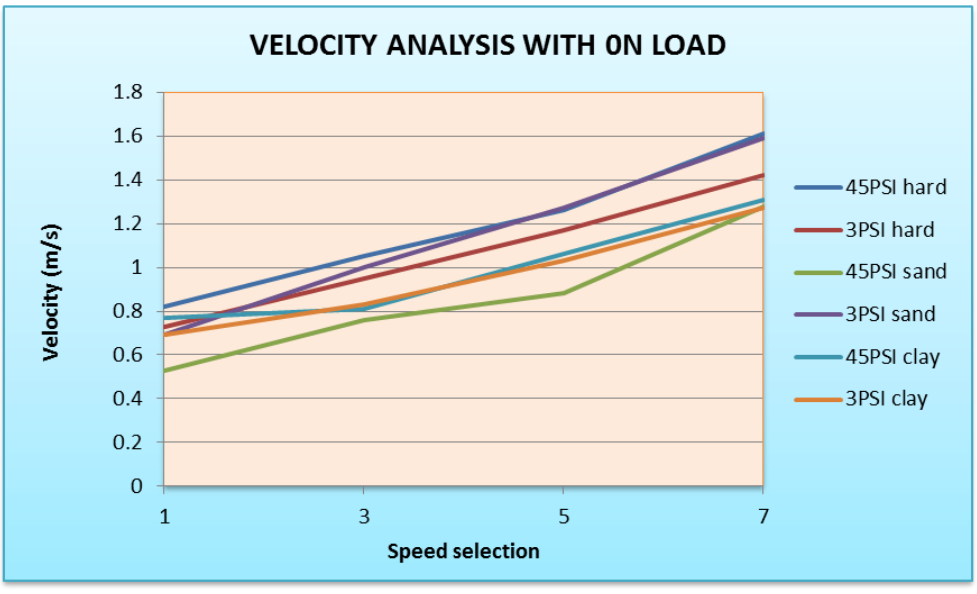

Figure 7.39: Velocity analysis of the machine for 0N applied load with all tyre pressures and all terrains

The velocity analysis in figure 7.39 above presents the results from the 0N applied load for all terrains in the experiment. It is driven by four selected speeds and two tyre pressures high and low, 45PSI and 3PSI respectively. With 0N and a self-weight of 784N there was a steady increase in velocity with increase in the speed selections which were 1, 3, 5 and 7.

The highest velocity of 1.61m/s attained was for the 45PSI tyre pressure on hard ground. The second highest velocity (1.59m/s) attained was that from the 3PSI tyre pressure running in sand bed. This is a very interesting result because the results confirm that the closest efficient terrain to normal pavement road in terms of velocity is the wet and dense sand with minimum tyre pressure. The tyre with lower inflation pressure provides wider contact area which improves the grip on the terrain.

The results suggest that there is less energy and fuel wastage for lightly loaded construction vehicles operating in dense sandy terrain. The least efficient velocity (0.53m/s) from the lowest speed selection was that of the 45PSI tyre pressure in wet and dense sandy terrain from the lowest speed selection. The smaller contact area created by high pressure results in deeper tyre rutting which in turn creates loss of energy due to motion resistance. Reduced tyre pressure or much wider tyres must be used to improve the velocity. Alternatively the terrain can be stabilised and compacted more to improve the performance.

7.4.2. Velocity data of the machine with 400N applied load for all speed selections and terrains

	Velocity in m/s					
Tyre Pressure & Terrain type	45PSI hard	3PSI hard	45PSI sand	3PSI sand	45PSI clay	3PSI clay
Speed Selection						
1	0.80	0.70	0.31	0.76	0.59	0.57
3	1.03	0.90	0.21	0.98	0.75	0.7
5	1.25	1.13	0.80	1.24	0.88	0.9
7	1.58	1.39	0.38	1.52	1.14	1.09

Table 7.12: Velocity data of the machine based on 400N applied load for all speed selections and all the three terrains

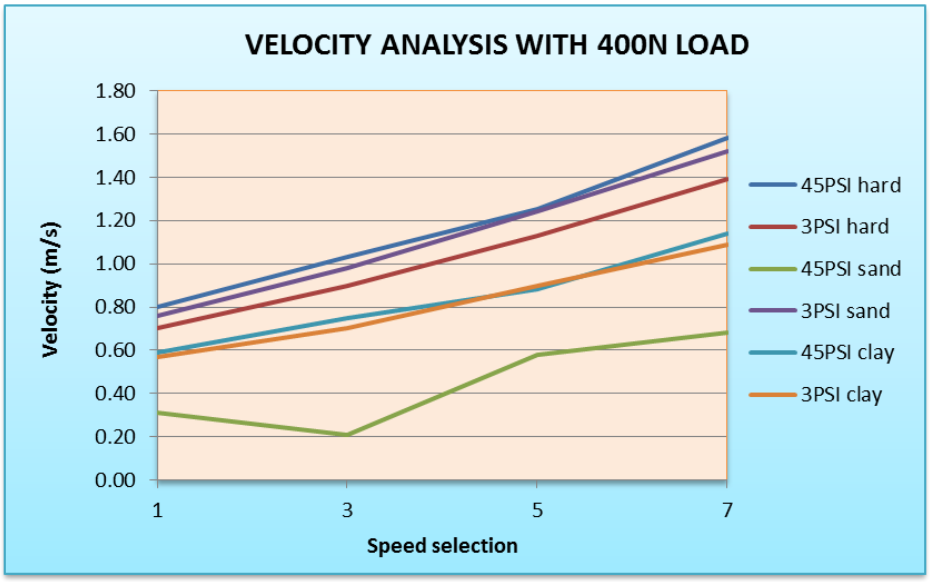

Figure 7.40: Velocity analysis of the machine under 400N applied load with all tyre pressures and all terrains

With the applied load of 400N load and self-weight of 784N shown in figure 7.40 the gradient of all the velocity graphs have a similar pattern with the 0N graphs from figure 7.40 but with some exceptions as discussed in the next paragraph.

There was a reduction in velocity for all speed selections used in the experiments. This was as a result of the introduced load. The 3PSI tyre pressure on hard ground gave a reduced velocity compared to the 45PSI tyre pressure due to the deflection experienced. Despite the reduced velocity it had more grip as seen in

the drawbar-pull analysis demonstrated in figures 7.45 and 7.46. The 3PSI tyre pressure in wet dense sand still remained efficient being second to the 45PSI tyre on the ground. The most significant change noticed was on the effect of the introduced load on the 45PSI tyre pressure on the sand test bed. The velocity reduced significantly to as low as 0.21m/s at speed selection 2 and 0.38m/s at speed 7. In this run, the vehicle did not even get to the end of the test bed. The motion resistance created by the sinkage was so high that it significantly reduces the power efficiency of the vehicle. The difference between the velocity produced by the 45PSI tyre pressure in sand and the 3PSI tyre pressure in sand was 1.14m/s which is very significant.

This result is very critical for wheeled construction vehicles with highly inflated tyres. The result suggests that wheeled plant should not operate in loose sandy soils because it would result into high waste of energy unless the tyre pressure is reduced. Wider tyres and reduced applied load with much larger diameter must be used in line with mathematical model recommendation in order to attain better performance results of wheeled plant traversing in unpaved and soft terrain.

7.4.3. Velocity analysis of the machine with 800N applied load for all speeds and terrains

	Velocity in m/s					
Tyre Pressure & Terrain type	45PSI hard	3PSI hard	45PSI sand	3PSI sand	45PSI clay	3PSI clay
Speed Selection						
1	0.78	0.67	0.45	0.52	0.50	0.47
3	1.01	0.87	0.12	0.98	0.52	0.63
5	1.23	1.05	0.24	1.21	0.77	0.79
7	1.53	1.32	0.35	1.71	0.93	1.00

Table 7.13: Velocity data of the machine based on 800N applied load for all speed selections and all the three terrains

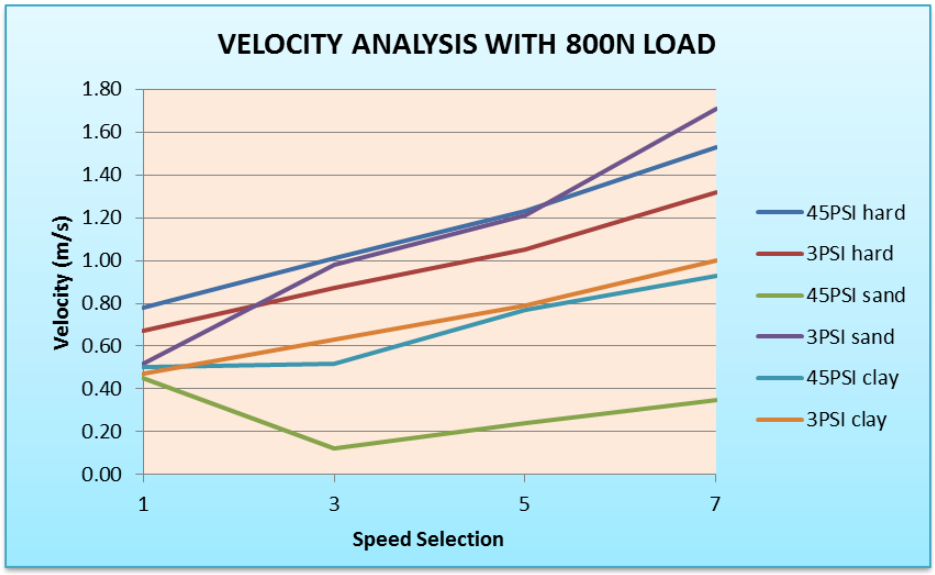

Figure 7.41: Velocity analysis of the machine under 800N applied load with all tyre pressures and all three terrains

Figure 7.41 above shows the results for velocity analysis based on the maximum (800N) load for all terrains. With the maximum load of 800N, all velocities reduced in magnitude except for the 3PSI tyre pressure in sand bed which increased the velocity to the maximum value of 1.71m/s. The load enabled it to be more stable and provides more traction. The difference between the highest velocity and the lowest velocity increased significantly.

In clay soil, the 3PSI tyre pressure performed better in velocity that the 45PSI tyre pressure due to better traction as seen from figures 7.43 and 7.44. This shows that even in clay terrain the tyre pressure should be reduced to maximise the tyre/terrain contact area. Alternatively wider tyres must be used in this case. The 45PSI tyre pressure still provided the least efficient in the sand terrain and slowest velocity with 0.35m/s at the maximum speed selection. The only economical velocity for this tyre pressure in the sand bed was at the lowest speed selection. This result suggests that heavily loaded wheeled construction plant should not exceed a particular velocity if energy is to be preserved in sand terrain. The 45PSI and 3PSI tyre pressure on the hard ground still provided consistent results despite a reduction in the velocity. Claims for lost time can be avoided in wet sandy terrain if the wheels contact area is kept to the maximum with wider tyres and minimum allowable pressure. Highly inflated but wider tyres may be used with reduced load and velocity to avoid deeper rutting that would eventually reduce the performance power output.

In loose sand however MOBILITY SF-3713 could not move at higher speed selections in the sand bed. This result suggests that wheeled plant should not be operated in loose sand weather wet or dry. It is suggested that tracked plant should be introduced or alternatively the sand will require stabilisation and compaction. The cost implications will determine the most economical option of the two routes.

7.4.4. Rut depth data of the machine with 0N applied load for all speed selections and terrains

	Rut Depth (mm)					
Tyre Pressure & Terrain type	45PSI hard	3PSI hard	45PSI sand	3PSI sand	45PSI clay	3PSI clay
Speed Selection						
1	0	0	21	13	8	11
3	0	0	25	2	7	6
5	0	0	27	2	7	4
7	0	0	22	3	4	8

Table 7.14: Rut depth data of the machine based on 0N load for all speed selections and terrains

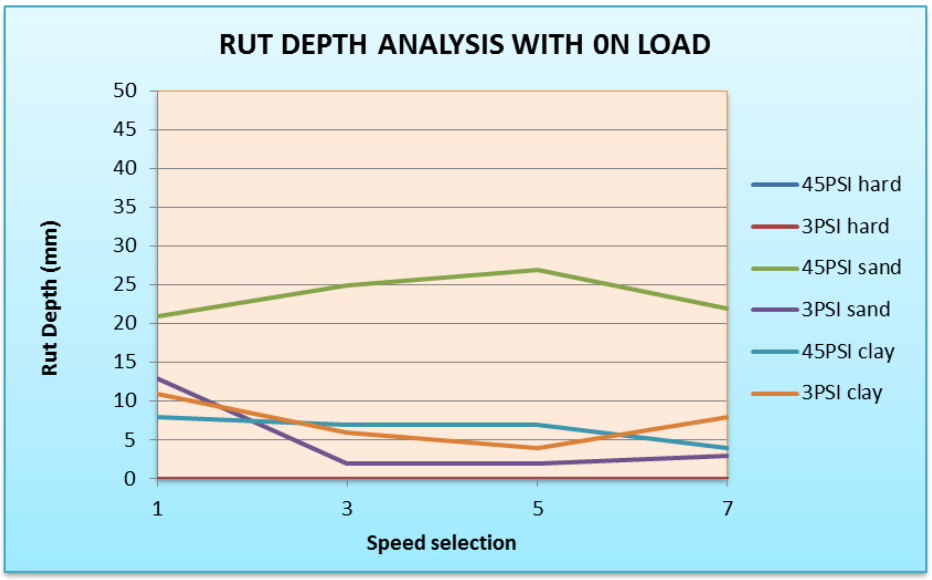

Figure 7.42: Rut depth analysis of the machine under 0N applied load with all tyre pressures and all three terrains

Figure 7.42 above provides data for the analysis of rut depth in all terrains under 0N applied load. With 0N load, tyre pressures of 45PSI and 3PSI operating on hard ground all runs produced 0mm rut depth as seen in figure 7.25. The deflection was recorded in terms of the tyre foot print for comparison with loaded tyres in order to capture the effect of the tyre loading in terms of contact area with the ground demonstrated in figure 7.28.

The deepest tyre rut depth recorded from the experiment was that of the 45PSI tyre inflation pressure running on the sand bed. Being the lowest in velocity value as well, it had the largest value of energy waste with the deepest rut being 27mm occurring on speed selection 3 even without any applied load. The conclusion for this result is that it is uneconomical to run wheeled construction plant on highly inflated tyres in sandy terrain because it behaves as a rigid wheel and thus other alternatives must be sought to reduce the rut depth.

The lowest rut depth (2mm) recorded during the experiments is the 3PSI in sand terrain due to better traction and wider contact areas between the tyres and the terrain. Higher friction angle and better compaction can also contribute to better performance of wheeled plant. Wheel multi pass effect discussed in chapters 2 and 4 can also help in the compaction and subsequent in the reduction of rutting in the sand terrain. This principle also applies to clay terrain.

7.4.5. Rut depth data of the machine with 400N applied load for all speed selections and terrains

	Rut Depth (m)					
Tyre Pressure & Terrain type	45PSI hard	3PSI hard	45PSI sand	3PSI sand	45PSI clay	3PSI clay
Speed Selection						
1	0	0	25	4	14	14
3	0	0	31	3	17	14
5	0	0	36	3	14	15
7	0	0	32	4	16	15

Table 7.15: Rut depth data of the machine based on 400N applied load for all speed selections, terrains and tyre pressures

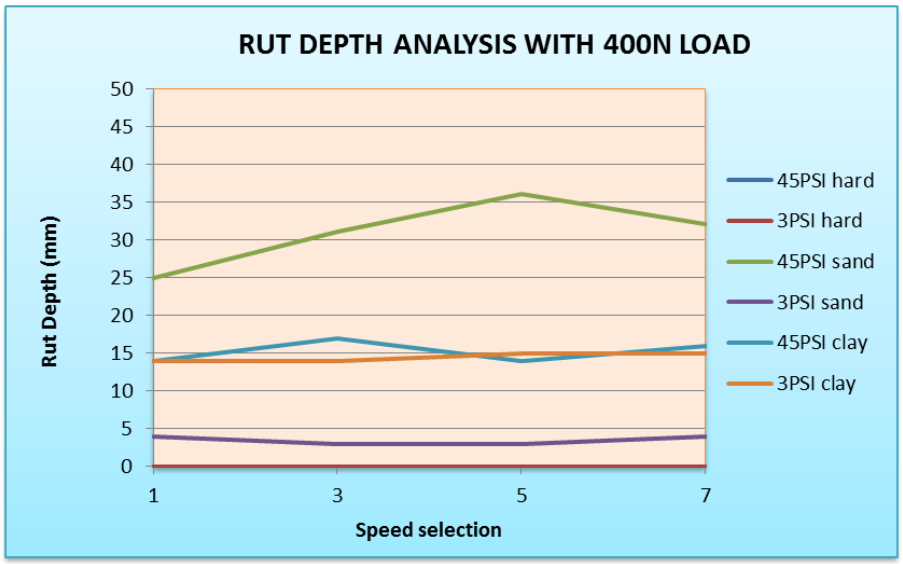

Figure 7.43: Rut depth analysis of the machine under applied load with all tyre pressures and all three terrains

Figure 7.43 provides the analysis of rut depth under the applied load of 400N. With the load of 400N, the tyre pressures of 45PSI and 3PSI on the hard ground still provided 0mm rut depth because the ground surface in non-deformable. The effect however is seen in the increase of the tyre foot print cause by deflection as illustrated in figure 7.28. The 45PSI tyre pressure running in the sand bed produced the deepest rut at 36mm. This is because the increased tyre pressure reduces the tyre/terrain contact area thereby increasing the tyre penetration power into the terrain. The velocity in this case was not enough to overcome the motion resistance caused by the deep rut.

The rut depth in clay terrain also increased by 100% from the previous applied loading. There is enough evidence to show that applied load has significant influence on the formation of rut in deformable terrain which sand and clay beds in this case. The lowest rut outside the hard surface was 3mm for the 3PSI tyre pressure in sand terrain bed followed by 45PSI and 3PSI tyre pressure in clay.

The difference among the two is only 1mm. This means that other factors other than rut depth have to be identified in order to determine the most efficient course of action for this tyre pressure in clay soil.

Increase in soil cohesion and friction angle, wider tyres and radius can all improve the vehicle performance and result in reduced rut depth which is good for energy conservation. A further combination of wider tyres, bigger tyre diameter and lower velocities would provide more efficient drive in sandy terrain.

7.4.6. Rut depth data of the machine with 800N applied load for all speed selections and terrains

	Rut Depth (m)					
Tyre Pressure & Terrain type	45PSI hard	3PSI hard	45PSI sand	3PSI sand	45PSI clay	3PSI clay
Speed Selection						
1	0	0	40	1	20	18
3	0	0	34	3	26	20
5	0	0	42	4	24	23
7	0	0	47	4	30	17

Table 7.16: Rut depth data of the machine based on 800N applied load for all speed selections, terrains and tyre pressures

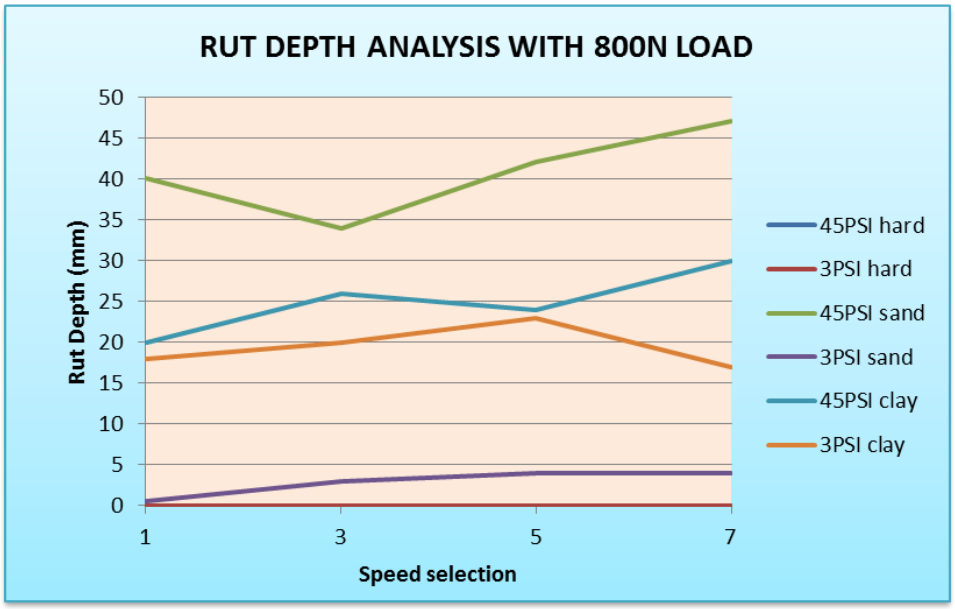

Figure 7.44: Rut depth analysis of the machine under 800N applied load with all tyre pressures and all three terrains

Figure 7.44 above provides the analysis of rut depth under the maximum load of 800N. With the maximum applied load of 800N, the rut depth for the hard ground surface in both tyre pressures remained 0mm. The effect was seen in the increased size of the tyre foot print as shown in figure 7.28. The 3PSI in sand terrain still gave the lowest rut depth of 4mm at maximum velocity. As for the clay terrain, there was a shift in the pattern because 45PSI tyre pressure produced 30mm rut depth while the 3PSI in clay produced a rut depth of 17mm which confirms that tyre contact area still plays an essential part in rut depth reduction especially for loaded tyres.

7.4.7. Drawbar-pull data of the machine with 0N applied load for all speed selections and terrains

	Drawbar-Pull (N)					
Tyre Pressure & Terrain type	45PSI hard	3PSI hard	45PSI sand	3PSI sand	45PSI clay	3PSI clay
Speed Selection						
1	380	410	5	200	300	500
3	380	420	0	150	530	430
5	380	420	1	90	280	500
7	330	410	0	23	190	550

Table 7.17: Drawbar-pull data of the machine based on 0N applied load for all speed selections, terrains and tyre pressures

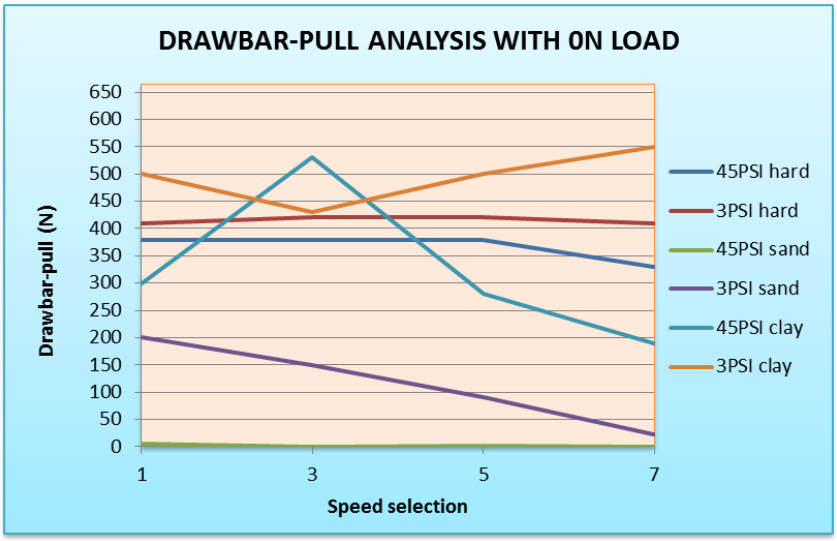

Figure 7.45: Drawbar-pull analysis of the machine under 0N applied load with all tyre pressures and all three terrains

For the 0N load 3PSI tyre pressure in the clay bed gives the highest power in the form of drawbar-pull available which is 550N as illustrated in the table 7.17 and figure 7.45 above. This was achieved with the lowest tyre pressure at the maximum speed. This is a very interesting finding because it confirms the results from the mathematical model that show that there is more traction generated in clay terrain than in sand terrain. In some cases the drawbar-pull in clay (530N) exceeded the drawbar-pull on the hard ground in the case where there was no applied load.

The second highest drawbar-pull generated was the 3PSI on hard ground because large contact area provides more power due to stability through better tyre grip and traction. Though consistent, increase in velocity did not increase the drawbar-pull. The lowest drawbar-pull was for 45PSI in sand bed because of poor traction and small contact area. There is literally no pulling power available. The drawbar-pull for 3PSI in sand should not exceed speed selection 2 because it diminished after this point. The lower tyre pressure again demonstrates that it has more traction than the higher pressure one. The highest drawbar-pull still remains in the clayey terrain provided the moisture content is not too much to make traversing impossible.

7.4.8. Drawbar-pull data of the machine with 400N applied load for all speed selections and terrains

	Drawbar-Pull (N)					
Tyre Pressure & Terrain type	45PSI hard	3PSI hard	45PSI sand	3PSI sand	45PSI clay	3PSI clay
Speed Selection						
1	530	615	5	210	530	450
3	630	640	0	200	550	500
5	630	640	1	150	430	530
7	630	660	0	160	440	530

Table 7.18: Drawbar-pull data of the machine based on 400N applied load for all speed selections, terrains and tyre pressures

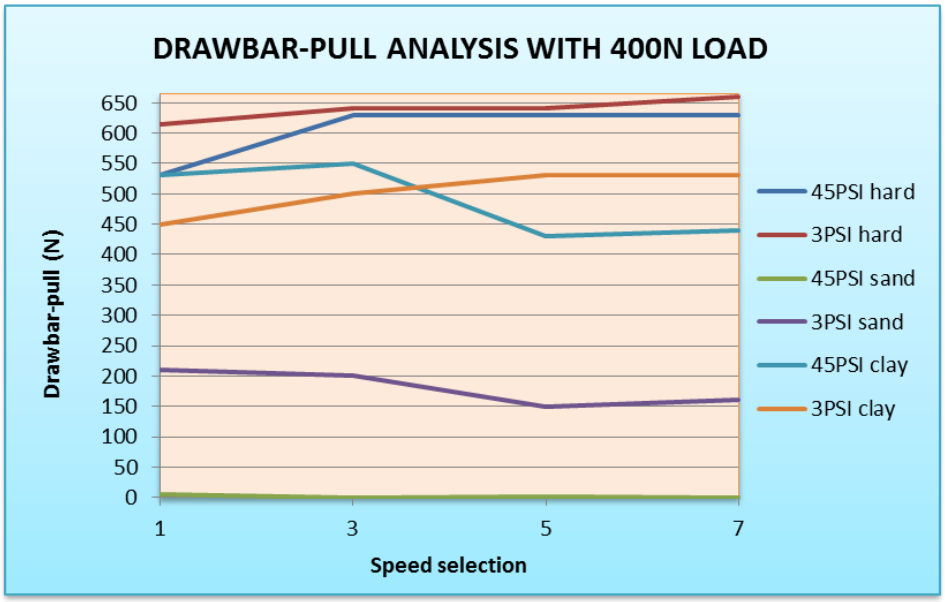

Figure 7.46: Drawbar-pull analysis of the machine under 400N applied load with all tyre pressures and all three terrains

With the applied load of 400N, 3PSI on hard ground provided the highest drawbar-pull overall with 660N at the maximum speed as shown in figure 7.46. The drawbar-pull (630N) for the 45PSI tyre pressure on the ground is second in the order due to the reduced contact area. This was followed by the 3PSI tyre pressure in clay soil, a confirmation that clay terrain provides better traction than sandy terrain.

The drawbar-pull in the sand bed was the lowest with the least value produced by the 45PSI tyre pressure which in fact did not generate any drawbar-pull at all. The 3PSI tyre in sand had a low drawbar-pull of 200N at speed 2 as its maximum efficiency.

The evidence continues to demonstrate that there is more drawbar-pull in clay than in sand due to tyre/terrain traction and grip when it comes to off-road conditions. At an applied load of 400N, the drawbar-pull for clay terrain this time is lower than the hard ground due to energy loss through motion resistance arising from the sinkage caused by the introduction of the applied 400N load.

7.4.9. Drawbar-pull data of the machine with 800N applied load for all speed selections and terrains

	Drawbar-Pull (N)					
Tyre Pressure & Terrain type	45PSI hard	3PSI hard	45PSI sand	3PSI sand	45PSI clay	3PSI clay
Speed Selection						
1	520	605	50	330	550	430
3	600	620	90	250	480	520
5	630	640	150	300	330	530
7	630	670	45	330	330	500

Table 7.19: Drawbar-pull data of the machine based on 800N applied load for all speed selections, all terrains and tyre pressures

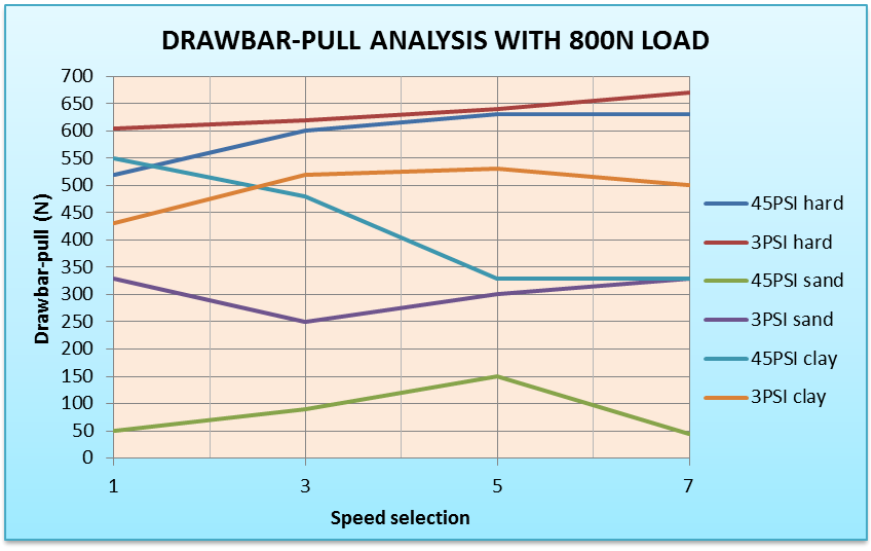

Figure 7.47: Drawbar-pull analysis of the machine under 800N applied load with all tyre pressures and all three terrains

With the 800N applied load and 734N self-weight, 3PSI and 45PSI tyre pressure on the hard ground had the highest drawbar-pull (670N and 630N respectively) due to stronger grip and traction created by larger contact area as seen in figure 7.47 above. The lowest drawbar-pull (45N) was that for the 45PSI in sandy terrain because the 800KN load had resulted in more rutting thereby reducing the drawbar-pull during the experiment. The 3PSI tyre pressure in clay bed still provided the highest drawbar-pull (500N) for the off-road conditions terrain when compared with the sand bed. The drawbar-pull for the 45PSI tyre pressure diminished with increase in speed as a result of increased rutting as illustrated in figure 7.47.

In the sand terrain, the 3PSI and 45 PSI tyre pressures gave lowest drawbar-pull with 3PSI having an upper hand (330N) due to higher contact area. The 45PSI tyre pressure only provides 45N drawbar-pull output at maximum velocity. Speed selection 5 however gave the best performance for this terrain with a drawbar-pull output of 150N. There was a small improvement in drawbar-pull for sand because of the increased power transmitted to the tyres by higher velocity. This high velocity still remains uneconomical taking into account the low value drawbar-pull generated given the high velocity input.

The clay terrain continues to give higher drawbar-pull than sand due to better traction. This as mentioned earlier is supported by the mathematical model outcome discussed in chapter 4.

7.5. Experimental wheel multi-pass rut depth from MOBILITY SF-3713

Wheel multi pass experimental were conducted on the laboratory terrain bed in order to verify the multi pass model results presented in 2.9 of chapter 2 and section 4.4.2 of chapter 4. The results from the experiments confirm the results from the mathematical model as shown in figures 7.48 and 7.49. These results are consistent with figure 4.19 from the mathematical model. The experimental results were consistent for both clay and sandy terrain beds.

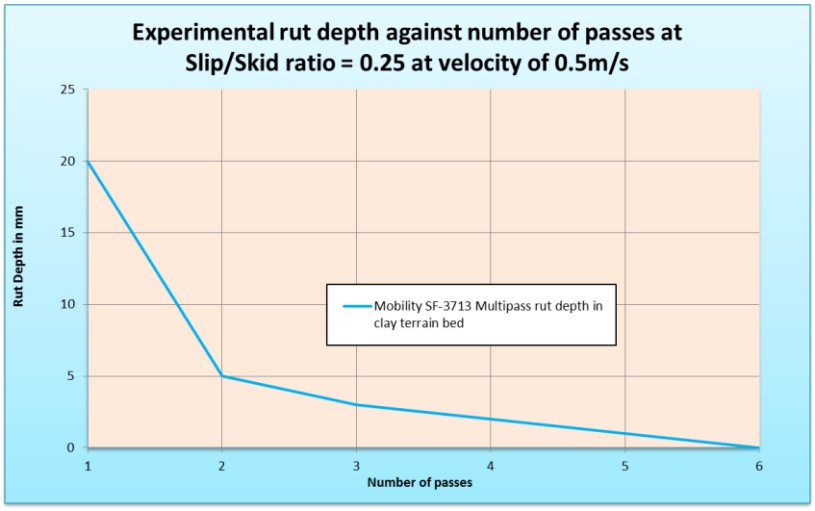

Figure 7.48: Experimental wheel multi-pass rut depth from MOBILITY SF-3713 on the clay terrain bed

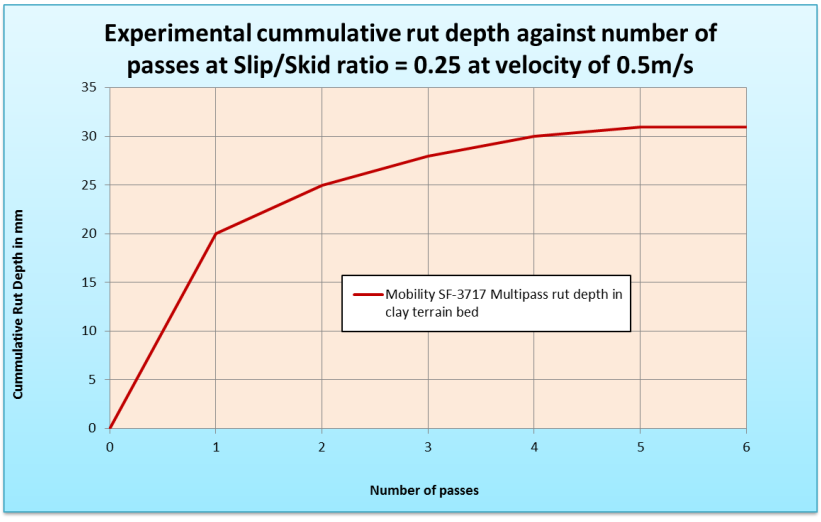

Figure 7.49: Experimental cumulative rut depth from MOBILITY SF-3713 on the clay terrain bed

7.6. Chapter Summary

This chapter has described and illustrated the experimental procedure aimed at establishing the relationship between velocity, rut depth and drawbar–pull on non-deformable ground, clay terrain bed and sand terrain bed. All the experiments deployed the powerful principle of isolated analysis through the use of different applied loads and tyre pressures in order to get a complete analytical view of the experiments. This approach also contributed to a more robust comparative approach between the mathematical model developed and the experimental outcome.

The chapter has demonstrated that there is a strong relationship between the results of the experiments and the mathematical model. The results from this chapter have also verified the results outcome from chapter 5 regarding the behaviour of flexible tyres operating in rigid and flexible modes. The chapter has confirmed and established that highly inflated tyres have a reduced contact area thereby resulting in deep rutting particularly in sand soil bed. Reducing the tyre pressure increases the contact patch area between the tyre and the terrain resulting in reduced rutting and more drawbar-pull generated. The effect of deep rutting is more prominent in the sand terrain bed than in clay.

The applied load also played a significant role in the generation of drawbar-pull in all cases but with the lowest values being obtained in highly inflated tyres operating in sand soil terrain bed. The direct comparison between the accuracy of the POWERSEV mathematical model and the experimental results is graphically and analytically addressed in detail in chapter 8, which is the next chapter.

CHAPTER 8

DISCUSSION OF RESULTS:

COMPARATIVE ANALYSIS FOR VARIABLE TRENDS AND PATTERNS

8.0. CHAPTER 8

DISCUSSION OF RESULTS: COMPERATIVE ANALYSIS FOR VARIABLE TRENDS AND PATTERNS

8.1. Introduction

This chapter discusses the analysis and application of results obtained from the experimental procedures. The output variables are compared with respect to their respective terrain. The results are then analysed in relation with the impact on wheeled construction plant. This chapter further compares the accuracy of the mathematical model presented in chapter 4 by comparing the output results of the model with the experimental results. Lastly the impact of the main variable outputs on the performance of wheeled construction plant is presented and discussed based on the model and experimental results.

8.2. Performance analysis of all variables based on the three terrains: Trends and patterns

Based on MOBILITY SF-3713 experimental results, the performance of velocity, rut depth and drawbar–pull are analysed with respect to hard ground, clay terrain bed and sand terrain bed. The results are then discussed in comparison with the existing theory and the mathematical model outcomes. This part of the thesis provides a practical perspective of the wheeled plant behaviour in the three different terrains investigated under different conditions in relation to the mathematical model results and other similar studies done before.

This section forms a very critical part of the economic analysis by categorising each of the three key variables namely velocity, rut depth and drawbar-pull with respect to the tyre pressure applied load and terrain in which the tyres are operating. The criteria for economic decision have been categorised in tables from figures 8.1 to 8.12 including their respective analysis.

8.2.1. Velocity trend and pattern analysis for speed selection 1

From figure 8.1, the velocity patterns for tyre pressure combinations and applied were all concentrated in one area indicating that the low speed selections does not affect the variance of velocity outputs for all the three terrains under investigation.

8.2.2. Rut depth trend and pattern analysis for speed selection 1

Figure 8.2 presents the rut depth patterns for the three terrains. On hard ground there was no rutting experienced by the tyres. In the clay terrain, rutting was seen to take place due to the deformable nature of wet clay. The deepest rut was produced by the combination of maximum load and maximum tyre pressure 800N and 45PSI respectively. In sand terrain, higher loads and higher tyres pressures produced deeper ruts than in clay due to small surface contact areas increasing the penetrating force. The two fully loaded tyres (800N) under minimum tyre pressure (3PSI) produced less rutting than clay due to increased surface area.

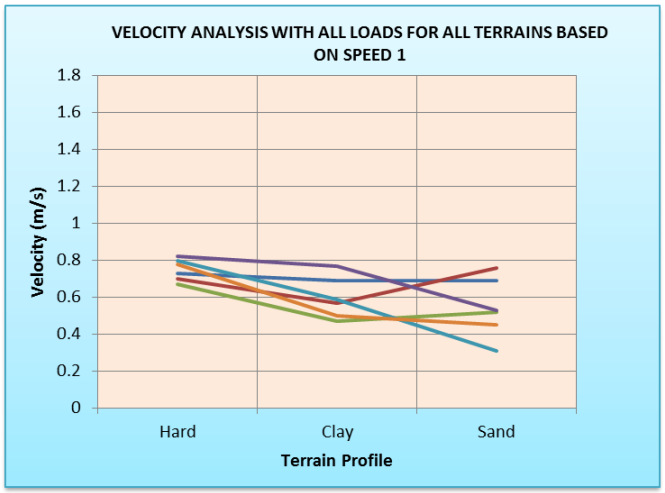

Figure 8.1: Velocity analysis at speed selection 1

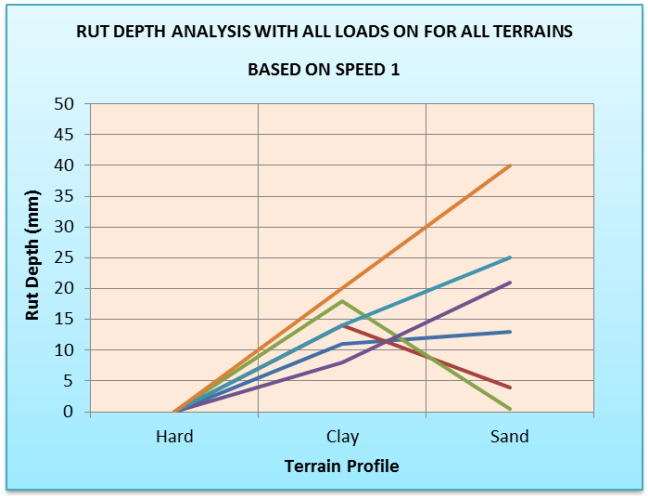

Figure 8.2: Rut depth analysis at speed selection 1

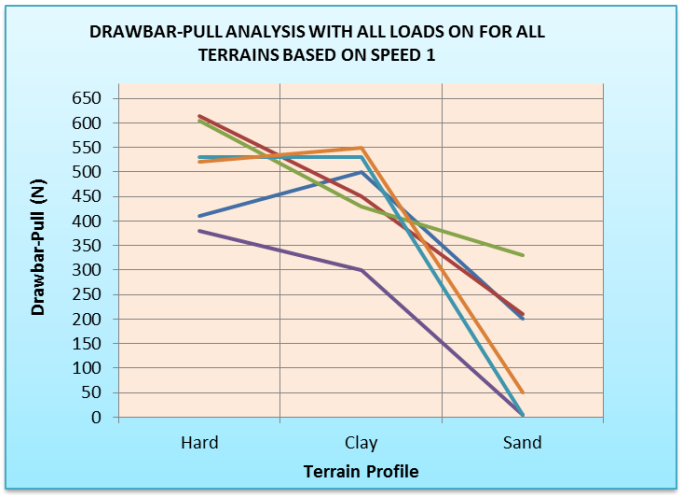

Figure 8.3: Drawbar-pull analysis at speed selection 1

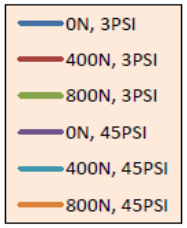

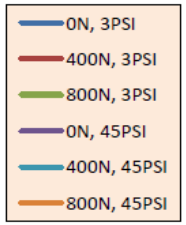

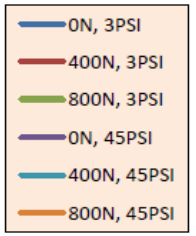

Applied Load & Tyre pressure	Velocity output based on speed selection 3		
	Hard	Clay	Sand
0N, 3PSI	High	High	High
400N, 3PSI	High	Low	High
800N, 3PSI	High	Low	Low
0N, 45PSI	High	High	Low
400N, 45PSI	High	Low	Lower
800N, 45PSI	High	Low	Low

Applied Load & Tyre pressure	Rut Depth output based on speed selection 3		
	Hard	Clay	Sand
0N, 3PSI	Lower	High	High
400N, 3PSI	Lower	High	Low
800N, 3PSI	Lower	High	Lower
0N, 45PSI	Lower	High	Higher
400N, 45PSI	Lower	High	Higher
800N, 45PSI	Lower	High	Higher

Applied Load & Tyre pressure	Drawbar-Pull output based on speed selection 3		
	Hard	Clay	Sand
0N, 3PSI	High	Higher	Low
400N, 3PSI	Higher	High	Low
800N, 3PSI	Higher	High	Low
0N, 45PSI	High	Low	Lower
400N, 45PSI	Higher	Higher	Lower
800N, 45PSI	Higher	Higher	Lower

8.2.3. Drawbar-pull trend and pattern analysis for speed selection 1

Figure 8.3 presents the behaviour pattern of the power performance of the machine and tyre in terms of drawbar-pull. On the hard ground generally all combinations of tyre pressure and applied load produced significant drawbar-pull with highly loaded tyres and maximum applied loads producing the highest drawbar-pull due to larger contact areas resulting in better grip and traction. In clay it is very interesting to note that the drawbar-pull values for all combinations were still high except for the high 45PSI and no load which had reduced drawbar-pull due to lack of traction. It is clear that additional load helps less inflated tyres to have more traction on the ground, whether hard or deformable. In sand terrain however the drawbar-pull reduced significantly for all combinations except the 800N, 3PSI tyre pressure. The highly inflated tyres and high applied loads provide the least desired results due to the deep tyre rutting in sand terrain as seen in figure 8.2.

Output comparisons of various applied load/tyre pressure combination with respect to velocity, rut depth and drawbar-pull in the three terrains can be deduced from the respective tables contained in figures 8.1 to 8.3.

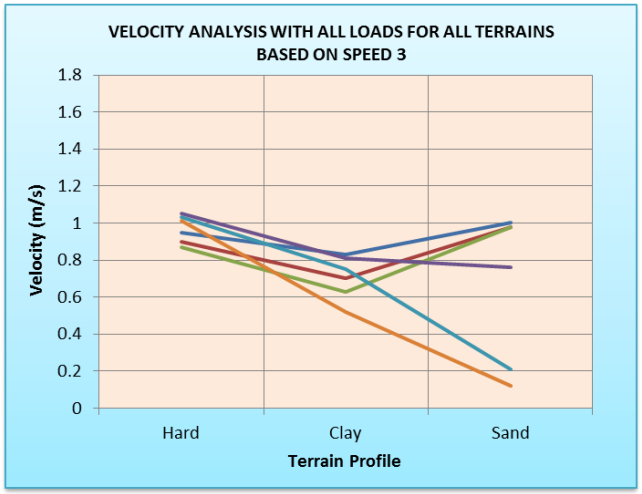

Figure 8.4: Velocity analysis at speed selection 3

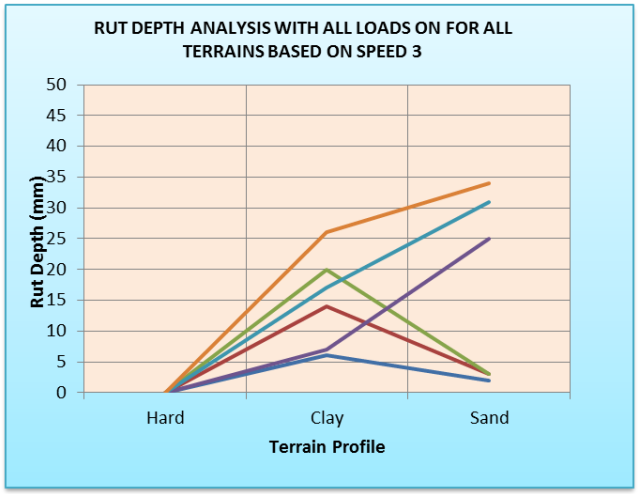

Figure 8.5: Rut depth analysis at speed selection 3

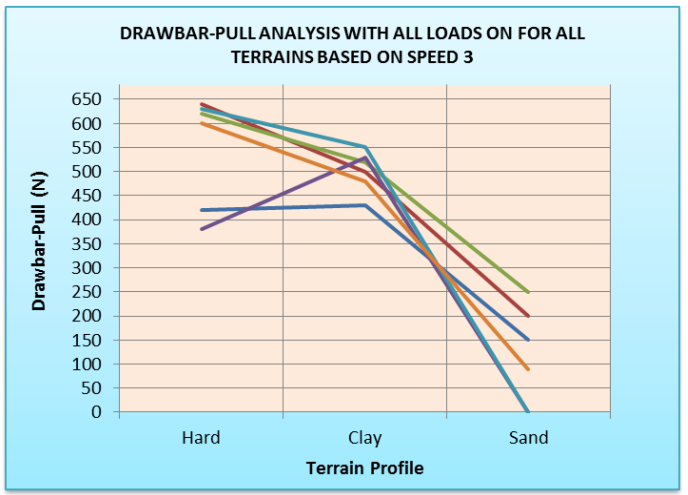

Figure 8.6: Drawbar-pull analysis at speed selection 3

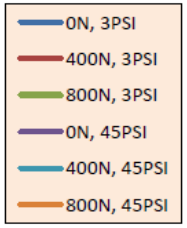

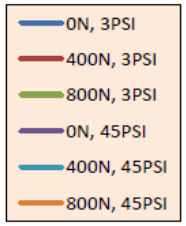

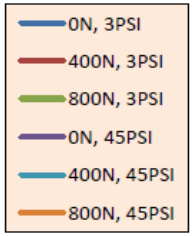

Applied Load & Tyre pressure	Velocity output based on speed selection 3		
	Hard	Clay	Sand
0N, 3PSI	High	Low	High
400N, 3PSI	High	Low	High
800N, 3PSI	High	Low	High
0N, 45PSI	High	Low	Low
400N, 45PSI	High	Low	Lower
800N, 45PSI	High	Low	Lower

Applied Load & Tyre pressure	Rut Depth output based on speed selection 3		
	Hard	Clay	Sand
0N, 3PSI	Lower	Low	Lower
400N, 3PSI	Lower	High	Lower
800N, 3PSI	Lower	High	Lower
0N, 45PSI	Lower	Low	Higher
400N, 45PSI	Lower	High	Higher
800N, 45PSI	Lower	High	Higher

Applied Load & Tyre pressure	Drawbar-Pull output based on speed selection 3		
	Hard	Clay	Sand
0N, 3PSI	High	High	Low
400N, 3PSI	Higher	High	Low
800N, 3PSI	Higher	High	Low
0N, 45PSI	High	Higher	Lower
400N, 45PSI	Higher	High	Lower
800N, 45PSI	Higher	High	Low

8.2.4. Velocity trend and pattern analysis for speed selection 3

From figure 8.4, the velocity patterns were now more distinguished and defined with the increase in the speed. In the hard ground, the velocity was high for all combinations with 0N applied loads producing the highest velocity for both 45PSI and 3PSI tyre pressures. The most loaded and least inflated tyres produced the least velocity. As for clay terrain bed there was a reduction in velocity compared to the hard ground for all inflation pressure/applied load combinations. In sand terrain however, all combinations produced higher velocity than in clay except for higher applied loads/high tyre pressure combinations.

8.2.5. Rut depth trend and pattern analysis for speed selection 3

Figure 8.5 presents the rut depth patterns for the three terrains. On hard ground there was no rutting experienced by the tyres. In the clay terrain, rutting was seen to take place due to the deformable nature of wet clay for all combinations as seen in figure 8.5. The least loaded tyres produced the lowest rut depths in clay with the highest rutting being produced by the 800N/3PSI combination. In sand terrain, all the three higher tyre pressures produce deeper ruts than in clay. The other three combinations characterised by lower tyre pressure/larger contact areas produce very low rutting.

8.2.6. Drawbar-pull trend and pattern analysis for speed selection 3

Figure 8.6 presents the behaviour pattern of the power performance of the machine and tyre in terms of drawbar-pull for speed 3. On the hard ground generally all combinations of tyre pressure and applied load produced significant

drawbar-pull. The lower values of these combinations are for the 0N applied loads for both 45PSI and 3PSI. Despite the slight reduction in drawbar-pull in clay compared to hard ground, the output was still high. It is clear that additional load helps less inflated tyres to have more traction on the ground, whether hard or deformable. In sand terrain however the drawbar-pull reduced significantly for all combinations except the 800N, 3PSI tyre pressure. Sandy terrain provided the poorest and lowest drawbar-pull of all the three terrains. Output comparisons of various applied load/tyre pressure combination with respect to velocity, rut depth and drawbar-pull in the three terrains can be deduced from the respective tables contained in figures 8.4 to 8.6.

8.2.7. Velocity trend and pattern analysis for speed selection 5

From figure 8.7, the velocity patterns are now more distinguished and defined with the increase in the speed. On the hard ground, the velocity was high for all combinations with 0N applied loads producing the highest velocity for both 45PSI and 3PSI tyre pressures just like in the previous speed selection 3. The most loaded/least inflated combination tyre produced the least velocity. As for clay the clay terrain bed there was a reduction in velocity compared to the hard ground for all combinations. In sand terrain however, all runs with low tyre pressure produce high velocity just like in hard ground regardless of the load. The other runs based on 45PSI produced the least velocity as seen in figure 8.7.

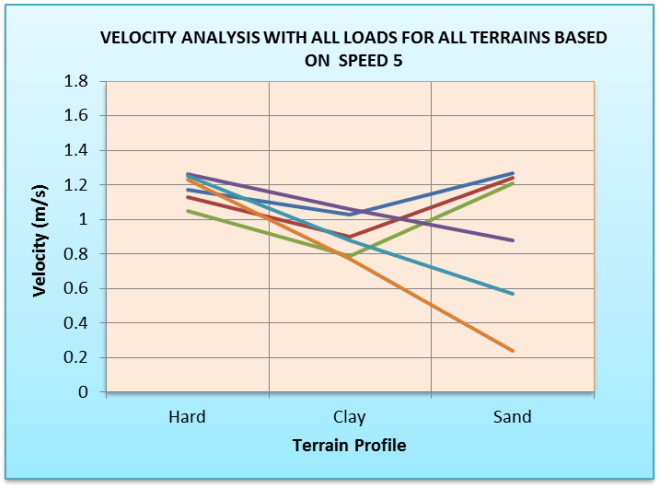

Figure 8.7: Velocity analysis at speed selection 5

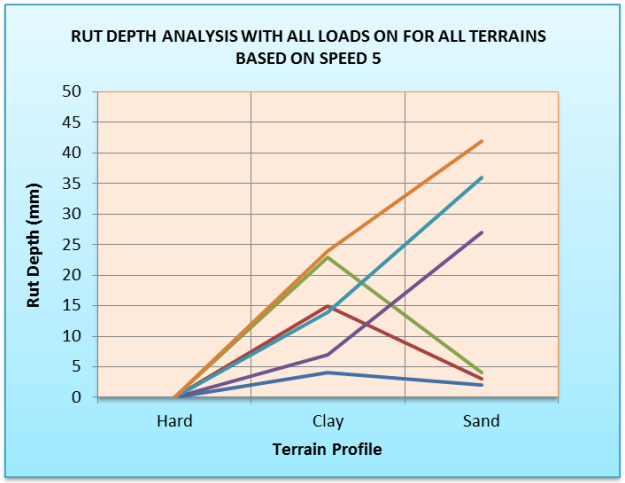

Figure 8.8: Rut depth analysis at speed selection 5

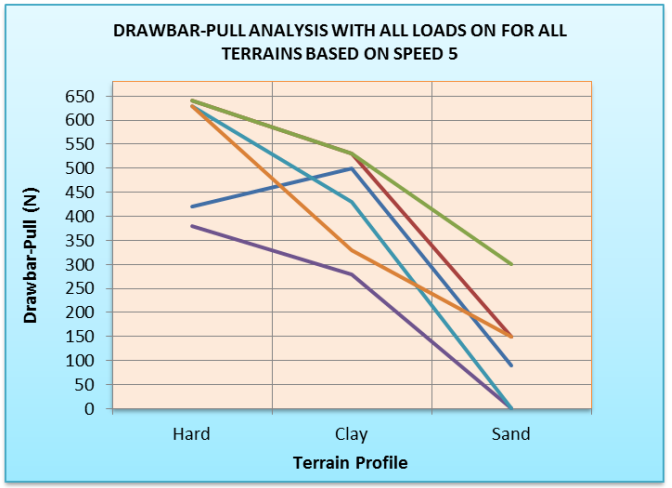

Figure 8.9: Drawbar-pull analysis at speed selection 5

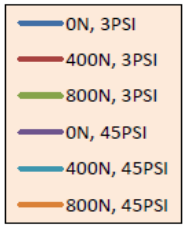

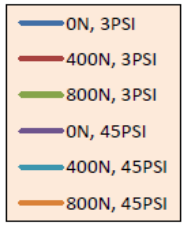

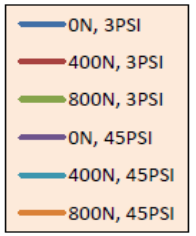

Applied Load & Tyre pressure	Velocity output based on speed selection 3		
	Hard	Clay	Sand
0N, 3PSI	Higher	High	Higher
400N, 3PSI	Higher	High	Higher
800N, 3PSI	Higher	High	Higher
0N, 45PSI	Higher	High	Low
400N, 45PSI	Higher	High	Lower
800N, 45PSI	Higher	High	Lower

Applied Load & Tyre pressure	Rut Depth output based on speed selection 3		
	Hard	Clay	Sand
0N, 3PSI	Lower	Low	Lower
400N, 3PSI	Lower	High	Lower
800N, 3PSI	Lower	High	Lower
0N, 45PSI	Lower	Low	Higher
400N, 45PSI	Lower	High	Higher
800N, 45PSI	Lower	High	Higher

Applied Load & Tyre pressure	Drawbar-Pull output based on speed selection 3		
	Hard	Clay	Sand
0N, 3PSI	High	Higher	Lower
400N, 3PSI	Higher	High	Lower
800N, 3PSI	Higher	High	Low
0N, 45PSI	High	Low	Lower
400N, 45PSI	Higher	High	Lower
800N, 45PSI	Higher	Low	Low

8.2.8. Rut depth trend and pattern analysis for speed selection 5

Figure 8.8 presents the rut depth patterns for the three terrains. On hard ground there was no rutting experienced by the tyres. In the clay terrain, rutting was seen to take place due to the deformable nature of wet clay for all combinations as seen in figure 8.8. The least loaded tyres produced the lowest rut depths in clay with the highest rutting being produced by the 800N/3PSI combination. In sand terrain, all the three higher tyres pressures based runs produced deeper rut depths than in clay. The other three combinations characterised by lower tyre pressure/larger contact areas produced very low rutting. These results are consistent with velocity results presented in figure 8.7

8.2.9. Drawbar-pull trend and pattern analysis for speed selection 5

Figure 8.9 presents the behaviour pattern of the power performance of the machine and tyre in terms of drawbar-pull for speed 5. On the hard ground generally all combinations of tyre pressure and applied load produced significant drawbar-pull. The lower outputs of these combinations were for the 0N applied loads for both 45PSI and 3PSI due to low contact area. Despite the slight reduction in drawbar-pull in the clay terrain compared to hard ground, the output was still high. In the sand terrain however the drawbar-pull reduced significantly for all combinations except the 800N/3PSI tyre pressure whose drop in value was not as significant as the other combinations. Sandy terrain provided the poorest and lowest drawbar-pull of all the three terrains. These results are also consistent with findings from other scholars presented in the literature review. Output trend and pattern analysis of various applied load/tyre pressure combinations with respect to velocity, rut depth and drawbar-pull in the three terrains can be deduced from the respective tables contained in figures 8.7 to 8.9.

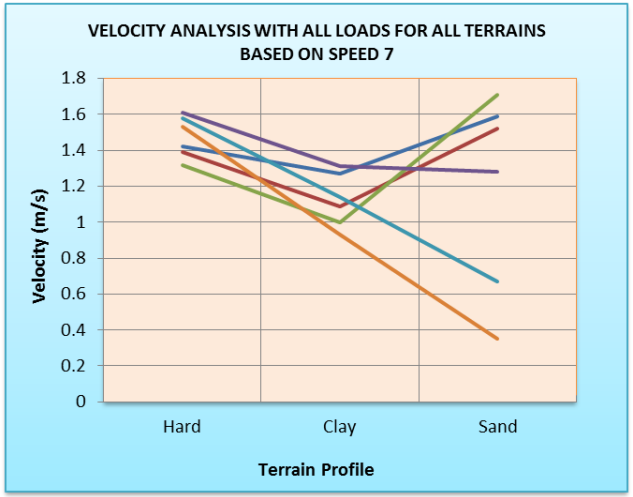

Figure 8.10: Velocity analysis at speed selection 7

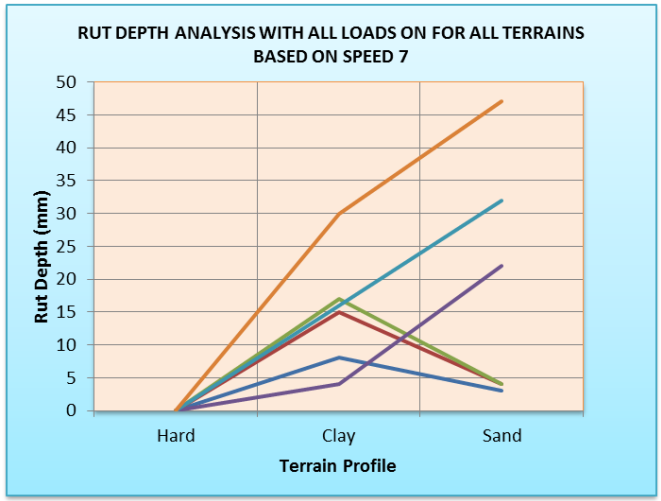

Figure 8.11: Rut depth analysis at speed selection 7

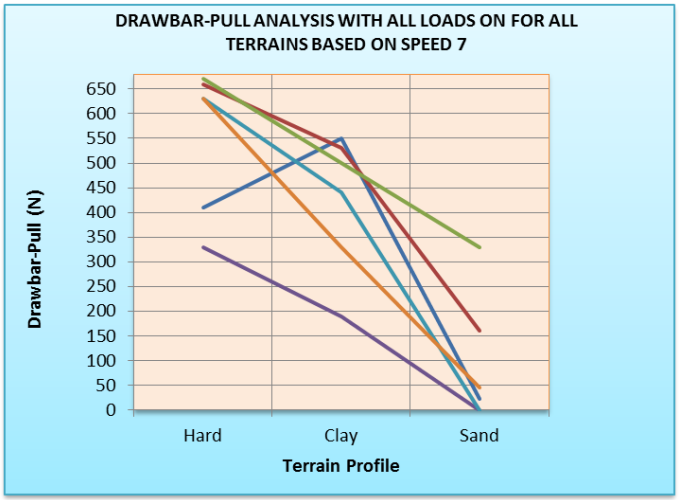

Figure 8.12: Drawbar-pull analysis at speed selection 7

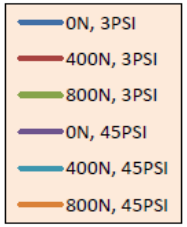

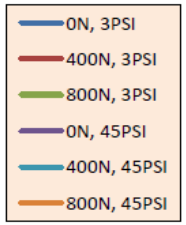

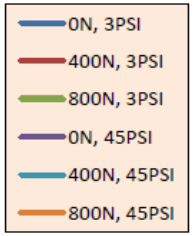

Applied Load & Tyre pressure	Velocity output based on speed selection 3		
	Hard	Clay	Sand
0N, 3PSI	Higher	High	Higher
400N, 3PSI	Higher	High	Higher
800N, 3PSI	Higher	High	Higher
0N, 45PSI	Higher	High	High
400N, 45PSI	Higher	High	Lower
800N, 45PSI	Higher	High	Lower

Applied Load & Tyre pressure	Rut Depth output based on speed selection 3		
	Hard	Clay	Sand
0N, 3PSI	Lower	Low	Lower
400N, 3PSI	Lower	High	Lower
800N, 3PSI	Lower	High	Lower
0N, 45PSI	Lower	Low	High
400N, 45PSI	Lower	High	Higher
800N, 45PSI	Lower	High	Higher

Applied Load & Tyre pressure	Drawbar-Pull output based on speed selection 3		
	Hard	Clay	Sand
0N, 3PSI	High	Higher	Lower
400N, 3PSI	Higher	High	Low
800N, 3PSI	Higher	High	Low
0N, 45PSI	High	Low	Lower
400N, 45PSI	Higher	Low	Lower
800N, 45PSI	Higher	Low	Lower

8.2.10. Velocity trend and pattern analysis for speed selection 7

The velocity trends and patterns for speed 7 are presented in figure 8.10. The entire pattern of graphs in this figure was similar to that produced by speed 5 selection. The only notable difference is that velocity values were higher on the hard ground and on the sandy terrain.

8.2.11. Rut depth trend and pattern analysis for speed selection 7

The rut depth patterns for speed 7 are presented in figure 8.11. The entire pattern of graphs in this figure was similar to that produced by speed 5 selection. The only notable difference is that rut depth in clay and sandy terrains were deeper than in speed selection 5. This indicates that velocity becomes uneconomical beyond a particular value because much of the energy is wasted on the effort in trying to overcome resistance. This results in further rutting as the motion resistance is too great to be overcome.

8.2.12. Drawbar-pull trend and pattern analysis for speed selection 7

The drawbar-pull patterns for speed 7 are presented in figure 8.12. The entire pattern of graphs in this figure was similar to that produced by speed 5 selection. The only difference observed is that there was a slight increase in drawbar-pull for all the terrains. This increase was uneconomical because it was not proportional to the amount on increase in the speed value. Much of the energy was wasted in the process of overcoming motion resistance. These results are also consistent with the outcome of the velocity and rut depth analysis discussed in chapter 6 where slip levels beyond 0.5 are uneconomical. Output comparisons of various applied

load/tyre pressure combination with respect to velocity, rut depth and drawbar-pull in the three terrains can be deduced from the respective tables contained in figures 8.10 to 8.12.

8.3. Comparative analysis of mathematical model results and experimental data results.

This section of the thesis forms one of the most critical parts of the research where the POWERSEV mathematical model is tested by comparing the power loss or output results with the results from the Mobility SF-3713 experiments. This section of work also fulfils the outlined objective number 6 which addresses the experimental procedure of model verification. The soil and machine parameters such as soil cohesion, friction angle, wheel slip/skid ratio, self and applied loads, tyre sizes and velocities were all entered in the mathematical model to calculate the available drawbar-pull. The final result for each run was compared with the respective drawbar-pull force (in Newtons) reading from PCE-1000 force gauge. The results were then compared in terms of value and percentage where appropriate.

It must be emphasised that scaling and correction factors have to be deployed when using the mathematical model for the live running of the wheeled plant. This is because the model factors and figures used are less that than those characterised by heavy duty wheeled plant. It is from this perspective that more refinement and live field experiments are required in order to increase the accuracy of the mathematical model. The tyre pressure adopted for this comparison was the 45PSI. This is because it is the one that simulates the rigid wheel, upon which the POWERSEV mathematical model was based on.

8.3.1. Mathematical and experimental model results comparison for speed selection 1 in the Clay terrain bed

	Drawbar-pull (N)			
	Applied Load, Tyre pressure	**0N, 45PSI**	**400N, 45PSI**	**800N, 45PSI**
1	Experimental Drawbar-pull	300	530	550
2	Mathematical model Drawbar-pull	322	629	561
	Difference (N)(%)	**22 (7%)**	**99 (19%)**	**11(2%)**

Table 8.1: Drawbar-pull Comparison/ Verification data for mathematical model results and experimental results on the clay terrain bed

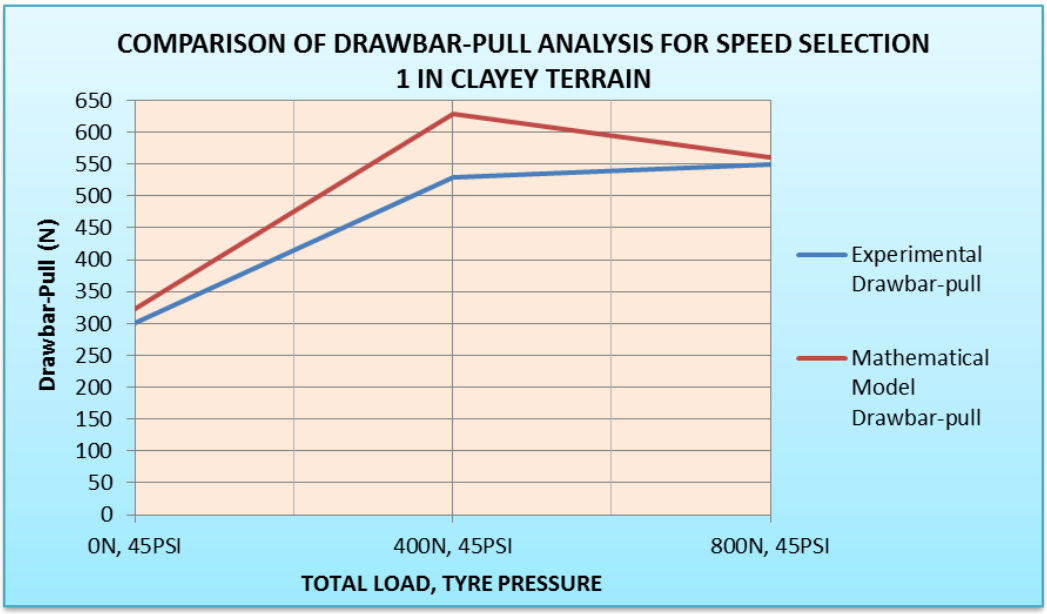

Figure 8.13: Drawbar-pull Comparative/Verification analysis between mathematical model results and experimental results

Figure 8.13 compares the drawbar-pull results of the POWERSEV mathematical model and the results from the instrument readings from the experiment in the clay terrain bed. The results show that for speed selection 1, the overall level of coloration between the results is very high with the best result being 2% (11N) or 1.1kg difference for the applied load of 800N run as seen from table 8.1. The least result was for the 400N applied load provided a difference of 19% (22N) or 2.2Kg. A difference of 22N between model result and actual practical result is acceptable considering that the natural terrain is involved

8.3.2. Mathematical and experimental model results comparison for speed selection 3 in the clay terrain bed

	Drawbar-pull (N)			
	Applied Load, Tyre pressure	**0N, 45PSI**	**400N, 45PSI**	**800N, 45PSI**
1	Experimental Drawbar-pull	530	550	480
2	Mathematical model Drawbar-pull	528	460	403
	Difference (N)(%)	**2 (0.3%)**	**90 (20%)**	**77(19%)**

Table 8.2: Drawbar-pull Comparison/ Verification data for mathematical model results and experimental results on the clay terrain bed

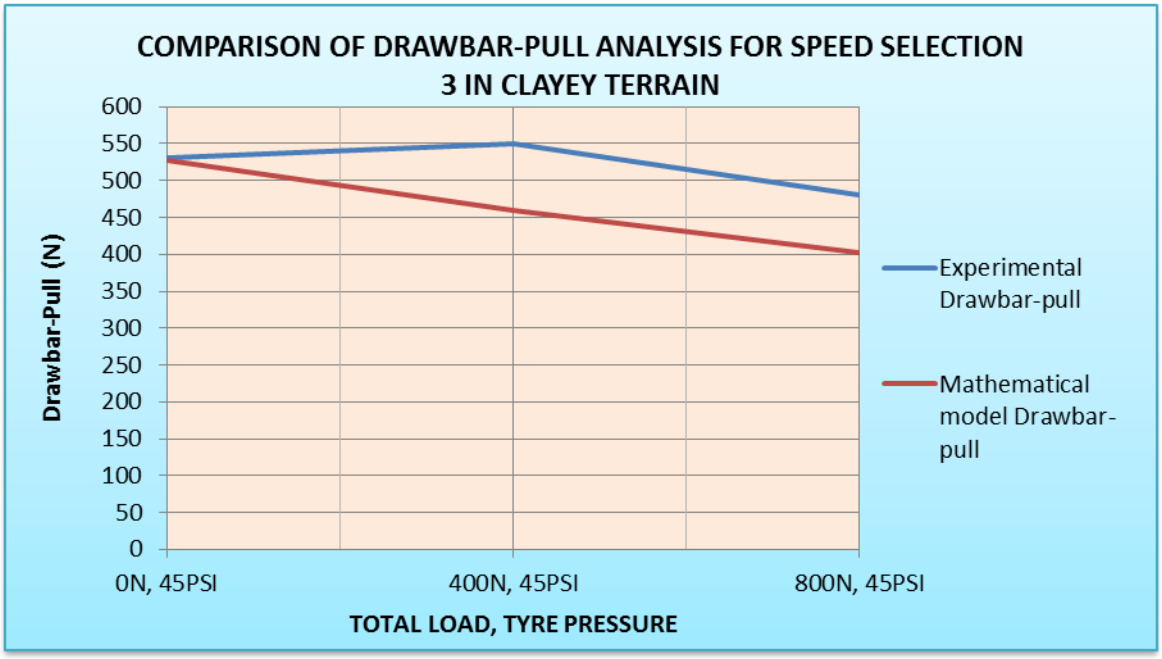

Figure 8.14: Drawbar-pull Comparative/Verification analysis between mathematical model results and experimental results on the cay terrain bed

Figure 8.14 compares the drawbar-pull results of the POWERSEV mathematical model and the results from the instrument readings from the experiment in the clay terrain bed. The results show that for speed selection 3, the level of correlation of the results was very high with the best result being 0.3% (2N) or 0.2kg difference for the 0N applied load run as seen from table 8.2. The least result was for the 400N applied load providing a difference of 20% (90N) or 9Kg. This result is equally more accurate than using other methods that utilise the constants such as

the Bekker method. A difference of 90N between model result and actual practical result is acceptable considering that the natural terrain is involved

8.3.3. Mathematical and experimental model results comparison for speed selection 5 on the clay terrain bed

	Drawbar-pull (N)			
	Applied Load, Tyre pressure	**0N, 45PSI**	**400N, 45PSI**	**800N, 45PSI**
1	Experimental Drawbar-pull	280	430	330
2	Mathematical model Drawbar-pull	306	498	384
	Difference (N)(%)	**26 (9.3%)**	**68 (15.8%)**	**54 (16.4%)**

Table 8.3: Drawbar-pull Comparison/ Verification data for mathematical model results and experimental results on the clay terrain bed

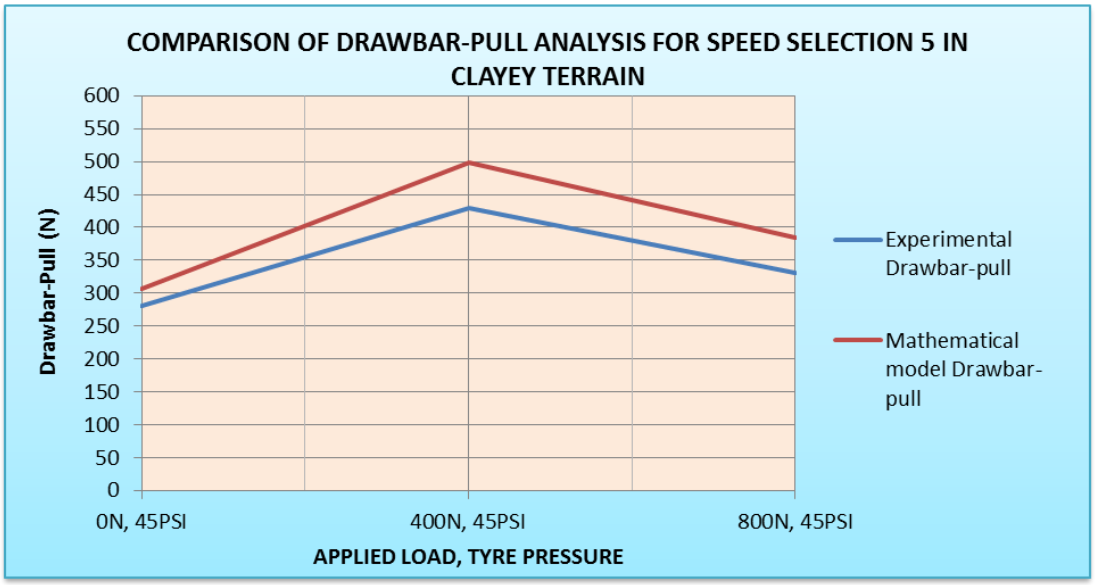

Figure 8.15: Drawbar-pull Comparative/Verification analysis between mathematical model results and experimental results on the clay terrain bed

Figure 8.15 compares the drawbar-pull results of the POWERSEV mathematical model and the results from the instrument readings from the experiment in the clay terrain bed as explained in chapter 7. The results show that for speed selection 5, the level of correlation of the results is acceptable with the best result being 9.3% (26N) or 2.6kg as the difference for the 0N applied load run as seen from table 8.3. The least result was for the 800N applied load providing a difference of 16.4%

(54N) or 5.4Kg. This result was equally more accurate than using other methods that utilise the constants. A difference of 54N between model result and actual practical result is acceptable considering that the natural terrain is involved

8.3.4. Mathematical and experimental model results comparison for speed selection 7 in the clay terrain bed

	Drawbar-pull (N)			
	Applied Load, Tyre pressure	**0N, 45PSI**	**400N, 45PSI**	**800N, 45PSI**
1	Experimental Drawbar-pull	190	440	330
2	Mathematical model Drawbar-pull	300	379	276
	Difference (N)(%)	**110 (59%)**	**61 (15.8%)**	**54 (19.6%)**

Table 8.4: Drawbar-pull Comparison/ Verification data for mathematical model results and experimental results on the clay terrain bed

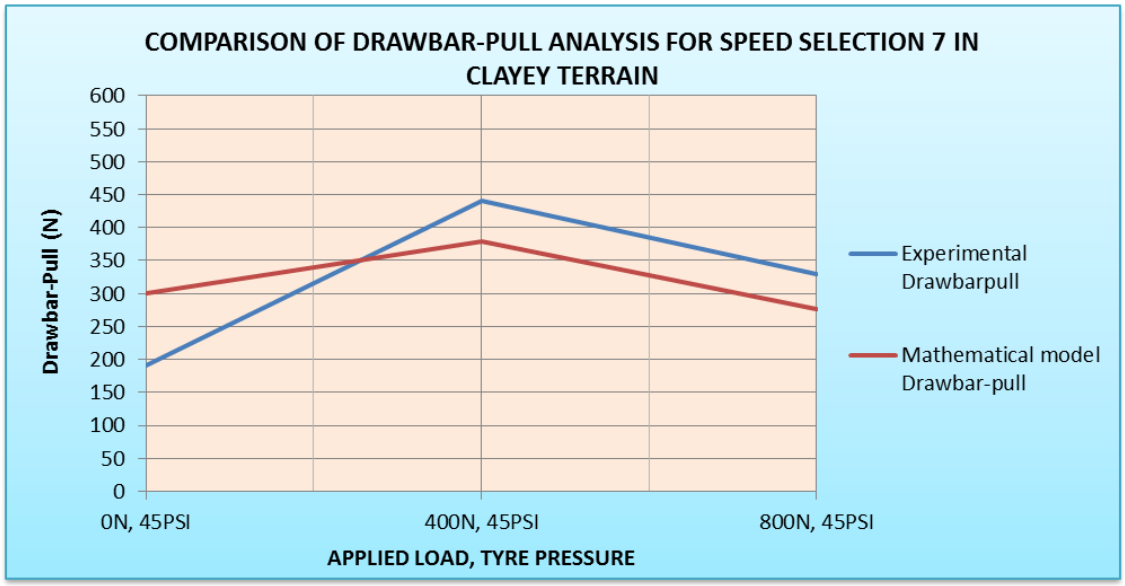

Figure 8.16: Drawbar-pull Comparative/Verification analysis between mathematical model results and experimental results on the clay terrain bed

Figure 8.16 compares the drawbar-pull results of the POWERSEV mathematical model and the results from the instrument readings from the experiment in the clay terrain bed as explained in chapter 7. The results show that for speed selection 7, the level of correlation of the results is acceptable with the best result being 15.8% (61N) or 6.1kg difference for the 400N applied load run as seen from table 8.4. The lowest result was for the 0N applied load providing a difference of 59% (110N)

or 11Kg. Although this result is acceptable based on the previous methods approaches speed selection 7 is less accurate compared to other earlier speed selections, particularly for the 0N applied load run. This can be attributed to the limitation of the vehicle and terrain combination to handle higher velocities.

8.4. Comparative analysis of mathematical model results and experimental data results in the sand terrain bed

The same procedure for the clay terrain bed was used for calculating the drawbar-pull except that the main engineering factor is the angle of shearing resistance. The results were the compared and discussed for each run recorded in the thesis

Figure 8.17 compares the drawbar-pull results of the POWERSEV mathematical model and the results from the instrument readings from the experiment in the sand terrain bed as explained in chapter 7. The results show that for speed selection 1, the level of correlation of the results is very high with the best result being 4.4% (4N) or 0.44kg difference for the 800N applied load run as seen from table 8.5. The least result is for the 0N applied load provides a difference of 3.7N or 0.37Kg. The results are acceptable when discussed in terms of Newton values and not percentage values as they are misleading due to the small drawbar-pull values involved. The drawbar-pull values were lower in the wet sandy terrain than in the wet clay terrain as seen in figures 8.13 to 8.17. . The graph on the right side is an expanded version of the same figure whose aim is to clearly see the relationship of the two results at a close range.

.

8.4.1. Mathematical and experimental model results comparison for speed selection 1 in the sand terrain bed

	Drawbar-pull (N)			
	Applied Load, Tyre pressure	**0N, 45PSI**	**400N, 45PSI**	**800N, 45PSI**
1	Experimental Drawbar-pull	5	5	90
2	Mathematical model Drawbar-pull	1.3	10	94
	Difference (N)	**3.7**	**5**	**4.4**

Table 8.5: Drawbar-pull Comparison/ Verification data for mathematical model results and experimental results on the sand terrain bed

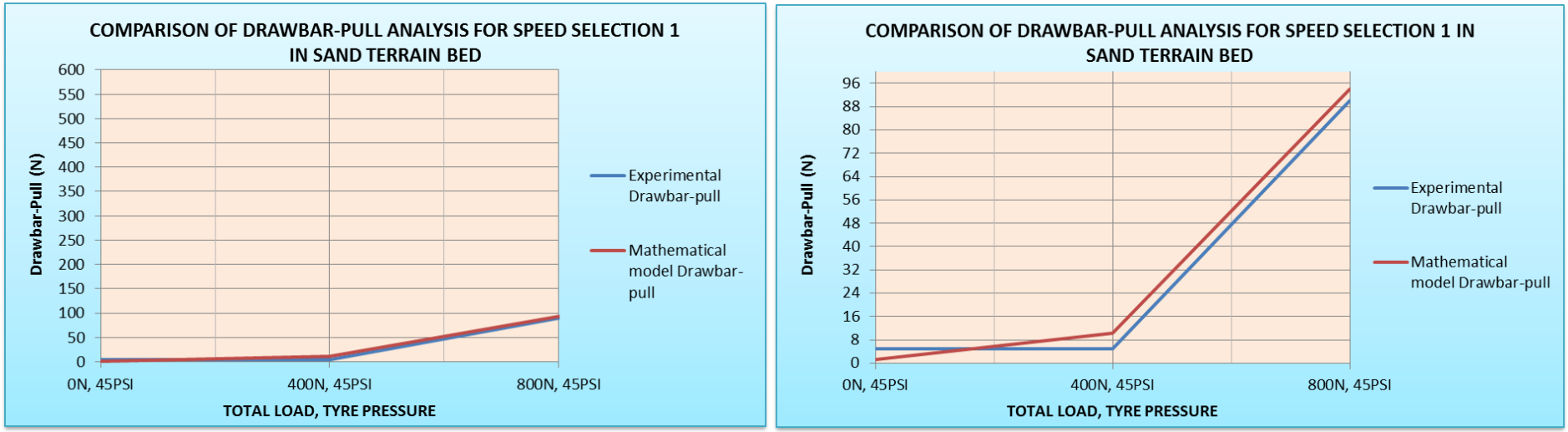

Figure 8.17: Drawbar-pull Comparative/Verification analysis between mathematical model results and experimental results on the sand terrain bed with the right pane showing expanded version

8.4.2. Mathematical and experimental model results comparison for speed selection 3 in the sand terrain bed

Figure 8.18 compares the drawbar-pull results of the POWERSEV mathematical model and the results from the experiment in the sand terrain. The results show that for speed selection 3, the level of correlation of the results is high with the best result being 0.4N or 0.04kg difference for the 800N applied load run as seen from table 8.6. The least result is for the 800N applied load provides a difference of 51N or 5.1Kg. The results are within acceptable means when discussed in terms of Newton values and not percentage values as they are misleading due to the small drawbar-pull values involved. The drawbar-pull values were lower in the wet sandy terrain than in the wet clay terrain as seen in figures 8.15 to 8.19. The graph on the right side is an expanded version of the same figure whose aim is to clearly see the relationship of the two results at a close range.

Figure 8.19 and table 8.7 compares the drawbar-pull results of the POWERSEV mathematical model and the results from the experiment in the sand terrain. The results show that for speed selection 5, the level of correlation of the results is high with all the three results differences between the mathematical model and the experiment outcome as follows: 0.8N, 0.5N and 6N from the runs of the combinations 0N/45PSI, 400N/45PSI and 800N/45PSI respectively. The 800N/45PSI run represented a percentage difference of 6N or 0.6kg which is very minimal. The results are further acceptable when discussed in terms of Newton values for the first two runs due to the small drawbar-pull values involved. The drawbar-pull values were lower in the wet sandy terrain than in the wet clay terrain as seen in figures 8.16 to 8.20.

Mathematical and experimental model results comparison for speed selection 3 in the sand terrain bed

	Drawbar-pull (N)			
	Applied Load, Tyre pressure	**0N, 45PSI**	**400N, 45PSI**	**800N, 45PSI**
1	Experimental Drawbar-pull	0	0	90
2	Mathematical model Drawbar-pull	0.4	7	141
	Difference (N)	**0.4**	**7**	**51**

Table 8.6: Drawbar-pull Comparison/ Verification data for mathematical model results and experimental results on the sand terrain bed

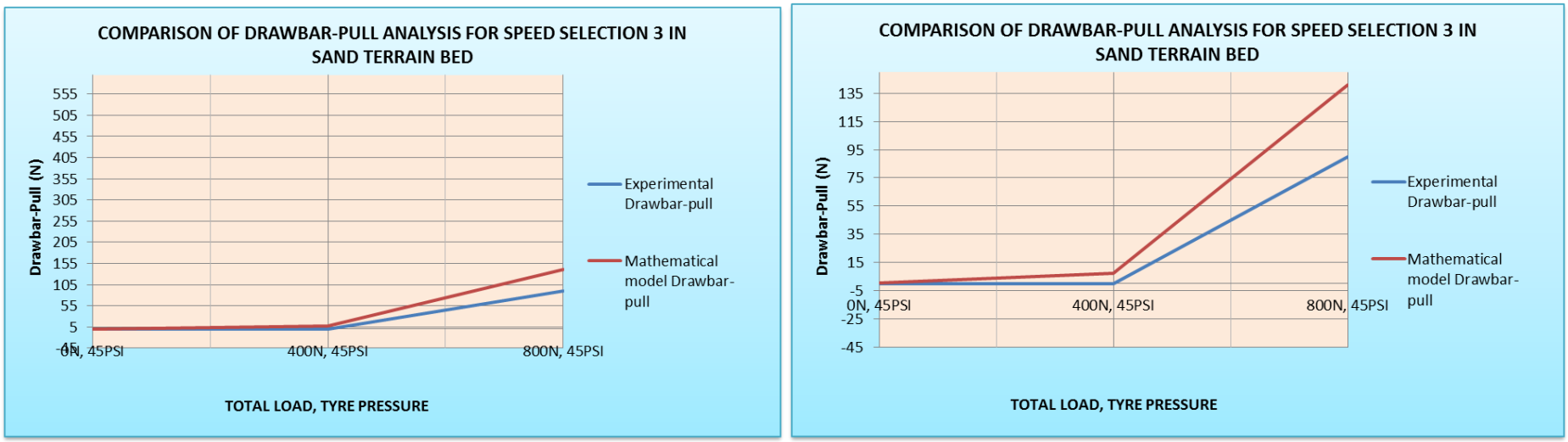

Figure 8.18: Drawbar-pull Comparative/Verification analysis between mathematical model results and experimental results on the sand terrain bed with the right pane showing expanded version

8.4.3. Mathematical and experimental model results comparison for speed selection 5 in the sand terrain bed

	Drawbar-pull (N)			
	Applied Load, Tyre pressure	**0N, 45PSI**	**400N, 45PSI**	**800N, 45PSI**
1	Experimental Drawbar-pull	1	1	150
2	Mathematical model Drawbar-pull	0.2	0.5	144
	Difference (N)	**0.8**	**0.5**	**6**

Table 8.7: Drawbar-pull Comparison/ Verification data for mathematical model results and experimental results on the clay terrain bed

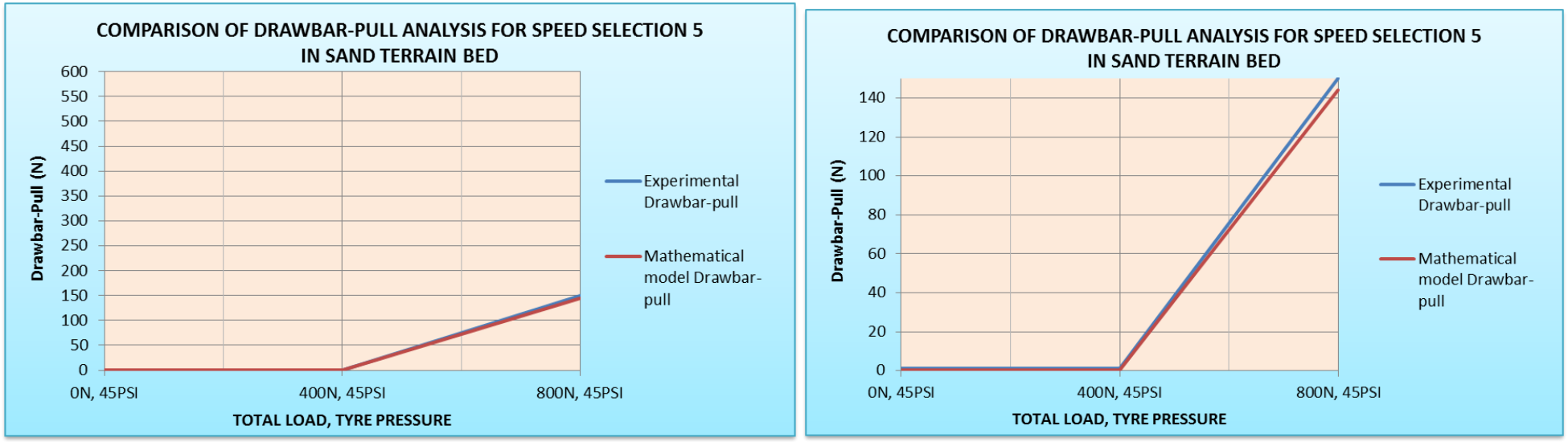

Figure 8.19: Drawbar-pull Comparative/Verification analysis between mathematical model results and experimental results on the sand terrain bed with the right pane showing expanded version

8.4.4. Mathematical and experimental model results comparison for speed selection 7 in the sand terrain bed

Figure 8.20 and table 8.8 compares the drawbar-pull results of the POWERSEV mathematical model and the results from the experiment in the sand terrain. The results show that for speed selection 7, the results provide excellent coloration for all the runs as seen from table 8.8 and figure 8.20. The best result was for the 0N applied load run which gave the same result as the experimental run. The 800N applied load provides difference of 4N (9%) or 0.4kg which is very significant. The drawbar-pull values were lower in the wet sandy terrain than in the wet clay terrain as seen in figures 8.13 to 8.19

Mathematical and experimental model results comparison for speed selection 7 in the sand terrain bed

	Drawbar-Pull (N)			
	Applied Load, Tyre pressure	**0N, 45PSI**	**400N, 45PSI**	**800N, 45PSI**
1	Experimental Drawbar-pull	0	0	45
2	Mathematical model Drawbar-pull	0	0.2	49
	Difference (N)	**0**	**0.2**	**4**

Table 8.8: Drawbar-pull Comparison/ Verification data for mathematical model results and experimental results on the clay terrain bed

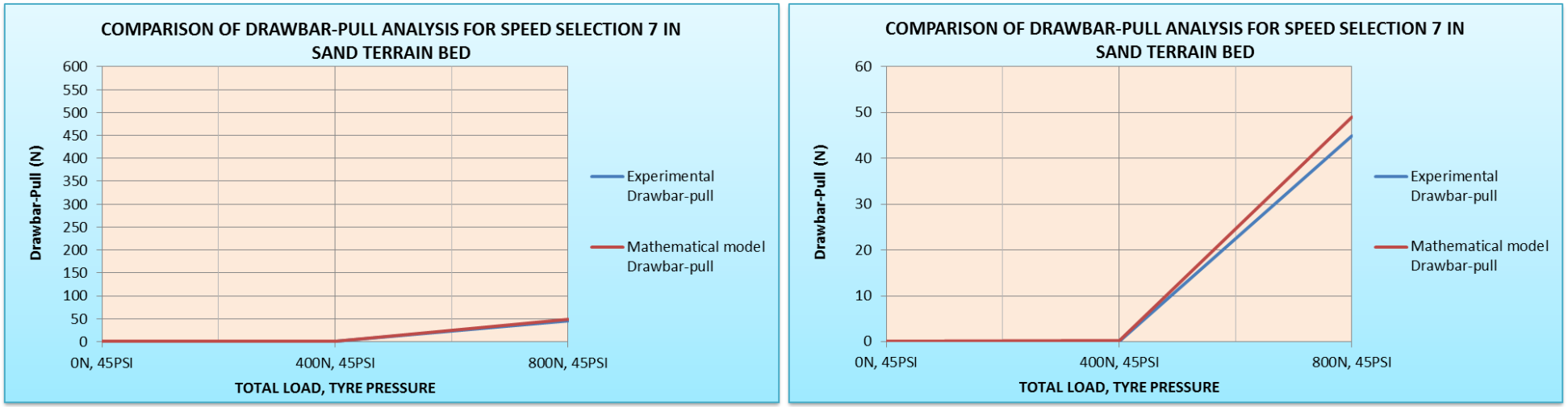

Figure 8.20: Drawbar-pull Comparative/Verification analysis between mathematical model results and experimental results in sand terrain bed with the right pane showing expanded version

8.5. Chapter Summary

This chapter has successfully demonstrated through laboratory experiments the relationship between velocity, rut depth and ultimate power available in terms of drawbar-pull. The relationship established in chapters 4, 5 and 6 has been confirmed by the outcome of the analytical comparison. These results have also verified other numerical studies that have been obtained before as discussed in the literature review chapter.

Secondly and most importantly the main aim of this research was to develop a model that would predict the power loss arising from the wheel; soil interface. The capability and reliability of the mathematical model (POWERSEV) developed in chapter 4 has been strongly verified in this chapter. This has been achieved by comparing the outcome of the Mathematical model and the Mobility SF-3713 experiments outcome. The level of correlation is very strong (99.8% in some cases) compared to the performance of other models developed before as demonstrated in chapter 6. The conclusion drawn is that this model can be refined further to be applied to the practical operations of wheeled construction plant in the economic and sustainable management of plant operating in deformable terrain particularly in clay and sandy terrains.

In practical terms the model can be used to predict most economic velocity, tyre contact area and applied load in order to attain the most efficient time and cost for the period that wheeled plant is expected to traverse the deformable section. In addition the mathematical model has demonstrated to have the capacity to

process terrain data which has a combination of both clay and sand by establishing the soil cohesion and angle of shearing resistance. The moisture content also played a critical role in this case. The successive progression of each factor namely velocity, rut depth and drawbar-pull is provided in appendices 21 to 23. These appendices demonstrate the trends and pattern of constancy in the analysis of each variable with respect to velocity increase.

CHAPTER 9

RESEARCH SUMMARY, ACHIEVEMENTS AND CONTRIBUTION TO KNOWLEDGE

9.0. CHAPTER 9

Research summary, achievements and contribution to knowledge

9.1. Introduction

This chapter presents the research summary, achievements and contribution to knowledge .The first section of the chapter outlines the main aim of the research and its associated objectives. Additionally, the achievement of each objective and the method used is presented thereby providing a comprehensive summary of the research. The last part of the section presents the principal contributions to the existing body of knowledge specifically on how the construction industry stands benefit from the study. The contribution to knowledge is based on the knowledge gap identified in chapter one.

9.2. Research summary and achievements

The aim of this study was to investigate the effect of ground conditions on the power loss of wheeled construction plant arising from the wheel-soil interaction. The focus of this study was on clay and sandy terrain. From the detailed assessment and outcome, it can be confidently stated that this aim was successfully achieved through the following objectives that were initially set out at the beginning of the research. These objectives are outlined as follows:

1. ***Objective 1***: To produce a predictive mathematical model which relates the loss of power and efficiency of wheeled construction plant to prevailing geotechnical ground conditions and soil properties using a single rigid

wheel mathematical model. This model was based on the work energy principle and the law of conservation energy incorporating vectors. ***This objective was successfully addressed in chapter four under the chapter heading mathematical model developed.***

The main reason for selecting the rigid wheel mode was based on the fact that most wheeled construction vehicles operate with highly inflated tyres due to the self-weight and applied load that they have to support. The model deployed demonstrated its powerful capacity to perform isolated analysis of variables in order to see the changing effect on the overall modelling results. Results indicated that increase in soil cohesion increased the drawbar-pull output for clay soil. Increase in the friction angle resulted in increased drawbar-pull for sandy terrain. Increase in tyre width and radius also resulted in improved drawbar-pull. The strength of the POWERSEV mathematical model in comparison with other models was in the accuracy of the rut depth variables that were derived from work energy and vector principles. This approach provided better accuracy of drawbar-pull predictions.

2. ***Objective 2:*** To critically review the existing literature in terramechanics and identify the knowledge gap associated with the subject's application to the construction sector. ***This objective was achieved in chapter two where existing terramechanics literature has been extensively reviewed and analysed from various sectors.***

As part of the important process of outlining and justifying the knowledge gap, an in-depth review of existing literature was carried out. Terramechanics related literature in the military sector was extensively reviewed being the pioneering field of terramechanics. Other areas fields studied included forestry, agricultural, planetary exploration and mining. The few construction related studies were also reviewed. Benefits and applications to the other sectors were equally discussed on selected research publications and projects. The chapter concluded by establishing that there is limited research and application of terramechanics in determining and predicting the performance of wheeled construction plant operating in deformable off road conditions in this case clay and sandy terrains. This result constituted part of the knowledge gap.

3. ***Objective 3:*** To formulate a research design and methods approach that will result in the successful execution of this doctoral research. ***This objective was achieved in chapter 3 where the detailed research design road map, research paradigms and associated methods deployed are described, explained and justified.*** Challenges associated with research methods have equally been outlined.

This section outlined and justified the main research paradigms adopted in this study. A mixed method approach dominated by quantitative methods was used to deliver the objectives of the research. Mathematical modelling was selected as the main and primary tool for obtaining research answers due to its unlimited nature in terms of the number of configurations that can

be set at each particular time. Computational analysis was selected as the main verification process due to its strength in unlimited model and variable configurations.

The third model verification process was achieved through controlled laboratory experiments as an applied method of testing the first two sets of results from non-physical modelling. Full scale site experiments were not considered as an option for verification of results due to restrictions regarding the health and safety regulations governing wheeled plant testing sites.

4. ***Objective 4:*** To demonstrate that the flexible tyre can operate in a rigid mode under certain off-road conditions using computational analysis. ***This objective was achieved in chapter five using real data obtained from the Canadian Defence department, Wong/Reece and Bekker terramechanics principles.***

In this this research, it was extremely important to demonstrate that a flexible tyre could behave as a rigid rim when highly inflated and operating in softer deformable terrain with less ground pressure; clay and sand in this case. This is because most tyres that are used for wheeled construction plant are characterised by high tyre inflation pressure. The analysis took the powerful form of isolated analysis by introducing different loads and different terrain parameters in order to demarcate the border line between rigid and flexible mode of the tyre.

The comprehensive graphical and numerical demonstration was successfully achieved through computational analysis. Mathematical modelling from POWERSEV and real experimental data from previous research were used in order to achieve this objective. These results justified the relevance of the mathematical model towards predicting the tractive performance of wheeled construction plant operating in deformable terrain.

5. ***Objective 5:*** To verify the mathematical model results using the computational analysis method based on real experimental data obtained from the Canadian Defence Department as recorded in Wong, (2010). ***This objective was achieved in chapter six using real data obtained from the Canadian Defence department, Wong/Reece and Bekker terramechanics principles compared with the developed mathematical model results.***

In order to confidently accept drawbar-pull results from the mathematical model, these results had to be compared with existing similar semi-empirical models that have been used as benchmarks in terramechanics, namely: the Bekker theory and the Wong/Reece motion of equilibrium. The mathematical model results were found to be between the boundaries of the two principles making the results to be accepted as an accurate estimate. This approach provided an opportunity to run multiple configurations which is difficult and almost impossible to attain similar runs during laboratory and full scale experiments.

6. ***Objective 6:*** To verify the mathematical model and computational analysis model results by carrying out laboratory experiments using a scaled down battery powered special vehicle called MOBILITY SF-3713. This vehicle was operated under controlled laboratory conditions. Measurements of variables during laboratory tests are taken using physical measurements, instrumentation and data computation. ***This objective was successfully achieved in chapter seven using clay terrain bed, sand terrain bed and non-deformable hard ground.***

   While the first two model verification processes provided strong and adequate confirmation of the mathematical model outcome, this section provided a platform for testing the overall results through live practical laboratory experiments. The deployment of MOBILITY SF-3713 to run on hard ground and deformable sand/clay terrains provided credible and consistent results with the mathematical and two verification models. The results from different experiment configurations were in form of tyre foot prints on hard ground, rut depth in deformable terrain and drawbar-pull for all terrains defined within the research boundary. The results were also consistent with many other studies recorded in the literature review.

7. ***Objective 7:*** To conduct an integrated variable trend and pattern of results from the research outcome. ***This objective was achieved in chapter eight by comparing the effect of the variables under discussion in each respective terrain based on the mathematical model and the experiments. The chapter further demonstrated using tyre***

manufacturing company data that tyre pressure and velocity guidelines are not enough to make economic decisions regarding wheeled plant traversing in deformable. This particularly true for clay and sandy terrains taking into account the varying moisture contents that they are subjected to in during different seasons.

The results from this section revealed that a strong relationship exists between tyre pressure, applied load, rut depth, velocity and drawbar-pull. Any combination of the factors proved to have significant influence on the power available at the wheels in the form of drawbar-pull. In practical terms the mathematical model could be used to predict most efficient velocity, tyre/terrain contact area and applied load in order to attain the optimum plant cycle time and traction for the existing deformable terrain conditions. Furthermore the contractors' claims against change of weather and subsequent deformable terrain could now be subject to more specific evaluation based on the principle trends and patterns obtained from the research. Despite the successful development of the mathematical model, there is need to refine it capacity by incorporating additional experimental data from different wheeled plants as outlined in the recommendations for future research section.

In addition to the aim and objectives laid down in the introductory chapter, three key research questions have been comprehensively answered. Below are the research questions as outlined from the onset of the research:

- How does construction plant performance and efficiency vary with response to prevailing ground conditions? ***This question has been answered in chapters' four to eight.***

- Can this model be used to predict costs, time variations and estimated completion dates resulting from research results? ***This question has been answered in chapters four to eight***

- Can the effects of varying ground conditions on cost associated with construction plant be modelled and quantified? ***This question has also been addressed in chapters' four to eight as well.***

9.3 Contribution to Knowledge

From the literature review, results analysis and variable trend analysis outcome the following have been drawn as significant contribution to knowledge towards modelling plant performance in the construction industry:

1. The limited application and utilisation of terramechanics in the construction sector has been demonstrated in a way that has not been discussed before, at least from the existing records. The case has been clearly made to highlight the relevance of terramechanics in the management of wheeled plant performance when affected by changing ground conditions.

2. The POWERSEV mathematical model was developed using a combination of the work energy model and the vector analysis approach. This approach improves the accuracy of measured drawbar-pull values in the model compared to many previous models that have been developed in the past as reported in the literature review.

3. The mathematical model results provides the practising project and cost engineers in construction with initial guidelines to solutions for soil wheel interaction problems such as subsequent plant power/efficiency loss. The model provides a starting point in developing measurable criteria for economic and technical decision making in the management of plant traversing on different off-road ground conditions.

4. The mathematical model developed can be used as a basis for assessing the mechanism for establishing contractors' claims and elimination of initial overestimating associated with wheeled construction plant operating in changing ground conditions. These measurable guidelines are currently unavailable.

5. The research has clearly demonstrated through computational analysis and experimental data that a fully inflated tyre can operate in rigid form when its inflation and carcass pressure exceeds that of the terrain in which it is operating in.

6. The research further demonstrated the practical application of the mathematical model through controlled laboratory experiments.

Figure 9.1 provides a simple guide on how the mathematical model developed could be used in the management of wheeled construction plant for optimum and efficient performance in soft and deformable terrain. This would be the first step towards developing a mechanism that would eliminate initial overestimating and any other economic decision making regarding better management of off road wheeled plant.

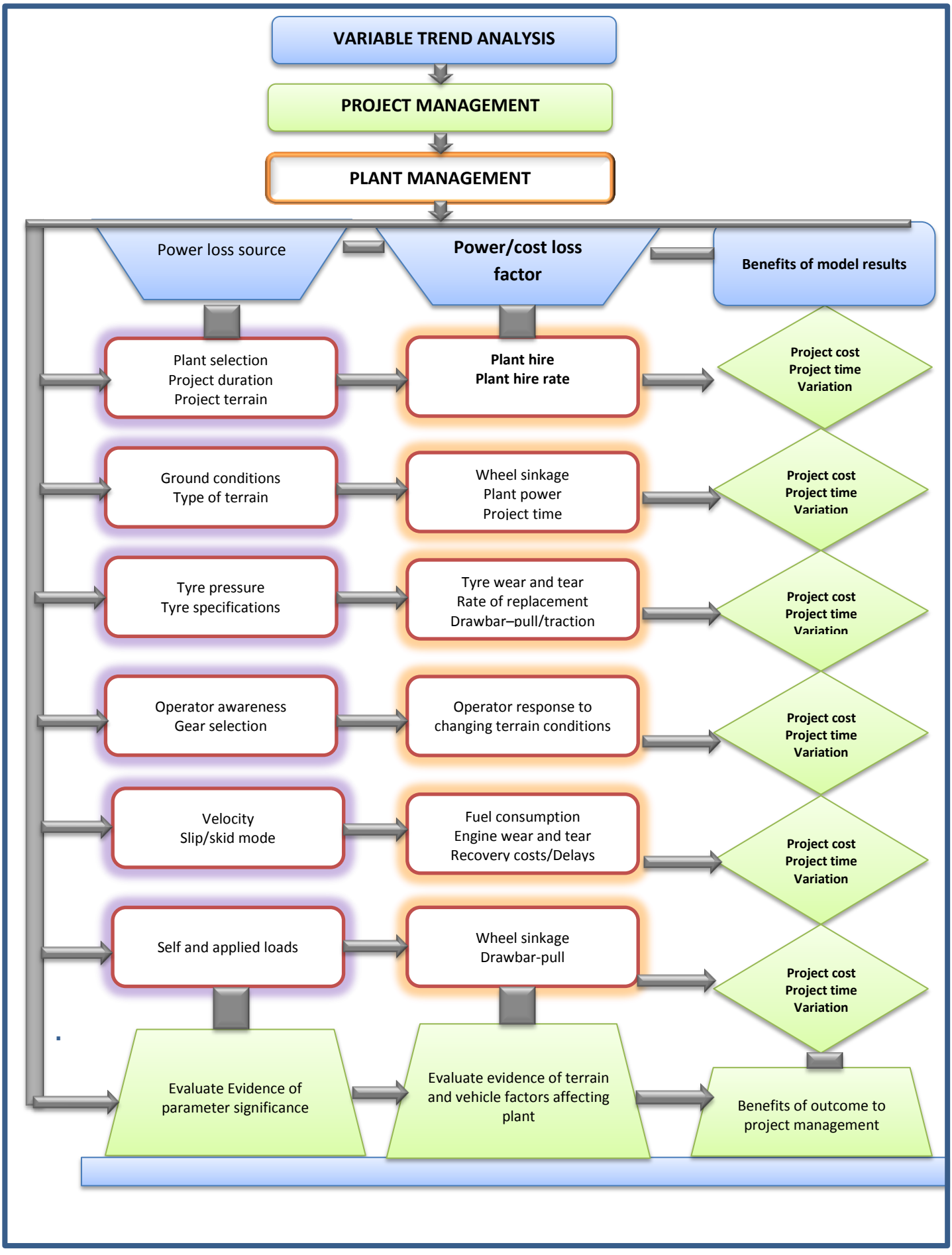

Figure 9.1: Benefits and relevance of the research results towards contribution to knowledge

Further variation management tools could become more feasible for institutions as follows:

- ***Clients and their consultants****:* The mathematical model provides an initial basis to clients and their teams of consultants to establish/verify contractors' claims towards time and cost variations arising from power losses resulting from changing ground conditions.

- ***Contractors and plant hire companies:*** The model further provides useful criteria for contractors' in planning the type of plant and contract duration depending on the given ground conditions. Plant hire companies can also have an opportunity to fairly price the hire rate per hour for each specific wheeled-equipment based on the terrain conditions in which it is to operate in.

CHAPTER 10

CONCLUSIONS AND RECOMMENDATIONS FOR FUTURE RESEARCH

10. CHAPTER 10

Conclusions and recommendations for future research

10.1. Conclusions

Based on the research objectives, results analysis and defined boundaries, the following conclusions have been drawn from the study:

1. The effect of changing ground conditions on the performance of construction related wheeled plant was successfully quantified and measured through mathematical modelling.

2. The mathematical model results were found to be consistent with the model verification results obtained through computational analysis. These results signify the credibility of the mathematical model.

3. The mathematical model and computational analysis results were found to be consistent with the controlled laboratory experiments. These experiments further verified the results obtained from previous research carried out in in pavement and off-road conditions.

4. The research results suggest that it is more efficient to operate wheeled construction plant in higher cohesive soils with relatively higher velocities. Low cohesion soils require stabilisation to avoid plant power loss due to high motion resistance. Lower velocities are also recommended on this type of soil.

5. Dry clay terrain has a higher capacity to support wheeled vehicular mobility. The introduction of moisture reduces that capacity leading to reduced soil cohesion. This eventually leads to reduced tractive effort.

6. The results from the research suggest that construction sites and deformable haulage roads with low angle of shearing resistance sandy terrain would require stabilisation and additional moisture in all vehicular routes/roads to avoid wheeled plant power losses during traversing on the sites.

7. As opposed to clay terrain, dry sandy terrain does not support wheeled vehicular mobility. Introduction of moisture stabilises the terrain in order to attain positive tractive effort. An optimum amount of moisture for saturation exists for maximum generation of tractive effort.

8. Applied load, wheel radius, wheel slip ratio, tyre-terrain contact area and wheel self-weight all have significant influence on the ultimate generation of wheel tractive effort.

9. The mathematical model results could be directly used in the variable management of variations on construction related projects that are characterised by deformable construction sites and haulage roads.

10. All the conclusions lead to one ultimate confirmation that the effect of terrain on the performance of wheeled plant can be modelled and quantified. This therefore means that factors such as power output, project time and fuel consumption can now be estimated with more certainty in order to price such works using much fairer criteria.

11. Managers, planners, estimators and Engineers all need to take into account the effect of ground conditions on wheeled construction plant in order to establish the most economic applied load, velocity, tyre with/radius and desired drawbar-pull for every situation on projects involving long stretches of vehicular movement. This will reduce the risk of overestimation and over claiming in terms of time and cost.

12. There must be a constant review of the projects with particular focus of the ground conditions of the time and cost factors arising from the wheel-soil interaction using the framework and principles form this mathematical model.

13. There is need to introduce training programs for wheeled plant operatives for them to appreciate and embrace this concept of terramechanics in optimising the performance of wheeled plant operating in soft and deformable terrain.

10.2. Recommendations for future research

This last section presents the identified and suggested areas for further research in order to develop better and more accurate modelling systems by improving the current mathematical model. Three suggested areas of further research have been identified at the end of this study.

10.2.1. Computational Analysis based on wheeled plant real data.

The absence of full scale testing of wheeled plant on soft, deformable and wet terrain by plant manufacturers resulted in the identification of significant gap in

construction sector body of knowledge. This knowledge gap needs to be closed up by sourcing financial and technical support to make special arrangements with plant manufactures to run full scale experiments under different conditions for a reasonably longer period. These results should then be processed using computational analysis. The results from the computational analysis can be used in combination with the mathematical model to make future predictions of wheeled plant performance in terms of terrain properties, desired drawbar-pull, tyre sinkage and the subsequent power loss, applied load, velocity and tyre properties.

10.2.2. Development of Tyre Pressure Control System (TPCS)

A useful extension to this study should consider TPCS involving the development of an algorithm that would be incorporated in the outcome of this study to automatically adjust tyre pressure based on real time terrain properties. This would require the collection of data from wheeled plant using the current specifications. Such a tool in the vehicle would be reliable enough to automatically regulate the tyre pressure in order to attain the desired parameters. This research will need a significant input from the automotive design and manufacture industry that will be required to design and build sensors that would meet the laid down objectives. Such technology already exists in the American Defence Department according to the Clemson University vehicular electronics laboratory in South Carolina.

10.2.3. Contract Pricing criteria for off-road terrain related works

Based on the findings, conclusions and recommendations from this research, it is clear that further research needs to be carried out on the pricing of unit rates and overall contracts involving wheeled plant traversing in soft and wet off-road terrain. As seen from the pre-research study in chapter 1, the pricing criteria for wheeled

plant operating on pavement roads and off-road condition is the same. This means that these particular sections of the contracts are either under-priced or overpriced. In case some correction factors have to be introduced to cover lost time and expenses. Additionally the extra fuel used by this plant in wet off-road conditions is usually not taken into account as ground conditions changes. Having established a strong relationship between wheeled plant power loss and terrain profile, Studies therefore need to be carried out by monitoring the fuel consumption in relation to gear selection and on a daily basis and details of the terrain in which the plant is operating. This data can now be used to develop models that will guide the pricing criteria based on the potential usage of fuel and wear/tear of plant traversing in soft terrain especially for distances exceeding one mile. This is even more significant in developing economies that are characterised by long non-pavement haulage roads. At present this a grey area for clients, contactors' and consultants who have to rely on experience as opposed to much more reliable models that have the power to predict and provide more accurate outputs.

10.3. References

1. Abebe, A., Tanaka, T. and Yamaza, M., (1989). *Passes of a rigid wheel relevant for optimisation of trafficability,* Journal of Terramechanics, 26 (2), pp.139-148. Accessed 10/08/2014.

2. Anderson, B.A., Palazzo, J.A., Ayers, D.P., Fehmi, S.J., Shoop, S. and Sullivan Patricia., (2005). *Assessing the impacts of military vehicle traffic on natural areas. Introduction to the special issue and review of the relevant military vehicle impact literature,* Journal of Terramechanics 42, pp. 143-158, Emerald Group Publishing Limited.

3. Apostolopoulos, S.D., (2001). *Analytical Configuration of wheeled robotic locomotion*, Doctoral Thesis, The Robotics Institute, Carnegie Mellon University, Pittsburg, Pennsylvania, USA.

4. Azimi, A., Holz, D., Kovecses, J., Angeles, A. and Teichmann, M., (2012). *Efficient Dynamics Modelling for Rover Simulation on Soft Terrain*, Proceedings of the 50th American Institute of Aeronautics and Astronautics, Aerospace Sciences Meeting.

5. Bacon, N.S., McDonald, V.E., Baker, E.S., Caldwell, G.T. and Stullenbarger, G., (2008). *Desert terrain characterisation of landforms and surface materials within vehicle test courses at US Army Yuma Proving Ground USA*, Journal of Terramechanics 45, pp. 167-183, Emerald Group Publishing Limited.

6. Baladi, Y.G. and Rohani, B., (1984). *Development of a soil-wheel interaction model*, proceedings of the 8th international conference on the performance of off road vehicles and machines volume 1, international society for terrain vehicle systems.

7. Barnes, G., (2010). *Soil mechanics: Principles and practice*, 3rd edition, Palgrave Macmillan

8. Ben, H.T., Scott, W.D., Francois, M.H., Mark, C.A., Jason, E.P. and Edward, A.R., (2004). *Concepts of Model Verification and Validation*, Los Alamos National Laboratory, University of California for the United States Department of Energy.

9. Blahova, K., Sevelova, L. and Pilarova., (2013). *Influence of water content on the shear strength parameters of clayey soil in relation to stability analysis of a hillside in Brno region*, Acta Universiatis Agriculturae et Silviculturae Mendelianae Brunensis, 2013, LXI, No.6, pp. 1583-1588, http://acta.mendelu.cz/pdf/actaun201361061583.pdf, accessed (8/12/2014)

10. Brown, C. and Sessions, J., (1999). *Variable Tyre Pressures for Tropical Forests, "Synthesis of Concepts and Applications",* Forestry department, Food and Agricultural Organisation of the United Nations, Corporate Document Repository. http://www.fao.org/docrep/w2809e/w2809e03.htm#TopOfPage, accessed (14/08/2014)

11. Bygdén, G. and Wästerlund, I., (2007). *Rutting and soil disturbance minimised by planning and using bogie tracks*. – Forestry Studies Metsanduslikud

12. Cook, D.T. and Shadish, R.W., (1994). *Social Experiments: Some Developments over the past fifteen years*, Annual Review Psychology, 45, pp.545-580, University of Idaho Library.

13. Cook, T.D. and Campbell, D.T., (1979). *Quasi- Experimentation: Design and analysis issues for field settings*, Houghton Mifflin, Boston, USA.

14. Cresswell, W.J., (2014). *Research Design*, 4th edition, Sage Publications, UK.

15. Cupera, J and Smerda, T., (2010). *Tyre inflation and its influence on drawbar characteristics and performance – Energetic indicators of a tractor set*, journal of terramechanics, volume 47 pp.395–400, Elsevier limited.

16. Dainty, A., (2008). *Methodological pluralism in construction management research*, in KNight, A. and Ruddock, L. (Eds.), advanced research methods in the built environment, 1-13, Wiley-Blackwell, Oxford, UK.

17. Ding, L., Gao, H., Deng, Z., Nagatani, K., Yoshida, K., (2010). *Experimental study and analysis on driving wheels performance for planetary exploration rovers moving in deformable soil*, Journal of Terramechanics, Elsevier Limited, volume 48, p27 – 45.

18. Edwards, D.J., Holt, G.D. and Harris, F.C., (2002). *An artificial intelligence approach for improving plant operator maintenance proficiency*, Journal of Quality in Maintenance Engineering, Vol. 8 Issue: 3, pp.239–252

19. Edwards, D.J., Holt, G.D. and Robinson, B., (2000). *A comparative analysis between the multilayer perception neural network and multiple regression analysis for predicting construction plant maintenance costs*. Journal of Quality in Maintenance Engineering, Vol. 6 Number 1, pp.45–60. MCB University press.

20. Edwards, D.J., Holt, G.D. and Robinson, B., (2002). *An artificial intelligence approach for improving plant operator maintenance proficiency and multiple regression analysis for predicting construction plant maintenance costs*. Journal of Quality in Maintenance Engineering, Vol. 8 Number 3, pp.239–252. MCB University press.

21. Ellery, A. and Scott, G.P., (2005). *Application of Bekker theory for planetary exploration through wheeled, tracked and legged vehicle locomotion*, , American Institute of Aeronautics and Astronautics

22. Ellis, T.J. and Levy, Y., (2009). *Towards a guide for novice researchers on research methodology: Review and proposed method*, Journal of Issues in Informing Science and Information Technology (IISIT), Volume 6, pp.323-337.

23. Farrar, D.M. and Darley, P., (1975). *The operation of earthmoving plant on wet fill*, Transport and Road Research laboratory (TRRL) report 688

24. Favaedi, Y., Pechev, A., Marco. And Richter, L., (2011). *Prediction of tractive response for flexible wheels with application to planetary rovers*, Journal of Terramechanics, Elsevier Limited, volume 48, pp.199–213.

25. Gerda, D.V., (2001). *modelling activities, answer keys*, http://www.math.ualberta.ca/devries/erc2001, accessed 12/06/2012

26. Gerda, D.V., (2001). *What is mathematical modelling,* University of Alberta, Canada, http://www.math.ualberta.ca/devries/erc2001, accessed, 10/06/2011.

27. Gibbesch, A. and Schafer, B., (2004). *Advanced Modelling and simulation methods of planetary rover mobility on soft terrain*, Proceedings of the 8th ESA Workshop on Advanced Space Technologies for Robotics and Automation The Netherlands, November 2 -4.

28. Grix, J., (2002). *Introducing students to the generic terminology of social research*, Politics journal, vol 22 (3) pp.175–186, Political studies association, Blackwell publishers, USA.

29. Grujicic, M.H., Marvi, G., Arakere, B.W.C. and Haque, I., (2009). *A finite element analysis of pneumatic-tyre/sand interactions during off-road vehicle travel*, International Centre for Automotive Research CU-ICAR, Multidiscipline Modelling in Materials and Structures, Vol. 6 No. 2, 2010 pp. 284-308 Emerald Group Publishing Limited.

30. Grujicic, M.H., Marvi, G., Arakere, B.W.C. and Haque, I., (2009). *The effect of up-armouring of high mobility multi-purpose wheeled vehicle (HMMWV) on the off-road vehicle performance*, Multidiscipline Modelling in Materials and Structures, Journal of Terramechanics ,Vol. 6 No. 2, 2010 pp. 229-256 Emerald Group Publishing Limited.

31. Gunnar, B., Eliasson, L. and Wasterlund, I., (2003). *Rut depth, soil compaction and rolling resistance when using bogie tracks*, Journal of Terramechanics 40, pp 179– 190. Elsevier Limited

32. Hambleton, J.P. and Drescher, A., (2009). *Modelling wheel-induced rutting in soils: Rolling*, Journal of terramechanics, Volume 46, pp.35–47, Elsevier Limited.

33. Hansen, J.D. and Ostler, W.K., (2005). *Assessment technique for evaluating military vehicular impacts to vegetation in the Mojave desert*, Journal of Terramechanics 42, pp. 193-205, Emerald Group Publishing Limited

34. Hellström, T., Ringdahl, O. and Wästerlund, I., (2008). *Estimating wheel slip for a forest machine Pre-study report*, Umea University, Sweden http://www8.cs.umu.se/research/ifor/en/files/slip_pre-study_1.pdf, accessed 12/02/2012.

35. Ishigami, G., Masatsugu, O., Takashi, K. and Iagnemma, K., (2011). *Modelling of Flexible and Rigid Wheels for Exploration Rover on Rough Terrain* Proceedings of the 28th International Symposium on Space Technology and Science (ISTS 2011), Okinawa, Japan, June 2006.

36. Janulevičius, A., Juostas, A. and Pupinis, G., (2010). *Tractor engine load and fuel consumption in road construction work*, Transport, 2010 25(4), 403 – 410.

37. Johnson, B. and Christenden, L., (2012). *Educational Research: Quantitative, Qualitative and Mixed Approaches*, 4th edition, Sage Publications.

38. Johnson, B., & Christensen, L., (2008). *Educational research: Quantitative, qualitative, and mixed approaches* Thousand Oaks, CA: Sage Publications.

39. Johnson, K.L., (1985). *Contact Mechanics*, Cambridge University Press, United Kingdom.

40. Jordan, G.D. and Lategan L.O.K., (2010). *Physical Modelling of Terrains and Structures*: *Modelling as Research Methodology*, Sun Press, Bloemfontein, South Africa, ISBN 978-920383-05-3.

41. Jun, H., Way, R.T., Lofgren, B., Landstrom, M.,, Bailey, C.A., Burt, C.E. and McDonald P.T., (2004). *Dynamic load and inflation pressure effects on contact pressures of a forestry forwarder tyre*, Journal of Terramechanics 41 pp. 209-222, Emerald Group Publishing Limited

42. Korlath, G., (2007). *Mobility analysis of off road vehicles: Benefits for development, procurement and operation*, Journal of Terramechanics 44, pp. 383-393, Emerald Group Publishing Limited.

43. Kumar, R., (2005). *Research Methodology: A step by step guide for beginners*, 1st edition, Sage Publications.

44. Lagnemma, K., (2011), Surface Interaction Modelling, Engineering methods, Massachusetts Institute of Technology, http://www.kiss.caltech.edu/workshops/xterramechanics2011/presentations/iagnemma_sc.pdf, accessed 25/01/2013

45. Lagnemma, K., Kang, S., Brooks, C. and Dubowsky, S., (2005). *Multi Sensor Estimation for Planetary Rovers*, Massachussetts Institute of Technology, USA.

46. Lysako, M., (2010). *Multi-Pass effect of off-road vehicle tractive performance*, Journal of Terramechanics, Elsevier Limited, volume 47, pp.275–294

47. Macmillan. R. H., (2002). *The Mechanics of Tractor - Implement Performance, Theory and Worked Examples: A textbook for students and engineers*, Chapter 4, http://bsesrv214.bse.vt.edu/Hop/Papers/Mechanics-Tractor-Implement.pdf

48. Madsen, J., Seidl, A. and Negrut, D., (2013). *Off-road vehicle dynamics mobility simulation with a compaction based deformable terrain model*, Proceedings of the ASME 2013 International Design Engineering Technical conferences and Computers and Information Engineering Conference, IDETC/CIE 2013, August 4-7, 2013, Oregon, USA.

49. Makineci, E., Demir, M., Comez, A. and Yilmaz, E., (2007). Effects of timber skidding on chemical characteristics of *herbaceous cover, forest floor and top soil on skid road in an oak forest*, Journal of Terramechanics 44, pp. 423-428, Emerald Group Publishing Limited

50. Naghdi, R., Bagheri, I., Lotfalian, M. and Setodeh, B., (2009). *Rutting and soil displacement caused by 450C Timber Jack wheeled skidder*, (Asalem forest Northern Iran Journal of forest science, *55*, 2009 (4): pp. 177–183.

51. Nguyen, V.N., Matsuo, T., Inaba, S. and Koumoto, (2008). *Experimental analysis of vertical soil reaction and stress distribution under off-road tyres*.

52. Noor, B.M.K. (2008), *Case Study: A strategic Research Methodology*, American Journal of applied Sciences, Volume 5 issue 11, pp.1602–1604.

53. Patel, N., Scott, G. and Ellery, A., (2004). *Application of Bekker Theory for planetary Exploration through wheeled, tracked and legged vehicle locomotion*, Space 2004 conference and exhibit, 28- 30 September 2004, San Diego, California, USA, American Institute of Aeronautics and Astronauts.

54. Radforth, R. J., (1993). *Book reviews*, Journal of terramechanics, volume 30, Number 1, pp.59–61, Pergamon Press, Great Britain.

55. Rajasekar, S., Philominathan, P. and Chinnathambi, V., (2006). *Research Methodology*, Cornell University Library, USA, arXiv:physics/0601009v2 [physics.ed-ph].

56. Rashidi and Gholami, (2011), *Non-Linear modelling of soil sinkage by multiple loadings using the Finite Element Method*, ARPN Journal of Agricultural and Biological Science, Vol 6 No.3 March 2011, Asian Research Publishing Network, ARPN.
57. Reid, D., (2000). *Doctoral thesis*, Edinburgh Napier University, Scotland.

58. Reid, D., Muleya, F. and Nwaubani, S., (2012), *Experimental study for determining wheel rut depth in clay and sandy soil terrain*, 2nd Annual Research & Scholarship Conference, Faculty of Science & Technology, Anglia Ruskin University.

59. Rohand, K., Kalb, A.A., Herbauts, J. and Verbrugge, J.C., (2004). *Changes in some mechanical properties of a loamy soil under the influence of mechanised forest exploitation in a beech forest of central Belgium*, Journal of Terramechanics 40, pp. 235-253, Emerald Group Publishing Limited

60. Saarilahti, M. and Anttila, T., (1999). *Rut depth model for timber transport on moraine soils*, Proceedings of the 9th International Conference of International Society for Terrain-Vehicle Systems, 14th - 17th September 1999, Munich, Germany. pp:29-37

61. Saarilahti, M., (2002). *Soil Interaction model – Evaluation of the Waterways experiment station method in assessing the trafficability of terrain and the mobility of forest tractors*, Appendix report number 2, University of Helsinki.

62. Saarilahti, M., (2002). *Soil Interaction model*, University of Helsinki.

63. Sandu, C. and Li, L., (2006). *Algorithm for the prediction of Traction performance of terrain vehicles*, Proceedings of the IMECE 2006 ASME International Mechanical Engineering Congress and RD & D Expo, November 5 – 10, Chicago.

64. Sandu, C. and Senatore, C., (2011). *Off-road tyre modelling and the multi-pass effect for vehicle dynamics simulation*, Journal of Terramechanics, Elsevier Limited, volume 48, pp. 265 – 276

65. Sandu, C., Worley, E.M. and Morgan, J.P., (2010). *Experimental study on the contact patch pressure and sinkage of a lightweight vehicle on sand*, Journal of Terramechanics, volume 47, pp 343.

66. Senatore, C. and Sandu, C., (2009). *Exit angle influence on energy efficiency of off road tyres*, 11thEuropean Regional Conference of the International society for Terrain-Vehicle Systems, Bremen, Germany, October 5 – 8, 2009.

67. Seung, C.O. and Sunil, K.S., (2006). *Construction equipment productivity estimation using artificial neural network model*, Construction Management and Economics, Volume 24, Issue 10, pp.1029–1044.
68. Shahangian., (2011), *Variable cohesion model for shear strength evaluation*, 2011 pan AM CGS Geotechnical conference,

69. Sohne, W., (1976). *Terramechanics and Its influence on the Concepts of Tractors, Tractor Power Development and Energy Consumption*, Journal of Terramechanics, volume 13, Number 1, pp.27–43, Pergamon Press, Great Britain.

70. The Aggregates and Recycling Information Network, *http://www.agg-net.com/news/pgc-calls-on-jcb-for-massive-groundworks-project*, accessed 16/06/2013

71. The Online business dictionary: http://www.businessdictionary.com/definition/research-design.html#ixzz2wE86Qg4Q

72. Thomson, R.J. and Visser, A.T., (2000). *The functional design of surface mine haul roads*, The Journal of the South African Institute of mining and metallurgy, May/June 2000.

73. Thomson, R.J., Visser, A.T. and Heyns, P.S., (2004). *Integrating Real-Time Mine Haul Road Maintenance Management with Mine-wide asset location and communication system*, Transportation Research Board of the national academies, 6th International conference on managing pavements, Brisbane, Australia.

74. Volvo Construction Equipment, *http://www.volvoce.com/dealers/en-gb/vcegb/products/articulatedhaulers/pages/introduction.aspx*, accessed 16/06/2013

75. Walker, R., (2010). *Computer Aided Engineering module guide*, Anglia Ruskin University, England.

76. Wang, W., Zhijiang, D. and Lining, S., (2007). *Obstacle performance analysis of mine research robot based on Terramechanics*, Proceedings of the IEEE international conference on mechatronics and Automation, August 5 – 8, Harbin, China.

77. Wong, J.Y. and Reece, A.R., (1967*). Prediction of rigid wheel performance based on the analysis of soil-wheel stresses, Part 1 Performance of driven rigid wheel*, Journal of Terramechanics, 4(2); pp.81-89.

78. Wong, J.Y., (1984). *An introduction to Terramechanics*, Journal of Terramechanics, 21, (1), pp.5-17, Pergamon Press

79. Wong, J.Y., (2010). *Terramechanics and off-road vehicle engineering. Terrain behaviour, vehicle design and performance*, Butterworth-Heinemann, Elsevier Ltd.

80. Xia, K., (2010). *Finite element modelling of tyre/terrain interaction: Application to predicting soil compaction and tyre mobility*, Journal of Terramechanics, Elsevier Limited.

81. Zebrowski, J., (2010). *Traction efficiency of a wheeled tractor in construction operations*, Journal of Automation in Construction, Vol 19 (2010), pp.100–108, Elsevier Science.

82. Zombori, J., (1967). Drawbar-pull tests of various traction devices on sandy soils, Journal of Terramechanics, volume 4, number 1, pp.9-17, Pergamon Press limited.

10.4 Bibliography.

1. Chiroux, R.C., Foster Jr, W.A., Johnson, C.E., Shoop, S.A. and. Raper, R.L., (2005). *Three-dimensional finite element analysis of soil interaction with a rigid wheel,* Journal of Applied Mathematics and Computation, 162, pp. 707–722.

2. Dubey, A., (2011). *Tyre pressure regulation system*, automotive electronics, The Clemson University vehicular electronics laboratory. http://www.cvel.clemson.edu/auto/AuE835_Projects_2011/Dubey_project.html, accessed 14/08/2014

3. El Pebrian, D. and Yahya, A., (2010). *Comparisons on engine power requirements of 6WD and 4WD prime movers for the oil palm plantation in Malaysia*, Journal of Terramechanics, Volume 47, Issue 3, June 2010, pp. 131–142., Elsevier limited.

4. Ellis, J.T. and Levy, T., (2009). *Towards a Guide for Novice Researchers on Research Methodology: Review and Proposed Methods*, Issues in Informing Science and Information Technology Volume 6, 2009.

5. Grahn, M., (1991). *Prediction of sinkage and rolling resistance for off the road vehicles considering penetration velocity*, Journal of terramechanics, Volume 28, Number 4, pp. 339–347, Pergamon Press plc.

6. Gyu, J.H., Way, R.T., Löfgren, B., Landström, M., Bailey, A.C., Burt, E.C. and McDonald, T.P., (2004). *Dynamic load and inflation pressure effects on contact pressures of a forestry forwarder* Journal of Terramechanics, Volume 41, Issue 4, October 2004, pp 209-222.

7. Hetherington, J.G., (2005). *Tracked vehicle operations on sand–investigations at model scale*, Journal of Terramechanics - J TERRAMECH 01/2005; 42(1):65-70. DOI: 10.1016/j.jterra.2004.05.003.

8. Heyns, T., Heyns,, P.S. and De Villiers, J.P., (2012). *A method for real-time condition monitoring of haul roads based on Bayesian parameter estimation,* Journal of Terramechanics Volume 49, Issue 2, April 2012, pp 103–113, Elsevier Limited.

9. Hutangkabodee, S., Zweiri, Y.H., Seneviratne, L.D. and Althoefer, K., (2006). *Soil parameter identification for wheel-terrain interaction dynamics and traversability prediction*, International Journal of Automation and Computing, July 2006, Volume 3, Issue 3, pp 244-251.

10. Ishigami, G., Miwa, A., Nagatani, K. and Yoshida, K., (2007). *Terramechanics-based model for steering maneuver of planetary exploration rovers on loose soil*, Journal of Field Robotics Special Issue: Special Issue on Space Robotics, Part I Volume 24, Issue 3, pp. 233–250, March 2007.

11. Kheiralla, A.F., Yahya, A., Zohadie, M. and Ishak, W., (2004). *Modelling power and energy requirements for tillage implements operating in serdang*, sandy, clay, loam in Malaysia, Soil and Tillage research, Journal of Terramechanics, volume 78, pp 21–34, Elsevier Limited.

12. Leite, A.C. and Schafer, B., (2012). *Mass, power and static stability optimization of a 4-wheeled planetary, exploration rover,* 2nd International Conference on Engineering Optimization September 6-9, 2010, Lisbon, Portugal.

13. Muro, T. and O'Brien, J., (2004). *Terramechanics: Land Locomotion Mechanics*, 1st edition CRC Press.

14. Nakashima, H. and Oida, A., (2004). *Algorithm and implementation of soil–tyre contact analysis code based on dynamic FE–DE method*, Journal of Terramechanics Volume 41, Issues 2–3, April–July 2004, pp. 127–137, Elsevier Limited.

15. Nakashima, H.; Takatsu, Y., Hisanori, S., , Hisanori, M. and Takahiro, K., (2009)

16. *FE-DEM Analysis of the Effect of Tread Pattern on the Tractive Performance of Tyres Operating on Sand*, Journal of Mechanical Systems for Transportation and Logistics, Volume 2, Issue 1, pp. 55-65.

17. Onafeko, O. and Reece, A.R. (1967). *Soil stresses and deformations beneath rigid wheels,* Journal of Terramechanics, Volume 4, Issue 1, 1967, pp. 59–80, Elsevier.

18. Quintus, V., Harold, H.L.; James, M.S., (2007). *Pavements; Pavements, Flexible; Pavements, Asphalt; Pavements,* Montana Department of Transportation; Applied Research Associates.

19. Ray, L.E., (2008). *Autonomous terrain parameter estimation for wheeled vehicles*, Proceedings of the SPIE, Volume 6962, article id. 69621H.

20. Shahangian, S., (2011). *Variable Cohesion Model for Soil Shear Strength Evaluation*, 2011 Pan-Am CGS Geotechnical Conference.

21. Van Wyk, D.J., de Klerk, J.H. and Spoelstra, J., (1996). *Mathematical modelling of the interaction between a tracked vehicle and the terrain*, Applied Mathematical Modelling Journal, Volume 20, Issue 11, November 1996, pp. 838–846 Elsevier.

22. Yong, R.N., Elmamlouk , H. and Della, L.M., (1980). *Evaluation and prediction of energy losses in track-terrain interaction*, Journal of Terramechanics Volume 17, Issue 2, June 1980, pp 79–100, Elsevier Limited.

APPENDICES

Appendix 1: Example of Drawbar-pull tabulation leading to graphical plotting

Rut			**eqn 30**				**eqn 25**	**eqn.13**	**eqn.14**	**eqn.16**
d (m)	d(m)	r (m)	alpha	W (N)	t (m)	C (N/m2)	sigma(N/m	H (N)	R (N)	D (N))
112	0.112	0.8	0.535527	5100	0.3	20000	36155.63	2449.411	1214.829	1235
94	0.094	0.8	0.489645	5100	0.3	25000	38936.89	2821.874	1098.02	1724
82	0.082	0.8	0.456729	5100	0.3	30000	41211.8	3175.304	1013.81	2161
73	0.073	0.8	0.430517	5100	0.3	35000	43264.99	3505.664	947.5033	2558
66	0.066	0.8	0.409048	5100	0.3	40000	45130.46	3818.263	893.5832	2925
61	0.061	0.8	0.393037	5100	0.3	45000	46524.64	4136.357	851.4009	3285
56	0.056	0.8	0.376383	5100	0.3	50000	48291.5	4410.714	811.2972	3599
52	0.052	0.8	0.362537	5100	0.3	55000	49838.19	4681.35	777.4758	3904
49	0.049	0.8	0.351812	5100	0.3	60000	51001.32	4962.225	749.7193	4213
46	0.046	0.8	0.340763	5100	0.3	65000	52400.29	5213.616	723.124	4490
43	0.043	0.8	0.329359	5100	0.3	70000	54067.86	5433.727	697.4754	4736
41	0.041	0.8	0.32154	5100	0.3	75000	55078.26	5688.497	677.4626	5011
39	0.039	0.8	0.313533	5100	0.3	80000	56254.3	5921.681	658.1753	5264
37	0.037	0.8	0.305323	5100	0.3	85000	57613.75	6132.26	639.5127	5493
36	0.036	0.8	0.301137	5100	0.3	90000	57989.43	6406.685	626.2858	5780
34	0.034	0.8	0.29259	5100	0.3	95000	59675.85	6576.279	608.6937	5968
33	0.033	0.8	0.288225	5100	0.3	100000	60246.12	6822.016	596.4366	6226
32	0.032	0.8	0.283794	5100	0.3	105000	60892.86	7056	584.5714	6471
31	0.031	0.8	0.279295	5100	0.3	110000	61620.77	7277.903	573.0732	6705
30	0.03	0.8	0.274724	5100	0.3	115000	62435.1	7487.374	561.9159	6925
29	0.029	0.8	0.270078	5100	0.3	120000	63341.68	7684.04	551.0726	7133
28	0.028	0.8	0.265353	5100	0.3	125000	64347.03	7867.496	540.515	7327
27	0.027	0.8	0.260544	5100	0.3	130000	65458.45	8037.312	530.2134	7507
26	0.026	0.8	0.255647	5100	0.3	135000	66684.19	8193.021	520.1367	7673
25	0.025	0.8	0.250656	5100	0.3	140000	68033.61	8334.117	510.252	7824
25	0.025	0.8	0.250656	5100	0.3	145000	67403.66	8631.764	505.5275	8126
24	0.024	0.8	0.245566	5100	0.3	150000	68900.29	8751.777	496.0821	8256
24	0.024	0.8	0.245566	5100	0.3	155000	68283.28	9043.503	491.6396	8552
23	0.023	0.8	0.24037	5100	0.3	160000	69939.81	9141.574	482.5847	8659
22	0.022	0.8	0.235062	5100	0.3	165000	71757.38	9222.954	473.5987	8749
22	0.022	0.8	0.235062	5100	0.3	170000	71167	9502.437	469.7022	9033
21	0.021	0.8	0.229633	5100	0.3	175000	73175.64	9560.047	461.0065	9099
21	0.021	0.8	0.229633	5100	0.3	180000	72599.02	9833.191	457.3738	9376
20	0.02	0.8	0.224075	5100	0.3	185000	74818.35	9865.896	448.9101	9417
20	0.02	0.8	0.224075	5100	0.3	190000	74255.8	10132.54	445.5348	9687
20	0.02	0.8	0.224075	5100	0.3	195000	73693.26	10399.19	442.1595	9957
19	0.019	0.8	0.218379	5100	0.3	200000	76160.75	10399.06	434.1163	9965
	DP at Velocity = 10m/s and i = 0.3									

Appendix 2: Example of Drawbar-pull graphs generated from the tabulated data derived from the equations

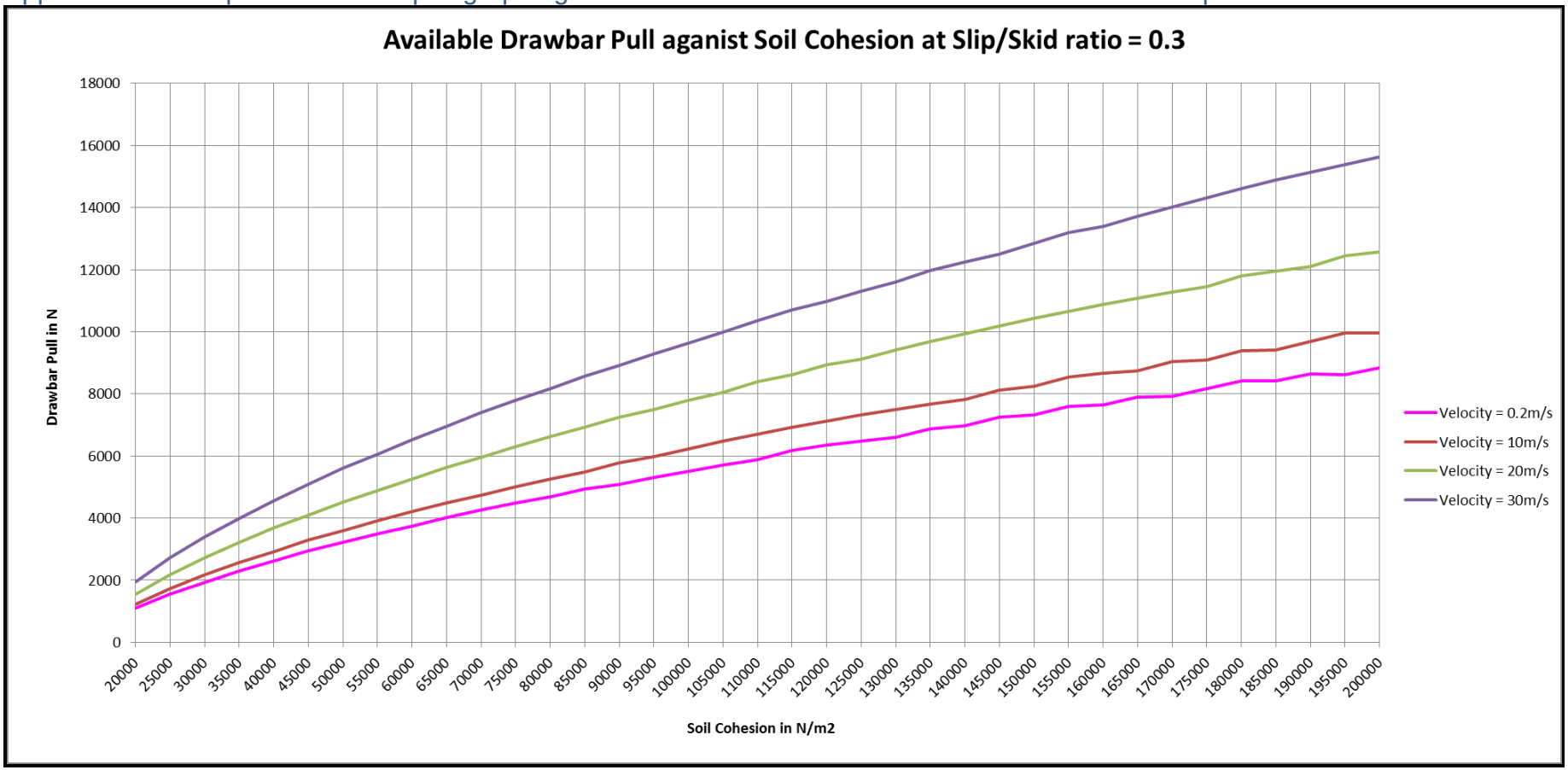

.Appendix 3: Example of wheel multi-pass data in tabular form based on Abebe's approach

	MULTI PASS EFFECT BASED ON ABEBES FORMULA			
Pass	Rut	Cummulative rut depth		
1	252	252		
2	63	315		
3	28	343		
4	15.75	358.75		
5	10.08	368.83		
6	7	375.83		
7	5.142857	380.9729		
8	3.9375	384.9104		
9	3.111111	388.0215		
10	2.52	390.5415		
Pass	Rut	Cummulative rut depth		
1	101	101		
2	6.3125	107.3125		
3	1.246914	108.5594		
4	0.394531	108.9539		
5	0.1616	109.1155		
6	0.077932	109.1935		
7	0.042066	109.2355		
8	0.024658	109.2602		
9	0.015394	109.2756		
10	0.0101	109.2857		
Pass	Rut	Cummulative rut depth		
1	62	62		
2	0.96875	62.96875		
3	0.085048	63.0538		
4	0.015137	63.06893		
5	0.003968	63.0729		
6	0.001329	63.07423		
7	0.000527	63.07476		
8	0.000237	63.075		
9	0.000117	63.07511		
10	0.000062	63.07517		

Appendix 4: Example of tabular data determining line separating rigid and flexible mode of a tyre in firmer soil

EXPERIMENT TYRE SET 1: 25KN

Tyre type: 12.5/75R20
Normal load: 25KN
Inflation pressure: 150 - 600Kpa
Tyre diameter: 1m
Section height: 0.245m
Tyre width: 0.327
Pressure sinkage parameters: K_c=29.76KN/m^2, K_ϕ=2083 KN/m^3 and n=0.8, D=1m
Critical ground pressure: 335Kpa
Medium soil

Inflation Pressure	AV Pg	Contact length	Sinkage	Deflection			
150	180	0.425	0.044	0.047			
200	220	0.348	0.057	0.031			
250	260	0.294	0.070	2.20E-02			
300	290	0.264	0.080	0.018			
						0.095m	zr
350	330	0.207	0.095	0.011			
400	360	0.204	0.095	0.011			
450	390	0.201	0.095	1.000E-02			
500	420	0.199	0.095	1.000E-02			
550	450	0.197	0.095	9.80E-03			
600	480	0.196	0.095	9.70E-03			

Appendix 5: Example of tabular data determining line separating rigid and flexible mode of a tyre in weaker soil

		EXPERIMENTAL TYRE SET 2: 25KN					
Tyre type: 12.5/75r220							
Normal load: 25KN							
Inflation pressure: 150 - 600Kpa							
Tyre diameter: 1m							
Section height: 0.245m							
Tyre width: 0.327m							
Pressure sinkage parameters: Kc=30.08KN/m2, Kφ= 499.7KN/m3 and n=0.6, D=1							
Critical ground pressure: 219Kpa							
Clayey soil							
Inflation Pressure	**AV Pg**	**Contact length**	**Sinkage**	**Deflection**			
150	180	0.425	0.138	0.047			
						0.191mm	zr
200	220	0.276	0.186	0.019			
250	260	0.273	0.185	0.019			
300	290	0.271	0.185	0.019			
350	330	0.270	0.185	0.019			
400	360	0.269	0.185	0.018			
450	390	0.266	0.185	0.018			
500	420	0.265	0.185	0.018			
550	450	0.263	0.184	0.018			
600	480	0.263	0.184	0.018			

Appendix 6: Example of data for testing the accuracy of the mathematical against other control models in the field in higher cohesion soil

EXPERIMENTAL TYRE SET 1 10KN

BEKKER FORMULA

d(m)	d(m)	r (m)	θ1 (rad)	Sin θ1	θ	Sin θ	i	t (m) or b	W (KN)	C (N/m2)	C (KPa)	ϕ	ϕrad	Tan ϕ	k	n	Kc	Kϕ	j	-j/k	Normal stress sigma(N/m2)	Shear Stress (s) or (τ)	H (KN)	R (KN)	D(KN)
46	0.046	0.5	0.4323	0.4190	0	0	0.1	0.327	10	8620	8.62	22.5	0.3928	0.4143	0.0254	0.8	29.76	2083	0.028	-1.0873562	185.13	56.55328415	3.873991702	2.617938369	1.256053333
46	0.046	0.5	0.4323	0.4190	0	0	0.2	0.327	10	8620	8.62	22.5	0.3928	0.4143	0.0254	0.8	29.76	2083	0.049	-1.9121006	185.13	72.70614249	4.9804887	2.617938369	2.362550331
46	0.046	0.5	0.4323	0.4190	0	0	0.3	0.327	10	8620	8.62	22.5	0.3928	0.4143	0.0254	0.8	29.76	2083	0.070	-2.736845	185.13	79.78669965	5.465518351	2.617938369	2.847579982
46	0.046	0.5	0.4323	0.4190	0	0	0.4	0.327	10	8620	8.62	22.5	0.3928	0.4143	0.0254	0.8	29.76	2083	0.090	-3.5615895	185.13	82.89044071	5.678129649	2.617938369	3.06019128
46	0.046	0.5	0.4323	0.4190	0	0	0.5	0.327	10	8620	8.62	22.5	0.3928	0.4143	0.0254	0.8	29.76	2083	0.111	-4.3863339	185.13	84.25095633	5.771327175	2.617938369	3.153388806
46	0.046	0.5	0.4323	0.4190	0	0	0.6	0.327	10	8620	8.62	22.5	0.3928	0.4143	0.0254	0.8	29.76	2083	0.132	-5.2110783	185.13	84.84733428	5.812180032	2.617938369	3.194241664
46	0.046	0.5	0.4323	0.4190	0	0	0.7	0.327	10	8620	8.62	22.5	0.3928	0.4143	0.0254	0.8	29.76	2083	0.153	-6.0358227	185.13	85.10875477	5.83008776	2.617938369	3.212149391
46	0.046	0.5	0.4323	0.4190	0	0	0.8	0.327	10	8620	8.62	22.5	0.3928	0.4143	0.0254	0.8	29.76	2083	0.174	-6.8605672	185.13	85.22334766	5.837937559	2.617938369	3.21999919
46	0.046	0.5	0.4323	0.4190	0	0	0.9	0.327	10	8620	8.62	22.5	0.3928	0.4143	0.0254	0.8	29.76	2083	0.195	-7.6853116	185.13	85.27357911	5.841378495	2.617938369	3.223440126

WONG AND REECE

d(m)	d(m)	r (m)	θ1 (rad)	Sin θ1	θ	Sin θ	i	t (m) or b	W (KN)	C (N/m2)	C (KPa)	ϕ	ϕrad	Tan ϕ	k	n	Kc	Kϕ	j	-j/k	Normal stress sigma(N/m2)	Shear Stress (s) or (τ)	H (KN)	R (KN)	D(KN)
33	0.033	0.5	0.3653	0.3573	0	0	0.1	0.327	10	8620	8.62	22.5	0.3928	0.4143	0.0254	0.8	29.76	2083	0.022	-0.8622216	169.60	45.5752448	2.662238562	1.830143267	0.832095295
33	0.033	0.5	0.3653	0.3573	0	0	0.2	0.327	10	8620	8.62	22.5	0.3928	0.4143	0.0254	0.8	29.76	2083	0.040	-1.5655149	169.60	62.39589772	3.644802474	1.830143267	1.814659207
33	0.033	0.5	0.3653	0.3573	0	0	0.3	0.327	10	8620	8.62	22.5	0.3928	0.4143	0.0254	0.8	29.76	2083	0.058	-2.2688082	169.60	70.7213233	4.131125018	1.830143267	2.300981751
33	0.033	0.5	0.3653	0.3573	0	0	0.4	0.327	10	8620	8.62	22.5	0.3928	0.4143	0.0254	0.8	29.76	2083	0.075	-2.9721016	169.60	74.84201418	4.371831617	1.830143267	2.54168835
33	0.033	0.5	0.3653	0.3573	0	0	0.5	0.327	10	8620	8.62	22.5	0.3928	0.4143	0.0254	0.8	29.76	2083	0.093	-3.6753949	169.60	76.88156077	4.490969969	1.830143267	2.660826702
33	0.033	0.5	0.3653	0.3573	0	0	0.6	0.327	10	8620	8.62	22.5	0.3928	0.4143	0.0254	0.8	29.76	2083	0.111	-4.3786882	169.60	77.89103962	4.549937804	1.830143267	2.719794537
33	0.033	0.5	0.3653	0.3573	0	0	0.7	0.327	10	8620	8.62	22.5	0.3928	0.4143	0.0254	0.8	29.76	2083	0.129	-5.0819815	169.60	78.39068378	4.579124086	1.830143267	2.748980819
33	0.033	0.5	0.3653	0.3573	0	0	0.8	0.327	10	8620	8.62	22.5	0.3928	0.4143	0.0254	0.8	29.76	2083	0.147	-5.7852748	169.60	78.63798394	4.593569912	1.830143267	2.763426645
33	0.033	0.5	0.3653	0.3573	0	0	0.9	0.327	10	8620	8.62	22.5	0.3928	0.4143	0.0254	0.8	29.76	2083	0.165	-6.4885681	169.60	78.7603858	4.600719911	1.830143267	2.770576644

MATHEMATICAL MODEL

d(m)	d(m)	r (m)	θ1 (rad)	Sin θ1	θ	Sin θ	i	t (m) or b	W (KN)	C (N/m2)	C (KPa)	ϕ	ϕrad	Tan ϕ	k	n	Kc	Kϕ	j	-j/k	Normal stress sigma(N/m2)	Shear Stress (s) or (τ)	H (KN)	R (KN)	D(KN)
45	0.045	0.5	0.4275	0.4146	0	0	0.1	0.327	10	8620	8.62	22.5	0.3928	0.4143	0.0254	0.8	29.76	2083	0.027	-1.070174	145.65	45.30859537	3.071399392	2.017593954	1.053805439
45	0.045	0.5	0.4275	0.4146	0	0	0.2	0.327	10	8620	8.62	22.5	0.3928	0.4143	0.0254	0.8	29.76	2083	0.048	-1.886332	145.65	58.50167006	3.965737459	2.017593954	1.948143505
45	0.045	0.5	0.4275	0.4146	0	0	0.3	0.327	10	8620	8.62	22.5	0.3928	0.4143	0.0254	0.8	29.76	2083	0.069	-2.70249	145.65	64.3346854	4.36114852	2.017593954	2.343554566
45	0.045	0.5	0.4275	0.4146	0	0	0.4	0.327	10	8620	8.62	22.5	0.3928	0.4143	0.0254	0.8	29.76	2083	0.089	-3.5186479	145.65	66.91361932	4.53597045	2.017593954	2.518376496
45	0.045	0.5	0.4275	0.4146	0	0	0.5	0.327	10	8620	8.62	22.5	0.3928	0.4143	0.0254	0.8	29.76	2083	0.110	-4.3348059	145.65	68.0538358	4.613263956	2.017593954	2.595670002
45	0.045	0.5	0.4275	0.4146	0	0	0.6	0.327	10	8620	8.62	22.5	0.3928	0.4143	0.0254	0.8	29.76	2083	0.131	-5.1509639	145.65	68.55795636	4.647437507	2.017593954	2.629843553
45	0.045	0.5	0.4275	0.4146	0	0	0.7	0.327	10	8620	8.62	22.5	0.3928	0.4143	0.0254	0.8	29.76	2083	0.152	-5.9671219	145.65	68.7808417	4.662546558	2.017593954	2.644952604
45	0.045	0.5	0.4275	0.4146	0	0	0.8	0.327	10	8620	8.62	22.5	0.3928	0.4143	0.0254	0.8	29.76	2083	0.172	-6.7832798	145.65	68.87938534	4.669226679	2.017593954	2.651632725
45	0.045	0.5	0.4275	0.4146	0	0	0.9	0.327	10	8620	8.62	22.5	0.3928	0.4143	0.0254	0.8	29.76	2083	0.193	-7.5994378	145.65	68.92295415	4.672180141	2.017593954	2.654586187

Appendix 7: Example of data for testing the effect of tyre radius on drawbar-pull in higher cohesion soil.

BEKKER FORMULA EXP TYRE 25KN HIGH COHESION RADIUS EFFECT

d(m)	d(m)	r (m)	θ1 (rad)	Sin θ1	θ	Sin θ	i	t (m) or b	W (KN)	C (N/m2)	C (KPa)	ϕ	ϕrad	Tan ϕ	k	n	Kc	Kϕ	j	-j/k	Normal stress sigma(N/m2)	Shear Stress (s) or (τ)	H (KN)	R (KN)	D(KN)
95	0.095	0.3	0.8185	0.7301	0	0	0.4	0.327	25	8620	8.62	22.5	0.3928	0.4143	0.0254	0.8	29.76	2083	0.114	-4.4930778	330.70	143.9931135	10.31328375	8.269388369	2.043895383
95	0.095	0.4	0.7036	0.6470	0	0	0.4	0.327	25	8620	8.62	22.5	0.3928	0.4143	0.0254	0.8	29.76	2083	0.126	-4.9674799	330.70	144.6084387	12.23764219	8.741946259	3.495695931
95	0.095	0.5	0.6266	0.5864	0	0	0.4	0.327	25	8620	8.62	22.5	0.3928	0.4143	0.0254	0.8	29.76	2083	0.137	-5.4091789	330.70	144.9703611	13.89994448	9.033960207	4.865984269
95	0.095	0.6	0.5704	0.5400	0	0	0.4	0.327	25	8620	8.62	22.5	0.3928	0.4143	0.0254	0.8	29.76	2083	0.148	-5.8213133	330.70	145.1904839	15.38256812	9.232379069	6.150189046
95	0.095	0.7	0.5271	0.5030	0	0	0.4	0.327	25	8620	8.62	22.5	0.3928	0.4143	0.0254	0.8	29.76	2083	0.158	-6.2081463	330.70	145.3289333	16.73273361	9.376007841	7.356725767
95	0.095	0.8	0.4923	0.4727	0	0	0.4	0.327	25	8620	8.62	22.5	0.3928	0.4143	0.0254	0.8	29.76	2083	0.167	-6.5734075	330.70	145.4186272	17.98033777	9.484795415	8.49554235
95	0.095	0.9	0.4636	0.4472	0	0	0.4	0.327	25	8620	8.62	22.5	0.3928	0.4143	0.0254	0.8	29.76	2083	0.176	-6.9201346	330.70	145.478235	19.14563479	9.570051394	9.575583395
95	0.095	1	0.4394	0.4254	0	0	0.4	0.327	25	8620	8.62	22.5	0.3928	0.4143	0.0254	0.8	29.76	2083	0.184	-7.2507743	330.70	145.5187284	20.24304947	9.638667283	10.60438219
95	0.095	1.1	0.4187	0.4065	0	0	0.4	0.327	25	8620	8.62	22.5	0.3928	0.4143	0.0254	0.8	29.76	2083	0.192	-7.567308	330.70	145.5467668	21.28326085	9.695082405	11.58817845

WONG AND REECE

d(m)	d(m)	r (m)	θ1 (rad)	Sin θ1	θ	Sin θ	i	t (m) or b	W (KN)	C (N/m2)	C (KPa)	ϕ	ϕrad	Tan ϕ	k	n	Kc	Kϕ	j	-j/k	Normal stress sigma(N/m2)	Shear Stress (s) or (τ)	H (KN)	R (KN)	D(KN)
79	0.079	0.3	0.7427	0.6763	0	0	0.4	0.327	25	8620	8.62	22.5	0.3928	0.4143	0.0254	0.8	29.76	2083	0.101	-3.9793083	373.49	160.2908672	10.63381103	9.648260166	0.985550866
79	0.079	0.4	0.6393	0.5967	0	0	0.4	0.327	25	8620	8.62	22.5	0.3928	0.4143	0.0254	0.8	29.76	2083	0.113	-4.4304176	317.49	138.4771197	10.80704481	8.20163117	2.605413641
79	0.079	0.5	0.5698	0.5395	0	0	0.4	0.327	25	8620	8.62	22.5	0.3928	0.4143	0.0254	0.8	29.76	2083	0.123	-4.8450778	280.91	124.0091042	10.93817037	7.256681337	3.681489035
79	0.079	0.6	0.5190	0.4960	0	0	0.4	0.327	25	8620	8.62	22.5	0.3928	0.4143	0.0254	0.8	29.76	2083	0.133	-5.2293462	254.62	113.4904432	11.04392368	6.577563676	4.466360002
79	0.079	0.7	0.4797	0.4615	0	0	0.4	0.327	25	8620	8.62	22.5	0.3928	0.4143	0.0254	0.8	29.76	2083	0.142	-5.5884968	234.55	105.3934455	11.13336148	6.059216335	5.074145142
79	0.079	0.8	0.4482	0.4333	0	0	0.4	0.327	25	8620	8.62	22.5	0.3928	0.4143	0.0254	0.8	29.76	2083	0.151	-5.926642	218.59	98.9110487	11.21168047	5.646811108	5.564869357
79	0.079	0.9	0.4221	0.4097	0	0	0.4	0.327	25	8620	8.62	22.5	0.3928	0.4143	0.0254	0.8	29.76	2083	0.159	-6.2469591	205.50	93.56980162	11.28203499	5.308568579	5.973466407
79	0.079	1	0.4002	0.3896	0	0	0.4	0.327	25	8620	8.62	22.5	0.3928	0.4143	0.0254	0.8	29.76	2083	0.166	-6.5519313	194.50	89.07062992	11.34643696	5.024631133	6.321805825
79	0.079	1.1	0.3813	0.3721	0	0	0.4	0.327	25	8620	8.62	22.5	0.3928	0.4143	0.0254	0.8	29.76	2083	0.174	-6.843531	185.11	85.2138823	11.40622632	4.781867445	6.624358877

MATHEMATICAL METHOD

d(m)	d(m)	r (m)	θ1 (rad)	Sin θ1	θ	Sin θ	i	t (m) or b	W (KN)	C (N/m2)	C (KPa)	ϕ	ϕrad	Tan ϕ	k	n	Kc	Kϕ	j	-j/k	Normal stress sigma(N/m2)	Shear Stress (s) or (τ)	H (KN)	R (KN)	D(KN)
97	0.097	0.3	0.8276	0.7363	0	0	0.4	0.327	25	8620	8.62	22.5	0.3928	0.4143	0.0254	0.8	29.76	2083	0.116	-4.5566536	342.33	148.859473	10.75211967	8.699078203	2.053041469
97	0.097	0.4	0.7113	0.6528	0	0	0.4	0.327	25	8620	8.62	22.5	0.3928	0.4143	0.0254	0.8	29.76	2083	0.128	-5.0333877	289.57	127.742964	10.90807891	7.788575106	3.119503804
97	0.097	0.5	0.6334	0.5919	0	0	0.4	0.327	25	8620	8.62	22.5	0.3928	0.4143	0.0254	0.8	29.76	2083	0.139	-5.4780324	255.50	113.9875718	11.03151087	7.106839509	3.924671357
97	0.097	0.6	0.5766	0.5452	0	0	0.4	0.327	25	8620	8.62	22.5	0.3928	0.4143	0.0254	0.8	29.76	2083	0.150	-5.8932935	231.18	104.1021239	11.1347627	6.574667244	4.56009546
97	0.097	0.7	0.5327	0.5079	0	0	0.4	0.327	25	8620	8.62	22.5	0.3928	0.4143	0.0254	0.8	29.76	2083	0.160	-6.2832789	212.70	96.55341314	11.22466681	6.145239202	5.079427605
97	0.097	0.8	0.4976	0.4773	0	0	0.4	0.327	25	8620	8.62	22.5	0.3928	0.4143	0.0254	0.8	29.76	2083	0.169	-6.6516555	198.04	90.5451773	11.30520478	5.789611981	5.515592802
97	0.097	0.9	0.4686	0.4516	0	0	0.4	0.327	25	8620	8.62	22.5	0.3928	0.4143	0.0254	0.8	29.76	2083	0.178	-7.0014347	186.05	85.61634274	11.37883018	5.488976555	5.889853625
97	0.097	1	0.4441	0.4296	0	0	0.4	0.327	25	8620	8.62	22.5	0.3928	0.4143	0.0254	0.8	29.76	2083	0.186	-7.335053	176.00	81.47863863	11.4471343	5.230563501	6.216570797
97	0.097	1.1	0.4231	0.4106	0	0	0.4	0.327	25	8620	8.62	22.5	0.3928	0.4143	0.0254	0.8	29.76	2083	0.194	-7.6544893	167.42	77.94122593	11.51119706	5.005378572	6.505818487

Appendix 8: Example of data for testing the effect of tyre radius on drawbar-pull in lower cohesion soil.

EXPERIMENTAL TYRE SET 2 25KN LOW COHESION RADIUS EFFECT

BEKKER FORMULA

d(m)	d(m)	r (m)	θ1 (rad)	Sin θ1	θ	Sin θ	i	t (m) or b	W (KN)	C (N/m2)	C (KPa)	ϕ	ϕrad	Tan ϕ	k	n	Kc	Kϕ	j	-j/k	Normal stress sigma(N/m2)	Shear Stress (s) or (τ)	H (KN)	R (KN)	D(KN)
185	0.185	0.3	1.1774	0.9236	0	0	0.4	0.327	25	7580	7.58	14	0.2444	0.2494	0.0254	0.6	30.08	499.7	0.187	-7.3609566	214.98	61.14857844	5.540437121	8.373679887	-2.833242767
185	0.185	0.4	1.0033	0.8433	0	0	0.2	0.327	25	7580	7.58	14	0.2444	0.2494	0.0254	0.6	30.08	499.7	0.131	-5.1766252	214.98	60.84194101	6.710799066	9.419126947	-2.708327881
185	0.185	0.5	0.8892	0.7766	0	0	0.3	0.327	25	7580	7.58	14	0.2444	0.2494	0.0254	0.6	30.08	499.7	0.173	-6.8036717	214.98	61.11956927	7.760553661	10.07708775	-2.316534087
185	0.185	0.6	0.8070	0.7222	0	0	0.4	0.327	25	7580	7.58	14	0.2444	0.2494	0.0254	0.6	30.08	499.7	0.224	-8.8268971	214.98	61.17849038	8.668927967	10.53028035	-1.861352381
185	0.185	0.7	0.7441	0.6773	0	0	0.5	0.327	25	7580	7.58	14	0.2444	0.2494	0.0254	0.6	30.08	499.7	0.284	-11.173257	214.98	61.18660922	9.485891272	10.86169563	-1.375804353
185	0.185	0.8	0.6939	0.6395	0	0	0.6	0.327	25	7580	7.58	14	0.2444	0.2494	0.0254	0.6	30.08	499.7	0.350	-13.79818	214.98	61.18740633	10.23702776	11.11469955	-0.877671791
185	0.185	0.9	0.6527	0.6073	0	0	0.7	0.327	25	7580	7.58	14	0.2444	0.2494	0.0254	0.6	30.08	499.7	0.423	-16.671366	214.98	61.18746507	10.93660033	11.31421528	-0.377614948
185	0.185	1	0.6181	0.5795	0	0	0.8	0.327	25	7580	7.58	14	0.2444	0.2494	0.0254	0.6	30.08	499.7	0.502	-19.770667	214.98	61.18746843	11.59402992	11.4756014	0.118428518
185	0.185	1.1	0.5884	0.5550	0	0	0.9	0.327	25	7580	7.58	14	0.2444	0.2494	0.0254	0.6	30.08	499.7	0.586	-23.079044	214.98	61.18746859	12.21612951	11.60884412	0.607285388

WONG AND REECE

d(m)	d(m)	r (m)	θ1 (rad)	Sin θ1	θ	Sin θ	i	t (m) or b	W (KN)	C (N/m2)	C (KPa)	ϕ	ϕrad	Tan ϕ	k	n	Kc	Kϕ	j	-j/k	Normal stress sigma(N/m2)	Shear Stress (s) or (τ)	H (KN)	R (KN)	D(KN)
152	0.152	0.3	1.0549	0.8698	0	0	0.1	0.327	25	7580	7.58	14	0.2444	0.2494	0.0254	0.6	30.08	499.7	0.082	-3.2128617	288.56	76.33526829	6.513790553	14.3426054	-7.828814845
152	0.152	0.4	0.9021	0.7846	0	0	0.2	0.327	25	7580	7.58	14	0.2444	0.2494	0.0254	0.6	30.08	499.7	0.110	-4.3208217	239.93	66.51403931	6.826064259	11.92558121	-5.099516948
152	0.152	0.5	0.8010	0.7180	0	0	0.3	0.327	25	7580	7.58	14	0.2444	0.2494	0.0254	0.6	30.08	499.7	0.149	-5.8731386	209.74	59.71218934	7.010200954	10.42483358	-3.41463263
152	0.152	0.6	0.7278	0.6652	0	0	0.4	0.327	25	7580	7.58	14	0.2444	0.2494	0.0254	0.6	30.08	499.7	0.197	-7.7631602	188.67	54.60299908	7.126342398	9.377485811	-2.251143413
152	0.152	0.7	0.6716	0.6222	0	0	0.5	0.327	25	7580	7.58	14	0.2444	0.2494	0.0254	0.6	30.08	499.7	0.252	-9.9336876	172.89	50.68953336	7.219300716	8.593295858	-1.373995142
152	0.152	0.8	0.6266	0.5864	0	0	0.6	0.327	25	7580	7.58	14	0.2444	0.2494	0.0254	0.6	30.08	499.7	0.314	-12.348733	160.51	47.60385053	7.302909361	7.977793232	-0.674883871
152	0.152	0.9	0.5897	0.5561	0	0	0.7	0.327	25	7580	7.58	14	0.2444	0.2494	0.0254	0.6	30.08	499.7	0.381	-14.983288	150.45	45.09687206	7.380649309	7.478051527	-0.097402218
152	0.152	1	0.5586	0.5300	0	0	0.8	0.327	25	7580	7.58	14	0.2444	0.2494	0.0254	0.6	30.08	499.7	0.453	-17.818774	142.08	43.00863297	7.453773109	7.061810732	0.391962378
152	0.152	1.1	0.5320	0.5072	0	0	0.9	0.327	25	7580	7.58	14	0.2444	0.2494	0.0254	0.6	30.08	499.7	0.529	-20.840719	134.96	41.23428837	7.523034034	6.708139429	0.814894605

MATHEMATICAL MODEL

d(m)	d(m)	r (m)	θ1 (rad)	Sin θ1	θ	Sin θ	i	t (m) or b	W (KN)	C (N/m2)	C (KPa)	ϕ	ϕrad	Tan ϕ	k	n	Kc	Kϕ	j	-j/k	Normal stress sigma(N/m2)	Shear Stress (s) or (τ)	H (KN)	R (KN)	D(KN)
176	0.176	0.3	1.1447	0.9106	0	0	0.1	0.327	25	7580	7.58	14	0.2444	0.2494	0.0254	0.6	30.08	499.7	0.098	-3.8405056	274.98	74.5145963	6.656230729	10.43192669	-3.775695959
176	0.176	0.4	0.9764	0.8285	0	0	0.2	0.327	25	7580	7.58	14	0.2444	0.2494	0.0254	0.6	30.08	499.7	0.125	-4.9388416	226.67	63.64420651	6.896921099	9.606564582	-2.709643484
176	0.176	0.5	0.8658	0.7616	0	0	0.3	0.327	25	7580	7.58	14	0.2444	0.2494	0.0254	0.6	30.08	499.7	0.166	-6.5490652	197.25	56.68646637	7.059063325	8.910824761	-1.851761435
176	0.176	0.6	0.7860	0.7075	0	0	0.4	0.327	25	7580	7.58	14	0.2444	0.2494	0.0254	0.6	30.08	499.7	0.217	-8.5391908	176.95	51.69342739	7.176115048	8.333463225	-1.157348177
176	0.176	0.7	0.7249	0.6631	0	0	0.5	0.327	25	7580	7.58	14	0.2444	0.2494	0.0254	0.6	30.08	499.7	0.275	-10.840749	161.85	47.93706228	7.275556392	7.849535248	-0.573978856
176	0.176	0.8	0.6761	0.6258	0	0	0.6	0.327	25	7580	7.58	14	0.2444	0.2494	0.0254	0.6	30.08	499.7	0.341	-13.411613	150.05	44.99662234	7.366123501	7.438187163	-0.072063663
176	0.176	0.9	0.6361	0.5940	0	0	0.7	0.327	25	7580	7.58	14	0.2444	0.2494	0.0254	0.6	30.08	499.7	0.412	-16.222972	140.51	42.61703098	7.450411998	7.083747757	0.36666424
176	0.176	1	0.6024	0.5666	0	0	0.8	0.327	25	7580	7.58	14	0.2444	0.2494	0.0254	0.6	30.08	499.7	0.489	-19.253677	132.58	40.64038737	7.52964225	6.774605973	0.755036277
176	0.176	1.1	0.5735	0.5426	0	0	0.9	0.327	25	7580	7.58	14	0.2444	0.2494	0.0254	0.6	30.08	499.7	0.571	-22.487398	125.86	38.96449198	7.604634734	6.50208624	1.102548494

Appendix 9: Levelling of sand in the sand terrain bed during laboratory experiments

Appendix 10: Procedure for obtaining the tyre foot print in relation to applied load and tyre pressure of Mobility SF-3713

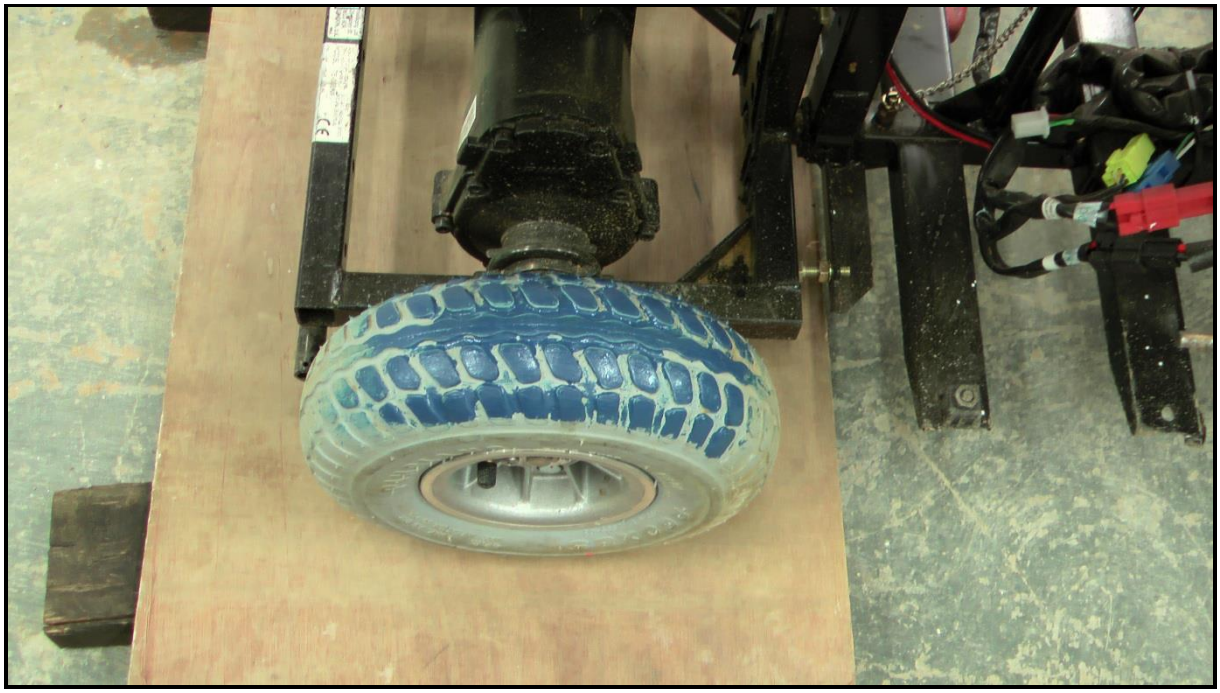

Appendix 11: Procedure for transferring the tyre foot print to the paper in relation to applied load and tyre pressure of Mobility SF-3713

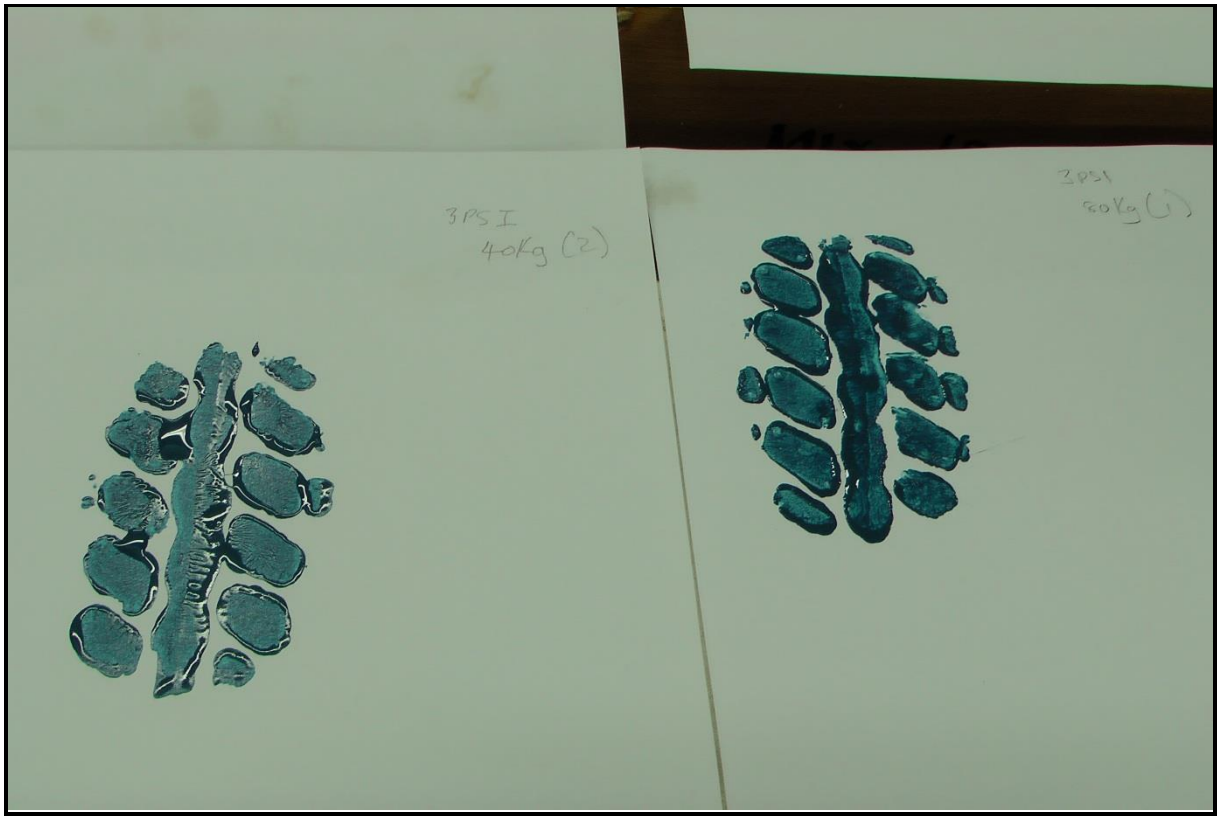

Appendix 12: Mobility SF-3713 in the process of modification in the Advanced Technology Centre at Anglia Ruskin University plate 1

Appendix 13: Mobility SF-3713 in the process of modification in the Advanced Technology Centre at Anglia Ruskin University plate 2

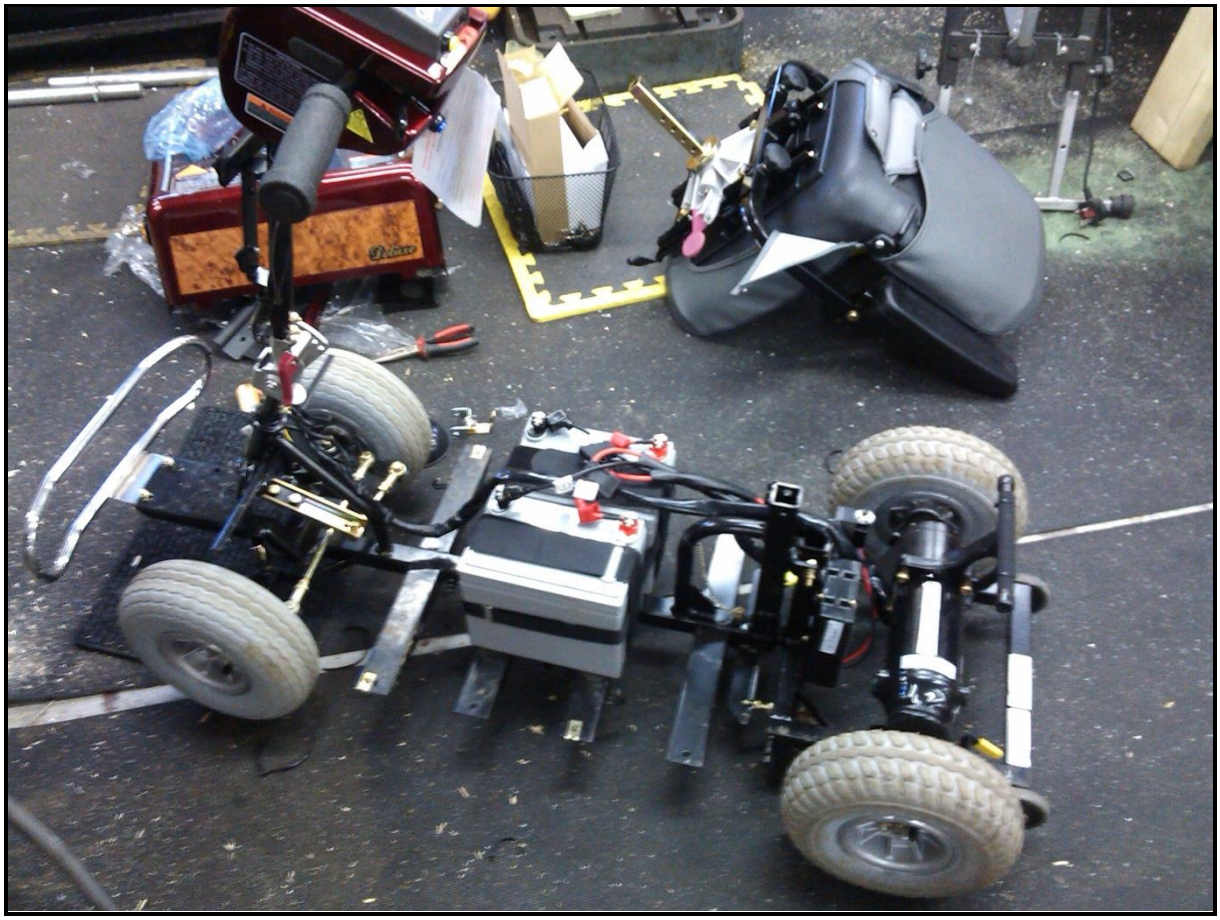

Appendix 14: Sieving process of the sand sample on a shaker

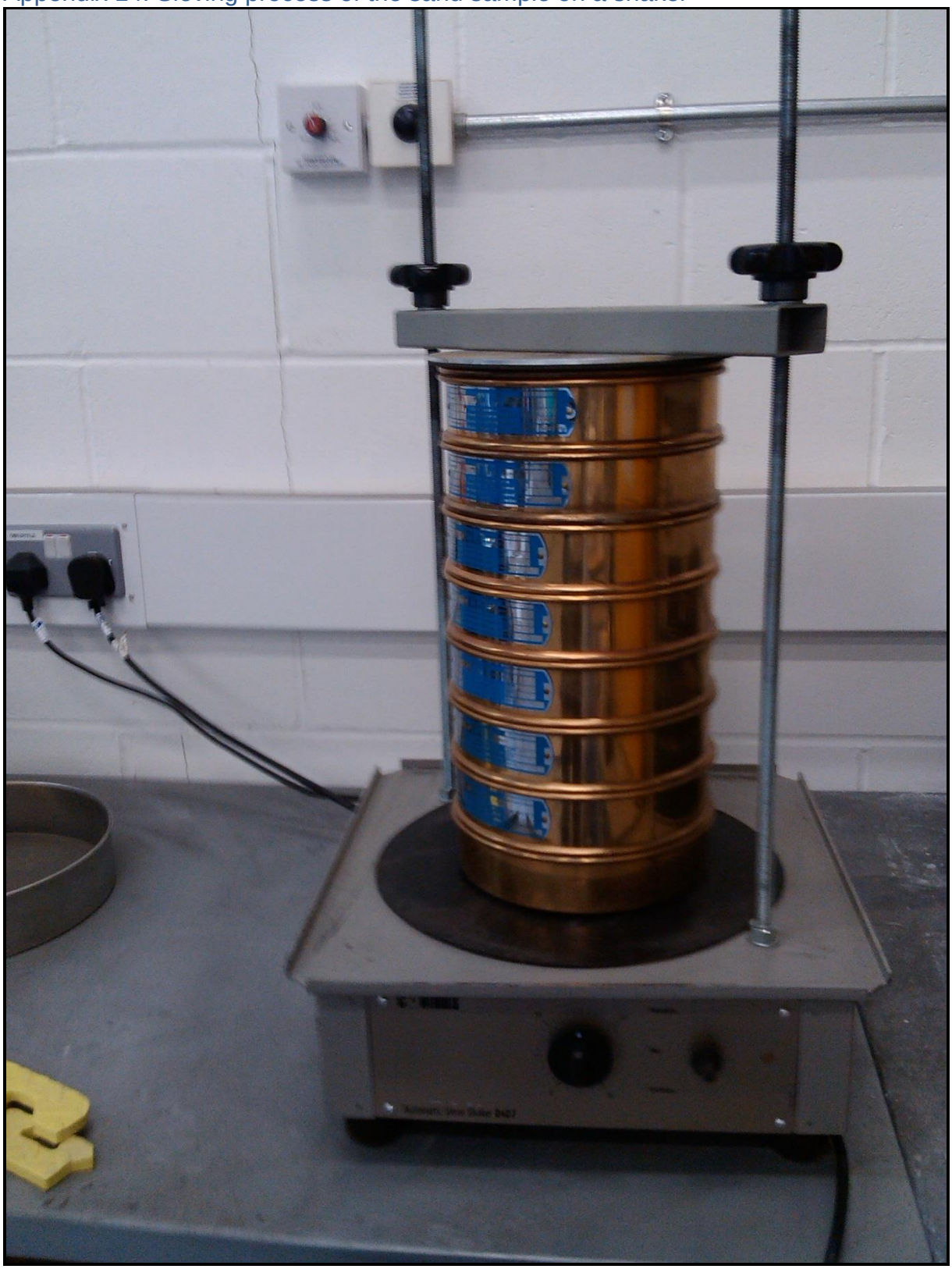

Appendix 15: Weighing procedure for the moulds used as applied load

Appendix 16: Particle size distribution picture of the sand sample after sieving

Appendix 17: Weighing of the sand samples after sieving using a sensitive scale for accurate establishment of the results

Appendix 18: Laboratory report containing the establishment of soil cohesion and angle of shearing resistance of the samples used in the laboratory experiments.1/4

Chelmer Geotechnical Laboratories

Chelmer Geotechnical Laboratories

Unit 15, East Hanningfield Industrial Estate
Old Church Road, East Hanningfield, Essex CM3 8AB
Telephone: 01245 400 930 **Fax:** 01245 400 933
Email: info@siteinvestigations.co.uk **Website**: www.soillabs.co.uk

Geotechnical Testing

Client : Franco Muleya
Site Name : Academic Research ARU
Client Reference : Franco Muleya
CGL Reference : CGL04316
Date of Completion : 16-May

Appendix 19: Laboratory report containing the establishment of soil cohesion and angle of shearing resistance of the samples used in the laboratory experiments.2/4

Chelmer Geotechnical Laboratories

Content Summary

This report contains all test results indicated on the attached test instruction/summary (Q17).

CGL Reference : CGL04316
Client Reference : N/A
For the attention of : Franco Muleya
This report comprises of the following : 1 Pages of Results

Notes :

General

Please refer to report summary notes for details pertaining to methods undertaken and their subsequent accreditations

Samples were supplied by Customer

All tests performed in-house unless otherwise stated

Deviant Samples

Samples were received in suitable containers	Yes
A date and time of sampling was provided	Yes
Arrived damaged and/or denatured	No

Appendix 20: Laboratory report containing the establishment of soil cohesion and angle of shearing resistance of the samples used in the laboratory experiments.3/4

DIRECT SHEAR / TRIAXIAL / ANGLE OF INTERNAL FRICTION

Sample No.	MOISTURE CONTENT (%)	BULK DENSITY (Mg/m^3)	LATERAL PRESSURE (kN/m^2)	COMPRESSIVE STRENGTH (kN/m^2)	COHESION (kN/m^2)	SHEAR VANE TEST RESULTS
Sample 1	31	1.98	70	139	74	111kn/m^2
			210	152		
			350	155		
Sample 2	6.3	1.52	Angle of internal Friction			-
			31°			
Comments:-						

SITE:	Testing for Franco Muleya				JOB NO:	N/A
DATE:	08/05/2014	TESTED BY:	MS	CHECKED:	GW	

TESTS CARRIED OUT UNDER UNDRAINED CONDITIONS UNLESS SPECIFIED

Appendix 18: Laboratory report containing the establishment of soil cohesion and angle of shearing resistance of the samples used in the laboratory experiments.4/4

Appendix 19: Good year tyre inflation data and velocities for off-the road haulage service plate 1

LOAD LIMITS AT COLD INFLATION PRESSURES																
30 MPH (50 KM/H) MAXIMUM SPEED OFF-THE-ROAD HAULAGE SERVICE																
	PSI	**40**	**44**	**46**	**51**	**54**	**58**	**62**	**65**	**69**	**73**	**76**	**80**	**83**		**94**
BIAS	KPA	275	300	325	350	375	400	425	450	475	500	525	550	575		650
16.00-25	**LBS**	**9650**	**10200**	**10700**	**11000**	**11700**	**12000(20)**	**12300**	**12800**	**13200(24)**	**13900**	**14300**	**14300**	**14800(28)**		**16100(32)**
	KG	4375	4625	4875	5000	5300	5450(20)	5600	5800	6000(24)	6300	6500	6500	6700(28)		7300(32)
	PSI	**65**	**69**	**73**	**76**	**80**	**83**	**87**	**91**	**94**	**98**	**102**				
RADIAL	KPA	450	475	500	525	550	575	600	625	650	675	700				
16.00R25	**LBS**	**11400**	**12000***	**12300**	**12800**	**13200**	**13900**	**14300**	**14800**	**15200**	**15700**	**16100****				
	KG	5150	5450*	5600	5800	6000	6300	6500	6700	6900	7100	7300**				
5 MPH (10 KM/H) MAXIMUM SPEED OFF-THE-ROAD SLOW SPEED SERVICE																
	PSI	**69**	**73**	**76**	**80**	**83**	**87**	**91**	**94**	**98**	**102**	**105**	**109**	**112**		
BIAS	KPA	475	500	525	550	575	600	625	650	675	700	725	750	775	Continued	
16.00-25	**LBS**	**19300**	**19800**	**20400**	**21500(20)**	**22000**	**22000**	**22700**	**23400(24)**	**24000**	**24700**	**24700**	**25400(28)**	**26000**		
	KG	8750	9000	9250	9750(20)	10000	10000	10300	10600(24)	10900	11200	11200	11500(28)	11800		
	PSI	**116**	**120**	**123**	**127**	**131**	**134**	**138**	**141**	**145**	**149**					
	KPA	800	825	850	875	900	925	950	975	1000	1025					
	LBS	**26800**	**26800**	**27600**	**27600(32)**	**28300**	**29100**	**29100**	**30000(36)**	**30000**	**30900**			**32000(40)▲**		
	KG	12150	12150	12500	12500(32)	12850	13200	13200	13600(36)	13600	14000			14500(40)▲		
	PSI	**76**	**80**	**83**	**87**	**91**	**94**	**98**	**102**	**105**	**109**	**112**	**116**	**120**		**131**
RADIAL	KPA	525	550	575	600	625	650	675	700	725	750	775	800	825		900
16.00R25	**LBS**	**19300**	**19800***	**20400**	**21500**	**22000**	**22700**	**23400**	**24000**	**24700**	**25400**	**26000**	**26800**	**26800****		**29100*****
	KG	8750	9000*	9250	9750	10000	10300	10600	10900	11200	11500	11800	12150	12150**		13200***

▲ Permafoam inflation or special rim required.

Appendix 21: Good year tyre inflation data and velocities for off-the road haulage service plate 2

LOAD LIMITS AT COLD INFLATION PRESSURES

5 MPH (10 KM/H) MAXIMUM OFF-THE-ROAD SLOW SPEED SERVICE

	PSI	58	62	65	69	73	76	80	83	87	91					
RADIAL	KPA	400	425	450	475	500	525	550	575	600	625					
25/55R25	LBS	17600	18700	19300	20400*											
	KG	8000	8500	8750	9250*											
550/65R25	LBS	16500	17600	18200	18700*	19800	20400	20900	22000	22700	23400**					
(22/65R25)	KG	7500	8000	8250	8500*	9000	9250	9500	10000	10300	10600**					
600/65R25	LBS	19300	19800	20900	21500*	22700	23400	24000	24700	26000	26800**					
	KG	8750	9000	9500	9750*	10300	10600	10900	11200	11800	12150**					
25/65R25	LBS	19800	20400	21500	22700*	23400	24000	25400	26000	26800	27600**					
	KG	9000	9500	9750	10300*	10600	10900	11500	11800	12150	12500**					
650/65R25	LBS	22000	23400	24000	25400*	26000	26800	28300	29100	30000	30900**					
	KG	10000	10600	10900	11500*	11800	12150	12850	13200	13600	14000**					
750/65R25	LBS	30000	30900	33100	34200*	35300	36400	37500	38600	39700	41900**					
(30/65R25)	KG	13600	14000	15000	15500*	16000	16500	17000	17500	18000	19000**					
775/65R29	LBS	33100	34200	35300	37500*	38600	39700	40800	41900	44100	45400**					
(800/65R29)	KG	14500	15500	16000	17000*	17500	18000	18500	19000	20000	20600**					
30/65R29	LBS	30900	32000	34200	35300*	36400	37500	38600	39700	40800	41900**					
	KG	14000	14500	15500	16000*	16500	17000	17500	18000	18500	19000**					
875/65R29	LBS	40800	43000	44100	46700*	48100	49400	52000	53600	55100	56800**					
	KG	18500	19500	20000	21200*	21800	22400	23600	24300	25000	25750**					

30 MPH (50 KM/H) MAXIMUM SPEED OFF-THE-ROAD ARTICULATED DUMP SERVICE

	PSI	29	33	36	40	44	47	51	54	58	62	65	69	73		
RADIAL	KPA	200	225	250	275	300	325	350	375	400	425	450	475	500		
600/65R25	LBS	8550	9350	10200	10700	11700	12300*	12800	13600	14300	15200**					
	KG	3875	4250	4625	4875	5300	5600*	5800	6150	6500	6900**					
25/65R25	LBS	8800	9650	10500	11000	12000	12800*	13600	13900	14800	15700**					
	KG	4000	4375	4750	5000	5450	5800*	6150	6300	6700	7100**					
650/65R25	LBS	9900	10700	11700	12300	13200	14300*	15200	15700	16500	17600**					
	KG	4500	4875	5300	5600	6000	6500*	6900	7100	7500	8000**					
750/65R25	LBS	13200	14300	15700	17100	18200	19300*	20400	21500	22700	23400**					
(30/65R25)	KG	6000	6500	7100	7750	8250	8750*	9250	9750	10000	10600**					
30/65R29	LBS	15700	17100	18200	19800	20900	22000*	23400	24700	26000	27600**					
	KG	7100	7750	8250	9000	9500	10000*	10600	11200	11800	12500**					
775/65R29	LBS	16100	17600	18700	20400	21500	22700*	24000	25400	26800	28300**					
	KG	7300	8000	8500	9250	9750	10300*	10900	11500	12150	12850**					
875/65R29	LBS	19300	20900	22700	24700	26000	27600*	29100	30900	32000	34200**					
	KG	8750	9500	10300	11200	11800	12500*	13200	14000*	14500	15500**					

Appendix 22: Velocity analysis results from Mobility SF-3713 laboratory experiments showing consistency with respect to increase in speed selections

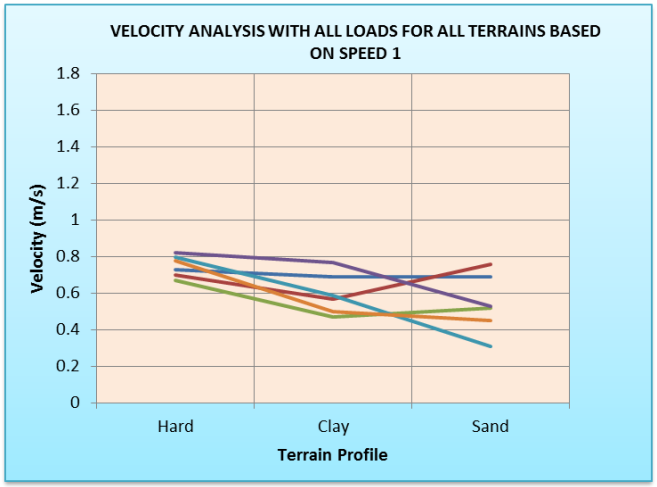

Velocity analysis at speed selection 1

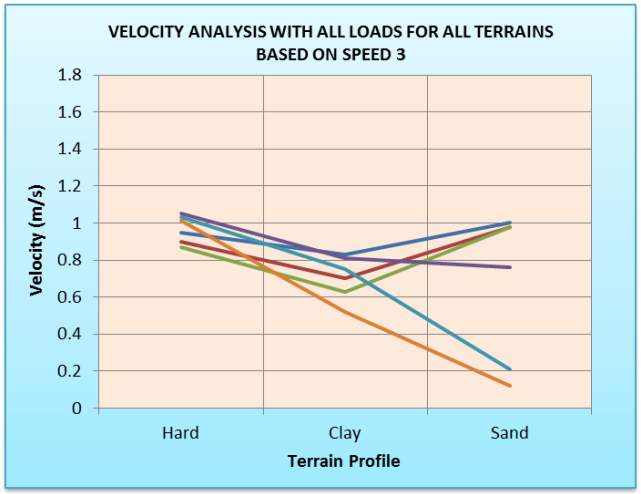

Velocity analysis at speed selection 3

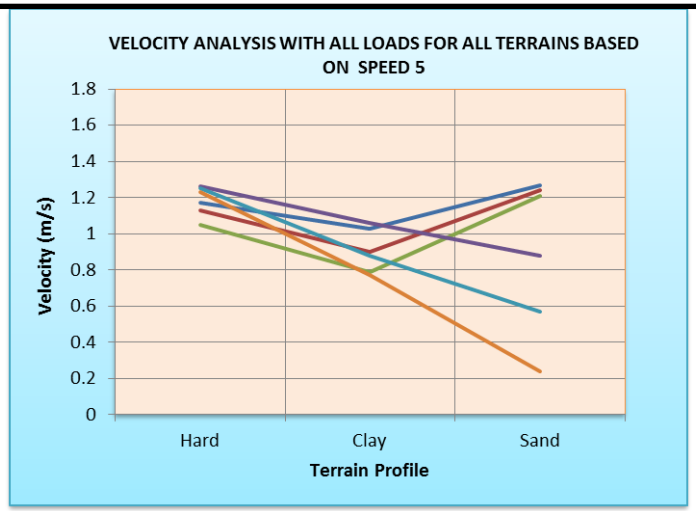

Velocity analysis at speed selection 5

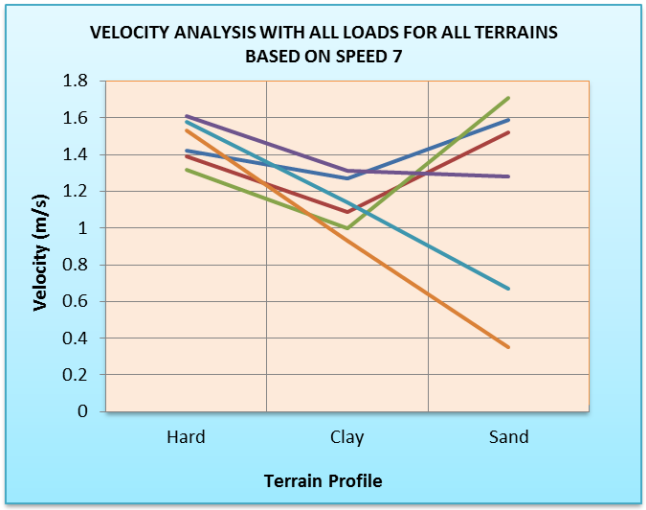

Velocity analysis at speed selection 7

Appendix 23: Rut depth analysis results from Mobility SF-3713 laboratory experiments showing consistency with respect to increase in speed selections

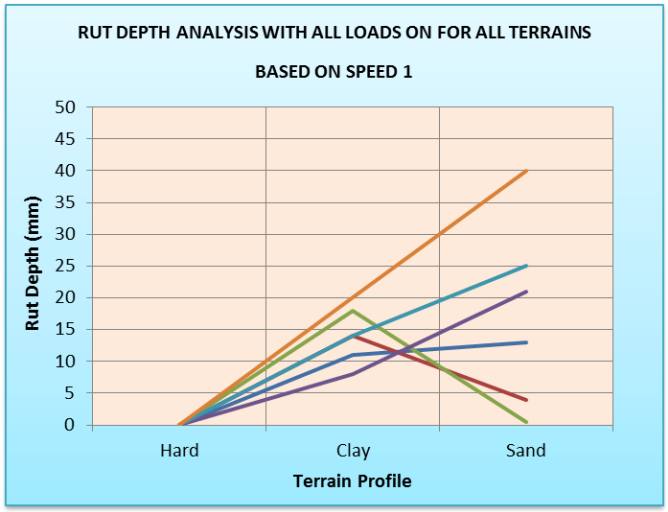

Rut depth analysis at speed selection 1

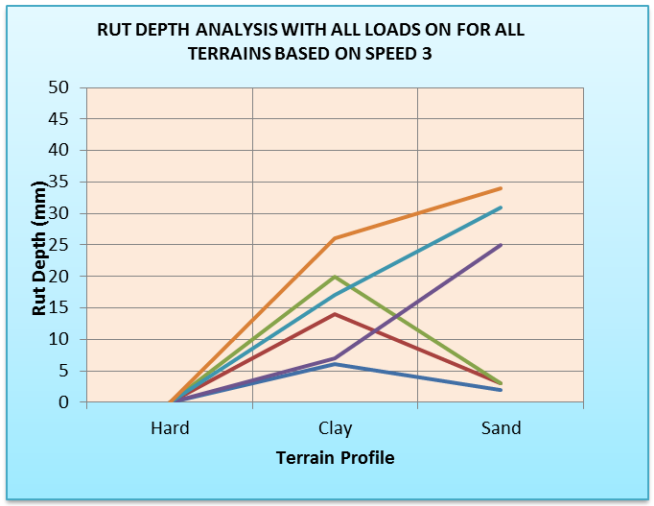

Rut depth analysis at speed selection 3

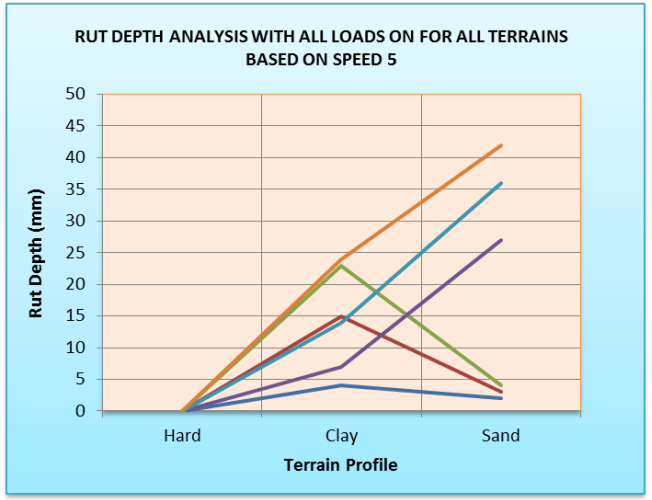

Rut depth analysis at speed selection 5

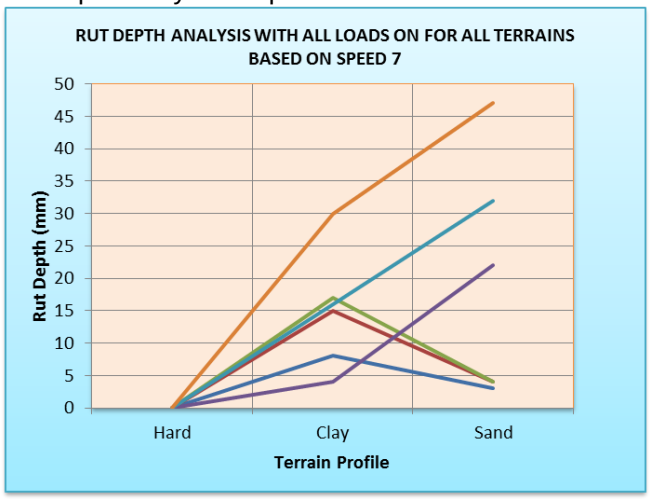

Rut depth analysis at speed selection 7

Appendix 24: Drawbar-pull analysis results from Mobility SF-3713 laboratory experiments showing consistency with respect to increase in speed selections

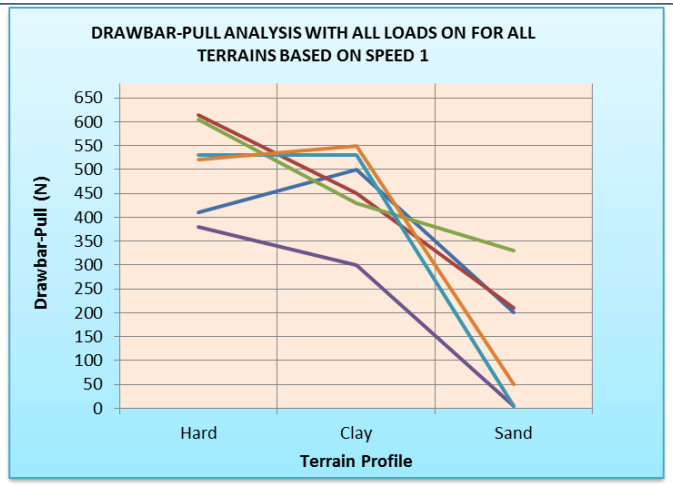

Drawbar-pull analysis at speed selection 1

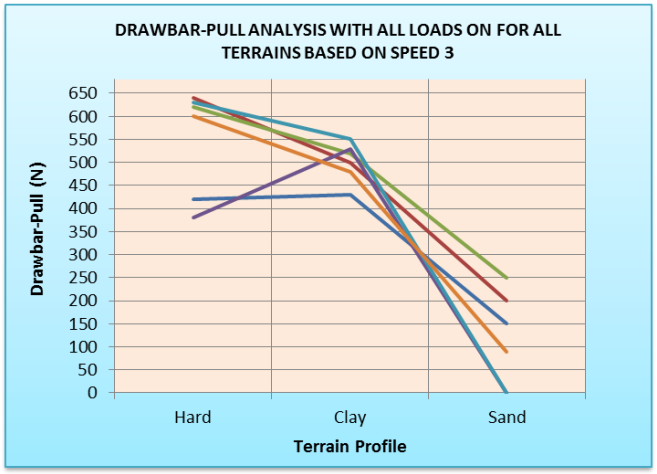

Drawbar-pull analysis at speed selection 1

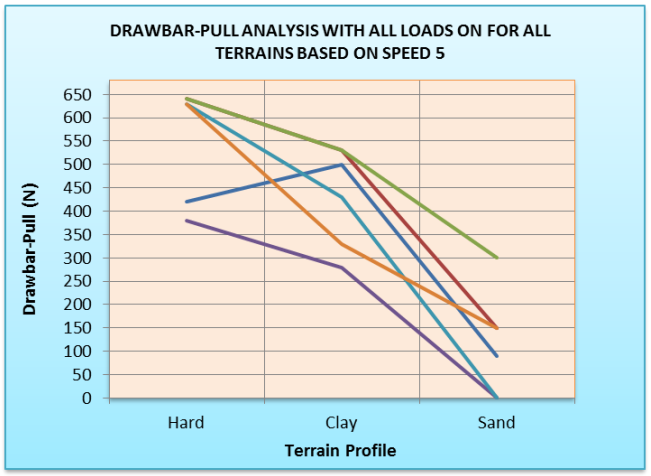

Drawbar-pull analysis at speed selection 1

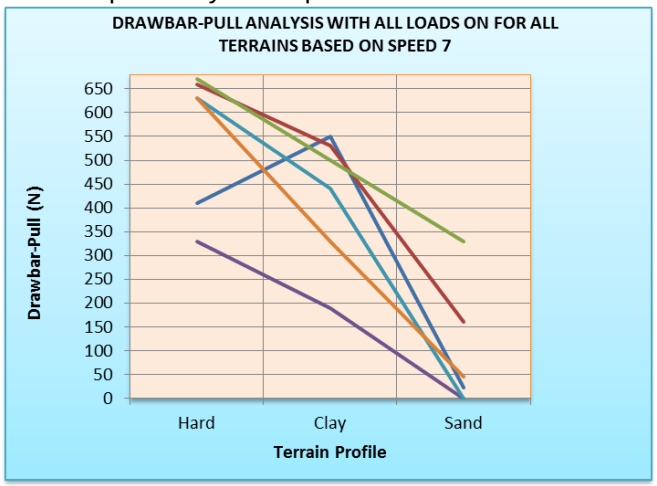

Drawbar-pull analysis at speed selection 1

Appendix 24: Description of the labelled image for the special instrumented vehicle Mobility SF-3713 used during controlled laboratory experiments

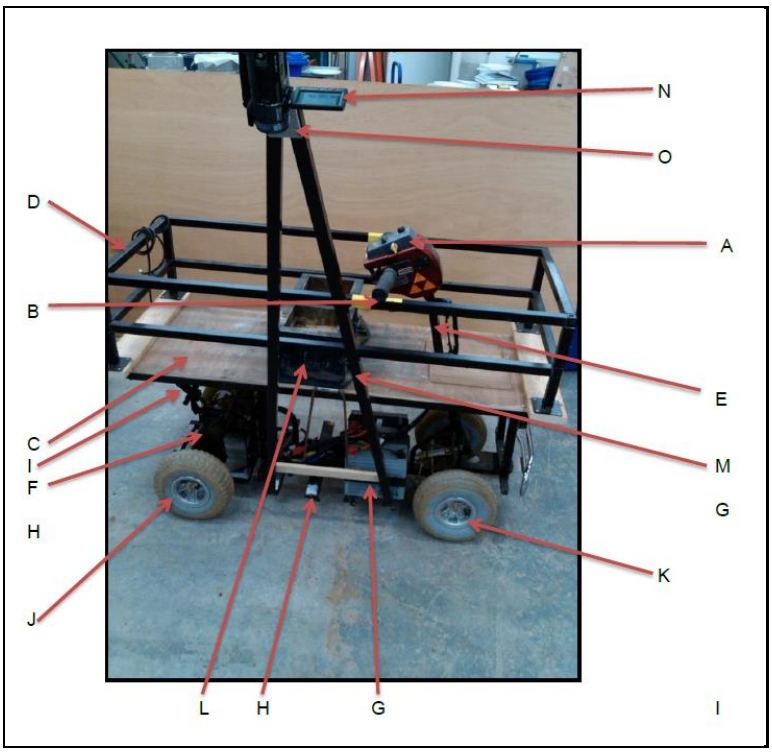

The following describe parts of the instrumented MOBILITY SF-3713 vehicle used

A. Speed control and manoeuvring unit
B. Forward gear lever and reverse gear lever
C. Softwood timber load supporting base
D. Light metal square tubular rails for load side support
E. Front tyre steering spindle
F. Battery powered motor
G. Batteries for power supply.
H. Battery support base
I. Power supply cutting mechanism.
J. Two rear tyres
K. Two Front tyres 260 x 85
L. Applied load of 20Kg of applied load each.
M. Camcorder stand and holder
N. Panasonic High Definition Camcorder
O. Unit for securing the camcorder.

Appendix 25: Description of David Reid's mathematical RUTSEV model for calculating rut depth

$$d_n = d_{n-1} - \frac{f(d)}{f'(d)}$$ Eqn 4.33 and Eqn 6.12

Where d_n is the rut depth.

$$f(d) = Ctd^2 - \frac{WVv^2d^2}{2gr^2(1-i)^2\arccos^2\left(\frac{r-d}{r}\right)} + 2C(2rd-d^2)^{0.5}d^2 + (W+L)\left(\frac{2}{\pi}-1\right)d + 2(W+L)\left(\frac{(1-\sin\phi)}{(1+\sin\phi)}\right)\tan\phi.d + \left(\frac{(W+L)\tan\phi\left(2rd-d^2\right)^{0.5}}{2r}\right)d$$ Eqn 4.34 and Eqn 6.13

$$f'(d) = 2Ctd - \left\{\frac{W\omega^2 d\left(\arccos\left(\frac{r-d}{r}\right) - \frac{d}{r\left(1-\left((r-d)/r\right)^2\right)^{0.5}}\right)}{g.\arccos^3\left(\frac{r-d}{r}\right)}\right\} + 4dc\left(2rd-d^2\right)^{0.5} + \frac{Cd^2(2r-2d)}{\left(2rd-d^2\right)^{0.5}} + \left(\frac{2}{\pi}-1\right)(W+L) + \frac{(W+L)\tan\phi(2rd-d^2)^{0.5}}{2r} + \frac{(W+L)\tan\phi.d(2r-2d)}{4r(2rd-d^2)^{0.5}} + 2(W+L)\left(\frac{(1-\sin\phi)}{(1+\sin\phi)}\right)\tan\phi$$ Eqn 4.35 and Eqn 6.14

Notation

d_n = rut depth

C = Cohesion (N/m^2)

t = wheel width (m)

r = wheel rolling radius (m)

L = Wheel applied load (N)

i = Slip/skid ratio

$\emptyset$ = Angle of shearing resistance (Degrees)

ω = Rotational velocity (rad/s)

d = wheel sinkage (m)

W = Wheel self-weight (N)

V_v = Forward velocity (m/s)

g = Acceleration (m/s^2)

Appendix 26: Development of David Reid's mathematical RUTSEV model for calculating rut depth. 1/8

Rut depth equation development part 1: The Soil Velocity Model

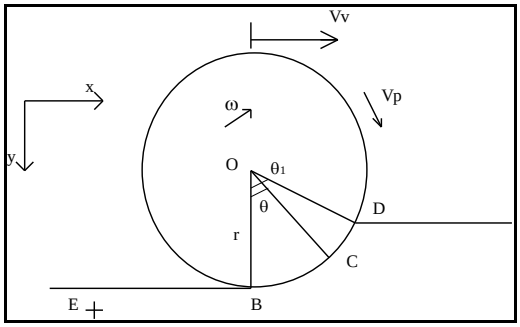

Figure 1: Wheel dynamics basic notation

$$i = \frac{Vp - Vv}{Vp} = \frac{\omega r - Vv}{\omega r}$$

$$\therefore Vv = \omega r(1-i) \qquad \text{Eqn. 1}$$

$$\left|(V_C)_E\right| = [\{\omega r(1-i)\}^2 + \{\omega r\}^2 - 2\{\omega r(1-i)(\omega r)\cos\theta\}]^{0.5} \qquad \text{Eqn. 2}$$

$$\left|(V_C)_E\right| = [\omega^2 r^2(1-i)^2 + \omega^2 r^2 - 2\omega^2 r^2(1-i)\cos\theta]^{0.5}$$

$$\therefore \left|(V_C)_E\right| = \omega r[(1-i)^2 + 1 - 2(1-i)\cos\theta]^{0.5} \qquad \text{Eqn. 3}$$

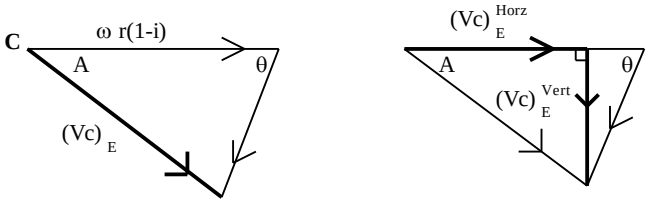

Figure 1a: Absolute velocity of C and 1b: Components of the velocity at C

As can be seen from Figure 1a, the vector describing the velocity at C relative to E can be expressed as the sum of the horizontal and vertical components as given in Equations 4 and 5.

$$\text{(a)}\quad (V_C)_E^{vert} = \omega r \sin\theta \downarrow \qquad \text{Eqn. 4}$$

$$\text{(b)}\quad (V_C)_E^{horz} = \omega r(1 - i - \cos\theta) \rightarrow \qquad \text{Eqn. 5}$$

From Figure 3 and Equations 4 and 5, the direction of the velocity vector at C can be expressed by Equations 6 and 7.

$$\angle A = \arctan\left\{\frac{\sin\theta}{(1-i-\cos\theta)}\right\} \qquad \text{Eqn. 6}$$

$$\angle A = \arccos\left\{\frac{(1-i-\cos\theta)}{[(1-i)^2 + 1 - 2(1-i)\cos\theta]^{0.5}}\right\} \qquad \text{Eqn. 7}$$

Appendix 27: Development of David Reid's mathematical RUTSEV model for calculating rut depth. 2/8

Equation 6 confirms the expression developed for the direction of the velocity vector developed from the rolling locus. The sum of the vertical velocities for all points 'C' between B and D can be found by integrating Equation 4 for θ between 0 and θ_1 resulting in Equation 9.

$$(V)_{tot}^{vert} = \int_0^{\theta_1} (\omega r \sin\theta).d\theta \qquad \text{Eqn. 8}$$

$$= [-\omega r \cos\theta]_0^{\theta_1}$$

$$= (-\omega r \cos\theta_1) - (-\omega r)$$

$$\therefore (V)_{tot}^{vert} = \omega r(1-\cos\theta_1) \qquad \text{Eqn. 9}$$

Thus an expression for the average vertical velocity of the wheel rim in the soil contact arc BD can be developed from Equation 10 and is expressed as Equation 11.

$$(V)_{aver}^{vert} = \frac{(V)_{tot}^{vert}}{\theta_1} \qquad \text{Eqn. 10}$$

$$= \frac{\omega r(1-\cos\theta_1)}{\theta_1}$$

$$= \frac{\omega r\left(1-\left(\frac{r-d}{r}\right)\right)}{\arccos\left(\frac{r-d}{r}\right)}$$

$$\therefore (V)_{aver}^{vert} = \frac{\omega d}{\arccos\left(\frac{r-d}{r}\right)} \qquad \text{Eqn. 11}$$

Substituting the rotational velocity term by the expression for forward velocity given by Equation 1, the average vertical velocity of the wheel rim in the soil contact arc can be expressed in terms of Vv, r, i and d as in Equation 12.

$$(V)_{aver}^{vert} = \frac{Vv.d}{r(1-i)\arccos\left(\frac{r-d}{r}\right)} \qquad \text{Eqn. 12}$$

Appendix 26: Development of David Reid's mathematical RUTSEV model for calculating rut depth. 3/8

Rut depth equation development part 2: The Soil Velocity Model

C:	Apparent cohesion (N/m^2)	W:	Wheel self-weight (N)
D:	Rrut depth (m)	WD:	Work done (J)
E_1:	Initial energy (J)	W_{soil}:	Work done by soil compression (J)
E_2;	Final energy (J)	W_{FB}:	Work done, friction wheel face (J)
I:	Slip skid ratio	W_{FS}:	Work done, friction wheel sides (J)
K_1:	Initial kinetic energy (J)	W_W:	Work done by wheel weight (J)
K_2:	Final kinetic energy (J)	W_L:	Work done by applied load (J)
L:	Applied load (N)	ϕ	Angle of shearing resistance (deg.)
R:	Wheel radius (m)	θ	Angular position of general point C (rad)
T:	Wheel width (m)	$\theta 1$	Angle subtending contact arc BD (rad)
Vv:	Translational velocity (m/s)	σ_n:	normal stress (N/m^2)
ω:	Rotational velocity (rad/s)		

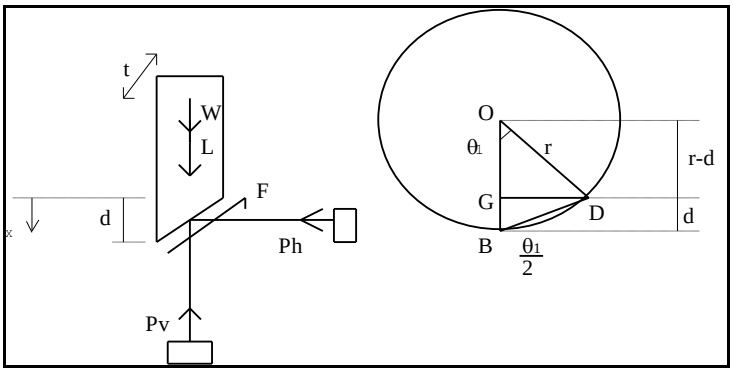

Figure 2a: Idealised free-body diagram of wheel and figure 2b Wheel geometry on the right

$$WD = W_{soil} + W_{FB} + W_{FS} + W_W + W_L \qquad \text{Eqn. 13}$$

Considering each element of Equation 13 separately.

(1) Work done by the vertical soil component (W_{soil})

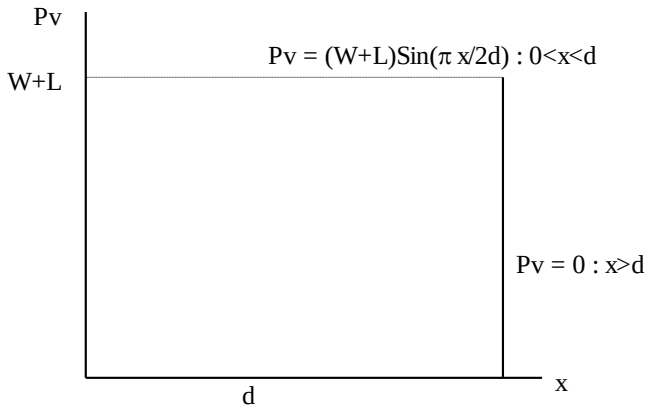

Figure 3: The vertical component of soil reaction

Appendix 26: Development of David Reid's mathematical RUTSEV model for calculating rut depth. 4/8

Work done by the vertical component of the soil reaction can be determined from the area under the curve shown in Figure 3 for displacement, x, between values of 0 and d.

Integrating Equation 14 leads to Equation 15.

$$W_{soil} = -\int_0^d (W+L)\sin\left(\frac{\pi x}{2d}\right)dx \qquad \text{Eqn. 14}$$

$$= -\left[-\frac{2d(W+L)}{\pi}\cos\left(\frac{\pi x}{2d}\right)\right]_0^d$$

$$= -\left[\left(-\frac{2d(W+L)}{\pi}\cos\frac{\pi}{2}\right)-\left(-\frac{2d(W+L)}{\pi}\cos 0\right)\right]$$

$$\therefore W_{soil} = -\frac{2d(W+L)}{\pi} \qquad \text{Eqn. 15}$$

(2) Work done by the friction on the wheel (underside and sides) (W_{FB} and W_{FS})

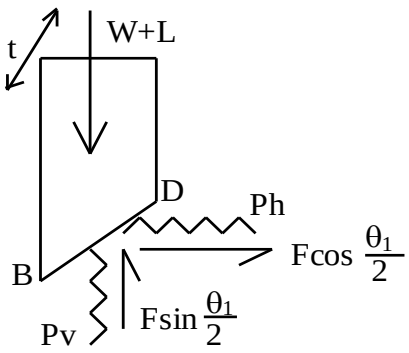

Figure 4: The soil-wheel frictional resistance

The soil-wheel frictional resistance term consists of two components, F_B and F_S, generated under the wheel and on the wheel sides respectively.

$$F = F_B + F_S \qquad \text{Eqn. 16}$$

Appendix 26: Development of David Reid's mathematical RUTSEV model for calculating rut depth. 5/8

The classical Mohr-Coulomb soil model for shear strength is written in terms of shear stress in Equation 17. The equation is presented in total stress parameters due to the nature of the loading. The moving wheel rapidly loads the soil, precluding the dissipation of pore water pressure.

$$F_B = (C + \sigma_n \tan\phi) t\sqrt{2rd} \qquad \text{Eqn. 17}$$

The normal stress on the plane BD is given by Equation 18.

$$\sigma_n = \frac{(W+L)\cos\frac{\theta_1}{2}}{t\sqrt{2rd}} \qquad \text{Eqn. 18}$$

Substituting Equation 18 into Equation 17 leads to Equation 19.

$$F_B = \left(C + \frac{(W+L)\cos\frac{\theta_1}{2}}{t\sqrt{2rd}} \tan\phi \right) t\sqrt{2rd}$$

$$= Ct\sqrt{2rd} + (W+L)\cos\frac{\theta_1}{2}\tan\phi$$

$$\therefore W_{FB} = -d\left(Ct\sqrt{2rd} + (W+L)\cos\frac{\theta_1}{2}\tan\phi\right)\sin\frac{\theta_1}{2} \qquad \text{Eqn. 19}$$

The trigonometric relationships of Equations 20, 21 and 22 are established by reference to Figure 2b.

$$\sin\frac{\theta_1}{2} = \frac{d}{\sqrt{2rd}} = \frac{d^{0.5}}{\sqrt{2r}} \qquad \text{Eqn. 20}$$

$$\cos\frac{\theta_1}{2} = \frac{(2rd - d^2)^{0.5}}{\sqrt{2rd}} \qquad \text{Eqn. 21}$$

$$\sin\frac{\theta_1}{2}\cos\frac{\theta_1}{2} = \frac{(2rd - d^2)^{0.5}}{2r} \qquad \text{Eqn. 22}$$

Substituting these relationships into Equation 19 leads to Equation 23

Appendix 26: Development of David Reid's mathematical RUTSEV model for calculating rut depth. 6/8

$$\therefore W_{FB} = -(Ct\sqrt{2r}\sin\frac{\theta_1}{2})d^{1.5} - (W+L)\cos\frac{\theta_1}{2}\sin\frac{\theta_1}{2}\tan\phi)d$$

$$W_{FB} = -Ctd^2 - \left(\frac{(W+L)\tan\phi(2rd-d^2)^{0.5}}{2r}\right)d \qquad \text{Eqn. 23}$$

The frictional resistance of the soil in the vertical plane near the wheel sides can be calculated from Equation 24.

$$F_S = 2\{\text{side area } (C+\sigma_3\tan\phi)\} \qquad \text{Eqn. 24}$$

The side area can be approximated by the triangle BGD on Figure 2b and σ_3 set equal to Ka.σ_1 giving Equation 25.

$$F_S = 2Cd\sqrt{2rd-d^2} + 2(W+L)\frac{(1-\sin\phi)}{(1+\sin\phi)}\tan\phi \qquad \text{Eqn. 25}$$

The assumption that the stress normal to the vertical face of the wheel sides, σ_3, can be replaced by the vertical stress σ_1 and the coefficient of active pressure Ka, implies that the predominant mode of interaction between the soil and the wheel sides is as shown on Figure 5.

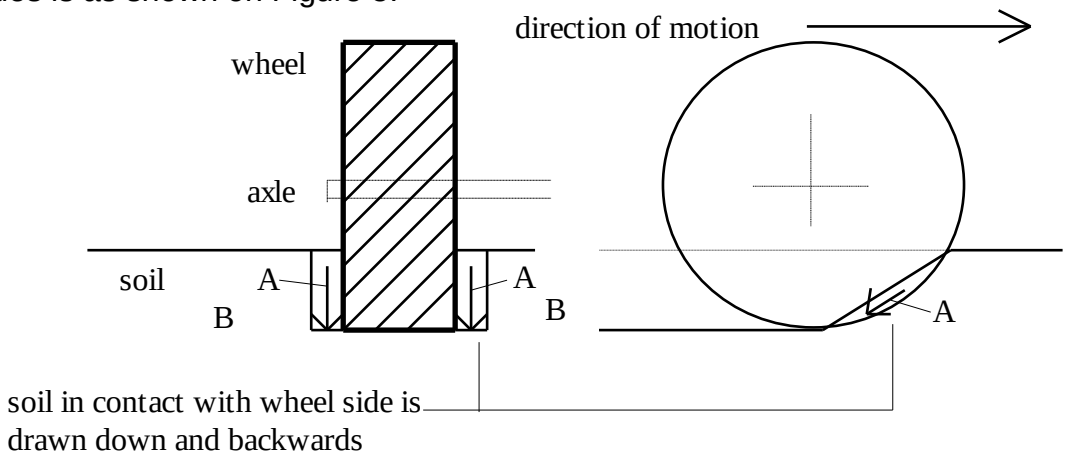

Figure 5: Transverse directions of soil flow during the passage of a wheel

As the wheel passes, soil close to the wheel sides, shown as A on figure 5, is drawn downwards and backwards with the wheel. As a consequence a horizontal expansion of the

Appendix 26: Development of David Reid's mathematical RUTSEV model for calculating rut depth. 7/8

soil at the rut edges, shown as B on Figure 5, takes place with the soil flowing into region A, thus dictating the adoption of the active pressure coefficient. Hence the work term due to side friction can be expressed by Equation 26.

$$\therefore W_{FS} = -2Cd^2\sqrt{2rd-d^2} - 2d(W+L)\frac{(1-\sin\phi)}{(1+\sin\phi)}\tan\phi \qquad \text{Eqn. 26}$$

(3) Work done by the wheel (W_W) is given by:

$$W_W = +Wd \qquad \text{Eqn. 27}$$

(4) Work done by the load (W_L) is given by:

$$W_L = +Ld \qquad \text{Eqn. 28}$$

The traditional work-energy relationship is stated in Equation 29. The relationship is satisfactory for systems where non-mechanical energy losses are negligible. Since the assumption here is that the wheel is solid, Equation 29 is valid. For a real wheel, energy losses in the form of heat developed from tyre distortions will be present. The effect will, however be small and can justifiably be ignored.

$$E_2 = E_1 + WD \qquad \text{Eqn. 29}$$

The energy terms are due purely to kinetic energy and thus lead to Equation 30.

$$K_2 = K_1 + WD \qquad \text{Eqn. 30}$$

For the model adopted, the final kinetic energy is zero and initial kinetic energy is purely translational and can be approximated using the wheel mass and the average vertical velocity term.

$$0 = 0.5m\{(V)_{aver}^{vert}\}^2 + W_{soil} + W_{FB} + W_{FS} + W_W + W_L \qquad \text{Eqn. 31}$$

Appendix 26: Development of David Reid's mathematical RUTSEV model for calculating rut depth. 8/8

Denoting the right hand side of Equation 31 by f(d) produces Equation 32.

$$f(d) = Ctd^2 - \frac{WVv^2d^2}{2gr^2(1-i)^2\arccos^2\left(\frac{r-d}{r}\right)} + 2C(2rd-d^2)^{0.5}d^2$$

$$+(W+L)\left(\frac{2}{\pi}-1\right)d + 2(W+L)\left(\frac{(1-\sin\phi)}{(1+\sin\phi)}\right)\tan\phi.d$$

$$+\left(\frac{(W+L)\tan\phi\left(2rd-d^2\right)^{0.5}}{2r}\right)d \qquad \text{Eqn. 32}$$

Differentiating Equation 32 with respect to d, provides Equation 33.

$$f'(d) = 2Ctd - \left\{\frac{W\omega^2 d\left(\arccos\left(\frac{r-d}{r}\right) - \frac{d}{r\left(1-\left((r-d)/r\right)^2\right)^{0.5}}\right)}{g.\arccos^3\left(\frac{r-d}{r}\right)}\right\}$$

$$+4dc\left(2rd-d^2\right)^{0.5} + \frac{Cd^2(2r-2d)}{\left(2rd-d^2\right)^{0.5}} + \left(\frac{2}{\pi}-1\right)(W+L)$$

$$+\frac{(W+L)\tan\phi(2rd-d^2)^{0.5}}{2r} + \frac{(W+L)\tan\phi.d(2r-2d)}{4r(2rd-d^2)^{0.5}}$$

$$+2(W+L)\left(\frac{(1-\sin\phi)}{(1+\sin\phi)}\right)\tan\phi \qquad \text{Eqn. 33}$$